

COBALT-CATALYZED C-H FUNCTIONALIZATION: FROM MECHANISTIC STUDIES TO SYNTHETIC METHODOLOGIES

Oriol Planas Fàbrega

Per citar o enllaçar aquest document:
Para citar o enlazar este documento:
Use this url to cite or link to this publication:
<http://hdl.handle.net/10803/482111>



<http://creativecommons.org/licenses/by-nc/4.0/deed.ca>

Aquesta obra està subjecta a una llicència Creative Commons Reconeixement-
NoComercial

Esta obra está bajo una licencia Creative Commons Reconocimiento-NoComercial

This work is licensed under a Creative Commons Attribution-NonCommercial licence



DOCTORAL THESIS

**COBALT-CATALYZED C-H
FUNCTIONALIZATION:
FROM MECHANISTIC STUDIES TO
SYNTHETIC METHODOLOGIES**

ORIOL PLANAS FÀBREGA

2017

Doctoral programme in Chemistry

Supervised by Dr. Xavi Ribas Salamaña and Dr. Anna Company Casadevall

Tutor: Dr. Xavi Ribas Salamaña

Presented in partial fulfillment of the requirements for a doctoral degree from the
Universitat de Girona.



Dr. Xavi Ribas Salamaña and Dr. Anna Company Casadevall, from Universitat de Girona,

WE DECLARE:

That the thesis entitled “Cobalt-catalyzed C-H Functionalization: From Mechanistic Studies to Synthetic Methodologies”, presented by Oriol Planas Fàbrega to obtain a doctoral degree, has been completed under our supervision and meets the requirements to opt for an International Doctorate.

For all intents and purposes, we hereby sign this document.

Dr. Xavi Ribas Salamaña

Dr. Anna Company Casadevall

Girona, 22nd November 2017

The scientific man does not aim at an immediate result. He does not expect that his advanced ideas will be readily taken up. His work is like that of the planter - for the future. His duty is to lay the foundation for those who are to come, and point the way.

Nikola Tesla (1856-1943)

Als meus pares i la meva germana

A la Mireia

I a tots amb els que he compartit alguna etapa d'aquest viatge

FULL LIST OF PUBLICATIONS

This thesis is based on a compendium of the following publications:

Chapter III

Isolation of Key Organometallic Aryl-Co(III) Intermediates in Cobalt-Catalyzed C(sp²)-H Functionalization and New Insights into Alkyne Annulation Reaction Mechanisms. **Oriol Planas**, Christopher J. Whiteoak, Vlad Martin-Diaconescu, Ilaria Gamba, Josep M. Luis, Teodor Parella, Anna Company and Xavi Ribas. *J. Am. Chem. Soc.* **2016**, *138*, 14388-14397. (Impact factor: 13.858, position 10/166 in Chemistry, multidisciplinary, 1st quartile).

Chapter IV

Carboxylate-Assisted Formation of Aryl-Co(III) Masked-Carbenes in Cobalt-Catalyzed C-H Functionalization with Diazo Esters. **Oriol Planas**, Steven Roldan-Gomez, Vlad Martin-Diaconescu, Teodor Parella, Josep M. Luis, Anna Company and Xavi Ribas. *J. Am. Chem. Soc.* **2017**, *139*, 14649-14655. (Impact factor: 13.858, position 10/166 in Chemistry, multidisciplinary, 1st quartile)

Chapter V

Regioselective Access to Sultam Motifs through Cobalt-Catalyzed Annulation of Aryl Sulfonamides and Alkynes using an 8-Aminoquinoline Directing Group. **Oriol Planas**, Christopher J. Whiteoak, Anna Company and Xavi Ribas. *Adv. Synth. Catal.* **2015**, *357*, 4003-4012. (Impact factor: 5.646, position 2/72 in Chemistry Applied and 4/59 in Chemistry Organic, 1st quartile)

Chapter VI

A First Example of Cobalt-Catalyzed Remote C-H Functionalization of 8-Aminoquinolines Operating through a Single Electron Transfer Mechanism. Christopher J. Whiteoak,* **Oriol Planas**,* Anna Company and Xavi Ribas. *Adv. Synth. Catal.* **2016**, *358*, 1679-1688. (Impact factor: 5.646, position 2/72 in Chemistry Applied and 4/59 in Chemistry Organic, 1st quartile) (*equal contribution)

All these papers have been published in journals that belong to the first quartile according to JCR.

Publications not included in this thesis:

Structural Modeling of Iron Halogenases: Synthesis and Reactivity of Halide-iron(IV)-oxo Compounds. Oriol Planas, Martin Clemancey, Jean-Marc Latour, Anna Company, Miquel Costas. *Chem. Commun.* **2014**, *50*, 10887-10890.

LIST OF ABBREVIATIONS

Å	Ångström
acac	Acetyl acetate
AcOEt	Ethyl acetate
AcOH	Acetic acid
AIBN	2,2'-Azobis(2-methylpropionitrile)
AMLA	Ambiphilic metal-ligand substitution
APO	2-aminopyridine-N-oxide
AQ	Aminoquinoline
Ar	Aryl
atm	Atmosphere
BDE	Bond dissociation energy
BHT	2,6-di- <i>tert</i> -butyl-4-methyl-phenol
bipy	2,2'-bipyridine
CAN	Cerium(IV) ammonium nitrate
cat	Catalyst
CDC	Cross-Dehydrogenative Coupling
CMD	Concerted Metalation-Deprotonation
COSY	Correlation Spectroscopy
Cp	cyclopentadiene
Cp*	1,2,3,4,5-pentamethylcyclopentadiene
dacoda	1,5-diazacyclooctane-N,N'-diacetic acid
DCB	Dichlorobutane
DCE	Dichloroethane
DCP	Dicumylperoxide
DFT	Density Functional Theory
DG	Directing Group
DHIQ	Dihydroisoquinoline
DIAD	Diisopropyl azodicarboxylate
dmpe	1,2-bis(dimethylphosphino)ethane
dppen	1,2-bis(diphenylphosphino)ethane
DMSO	Dimethylsulfoxide
DTBP	Di- <i>tert</i> -butyl peroxide
EA	Elemental analysis
EDA	Ethyl diazoacetate
EDG	Electron-Donating Group
EPR	Electron Paramagnetic Resonance spectroscopy
ESI-MS	Electrospray Ionization Mass spectrometry
ET	Electron Transfer
EtOH	Ethanol

equiv.	Equivalent
EWG	Electron-Withdrawing Group
EXAFS	Extended X-ray Absorption Fine Structure
FT-IR	Fourier Transform Infrared spectroscopy
GC	Gas Chromatography
h	Hour
HAT	Hydrogen Atom Transfer
HFIP	1,1,1,3,3,3-hexafluoroisopropanol
HMBC	Heteronuclear multiple-bond correlation spectroscopy
HOMO	Highest occupied molecular orbital
HRMS	High-resolution mass spectrometry
HSQC	Heteronuclear single-quantum correlation spectroscopy
IES	Internal electrophilic substitution
kcal	Kilocalorie
KIE	Kinetic Isotope Effect
L	Ligand
LUMO	Lowest unoccupied molecular orbital
M	Metal
MeCN	Acetonitrile
MeOH	Methanol
min	Minute
mM	Millimolar
MO	Molecular orbital
m.p.	Melting point
MS/MS	Tandem mass spectrometry
n.d.	Not-detected
NMR	Nuclear Magnetic Resonance
NOESY	Nuclear Overhauser effect spectroscopy
OLED	Organic light-emitting diode
OTf	Trifluoromethanesulfonate anion (CF ₃ SO ₃)
OX	Oxidant
OZ	2-(4,5-dihydrooxazol-2-yl)aniline
PA	Picolinamide
PCET	Proton-Coupled Electron Transfer
PEG	Polyethylene glycol
PIP	2-pyridinylisopropyl
PivOH	Trimethylacetic acid, Pivalic acid
PO	Pyridine-N-oxide
py	Pyridine
Q	Quinoline
QTOF	Quadrupole Time-of-flight

rds	Rate determining step
Rf	Retardation factor
rt	Room temperature
SN	Nucleophilic substitution
tabcod	1,4,8,11-tetraazabicyclo[9-5-2]octadecane
tacn	triazacyclononane
TBA	tetrabutylammonium
TBAI	tetrabutylammonium iodide
TBPB	tert-butyl peroxybenzoate
tBuONO	tert-butyl nitrite
TEMPO	(2,2,6,6-Tetramethyl-piperidin-1-yl)oxyl
TFA	Trifluoroacetic acid
TFE	2,2,2-Trifluoroethanol
THF	tetrahydrofuran
TMB	1,3,5-trimethoxybenzene
TMEDA	Tetramethylethylenediamine
TMG	1,1,3,3-Tetramethylguanidine
TON	Turnover number
TOF	Turnover frequency
TS	Transition State
Ts	Tosyl
XAS	X-ray Absorption Spectroscopy
XANES	X-ray Absorption Near Edge Structure
XRD	X-ray Diffraction

LIST OF FIGURES

- Figure I.1.** Reactivity of a variety of C-H bonds in a simple organic molecule8
- Figure I.2.** Nucleophilic and electrophilic C-H activation. 10
- Figure I.3.** Publications of Cobalt-catalyzed C-H activation *per year*. In purple, low-valent catalysis; in red, high-valent catalysis. Number of publications obtained from ISI WoS (Search criteria used: cobalt AND C-H activation). 16
- Figure I.4.** Cp*Co(III) complexes used in C-H functionalization methodologies..... 21
- Figure VII.1** Solid state structures of Co(II) coordination complexes. H-atoms and solvent molecules have been omitted for clarity; ellipsoids are set at 50% probability level. (A) Crystal data for **3b-OAc**. Selected bond distances [Å] and angles [°]: Co-C(1) 3.321(5), Co-H(1) 2.945(5), Co-N(1) 2.159(4), Co-N(2) 2.112(6), Co-N(3) 4.614(6), Co-O(1) 2.085(5), Co-O(2) 2.136(4); C(1)-Co-H(1) 58.90(1). (B) Crystal data for **3c-Br**. Selected bond distances [Å] and angles [°]: Co-C(1) 2.599(1), Co-H(1) 2.368(9), Co-N(1) 2.267(1), Co-N(2) 2.067(8), Co-N(3) 2.271(6), Co-Br(1) 2.476(2), Co-Br(2) 2.491(3); C(1)-Co-H(1) 65.49(5). 120
- Figure VII.2.** Characterization of aryl-Co(III) compounds through XAS spectroscopy. (A) XAS spectra at the Co K-edge highlighting the XANES region of the spectrum, and the 1s → 3d pre-edge transitions (inset). (B) EXAFS analysis of **4b-OAc**. Shown are Fourier-transformed EXAFS spectra (no phase correction, k-window = 2 -12.5 Å⁻¹), as well as the k³-weighted unfiltered EXAFS spectra (inset). (C) EXAFS analysis of **4c-OAc**. Shown are Fourier-transformed EXAFS spectra (no phase correction, k-window = 2 -12.5 Å⁻¹) as well as the k³-weighted unfiltered EXAFS spectra (inset). (D) Geometry optimized structure for **4b-OAc**. Selected bond distances [Å] and angles [°]: Co-C(1) 1.85, Co-N(1) 1.85, Co-N(2) 2.00, Co-N(3) 2.00, Co-O(1) 1.96, Co-O(2) 2.11; C(1)-Co-N(1) 89.8, C(1)-Co-N(2) 84.5, C(1)-Co-N(3) 84.4, C(1)-Co-O(1) 99.6, C(1)-Co-O(2) 164.9. (E) Geometry optimized structure for **4c-OAc**. Selected bond distances [Å] and angles [°]: Co-C(1) 1.85, Co-N(1) 1.85, Co-N(2) 2.05, Co-N(3) 2.05, Co-O(1) 1.96, Co-O(2) 2.11; C(1)-Co-N(1) 86.5, C(1)-Co-N(2) 84.6, C(1)-Co-N(3) 84.6, C(1)-Co-O(1) 101.0, C(1)-Co-O(2) 166.3..... 123
- Figure VII.3.** Solid state structures of aryl-Co(III) complexes **4b-CH₃CN** and **4c-CH₃CN**. Hydrogen atoms, perchlorate anions and solvent molecules have been omitted for clarity; ellipsoids are set at 50% probability. (A) Crystal data for **4b-CH₃CN**. Selected bond distances [Å] and angles [°]: Co-C(1) 1.876(7), Co-N(1) 1.853(4), Co-N(2) 1.997(6), Co-N(3) 2.008(5), Co-N(4) 2.025(6), Co-N(5) 1.897(4); C(1)-Co-N(1) 90.55(2), C(1)-Co-N(2) 83.68(2), C(1)-Co-N(3) 83.66(2), C(1)-Co-N(4) 177.87 (2), C(1)-Co-N(5) 88.40(2). (B) Crystal data for **4c-CH₃CN**. Selected bond distances [Å] and angles [°]: Co-C(1) 1.865(2), Co-N(1) 1.856(2), Co-N(2) 2.029(2), Co-N(3) 2.027(2), Co-N(4) 1.999(2), Co-N(5) 1.927(2); C(1)-Co-N(1) 88.16(9), C(1)-Co-N(2) 84.13(9), C(1)-Co-N(3) 84.26(9), C(1)-Co-N(4) 178.30(9), C(1)-Co-N(5) 91.30(9)..... 125
- Figure VII.4.** Solid state structure of aryl-Co(III) species **8**. Selected bond distances [Å] and angles [°]: Co-C(1) 1.919(2), Co-N(1) 1.889(2), Co-N(2) 2.007(2), Co-N(3) 1.934(2), Co-N(4) 1.931(2), Co-O(1) 1.932(2); C(1)-Co-N(1) 84.24(9), C(1)-Co-N(2) 166.33(9), C(1)-Co-N(3) 97.67(9), C(1)-Co-N(4) 88.88(9), C(1)-Co-O(1) 87.48(8). 127

Figure VII.5. HRMS analysis of the crude reaction of **2b-OAc** and EDA in presence of water after 24h in TFE (main peaks). Peak at $m/z = 384.1150$ corresponds to **2b-OAc**; peak at $m/z = 354.2188$ corresponds to **4** and peak at $m/z = 470.1506$ corresponds to **5b-OAc**.135

Figure VII.6. Solid state structures of **5a-OBz-R**. Hydrogen-atoms, anions and solvent molecules have been omitted and only one of the enantiomers is depicted for clarity; ellipsoids displayed at 50% (**5a-OBz-Cl**) and 30% (**5a-OBz-OMe**) probability. (A) **5a-OBz-OMe**. Selected bond distances [Å] and angles [°]: Co-C(1) 1.82(2), Co-C2 1.97(4), Co-N(1) 2.02(4), Co-N(2) 1.88(3), Co-N(3) 1.99(4), Co-O(1) 2.01(4), C(2)-O(2) 1.50(7); C(1)-Co-C(2) 95.6(1), C(1)-Co-O(1) 179.2(2). (B) **5a-OBz-Cl**. Selected bond distances [Å] and angles [°]: Co-C(1) 1.82(2), Co-C2 1.97(4), Co-N(1) 2.02(4), Co-N(2) 1.88(3), Co-N(3) 1.99(4), Co-O(1) 2.01(4), C(2)-O(2) 1.50(7); C(1)-Co-C(2) 95.6(1), C(1)-Co-O(1) 179.2(2). 138

Figure VII.7. ^1H NMR spectrum of $[\text{D}]_n\text{-3}$ (up, blue) and **3** (down, black) recorded at 298K using CDCl_3 as solvent. 36% of D-incorporation was observed (Table VII.6, entry 1). 139

Figure VII.8. Solid state structures of synthesized sultam motifs. Hydrogen-atoms and solvent molecules have been omitted for clarity; ellipsoids displayed at 50% probability. (A) **1aa**. Selected bond distances [Å] and angles [°]: S-O(1) 1.428(1), S-O(2) 1.429(1), S-N(1) 1.658(1); O(1)-S-O(2) 119.1(2). (B) **1ah'**. Selected bond distances [Å] and angles [°]: S-O(1) 1.415(5), S-O(2) 1.434(4), S-N(1) 1.647(5); O(1)-S-O(2) 119.5(2). 148

Figure VII.9. Unsuccessful substrates using the optimized reaction conditions.157

Figure VII.10. Solid state structures of C5- (A, **15a**) and C7- (B, **13b**) nitration products. Hydrogen-atoms have been omitted for clarity; ellipsoids displayed at 50% probability. 158

LIST OF TABLES

Table VII.1. Stoichiometric reaction of 4b-OAc with terminal alkynes for the synthesis of dihydroisoquinoline (9a and 10a) or dihydroisoindoline (9b and 10b) products.....	128
Table VII.2. Catalytic transformation of 2b-H with terminal alkynes for the synthesis of dihydroisoquinoline (9a) or dihydroisoindoline (9b) products.....	129
Table VII.3. Optimization of stoichiometric reaction (see Table S13, Annex II).	134
Table VII.4. Optimization of catalytic reaction using a variety of cobalt salts as catalysts and water or Lewis acids as additives (see Table S16, Annex II).	136
Table VII.5. Use of a variety of additives in the formation of 3 from 5a-OAc species.	139
Table VII.6. Deuterium-labeling experiments with deuterated TFE as solvent or labeled D ₂ O and Lewis acids as additives.	141
Table VII.7. Optimization of the reaction conditions for the synthesis of sultam motifs.....	146
Table VII.8. Scope of Co(II)-catalyzed coupling of phenyl acetylene (blue) to aryl sulfonamide derivatives forming functionalized sultams (1aa-1ao).	147
Table VII.9. Scope of Co(II)-catalyzed coupling of a variety of alkynes (blue) to tosyl sulfonamide forming functionalized sultams (1ab-1at).	149
Table VII.10. Reaction in the presence of radical scavengers.....	152
Table VII.11. Optimization of the reaction conditions for the nitration of 8-aminoquinoline	156
Table VII.12. Screening of different ancillary groups (1y-16y).	158
Table VII.13. Screening of different 8-aminoquinoline scaffolds.	160

LIST OF SCHEMES

Scheme I.1. Direct C-H bond transformation technologies allow the transformation of natural gas and petroleum feedstocks to more complex products.....	7
Scheme I.2. Inner-sphere (top) and Outer-sphere C-H functionalization (bottom).	9
Scheme I.3. (A) Concerted Oxidative Addition general mechanism. (B) Early examples of organometallic C-H activation described by Chatt and co-workers.	11
Scheme I.4. (A) General mechanism of arene σ -bond metathesis. (B) Crabtree's mechanistic proposal of Shilov's methane conversion to methanol.	12
Scheme I.5. General mechanism of metal-mediated electrophilic aromatic C-H activation....	12
Scheme I.6. (A) General mechanism of metal-mediated Concerted Metalation-Deprotonation (CMD) and (B) Fagnou's mechanistic study of Pd-catalyzed C-H arylation.	13
Scheme I.7. Catalytic C-H activation examples using the Directing Group strategy with <i>ortho</i> -directing (mono and bidentate ligands) as well as <i>meta</i> -directing groups.	14
Scheme I.8. Recent C-H activation and functionalization methodologies using first-row transition metals as catalysts and 8-aminoquinoline as directing groups.	15
Scheme I.9. Early reports on cobalt C-H functionalization by (A) Murahashi, (B) Kochi, (C) Kisch and (D) Brookhart.....	17
Scheme I.10. Renaissance of high-valent Co-catalyzed C-H activation enabled by Matsunaga and Kanai's (left) and Daugulis' (right) reports.	19
Scheme I.11. Early examples of high-valent cobalt-mediated C-H activation reported by (A) Broderick and Legg, (B) Aviles and (C) Jackson. Colour code: Co(II), pink; Co(III), orange....	20
Scheme I.12. Selected Cp*Co(III)-catalyzed C(sp ²)-C bond-forming reactions using indole-based substrates (blue); 2-arylpyridine related substrates (green), amine, alcohol and imine related substrates (red); and pyrazole-based substrates (orange). General conditions for each example can be found in the corresponding reference.	22
Scheme I.13. Selected Cp*Co(III)-catalyzed C(sp ²)-N bond-forming reactions (in blue), C(sp ²)-(pseudo)Halogen bond-forming transformations (in green), C(sp ²)-S bond-forming protocols (in red) and the only example of Cp*Co(III)-catalyzed C(sp ²)-H carbonylation reaction with CO _(g) . General conditions for each example can be found in the corresponding reference.....	24
Scheme I.14. Cp*Co(III)-catalyzed C(sp ³)-H functionalization reactions with dioxazolone (A), alkynes (B) and diazo compounds (C). General conditions for each example can be found in the corresponding reference.	25
Scheme I.15. Cobalt-catalyzed 8-aminoquinoline-directed C-H functionalization with alkynes.....	27
Scheme I.16. Cobalt-catalyzed N-pyridine-oxide-directed functionalization of C-H bond with alkynes as coupling partners described by Niu and Song.	28
Scheme I.17. Cobalt-catalyzed picolinamide-directed C-H functionalization with alkynes. ..	28

Scheme I.18. Traceless heterocycle synthesis through cobalt-catalyzed pyridinylhydrazine-directed functionalization of C-H bonds with alkynes as coupling partners described by Zhu.....	29
Scheme I.19. Cobalt-catalyzed functionalization of C-H bonds with alkenes.	30
Scheme I.20. General Mechanisms for cobalt-catalyzed C-H functionalization with alkynes and alkenes. Colour code: Co(I), green; Co(II), pink; Co(III), orange; Co(IV), blue.	31
Scheme I.21. Cobalt-catalyzed functionalization of C-H bonds with allenes as coupling partners using 8-aminoquinoline (AQ) as directing group.	32
Scheme I.22. Cobalt-catalyzed functionalization of C-H bonds with allenes as coupling partners using 8-aminoquinoline (AQ) as directing groups.	33
Scheme I.23. Cobalt-catalyzed functionalization of C-H bonds with carbon monoxide (CO _(g)) and CO-surrogates as coupling partners using 8-aminoquinoline as directing group.....	34
Scheme I.24. Traceless heterocycle synthesis through cobalt-catalyzed PH-directed functionalization of C-H bonds with alkynes as coupling partners described by Zhu.	35
Scheme I.25. Cobalt-catalyzed C-H functionalization with isocyanates using 8-aminoquinoline as DG and upgrading to phthalimide through hydrolysis of the imine unit.	36
Scheme I.26. General mechanisms for cobalt-catalyzed C-H functionalization with CO(g) (or surrogates) and isocyanates. Usually proposed Co(II)/Co(IV) (left) and Co(I)/Co(III) (right) pathways. Colour code: Co(I), green; Co(II), pink; Co(III), orange; Co(IV), blue.	37
Scheme I.27. Cobalt-mediated arylation and alkylation of C-H bonds with bidentate (A, B and C) and monodentate (D and E) directing groups.	38
Scheme I.28. General Mechanisms for Q-assisted cobalt-catalyzed C-H alkylation and arylation of C(sp ²)-H bonds through either homocoupling or transmetalating reagents. Two mechanistic scenarios are possible: σ -bond metathesis (left) and base-assisted CMD pathway (right). Colour code: Co(I), green; Co(II), pink; Co(III), orange.	39
Scheme I.29. Cobalt-catalyzed C-H alkylation reported by Lu and Li (top) and General Mechanisms for PIP-assisted cobalt-catalyzed C-H alkylation of C(sp ²)-H bonds through a Co(II)/Co(III)/Co(IV) catalytic cycle (bottom). Colour code: Co(II), pink; Co(III), orange.....	40
Scheme I.30. Niu and Song's amination (left) and Li and Ge's amidation (intramolecular, right up; intermolecular, right down) of C-H bonds with anilines and amides as coupling partners, respectively.	41
Scheme I.31. Mechanisms for cobalt-catalyzed C-H amination and amidation reactions, including intra- and intermolecular transformations. Colour code: Co(I), green; Co(II), pink; Co(III), orange; Co(IV), blue.....	42
Scheme I.32 Zeng's cross-dehydrogenative coupling of arene and carboxylic acids (top). A Co(I)/Co(III) catalytic cycle was proposed (bottom). Colour code: Co(I), green; Co(III), orange.....	43
Scheme I.33. Detected organometallic Co(III) species containing the 8-aminoquinoline directing group through spectroscopic and spectrometric techniques.	45

Scheme I.34. Maiti's synthesis of aryl-Co(III) intermediates (up) and the XRD structure (solvent and H-atoms omitted for clarity; ellipsoids set at 50% probability level; down).....	46
Scheme I.35. Niu and Song's synthesis of organometallic aryl-Co(III)-amino intermediates (up) and XRD structure of the isolated intermediate (solvent and H-atoms omitted for clarity; ellipsoids set at 30% probability level; down).....	46
Scheme I.36. C-H activation via a Single-Electron Transfer and PCET pathway and representative reaction types of radical C-H functionalization.....	48
Scheme I.37. Ribas' Cu(II) C-H activation in triazamacrocyclic in the absence (upper reaction) or in presence of TEMPO (lower reaction). Color code: Cu(I), green; Cu(II), blue; Cu(III), red.....	49
Scheme I.38. Stahl's control of governing pathway in Cu(II) C-H functionalization: Organometallic pathway (left, blue) and SET pathway (right, red).....	49
Scheme I.39. Niu and Song's alkoxylation and amination of C-H bonds through a Single Electron Transfer (SET).	51
Scheme I.40. Song' nitration of C(sp ³)-H bonds through a Single Electron Transfer (SET)....	52
Scheme I.41. Das' nitration and methoxylation of arenes through a Proton-Coupled Electron Transfer (PCET) pathway (aminopyridine as DG is depicted).	53
Scheme I.42. Niu and Song' mixed strategy for the arylation of arenes (top) and its proposed mechanism (bottom). Colour code: Co(II), pink; Co(III), orange; Co(IV), blue.	54
Scheme I.43. Niu and Song's perfluoroalkylation of quinolone amides at C5 position through a Single Electron Transfer (SET) pathway.....	55
Scheme II.1. Use of macrocyclic model substrate for the formation of organometallic aryl-Co(III) complexes through C-H activation. Reactivity of aryl-Co(III) with alkynes (blue) and ethyl diazoacetate (red).	67
Scheme II.2. Cobalt-catalyzed organometallic C-H activation and functionalization with alkynes for the synthesis of cyclic sulfonamide (sultam) motifs.	68
Scheme II.3. Remote nitration of 8-aminoquinoline scaffolds through cobalt-catalyzed C-H functionalization via Single Electron Transfer (SET).	68
Scheme VII.1. Synthesis of building blocks 1 , 2a-H and ligands 2b-H and 2c-H	119
Scheme VII.2. (A) Synthesis of Co(II) precursors 3b-X (X = OAc) and 3c-X (X = OAc, Br). (B) Bending of the targeted C-H bond through interaction with the Co(II) centre	120
Scheme VII.3. Synthesis of aryl-Co(III) intermediates 4b-X and 4c-X	121
Scheme VII.4. Formation of aryl-Co(III) intermediates.....	124
Scheme VII.5. (A) Synthesis of organometallic aryl-Rh(III)Cl ₂ species. (B) Solid state structure of aryl-Rh(III) complex 5c-Cl . Hydrogen atoms and solvent molecules have been omitted for clarity; ellipsoids are set at 50% probability. Selected bond distances [Å] and angles [°]: Rh-C(1)	

1.929(2), Rh-N(1) 2.113(2), Rh-N(2) 1.953(2), Rh-N(3) 2.120(2), Rh-Cl(1) 2.525(7), Rh-Cl(2) 2.376(4); C(1)-Rh-N(1) 82.99(2), C(1)-Rh-Cl(1) 175.71(2), C(1)-Rh-Cl(2) 91.34(2).....	126
Scheme VII.6. Synthesis of aryl-Co(III) complexes 7 and 8 containing benzamide 6 bearing an 8-aminoquinoline directing group.....	126
Scheme VII.7. Mechanistic proposal for the formation of 5- and 6-membered ring products through the “acetylide pathway”. This mechanism was supported by DFT calculations.	131
Scheme VII.8. Mechanistic proposal for the formation of 5- and 6-membered ring products through the “migratory insertion pathway”	132
Scheme VII.9. Reactivity of bench-top stable aryl-Co(III) organometallic compounds with diazoacetates and formation of hypothesized intermediates A (aryl-Co(III)-carbene) and B (Aryl-EDA-Co(III), or the actual intermediate, C (Aryl-Co(III)-alkyl).	137
Scheme VII.10. (A) Use of 5a-X as catalysts for the construction of macrocyclic amide 3 and (B) role of acetate anions in this transformation.	140
Scheme VII.11. Mechanistic proposal for the formation 6-membered ring cyclic amide 3 by reaction of 2a-OAc with EDA as coupling partner. This mechanism was supported by DFT calculations.	142
Scheme VII.12. Drugs containing cyclic sulfonamide motifs.	145
Scheme VII.13. Attempted upgrading of sultam 1aa	149
Scheme VII.14. Intermolecular competition experiments using standard conditions. Yields were calculated by ¹ H NMR analysis using mesitylene as internal standard.	150
Scheme VII.15. Deuterium labeling experiments using standard conditions. Deuterium incorporation was obtained from ¹ H NMR integration of signals.	151
Scheme VII.16. Proposed reaction mechanism for the Co(II)-catalyzed synthesis of sultam motifs from sulfonamides and alkynes. Color code: Co(I), green; Co(II), pink; Co(III), orange.....	152
Scheme VII.17. Antimalarial drugs containing the 8-aminoquinoline scaffold.	155
Scheme VII.18. Gram-scale nitration reaction and product upgrading (isolated yields reported). Reaction conditions for gram-scale nitration reaction: 1 (1.89 g, 7.6 mmol), Co(NO ₃) ₂ ·6H ₂ O (443 mg, 1.5 mmol, 20 mol%), TBN (4.1 mL, 90%, 4.0 equiv., 30.4 mmol), acetic acid (50 mL), RT, 18 h. ^a Isolated yield starting from 300 mg of 1a . ^b Isolated yield starting from 1.0 g of 1a . ^c Isolated yield starting from 500 mg of A . ^d Isolated yield starting from 320 mg of 1b	159
Scheme VII.19. (A) Competition reactions performed to investigate relative reactivity of substrates 17 and 19 . Yields calculated from ¹ H NMR of crude reaction mixture using 1,3,5-trimethoxy benzene as internal standard and are based on conversion of corresponding substrate. Reaction conditions: substrate (0.5 mmol; 0.25 mmol of each substrate), Co(NO ₃) ₂ ·6H ₂ O (29.1 mg, 0.1 mmol, 20 mol%), TBN (267 μL, 90%, 4.0 equiv., 2.0 mmol), acetic acid (3.5 mL), RT, 18 h. (B) Summary of Kinetic Isotope Experiment (KIE); for further details see Supporting Information.	161
Scheme VII.20. Proposed mechanism for the C5-H nitration of substrate A	162

ACKNOWLEDGMENT

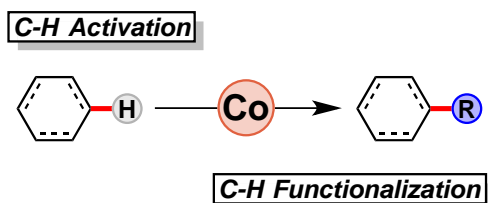
This work would have not been possible without the following collaborations:

- Serveis Tècnics de Recerca from Universitat de Girona for technical support, with especial remark to Dr. Laura Gomez and Xavi Fontrodona, for their dedication in setting up the mass spectrometer and the X-Ray Diffractometer, respectively.
- Dr. Josep Maria Luis and Steven Roldán Gomez from the Insitut de Química Computacional i Catàlisi of Universitat de Girona for the theoretical studies.
- Dr. Teodor Parella from Servei de RMN at Universitat Autònoma de Barcelona for NMR experiments, structure elucidation and fruitful discussions.
- Dr. Christopher J. Whiteoak (currently at Sheffield Hallam University, UK) for collaboration in the project design, mentoring and English grammar corrections
- Dr. Vlad Martin-Diaconescu (currently at Institut Català d'Investigació Química, ES) for XAS studies, EXAFS analysis, DFT calculations and fruitful discussions.
- Prof. Dr. Vy M. Dong for her hosting, mentoring and support during the 3-month scientific visit at University of California at Irvine (UCI), CA, US.
- Financial support from the Ministerio de Educación, Cultura y Deporte (MECD) for a Pre-doctoral FPU grant Ref. FPU13/04099 and MINECO for CTQ2013-43012-P and CTQ2016-77989-P project to Dr. Anna Company and Dr. Xavi Ribas.
- Financial support from the Ministerio de Educación, Cultura y Deporte (MECD) for the mobility grant Ref. EST15/00493.
- Generalitat de Catalunya for project 2014SGR862.
- European Research Council for the Starting Grant Project ERC-2011-StG-277801 to Dr. Xavi Ribas

GRAPHICAL ABSTRACT

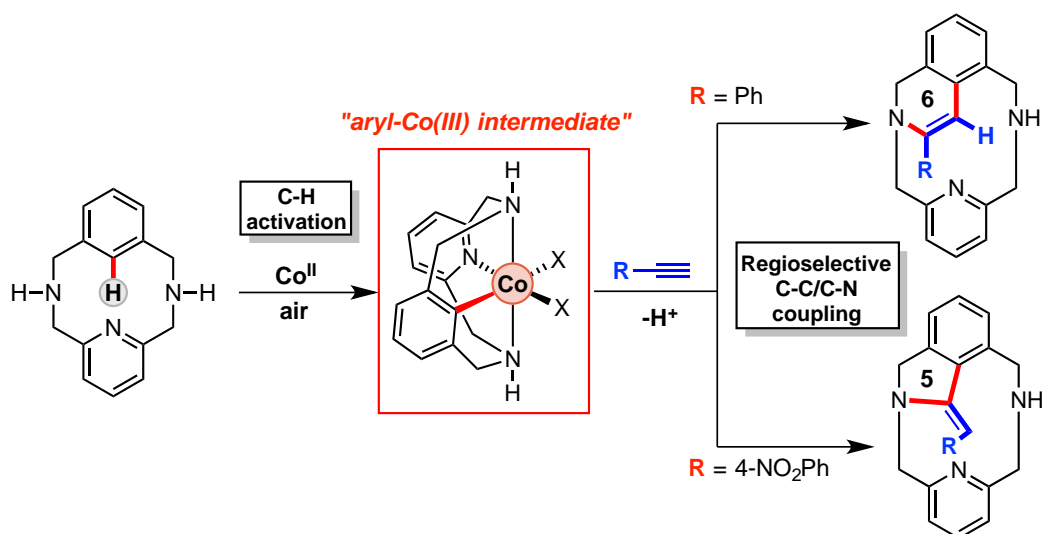
Summary (p. 1)

Chapter I. General Introduction (p. 5)

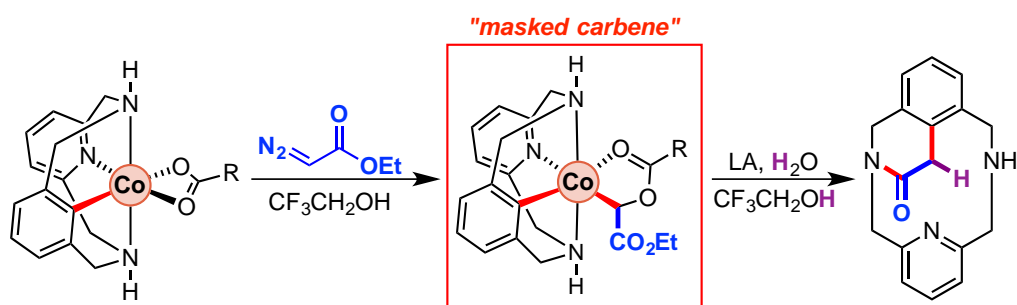


Chapter II. General Objectives (p. 65)

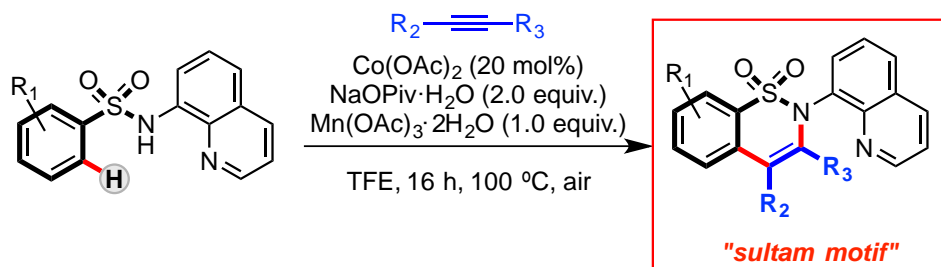
Chapter III. Isolation of Key Organometallic Aryl-Co(III) Intermediates in Cobalt-Catalyzed C(sp²)-H Functionalization and New Insights into Alkyne Annulation Reaction Mechanisms. (p. 69)



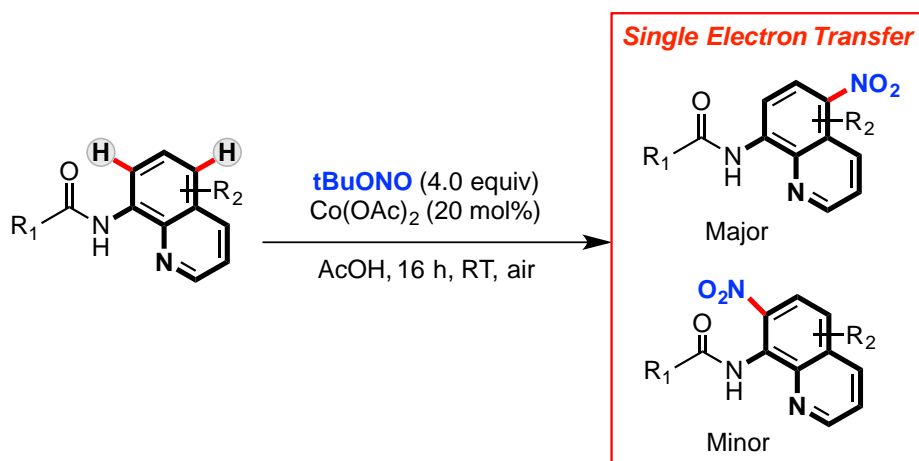
Chapter IV. Carboxylate-Assisted Formation of Aryl-Co(III) Masked-Carbenes in Cobalt-Catalyzed C-H Functionalization with Diazo Esters. (p. 81)



Chapter V. Regioselective Access to Sultam Motifs through Cobalt-Catalyzed Annulation of Aryl Sulfonamides and Alkynes using an 8-Aminoquinoline Directing Group. (p. 91)



Chapter VI. A First Example of Cobalt-Catalyzed Remote C-H Functionalization of 8-Aminoquinolines Operating through a Single Electron Transfer Mechanism. (p. 103)



Chapter VII. Results and Discussion (p. 115)

Chapter VIII. General Conclusions (p. 165)

Annex (p. 169)

CONTENTS

Summary	1
Resum	2
Resumen	3
Chapter I. General Introduction	5
I.1. Organometallic C-H Activation	7
<i>I.1.1 Challenges and Definitions</i>	7
<i>I.1.2 Mechanisms of Activation and Early Examples</i>	9
<i>I.1.3 First-Row Transition Metals in C-H Activation</i>	15
I.2. Cobalt in C-H Activation	16
<i>I.2.1 Early Examples of Cobalt-Catalyzed C-H Functionalization Reactions</i>	17
I.3. High-Valent Cobalt-Mediated C-H Activation	19
<i>I.3.1 Early Stoichiometric Examples</i>	19
<i>I.3.2 Half-Sandwich Co(III)-Catalyzed C-H Activation</i>	21
<i>I.3.3 Oxidative C-H Activation and Functionalization</i>	26
I.4. One-Electron Redox Processes for C-H Functionalization	48
<i>I.4.1 Cobalt-Catalyzed C-H Functionalization through SET and PCET</i>	50
I.5. References	56
Chapter II. General Objectives	65
Chapter III. Isolation of Key Organometallic Aryl-Co(III) Intermediates in Cobalt-Catalyzed C(sp²)-H Functionalization and New Insights into Alkyne Annulation Reaction Mechanisms.	69
Chapter IV. Carboxylate-Assisted Formation of Aryl-Co(III) Masked-Carbenes in Cobalt-Catalyzed C-H Functionalization with Diazo Esters	81
Chapter V. Regioselective Access to Sultam Motifs through Cobalt-Catalyzed Annulation of Aryl Sulfonamides and Alkynes using an 8-Aminoquinoline Directing Group	91
Chapter VI. A First Example of Cobalt-Catalyzed Remote C-H Functionalization of 8-Aminoquinolines Operating through a Single Electron Transfer Mechanism	103

Chapter VII. Results and Discussions.....	115
VII.1 Isolation of Key Organometallic Aryl-Co(III) Intermediates in Cobalt-Catalyzed C(sp ²)-H Functionalization and New Insights into Alkyne Annulation Reaction Mechanisms.	119
<i>VII.1.1 Synthesis of macrocyclic model substrates and Co(II) precursors.</i>	<i>119</i>
<i>VII.1.2 Synthesis and characterization of aryl-Co(III) complexes.....</i>	<i>121</i>
<i>VII.1.3 Reactivity of aryl-Co(III) complexes with terminal alkynes.....</i>	<i>127</i>
<i>VII.1.4 Theoretical studies and reaction mechanism.....</i>	<i>130</i>
VII.2 Carboxylate-Assisted Formation of Aryl-Co(III) Masked-Carbenes in Cobalt-Catalyzed C-H Functionalization with Diazo Esters.	133
<i>VI.2.1 Reactivity with ethyl diazo acetate (EDA).....</i>	<i>133</i>
<i>VI.2.2 Mechanistic Insight.....</i>	<i>136</i>
VII.3 Regioselective Access to Sultam Motifs through Cobalt-Catalyzed Annulation of Aryl Sulfonamides and Alkynes using an 8-Aminoquinoline Directing Group.....	145
<i>VII.3.1 Optimization of reaction conditions.....</i>	<i>145</i>
<i>VII.3.2 Substrate scope and product upgrading.....</i>	<i>147</i>
<i>VII.3.3 Mechanistic experiments and possible reaction pathway.....</i>	<i>150</i>
VII.4 A First Example of Cobalt-Catalyzed Remote C-H Functionalization of 8-Aminoquinolines Operating through a Single Electron Transfer Mechanism.....	155
<i>VII.4.1 Optimization of reaction conditions.....</i>	<i>155</i>
<i>VII.4.2 Substrate scope and upgrading.....</i>	<i>157</i>
<i>VII.4.3 Mechanistic experiments and possible reaction pathway.....</i>	<i>161</i>
<i>VII.5 References.....</i>	<i>163</i>
Chapter VIII. General Conclusions	165
Annex.....	169
A.1 Supporting Information for Chapter III	S1
A.2 Supporting Information for Chapter IV	S41
A.3 Supporting Information for Chapter V.....	S79
A.4 Supporting Information for Chapter VI	S113

Supplementary Digital Material

The material listed below can be found in the attached CD:

- PDF file of the PhD dissertation
- PDF files containing complete spectroscopic and spectrometric characterization corresponding to Chapters III, IV, V and VI. Each file is labeled as *SuppInfo_ChapterX*, where X correspond to the respective chapter number. Each file can be found in the folder named as the corresponding file.
- CIF files for each crystal structure presented in this thesis. They can be found at the folder named *CIF Files* and they are organized as indicated in the following table:

Chapter	File name
III	3b-OAc
III	3c-Br
III	4b-CH ₃ CN
III	4c-CH ₃ CN
III	5c-Cl
III	8
IV	5a-OBz-Cl
IV	5a-OBz-OMe
V	1aa
V	1aaH4
V	1ah
V	1ar
VI	11b
VI	13b
VI	15a

SUMMARY

Synthetic methodologies involving the cleavage of Carbon-Hydrogen (C-H) bonds are currently attracting significant interest. Most of the achievements in this field have been accomplished with second- and third-row transition metals such as Rh, Ru and Pd. However, methodologies using more abundant and cost-efficient 3d transition metal catalysts have attracted the attention of the catalysis community in directed C-H functionalization methodologies. In particular, cobalt catalysis has emerged as a valuable approach for the construction of a wide variety of organic molecules. Even though cobalt catalysis has remained as a dormant methodology mainly dominated by low-valent cobalt-catalyzed protocols, the field recently experimented an explosion of activity due to the use of high-valent catalysts. Unfortunately, mechanistic understanding concerning how these new high-valent cobalt-catalyzed protocols operate is significantly underdeveloped. This is likely a consequence of the instability of key reaction intermediates, although there is an increasing interest in their detection and isolation.

Thus, the main goal of this Ph.D. dissertation is the synthesis and characterization of bench-top stable aryl-Co(III) organometallic species using commercially available cobalt(II) salts and a macrocyclic model substrate as a model platform. Special attention will be paid to the C-H activation step to elucidate the operating mechanism in the high-valent cobalt-mediated cleavage of C-H bonds. Moreover, this mechanistic study will also be performed in substrates bearing an 8-aminoquinoline directing group, which has been proven to be successful in cobalt-catalyzed C-H activation protocols.

Mechanistic experiments, as well as spectroscopic characterization of intermediates will be useful to give light to a basic underdeveloped step in cobalt C-H activation methodologies. In addition, reactivity of the isolated organometallic aryl-Co(III) intermediates towards a variety of coupling partners will be tested. On one hand, annulation reaction using alkynes will be studied, as their use as coupling partners in cobalt-catalyzed protocols has attracted increasing attention. On the other hand, cobalt-mediated insertion of metal-carbenoids into C-H bonds will be studied using ethyl diazoacetates as coupling partners. The mechanism of these transformation is poorly understood and no experimental evidences of reactive intermediates are reported in the literature. Moreover, both transformation will be extrapolated to substrates bearing an 8-aminoquinoline group in cobalt-catalyzed C-H activation and functionalization methodologies with alkynes and alkyl nitrites for the synthesis of cyclic sulfonamide motifs and 5- and 7-nitro-8-aminoquinolines, respectively.

RESUM

Les metodologies sintètiques que inclouen el trencament d'enllaços Carboni-Hidrogen (C-H) han patit un interès creixent per part de la comunitat científica. La majoria dels èxits d'aquest camp s'han portat a terme amb metalls de la segona i tercera sèrie de transició com Rh, Ru i Pd. No obstant, les metodologies que fan servir metalls amb configuració electrònica 3d, els quals són més abundants i barats, recentment han esdevingut més populars i la comunitat científica hi ha centrat esforços importants per a desenvolupar-les. En particular, el camp de catàlisi amb cobalt ha emergit com una metodologia útil i eficient per la construcció de molècules orgàniques. Tot i que la catàlisi amb cobalt ha estat poc estudiada fins ara i principalment dominada per processos catalitzats per cobalt en baix estat d'oxidació, el camp ha experimentat una explosió degut a l'ús de catalitzadors en alt estat d'oxidació. Desafortunadament, el mecanisme d'acció d'aquestes espècies en alt estat d'oxidació és encara molt poc conegut. Probablement, aquest fet és conseqüència de la poca estabilitat dels intermedis de reacció, tot i que diversos grups de recerca estan focalitzant els seus esforços en aïllar aquestes espècies reactives.

D'aquesta manera, l'objectiu principal d'aquesta tesi doctoral és la síntesis i la caracterització d'espècies organometàl·liques i estables aril-Co(III), fent ús de salts de cobalt(II) i d'un lligand macrocíclic com a substrat model. Concretament, es focalitza l'atenció en el pas d'activació de l'enllaç C-H per tal d'esbrinar quin és el mecanisme que opera en la activació d'enllaços C-H catalitzada per espècies de cobalt en alt estat d'oxidació. A més a més, aquest estudi mecanístic també es porta a terme en substrats que contenen el grup director 8-aminoquinolina, el qual ha demostrat ser molt útil en la funcionalització d'enllaços C-H catalitzada per cobalt.

Els experiments mecanístics, així com la caracterització espectroscòpica dels intermedis, és extremadament útil per entendre un pas bàsic en les metodologies d'activació d'enllaços C-H amb cobalt. Tanmateix, també es porta a terme l'estudi de la reactivitat de les espècies organometàl·liques aril-Co(III) amb diferents parelles d'acoblament. D'una banda, s'estudia la formació d'anells fent ús d'alquins, ja que el seu ús com a parelles d'acoblament en reaccions catalitzades per cobalt ha patit un gran increment de manera recent. D'altra banda, s'estudia la inserció d'espècies metall-carbenoid en enllaços C-H catalitzada per cobalt, fent ús d'etil diazo acetat com a parella d'acoblament. El mecanisme d'aquesta reacció no s'ha estudiat en profunditat i mai s'ha caracteritzat cap espècie intermèdia. Finalment, aquesta reactivitat s'extrapola a substrats que contenen el grup 8-aminoquinolina. Finalment, es desenvolupen metodologies per la síntesis de sulfonamides cícliques així com per la formació de 5- i 7-nitro-8-aminoquinolines fent ús d'alquins i nitrit de tert-butil, respectivament.

RESUMEN

Las metodologías sintéticas que incluyen la rotura de enlaces Carbono-Hidrógeno (C-H) ha sufrido un interés creciente por parte de la comunidad científica. La mayoría de los éxitos en este campo se deben al uso de metales de la segunda y tercera serie de transición tales como Rh, Ru y Pd. No obstante, las metodologías que usan metales con configuración electrónica 3d, los cuales son más abundantes y baratos, recientemente han devenido más populares y la comunidad científica ha centrado esfuerzos importantes para su desarrollo. Particularmente, la catálisis con cobalto ha surgido como una metodología útil y eficiente para la construcción de moléculas orgánicas. Aunque este campo ha sido poco estudiado y mayormente dominado por procesos que usan cobalto en bajo estado de oxidación, el uso de especies de alto estado de oxidación ha provocado un aumento sustancial en su uso. Desafortunadamente, el mecanismo de acción de estas especies de alto estado de oxidación es todavía poco conocido. Probablemente, este hecho es consecuencia la poca estabilidad de los intermedios de reacción, aunque varios grupos de investigación están centrando sus esfuerzos en aislar estas especies reactivas.

Así pues, el objetivo principal de esta tesis doctoral es la síntesis y la caracterización de especies organometálicas arilo-Co(III), usando sales de cobalto(II) i un ligando macrocíclico como sustrato modelo. Concretamente, se centra la atención en el paso de activación del enlace C-H para entender cuál es el mecanismo que opera en la activación de enlaces C-H catalizada por especies de cobalto en alto estado de oxidación. Además, este estudio mecanístico también se lleva a cabo con sustratos que contienen el grupo director 8-aminoquinolina, el cual se ha utilizado satisfactoriamente en la funcionalización de enlaces C-H con cobalto como catalizador.

Los experimentos mecanísticos, así como la caracterización espectroscópica de los intermedios es muy útil para entender un paso básico en las metodologías de activación de enlaces C-H con cobalto. En este trabajo también se lleva a cabo el estudio de la reactividad de les especies arilo-Co(III) con varias parejas de acoplamiento. Por una parte, se estudia la formación de anillos usando alquinos, ya que su uso como pareja de acoplamiento en reacciones catalizadas por cobalto ha ganado popularidad recientemente. Por otra parte, también se estudia la inserción de especies metal-carbenoide en enlaces C-H catalizada por cobalto, usando diazo acetato de etilo. El mecanismo de esta reacción no se ha estudiado en profundidad y nunca se ha caracterizado ninguna especie intermedia. Finalmente, se desarrollan metodologías para la síntesis de sulfonamidas cíclicas, así como para la formación de 5- y 7-nitro-8-aminoquinolinas usando alquinos y nitrito de *tert*-butilo, respectivamente.

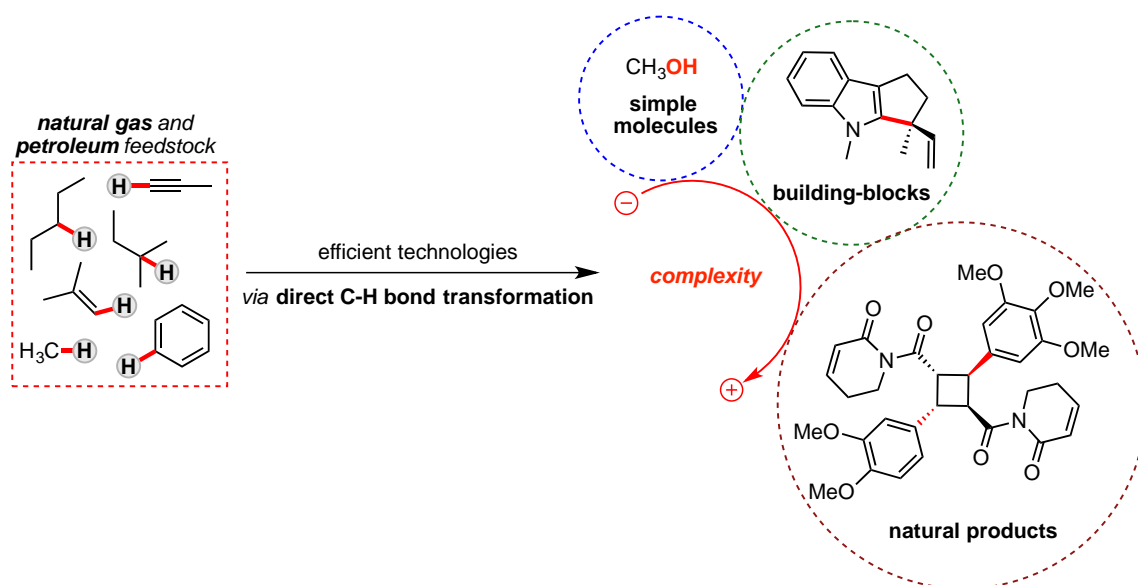
Chapter I

General Introduction

I.1 Organometallic C-H Activation

I.1.1 Challenges and Definitions

The discovery of new approaches and technologies that either improve the step and atom economy of existing processes or introduce novel and innovative methods to construct complex molecules is the main goal of synthetic chemists. As it is widely known, the majority of fuels, chemicals and materials are derived from petroleum feedstocks, which are mainly constituted by saturated and unsaturated hydrocarbons. However, exploitation of such resources is impeded by the high cost of gas transportation, as the main world's established gas resource locations are remote, in sites where there is no demand.¹ Furthermore, in spite of the relative abundance of these nonrenewable resources, very few practical processes for converting them into more valuable products are available due to their lack of reactivity. This chemical inertness arises from the constituent atoms of hydrocarbons being held together by strong C-C and C-H bonds. The latter bond, with a BDE of 100 kcal mol⁻¹ in alkanes and around 110 kcal mol⁻¹ in arenes and olefins,² can be understood as the un-functional group. Indeed, the presence of a C-H bond in organic molecules is indicated by the absence of any other bonds. As Goldman and Goldberg exposed in 2004,³ this invisibility clearly reflects their ubiquitous presence in organic molecules as well as their inert character. Thus, the possibility of direct introduction of a new functionality, including C-C bonds, via direct and selective C-H bond transformation is a highly attractive strategy. In fact, realization of such potential is revolutionizing the synthesis of organic molecules ranging from methanol to complex natural or unnatural products (Scheme I.1).^{4,5}



Scheme I.1. Direct C-H bond transformation technologies allow the transformation of natural gas and petroleum feedstocks to more complex products.

Despite the fact that C-H bonds are more difficult to cleave than other types of linkages, they are not completely inert. In fact, current industrial processes used to functionalize C-H bonds typically involve free radicals, carbocations, organometallic reagents or superacid electrophiles.⁶ Some critical features of these processes, however, are the requirement of high temperatures, which increase costs and emissions, and their relative unselectivity. Mainly, two problems concerning selectivity are encountered. The first issue involves the capacity of certain reagents to react faster towards one type of C-H bonds in preference to others. For example, free radical reagents exhibit preference for reaction of tertiary C-H bonds over primary ones, and reagents that exhibit the reverse selectivity are extremely rare. On the other hand, a second type of selectivity is defined as the ability to convert hydrocarbons into a functionalized product which does not undergo an even faster reaction than the initial hydrocarbon. The introduction of transition metals to the organic toolbox of reagents solved some of these problems and unlocked new opportunities in this area.⁷ Thus, novel reactions were discovered and the term “C-H bond activation” was coined and used to describe C-H cleavage processes.⁸ With time, this term has become very popular and its frequent usage has led to some misleading interpretations. Organic molecules contain a wide variety of C-H bonds of different reactivity and as a consequence many mechanistic pathways exist for an overall C-H functionalization process (Figure I.1).

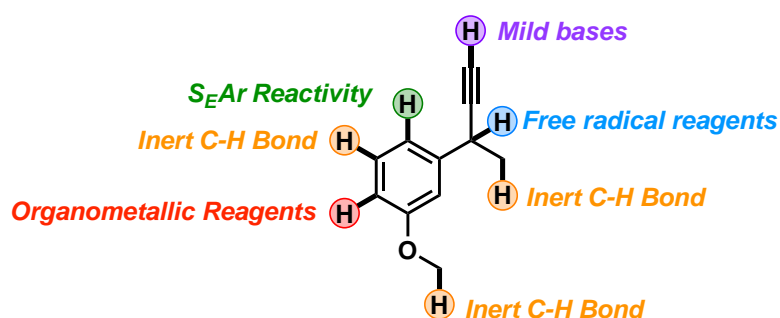
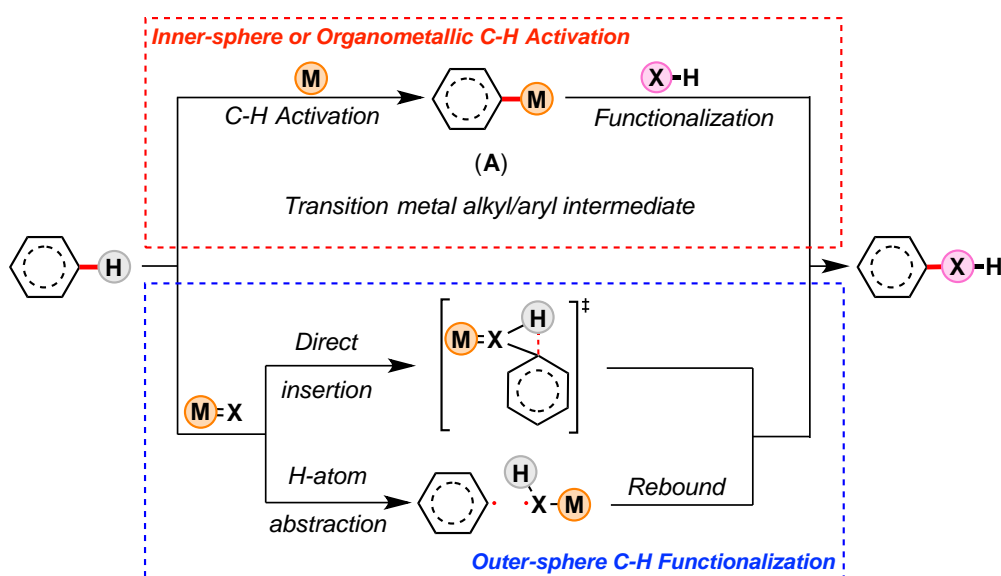


Figure I.1. Reactivity of a variety of C-H bonds in a simple organic molecule.

Before going into deeper detail about the possible mechanistic scenarios of C-H bond cleavage, a brief discussion of the term “activation” is necessary. Activation is considered to be the binding of a substrate to a metal center and this can be followed by a functionalization step in which the substrate is transformed. Indeed, the term “activation of a substrate/bond” refers to any process or phenomenon by which the reactivity of a substrate/bond is increased.⁹ The term “C-H bond activation” is frequently used as an organometallic term to describe certain metal-mediated processes and it was introduced with the clear purpose to distinguish metal-mediated C-H cleavage from hydrogen atom transfer (HAT), traditional radical and ionic substitution. Thus, according to this *organometallic approach* (Scheme I.2, top), the term C-H bond activation refers to the formulation of a complex wherein the C-H bond interacts directly with the metal reagent or catalyst. Then, these complexes often evolve to form

a carbon-metal intermediate in the absence of free radicals or ionic intermediates. In fact, this type of C-H activation can be explained through an inner-sphere mechanism event, which usually involve a first cleavage of a carbon-hydrogen bond to afford an alkyl/aryl-M intermediate species (Scheme I.2A). The latter will afford a particular product after reaction with either an external reagent or at the metal center. The electronic and structural properties of the intermediate will dictate the regio- and stereoselectivity of these functionalizations. In addition, factors such as the ligand environment or the mechanism of the C-H bond cleavage step can also influence selectivity.



Scheme I.2. Inner-sphere (top) and Outer-sphere C-H functionalization (bottom).

The organometallic or inner-sphere definition of C-H bond activation should be clearly distinguished from the coordination chemistry approach or outer-sphere definition of C-H functionalization (Scheme I.2, bottom).¹⁰⁻¹² This approach mimics biological reactions catalyzed by a variety of enzymes and two types of mechanisms can occur. After the high valent metal species containing and activated ligand X (X = oxo, carbene, imido) is formed, ligand X will react with a C-H bond. This step could proceed by either direct insertion or H-atom abstraction and radical rebound, which tends to have a selectivity that resembles radical reactions unless fast rebound occurs.

I.1.2 Mechanisms of Activation and Early Examples

The cleavage of a $\sigma(\text{C-H})$ bond in the inner coordination sphere of a transition metal complex results generally from two synergistic transfers of electron density (Figure I.2): σ -donation from the bonding $\sigma(\text{C-H})$ molecular orbital (MO) into a symmetry-adapted vacant orbital on $L_n\text{M}$ (electrophilic C-H activation); and π -backdonation from an occupied d_π MO on $L_n\text{M}$ into the antibonding $\sigma^*(\text{C-H})$ MO

(nucleophilic C-H activation). Both factors weaken the sigma bond leading eventually to bond cleavage, but a vacant site needs to be created on the metal to allow coordination of the σ bond. In spite of the experimental observation that formation of a σ -complex is challenging because the interaction between the metal and the C-H bond is usually weak, several examples, including agostic C-H bond interactions,^{13,14} have been characterized. Such intermediates are usually encountered prior to the C-H cleavage step, which will proceed through a variety of different mechanisms. In this section, some fundamental mechanisms of C-H activation, such as oxidative addition, σ -bond metathesis and electrophilic activation will be presented together with early discoveries. Nevertheless, mechanisms such as 1,2-addition will not be discussed in this thesis and radical C-H activation will be disclosed in Section I.4.

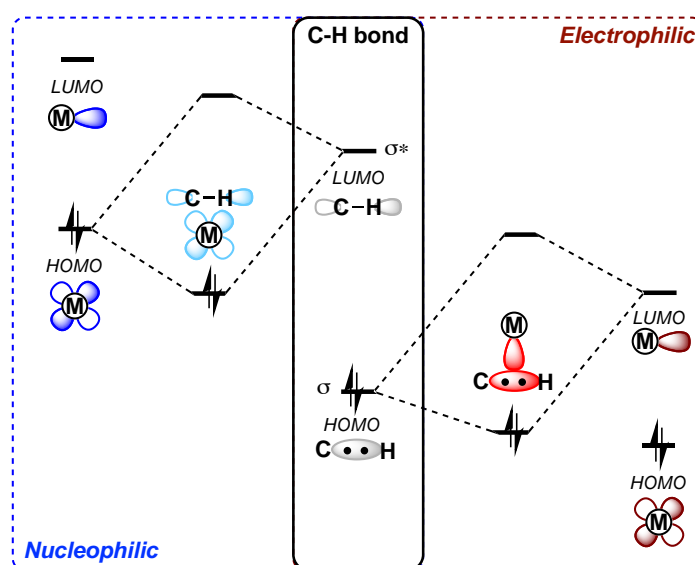
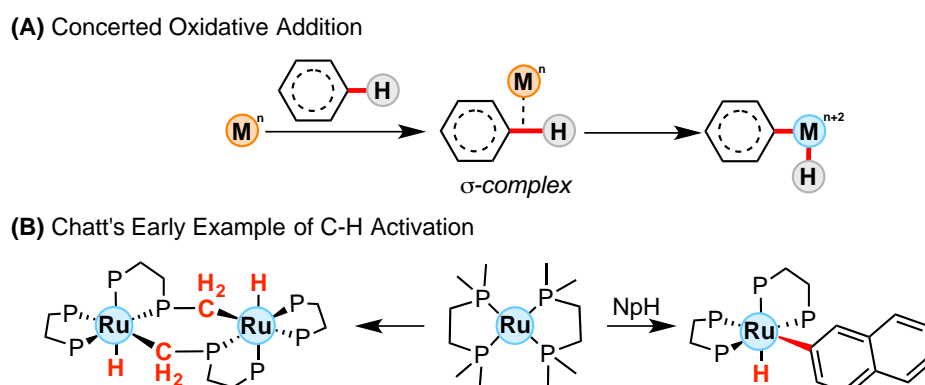


Figure I.2. Nucleophilic and electrophilic C-H activation.

1.1.2.1 Chatt's Example and Oxidative Addition into C-H bonds

The first metal containing system capable of reacting with hydrocarbons and other C-H compounds, the Fenton's reagent, was discovered as early as the end of the nineteenth century.¹⁵ At the same time, Dimroth reported one of the oldest known organometallic reactions, which is the facile electrophilic substitution of benzene by Hg(II) salts in acidic solvents to generate a stable Ar-Hg(II) species.¹⁶ Despite this important advance in the functionalization of C-H bonds, the latter example is not usually considered as a C-H activation process, as it involves the direct attachment at the aromatic ring and not a direct interaction with the targeted σ (C-H) bond (Further discussion in Section I.1.2.3). Indeed, one of the early uses of "C-H bond activation" is attributed to Taylor, who described the H-D exchange in methane catalyzed by a heterogeneous Ni⁰ catalyst.⁸ However, the first example of C-H activation is usually attributed to Chatt,^{17,18} who reported the properties of a zerovalent and extremely

electron-rich $[\text{Ru}(\text{dmpe})_2]$ back in 1965. When this complex was reacted with naphthalene, the hydride complex $[\text{Ru}(\text{H})(\text{Np})(\text{dmpe})_2]$ was observed by NMR as well as by FT-IR (Scheme I.3B). Moreover, this complex thermally decomposed to a dimer which indeed corresponds to the first cyclometalation involving a $\text{C}(\text{sp}^3)\text{-H}$ bond. These reactions are clear examples of oxidative addition,¹⁹ whose mechanism consists in the concerted cleavage of a C-H bond which was previously interacting with the metal center (σ -complex, Scheme I.3A). The next step involves the formation of M-C and M-H bonds in the transition state (TS), with a formal increase by two units of the oxidation state of the metal center and the change of geometry of the complex to accommodate the two new bonds. This mechanism is prevalent with d^{10} and d^8 configurations.²⁰



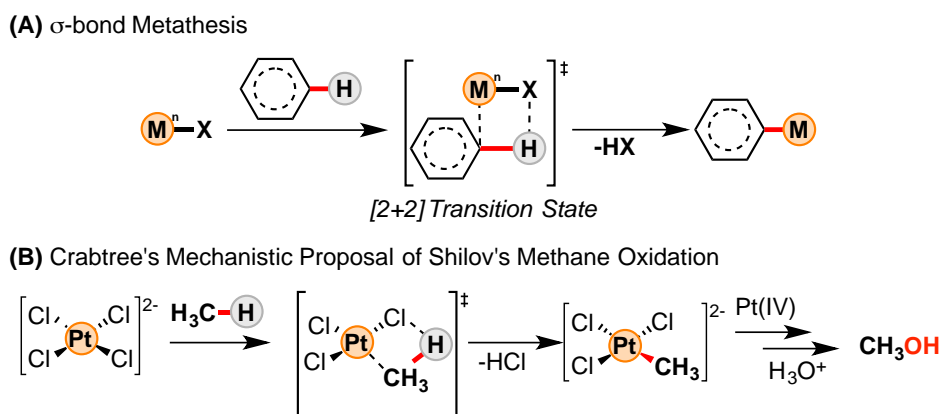
Scheme I.3. (A) Concerted Oxidative Addition general mechanism. (B) Early examples of organometallic C-H activation described by Chatt and co-workers.

Led by this elegant study, several other examples were reported in which electron-rich metal centers were found capable of adding into C-H bonds, including intra- and intermolecular additions.²¹⁻²⁵ One of these examples, which was believed to proceed via oxidative addition, is the Shilov's C-H activation chemistry with platinum.²⁶

1.1.2.2 Shilov's example and σ -bond Metathesis

Garnett and Hodges originally discovered that PtCl_4^{2-} promoted H/D isotope exchange in arenes.²⁷ Following this work, in 1972 Shilov published a dramatic advance on his earlier report of C-H activation mediated by Pt(II).²⁸ The addition of Pt(IV) salts to the aqueous reaction of PtCl_4^{2-} with methane led to the production of the oxidized species methanol and methyl chloride. This reaction is catalytic in Pt(II), but is, unfortunately, stoichiometric in Pt(IV). A significant fraction of research has concentrated on determining the mechanism of this C-H bond activation and, indeed, a reasonable mechanistic scheme was proposed by Shilov not long after his initial report.²⁹ The selectivity of the reaction (primary C-H > secondary C-H > tertiary C-H) suggested that the C-H bond is cleaved through oxidative addition, but this was felt to be unlikely since it would involve the oxidation of Pt(II) to Pt(IV). Despite the fact that

some DFT calculations pointed towards this direction, Crabtree and Siegbahn suggested a σ -bond metathesis (Scheme I.4A),³⁰ in which one hydrogen of methane is transferred to a Cl ligand, yielding HCl and a Pt-CH₃ bond (Scheme I.4B). The essential aspect of this mechanism is the redox neutral concerted formation (Pt-C(sp³)) and Cl-H) and breaking (Pt-Cl and C(sp³)-H) of bonds at the transition state ([2+2] cycloaddition).

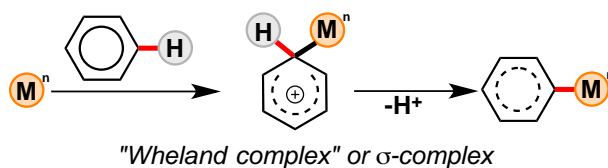


Scheme I.4. (A) General mechanism of arene σ -bond metathesis. (B) Crabtree's mechanistic proposal of Shilov's methane conversion to methanol.

This mechanism is more common for early transition metals and, indeed, it was first observed by Watson in 1983 using Lutetium and Yttrium³¹ and several examples have been reported since then.³² In spite of the fundamental importance of both oxidative addition and σ -bond metathesis, the following sections will be focused on pure electrophilic C-H activation of arenes and strategies to control site-selectivity.

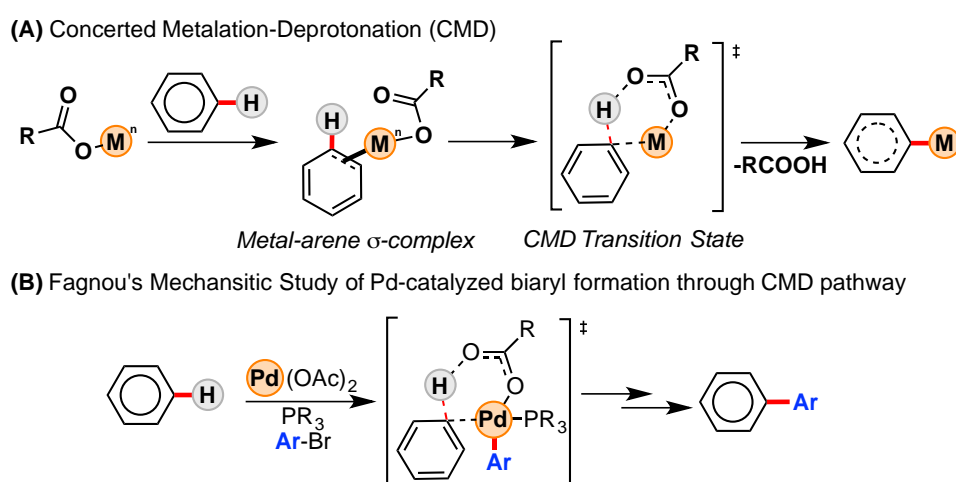
I.1.2.3 Fagnou's Concerted Metalation-Deprotonation

A particular scenario is found when considering the metalation of arenes. There are two distinct mechanisms for the metalation of aromatic C-H bonds: oxidative addition (see above) and electrophilic activation. As it has been exposed before, the early mercuriation of benzene to generate stable Ar-Hg(II) species is not usually considered a "C-H activation" process because there is no direct interaction with the σ (C-H) but with the π -aromatic system. However, this electrophilic substitution furnishes the so called "Wheland intermediate"³³ (Scheme I.5) and, indeed, it is hard to argue that the C-H bond in the cationic σ -complex is not activated.



Scheme I.5. General mechanism of metal-mediated electrophilic aromatic C-H activation.

As shown in Scheme I.5, a proton is released after the generation of the M-C complex, and consequently, the presence of a base will promote and accelerate these transformations. Indeed, Roberts and co-workers published an elegant mechanistic study on this subject.³⁴ First, the structure of the intermediate was initially assumed to be a “Wheland complex”.³⁵ However, Olah studied the nature of the intermediate through NMR spectroscopy and concluded that the species was a weakly bonded π -complex.³⁶ Roberts determined discrete KIEs of the reaction of the π -complex to form Ar-Hg species, which together with the negative entropy of the process at the TS, were indicative of a very organized TS. This data was consistent with a simultaneous C-H bond cleavage and a C-Hg bond formation mechanism, previously proposed by Winstein and Taylor in 1955.³⁷



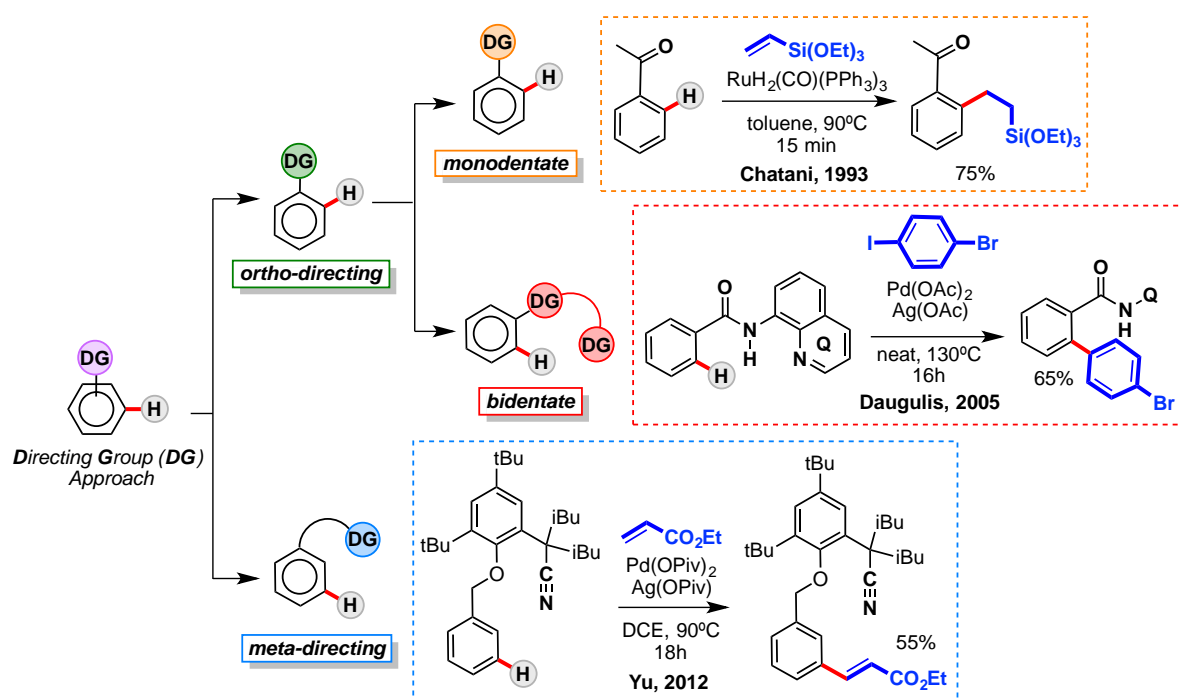
Scheme I.6. (A) General mechanism of metal-mediated Concerted Metalation-Deprotonation (CMD) and (B) Fagnou's mechanistic study of Pd-catalyzed C-H arylation.

This mechanism was also recognized in palladation of benzene by Davidson and Triggs in 1968,³⁸ and its name was coined by Fagnou as Concerted Metalation-Deprotonation (CMD, Scheme I.6),³⁹⁻⁴¹ albeit some authors used other names such as internal electrophilic substitution (IES)⁴² and ambiphilic metal-ligand activation (AMLA).⁴³ Several examples of base-assisted C-H activation and functionalization using Pd-based catalysts have been reported,^{44,45} and the field is still growing at astonishing rates using other second- and third-row transition metals such as Rh^{46,47} and Ir.⁴⁸⁻⁵¹

1.1.2.4 Murai's and Chatani's Directing Group Strategy

In order to be of broad utility, one of the critical requirements of C-H functionalization methods is to control site selectivity, as most molecules contain multiple C-H bonds and functional groups. Obviously, this issue can be solved by employing molecules with C-H bonds of different reactivity, and indeed this strategy has already been applied in the functionalization of heterocycles.^{52,53} However, in

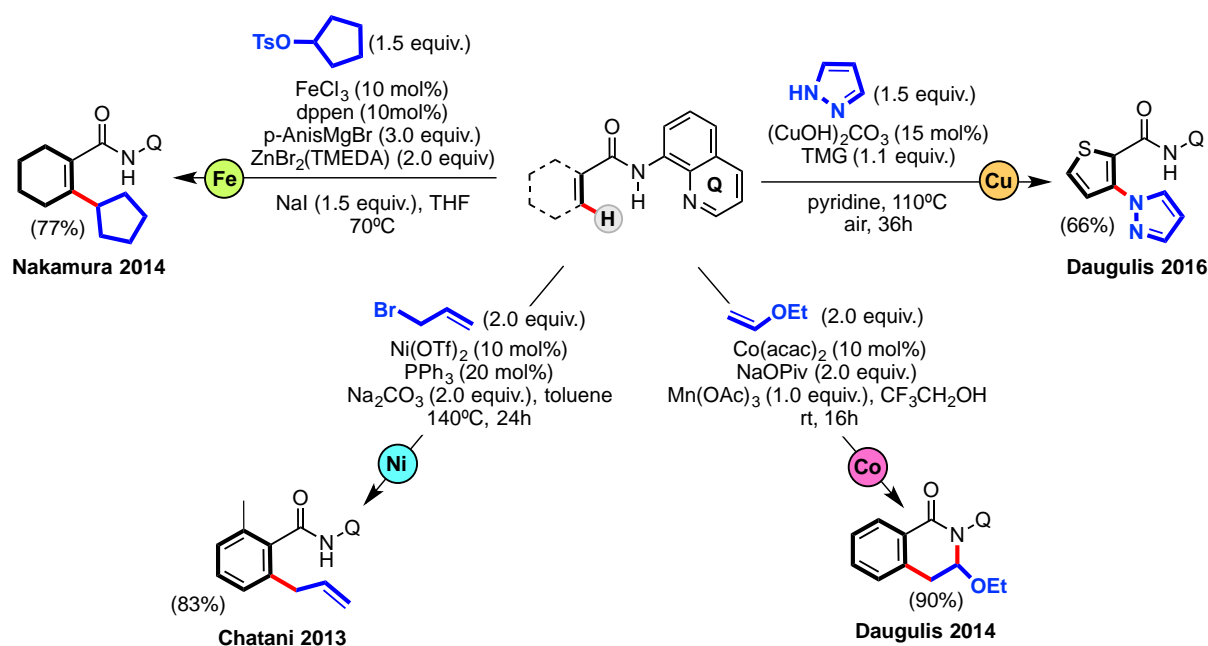
benzene derivatives the discrepancy between different C-H bonds is less pronounced and other regioselectivity-controlling strategies are required. The most successful approach, which consists in the use of directing groups (DGs), was pioneered by Lewis and Smith, who reported a Ru-catalyzed C-C bond formation protocol and proved the existence of *ortho*-metalated intermediates.⁵⁴ This proof-of-concept methodology was later popularized by Murai and Chatani,^{55,56} who utilized *ortho*-directing groups such as amines, amides, pyridines and alcohols (Scheme I.7, monodentate). Because of their coordination ability, DGs direct the metal into close proximity to the C-H bond to be activated, thus increasing its effective concentration at the site of interest,⁵⁷ which is translated in higher reactivity and regioselectivity. Then, since Murai's and Chatani's seminal work in the late 1990s, this area of chemistry has become extremely active, leading to a wide variety of solutions with broad utility in organic synthesis, including *ortho*- as well as *meta*-selective C-H activation protocols (Scheme I.7, *meta*-directing).⁵⁸⁻⁷⁰ The latter protocols were pioneered by Yu using T-shape directing groups such the one depicted in Scheme I.7. Regarding the *ortho*-selective C-H activation, in 2005, Daugulis and co-workers reported the use of the N,N-bi-dentate 8-aminoquinoline and picolinamide DGs for the direct arylation of non-activated C(sp²)-H and C(sp³)-H bonds using Pd(OAc)₂ as catalyst (Scheme I.7, bidentate).⁷¹ This pioneering study opened new horizons in the field of C-H activation, as the 8-aminoquinoline DG proved to be rigid enough to stabilize several intermediates and to enable the functionalization of C-H bonds with a wide range of coupling partners.^{72,73}



Scheme I.7. Catalytic C-H activation examples using the Directing Group strategy with *ortho*-directing (mono and bidentate ligands) as well as *meta*-directing groups.

I.1.3 First-Row Transition Metals in C-H Activation

As it has been explained above, late and noble transition metals, which are usually not abundant on earth, have traditionally played a key role in the activation of inert bonds, including C-H bonds. In contrast, first-row transition metals, which are more abundant, cheaper and less toxic, have been thus far underutilized despite their prevalence in the active center of enzymes. Nevertheless, in the recent years the application of metals such as Ni,^{74,75} Fe,⁷⁶⁻⁷⁸ Mn,^{79,80} Cu^{81,82} and Co⁸³⁻⁸⁶ have gained more prominence. Moreover, recent methodologies using rigid chelating groups such as 8-aminoquinoline (Scheme I.8) promoted their use in C-H activation catalysis and a variety of publications flourished.^{87,88}



Scheme I.8. Recent C-H activation and functionalization methodologies using first-row transition metals as catalysts and 8-aminoquinoline as directing groups.

Particularly interesting is the case of Co, which has recently received a lot of attention after Daugulis' alkylation⁸⁹ in 2014 and the use of high-valent Cp*Co(III) catalysts and their application in C-H functionalization in 2013 by Kanai and Matsunaga (see Scheme I.10).⁹⁰ Next sections of this thesis will be focused on the use of cobalt in cross-coupling catalysis and, particularly, in C-H activation and functionalization.

I.2 Cobalt in C-H Activation

The necessary development of mild and cost-effective catalysis triggered the engagement of the C-H activation community towards the application of 3d transition metals in these important transformations. In this context, environmentally benign cobalt complexes bear tremendous potential for applications in homogeneous catalysis.⁹¹ In fact, their application in metal-mediated C-H activation is not surprising if we consider the widely developed field of rhodium-catalyzed C-H activation.^{45,92} Moreover, the reduced electronegativity of cobalt as compared to rhodium translates in more nucleophilic organometallic cobalt complexes, allowing new reactivities and improved chemo- and regioselectivities. The use of cobalt remained exclusive to low-valent catalyzed processes since its discovery,⁹³ but new methodologies regarding high-valent cobalt catalysis have recently emerged as a powerful tool for the organic synthesis, being its reactivity comparable to analogous high-valent rhodium catalysts. This is evidenced by the increasing number of protocols on high-valent cobalt-catalyzed C-H activation that have been recently disclosed (Figure I.3). This research field can be divided in two categories depending on the oxidation state of the catalysts: a low-valent approach, where the active catalyst corresponds to cobalt(0) or cobalt(I) species,⁹⁴ and a high-valent approach, where the active catalysts typically contains a cobalt center in the +3 oxidation state. In this thesis, the low-valent approach will be briefly disclosed, highlighting some early examples, and the next sections will be focused on the high-valent approach.

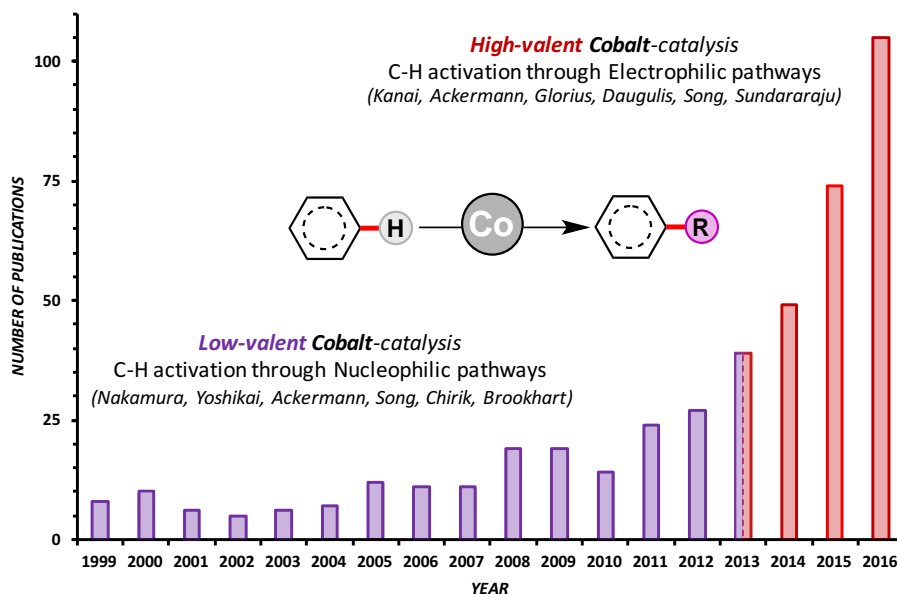
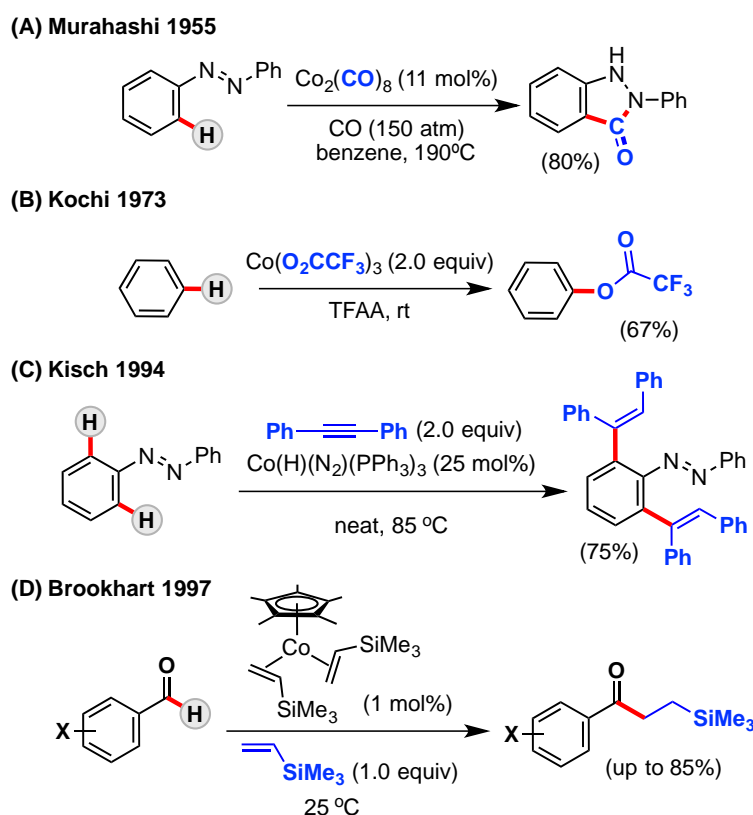


Figure I.3. Publications of Cobalt-catalyzed C-H activation *per* year. In purple, low-valent catalysis; in read, high-valent catalysis. Number of publications obtained from ISI WoS (Search criteria used: cobalt AND C-H activation).

I.2.1 Early Examples of Cobalt-Catalyzed C-H Functionalization Reactions

Cobalt-catalyzed bond formation dates back to 1941 when Kharasch and Fields reported the Co(II)-catalyzed coupling of organic halides with Grignard reagents.⁹⁵ Although this methodology is not a C-H functionalization protocol, it provided the basis of cobalt-catalyzed formation of new bonds together with subsequent works from the same authors.^{96,97} Actually, the carbonylation of azobenene and Schiff bases disclosed by Murahashi is the earliest examples of C-H activation and functionalization through low-valent cobalt-catalysis (Scheme I.9A).⁹⁸ This report demonstrated how $\text{Co}_2(\text{CO})_8$ could be used to catalyze the coupling of Schiff-bases and carbon monoxide to readily form isoindole derivatives, clearly operating through a different mechanism from the previous report of Kharasch and Fields. Subsequent to these pioneer findings, cobalt became a powerful alternative to late and noble metals in applications such as hydroformylation,^{99,100} Pauson-Khand¹⁰¹⁻¹⁰⁴ reaction and cross-coupling reactions with aryl/alkyl halides.⁹³ About twenty years later, further advances were made in the field of cobalt-catalyzed C-H functionalization. In 1973, Kochi discovered the first example of high-valent approach towards the preparation of aromatic trifluoroacetates (Scheme I.9B). In this work, benzene was oxidized in trifluoroacetic acid (TFA) through a Single-Electron Transfer (SET).^{105,106}



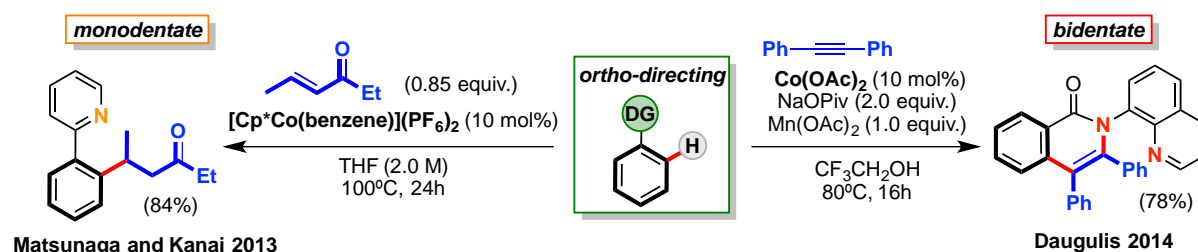
Scheme I.9. Early reports on cobalt C-H functionalization by (A) Murahashi, (B) Kochi, (C) Kisch and (D) Brookhart.

Despite these exciting breakthroughs, the field of Co-catalyzed cross-couplings was still relatively dormant, and only a few reactions were reported. In 1994, Kisch described the *ortho*-alkenylation of aromatic azo compounds using a Co(I)-catalyzed protocol (Scheme I.9C), with the product dependent on the substituents of the aromatic rings.¹⁰⁷ Following this work, Brookhart reported Cp*Co(I)-catalyzed hydroacylation of olefins (Scheme I.9D),^{108,109} C-H activation of vinyl(dimethyl)silyl amines¹¹⁰ and C-H activation of benzene.¹¹¹ These latter low-valent approaches have provided several useful bond forming methodologies⁹⁴ while high-valent approaches remained as proof-of-concept examples reported by Broderick/Legg and Avilés (see Section I.3.1).^{112,113}

The field of Co-catalyzed C-H activation protocols has recently been well reviewed by Ackermann,⁸³ Niu and Song,¹¹⁴ Yu,⁸⁶ Whiteoak⁸⁵ and Yoshino and Matsunaga.¹¹⁵ These reviews provide a broad account of developments in this field. Thus, an overview of this rapidly growing field will be provided using selected examples to highlight the potential of cobalt for expanding the synthetic chemistry tool-box. In particular, next sections will be focused on the exponential growth of the high-valent approach and its consequences in synthetic methodologies. Moreover, different mechanistic scenarios to explain the wide range of cobalt-catalyzed transformations will be disclosed.

I.3 High-valent Cobalt-mediated C-H activation

In contrast to the prevalence of low-valent cobalt-catalyzed C-H activation and functionalization field,^{93,94} high-valent systems were completely underdeveloped five years ago. However, a significant breakthrough was made in the field between 2013 and 2014 (See Figure I.3) by Matsunaga/Kanai and Daugulis (Scheme I10). In 2013, Matsunaga and Kanai reported the use of half sandwich Cp*Co(III) system,¹¹⁶ which is analogous to the Cp*Rh(III) complex reported by Miura in 2007.¹¹⁷ Cp*Co(III) systems proved to be very efficient in the coupling of monodentate 2-arylpyridines with a variety of electrophiles such as sulfonyl imines and α,β -unsaturated ketones. A year later, in 2014, the application of cheaper Co(II) salts such as Co(OAc)₂ as catalysts demonstrated to be highly productive in the directed C-H functionalization of phenyl amides with alkynes.⁸⁹ This methodology reported by Daugulis took advantage of the powerful bidentate DGs 8-aminoquinoline (AQ) and picolinamide (PA).



Scheme I.10. Renaissance of high-valent Co-catalyzed C-H activation enabled by Matsunaga and Kanai's (left) and Daugulis' (right) reports.

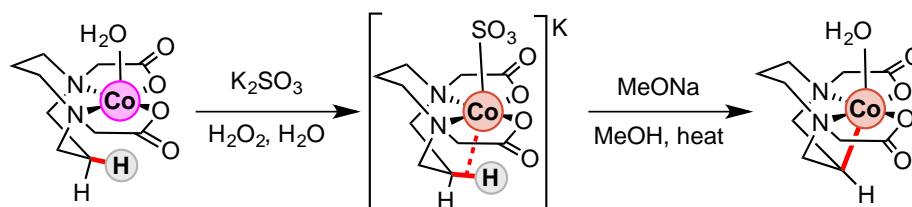
Although both methodologies exposed above overcame some challenges and opened new horizons of the high-valent cobalt-catalyzed C-H activation approach, some early examples are found in the literature. These stoichiometric proof-of-concept studies are fundamental in the understanding some mechanistic aspects of the modern cobalt-catalysis, and for this reason they deserve to be disclosed in more detail.

I.3.1 Early Stoichiometric Examples

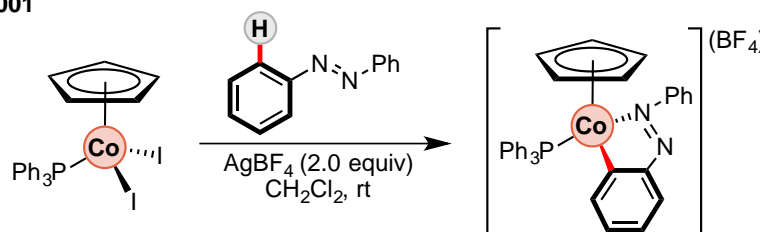
The first high-valent cobalt-mediated C-H activation was reported as early as 1986 by Broderick and Legg.¹¹² In this elegant work, the authors were able to synthesize an organometallic Co(III)-alkyl complex in an aqueous environment using a quadridentate or tetradentate macrocyclic ligand, "dacoda" (1,5-diazacyclooctane-N,N'-diacetic acid). In a subsequent study,¹¹⁸ the authors were able to identify a weak agostic interaction between the oxidized Co(III) coordination complex and the C-H bond to be activated (Scheme I.11A), which was favored when Co(III) was bearing relatively strong field ligands such as SO₃²⁻. Thus, this study was the first example of stepwise activation of C-H bonds through an electrophilic attack of Co(III), indicating that this is the actual

species that activates the C-H bond through a weak two-electron, three-center intermediate corresponding to an agostic interaction. Ten years after Broderick and Legg, another example of Co(III)-mediated stoichiometric C-H activation was reported by Avilés,¹¹³ where the first example of C-H activation using a CpCo(III) complex (CpCo(PPh₃)I₂) was described, obtaining the corresponding cyclometalated product (Scheme I.IIB). Conclusive evidence for the formation of the organometallic product was provided by X-ray diffraction (XRD). Similarly to these early examples, in 2003 Jackson reported a series of macrocyclic ligands based on the 1,4,8,11-tetrazabicyclo[9-5-2]octadecane (tabcod, Scheme I.IIC) and triazacyclonane scaffold (tacn) which were able to undergo base-assisted ligand-substitution reaction on a Co(III) center furnishing Co(III)-alkyl complexes.^{119,120}

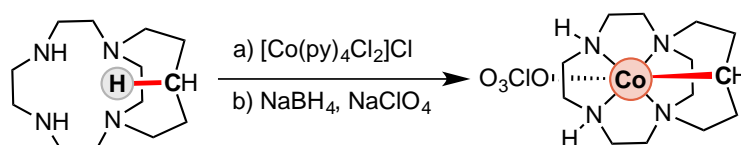
(A) Broderick and Legg 1986 and 1991



(B) Avilés 2001



(C) Jackson 2003



Scheme I.II. Early examples of high-valent cobalt-mediated C-H activation reported by (A) Broderick and Legg, (B) Avilés and (C) Jackson. Color code: Co(II), pink; Co(III), orange.

It should be noticed that in all of these examples, the hydrogen is removed as a proton, probably through an electrophilic pathway such as CMD, and thus the mechanism clearly differs from that of the low-valent cobalt chemistry in which cobalt-hydride intermediates are typically involved. Moreover, although the reactivity of these early isolated organometallic aryl/alkyl-Co(III) complexes was never tested, they indicate the strong potential of high-valent cobalt chemistry for chelation-assisted C-H activation. However, as it was mentioned above, catalytic synthetic reactions were not reported until 2013 by Matsunaga and Kanai.

I.3.2 Half-Sandwich Co(III)-catalyzed C-H Activation

In this field, the Cp*Co(III) family (Figure I.4) has demonstrated unprecedented capability for a vast variety of directed C-H bond functionalization reactions, mainly through electrophilic base-assisted mechanisms such as CMD. This section will give a brief discussion of selected examples of this field, with the objective of providing a wide view of the state of Cp*Co(III) functionalization.

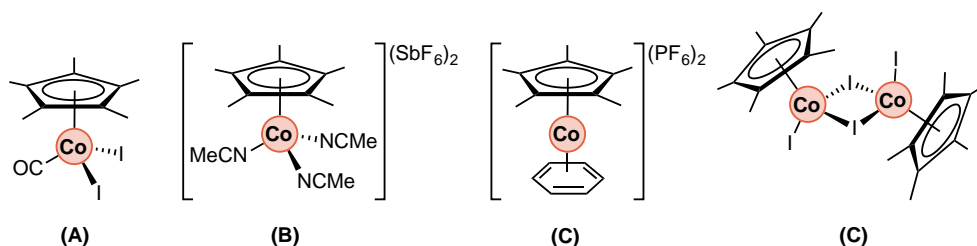
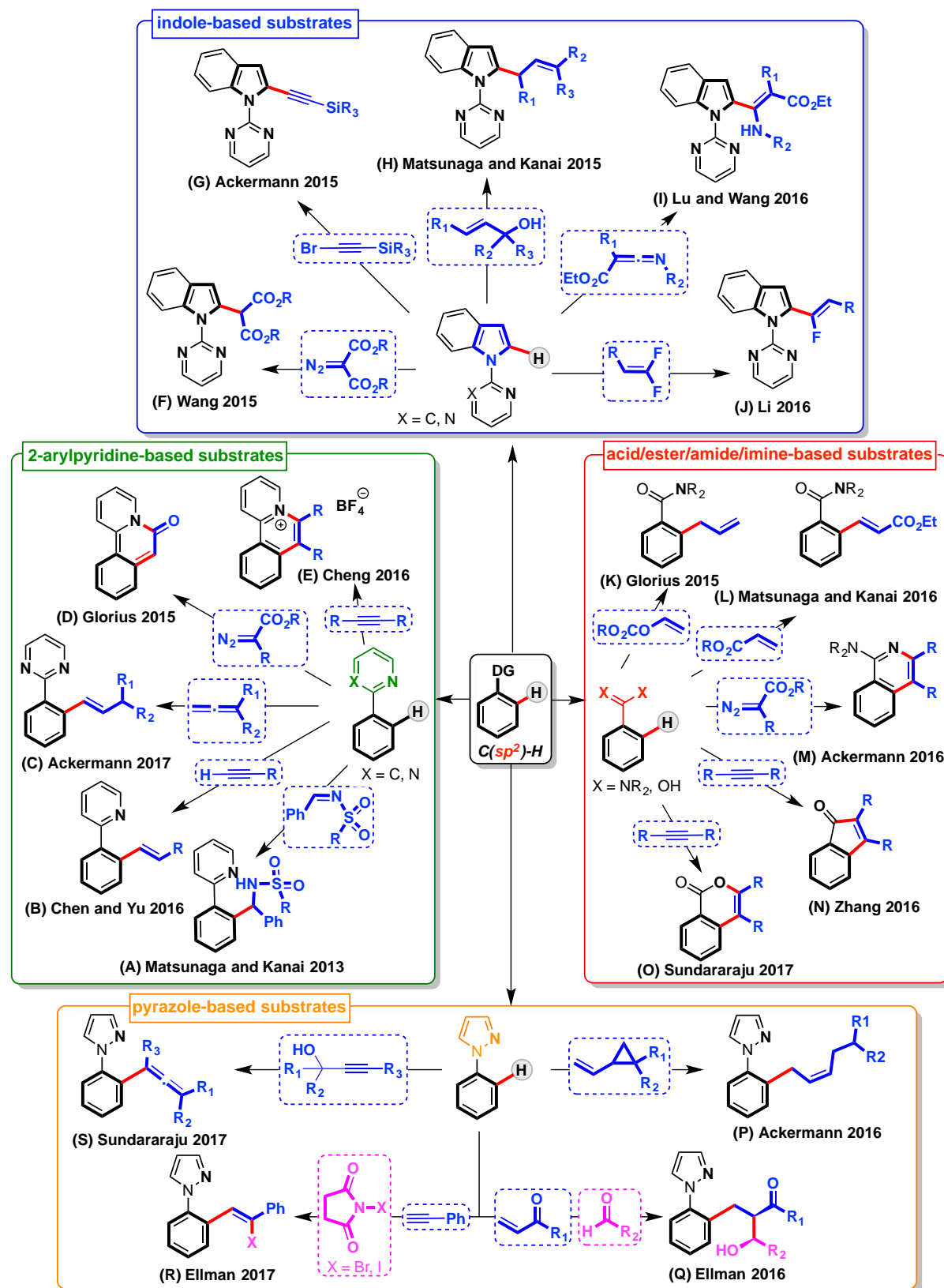


Figure I.4. Cp*Co(III) complexes used in C-H functionalization methodologies.

As mentioned above, it was not until 2013 when Matsunaga and Kanai reported the use of a readily accessible Cp*Co(III) complex to selectively cross-couple arylpyridines and imines in a selective fashion (Scheme I.12A),¹¹⁶ thus showcasing the applicability of high valent Co-catalyzed cross-coupling protocols. After this publication, the use of Cp*Co(III) complexes became popular, mostly for the construction of C(sp²)-C bonds, (Scheme I.12) and a wide variety of monodentate DGs has proven to efficiently assist these transformations. In this line, 2-arylpyridine-based substrates have been extensively used (Scheme I.12, left-green) in alkenylation reactions with triple bonds¹²¹ (Scheme I.12B) or even allene¹²² motifs (Scheme I.12C). Glorius pioneered the use of diazo compounds (Scheme I.12D) and reported several protocols for the synthesis of fluorescent π -extended systems.^{123,124} Furthermore, 2-arylpyridine-based substrates, among others,^{125,126} have been widely used for the synthesis of quaternary ammonium salts (Scheme I.12E),¹²⁷ Interestingly, the compounds obtained from azobenzene displayed strong blue photoluminescence, making them potential compounds as organic light-emitting diodes (OLEDs).

Matsunaga and Kanai not only pioneered the general use of Cp*Co(III), but also its applicability in indole and pyrrole C2 functionalization.¹²⁸⁻¹³⁰ Since then, several authors take advantage of the acidity of indole-based substrates (Scheme I.12, top-blue) and a wide variety of coupling partners have been employed. For instance, these substrates have been exploited in the insertion of diazo compounds (Scheme I.12F),¹³¹ oxidative alkynylation (Scheme I.12G),^{132,133} allylation reactions (Scheme I.12H),^{121,134-136} enaminylation¹³⁷ (Scheme I.12I) and α -fluoroalkenylations (Scheme I.12J),¹³⁸ among other practical and versatile transformations with a vast array of electrophiles as coupling partners.¹³⁹⁻¹⁴⁴



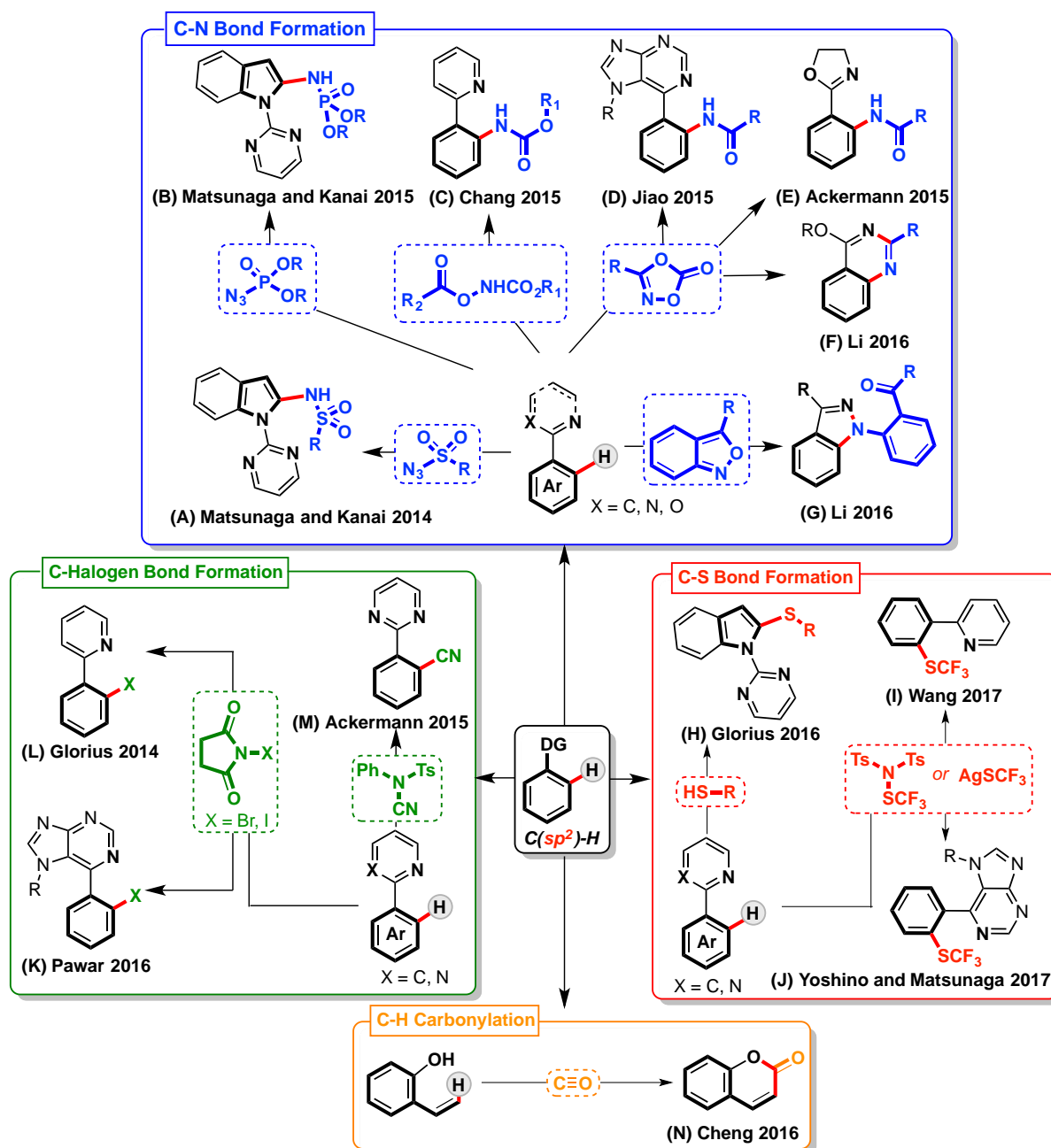
Scheme I.12. Selected Cp*Co(III)-catalyzed C(sp²)-C bond-forming reactions using indole-based substrates (blue); 2-arylpyridine related substrates (green), amine, alcohol and imine related substrates (red); and pyrazole-based substrates (orange). General conditions for each example can be found in the corresponding reference.

Other functionalities, such as carboxylic acids, esters, amides and imines have efficiently been employed as directing groups (Scheme I.12, right-red). Amides have demonstrated to be excellent directing groups and provided a vast array of transformations including allylation¹⁴⁵ (Scheme I.12K) and alkenylation^{134,146} (Scheme I.12L) reactions. An interesting reaction was recently reported by Glorius, in which the amide directing group is transferred within the substrate itself furnishing unnatural protected amino acids.¹⁴⁷ Moreover, ring-closing reactions using amide functionalities allowed the synthesis of 6- and 5-membered ring products such as isoquinoline¹⁴⁸ and isoquinolin-1(2H)-ones^{149,150} or isoindolines and pyrroles,^{151,152} respectively.¹⁵³ Imines have also been employed as monochelating directing groups in a variety of half-sandwich cobalt-catalyzed C-H functionalizations, such as α -fluoroalkenylation reactions,¹³⁸ albeit their reactivity in ring-closing transformations is the most relevant application. For example, 6-membered ring isoquinoline motifs can be furnished starting from imines and diazo compounds (Scheme I.12M)¹⁵⁴, alkynes¹⁵⁵⁻¹⁵⁸ and allylic carbonates¹⁵⁹ as coupling partners. Ester moieties have proved to be good functional groups for the synthesis of indenone motifs with alkynes,¹⁶⁰ which have also been successfully coupled with carboxylic acids furnishing isochromenone motifs.¹⁶¹

Another directing-group that has become important in the field of Cp*Co(III) catalysis is the pyrazole moiety (Scheme I.12, bottom-orange). Despite pyrazole-based substrates seem similar to 2-arylpiperidine substrates, they present different reactivity with a wide scope of coupling partners. The most relevant C-H functionalizations using these motifs include C-H/C-C activation and allylation,¹⁶² three component reactions,^{163,164} which require two different electrophiles as coupling partners, allenylations using alkynes,¹⁶⁵ hydroarylations with allenes¹²² and α -fluoroalkenylations.¹³⁸ Furthermore, despite being less exploited, substrates such as azobenzene^{166,167} and quinoline N-oxide^{168,169} also have their own place in this field.

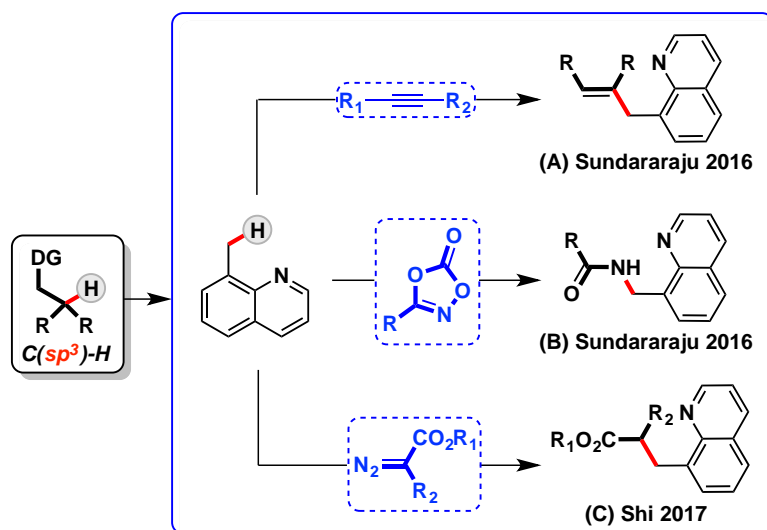
Although the formation of C(sp²)-C bonds has attracted increasing attention in the field of Cp*Co(III) C-H functionalization, C-X (X = N, Halogen, S, etc.) bond formation methodologies have also flourished and several examples have recently been reported. The construction of C-N bonds (Scheme I.13, top-blue) can be achieved by different amidation/amination technologies such as the early report from Matsunaga and Kanai with sulfonyl azides (Scheme I.13A).¹⁷⁰ Phosphorazides (Scheme I.13B) have also proven to be good aminating agents,¹⁷¹ but the use of carbamates¹⁷² (Scheme I.13C), dioxazolone (Scheme I.13D, I.13E and I.13F) and anthranil (I.13G) has been decisive for the advance on C-H bond amidation/amination¹⁷³⁻¹⁷⁵ (and annulation protocols).¹⁷⁶⁻¹⁸⁰ Furthermore, a few C-S bond formation methodologies have been recently reported (Scheme I.13, right-green), including a dehydrogenative coupling with thiols¹⁸¹ and the insertion of trifluoromethylthiolates with silver salts among other reagents.^{182,183} The

versatility of $\text{Cp}^*\text{Co(III)}$ C-H functionalization becomes clear if we consider the reported C-Halogen bond reactions using N-halide succinimides^{184,185} (Scheme I.13K and I.13L) as well as N-cyanosulfonamides,^{186,187} considering the cyano functional group as a pseudohalogen (Scheme I.13M). Moreover, direct carbonylation to yield 2H-chromen-2-one derivatives with carbon monoxide can be achieved with 2-vinylphenol as substrate,¹⁸⁸ which can also be functionalized with other coupling partners.¹⁸⁹



Scheme I.13. Selected $\text{Cp}^*\text{Co(III)}$ -catalyzed $\text{C(sp}^2\text{)-N}$ bond-forming reactions (in blue), $\text{C(sp}^2\text{)-}$ (pseudo)Halogen bond-forming transformations (in green), $\text{C(sp}^2\text{)-S}$ bond-forming protocols (in red) and the only example of $\text{Cp}^*\text{Co(III)}$ -catalyzed $\text{C(sp}^2\text{)-H}$ carbonylation reaction with CO(g) . General conditions for each example can be found in the corresponding reference.

The activation of C-H bonds using Cp*Co(III) catalysts has been mainly focused on the functionalization of C(sp²)-H bonds, probably due to their higher acidity as well as the higher stability of the resulting organometallic intermediate. In fact, C(sp³)-H functionalization protocols are scarce and limited to the rigid 8-methylquinoline monodentate substrate (Scheme I.14). Sundararaju pioneered this field with the publication of two methodologies. In the first one, alkynes proved to be an efficient coupling partner for the alkenylation of 8-methylquinoline. This work is the first example of C(sp³)-H catalytic functionalization with Cp*Co(III) catalysts (Scheme I.14A).¹⁹⁰ In the same year, a C(sp³)-H amidation reaction with dioxazolone was described (Scheme I.14B).¹⁹¹ Finally, another example disclosing the alkylation of 8-methylquinoline using diazo compounds has been recently reported and represents the last example of Cp*Co(III)-catalyzed C(sp³)-H bond functionalization reactions (Scheme I.14C).¹⁹²



Scheme I.14. Cp*Co(III)-catalyzed C(sp³)-H functionalization reactions with dioxazolone (A), alkynes (B) and diazo compounds (C). General conditions for each example can be found in the corresponding reference.

As stated in this section, Cp*Co(III) catalysts have demonstrated their tremendous capability for functionalization of C(sp²)-H and C(sp³)-H bonds, albeit the latter protocols still need more development. Indeed, recent studies prove their practicality in the construction of complex motifs^{149,193} total synthesis of natural products and some analogues,¹⁹⁴ as well as polyaromatic highly conjugated organic frameworks.¹⁹⁵ Despite the field experimented significant advances, limited information about the C-H activation modes and operating mechanisms is known.¹⁹⁶ In fact, there still remains significant room for further discovery, and future efforts should be directed towards the mechanistic understanding of the transformations, the design of more effective and robust catalysts as well as the development of more stereoselective transformations.

I.3.3 Oxidative C-H Activation and Functionalization

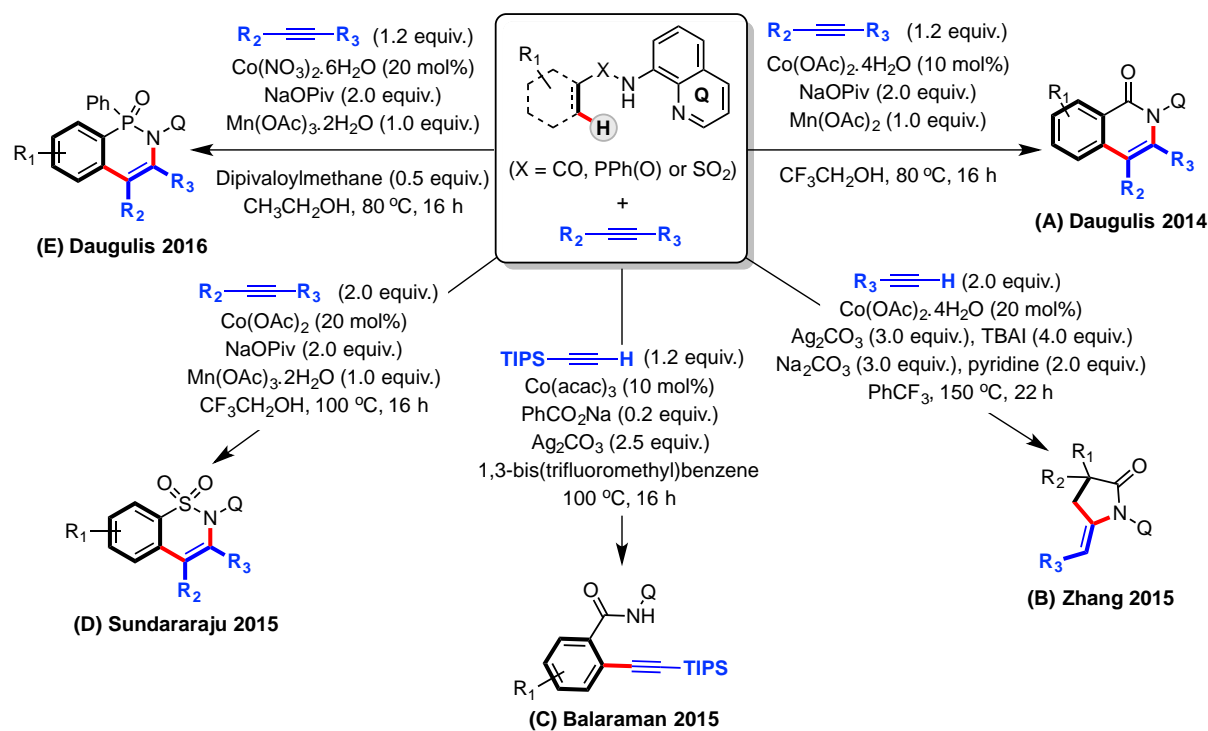
While the field of Cp*Co(III)-catalyzed C-H activation and functionalization started to grow after the publication of Matsunaga and Kanai,^{85,171,197} Daugulis identified another productive route towards high-valent cobalt-catalyzed C-H functionalization using the mono-anionic bidentate 8-aminoquinoline (AQ) and picolinamide (PA) directing groups.^{89,198,199} In this route, the precatalyst Co(II) was proposed to be oxidized to Co(III) by an external oxidant such as Ag(I), Mn salts or air. Then, the electrophilic Co(III) center initiates the catalytic cycle by a non-oxidative C-H cleavage, usually proposed to follow a Concerted Metalation-Deprotonation (CMD) pathway, which is remarkably different from the oxidative C-H activation proposed in low-valent cobalt catalytic systems (see above). Subsequently, an organometallic aryl-Co(III) species is obtained and its nucleophilic character can be exploited in reactions with coupling partners such as unsaturated C-C bonds or isocyanates. Moreover, nucleophiles such as amines and amides can also coordinate the electrophilic Co(III) center, promoting a plausible reductive elimination to Co(I). Nevertheless, in some particular cases oxidation of aryl-Co(III) intermediates is proposed to furnish aryl-Co(IV) species, which might be the key intermediates in Co(II)/Co(IV) catalytic transformations.

Since the discovery of bidentate directing group-assisted high-valent Co C-H activation in 2014, many other methodologies have been reported showing the potential of this methodology starting from readily available Co(II) salts and co-oxidants. Next sections of this thesis will be focused on the progress of C-H functionalization catalyzed by Co(II) and Co(III) species, particularly Co(II)-oxidant cooperative catalysis. Moreover, general mechanistic details of some transformations as well as experimental evidences of intermediates will be disclosed.

1.3.3.1 C-H Functionalization with Alkynes, Alkenes and Allenes

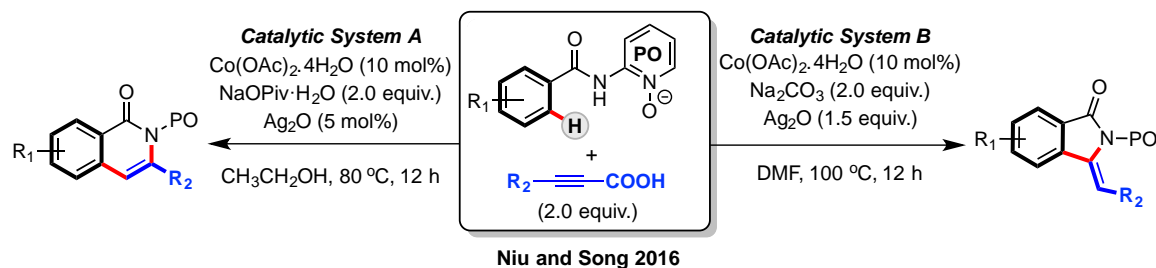
As discussed above, Co(III) complexes can participate in electrophilic C-H activation furnishing aryl-Co(III) intermediates, followed by the insertion of unsaturated C-C bonds. In a similar vein, Daugulis reported on the cobalt-catalyzed alkyne annulation taking advantage of the bidentate AQ-directing group (Scheme I.15A).⁸⁹ The alkyne annulation reaction of the starting benzamide worked best when Co(OAc)₂·4H₂O was used as catalyst together with Mn(OAc)₂ as oxidant in 2,2,2-trifluoroethanol (TFE) as solvent, which has proven to be key in C-H bond functionalization reactions.²⁰⁰ Interestingly, the quinoline-auxiliary can be oxidatively removed by treatment with cerium(IV) ammonium nitrate (CAN) at room temperature, and oxidation of the double bond affords ketolactone products. In contrast to the 6-membered rings obtained through the coupling of alkenes reported by Daugulis, later

work by Zhang has shown that 5-membered rings are also accessible through C(sp³)-H activation using terminal alkynes as coupling partners and silver salts as oxidants (Scheme I.15B).²⁰¹ Even though the cyclization reaction seemed to be very favoured in these methodologies, alkynes can be also coupled in a linear fashion, as reported by Balaraman, using ethynyltriisopropylsilane as coupling partner and Co(acac)₃ as catalyst (Scheme I.15C).²⁰² Also building on the work by Daugulis, in 2015 Sundararaju reported the preparation of benzosultam motifs using benzosulfonamides as starting materials and either terminal and internal alkynes as starting materials (Scheme I.15D), concomitantly with Chapter V of this thesis.²⁰³ Most recently, the AQ-assisted oxidative alkyne annulation has been extended still further by Daugulis using phosphinic acid amides, providing a new route towards arylazaphosphinine oxides (Scheme I.15E), among other useful transformations.²⁰⁴



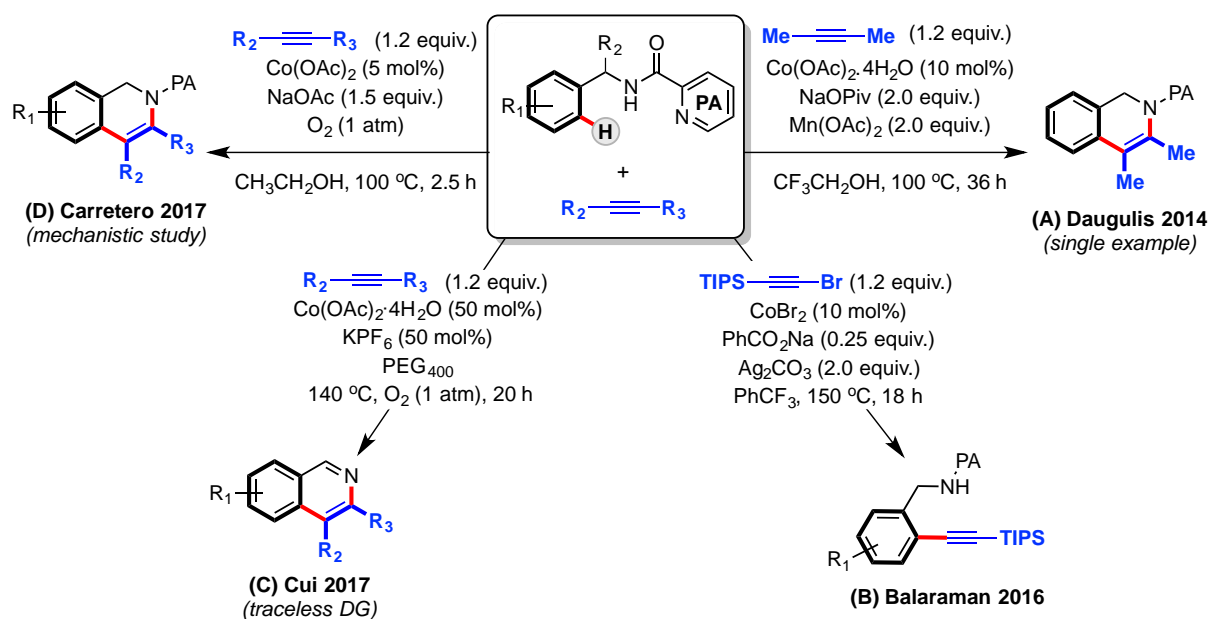
Scheme I.15. Cobalt-catalyzed 8-aminoquinoline-directed C-H functionalization with alkynes.

In 2016, Niu and Song reported a C-H functionalization with controllable regioselectivity towards 5- or 6-membered rings using Co(OAc)₂·4H₂O as catalyst, alkynyl carboxylic acids as coupling partners and 2-aminopyridine-1-oxide (APO) as directing group (Scheme I.16).²⁰⁵ Depending on the catalytic system, this strategy could afford isoquinolones (Scheme I.16, catalytic system A) or isoindolinones (Scheme I.16, catalytic system B) divergently with excellent selectivity. Remarkably, the synthesis of isoquinolones was achieved under air with catalytic amounts of Ag₂O as co-catalysts, while the construction of 5-membered ring isoindolinones needed stoichiometric amounts of silver, higher temperature and non-protic solvents.



Scheme I.16. Cobalt-catalyzed N-pyridine-oxide-directed functionalization of C-H bond with alkynes as coupling partners described by Niu and Song.

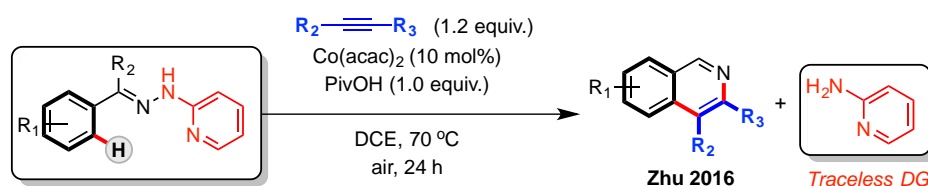
Other directing groups, such as picolinamide (PA), can also assist alkyne oxidative annulations catalyzed by binary Co(II)-oxidant systems (Scheme I.17). Indeed, the first example of PA-directed C-H functionalization with Co(OAc)₂ as catalyst was reported by Daugulis in 2014.⁸⁹ Despite disclosing just one example using 2-butyne as coupling partner (Scheme I.17A), this protocol showed the potential of cobalt-catalyzed PA-directed C-H functionalizations. Indeed, two years later, Balaraman reported the *ortho*-alkynylation of benzylamines with CoBr₂ as catalyst and (bromoethynyl)triisopropylsilane (Scheme I.17B).²⁰⁶ Interestingly, PA can be easily removed using Lewis acid-catalysts or by acid/base hydrolysis. This property as easily removable unit has been recently exploited by Cui,²⁰⁷ who reported the synthesis of isoquinolines through a traceless directing group-strategy with PA (Scheme I.17C). Analogously to Daugulis' work, a catalytic system composed of Co(OAc)₂·4H₂O as catalyst and catalytic amounts of KPF₆ under O₂ atmosphere efficiently furnished isoquinoline motifs without containing the PA-directing group.



Scheme I.17. Cobalt-catalyzed picolinamide-directed C-H functionalization with alkynes.

Another related catalytic system using alkynes as coupling partners was reported by Carretero in 2017.²⁰⁸ In this work, the authors disclosed the synthesis of dihydroisoquinoline (DHIQ) motifs, still containing the PA-directing group (Scheme I.17D). The reaction was tolerant to a wide scope of substrates, with no appreciable loss of enantiomeric purity when starting from chiral non-racemic substrates, subsequently allowing the synthesis of chiral DHIQ motifs. Moreover, Carretero performed elegant mechanistic experiments, including kinetic and labelling studies, which provided valuable information about the operating mechanism and the structure of some presumed intermediates.

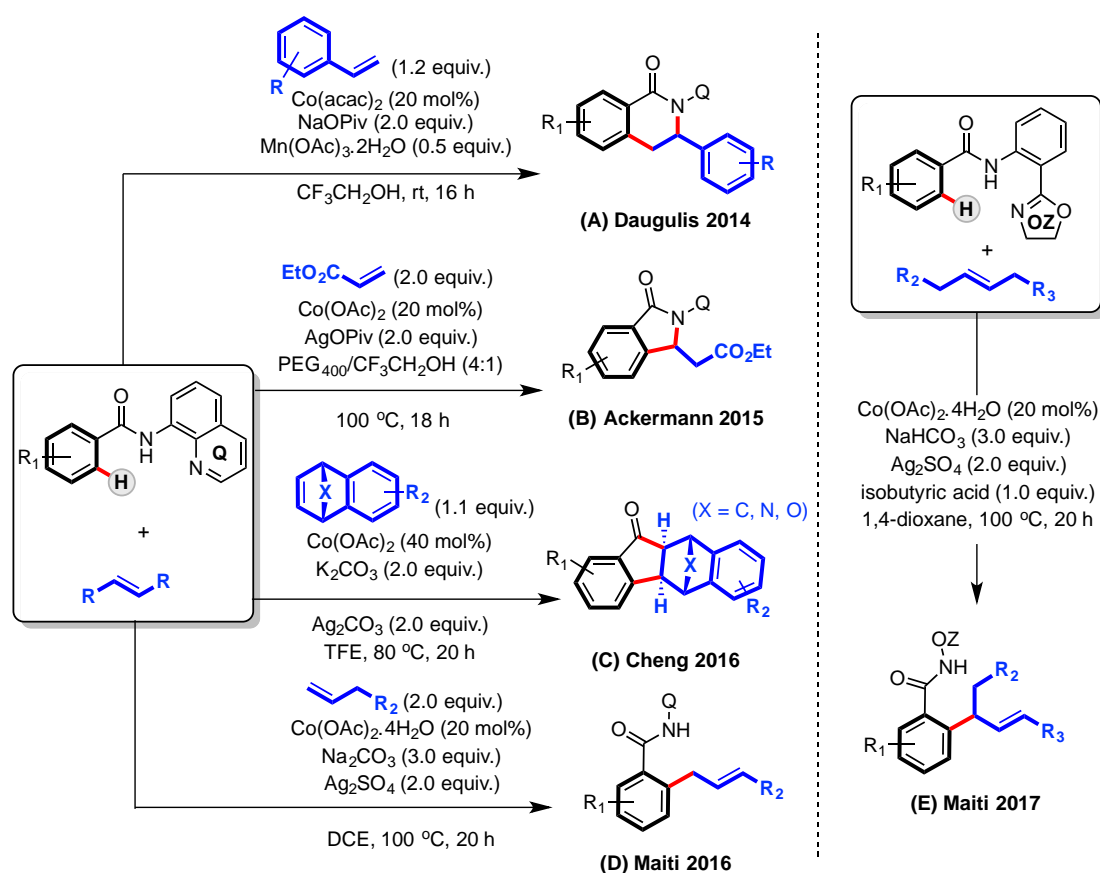
The concept of traceless directing group in high-valent cobalt-catalyzed C-H functionalization protocols was further developed by Zhu.²⁰⁹ Indeed, Zhu's example is the first bidentate directing group-enabled, traceless isoquinolone synthesis (Scheme I.18). A new directing group, 2-hydrazinylpyridine, was used in a catalytic system composed by $\text{Co}(\text{acac})_2$, pivalic acid and alkynes as coupling partners. This methodology constitutes a convenient example of directing group installation through hydrazone formation with ubiquitous ketones, allowing the synthesis of 6-membered rings. The synthetic utility of this protocol relies on the ability to directly furnish isoquinoline motifs through a traceless directing group strategy.⁵⁸



Scheme I.18. Traceless heterocycle synthesis through cobalt-catalyzed pyridinylhydrazone-directed functionalization of C-H bonds with alkynes as coupling partners described by Zhu.

Other unsaturated hydrocarbons can be selected as coupling partners in cobalt-catalyzed C-H transformations. The annulation reaction using alkenes as coupling partners was also introduced by Daugulis in 2014.¹⁹⁸ In this work, 6-membered dihydroisoquinoline motifs were synthesized using similar reaction conditions reported by Daugulis in the pioneer cobalt-catalyzed alkenylation of C-H bonds (Scheme I.19A). In addition, this elegant work showed that the AQ-auxiliary containing a methoxy group can be oxidatively cleaved in a traceless fashion with ceric(IV) ammonium nitrate (CAN). While Daugulis' system furnished 6-membered rings, Ackermann accomplished the ring-closure reaction to furnish 5-membered isoindolin-1-ones (Scheme I.19B).²¹⁰ Remarkably, Ackermann employed a mixture of TFE and polyethylene glycol (PEG400) as solvent and a catalytic system composed by $\text{Co}(\text{OAc})_2$ and stoichiometric amounts of AgOPiv as oxidant. Another 5-membered-ring-forming methodology was described by Cheng in 2016. The authors discovered a highly diastereoselective method for the

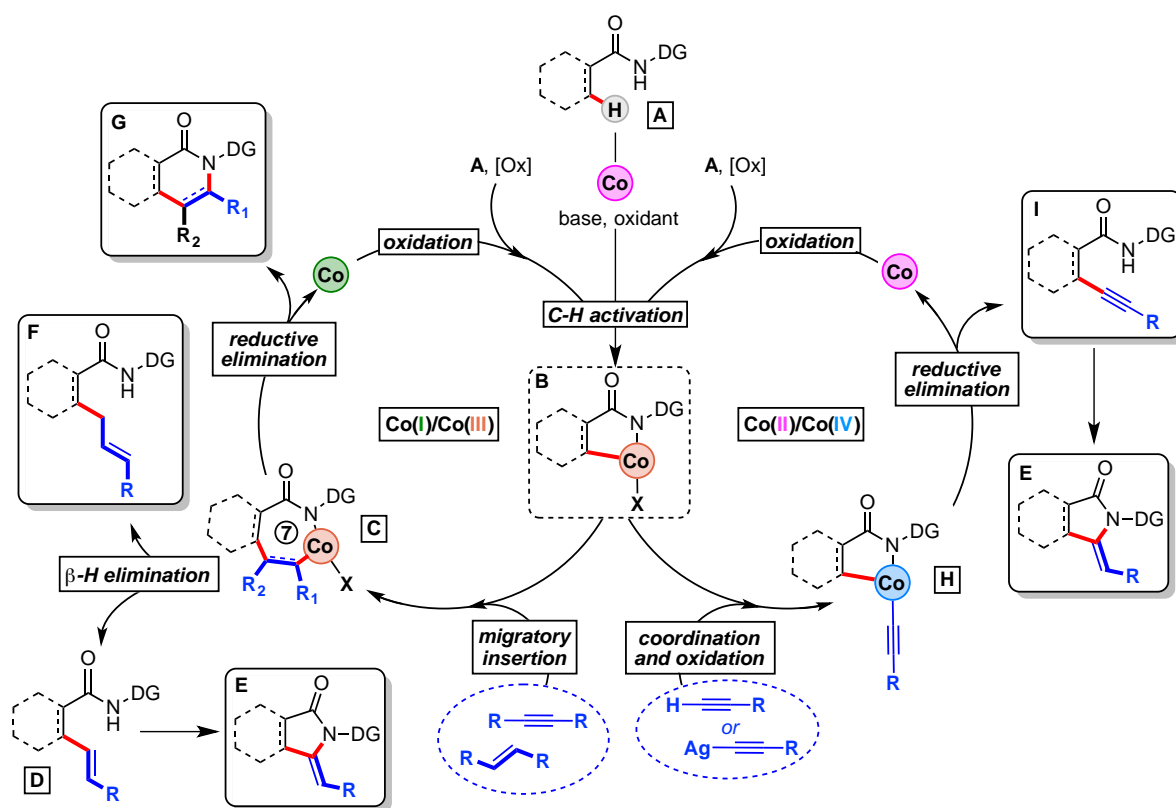
synthesis of dihydrobenzofluorenone motifs (Scheme I.19C) through a unique cobalt-catalyzed [3+2] annulation protocol.²¹¹ Non-annulated products can also be obtained using alkenes as coupling partners, as recently reported Maiti with terminal²¹² and internal alkenes.²¹³ In the former study (Scheme I.19D), aliphatic olefins were used to functionalize C-H bonds, obtaining a highly unusual allylic selectivity with a wide range of substrate combinations. In the latter work from 2017, Maiti developed a cobalt-catalyzed allylic selective dehydrogenative Heck reaction with internal aliphatic olefins (Scheme I.19E). The AQ-auxiliary group was substituted by the 1,5-bischelating system 2-(4,5-dihydrooxazol-2-yl)aniline (OZ), which considerably increased the efficiency of the method.



Scheme I.19. Cobalt-catalyzed functionalization of C-H bonds with alkenes.

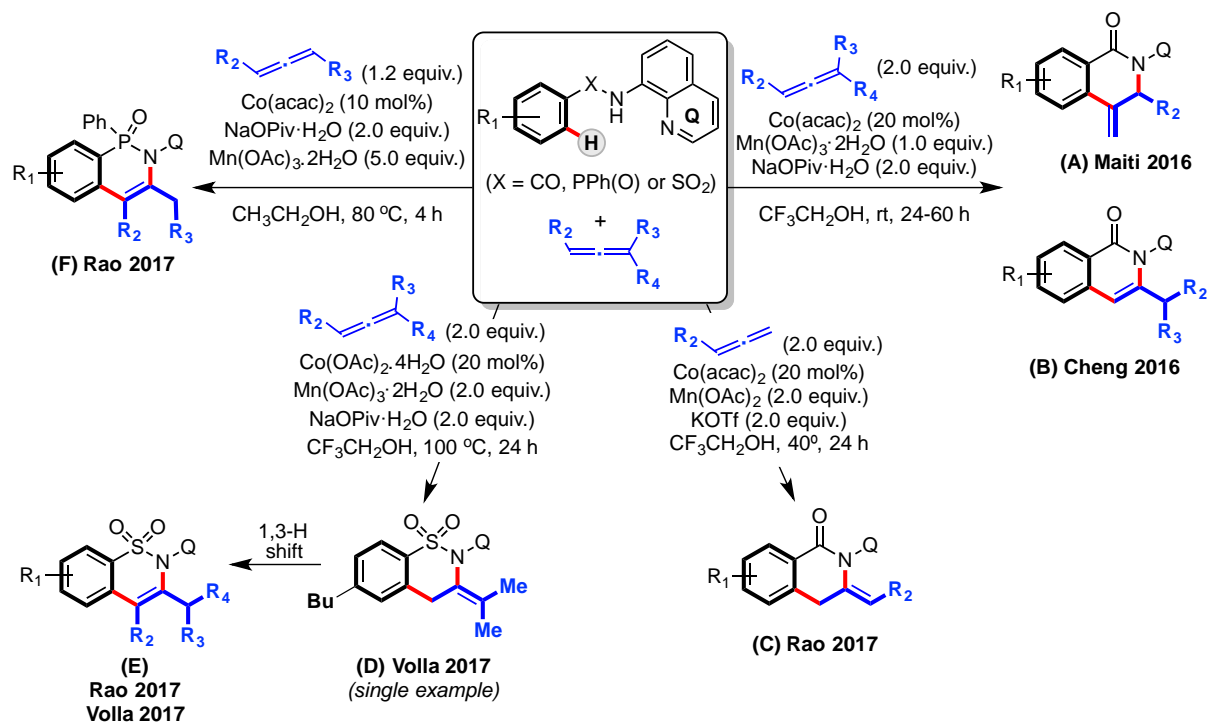
Regarding the mechanistic details of cobalt-catalyzed C-H functionalization with alkynes and alkenes, a variety of pathways, which are depicted in Scheme I.20, have been proposed. The mechanistic cycle starts with the coordination of Co(II) salts to benzamide **A**, oxidation and base-assisted C-H activation to furnish the organometallic aryl-Co(III) intermediate **B**. At this point, the mechanism splits in two different pathways. On one hand, alkynes and alkenes can undergo migratory insertion into the carbon-cobalt bond, furnishing a plausible organometallic 7-membered cobaltacycle **C**. After β -hydride elimination, **D** and **E** are furnished depending on the position of the

hydride that is abstracted. Product **D**, which has been reported by Maiti,^{212,213} is obtained after β -hydride elimination on the benzylic position. In the case of **E**, it can further react through a ring-closing transformation to furnish isoindolin-1-one **F**, described by Ackermann.²¹⁰ If instead of β -hydride elimination, cobaltacycle **C** undergoes reductive elimination, isoquinoline-1-ones and dihydroisoquinoline-1-ones **G** are furnished when alkynes and alkenes are used as coupling partners, respectively. Then, Co(I) is reoxidized and C-H activation occurs again to give the organometallic aryl-Co(III) intermediate **B**. Thus, in this case, a two-electron Co(I)/Co(III)-redox catalytic cycle is proposed to enable the synthesis of a variety of products. On the other hand, the aryl-Co(III) intermediate **B** is proposed to react with either terminal alkynes or alkynyl silver(I) species to furnish a rare aryl-Co(IV)-alkynyl intermediate **H**. Then, **H** undergoes reductive elimination to furnish the linear coupling product **I**, which has been described by Balaraman when R = triisopropylsilyl group.²⁰² Finally, a ring-closing reaction can occur on **I** to furnish the 5-membered isoindolin-1-one **E**. This latter mechanism has been proposed by Zhang, obtaining pyrrolidin-1-ones **E** through C(sp³)-H functionalization.²⁰¹ Afterwards, Co(II) is chelated again by **A** and oxidation to Co(III) promotes C-H activation to furnish **B** and restart the catalytic cycle. An unusual two-electron Co(II)/Co(IV) redox catalytic cycle is proposed to produce linear alkynes **I** or 5-membered cyclic motifs such as **E**.



Scheme I.20. General mechanisms for cobalt-catalyzed C-H functionalization with alkynes and alkenes. Color code: Co(I), green; Co(II), pink; Co(III), orange; Co(IV), blue.

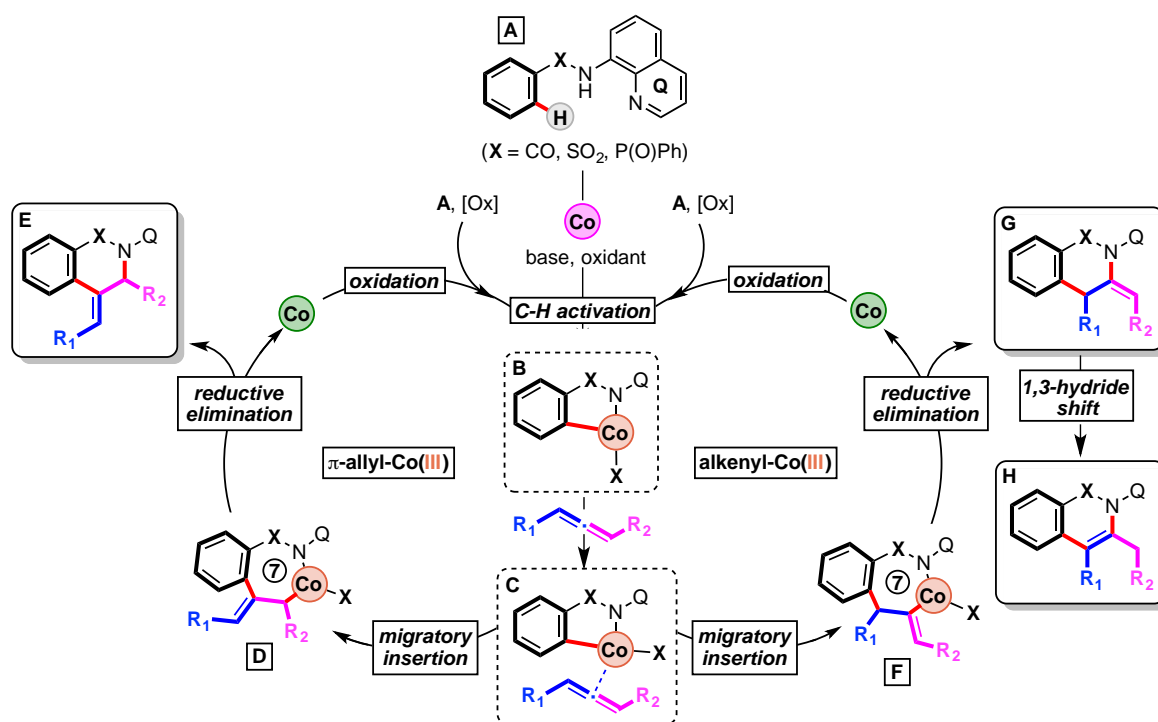
Allenes have recently proved to be suitable coupling partners for C-H functionalization using cobalt as catalyst (Scheme I.21). Indeed, due to the special reactivity and properties of 1,2-diene motifs, allenes have been extensively exploited in organic transformations.^{214–216} Taking advantage of the unique features of allenes, Maiti, Volla, Rao and Cheng pioneered the use of high-valent cobalt catalysis. In 2016, Maiti and Volla reported a mild heterocyclization of arylamides and alkenyl amides with mono- and disubstituted allenes (Scheme I.21A).²¹⁷ The authors were able to change the reactivity pattern for the regioselective cyclization, leading to the formation of dihydroisoquinoline-1-ones, isoquinolin-1-ones, dihydropyridones and pyridones. Independently, Cheng in 2016 reported a similar protocol for the synthesis of isoquinolin-1-ones and pyridones (Scheme I.21B).²¹⁸ Cheng's methodology, however, was limited by the use of monosubstituted allene motifs, which lead to the synthesis of *endo*-cyclic instead of *exo*-cyclic isoquinolines. Regarding the construction of isoquinolines, Rao reported the synthesis of *endo*- and *exo*-cyclic isoquinolines depending on the base.²¹⁹ Interestingly, the authors found potassium trifluoromethanesulfonate (KOTf) as suitable base for furnishing dihydroisoquinoline-1-ones (Scheme I.21C). It should be noticed that the methylene group in Rao's hydroisoquinoline motif is located in 3- instead of 4-position, which is opposite to Maiti's protocol. On the basis of Maiti's work, in 2017 Rao²²⁰ and Volla²²¹ reported the synthesis of sultam motifs using allenes (Scheme I.21D and I.21E).



Scheme I.21. Cobalt-catalyzed functionalization of C-H bonds with allenes as coupling partners using 8-aminoquinoline (AQ) as directing group.

Interestingly, when 1,1-dimethylallene was added as coupling partner, Volla was able to isolate the heteroannulated sultam depicted in Scheme I.21D, which is the only example that did not undergo 1,3-hydrogen shift to furnish the corresponding cyclic π -allyl product depicted in Scheme I.21E. Furthermore, reaction conditions proved to be amenable to scale up and further development of one-pot three component protocol illustrates the versatility of these methods. However, this methodology was not limited to the functionalization of benzamides and benzosulfonamides. In fact, Rao demonstrated its versatility by developing an efficient annulation reaction for the synthesis of phosphaisoquinolin-1-ones which represents another example of C-H functionalization of benzophosphinamides (Scheme I.21F). From all of these methodologies one should notice the ubiquitous use of manganese salts as cooxidants, as well as trifluoroethanol (TFE) as solvent. Indeed, TFE as well as other fluorinated solvents demonstrated to be key in many other metal-catalyzed transformations.²⁰⁰

Based on experimental evidences, a plausible mechanism for the construction of different 6-membered motifs with allenes as building blocks is depicted in Scheme I.22.



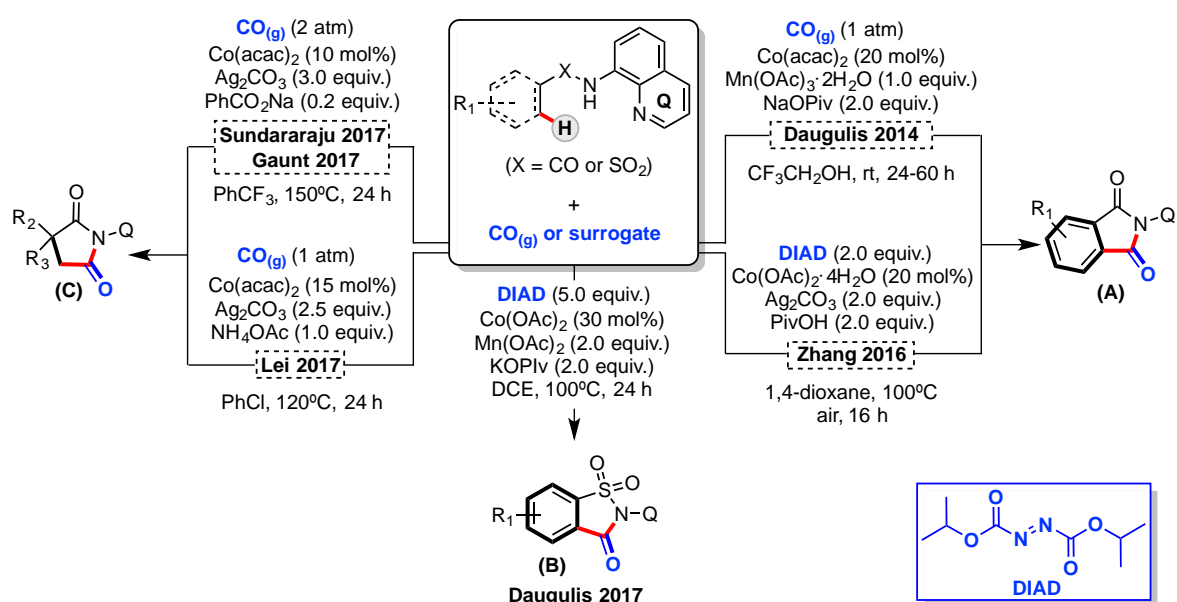
Scheme I.22. Cobalt-catalyzed functionalization of C-H bonds with allenes as coupling partners using 8-aminoquinoline (AQ) as directing groups.

In the first step, Co(II) is oxidized to Co(III) with the assistance of manganese salts such as $\text{Mn}(\text{OAc})_2$ and $\text{Mn}(\text{OAc})_3 \cdot 2\text{H}_2\text{O}$. Next, aminoquinoline A chelates in a bidentate fashion the Co(III) center, and subsequent base-assisted C-H activation forms the commonly proposed aryl-Co(III) intermediate B. Coordination of the allene moiety to

the Co(III) center yields the π -complex aryl-Co(III)-allene **C**. Then, migratory insertion into the carbon-Co(III) bond can proceed in two different ways. Insertion of allene can produce the π -allyl complex **D**. Reductive elimination of intermediate **D** yields the corresponding isoquinolin-1-ones **E** containing *exo*-cyclic double bonds in 4-position. Subsequently, Co(I) is reoxidized to Co(III) and C-H activation regenerates the key organometallic aryl-Co(III) species **B**. In contrast, carbometalation of allenes can proceed through the organometallic alkenyl-Co(III) intermediate **F**. This species will then undergo reductive elimination to furnish the corresponding isoquinolin-1-ones **G** with *exo*-cyclic double bonds in 3-position. Furthermore, after 1,3-hydride shift, isoquinolin-1-ones with *endo*-cyclic double bonds **H** can be observed. Both mechanisms involve a two-electron Co(I)/Co(III)-redox catalytic cycle.

1.3.3.2 C-H Functionalization with Carbon Monoxide (CO) or CO-Surrogates

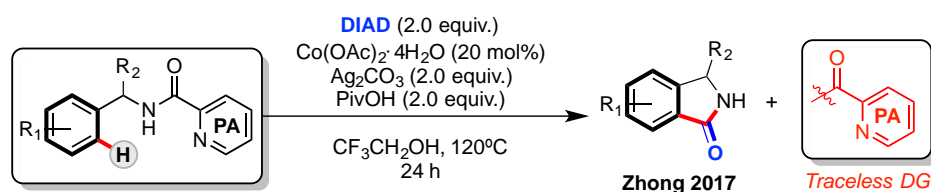
Transition-metal catalyzed C-H functionalization with carbon monoxide (CO) proved to be a useful strategy for the construction of new C-C bonds as well as annulated products.^{222–224} Indeed, as it has been explained in *Section I.2.1* (Scheme I.9), the cobalt-catalyzed C-H carbonylation of azobenzene disclosed by Murahashi in 1955 is one of the earliest examples of directed C-H bond functionalization.⁹⁸ Although this low-valent early precedent, several Co(II)-catalyzed carbonylations have been recently reported using the AQ-auxiliary DG (Scheme I.23). Although these methodologies demonstrated to be synthetically useful, they still need stoichiometric amounts of silver, the use of toxic CO gas as carbonyl source and high temperatures to operate efficiently.



Scheme I.23. Cobalt-catalyzed functionalization of C-H bonds with carbon monoxide (CO_(g)) and CO-surrogates as coupling partners using 8-aminoquinoline as directing group.

In fact, in 2014 Daugulis was the first to report the carbonylation of C-H bonds using a bidentate directing group strategy with binary Co(II)-oxidant systems as catalysts.¹⁹⁹ In this work, the authors were able to synthesize benzophthalimide derivatives (Scheme I.23A) at room temperature by using $\text{Co}(\text{acac})_2$ and $\text{Mn}(\text{OAc})_3 \cdot 2\text{H}_2\text{O}$ as catalyst and co-catalyst, respectively, under 1 atm of CO as the carbonyl source. Despite the practicality of this method, the use of toxic CO gas limited its further application. To overcome this drawback, Zhang developed a novel strategy taking advantage of the properties of azadicarboxylate esters,²²⁵ which are known to decompose at elevated temperatures releasing carbon monoxide.²²⁶ Thus, use of diisopropylazodicarboxylate (DIAD) proved to be efficient for the convenient formation of a library of functionalized phthalimides in a safer and environmentally friendly manner, albeit stoichiometric amounts of silver salts were used as oxidant. On the basis of Zhang's protocol, in 2017 Daugulis reported the carbonylation of benzosulfonamides using DIAD as carbonyl source (Scheme I.23B).²²⁷ Interestingly, when 8-amino-5-methoxyquinoline was used as auxiliary bidentate directing group, the DG could be removed after the carbonylation through an oxidative procedure with BBr_3 followed by an iodine(III) reagent. Subsequently, a vast variety of saccharin derivatives could be efficiently obtained through a method that tolerates halogen, ester and amide functionalities. Further development of high-valent cobalt-catalysis in this field allowed the discovery of $\text{C}(\text{sp}^3)\text{-H}$ carbonylation technologies, which were assisted by the AQ-auxiliary too. Sundararaju, Gaunt and Lei in 2017 independently reported a regio- and site-elective cobalt-catalyzed carbonylation of unactivated $\text{C}(\text{sp}^3)\text{-H}$ bonds (Scheme I.23C), including terminal and internal C-H bonds connected to $\alpha\text{-1}^\circ$, 2° and 3° carbons.²²⁸⁻²³⁰

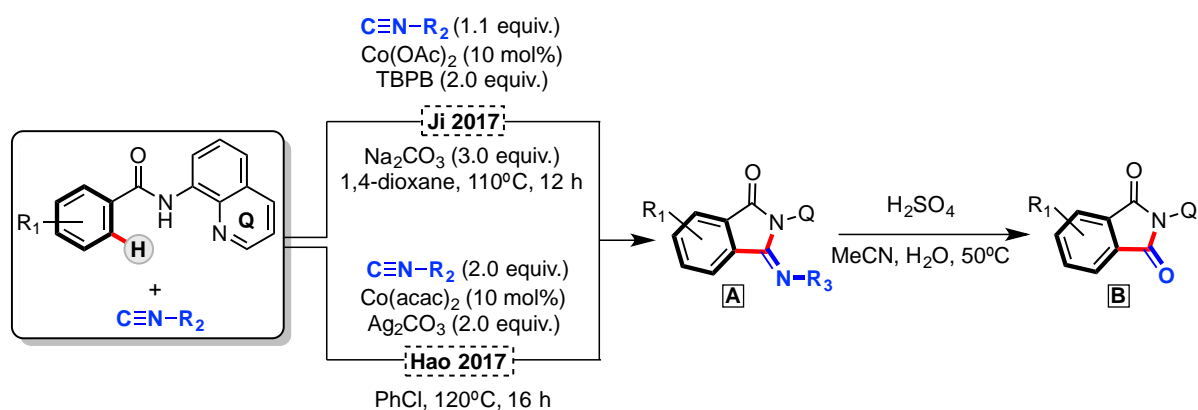
Recently, the concept of traceless directing-group has been applied to high-valent cobalt-catalyzed C-H carbonylation reactions by Zhong (Scheme I.24).²³¹ In fact, the authors reported the first example of carbonylation of benzamines using PA as traceless group for the synthesis of isoindolines. Moreover, this protocol provides an efficient method for the synthesis of biologically active compounds such as (+)-garenoxacin.



Scheme I.24. Traceless heterocycle synthesis through cobalt-catalyzed pyridinylhydrazone-directed functionalization of C-H bonds with alkynes as coupling partners described by Zhu.

A completely different strategy for the carbonylation of C-H bonds using surrogates consists in the insertion of isocyanides. Such compounds are considered an

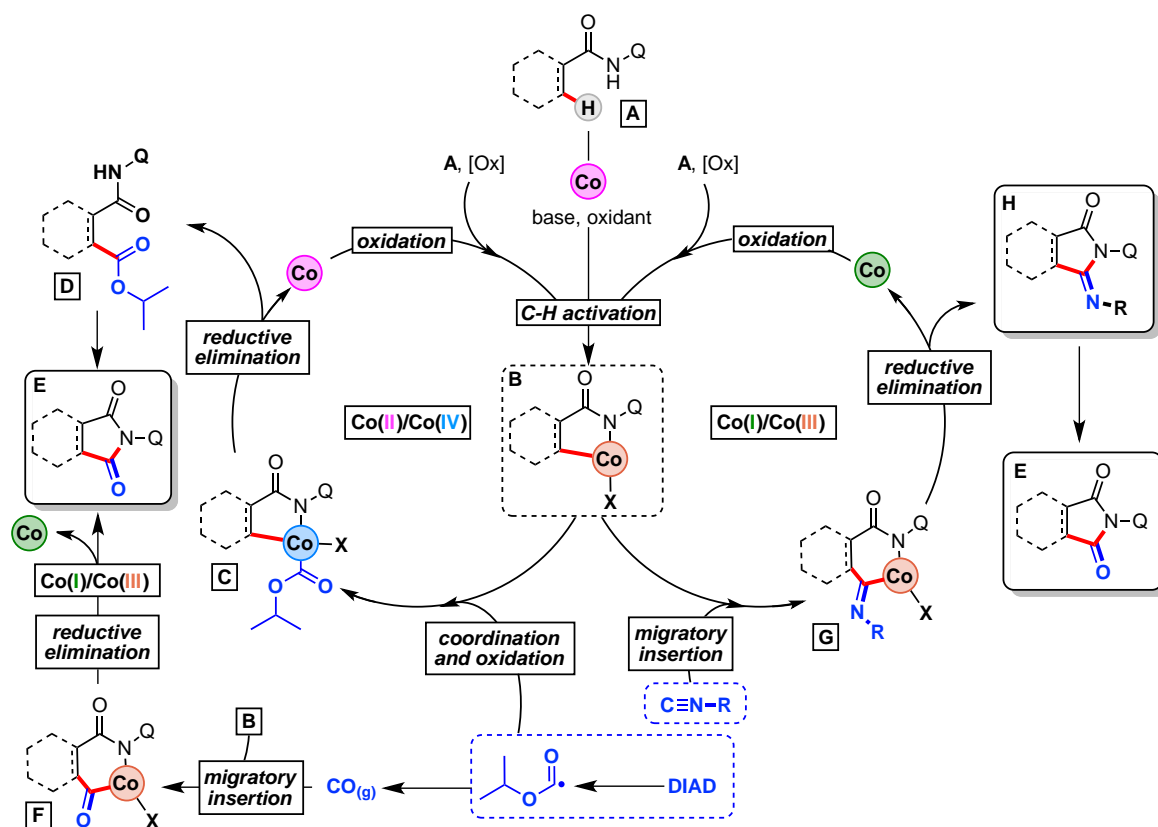
important source of carbon in metal-mediated organic synthesis due to their exceptional and valuable properties.²³² Based on these properties, in 2017 Ji²³³ and Hao²³⁴ independently developed a cobalt-catalyzed [4+1] cycloaddition of benzamides and isocyanides for the synthesis of 3-iminoisoindolinone derivatives (Scheme I.25A). Similar conditions were reported in both examples, but Ji avoided the use of expensive silver salts by adding *tert*-butyl peroxybenzoate (TBPB) as oxidant. Moreover, in his methodology Ji demonstrated that strongly coordinating N-heterocyclic directing groups such as pyridine, pyrimidine, and pyrazole were fully tolerated. Despite the versatility of the imines obtained, the synthetic applicability of these methodologies relies on the transformation of the imines motifs into carbonyl functionalities through acid hydrolysis with H₂SO₄ in acetonitrile (Scheme I.25B). Thus, these methods are considered appropriate for practical applications in terms of low cost, low toxicity, availability and efficiency to furnish cyclic carbonylated compounds.



Scheme I.25. Cobalt-catalyzed C-H functionalization with isocyanates using 8-aminoquinoline as DG and upgrading to phthalimide through hydrolysis of the imine unit.

Although different mechanistic scenarios should be considered depending on the carbonyl source employed, the first step is similar to other functionalizations. Thus, on the basis of several experimental results, a plausible mechanism is put forward in Scheme I.26. As in previous disclosed mechanisms, Co(II) coordinates with the substrate **A** and is then oxidized to Co(III) by either TBPB silver or manganese salts. Then, with the help of a base, C-H activation takes place to generate the corresponding organometallic alkyl/aryl-Co(III) complex **B**. In the reaction with CO (Scheme I.26, left cycle), two scenarios should be considered. As explained above, DIAD is known to decompose, generating carbonyl-centered radical species. These highly reactive radicals may combine with Co(III), furnishing an unstable Co(IV)-carbonyl intermediate **C**, which will rapidly undergo reductive elimination to yield **D**. Ring-closure condensation will finally generate phthalimide **E**. Alternatively, carbonyl-centered radicals could further experience decomposition to yield carbon monoxide gas. Thereafter, 1,1-migratory insertion of CO to the alkyl/aryl-Co(III) bond will generate intermediate **F**

which after reductive elimination also yields phthalimide E. Regarding isocyanides (Scheme I.26, right cycle), their reactivity is similar to CO. The corresponding isocyanide will insert into the alkyl/aryl-Co(III) bond in a 1,1-fashion to yield intermediate G. Then, reductive elimination yields imine H, which after an acid hydrolysis finally generates the corresponding phthalimide product E. Even though a Co(I)/Co(III) cycle is plausible, an oxidation step at some point of the mechanism cannot be discarded, which would promote an unusual Co(II)/Co(IV) cycle.

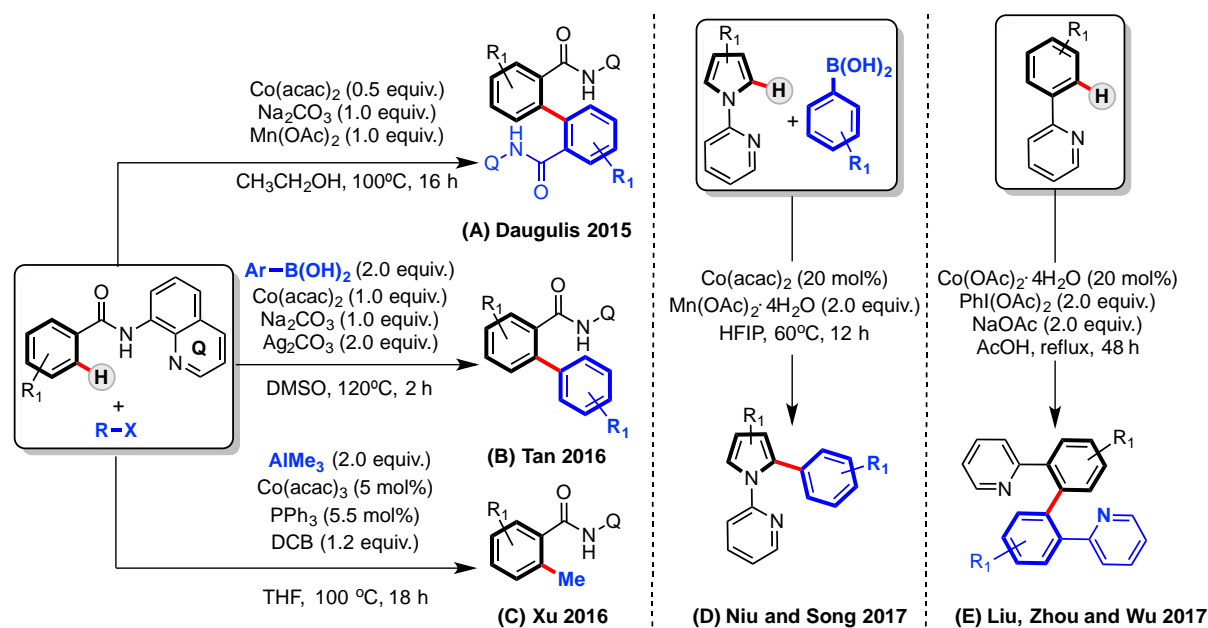


Scheme I.26. General mechanisms for cobalt-catalyzed C-H functionalization with CO(g) (or surrogates) and isocyanates. Usually proposed Co(II)/Co(IV) (left) and Co(I)/Co(III) (right) pathways. Color code: Co(I), green; Co(II), pink; Co(III), orange; Co(IV), blue.

1.3.3.3 C-H Alkylation and Arylation

Direct alkylation and arylation of C-H bonds typically proceeded through the reaction between organometallic reagents and organic electrophiles.^{51,235} However, directing-group based coupling via C-H activation has recently emerged as a practical alternative.²³⁶ Transition-metal-catalyzed homocoupling of C-H/C-H bonds has recently been developed as a straightforward methodology for constructing biaryl motifs.²³⁷ One of the main advantages of this method consists in avoiding prefunctionalized starting materials, which reduces the synthetic steps and amount of byproducts. Following this research line, in 2015 Daugulis reported the dimerization of

bidentate aminoquinoline benzamides through a cobalt-mediated methodology (Scheme I.27A).²³⁸ Although substoichiometric amounts of $\text{Co}(\text{acac})_2$ are needed, cross-coupling of benzamide proceeds efficiently and good selectivity is obtained if electronically different amides are used. This work, which can be considered as the first report of high-valent cobalt-mediated C-H/C-H bond coupling, was further extended to monodentate substrates such as 2-arylpyridines by Liu, Zou and Wu (Scheme I.27E).²³⁸ In this case, catalytic amounts of $\text{Co}(\text{OAc})_2 \cdot 4\text{H}_2\text{O}$ (5-10 mol%) were enough to generate biaryl compounds under mild conditions. However, cross-coupling of two different 2-arylpyridines proceeded with modest yields and selectivities. Another strategy for the construction of biaryl motifs is based on transition-metal catalyzed or promoted C-H activation using organoboronic acids as coupling partners, which are important actors in the field of cross-coupling reactions.^{239,240} In 2016, Tan took advantage of the reactivity and versatility of these compounds to promote the *ortho*-arylation of benzamides using readily available $\text{Co}(\text{acac})_2$ and Ag_2CO_3 as reagents of choice (Scheme I.27B).²⁴¹ While *ortho*-arylated benzamides were efficiently synthesized in good to excellent yields, stoichiometric amounts of silver and cobalt were needed, as well as high temperatures.

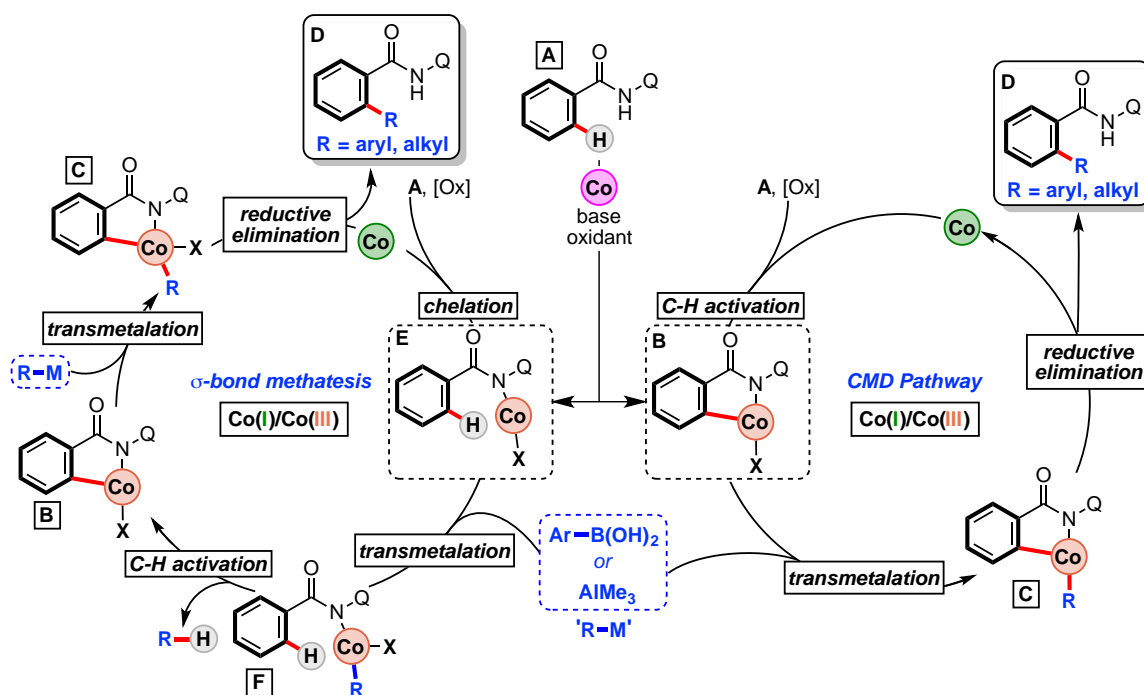


Scheme I.27. Cobalt-mediated arylation and alkylation of C-H bonds with bidentate (A, B and C) and monodentate (D and E) directing groups.

In the same year, the use of stoichiometric amounts cobalt salts was overcome by Niu and Song, who disclosed the cobalt-catalyzed direct C-H bond arylation of indoles and pyrroles with boronic acids through monodentate chelation (Scheme I.27D).²⁴² Moreover, these reactions were performed under mild conditions, avoiding the use of silver as oxidant and employing a Grignard reagent-free catalytic system. While cobalt-

catalyzed C-H arylation methodologies have recently received a lot of attention, high-valent strategies for C-H alkylation examples are really scarce. In fact, only one example of Q-directed methylation of C-H bonds can be found in the literature. In 2016 Xu detected in organoaluminium compounds a good alternative to Grignard reagents considering their functional group compatibility, availability and low cost.²⁴³ Precedents of trimethylaluminium compounds in iron cross-coupling^{244,245} as a suitable methyl donor turned out to be also valid in high-valent cobalt-catalyzed direct C-H methylation (Scheme I.27C). A catalytic system consisting in $\text{Co}(\text{acac})_3$ and PPh_3 , together with dichlorobutane (DCB) as oxidant was able to perform the mono-methylation of benzamides.

A plausible mechanism for the AQ-auxiliary cobalt-promoted arylation/alkylation of C-H bonds is depicted in Scheme I.28. The reaction is initiated by the oxidation of Co(II) to Co(III) by the corresponding oxidant. Then, two different pathways should be considered.

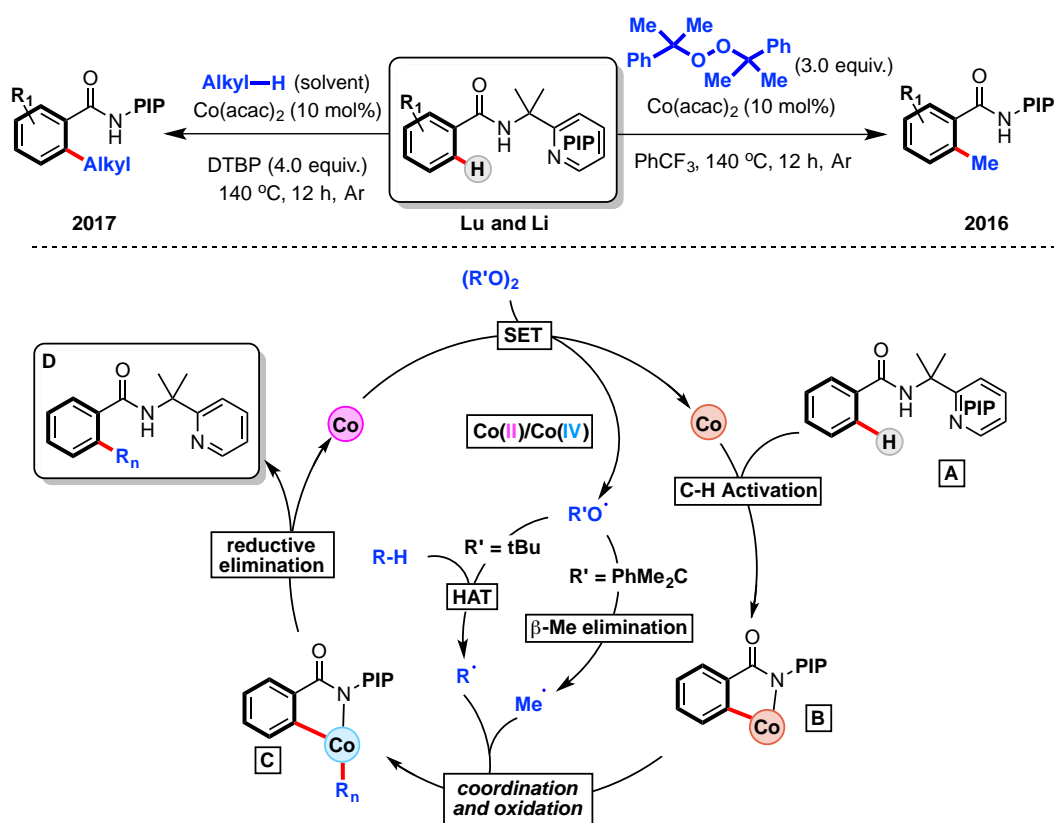


Scheme I.28. General Mechanisms for Q-assisted cobalt-catalyzed C-H alkylation and arylation of $\text{C}(\text{sp}^2)\text{-H}$ bonds through either homocoupling or transmetalating reagents. Two mechanistic scenarios are possible: σ -bond metathesis (left) and base-assisted CMD pathway (right). Color code: Co(I), green; Co(II), pink; Co(III), orange.

On one hand, Co(III) base-assisted C-H activation yields intermediate **B** through a CMD pathway (Scheme I.28, right). Then, transmetalation of organoaluminum and organoboron compounds to **B** furnishes aryl-Co(III)-alkyl/aryl intermediate **C**. After reductive elimination, the arylated/alkylated product is expelled from the catalytic

cycle, regenerating Co(III) after oxidation of Co(I). On the other hand, Co(III) coordinates substrate **A**, furnishing coordination complex **E**. Then, transmetalation of trimethylaluminium or boronic acids to **E** yields organocobalt complex **F**, which will promote C-H activation through a σ -bond metathesis mechanism (Scheme I.28, left), releasing the corresponding protonated arene or alkane fragment. This last step, which is the rate determining step in Xu's methylation (intermolecular KIE value of 3.3)²⁴³, furnishes aryl-Co(III) intermediate **B**, which is the same species generated through electrophilic base-assisted C-H activation. Thereafter, similarly to the mechanism depicted on the right side of Scheme I.27, another transmetalation step generates intermediate **C**, which undergoes reductive elimination to furnish arylated/alkylated benzamide **D** and Co(I).

Other strategies to construct C(sp²)-C(sp³) bonds were reported by Lu and Li. In their first work, the authors described a cobalt-catalyzed direct methylation of C(sp²)-H bonds using dicumyl peroxide (DCP) as the methylating (Scheme I.29, top right).²⁴⁶



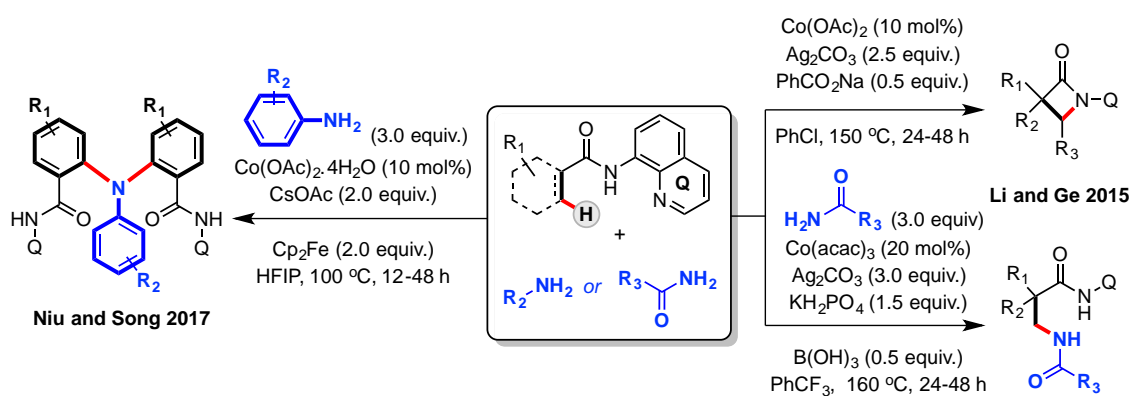
Scheme I.29. Cobalt-catalyzed C-H alkylation reported by Lu and Li (top) and General Mechanisms for PIP-assisted cobalt-catalyzed C-H alkylation of C(sp²)-H bonds through a Co(II)/Co(III)/Co(IV) catalytic cycle (bottom). Color code: Co(II), pink; Co(III), orange.

In this case, the reaction was applicable to various amides bearing a 2-pyridinylisopropyl DG (PIP) and proved to be efficient for the synthesis of *o*-methyl aryl

amides with high functional-group tolerance. In this transformation, the authors reported experimental evidences for the generation of radical intermediates through β -methyl elimination from DCP, which combine with the key aryl-Co(III) species (Scheme I.29, **B**) to generate aryl-Co(IV)-methyl species (Scheme I.29, **C**). Product **D** was finally obtained by a reductive elimination step. The same authors, in 2017, further exploited the reactivity with peroxides and developed a catalytic oxidative cross-dehydrogenative coupling (CDC) between arenes and alkanes.²⁴⁷ In this study, they achieved the *o*-alkylation of aromatic carboxamides containing the PIP-DG with di-*tert*-butyl peroxide (DTBP) (Scheme I.29, top left). In this case, a similar mechanistic scenario in which a radical was generated after hydrogen-atom transfer (HAT) to yield the same aryl-Co(IV)-alkyl intermediate was reported (Scheme I.29, **C**).

1.3.3.4 C-H Amination and Esterification

During the last five years, a great step forward towards catalytic systems that allow the construction of C-X bonds (X = N, O, S, P, B, Cl, Br, I) using catalytic systems based on cobalt has been reported. While hydrosilylation,²⁴⁸ hydrophosphination,²⁴⁹ hydroboration²⁵⁰⁻²⁵² and borylation^{253,254} reactions are established, direct C-H bond functionalization to furnish C-X bonds is underdeveloped,^{93,255} especially for high-valent cobalt-catalyzed C-N bond formation *via* C-H activation. Alkyl and aryl azides have been recognized as important reagents for C-N bond formation reactions,²⁵⁶⁻²⁶⁰ but cobalt-mediated coupling of arenes with differently substituted amines is still in its infancy (Scheme I.30).

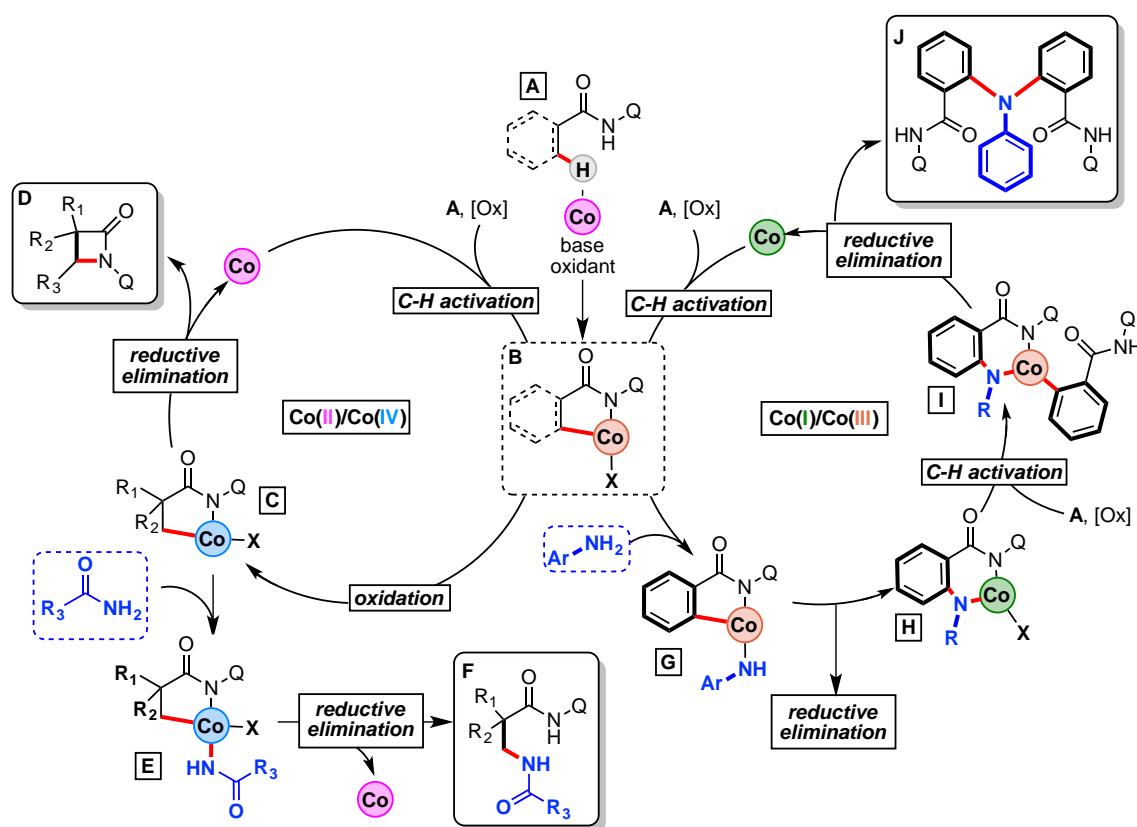


Scheme I.30. Niu and Song's amination (left) and Li and Ge's amidation (intramolecular, right up; intermolecular, right down) of C-H bonds with anilines and amides as coupling partners, respectively.

Li and Ge pioneered the field by reporting a highly regioselective intramolecular amination of propionamide and butyramide derivatives with a bidentate Q-auxiliary *via* C(sp³)-H bond functionalization process (Scheme I.30, right and up),²⁶¹ which yields 4- and 5-membered ring β -lactam derivatives in a highly site- and diastereo-selective

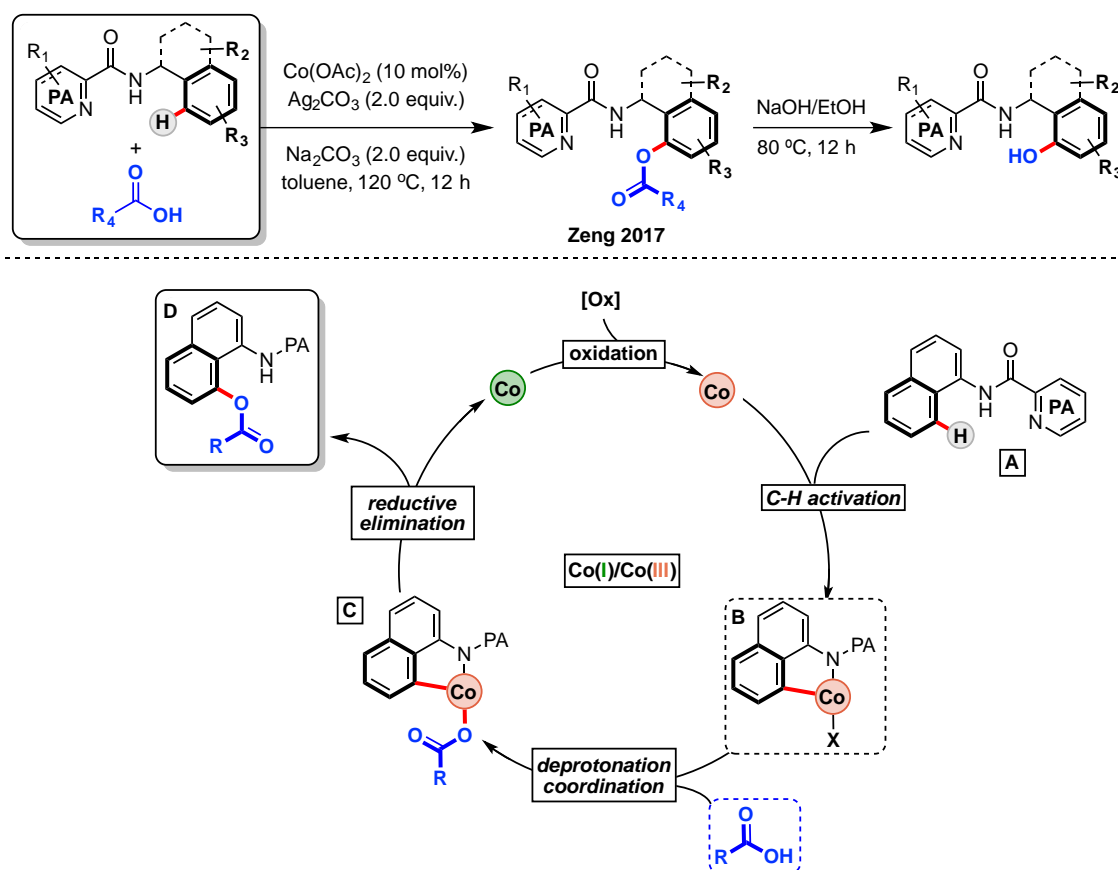
manner. In the same work, the authors also described an intermolecular protocol for the C(sp³)-H bond amidation with electron poor amides (Scheme I.30, right down). The latter protocol finds important applications in the synthesis of a library of differently α -substituted β -aminoacids. The first example of C-N bond formation using amines through C-H activation (see Section I.5.2 for one-electron C-heteroatom bond formations with high-valent cobalt catalysis) has been recently reported by Niu and Song (Scheme I.30, left).²⁶² The authors developed an oxidative C-H/N-H cross-coupling reaction between unactivated arenes and simple aniline substrates to accomplish the synthesis of triarylmines. Furthermore, sterically congested triarylmines were obtained via CDC-amination, which opens the gate to other cobalt catalyzed C-H bond functionalization reactions.

Based on several control experiments and mechanistic studies from the works presented above, a general mechanistic picture is shown in Scheme I.31. As in other mechanistic scenarios shown in past sections, Co(II) is oxidized to Co(III) after coordination of A, and intermediate B is furnished through organometallic C-H activation.



Scheme I.31. Mechanisms for cobalt-catalyzed C-H amination and amidation reactions, including intra- and intermolecular transformations. Color code: Co(I), green; Co(II), pink; Co(III), orange; Co(IV), blue.

In their protocol, Li and Ge suggested an oxidation of intermediate **B** to **C**, which corresponds to an aryl-Co(IV) organometallic complex.²⁶³ This step is based on the lack of reactivity observed when the reaction was performed starting from Co(III) salts such as $\text{Co}(\text{acac})_3$. Thus, this experiments led the authors to exclude a possible Co(I)/Co(III) catalytic cycle. Then, reductive elimination from **C** furnishes the new C-N bond in an intramolecular fashion, yielding 4-membered ring lactam derivatives. In contrast, another amide present in the media could also coordinate to the Co(IV) center furnishing **E**. Afterwards, the aryl-Co(IV)-amido intermediate **E** undergoes reductive elimination to yield the final C(sp³)-amidated product **F** through a Co(II)/Co(IV) catalytic cycle. Contrariwise, Niu and Song proposed a Co(I)/Co(III) mechanistic scenario in their amination reaction with anilines,²⁶² being able to isolate some of the reaction intermediates (see below). Subsequently, after C-H activation, **B** coordinates aniline to yield aryl-Co(III)-amine complex **G**, which will undergo a first reductive elimination to furnish Co(I)-amino complex **H**. As a result of reoxidation and C-H activation of another substrate molecule (**A**), the aryl-Co(III)-amino complex **I** is obtained. Afterwards, a second reductive elimination step takes place, releasing Co(I) and the desired product, triarylamine **J**.



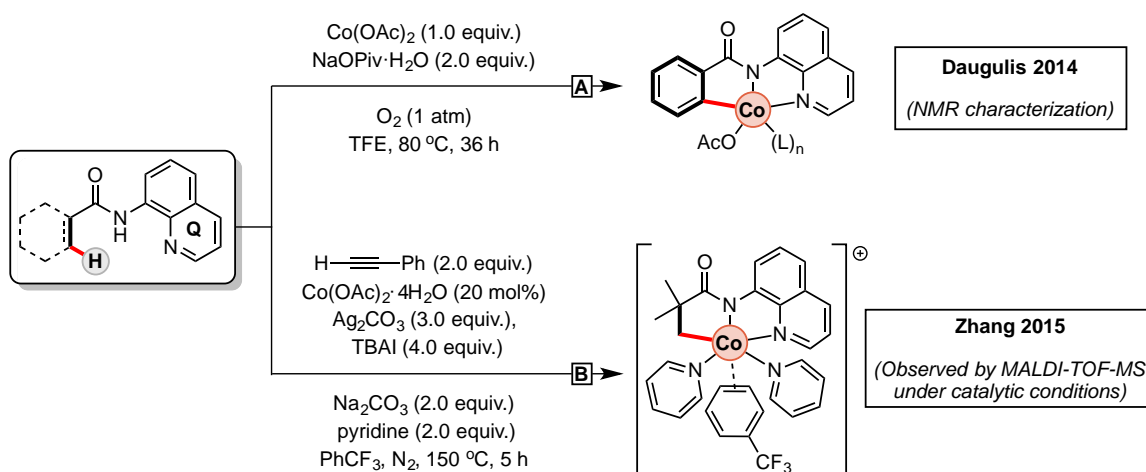
Scheme I.32 Zeng's cross-dehydrogenative coupling of arene and carboxylic acids (top). A Co(I)/Co(III) catalytic cycle was proposed (bottom). Color code: Co(I), green; Co(III), orange.

The synthesis of C-O bonds is one of the fundamental processes in organic chemistry, and ether- containing groups are widely employed in the synthesis of pharmaceuticals and functional materials.²⁶⁴⁻²⁶⁷ As it has been exposed in Section I.2.1, Co-mediated C-O bond formation was discovered by Kochi and further protocols have been developed taking advantage of one-electron processes mediated by Co(III) catalysts. Despite these great advances, just one recent example of high-valent cobalt-catalyzed C-O bond formation is found in the literature. Thus, in 2017, Zheng reported a cobalt-catalyzed cross-dehydrogenative coupling of arenes with carboxylic acids to furnish a variety of aryl esters (Scheme I.32).²⁶⁸ Additionally, the applicability of this methodology relies in the conversion of the ester moieties into free-hydroxyl groups, furnishing an entirely new library of substituted phenol derivatives. Several control experiments revealed that the transformation proceeds through an organometallic mechanism, in which an aryl-Co(III) species is involved (Scheme I.32, **B**). Indeed, coordination of carboxylic acids (Scheme I.32, **C**) after a deprotonation step and a subsequent reductive elimination yields the corresponding aryl ester (Scheme I.32, **D**). While this mechanistic scenario is well established, results from control experiments suggest that a radical mechanism cannot be completely ruled out.

1.3.3.5 Experimental Evidences of Organometallic Intermediates

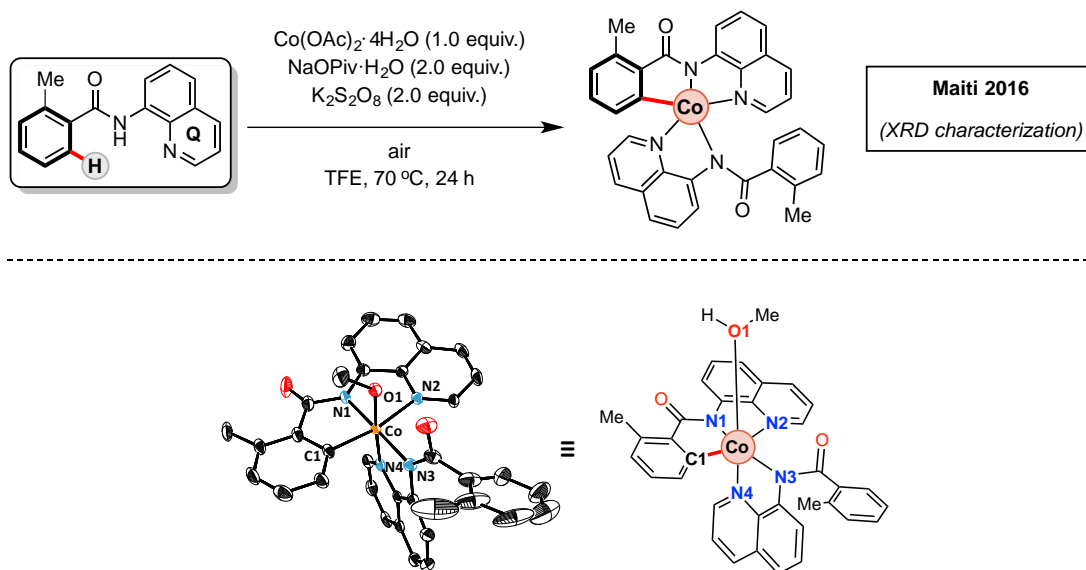
As disclosed in previous sections of this thesis, the use of bidentate chelating groups in high-valent cobalt-catalyzed functionalization of C-H bonds prospered and several methodologies have recently been reported. Novel protocols include C-C bond formation, among them annulation and ring-closure transformations, as well as C-Heteroatom bond construction reactions, which enabled the synthesis of products such as aryl esters, tertiary amines and secondary amides. However, despite the exponential growth in protocols published and the practicality of these methods, scarce mechanistic information is known. Although control studies such as kinetic isotope effects (KIE), evaluation of reaction kinetics, competition experiments and radical traps are useful to understand the mechanistic details of a transformation, solid state structures of reaction intermediates usually set definitive proof of the operating mechanism.²⁶⁹⁻²⁷² However, a very limited number of aryl-Co(III) intermediates involved in catalytic C-H activation have been detected or isolated since the rise of high-valent cobalt methodologies. This is an intriguing fact if one considers that early examples of high-valent cobalt C-H activation consisted in stoichiometric proof-of-concept studies in which the intermediates, typically aryl- and alkyl-Co(III) organometallic complexes, were stable enough to be fully characterized, including crystallographic evidence. Thus, the elusive nature of these intermediates in C-H functionalization stands in the way of their characterization, but some of them have been either detected or isolated.

In his landmark study from 2014,⁸⁹ Daugulis was able to isolate an organometallic intermediate using cobalt(II) salts and O₂ to generate a highly electrophilic Co(III) species, such as in the example of Broderick and Legg.¹¹² Then, with assistance of a sodium pivalate hydrate (NaOPiv·H₂O), C-H activation takes place to furnish an aryl-Co(III) intermediate stabilized by the presence of the popular 8-aminoquinoline bidentate chelating group (Scheme I.33, A). Even though the characterization of this aryl-Co(III) was limited to ¹H NMR spectroscopy, it represents the first example of aryl-Co(III) complex involved in catalytic C-H activation. Unfortunately, the reactivity of the isolated aryl-Co(III) complex towards alkynes was not tested, but the authors assumed its intermediacy in the alkenylation reaction reported. Nevertheless, one year later Zhang detected another organometallic intermediate by mass spectrometry (Scheme I.33, B). In this case, when a *tert*-butyl amide bearing an 8-aminoquinoline directing group was subjected to the corresponding catalytic conditions, including alkynes in the reaction medium, an alkyl-Co(III) species could be detected. Thus, this experiment, is the first report that demonstrates the direct intermediacy of organometallic Co(III) species in catalytic C-H functionalization reactions.



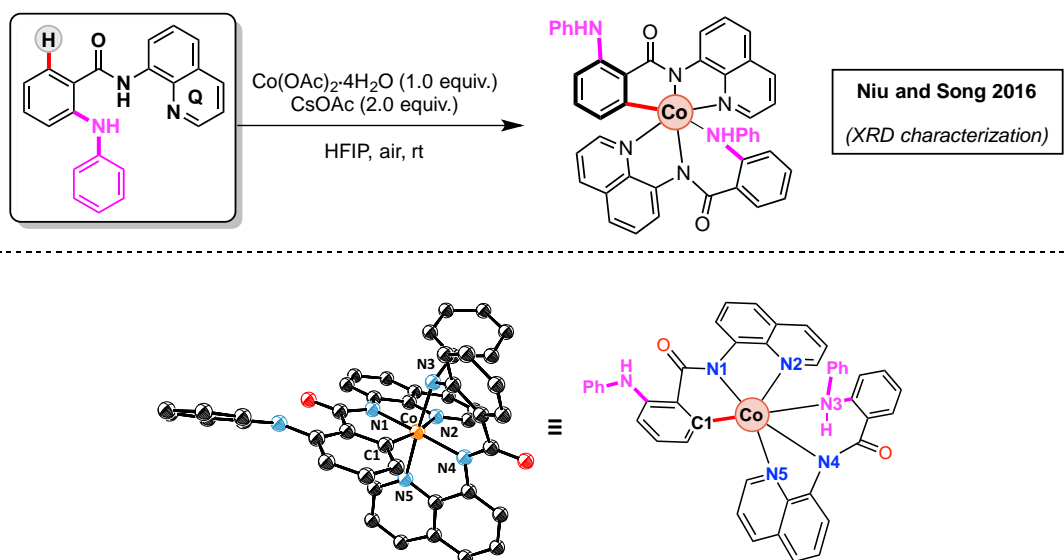
Scheme I.33. Detected organometallic Co(III) species containing the 8-aminoquinoline directing group through spectroscopic and spectrometric techniques.

Crystallographic evidence of aryl-Co(III) intermediates involved in high-valent cobalt C-H functionalization was first reported by Maiti in 2016, together with the results disclosed in Chapter III of this thesis.²¹² In this work, several mechanistic studies were performed, including kinetic analysis, radical trap experiments and deuterium-labeling experiments. However, the key experiment of Maiti's protocol was the synthesis and isolation of an organometallic aryl-Co(III) complex with Co(OAc)₂·4H₂O and an external oxidant such as K₂S₂O₈ (Scheme I.34).



Scheme I.34. Maiti's synthesis of aryl-Co(III) intermediates (up) and the XRD structure (solvent and H-atoms omitted for clarity; ellipsoids set at 50% probability level; down).

On the basis of Maiti's work, in 2017 Niu and Song were able to detect and isolate the reaction intermediate corresponding to the cobalt-catalyzed amination of $\text{C}(\text{sp}^2)\text{-H}$ bonds.²⁶² Starting from the previously aminated substrate (Scheme I.35, up), the authors were able to synthesize an organometallic aryl-Co(III)-amino complex and they reported its crystallographic solid state structure (Scheme I.35, down). Furthermore, when this organometallic complex is subjected to high temperatures, reductive elimination occurs furnishing the corresponding triaryl amines, thus supporting the Co(I)/Co(III) mechanistic scenario depicted in Scheme I.31.



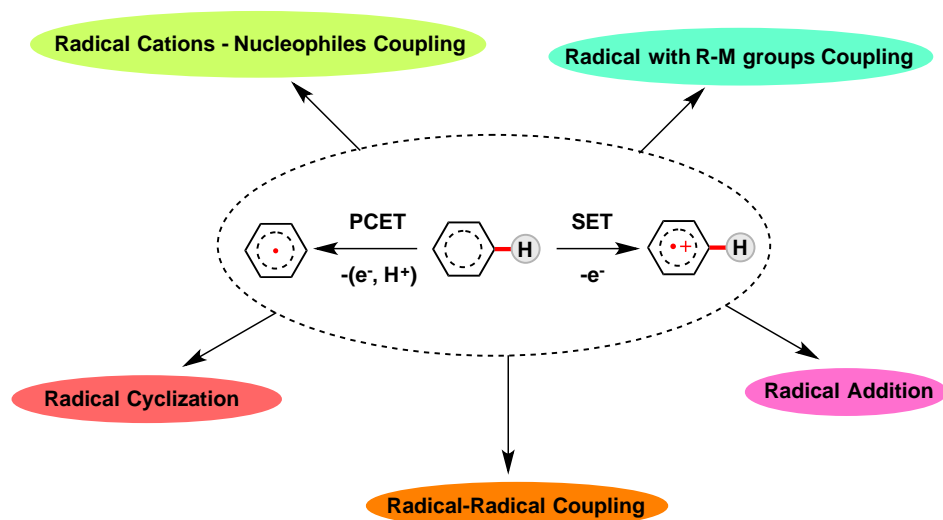
Scheme I.35. Niu and Song's synthesis of organometallic aryl-Co(III)-amino intermediates (up) and XRD structure of the isolated intermediate (solvent and H-atoms omitted for clarity; ellipsoids set at 30% probability level; down).

Recently, Carretero detected aryl-Co(III) intermediates using picolinamide as directing group in the synthesis of dihydroisoquinolines with alkynes as coupling partners (Scheme I.17D). Despite the fact that the organometallic complex was not fully characterized, its interception by mass spectrometry provided valuable insights about the reaction mechanism and the structure of some elusive cobalt species involved in the catalytic cycle.

To summarize, recent efforts have been made towards the mechanistic understanding of high-valent cobalt-catalyzed organometallic C-H activation, pointing towards a Co(III)-mediated CMD C-H activation pathway and including the isolation and characterization of key reaction intermediates. Notwithstanding, probably due to the instability of organometallic species and their low-yielding synthetic protocols, there is still a lack of knowledge on how they react with different coupling partners. Future efforts on this field are required to understand and elucidate reaction pathways and discover new possible reactivity modes.

I.4 One-electron redox processes for C-H Functionalization

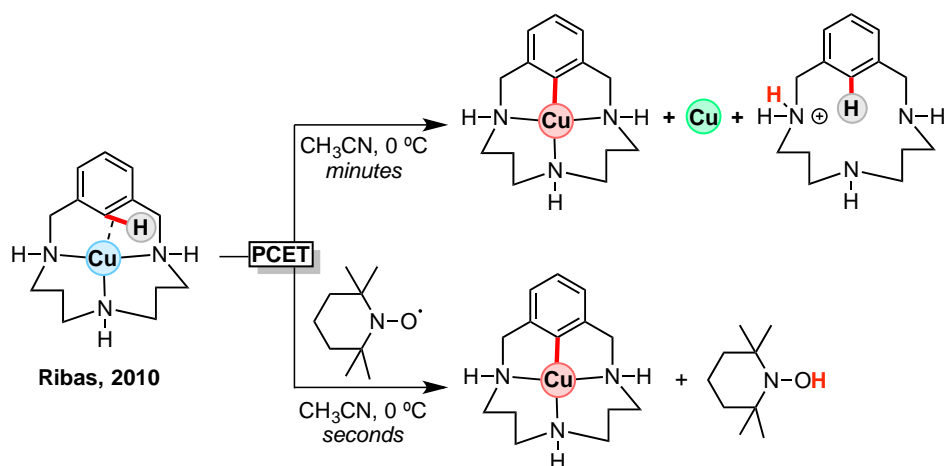
Organometallic C-H activation has demonstrated to be a tremendously powerful tool for the synthesis of a vast array of products and different functionalities. However, as it has been stated in the first sections of this thesis, C-H functionalization can be achieved through outer sphere mechanisms which exclude the formation of organometallic intermediates. Hydrogen Atom Transfer reactions are well established and represent one example of C-H functionalization.²⁷³ In this field, high-valent oxo/imido complexes,^{10,274} including metal centers found in natural enzymes, play a key role in C-H oxidation chemistry.²⁷⁵ Pure electron-transfer processes are also important for the formation of new C-X bonds from C-H bonds using first-row transition metals.²⁷⁶ Electron-transfer (ET) occurs when an electron relocates from an atom, typically a transition metal complex, to another chemical entity. This process constitutes a mechanistic description of a redox reaction typically more favored for first row transition metals, wherein the oxidation state of reactant and product changes.²⁷² Furthermore, this electron transfer can be coupled with a simultaneous loss of a proton forming a radical through a process called Proton-Coupled Electron transfer (PCET).^{277,278} The radical or radical cation generated through this process serve then as a key intermediate in several C-H functionalization reactions (Scheme I.36).^{279,280} Thus, C-H functionalization via a radical pathway has emerged as a promising methodology with high atom- and step-economy.



Scheme I.36. C-H activation via a Single-Electron Transfer and PCET pathway and representative reaction types of radical C-H functionalization.

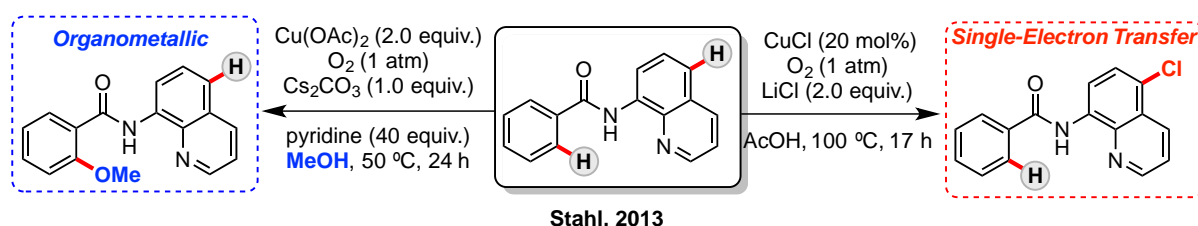
An interesting pathway that might follow a radical species after an electron transfer step is the coupling with a metal center furnishing an organometallic intermediate. An elegant example of this reactivity comes from Ribas, who identified a

mild aromatic C-H activation through a rate-limiting PCET as the key C-H activation step (Scheme I.37).²⁸¹ Furthermore, a three-center, three-electron C-H—Cu(II) interaction was identified (Scheme I.37), and kinetic and computational studies support the PCET, which indeed does not conform to any previously proposed C-H activation mechanisms. In this example, C-H bond cleavage is coupled with copper oxidation and thereby an aryl-Cu(III) species is formed. Furthermore, this reaction proceeds through either a copper disproportionation or, alternatively, even faster in the presence of a stable radical such as TEMPO.



Scheme I.37. Ribas' Cu(II) C-H activation in triazamacrocyclic in the absence (upper reaction) or in presence of TEMPO (lower reaction). Color code: Cu(I), green; Cu(II), blue; Cu(III), red.

Copper(II) is known to catalyze a variety of aerobic C-H functionalization reactions^{282,283} through a SET mechanisms as Yu proposed in 2006.²⁸⁴ However, other mechanisms have been found to operate in these transformations and the possibility of controlling these mechanisms recently became a possibility. In this line, in 2013, Stahl identified divergent mechanisms of C-H functionalization using copper(II) salts as catalysts and N-(8-quinoliny)benzamide substrates depending on the reaction conditions (Scheme I.38).²⁸⁵ Interestingly, when basic Cs₂CO₃ was added, an organometallic mechanism controls the reactivity. On the contrary, when acidic conditions are used, Cu(II) reduction potential is enhanced and a SET is favored. Subsequently, through a SET, the authors achieved the C5-halogenation of the DG.

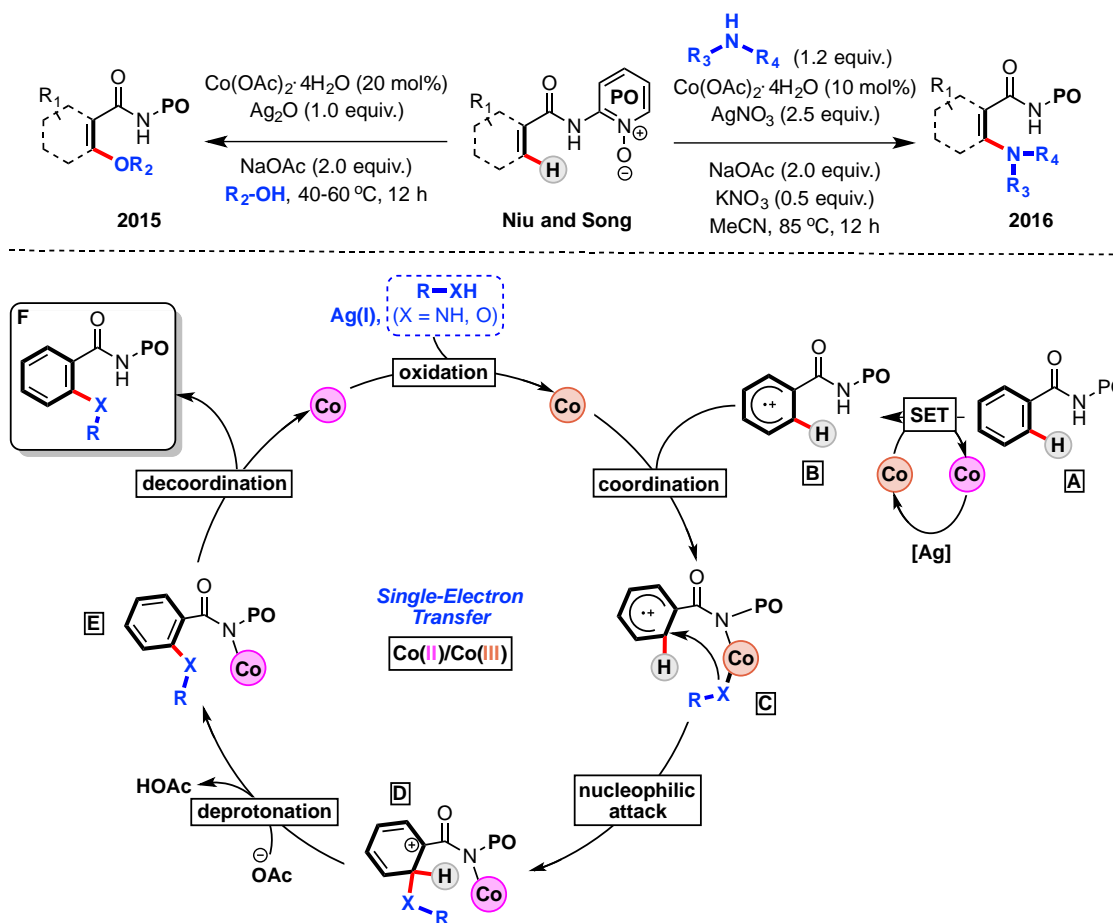


Scheme I.38. Stahl's control of governing pathway in Cu(II) C-H functionalization: Organometallic pathway (left, blue) and SET pathway (right, red).

Since the discovery of this electron-transfer mechanism, several C-H functionalization of 8-aminoquinoline directing groups using copper as catalysts have been reported. Halogenation,^{286,287} sulfonylation,²⁸⁸⁻²⁹⁰ nitration,^{291,292} thio/selenocyanation,²⁹³ amination²⁹⁴ selenylation,²⁹⁵ and esterification.²⁹⁶ However, other first row transition metals such as iron²⁹⁷⁻³⁰⁰ and nickel^{301,302} have also been used as efficient catalysts for remote C-H functionalization of aminoquinolines and related aromatic substrates. The use of cobalt in this field is still in its infancy, albeit some recent and elegant examples have been reported. In the next section of this thesis, these examples will be disclosed together with some mechanistic considerations.

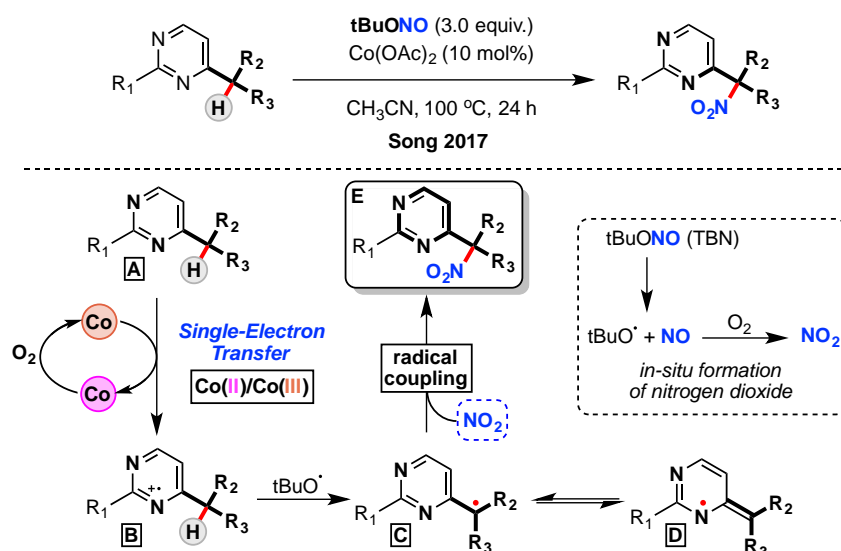
I.4.1 Cobalt-Catalyzed C-H Functionalization through SET and PCET

The powerful abilities of cobalt for C-H functionalization through one-electron processes were initially proven by Kochi's.¹⁰⁶ As disclosed in *Section I.2.1* of this thesis (Scheme I.9), benzene was oxidized in trifluoroacetic acid (TFA) at room temperature through a Single-Electron Transfer (SET) using stoichiometric amounts of Co(OTf)₃. Since this report, one-electron cobalt catalyzed C-H functionalization remained a hurdle to overcome until the groundbreaking study from Niu and Song in 2015.³⁰³ In this protocol, alkoxylation of C(sp²)-H aromatic and olefinic benzamides assisted by a 2-aminopyridine-1-oxide group (APO) was carried out using Co(OAc)₂·4H₂O as the catalyst and Ag₂O as the oxidant. EPR spectroscopy studies as well as experiments with radical quenchers suggested that a SET pathway was likely to be operative. Furthermore, DFT calculations performed by Wei and Niu provided further support for this hypothesis and provided valuable insights into rational prediction of catalyst design and reactivity using cobalt.³⁰⁴ Furthermore, the same authors described a new method for the amination of arylamides with secondary alkylamines through C(sp²)-H bond functionalization assisted by APO.³⁰⁵ Based on previous reports, control experiments with radical traps, low kinetic isotope effects (KIE values around 1.0) and DFT studies, a Single Electron Transfer (SET) is suggested again as a tentative reaction mechanism. As depicted in Scheme I.39, after Co(II) oxidation to Co(III), a SET occurs to **A** to furnish an arene radical cation **B**. Then, Co(III) coordinates **B** to yield **C**, and the nucleophilic attack of the alcohol/amine to the arene ring, together with an electron transfer furnishes a Co(II) Wheland species **D**. Afterwards, deprotonation of the arene ring yields the complex **E**, which after decoordination constructs the alkoxylated/aminated product **F**. In spite of these pioneer protocols, in 2016, Zhang independently reported a similar amination reaction using the 8-aminoquinoline directing group pioneered by Daugulis.³⁰⁶ In this case, mechanistic observations, such as a Kinetic Isotope Effect (KIE) value of 1.3 and radical scavenger inhibition, suggested that the reaction proceeds by a SET mechanism through a unique Co(II)/Co(IV) catalytic amination pathway.



Scheme I.39. Niu and Song's alkoxylation and amination of C-H bonds through a Single Electron Transfer (SET).

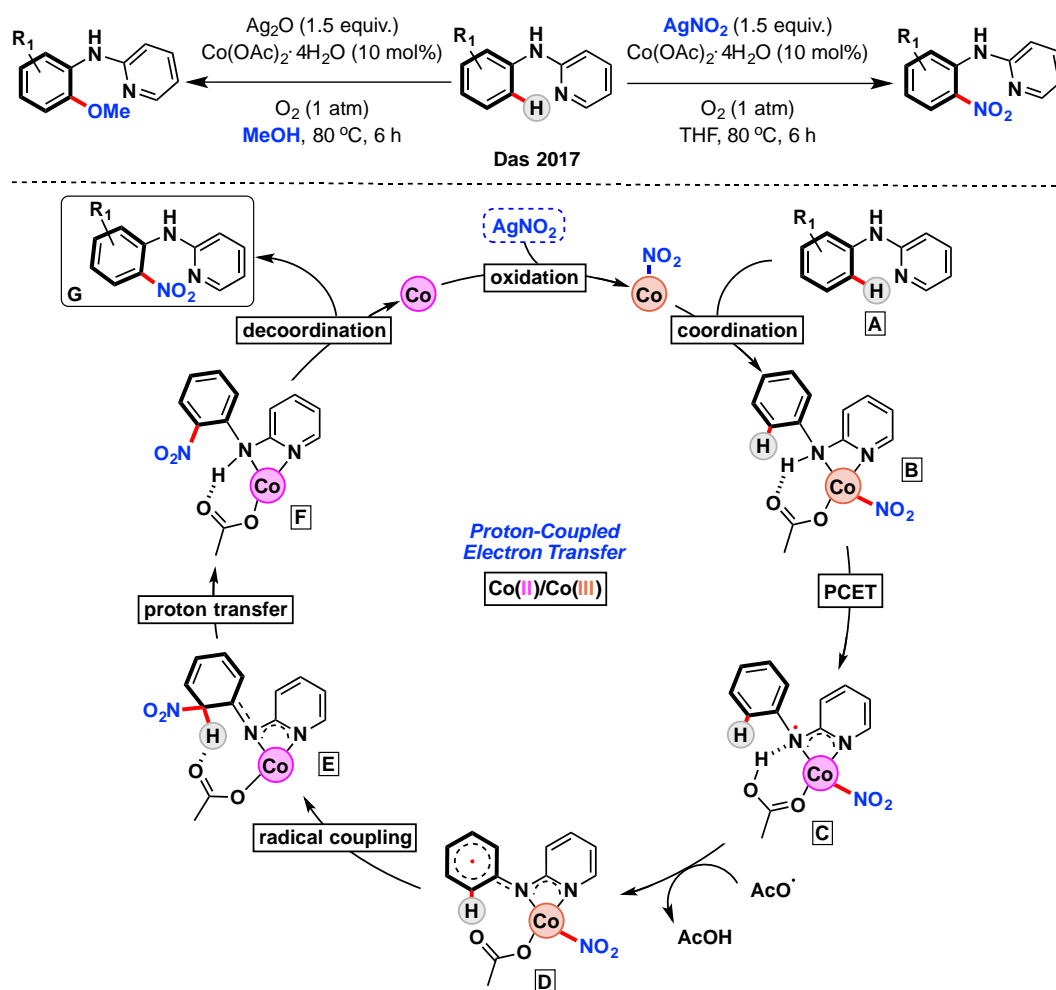
Recently, high-valent cobalt-catalyzed C-X (X = N, O) bond formation through one-electron processes has attracted increasing attention and novel procedures have been reported. In this line, Song disclosed a highly chemo- and regioselective nitration of $\text{C}(\text{sp}^3)\text{-H}$ bonds using $\text{Co}(\text{OAc})_2$ as catalyst and *tert*-butyl nitrite (tBuONO) as nitro source (Scheme I.40).³⁰⁷ Although the protocol was limited to the use of pyrimidine derivatives, it showed a broad spectrum of functional group tolerance. Based on previous reports and radical scavenging experiments using TEMPO, the authors disclosed a plausible reaction mechanism for this cobalt-catalyzed $\text{C}(\text{sp}^3)\text{-H}$ nitration, depicted in Scheme I.40. First, the NO radical coming from thermal decomposition of tBuONO is directly oxidized to NO_2 under aerobic conditions. Then, after the $\text{Co}(\text{II})$ complex is aerobically oxidized, $\text{Co}(\text{III})$ undergoes SET from pyrimidine A to yield a cationic radical intermediate B. Then, hydrogen-atom abstraction of intermediate B with the help of tBuO· radical affords the C-centered radical species C, which may be in equilibrium with N-centered radical species D. Finally, radical intermediate C delivers the nitrated product E via coupling with NO_2 radical.



Scheme I.40. Song' nitration of C(sp³)-H bonds through a Single Electron Transfer (SET).

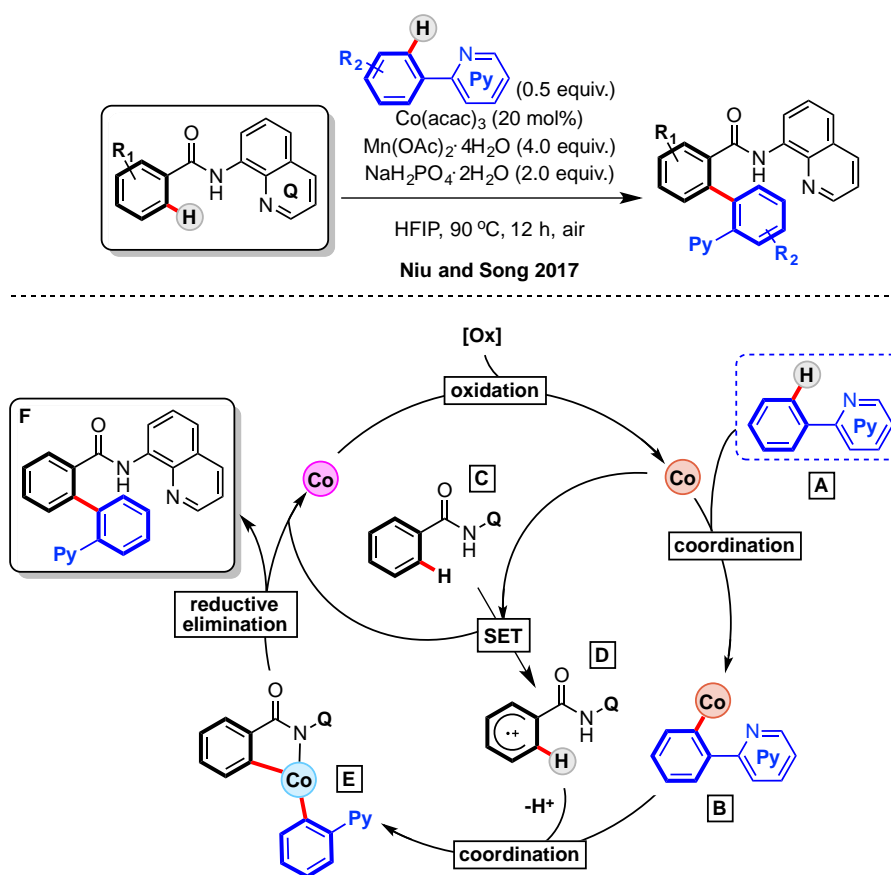
In the same vein, Das and co-workers reported a cobalt-catalyzed regioselective *ortho*-C(sp²)-H bond nitration (Scheme I.41, right) and alkoxylation (Scheme I.41, left) though a Proton-Coupled Electron Transfer mechanism.³⁰⁸ Interestingly, the reaction proceeded under mild reaction conditions in presence of Co(OAc)₂·4H₂O as the catalyst and AgNO₂ as nitro source as well as terminal oxidant, together with atmospheric O₂. In this case, the nitration reaction is assisted by bidentate removable vicinal diamine groups, such as 2-aminopyrimidine, 2-aminopyridine, 2-aminoisoquinoline or 2-aminobenzothiazole and produced pharmaceutically relevant compounds. Control experiments clearly indicate the intermediacy of radical species, and DFT calculations revealed that the reaction proceeds through a Proton-Coupled Electron Transfer promoted by a nitro-transfer pathway (Scheme I.41). Thus, the most relevant step of this mechanism comes after coordination of Co(III)-NO₂ to A to furnish coordination complex B. Then, PCET takes place while the acetate anion acts as a base and Co(III) as electron acceptor to yield C. After radical coupling (D and E), proton transfer (F) and decooordination, nitrated product G is finally released.

Despite the field of one-electron high-valent cobalt-catalyzed C-H functionalization has mainly focused on the construction of new C-N and C-O bonds, some examples of C-C bond formation have been recently reported by Niu and Song. In 2016, the authors described a practical mixed directing-group strategy using Co(acac)₃ as inexpensive and readily available catalyst for the arylation of unactivated arenes (Scheme I.42).³⁰⁹ Interestingly, the authors identified two different pathways governing this transformation. While a single-electron-transmetalation process occurs in the 8-aminoquinolinebenzamide moiety, a CMD process is proposed to proceed in the 2-arylpyridine motif.



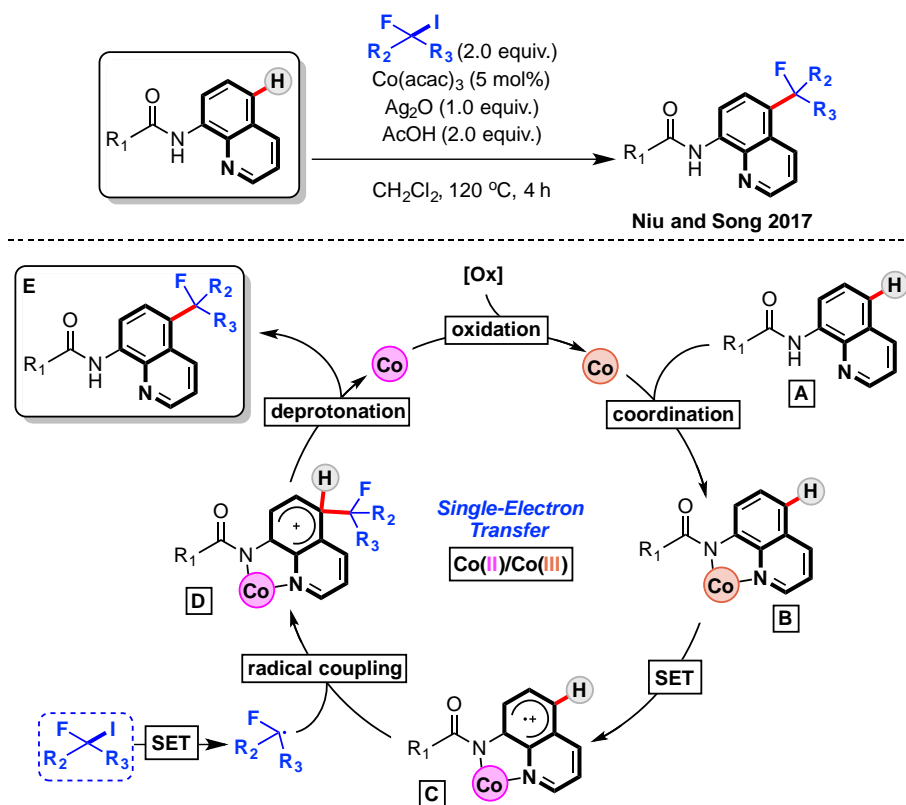
Scheme I.41. Das' nitration and methoxylation of arenes through a Proton-Coupled Electron Transfer (PCET) pathway (aminopyridine as DG is depicted).

Moreover, radical scavenging experiments with 2,6-di-*tert*-butyl-4-methyl-phenol (BHT) have proved the presence of aryl radical as benzylated products were formed. Based on these mechanistic studies, the authors proposed the mechanism depicted in Scheme I.42. The reaction starts with the oxidation of Co(II) precatalyst to Co(III). Then Co(III) interacts with both substrates **A** and **B** through different pathways. First, directed C-H activation of 2-arylpyridine **A** furnishes the organometallic complex **B**. In the second catalytic cycle, an intramolecular process between **C** and Co(II) provides the intermediate **D**, which will combine with **B** to generate the organometallic aryl-Co(IV)-aryl complex **E**. Then, the cross-coupling product **F** is obtained by reductive elimination and Co(III) is regenerated by the oxidant system (O_2 and $Mn(OAc)_2$). Thus, this mechanism represents a combination of the main proposed pathways for high-valent cobalt-catalyzed C-H functionalization: Concerted Metalation-Deprotonation (CMD) and Single-Electron Transfer (SET), for the synthesis of biaryl products through a cross-dehydrogenative coupling.



Scheme I.42. Niu and Song' mixed strategy for the arylation of arenes (top) and its proposed mechanism (bottom). Color code: Co(II), pink; Co(III), orange; Co(IV), blue.

One year later, in 2017, Niu and Song reported another protocol for the construction of C-C bonds through a remote perfluoroalkylation of quinolone amides (Scheme I.43).³¹⁰ This protocol consists in a catalytic system constituted by Co(acac)_3 , Ag_2O as oxidant and acetic acid as additive and represents one of the few examples of C5-alkylation of 8-aminoquinoline.³¹¹ To rationalize the observed reactivity, the authors proposed the mechanism depicted in Scheme I.43. In first place, Co(III) species coordinates to **A** to form a chelated complex **B**. Then, a SET drags an electron from the quinoline motif, furnishing a radical cation Co(II) complex **C**. On the other hand, through a thermal SET process,³¹² the heptafluoroisopropyl radical is generated from heptafluoroisopropyl iodide. Afterwards, complex **C** bearing a radical cation reacts with heptafluoroisopropyl radical to yield the cationic complex **D**, which undergoes deprotonation to furnish **E**. Finally, Co(III) is regenerated in the presence of Ag_2O for the next catalytic cycle.



Scheme I.43. Niu and Song's perfluoroalkylation of quinolone amides at C5 position through a Single Electron Transfer (SET) pathway.

1.5 References

- (1) Gradassi, M. J.; Wayne Green, N. *Fuel Process. Technol.* **1995**, *42*, 65.
- (2) Anslyn, E. V.; Dougherty, D. A. *Modern Physical Organic Chemistry*; University Science Books: Sausalito, CA, 2006.
- (3) Goldman, A. S.; Goldberg, K. I. In *Activation and Functionalization of C—H Bonds*; ACS Symposium Series; American Chemical Society, **2004**, 885, 1.
- (4) McMurray, L.; O'Hara, F.; Gaunt, M. J. *Chem. Soc. Rev.* **2011**, *40*, 1885.
- (5) Chen, D. Y.-K.; Youn, S. W. *Chem. Eur. J.* **2012**, *18*, 9452.
- (6) Sommer, J.; Bukala, J. *Acc. Chem. Res.* **1993**, *26*, 370.
- (7) Dyker, G. *Angew. Chem. Int. Ed.* **1999**, *38*, 1698.
- (8) Morikawa, K.; Benedict, W. S.; Taylor, H. S. *J. Am. Chem. Soc.* **1936**, *58*, 1445.
- (9) Bergman, R. G. *Nature* **2007**, *446*, 391.
- (10) Olivo, G.; Cussó, O.; Costas, M. *Chem. Asian J.* **2016**, *11*, 3148.
- (11) Talsi, E. P.; Bryliakov, K. P. *Coord. Chem. Rev.* **2012**, *256*, 1418.
- (12) Shul'Pin, G. B. In *Transition Metals for Organic Synthesis*; **2008**, 215.
- (13) Brookhart, M.; Green, M. L. H.; Parkin, G. *Proc. Natl. Acad. Sci.* **2007**, *104*, 6908.
- (14) Brookhart, M.; Green, M. L. H. *J. Organomet. Chem.* **1983**, *250*, 395.
- (15) Fenton, H. J. H. *J. Chem. Soc. Trans.* **1894**, *65*, 899.
- (16) Dimroth, O. *Ber. Dtsch. Chem. Ges.* **1899**, *32*, 758.
- (17) Chatt, J.; Watson, H. R. *J. Chem. Soc.* **1962**, 2545.
- (18) Chatt, J.; Davidson, J. M. *J. Chem. Soc.* **1965**, 843.
- (19) Halpern, J. *Acc. Chem. Res.* **1970**, *3*, 386.
- (20) Dedieu, A. *Chem. Rev.* **2000**, *100*, 543.
- (21) Crabtree, R. H. *J. Organomet. Chem.* **2004**, *689*, 4083.
- (22) Crabtree, R. H. *J. Chem. Soc. Dalton Trans.* **2001**, *17*, 2437.
- (23) Janowicz, A. H.; Bergman, R. G. *J. Am. Chem. Soc.* **1982**, *104*, 352.
- (24) Hoyano, J. K.; Graham, W. A. G. *J. Am. Chem. Soc.* **1982**, *104*, 3723.
- (25) Bergman, R. G. *Science* **1984**, *223*, 902.
- (26) Shilov, A. E.; Shul'pin, G. B. *Chem. Rev.* **1997**, *97*, 2879.
- (27) Garnett, J. L.; Hodges, R. J. *J. Am. Chem. Soc.* **1967**, *89*, 4546.
- (28) Shul'pin, A. E. S. and G. B. *Russ. Chem. Rev.* **1987**, *56*, 442.
- (29) Shilov, A. E.; Shteinman, A. A. *Coord. Chem. Rev.* **1977**, *24*, 97.
- (30) Siegbahn, P. E. M.; Crabtree, R. H. *J. Am. Chem. Soc.* **1996**, *118*, 4442.
- (31) Watson, P. L. *J. Am. Chem. Soc.* **1983**, *105*, 6491.
- (32) Waterman, R. *Organometallics* **2013**, *32*, 7249.
- (33) Wheland, G. W. *J. Am. Chem. Soc.* **1942**, *64*, 900.
- (34) Fung, C. W.; Khorramdel-Vahed, M.; Ranson, R. J.; Roberts, R. M. G. *J. Chem. Soc. Perkin Trans. 2* **1980**, *2*, 267.
- (35) Kresge, A.; Brennan, J. *J. Org. Chem.* **1967**, *32*, 752.
- (36) Olah, G. A.; Yu, S. H.; Parker, D. G. *J. Org. Chem.* **1976**, *41*, 1983.
- (37) Winstein, S.; Traylor, T. G. *J. Am. Chem. Soc.* **1955**, *77*, 3747.
- (38) Davidson, J. M.; Triggs, C. *J. Chem. Soc. A* **1968**, 1324.
- (39) Lapointe, D.; Markiewicz, T.; Whipp, C. J.; Toderian, A.; Fagnou, K. *J. Org. Chem.* **2011**, *76*, 749.
- (40) Gorelsky, S. I.; Lapointe, D.; Fagnou, K. *J. Am. Chem. Soc.* **2008**, *130*, 10848.
- (41) Lapointe, D.; Fagnou, K. *Chem. Lett.* **2010**, *39*, 1118.
- (42) Oxgaard, J.; Tenn, W. J.; Nielsen, R. J.; Periana, R. A.; Goddard, W. A. *Organometallics* **2007**, *26*, 1565.

- (43) Boutadla, Y.; Davies, D. L.; Macgregor, S. A.; Poblador-Bahamonde, A. I. *Dalt. Trans.* **2009**, *30*, 5887.
- (44) Chen, X.; Engle, K. M.; Wang, D.-H.; Yu, J.-Q. *Angew. Chem. Int. Ed.* **2009**, *48*, 5094.
- (45) Song, G.; Li, X. *Acc. Chem. Res.* **2015**, *48*, 1007.
- (46) Kuhl, N.; Schröder, N.; Glorius, F. *Adv. Synth. Catal.* **2014**, *356*, 1443.
- (47) Colby, D. A.; Bergman, R. G.; Ellman, J. A. *Chem. Rev.* **2010**, *110*, 624.
- (48) Cheng, C.; Hartwig, J. F. *Chem. Rev.* **2015**, *115*, 8946.
- (49) Larsen, M. A.; Hartwig, J. F. *J. Am. Chem. Soc.* **2014**, *136*, 4287.
- (50) Hartwig, J. F. *J. Am. Chem. Soc.* **2016**, *138*, 2.
- (51) Alberico, D.; Scott, M. E.; Lautens, M. *Chem. Rev.* **2007**, *107*, 174.
- (52) Cho, S. H.; Kim, J. Y.; Kwak, J.; Chang, S. *Chem. Soc. Rev.* **2011**, *40*, 5068.
- (53) Bugaut, X.; Glorius, F. *Angew. Chem. Int. Ed.* **2011**, *50*, 7479.
- (54) Lewis, L. N.; Smith, J. F. *J. Am. Chem. Soc.* **1986**, *108*, 2728.
- (55) Kakiuchi, F.; Kan, S.; Igi, K.; Chatani, N.; Murai, S. *J. Am. Chem. Soc.* **2003**, *125*, 1698.
- (56) Murai, S.; Kakiuchi, F.; Sekine, S.; Tanaka, Y.; Kamatani, A.; Sonoda, M.; Chatani, N. *Nature* **1993**, *366*, 529.
- (57) Ryabov, A. D. *Chem. Rev.* **1990**, *90*, 403.
- (58) Zhang, F.; Spring, D. R. *Chem. Soc. Rev.* **2014**, *43*, 6906.
- (59) Chen, Z.; Wang, B.; Zhang, J.; Yu, W.; Liu, Z.; Zhang, Y. *Org. Chem. Front.* **2015**, *2*, 1107.
- (60) Wang, K.; Hu, F.; Zhang, Y.; Wang, J. *Sci. China Chem.* **2015**, *58*, 1252.
- (61) Rao, Y.; Shan, G.; Yang, X. *Sci. China Chem.* **2014**, *57*, 930.
- (62) Yang, J. *Org. Biomol. Chem.* **2015**, *13*, 1930.
- (63) Tasker, S. Z.; Standley, E. A.; Jamison, T. F. *Nature* **2014**, *509*, 299.
- (64) Zhang, Z.; Tanaka, K.; Yu, J.-Q. *Nature* **2017**, *543*, 538.
- (65) Kuninobu, Y.; Ida, H.; Nishi, M.; Kanai, M. *Nat Chem* **2015**, *7*, 712.
- (66) Chu, L.; Shang, M.; Tanaka, K.; Chen, Q.; Pissarnitski, N.; Streckfuss, E.; Yu, J.-Q. *ACS Cent. Sci.* **2015**, *1*, 394.
- (67) Tang, R.-Y.; Li, G.; Yu, J.-Q. *Nature* **2014**, *507*, 215.
- (68) Leow, D.; Li, G.; Mei, T.-S.; Yu, J.-Q. *Nature* **2012**, *486*, 518.
- (69) Xu, H.; Shang, M.; Dai, H.-X.; Yu, J.-Q. *Org. Lett.* **2015**, *17*, 3830.
- (70) Wang, X.; Leow, D.; Yu, J.-Q. *J. Am. Chem. Soc.* **2011**, *133*, 13864.
- (71) Zaitsev, V. G.; Shabashov, D.; Daugulis, O. *J. Am. Chem. Soc.* **2005**, *127*, 13154.
- (72) Wan, J.-P.; Li, Y.; Liu, Y. *Org. Chem. Front.* **2016**, *3*, 768.
- (73) Daugulis, O.; Roane, J.; Tran, L. D. *Acc. Chem. Res.* **2015**, *48*, 1053.
- (74) Yamaguchi, J.; Muto, K.; Itami, K. *Top. Curr. Chem.* **2016**, *374*, 55.
- (75) Becker, R.; Jones, W. D. In *Catalysis without Precious Metals*; **2010**, 143.
- (76) Nakamura, E.; Hatakeyama, T.; Ito, S.; Ishizuka, K.; Ilies, L.; Nakamura, M. Iron-catalyzed Cross-Coupling Reactions. In *Organic Reactions*. John Wiley & Sons, Inc.: Hoboken, NJ, 2013; 1-210.
- (77) Ilies, L.; Nakamura, E. In *C-H Bond Activation and Catalytic Functionalization II*; Dixneuf, P. H., Doucet, H., Eds.; Springer International Publishing: Cham, 2016; 1-18.
- (78) Shang, R.; Ilies, L.; Nakamura, E. *Chem. Rev.* **2017**, *117*, 9086.
- (79) Liu, W.; Groves, J. T. *Acc. Chem. Res.* **2015**, *48*, 1727.
- (80) Liu, W.; Ackermann, L. *ACS Catal.* **2016**, *6*, 3743.
- (81) King, A. E.; Huffman, L. M.; Casitas, A.; Costas, M.; Ribas, X.; Stahl, S. S. *J. Am. Chem. Soc.* **2010**, *132*, 12068.
- (82) Guo, X.-X.; Gu, D.-W.; Wu, Z.; Zhang, W. *Chem. Rev.* **2015**, *115*, 1622.
- (83) Moselage, M.; Li, J.; Ackermann, L. *ACS Catal.* **2016**, *6*, 498.
- (84) Wei, D.; Zhu, X.; Niu, J. L.; Song, M. P. *ChemCatChem* **2016**, *8*, 1242.
- (85) Chirila, P. G.; Whiteoak, C. J. *Dalt. Trans.* **2017**, *46*, 9721.

- (86) Wang, S.; Chen, S.-Y.; Yu, X.-Q. *Chem. Commun.* **2017**, 53, 3165.
- (87) Pototschnig, G.; Maulide, N.; Schnürch, M. *Chem. Eur. J.* **2017**, 23, 9206.
- (88) Su, B.; Cao, Z.-C.; Shi, Z.-J. *Acc. Chem. Res.* **2015**, 48, 886.
- (89) Grigorjeva, L.; Daugulis, O. *Angew. Chem. Int. Ed.* **2014**, 53, 10209.
- (90) Yoshino, T.; Ikemoto, H.; Matsunaga, S.; Kanai, M. *Angew. Chem. Int. Ed.* **2013**, 52, 2207.
- (91) Tchounwou, P. B.; Yedjou, C. G.; Patlolla, A. K.; Sutton, D. J. in *Molecular, Clinical and Environmental Toxicology: Vol. 3: Environmental Toxicology*. Luch, A., Ed.; Springer Basel: Basel, 2012; 133–164.
- (92) Song, G.; Wang, F.; Li, X. *Chem. Soc. Rev.* **2012**, 41, 3651.
- (93) Cahiez, G.; Moyeux, A. *Chem. Rev.* **2010**, 110, 1435.
- (94) Gao, K.; Yoshikai, N. *Acc. Chem. Res.* **2014**, 47, 1208.
- (95) Kharasch, M. S.; Fields, E. K. *J. Am. Chem. Soc.* **1941**, 63, 2316.
- (96) Kharasch, M. S.; Fuchs, C. F. *J. Am. Chem. Soc.* **1943**, 65, 504.
- (97) Kharasch, M. S.; Lambert, F. L.; Urry, W. H. *J. Org. Chem.* **1945**, 10, 298.
- (98) Murahashi, S. *J. Am. Chem. Soc.* **1955**, 77, 6403.
- (99) Hebrard, F.; Kalck, P. *Chem. Rev.* **2009**, 109, 4272.
- (100) Vilches-Herrera, M.; Domke, L.; Börner, A. *ACS Catal.* **2014**, 4, 1706.
- (101) Blanco-Urgoiti, J.; Anorbe, L.; Perez-Serrano, L.; Dominguez, G.; Perez-Castells, J. *Chem. Soc. Rev.* **2004**, 33, 32.
- (102) Ricker, J. D.; Geary, L. M. *Top. Catal.* **2017**, 60, 609.
- (103) Shibata, T. *Adv. Synth. Catal.* **2006**, 348, 2328.
- (104) Blanco-Urgoiti, J.; Añorbe, L.; Pérez-Serrano, L.; Domínguez, G.; Pérez-Castells, J. *Chem. Soc. Rev.* **2004**, 33, 32.
- (105) Tang, R.; Kochi, J. K. *J. Inorg. Nucl. Chem.* **1973**, 35, 3845.
- (106) Kochi, J. K.; Tang, R. T.; Bernath, T. *J. Am. Chem. Soc.* **1973**, 95, 7114.
- (107) Halbritter, G.; Knoch, F.; Wolski, A.; Kisch, H. *Angew. Chem. Int. Ed. Engl.* **1994**, 33, 1603.
- (108) Lenges, C. P.; Brookhart, M. *J. Am. Chem. Soc.* **1997**, 119, 3165.
- (109) Lenges, C. P.; White, P. S.; Brookhart, M. *J. Am. Chem. Soc.* **1998**, 120, 6965.
- (110) Bolig, A. D.; Brookhart, M. *J. Am. Chem. Soc.* **2007**, 129, 14544.
- (111) Lenges, C. P.; Brookhart, M.; Grant, B. E. *J. Organomet. Chem.* **1997**, 528, 199.
- (112) Kanamori, K.; Broderick, W. E.; Jordan, R. F.; Willett, R. D.; Legg, J. I. *J. Am. Chem. Soc.* **1986**, 108, 7122.
- (113) Avilés, T.; Dinis, A.; Calhorda, M. J.; Pinto, P.; Félix, V.; Drew, M. G. B. *J. Organomet. Chem.* **2001**, 625, 186.
- (114) Wei, D.; Zhu, X.; Niu, J.-L.; Song, M.-P. *ChemCatChem* **2016**, 8, 1242.
- (115) Yoshino, T.; Matsunaga, S. *Adv. Synth. Catal.* **2017**, 359, 1245.
- (116) Yoshino, T.; Ikemoto, H.; Matsunaga, S.; Kanai, M. *Angew. Chem. Int. Ed.* **2013**, 52, 2207.
- (117) Ueura, K.; Satoh, T.; Miura, M. *Org. Lett.* **2007**, 9, 1407.
- (118) Broderick, W. E.; Kanamori, K.; Willett, R. D.; Legg, J. I. *Inorg. Chem.* **1991**, 30, 3875.
- (119) Zhou, X.; Day, A. I.; Willis, A. C.; Jackson, W. G. *Chem. Commun.* **2003**, 18, 2386.
- (120) Jackson, W. G.; McKeon, J. A.; Hockless, D. C. R.; Willis, A. C. *Inorg. Chem.* **2006**, 45, 4119.
- (121) Wang, S.; Hou, J.-T.; Feng, M.-L.; Zhang, X.-Z.; Chen, S.-Y.; Yu, X.-Q.; Shen, Y.; Shi, J.; Tian, H.; Zhu, W. *Chem. Commun.* **2016**, 52, 2709.
- (122) Nakanowatari, S.; Mei, R.; Feldt, M.; Ackermann, L. *ACS Catal.* **2017**, 7, 2511.
- (123) Zhao, D.; Kim, J. H.; Stegemann, L.; Strassert, C. A.; Glorius, F. *Angew. Chem. Int. Ed.* **2015**, 54, 4508.
- (124) Kim, J. H.; Greßies, S.; Glorius, F. *Angew. Chem. Int. Ed.* **2016**, 55, 5577.
- (125) Lao, Y.-X.; Zhang, S.-S.; Liu, X.-G.; Jiang, C.-Y.; Wu, J.-Q.; Li, Q.; Huang, Z.-S.; Wang, H. *Adv. Synth. Catal.* **2016**, 358, 2186.

- (126) Yang, Y.; Li, B.; Liu, W.; Zhang, R.; Yu, L.; Ma, Q.-G.; Lv, R.; Du, D.; Li, T. *J. Org. Chem.* **2016**, *81*, 11335.
- (127) Prakash, S.; Muralirajan, K.; Cheng, C.-H. *Angew. Chem. Int. Ed.* **2016**, *55*, 1844.
- (128) Yoshino, T.; Ikemoto, H.; Matsunaga, S.; Kanai, M. *Chem. Eur. J.* **2013**, *19*, 9142.
- (129) Ikemoto, H.; Yoshino, T.; Sakata, K.; Matsunaga, S.; Kanai, M. *J. Am. Chem. Soc.* **2014**, *136*, 5424.
- (130) Tanaka, R.; Ikemoto, H.; Kanai, M.; Yoshino, T.; Matsunaga, S. *Org. Lett.* **2016**, *18*, 5732.
- (131) Liu, X.-G.; Zhang, S.-S.; Wu, J.-Q.; Li, Q.; Wang, H. *Tetrahedron Lett.* **2015**, *56*, 4093.
- (132) Sauermann, N.; González, M. J.; Ackermann, L. *Org. Lett.* **2015**, *17*, 5316.
- (133) Zhang, Z.-Z.; Liu, B.; Wang, C.-Y.; Shi, B.-F. *Org. Lett.* **2015**, *17*, 4094.
- (134) Suzuki, Y.; Sun, B.; Sakata, K.; Yoshino, T.; Matsunaga, S.; Kanai, M. *Angew. Chem. Int. Ed.* **2015**, *54*, 9944.
- (135) Zell, D.; Müller, V.; Dhawa, U.; Bursch, M.; Presa, R. R.; Grimme, S.; Ackermann, L. *Chem. Eur. J.* **2017**, *23*, 12145.
- (136) Moselage, M.; Sauermann, N.; Koeller, J.; Liu, W.; Gelman, D.; Ackermann, L. *Synlett* **2015**, *26*, 1596.
- (137) Zhou, X.; Fan, Z.; Zhang, Z.; Lu, P.; Wang, Y. *Org. Lett.* **2016**, *18*, 4706.
- (138) Kong, L.; Zhou, X.; Li, X. *Org. Lett.* **2016**, *18*, 6320.
- (139) Zell, D.; Bursch, M.; Müller, V.; Grimme, S.; Ackermann, L. *Angew. Chem. Int. Ed.* **2017**, *56*, 10378.
- (140) Li, J.; Zhang, Z.; Ma, W.; Tang, M.; Wang, D.; Zou, L. H. *Adv. Synth. Catal.* **2017**, *359*, 1717.
- (141) Muniraj, N.; Prabhu, K. R. *ACS Omega* **2017**, *2*, 4470.
- (142) Yu, W.; Zhang, W.; Liu, Y.; Liu, Z.; Zhang, Y. *Org. Chem. Front.* **2017**, *4*, 77.
- (143) Hummel, J. R.; Ellman, J. A. *Org. Lett.* **2015**, *17*, 2400.
- (144) Li, J.; Ackermann, L. *Angew. Chem. Int. Ed.* **2015**, *54*, 8551.
- (145) Gensch, T.; Vásquez-Céspedes, S.; Yu, D.-G.; Glorius, F. *Org. Lett.* **2015**, *17*, 3714.
- (146) Suzuki, Y.; Sun, B.; Yoshino, T.; Kanai, M.; Matsunaga, S. *Tetrahedron* **2015**, *71*, 4552.
- (147) Lerchen, A.; Knecht, T.; Daniliuc, C. G.; Glorius, F. *Angew. Chem. Int. Ed.* **2016**, *55*, 15166.
- (148) Kong, L.; Yu, S.; Zhou, X.; Li, X. *Org. Lett.* **2016**, *18*, 588.
- (149) Chavan, L. N.; Gollapelli, K. K.; Chegondi, R.; Pawar, A. B. *Org. Lett.* **2017**, *19*, 2186.
- (150) Sivakumar, G.; Vijeta, A.; Jeganmohan, M. *Chem. Eur. J.* **2016**, *22*, 5899.
- (151) Yu, W.; Zhang, W.; Liu, Y.; Zhou, Y.; Liu, Z.; Zhang, Y. *RSC Adv.* **2016**, *6*, 24768.
- (152) Zhang, Z.-Z.; Liu, B.; Xu, J.-W.; Yan, S.-Y.; Shi, B.-F. *Org. Lett.* **2016**, *18*, 1776.
- (153) Lu, Q.; Vásquez-Céspedes, S.; Gensch, T.; Glorius, F. *ACS Catal.* **2016**, *6*, 2352.
- (154) Li, J.; Tang, M.; Zang, L.; Zhang, X.; Zhang, Z.; Ackermann, L. *Org. Lett.* **2016**, *18*, 2742.
- (155) Wang, H.; Koeller, J.; Liu, W.; Ackermann, L. *Chem. Eur. J.* **2015**, *21*, 15525.
- (156) Sun, B.; Yoshino, T.; Kanai, M.; Matsunaga, S. *Angew. Chem. Int. Ed.* **2015**, *54*, 12968.
- (157) Wang, F.; Wang, Q.; Bao, M.; Li, X. *Chinese J. Catal.* **2016**, *37*, 1423.
- (158) Pawar, A. B.; Agarwal, D.; Lade, D. M. *J. Org. Chem.* **2016**, *81*, 11409.
- (159) Wang, H.; Lorion, M. M.; Ackermann, L. *ACS Catal.* **2017**, *7*, 3430.
- (160) Yu, W.; Zhang, W.; Liu, Z.; Zhang, Y. *Chem. Commun.* **2016**, *52*, 6837.
- (161) Mandal, R.; Sundararaju, B. *Org. Lett.* **2017**, *19*, 2544.
- (162) Zell, D.; Bu, Q.; Feldt, M.; Ackermann, L. *Angew. Chem. Int. Ed.* **2016**, *55*, 7408.
- (163) Boerth, J. A.; Ellman, J. A. *Angew. Chem. Int. Ed.* **2017**, *56*, 9976.
- (164) Boerth, J. A.; Hummel, J. R.; Ellman, J. A. *Angew. Chem. Int. Ed.* **2016**, *55*, 12650.
- (165) Sen, M.; Dahiya, P.; Premkumar, J. R.; Sundararaju, B. *Org. Lett.* **2017**, *19*, 3699.
- (166) Muniraj, N.; Prabhu, K. R. *J. Org. Chem.* **2017**, *82*, 6913.
- (167) Hummel, J. R.; Ellman, J. A. *J. Am. Chem. Soc.* **2015**, *137*, 490.
- (168) Barsu, N.; Sen, M.; Premkumar, J. R.; Sundararaju, B. *Chem. Commun.* **2016**, *52*, 1338.
- (169) Kalsi, D.; Laskar, R. A.; Barsu, N.; Premkumar, J. R.; Sundararaju, B. *Org. Lett.* **2016**, *18*, 4198.
- (170) Sun, B.; Yoshino, T.; Matsunaga, S.; Kanai, M. *Adv. Synth. Catal.* **2014**, *356*, 1491.

- (171) Sun, B.; Yoshino, T.; Matsunaga, S.; Kanai, M. *Chem. Commun.* **2015**, *51*, 4659.
- (172) Patel, P.; Chang, S. *ACS Catal.* **2015**, *5*, 853.
- (173) Borah, G.; Borah, P.; Patel, P. *Org. Biomol. Chem.* **2017**, *15*, 3854.
- (174) Liang, Y.; Liang, Y.-F.; Tang, C.; Yuan, Y.; Jiao, N. *Chem. Eur. J.* **2015**, *21*, 16395.
- (175) Mei, R.; Loup, J.; Ackermann, L. *ACS Catal.* **2016**, *6*, 793.
- (176) Wang, H.; Li, L.; Yu, S.; Li, Y.; Li, X. *Org. Lett.* **2016**, *18*, 2914.
- (177) Wang, F.; Wang, H.; Wang, Q.; Yu, S.; Li, X. *Org. Lett.* **2016**, *18*, 1306.
- (178) Huang, J.; Huang, Y.; Wang, T.; Huang, Q.; Wang, Z.; Chen, Z. *Org. Lett.* **2017**, *19*, 1128.
- (179) Wang, F.; Jin, L.; Kong, L.; Li, X. *Org. Lett.* **2017**, *19*, 1812.
- (180) Shi, P.; Wang, L.; Chen, K.; Wang, J.; Zhu, J. *Org. Lett.* **2017**, *19*, 2418.
- (181) Gensch, T.; Klauck, F. J. R.; Glorius, F. *Angew. Chem. Int. Ed.* **2016**, *55*, 11287.
- (182) Liu, X. G.; Li, Q.; Wang, H. *Adv. Synth. Catal.* **2017**, *359*, 1942.
- (183) Yoshida, M.; Kawai, K.; Tanaka, R.; Yoshino, T.; Matsunaga, S. *Chem. Commun.* **2017**, *53*, 5974.
- (184) Yu, D.-G.; Gensch, T.; de Azambuja, F.; Vásquez-Céspedes, S.; Glorius, F. *J. Am. Chem. Soc.* **2014**, *136*, 17722.
- (185) Pawar, A. B.; Lade, D. M. *Org. Biomol. Chem.* **2016**, *14*, 3275.
- (186) Pawar, A. B.; Chang, S. *Org. Lett.* **2015**, *17*, 660.
- (187) Li, J.; Ackermann, L. *Angew. Chem. Int. Ed.* **2015**, *54*, 3635.
- (188) Liu, X.-G.; Zhang, S.-S.; Jiang, C.-Y.; Wu, J.-Q.; Li, Q.; Wang, H. *Org. Lett.* **2015**, *17*, 5404.
- (189) Kuppusamy, R.; Muralirajan, K.; Cheng, C.-H. *ACS Catal.* **2016**, *6*, 3909.
- (190) Sen, M.; Emayavaramban, B.; Barsu, N.; Premkumar, J. R.; Sundararaju, B. *ACS Catal.* **2016**, *6*, 2792.
- (191) Barsu, N.; Rahman, M. A.; Sen, M.; Sundararaju, B. *Chem. Eur. J.* **2016**, *22*, 9135.
- (192) Yan, S.-Y.; Ling, P.-X.; Shi, B.-F. *Adv. Synth. Catal.* **2017**, *359*, 2912.
- (193) Zhang, Z.-Z.; Han, Y.-Q.; Zhan, B.-B.; Wang, S.; Shi, B.-F. *Angew. Chem. Int. Ed.* **2017**, *56*, 13145.
- (194) Lerchen, A.; Knecht, T.; Koy, M.; Daniliuc, C. G.; Glorius, F. *Chem. Eur. J.* **2017**, *23*, 12149.
- (195) Bera, S. S.; Debbarma, S.; Ghosh, A. K.; Chand, S.; Maji, M. S. *J. Org. Chem.* **2017**, *82*, 420.
- (196) Sanjosé-Orduna, J.; Gallego, D.; Garcia-Roca, A.; Martin, E.; Benet-Buchholz, J.; Pérez-Temprano, M. H. *Angew. Chem. Int. Ed.* **2017**, *56*, 12137.
- (197) Wang, S.; Chen, S.-Y.; Yu, X.-Q. *Chem. Commun.* **2017**, *53*, 3165.
- (198) Grigorjeva, L.; Daugulis, O. *Org. Lett.* **2014**, *16*, 4684.
- (199) Grigorjeva, L.; Daugulis, O. *Org. Lett.* **2014**, *16*, 4688.
- (200) Wencel-Delord, J.; Colobert, F. *Org. Chem. Front.* **2016**, *3*, 394.
- (201) Zhang, J.; Chen, H.; Lin, C.; Liu, Z.; Wang, C.; Zhang, Y. *J. Am. Chem. Soc.* **2015**, *137*, 12990.
- (202) Landge, V. G.; Jaiswal, G.; Balaraman, E. *Org. Lett.* **2016**, *18*, 812.
- (203) Planas, O.; Whiteoak, C. J.; Company, A.; Ribas, X. *Adv. Synth. Catal.* **2015**, *357*, 4003.
- (204) Kathiravan, S.; Nicholls, I. A. *Org. Lett.* **2017**, *19*, 4758.
- (205) Hao, X.-Q.; Du, C.; Zhu, X.; Li, P.-X.; Zhang, J.-H.; Niu, J.-L.; Song, M.-P. *Org. Lett.* **2016**, *18*, 3610.
- (206) Landge, V. G.; Midya, S. P.; Rana, J.; Shinde, D. R.; Balaraman, E. *Org. Lett.* **2016**, *18*, 5252.
- (207) Kuai, C.; Wang, L.; Li, B.; Yang, Z.; Cui, X. *Org. Lett.* **2017**, *19*, 2102.
- (208) Martínez, A. M.; Rodríguez, N.; Gomez-Arrayas, R.; Carretero, J. C. *Chem. Eur. J.* **2017**, *23*, 11669.
- (209) Zhou, S.; Wang, M.; Wang, L.; Chen, K.; Wang, J.; Song, C.; Zhu, J. *Org. Lett.* **2016**, *18*, 5632.
- (210) Ma, W.; Ackermann, L. *ACS Catal.* **2015**, *5*, 2822.
- (211) Gandeepan, P.; Rajamalli, P.; Cheng, C.-H. *Angew. Chem. Int. Ed.* **2016**, *55*, 4308.
- (212) Maity, S.; Kancherla, R.; Dhawa, U.; Hoque, E.; Pimparkar, S.; Maiti, D. *ACS Catal.* **2016**, *6*, 5493.
- (213) Maity, S.; Dolui, P.; Kancherla, R.; Maiti, D. *Chem. Sci.* **2017**, *8*, 5181.
- (214) Ye, J.; Ma, S. *Acc. Chem. Res.* **2014**, *47*, 989.
- (215) Alcaide, B.; Almendros, P.; Aragoncillo, C. *Chem. Soc. Rev.* **2014**, *43*, 3106.
- (216) Neff, R. K.; Frantz, D. E. *Tetrahedron* **2015**, *71*, 7.

- (217) Thrimurtulu, N.; Dey, A.; Maiti, D.; Volla, C. M. R. *Angew. Chem. Int. Ed.* **2016**, *55*, 12361.
- (218) Muralirajan, K.; Prakash, S.; Cheng, C. H. *Adv. Synth. Catal.* **2017**, *359*, 513.
- (219) Li, T.; Zhang, C.; Tan, Y.; Pan, W.; Rao, Y. *Org. Chem. Front.* **2017**, *4*, 204.
- (220) Lan, T.; Wang, L.; Rao, Y. *Org. Lett.* **2017**, *19*, 972.
- (221) Thrimurtulu, N.; Nallagonda, R.; Volla, C. M. R. *Chem. Commun.* **2017**, *53*, 1872.
- (222) Fukuyama, T.; Maetani, S.; Ryu, I. In *Comprehensive Organic Synthesis: Second Edition*; Knochel, P.; Molander, G.; ed. Elsevier, Amsterdam, Netherlands, 2014; 1073–1100.
- (223) Beller, M.; Wu, X. F. *Transition metal catalyzed carbonylation reactions*. Springer-Verlag Berlin Heidelberg, Germany, 2013.
- (224) Wu, L.; Fang, X.; Liu, Q.; Jackstell, R.; Beller, M.; Wu, X.-F. *ACS Catal.* **2014**, *4*, 2977.
- (225) Ni, J.; Li, J.; Fan, Z.; Zhang, A. *Org. Lett.* **2016**, *18*, 5960.
- (226) Stollé, R.; Reichert, W. *J. für Prakt. Chem.* **1929**, *123*, 82.
- (227) Nguyen, T. T.; Grigorjeva, L.; Daugulis, O. *Chem. Commun.* **2017**, *53*, 5136.
- (228) Barsu, N.; Bolli, S. K.; Sundararaju, B. *Chem. Sci.* **2017**, *8*, 2431.
- (229) Zeng, L.; Tang, S.; Wang, D.; Deng, Y.; Chen, J. L.; Lee, J. F.; Lei, A. *Org. Lett.* **2017**, *19*, 2170.
- (230) Williamson, P.; Galvan, A.; Gaunt, M. J. *Chem. Sci.* **2017**, *8*, 2588.
- (231) Ling, F.; Ai, C.; Lv, Y.; Zhong, W. *Adv. Synth. Catal.* **2017**, *in press*, DOI: 10.1002/adsc.201700780.
- (232) Boyarskiy, V. P.; Bokach, N. A.; Luzyanin, K. V.; Kukushkin, V. Y. *Chem. Rev.* **2015**, *115*, 2698.
- (233) Gu, Z. Y.; Liu, C. G.; Wang, S. Y.; Ji, S. J. *J. Org. Chem.* **2017**, *82*, 2223.
- (234) Zou, F.; Chen, X.; Hao, W. *Tetrahedron* **2017**, *73*, 758.
- (235) A. de Meijere, F. D. *Metal-Catalyzed Cross-Coupling Reactions*; Wiley-VCH, Weinheim, Germany, 2008.
- (236) Ball, L. T.; Lloyd-Jones, G. C.; Russell, C. A. *Science.* **2012**, *337*, 1644.
- (237) Li, B.-J.; Shi, Z.-J. *Chem. Soc. Rev.* **2012**, *41*, 5588.
- (238) Xie, Y.; Xu, D.; Sun, W. W.; Zhang, S. J.; Dong, X. P.; Liu, B.; Zhou, Y.; Wu, B. *Asian J. Org. Chem.* **2016**, *5*, 961.
- (239) Suzuki, A. *J. Organomet. Chem.* **2002**, *653*, 83.
- (240) Hall, D. G. In *Boronic Acids: Preparation and Applications in Organic Synthesis and Medicine*; Wiley-VCH, Weinheim, Germany, 2006; 1–99.
- (241) Hu, L.; Gui, Q.; Chen, X.; Tan, Z.; Zhu, G. *Org. Biomol. Chem.* **2016**, *14*, 11070.
- (242) Zhu, X.; Su, J.-H.; Du, C.; Wang, Z.-L.; Ren, C.-J.; Niu, J.-L.; Song, M.-P. *Org. Lett.* **2017**, *19*, 596.
- (243) Wang, H.; Zhang, S.; Wang, Z.; He, M.; Xu, K. *Org. Lett.* **2016**, *18*, 5628.
- (244) Shang, R.; Ilies, L.; Nakamura, E. *J. Am. Chem. Soc.* **2016**, *138*, 10132.
- (245) Ohmiya, H.; Yorimitsu, H.; Oshima, K. *Org. Lett.* **2006**, *8*, 3093.
- (246) Li, Q.; Li, Y.; Hu, W.; Hu, R.; Li, G.; Lu, H. *Chem. Eur. J.* **2016**, *22*, 12286.
- (247) Li, Q.; Hu, W.; Hu, R.; Lu, H.; Li, G. *Org. Lett.* **2017**, *19*, 4676.
- (248) Sun, J.; Deng, L. *ACS Catal.* **2016**, *6*, 290.
- (249) Ohmiya, H.; Yorimitsu, H.; Oshima, K. *Angew. Chem. Int. Ed.* **2005**, *44*, 2368.
- (250) Zuo, Z.; Huang, Z. *Org. Chem. Front.* **2016**, *3*, 434.
- (251) Obligacion, J. V.; Neely, J. M.; Yazdani, A. N.; Pappas, I.; Chirik, P. J. *J. Am. Chem. Soc.* **2015**, *137*, 5855.
- (252) Zhang, L.; Zuo, Z.; Leng, X.; Huang, Z. *Angew. Chem. Int. Ed.* **2014**, *53*, 2696.
- (253) Obligacion, J. V.; Semproni, S. P.; Chirik, P. J. *J. Am. Chem. Soc.* **2014**, *136*, 4133.
- (254) Palmer, W. N.; Obligacion, J. V.; Pappas, I.; Chirik, P. J. *J. Am. Chem. Soc.* **2016**, *138*, 766.
- (255) Gandeepan, P.; Cheng, C.-H. *Acc. Chem. Res.* **2015**, *48*, 1194.
- (256) Cenini, S.; Gallo, E.; Penoni, A.; Ragaini, F.; Tollari, S. *Chem. Commun.* **2000**, *22*, 2265.
- (257) Ragaini, F.; Penoni, A.; Gallo, E.; Tollari, S.; Li Gotti, C.; Lapadula, M.; Mangioni, E.; Cenini, S. *Chem. Eur. J.* **2003**, *9*, 249.

- (258) Lyaskovskyy, V.; Suarez, A. I. O.; Lu, H.; Jiang, H.; Zhang, X. P.; de Bruin, B. J. *Am. Chem. Soc.* **2011**, *133*, 12264.
- (259) Lu, H.; Hu, Y.; Jiang, H.; Wojtas, L.; Zhang, X. P. *Org. Lett.* **2012**, *14*, 5158.
- (260) Villanueva, O.; Weldy, N. M.; Blakey, S. B.; MacBeth, C. E. *Chem. Sci.* **2015**, *6*, 6672.
- (261) Wu, X.; Yang, K.; Zhao, Y.; Sun, H.; Li, G.; Ge, H. *Nat. Commun.* **2015**, *6*, 6462.
- (262) Du, C.; Li, P.-X.; Zhu, X.; Han, J.-N.; Niu, J.-L.; Song, M.-P. *ACS Catal.* **2017**, *7*, 2810.
- (263) Wu, X.; Miao, J.; Li, Y.; Li, G.; Ge, H. *Chem. Sci.* **2016**, *7*, 5260.
- (264) Enthaler, S.; Company, A. *Chem. Soc. Rev.* **2011**, *40*, 4912.
- (265) Li, J. J.; Johnson, D. S. *Modern Drug Synthesis*; Wiley: Hoboken, NJ, 2010.
- (266) Li, J. J.; Johnson, D. S.; Sliskovic, D. R.; Roth, B. D. *Contemporary Drug Synthesis*; Wiley: Hoboken, NJ, 2004.
- (267) Müller, F. *Agrochemicals*; Wiley-VCH: Weinheim, Germany, 1999.
- (268) Lan, J.; Xie, H.; Lu, X.; Deng, Y.; Jiang, H.; Zeng, W. *Org. Lett.* **2017**, *19*, 4279.
- (269) Ananikov, V. P. *Understanding Organometallic Reaction Mechanisms and Catalysis: Computational and Experimental Tools*; Wiley-VCH, Weinheim, Germany, 2014.
- (270) Atwood, J. D.; Rosenberg, E. In *Encyclopedia of Inorganic and Bioinorganic Chemistry*; John Wiley & Sons, Inc.; Hoboken, NJ, 2011.
- (271) Crabtree, R. H. *The Organometallic Chemistry of the Transition Metals*; John Wiley & Sons, Inc.; Hoboken, NJ, 2005; Vol. 18.
- (272) Hartwig, J. F. *Organotransition Metal Chemistry. From Bonding to Catalysis*. University Science Books; Sausalito, CA, 2010; Vol. 49.
- (273) Wang, L.; Xiao, J. *Top. Curr. Chem.* **2016**, *374*, 17.
- (274) Nam, W. *Acc. Chem. Res.* **2007**, *40*, 522.
- (275) Costas, M.; Mehn, M. P.; Jensen, M. P.; Que, L. *Chem. Rev.* **2004**, *104*, 939.
- (276) Cannon, R. D.; *Electron Transfer Reactions*; Butterworth-Heinemann: Oxford, 1997.
- (277) Weinberg, D. R.; Gagliardi, C. J.; Hull, J. F.; Murphy, C. F.; Kent, C. A.; Westlake, B. C.; Paul, A.; Ess, D. H.; McCafferty, D. G.; Meyer, T. J. *Chem. Rev.* **2012**, *112*, 4016.
- (278) Costentin, C.; Robert, M.; Savéant, J.-M. *Acc. Chem. Res.* **2010**, *43*, 1019.
- (279) Yi, H.; Zhang, G.; Wang, H.; Huang, Z.; Wang, J.; Singh, A. K.; Lei, A. *Chem. Rev.* **2017**, *117*, 9016.
- (280) Kaga, A.; Chiba, S. *ACS Catal.* **2017**, *7*, 4697.
- (281) Ribas, X.; Calle, C.; Poater, A.; Casitas, A.; Gómez, L.; Xifra, R.; Parella, T.; Benet-Buchholz, J.; Schweiger, A.; Mitrikas, G.; Solà, M.; Llobet, A.; Stack, T. D. P. *J. Am. Chem. Soc.* **2010**, *132*, 12299.
- (282) Shi, Z.; Zhang, C.; Tang, C.; Jiao, N. *Chem. Soc. Rev.* **2012**, *41*, 3381.
- (283) Gamez, P.; Aubel, P. G.; Driessen, W. L.; Reedijk, J. *Chem. Soc. Rev.* **2001**, *30*, 376.
- (284) Chen, X.; Hao, X.-S.; Goodhue, C. E.; Yu, J.-Q. *J. Am. Chem. Soc.* **2006**, *128*, 6790.
- (285) Suess, A. M.; Ertem, M. Z.; Cramer, C. J.; Stahl, S. S. *J. Am. Chem. Soc.* **2013**, *135*, 9797.
- (286) Rao, N. S.; Reddy, G. M.; Sridhar, B.; Sarma, M. H. *European J. Org. Chem.* **2017**, *2017*, 438.
- (287) Zhang, S.; Ullah, A.; Yamamoto, Y.; Almansour, A. I.; Arumugam, N.; Kumar, R. S.; Bao, M. *ChemistrySelect* **2017**, *2*, 3414.
- (288) Wei, J.; Jiang, J.; Xiao, X.; Lin, D.; Deng, Y.; Ke, Z.; Jiang, H.; Zeng, W. *J. Org. Chem.* **2016**, *81*, 946.
- (289) Qiao, H.; Sun, S.; Yang, F.; Zhu, Y.; Zhu, W.; Dong, Y.; Wu, Y.; Kong, X.; Jiang, L.; Wu, Y. *Org. Lett.* **2015**, *17*, 6086.
- (290) Chen, G.; Zhang, X.; Zeng, Z.; Peng, W.; Liang, Q.; Liu, J. *ChemistrySelect* **2017**, *2*, 1979.
- (291) Zhu, X.; Qiao, L.; Ye, P.; Ying, B.; Xu, J.; Shen, C.; Zhang, P. *RSC Adv.* **2016**, *6*, 89979.
- (292) Khan, B.; Khan, A. A.; Bora, D.; Verma, D.; Koley, D. *ChemistrySelect* **2017**, *2*, 260.
- (293) Chen, J.; Wang, T.; Wang, T.; Lin, A.; Yao, H.; Xu, J. *Org. Chem. Front.* **2017**, *4*, 130.
- (294) Yin, Y.; Xie, J.; Huang, F.-Q.; Qi, L.-W.; Zhang, B. *Adv. Synth. Catal.* **2017**, *359*, 1037.
- (295) Sahoo, H.; Mandal, A.; Selvakumar, J.; Baidya, M. *European J. Org. Chem.* **2016**, *2016*, 4321.

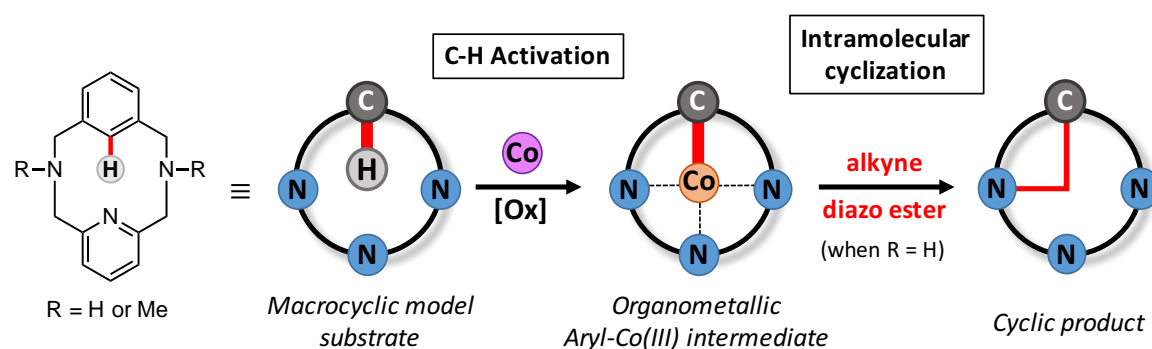
- (296) Xia, C.; Wang, K.; Xu, J.; Shen, C.; Sun, D.; Li, H.; Wang, G.; Zhang, P. *Org. Biomol. Chem.* **2017**, *15*, 531.
- (297) Cong, X.; Zeng, X. *Org. Lett.* **2014**, *16*, 3716.
- (298) Guan, Y.; Wang, K.; Shen, J.; Xu, J.; Shen, C.; Zhang, P. *Catal. Lett.* **2017**, *147*, 1574.
- (299) Cui, M.; Liu, J.-H.; Lu, X.-Y.; Lu, X.; Zhang, Z.-Q.; Xiao, B.; Fu, Y. *Tetrahedron Lett.* **2017**, *58*, 1912.
- (300) He, Y.; Zhao, N.; Qiu, L.; Zhang, X.; Fan, X. *Org. Lett.* **2016**, *18*, 6054.
- (301) Wan, L.; Qiao, K.; Yuan, X.; Zheng, M.-W.; Fan, B.-B.; Di, Z. C.; Zhang, D.; Fang, Z.; Guo, K. *Adv. Synth. Catal.* **2017**, *359*, 2596.
- (302) Ding, J.; Zhang, Y.; Li, J. *Org. Chem. Front.* **2017**, *4*, 1528.
- (303) Zhang, L.-B.; Hao, X.-Q.; Zhang, S.-K.; Liu, Z.-J.; Zheng, X.-X.; Gong, J.-F.; Niu, J.-L.; Song, M.-P. *Angew. Chem. Int. Ed.* **2015**, *54*, 272.
- (304) Guo, X.-K.; Zhang, L.-B.; Wei, D.; Niu, J.-L. *Chem. Sci.* **2015**, *6*, 7059.
- (305) Zhang, L.-B.; Zhang, S.-K.; Wei, D.; Zhu, X.; Hao, X.-Q.; Su, J.-H.; Niu, J.-L.; Song, M.-P. *Org. Lett.* **2016**, *18*, 1318.
- (306) Yan, Q.; Xiao, T.; Liu, Z.; Zhang, Y. *Adv. Synth. Catal.* **2016**, *358*, 2707.
- (307) Zhou, Y.; Tang, Z.; Song, Q. *Chem. Commun.* **2017**, *53*, 8972.
- (308) Nageswar Rao, D.; Rasheed, S.; Raina, G.; Ahmed, Q. N.; Jaladanki, C. K.; Bharatam, P. V.; Das, P. *J. Org. Chem.* **2017**, *82*, 7234.
- (309) Du, C.; Li, P. X.; Zhu, X.; Suo, J. F.; Niu, J. L.; Song, M. P. *Angew. Chem. Int. Ed.* **2016**, *55*, 13571.
- (310) Suo, J. F.; Zhao, X. M.; Zhang, K. X.; Zhou, S. L.; Niu, J. L.; Song, M. P. *Synth.* **2017**, *49*, 3916.
- (311) Iwai, T.; Sawamura, M. *ACS Catal.* **2015**, *5*, 5031.
- (312) Aihara, Y.; Tobisu, M.; Fukumoto, Y.; Chatani, N. *J. Am. Chem. Soc.* **2014**, *136*, 15509.

Chapter II

General Objectives

The development of new synthetic methodologies using earth abundant and cost-efficient 3d transition-metals has recently attracted increasing attention. Particularly, cobalt has become an actual alternative to precious metals in catalysis, displaying similar and improved reactivity patterns and unique transformations, specifically in C-H activation and functionalization. Since the discovery of cobalt-catalyzed C-H functionalization reactions in 1955, the field has been dominated by low-valent approaches using either low-valent catalysts or binary systems consisting in cobalt(II) salts and Grignard reagents. In spite of the prevalence of the low-valent approach in the cobalt C-H activation realm, new methodologies consisting in high-valent catalysts allowed for novel strategies in the field. Between 2013 and 2014, Kanai and Daugulis pioneered the field and since then a tremendous amount of synthetic protocols has been published, including novel and unique C-C, C-N, C-O and C-Halogen bond forming transformations. Despite the recent flourishing of the high-valent approach, there is still room for new reactivity and more mechanistic understanding is needed. Indeed, just a few examples of organometallic aryl-Co(III) species have been furnished through C-H activation and their role as intermediates in some transformation is not clear.

Thus, taking into account the lack of organometallic intermediates synthesized and the few existing evidences for the C-H activation step, in *Chapter III* we will focus on the synthesis and characterization of bench-stable stable model macrocyclic aryl-Co(III) compounds obtained through C(sp²)-H activation (Scheme II.2).

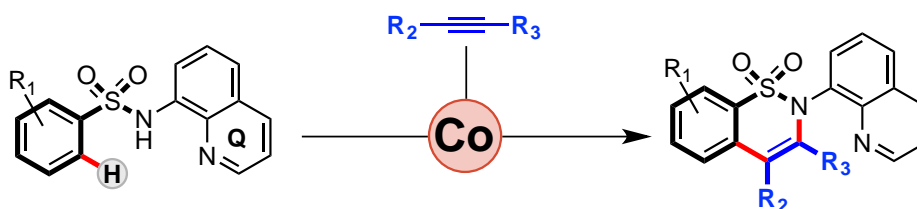


Scheme II.1. Use of model macrocyclic substrates for the formation of organometallic aryl-Co(III) complexes through C-H activation. Reactivity of aryl-Co(III) with alkynes (blue) and ethyl diazoacetate (red).

To do so, we will use a 12-membered macrocyclic model substrate, which has proved to be an excellent platform for the synthesis and characterization of high-valent Pd and Ni organometallic species. Subsequent insights obtained from the application of these organometallic aryl-Co(III) intermediates in alkyne annulation reactions will also be studied (Scheme II.2, blue). We will also evaluate the relevance of these aryl-Co(III) species in the context of 8-aminoquinoline directed oxidative Co(II)-catalyzed C-H

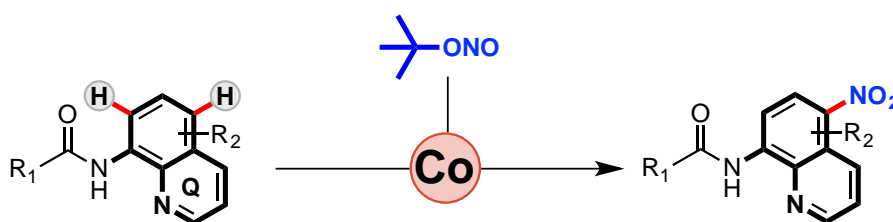
activation processes. Furthermore, in *Chapter IV* we will test the reactivity of aryl-Co(III) complexes with ethyl diazoacetate (EDA) to provide novel insight in cobalt-catalyzed C-H functionalization reactions with carbene precursors (Scheme II.1, red). The characterization of novel intermediate species will be sought in order to improve the understanding of the reactivity of putative cobalt-carbenes to construct C-C bonds.

The knowledge acquired using the macrocyclic model platform will be applied in different protocols for the construction of new C-C and C-N bonds. In *Chapter V*, we will attempt the synthesis of cyclic sulfonamides (sultams). Specifically, aryl sulfonamides, which bear an 8-aminoquinoline (Q) directing group, and alkynes will be reacted with Co(II) salts in presence of oxidants to attempt the synthesis of sultam derivatives.



Scheme II.2. Cobalt-catalyzed organometallic C-H activation and functionalization with alkynes for the synthesis of cyclic sulfonamide (sultam) motifs.

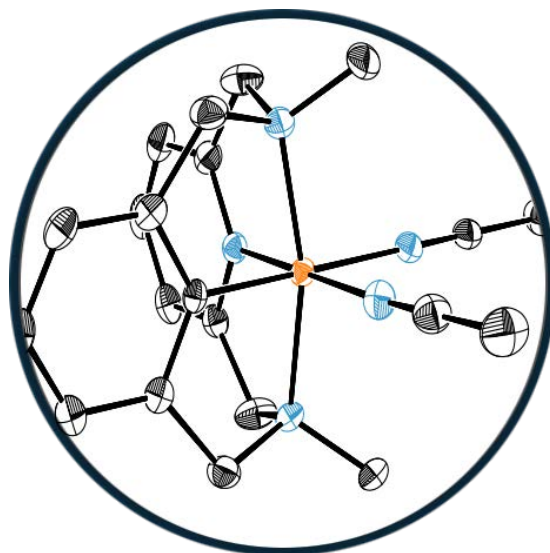
Finally, in *Chapter VI* we will attempt the remote C-H functionalization of the 8-aminoquinoline (Q) directing group using tert-butyl nitrite as nitro source and commercially available cobalt salts as catalysts.



Scheme II.3. Remote nitration of 8-aminoquinoline scaffolds through cobalt-catalyzed C-H functionalization.

Chapter III

Isolation of Key Organometallic Aryl-Co(III) Intermediates in Cobalt-Catalyzed C(sp²)-H Functionalization and New Insights into Alkyne Annulation Reaction Mechanisms



This chapter corresponds to the following publication:

Oriol Planas, Christopher J. Whiteoak, Vlad Martin-Diaconescu, Ilaria Gamba, Josep M. Luis, Teodor Parella, Anna Company and Xavi Ribas.

J. Am. Chem. Soc. **2016**, *138*, 14388-14397.

For this publication O.P. synthesized and characterized all the ligands and the organometallic complexes. Moreover, O.P. performed the reactivity studies which include stoichiometric and catalytic reactions with alkynes and the characterization of the resulting products. T.P. supervised the NMR experiments. V. M.-D. and I. G. collected and analyzed the XAS data. J.M.L. supervised the DFT studies. C.J.W., A.C. and X.R. designed the project. Besides, O.P. contributed in writing the manuscript and was involved in argumentations and discussions.

Reproduced with permission from:

Oriol Planas, Christopher J. Whiteoak, Vlad Martin-Diaconescu, Ilaria Gamba, Josep M. Luis, Teodor Parella, Anna Company, and Xavi Ribas. "Isolation of Key Organometallic Aryl-Co(III) Intermediates in Cobalt-Catalyzed C(sp²)-H Functionalizations and New Insights into Alkyne Annulation Reaction Mechanisms". *Journal of the American Chemical Society*. Vol. 138, Issue 43 (2016) : 14388-14397.

<http://dx.doi.org/10.1021/jacs.6b08593>

Copyright © 2016 American Chemical Society

Isolation of Key Organometallic Aryl-Co(III) Intermediates in Cobalt-Catalyzed C(sp²)-H Functionalizations and New Insights into Alkyne Annulation Reaction Mechanisms

Oriol Planas,[†] Christopher J. Whiteoak,^{†,‡} Vlad Martin-Diaconescu,[†] Ilaria Gamba,[†] Josep M. Luis,[†] Teodor Parella,[§] Anna Company,[†] and Xavi Ribas^{*,†}

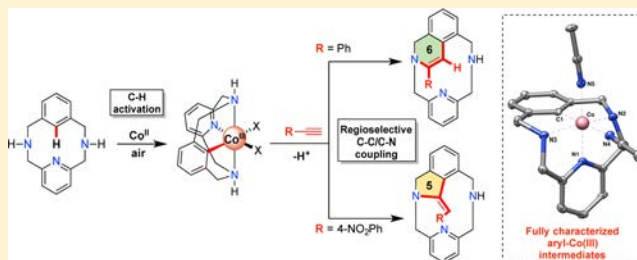
[†]Institut de Química Computacional i Catàlisi (IQCC) and Departament de Química, Universitat de Girona, Campus Montilivi, Girona, E-17071 Catalonia, Spain

[‡]Biomolecular Sciences Research Centre, Faculty of Health and Wellbeing, Sheffield Hallam University, City Campus, Sheffield S1 1WB, England

[§]Servei de RMN, Facultat de Ciències, Universitat Autònoma de Barcelona, Campus UAB, Bellaterra, E-08193 Catalonia, Spain

Supporting Information

ABSTRACT: The selective annulation reaction of alkynes with substrates containing inert C–H bonds using cobalt as catalyst is currently a topic attracting significant interest. Unfortunately, the mechanism of this transformation is still relatively poorly understood, with little experimental evidence for intermediates, although an organometallic Co(III) species is generally implicated. Herein, we describe a rare example of the preparation and characterization of benchtop-stable organometallic aryl-Co(III) compounds (NMR, HRMS, XAS, and XRD) prepared through a C(sp²)-H activation, using a model macrocyclic arene substrate. Furthermore, we provide crystallographic evidence of an organometallic aryl-Co(III) intermediate proposed in 8-aminoquinoline-directed Co-catalyzed C–H activation processes. Subsequent insights obtained from the application of our new organometallic aryl-Co(III) compounds in alkyne annulation reactions are also disclosed. Evidence obtained from the resulting regioselectivity of the annulation reactions and DFT studies indicates that a mechanism involving an organometallic aryl-Co(III)-alkynyl intermediate species is preferred for terminal alkynes, in contrast to the generally accepted migratory insertion pathway.



INTRODUCTION

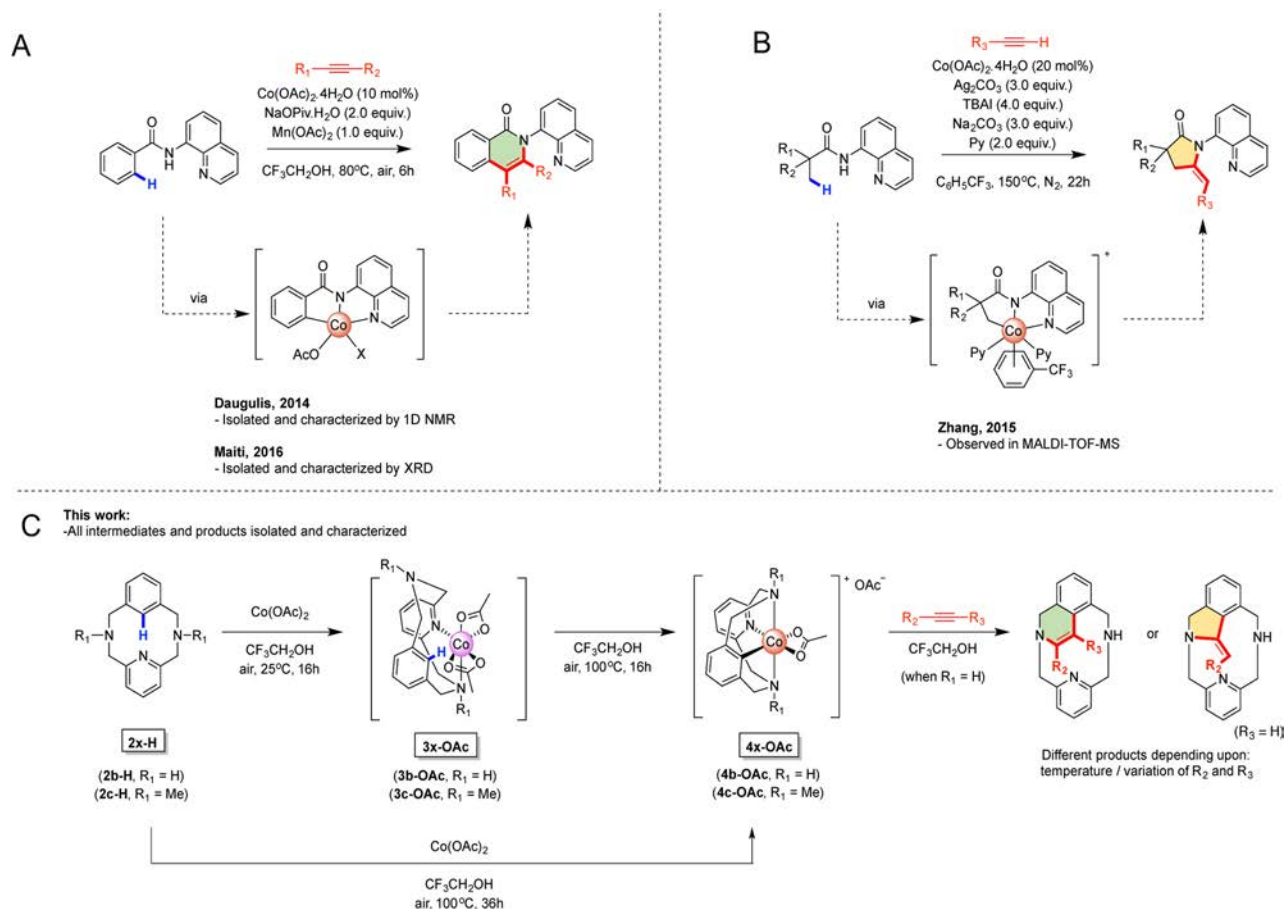
Selective functionalization of inert C–H bonds is currently attracting significant interest as the desire to develop new simplified protocols for the synthesis of complex pharmaceuticals, agrochemicals and natural products gathers pace.¹ Historically, most C–H activation and coupling protocols have been based on expensive, precious second- and third-row transition metals, most notably Pd.² More recently, the development of catalytic C–H functionalization protocols based on naturally more abundant and cheaper first-row transition metals, including Fe,³ Cu,⁴ Co,⁵ and Ni,⁶ has seen an explosion of activity. Unfortunately, mechanistic understanding concerning how these new first-row transition metal based protocols operate is significantly less advanced than their second- and third-row analogues. This is likely a consequence of the elusiveness and instability of key reaction intermediates, although there is an increasing interest in their detection and isolation.⁷ One reaction which is receiving particular interest at the current time is the annulation reaction of alkynes to substrates with inert C–H bonds, providing a facile route toward a variety of biologically and pharmaceutically relevant heterocyclic compounds. To date, Rh-catalysis has provided

significant success in this field,⁸ although the replacement of expensive Rh with a cheaper first-row transition metal has remained a challenge until recently. In this context, in 2013, Yoshikai reported the first synthesis of polysubstituted dihydropyridine derivatives, through a mild and facile cobalt-catalyzed alkyne annulation reaction.⁹ Since this report, an increasing number of Co-catalyzed annulation protocols have been reported using a range of coupling partners,¹⁰ including several examples highlighting the potential of alkynes.¹¹ Unfortunately, the mechanisms of these reactions are still relatively poorly understood, although organometallic Co(III) intermediates are generally implicated.⁵ Stable organometallic aryl-Co(III) compounds have been prepared via transmetalation reactions in the past,^{11g,12} although examples of the preparation of stable organometallic Co(III) compounds through direct C–H activation are still extremely rare, which has limited the understanding of this field. Organometallic aryl-Co(III) compounds derived from N-confused porphyrins and *m*-benzophthalocyanines have been metalated using Co(II) salts

Received: August 17, 2016

Published: October 10, 2016

Scheme 1. Characterized Organometallic Co(III) Intermediates in Co-Catalyzed Alkyne Annulation Protocols: (A) C(sp²)-H Activation and the Organometallic Aryl-Co(III) Intermediate Isolated by Daugulis and Co-workers and Maiti and Co-workers; (B) C(sp³)-H Activation and Organometallic Alkyl-Co(III) Intermediate Reported by Zhang and Co-workers; (C) Overview of This Work, with Co(II) and Co(III) Intermediates and Annulation Products Characterized by 1D and 2D NMR, HRMS, XRD, and XAS



furnishing the Co(III) C-H activated products,¹³ although further reactivity studies were somewhat limited as a result of their stability.¹⁴

In the field of Co-catalyzed alkyne annulation protocols through C-H activation, the most solid experimental evidence so far of reaction intermediates has been provided by succinct NMR, MALDI-TOF, and most recently X-ray diffraction (XRD). In 2014, Daugulis and co-workers reported the preparation and characterization (1D NMR) of an organometallic aryl-Co(III) compound, obtained through C(sp²)-H activation, which was implicated as the key intermediate in a Co-catalyzed annulation protocol (Scheme 1A).^{11b} In 2015, Zhang and co-workers observed, by MALDI-TOF analysis of a crude reaction mixture during a Co(II)-catalyzed annulation reaction, evidence of an organometallic C(sp³)-Co(III) intermediate, resulting from direct activation of C(sp³)-H bonds (Scheme 1B).^{11a} Very recently, in a related study, Maiti and co-workers have successfully provided XRD evidence of a species invoked as an intermediate in Co-catalyzed alkene coupling reactions.¹⁵

Taking into account the increasing interest in Co-catalyzed transformations and the absence of benchtop-stable organometallic aryl-Co(III) compounds prepared through direct C-H activation, we became interested in the possibility of isolating organometallic aryl-Co(III) compounds, in order to understand

their synthesis, features and reactivity. Our approach was based on expertise within our laboratory using model macrocyclic arene substrates to successfully stabilize organometallic aryl-metal intermediate species, including Ni(II)¹⁶ and Cu(III).^{16,17} These isolable compounds have now been implicated as the intermediate species in a wide variety of cross-coupling transformations.

Herein, we will describe the synthesis and characterization of benchtop-stable organometallic aryl-Co(III) compounds obtained through C(sp²)-H activation, in a clear stepwise manner, using a 12-membered macrocyclic model substrate, which have been fully crystallographically and spectroscopically characterized. A similar macrocyclic substrate has previously been utilized to investigate the reactivity of organometallic Ni(III) intermediates.¹⁸ Subsequent insights obtained from the application of these isolable organometallic aryl-Co(III) intermediates in alkyne annulation reactions, in which they are proposed as key reaction intermediate (Scheme 1C) will also be disclosed, including evidence for an unprecedented “acetylide pathway” for terminal alkynes in annulation reactions. Putting this work into context, we also report crystallographic evidence of the sought-after organometallic aryl-Co(III) intermediate proposed in 8-aminoquinoline directed Co-catalyzed C-H activation processes.

RESULTS

Synthesis and Characterization of Organometallic Aryl-Co(III) Compounds. Macrocyclic model arene substrates **2b-H** and **2c-H** were synthesized through cyclization of the tosyl-protected amine **1** with 2,6-bis(bromoethyl)pyridine, followed by a deprotection of tosylated macrocyclic compound **2a-H**, furnishing **2b-H**, which could be further methylated at the secondary amines to obtain **2c-H** (see [Scheme S1](#)). Thereafter, Co(II) coordination compounds were prepared by reaction of Co(OAc)₂ with **2b-H** and **2c-H** ([Scheme 1C](#)), at 25 °C, using 2,2,2-trifluoroethanol (TFE) as solvent ([(**2b-H**)Co(II)(OAc)₂] (**3b-OAc**) and [(**2c-H**)Co(II)(OAc)₂] (**3c-OAc**)). The structure of **3b-OAc** was initially confirmed by HRMS ([M - OAc]⁺; calcd *m/z* = 357.0882; found 357.0874) and XRD analysis (see [Figure S15](#)). The solid-state molecular structure of **3b-OAc** indicated that the compound has two acetates coordinated in a bidentate fashion and that the potentially tridentate macrocycle acts as bidentate ligand (coordinated through only the pyridine and one amine). Upon performing the same reaction with CoBr₂ and **2c-H**, complex **3c-Br** was obtained, which in contrast, had both amines of the macrocyclic ligand coordinated (XRD, see [Figure S16](#)). Careful analysis of these crystal structures shows that the aryl C-H bond is out of plane (torsion angles of 14° for **3b-OAc** and 21° for **3c-Br**), indicating an incipient interaction between the Co(II) and hydrogen of the arene.

Upon reacting Co(OAc)₂ with **2b-H** and **2c-H** in TFE at 100 °C (or heating of the preformed **3b-OAc** and **3c-OAc**), complete conversion to the target organometallic aryl-Co(III) complexes, [(**2b**)Co(III)(η²-OAc)](OAc) (**4b-OAc**) and [(**2c**)Co(III)(η²-OAc)](OAc) (**4c-OAc**), was achieved ([Scheme 1C](#)). Due to the stability of the isolated organometallic aryl-Co(III) compounds, it was possible to characterize them by NMR and HRMS ([Figure 1](#) and [Figures S36–S45](#)),

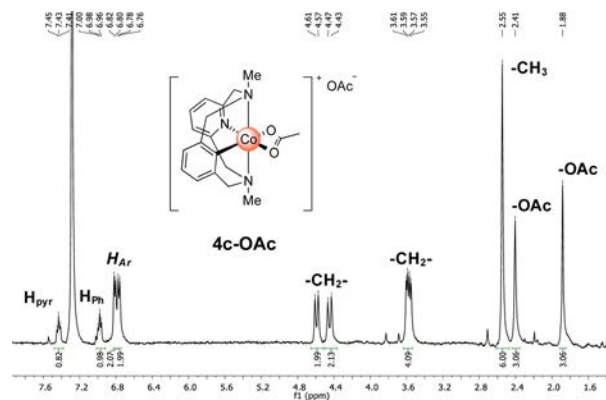


Figure 1. ¹H NMR spectrum with assignments for **4c-OAc** in CDCl₃ at 298 K.

providing spectra consistent with a low spin diamagnetic Co(III) metal center. Two nonequivalent acetate signals were observed, indicating that only one acetate is likely to be coordinated to the Co complex with the second acetate displaced as an outer-sphere counterion. The proposed structure was further supported by HRMS studies of **4b-OAc** and **4c-OAc**, which afforded clean spectra with major signals corresponding to the [(**2**)Co(III)(OAc)]⁺ ions (**4b-OAc**, [M - OAc]⁺; calcd *m/z* = 356.0804; found 356.0802; **4c-OAc**, [M - OAc]⁺; calcd *m/z* = 384.1117; found 384.1122). An analogous

organometallic Rh(III) complex (**5c-Cl**) was also prepared following a similar protocol (see [Scheme S15](#) and [Figure S17](#)).

In our initial studies, XRD characterization of **4b-OAc** and **4c-OAc** remained elusive and as a result we turned to X-ray absorption spectroscopy (XAS) at the Co K-edge, in order to probe the electronic structure (XANES) and coordination environment (EXAFS) ([Figure 2A–C](#) and [Figures S19–S22](#)). [Figure 2A](#) shows the rising edge spectra for the starting material and the organometallic aryl-Co(III) **4b-OAc** and **4c-OAc** analogues. **3c-OAc** shows a weak pre-edge feature due to 1s →

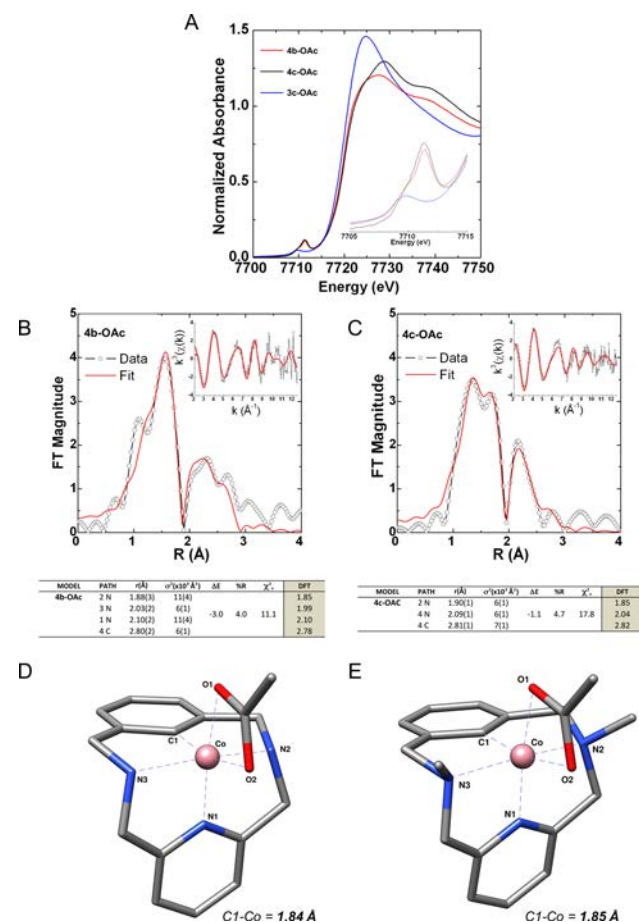
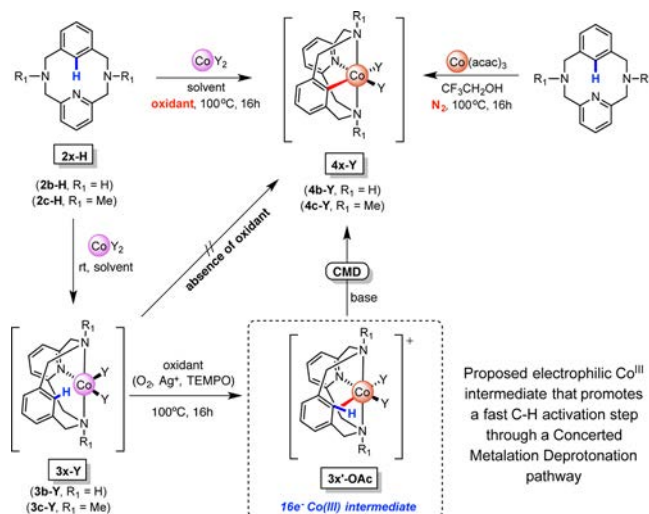


Figure 2. Characterization of aryl-Co(III) compounds through EXAFS spectroscopy. (A) XAS spectra at the Co K-edge highlighting the XANES region of the spectrum, and the 1s → 3d pre-edge transitions (inset). (B) EXAFS analysis of **4b-OAc**. Shown are Fourier-transformed EXAFS spectra (no phase correction, k-window = 2–12.5 Å⁻¹) as well as the k³-weighted unfiltered EXAFS spectra (inset) and comparison of selected EXAFS derived and theoretical bond distances (bottom table). (C) EXAFS analysis of **4c-OAc**. Shown are Fourier-transformed EXAFS spectra (no phase correction, k-window = 2–12.5 Å⁻¹) as well as the k³-weighted unfiltered EXAFS spectra (inset) and comparison of selected EXAFS derived and theoretical bond distances (bottom table). (D) Geometry optimized structure for **4b-OAc**. Selected bond distances [Å] and angles [°]: Co–C(1) 1.85, Co–N(1) 1.85, Co–N(2) 2.00, Co–N(3) 2.00, Co–O(1) 1.96, Co–O(2) 2.11; C(1)–Co–N(1) 89.8, C(1)–Co–N(2) 84.5, C(1)–Co–N(3) 84.4, C(1)–Co–O(1) 99.6, C(1)–Co–O(2) 164.9. (E) Geometry optimized structure for **4c-OAc**. Selected bond distances [Å] and angles [°]: Co–C(1) 1.85, Co–N(1) 1.85, Co–N(2) 2.05, Co–N(3) 2.05, Co–O(1) 1.96, Co–O(2) 2.11; C(1)–Co–N(1) 86.5, C(1)–Co–N(2) 84.6, C(1)–Co–N(3) 84.6, C(1)–Co–O(1) 101.0, C(1)–Co–O(2) 166.3.

3d transitions at ~ 7709.8 eV consistent with a Co(II) center having a centrosymmetric local environment.¹⁹ EXAFS analysis of **3c-OAc** shows a six coordinate complex with three pairs of Co–N/O scattering shells at 2.04, 2.22, and 2.35 Å, suggesting a distorted octahedral coordination environment at the metal center (Figure S20 and Table S15). XAS data for **3c-Br**, on the other hand, are consistent with the proposed 5-coordinate crystal structure (Figure S19 and Table S14). Upon C–H activation, a 0.5 eV shift in the rising edge at half height is observed for both **3c-OAc** and the **3b-OAc** analogue, concomitant with a ~ 1.6 eV shift to higher energy of the pre-edge, indicating oxidation of the metal center to Co(III).¹⁹ Additionally, the increase in intensity of the pre-edge feature observed, not only accounts for the increase in oxidation state and the extra electron hole, but also suggests a coordination geometry more favorable to p–d mixing. EXAFS analysis of **4b-OAc** and **4c-OAc** (Figure 2B,C) intermediates indicates the presence of two short N/O/C scattering atoms at ~ 1.89 Å and four longer N/O/C scattering paths with an average effective path length spanning ~ 2.04 – 2.09 Å. This is consistent with the proposed theoretical models that predict two short N/O/C pyridine nitrogen and C–H activated carbon (C_{phenyl}) and four longer scattering paths (~ 2.0 Å) coming from the tertiary amines and an acetate, resulting in a trigonal bipyramidal geometry at the metal center. The proposed structures for the **4b-OAc** and **4c-OAc** complexes are in agreement with the NMR and HRMS data (vide supra) and help to explain the intense pre-edge features from XAS, whereby a trigonal bipyramidal local metal geometry facilitates p–mixing into the d-manifold resulting in a more intense pre-edge.

Thereafter, formation of the organometallic aryl-Co(III) compounds was further studied (see Scheme 2 and Schemes S17–S19). It was found that the addition of 2.0 equiv of KOAc to a mixture of **2c-H** and CoBr_2 in MeCN resulted in complete conversion to **4c-OAc**, whereas in the absence of base a mixture of Co(II) complex **3c-Br** and Co(III) organometallic **4c-Br** was obtained, suggesting that both solvent and base have an important role in the C–H activation step. In particular,

Scheme 2. Formation of Aryl-Co(III) Intermediates: Optimization and Evaluation of Conditions Using Different Solvents (TFE, CH_3CN) and Oxidants (Air, Silver Salts, TEMPO) To Furnish Organometallic Aryl-Co(III) Intermediates through a C–H Activation Approach



fluorinated alcohols appear to be crucial (Table S2), as has previously been identified for a number of other metal-catalyzed transformations.²⁰ Preparation of the organometallic aryl-Co(III) compounds was also attempted under an inert atmosphere (N_2), but the reaction did not proceed when starting from Co(II) salts and **2c-H**. However, if the reaction was performed under an inert atmosphere in the presence of oxidants, such as silver salts or TEMPO, organometallic aryl-Co(III) intermediates could be detected using HRMS (Scheme S19 and Figures S5–S10). When $\text{Co}(\text{acac})_3$ was used as Co source, under an inert atmosphere, the corresponding organometallic aryl-Co(III) species (**4c-acac**) was formed as the major product (Figure S4). These observations indicate that Co(II) is likely first oxidized before the C–H activation step, forming a highly electrophilic penta-coordinated Co(III) $16e^-$ complex (Scheme 2, **3x'-OAc**). Interaction of Co(III) with the corresponding C–H bond promotes its deprotonation by the base (acetate, bromide or perchlorate in this study). These experimental observations lead us to propose that C–H bond cobaltation is likely to proceed via a concerted metalation–deprotonation (CMD) pathway.

As mentioned, it was not possible to obtain suitable crystals of **4x-OAc** for XRD studies. As reaction using silver salts as oxidant was also satisfactory, another strategy to grow crystals was followed; **3x-Br** was mixed with AgClO_4 (3.0 equiv) in an $\text{CH}_3\text{CN}/\text{TFE}$ (10:1) mixture at 100°C , whereby the corresponding organometallic complex **4x- CH_3CN** was obtained (see Schemes S13 and S14 and Figures S13 and S14). Crystals of **4b- CH_3CN** , as well as **4c- CH_3CN** , suitable for XRD studies were this time obtained and fully characterized using XRD and other techniques (Figure 3A,B and Figures S46–S55). The experimentally determined EXAFS Co– C_{phenyl} bond distances of 1.88 Å for **4b-OAc** and 1.90 Å for **4c-OAc** (Figure 2B–E) are consistent with the Co(III)– C_{phenyl} distance of 1.86

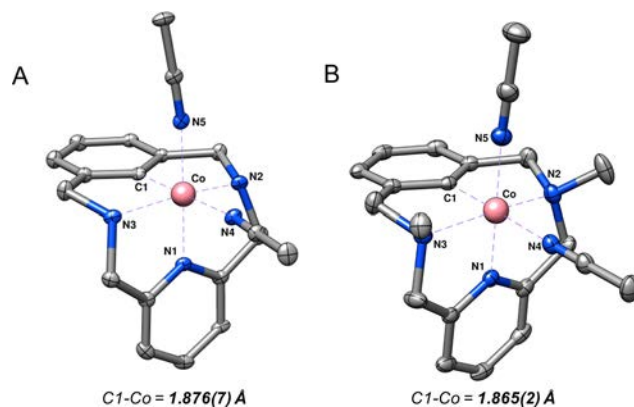



Figure 3. Solid-state structures of organometallic aryl-Co(III) compounds. Hydrogen atoms, perchlorate anions and solvent molecules have been omitted for clarity; ellipsoids are set at 50% probability. (A) Crystal data for **4b- CH_3CN** . Selected bond distances [Å] and angles [°]: Co–C(1) 1.876(7), Co–N(1) 1.853(4), Co–N(2) 1.997(6), Co–N(3) 2.008(5), Co–N(4) 2.025(6), Co–N(5) 1.897(4); C(1)–Co–N(1) 90.55(2), C(1)–Co–N(2) 83.68(2), C(1)–Co–N(3) 83.66(2), C(1)–Co–N(4) 177.87(2), C(1)–Co–N(5) 88.40(2). (B) Crystal data for **4c- CH_3CN** . Selected bond distances [Å] and angles [°]: Co–C(1) 1.865(2), Co–N(1) 1.856(2), Co–N(2) 2.029(2), Co–N(3) 2.027(2), Co–N(4) 1.999(2), Co–N(5) 1.927(2); C(1)–Co–N(1) 88.16(9), C(1)–Co–N(2) 84.13(9), C(1)–Co–N(3) 84.26(9), C(1)–Co–N(4) 178.30(9), C(1)–Co–N(5) 91.30(9).

Å determined for both **4b-CH₃CN** and **4c-CH₃CN** from their crystal structures (Figure 3A,B). In order to put our new organometallic aryl-Co(III) compounds into context, we have also been able to obtain XRD evidence of an aryl-Co(III) intermediate furnished through assistance of the 8-aminoquinoline directing group.²¹ Using a nitro-derivative of the aminoquinoline scaffold (**6**),²² together with the addition of 2,2'-bipyridine (bipy), we were able to successfully crystallize this sought-after intermediate, [(**6**)Co(III)(bipy)(OAc)] (**8**) (Scheme S16 and Figure S18). This result sets definitive proof of the structure of this intermediate organometallic species and highlights the relevance of our new isolable organometallic aryl-Co(III) compounds for studying high-valent Co-catalyzed C(sp²)-H annulation reactions.

Study of Isolated Organometallic Aryl-Co(III) Compounds in Stoichiometric Alkyne Annulation Reactions.

With the isolated organometallic aryl-Co(III) compounds in hand, we then turned our attention toward the reactivity of **4b-OAc** using alkynes as coupling partners to furnish annulated products. We envisioned that this compound may provide similar products to the previously reported Co-catalyzed annulation reactions with alkynes,¹¹ which are believed to proceed via β -migratory insertion of the alkyne into the organometallic aryl-Co(III) bond, furnishing a dihydroisoquinoline product (6-membered ring, **9a** and **10a**) upon reductive elimination of the Co with our macrocyclic ligand. However, reaction of **4b-OAc** with 1-ethynyl-4-nitrobenzene at 100 °C in TFE unexpectedly resulted in the regioselective formation of the dihydroisoindoline product **9b** (5-membered ring) in good yields (Table 1, entry 1). The unexpected formation of **9b** led

Table 1. Reactivity of Organometallic Aryl-Co(III) Complex **4b-OAc with Terminal Alkynes as Coupling Partners**



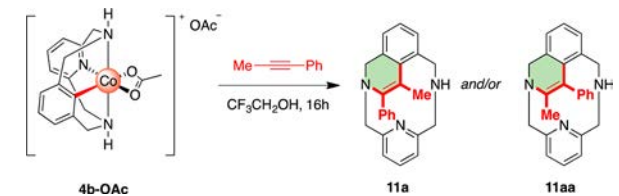
entry ^a	R	atm	temp (°C)	yield ^b (%)	ratio (a:b) ^c
1	4-NO ₂ Ph	air	100	54	1:99 (9a:9b)
2	4-NO ₂ Ph	air	60	66	1:12
3	4-NO ₂ Ph	air	rt	63	1:1.5
4	4-NO ₂ Ph	N ₂	60	60	1:12
5	Ph	air	100	30	99:1 (10a:10b)
6	Ph	air	60	36	99:1
7	Ph	air	rt	40	4:1
8	Ph	N ₂	60	34	99:1

^aReaction conditions: **4b-OAc** (40 mg, 0.077 mmol) and alkyne (2.0 equiv) were mixed in TFE and stirred at different temperatures and atmospheres over 16 h. ^bProducts were isolated using silica-gel chromatography. ^cRatios were determined by NMR spectrometry.

us to explore this reactivity further, changing the reaction conditions, such as temperature and electronic properties of the alkyne coupling partner. Thus, reactions with 1-ethynyl-4-nitrobenzene were carried out at lower temperatures (Table 1, entries 2 and 3) and interestingly, mixtures of **9a** and **9b** were obtained, with increasing ratio of **9a** with decreasing temperature.

This result suggests that **9b** is the thermodynamic product, while **9a** is the kinetic product. The structure of **9a** and **9b** were unambiguously determined using NMR and MS techniques (see Supporting Information for more details). Interestingly, under an inert atmosphere it was also possible to obtain products (Table 1, entry 4), indicating that no oxidant is required in the annulation reaction. Thereafter, reaction of **4b-OAc** with phenylacetylene was tested at 100 °C in TFE, which resulted in the selective formation of the 6-membered ring product **10a** (Table 1, entry 5). Surprisingly, other 6-membered ring isomers were never observed, showing that the reaction is regioselective toward the dihydroisoquinoline product **10a**. The same results were obtained when reactions were carried out at 60 °C in TFE, under air or N₂ atmospheres. However, when reactions were carried out at room temperature, a mixture of **10a** and **10b** was obtained (Table 1, entries 6 and 7). Therefore, contrary to the reaction with 1-ethynyl-4-nitrobenzene, for the reaction with phenylacetylene the thermodynamic product is **10a**, while **10b** is the kinetic product. Finally, the reactivity of the aryl-Co(III) compounds with an internal alkyne, 1-phenyl-1-propyne, was also evaluated. At 100 °C in TFE the reaction furnished 1,2-dihydroisoquinoline product (**11a**) in good yield (Table 2, entry 1). Variation of temperature resulted in the formation of both regioisomers, **11a** and **11aa** (Table 2, entries 2 and 3), suggesting again kinetic and thermodynamic products.

Table 2. Reactivity of Organometallic Aryl-Co(III) Complex **4b-OAc with 1-Phenyl-1-propyne as Coupling Partner**

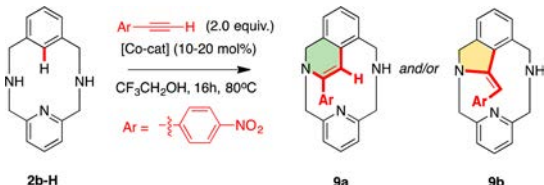


entry ^a	atm	temp (°C)	yield ^b (%)	Ratio ^c (11a:11aa)
1	air	100	72	99:1
2	air	60	70	4:1
3	air	rt	54	2:1
4	N ₂	60	65	4:1

^aReaction conditions: **4b-OAc** (0.077 mmol) and 1-phenyl-1-propyne (1.0 equiv) were mixed in TFE and stirred at different temperatures and atmospheres over 16 h. ^bProducts were isolated using silica-gel chromatography. ^cRatios were determined by ¹H NMR.

Study of Isolated Aryl-Co(III) Compounds in Catalytic Alkyne Annulation Reactions.

The annulation reaction was also studied in a catalytic fashion using **2b-H** and terminal alkynes. Initial tests were performed using catalytic quantities of Co(OAc)₂, **3b-OAc** and **4b-OAc**, together with 1-ethynyl-4-nitrobenzene and **2b-H** (Table 3). At room temperature, starting from Co(OAc)₂ the reactions did not proceed, in contrast to the stoichiometric experiments described above (Table 1, entries 3 and 7). This result indicates that C-H activation is the rate-determining step for these transformations, in agreement with what is suggested for most studies in this field. 1-ethynyl-4-nitrobenzene was successfully coupled to **2b-H** at 80 °C using TFE as solvent, under an oxygenated atmosphere, with 20 mol% of Co(OAc)₂, **3b-OAc** or **4b-OAc** (Table 3, entries 1, 3, and 7).

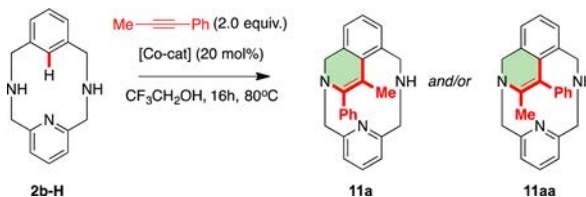
Table 3. Study of off-Cycle Intermediates in Catalytic Reactions Starting from 2b-H and Terminal Alkynes


entry ^a	[Co] (x mol%)	atm	yield ^b (%)	ratio ^c (9a:9b)
1	Co(OAc) ₂ (20)	air	66	1:99
2	Co(OAc) ₂ (20)	N ₂	5 ^d	n.d.
3	4b-OAc (20)	air	69	1:99
4	4b-OAc (20)	N ₂	13 ^d	1:99
5	4b-OAc (10)	air	43	1:99
6	4b-OAc (10)	N ₂	trace ^d	n.d.
7	3b-OAc (20)	air	58	1:99
8	3b-OAc (20)	N ₂	7 ^d	n.d.

^aReaction conditions: 2b-H (0.077 mmol) and 1-phenyl-1-propyne (2.0 equiv) were mixed in TFE with 10–20 mol% of 4b-OAc and stirred at 100 °C under different atmospheres over 16 h. ^bProducts were isolated using silica-gel chromatography. ^cRatios were determined by ¹H NMR. ^dYield determined using 1,3,5-trimethoxybenzene as internal standard.

Under an inert atmosphere the reaction was significantly retarded when starting from both Co(II) precursors or the off-cycle intermediate 4b-OAc (Table 3, entries 2, 4 and 8), suggesting that an external oxidant is needed to regenerate the catalyst.

Next, the annulation reaction with internal alkynes was tested in a catalytic fashion. At 80 °C, 1-phenyl-1-propyne could be coupled to 2b-H in good yields under air using 20 mol% of Co(OAc)₂ or the proposed off-cycle intermediates 3b-OAc and 4b-OAc, obtaining similar yields and regioselectivities (Table 4, entries 1, 3, and 5). As with the terminal alkynes, under an inert

Table 4. Study of off-Cycle Intermediates in Catalytic Reactions Starting from 2b-H and 1-Phenyl-1-propyne


entry ^a	[Co] (20 mol%)	atm	yield ^b (%)	ratio ^c (11a:11aa)
1	Co(OAc) ₂	air	67	5:1
2	Co(OAc) ₂	N ₂	trace ^d	n.d.
3	4b-OAc	air	64	5:1
4	4b-OAc	N ₂	14 ^d	5:1
5	3b-OAc	air	66	5:1
6	3b-OAc	N ₂	trace ^d	n.d.

^aReaction conditions: 2b-H (0.077 mmol) and internal alkyne (2.0 equiv) were mixed in TFE with 20 mol% of 4b-OAc and stirred at 100 °C under different atmospheres over 16 h. ^bProducts were isolated using silica-gel chromatography. ^cRatios were determined by ¹H NMR. ^dYield determined using 1,3,5-trimethoxybenzene as internal standard.

atmosphere the reaction did not proceed starting from 3b-OAc or Co(OAc)₂ (Table 4, entries 2 and 6) and a 14% yield was obtained starting from 4b-OAc (Table 4, entry 4), highlighting the necessity for air to regenerate the required +3 oxidation state of Co for catalytic turnover.

Mechanistic Insights. From the experimental studies we can conclude that initially Co(OAc)₂ coordinates to 2b-H to furnish 3b-OAc. The new ligand environment permits facile oxidation to Co(III) followed by C–H cobaltation, which we propose proceeds through a concerted metalation deprotonation (CMD) process, furnishing 4b-OAc. Starting from the key aryl-Co(III) intermediates, BP86/B3LYP calculations (Figures 4–6) revealed that reaction with terminal alkynes proceeds following detachment of the η²-OAc resulting in a mono-coordinated acetate (A, ΔG = 18.5 kcal mol⁻¹), followed by a formation of an adduct with the incoming terminal alkyne with the metal complex (B, ΔG = 20.6 kcal mol⁻¹) and finally coordination of the alkyne to furnish a cationic π-complex (Figure 4, 4b-alkyne-OAc, ΔG = 19.1 kcal mol⁻¹). At this point

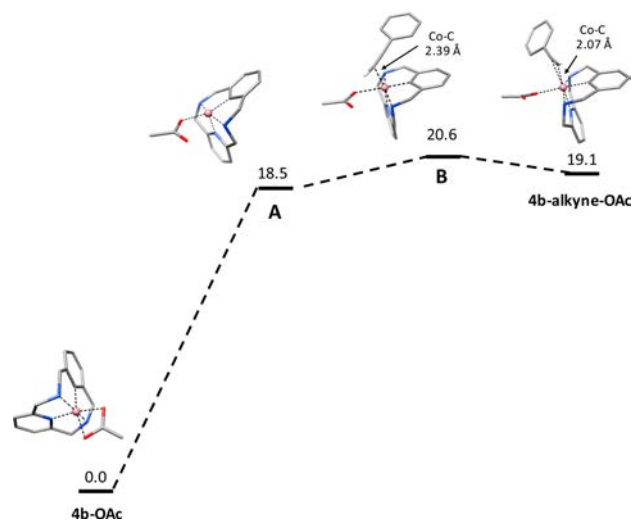
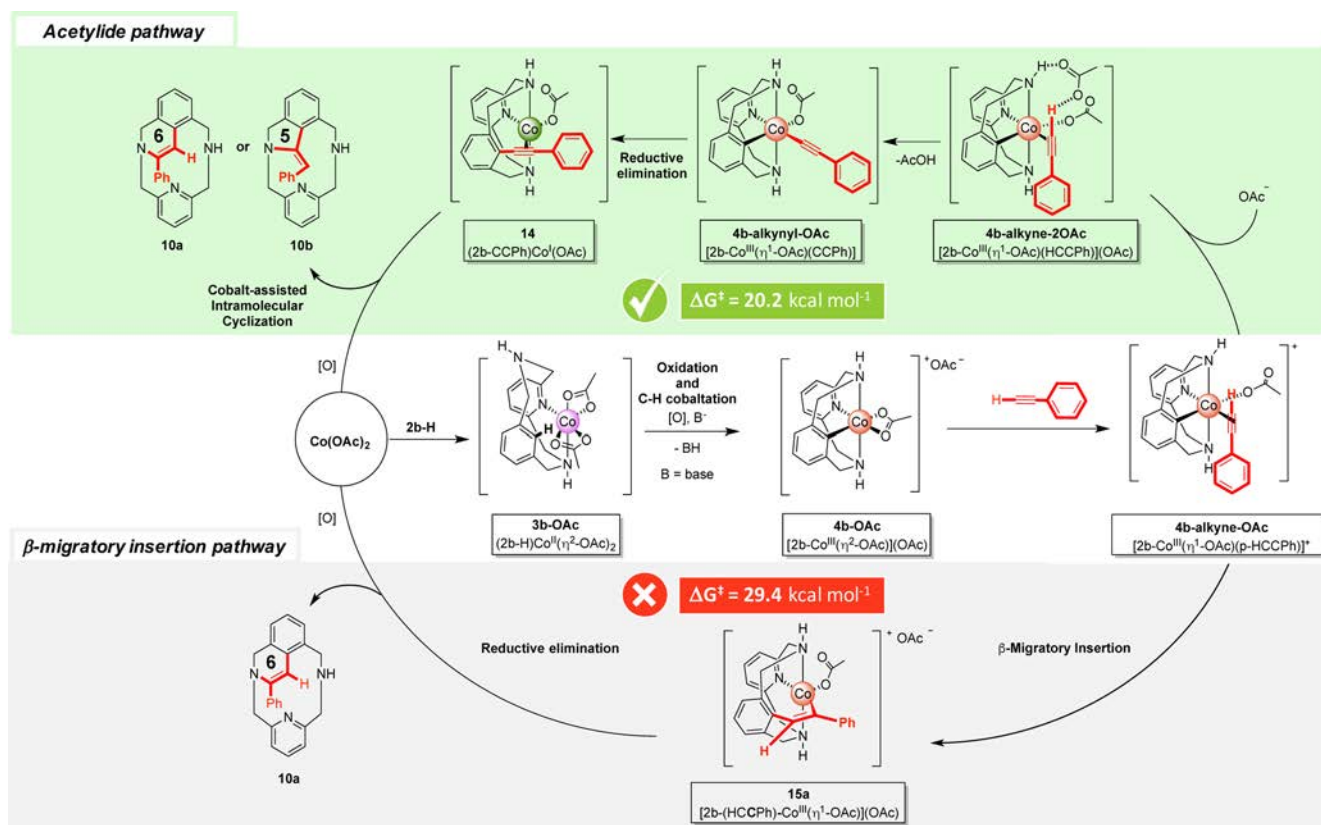


Figure 4. Gibbs energy profile of the formation of 4b-alkyne-OAc. Relative Gibbs energy values are given in kcal mol⁻¹ and selected bond distances in Å. Hydrogens not involved in reactivity are omitted for clarity (N, blue; O, red; Co(III), orange; C, gray; H, white).

the mechanism can diverge to two different pathways, i.e., the “acetylide pathway” (Scheme 3, upper green highlighted route) and the “migratory insertion pathway” (Scheme 3, lower gray highlighted route). In order to fully understand the implication of our experimental results, DFT studies were applied to distinguish whether the 6-membered ring products 9a and 10a were formed via the “acetylide pathway” or the prototypical β-migratory insertion when using phenylacetylene as alkyne coupling partner.

In the “acetylide pathway” (Figure 5), acetate-assisted deprotonation of the alkyne occurs via 4b-alkyne-2OAc (ΔG = 17.5 kcal mol⁻¹), which presents a hydrogen bond between the alkyne and one acetate anion. Subsequent proton transfer from the alkyne to the acetate anion and loss of acetic acid results in a low spin Co(III) acetylide intermediate, 4b-alkynyl-OAc (ΔG = 3.7 kcal/mol), through a 20.2 kcal mol⁻¹ transition state. Then, reductive elimination from 4b-alkynyl-OAc produces [(2b-CCPh)Co^I](OAc) (14), which is computed to be most stable as a triplet state by 19.3 kcal mol⁻¹. The most accessible C–C coupling pathway then proceeds from the

Scheme 3. Proposed Mechanistic Cycle of Co-Catalyzed Phenylacetylene Annulation through Aryl-Co(III) Intermediates Starting from Co(OAc)₂ and Macrocyclic Ligand 2b-H^a

^aThe highest energy barrier for each pathway indicated. Color code for Co oxidation state: green, (I); pink, (II); and orange, (III).

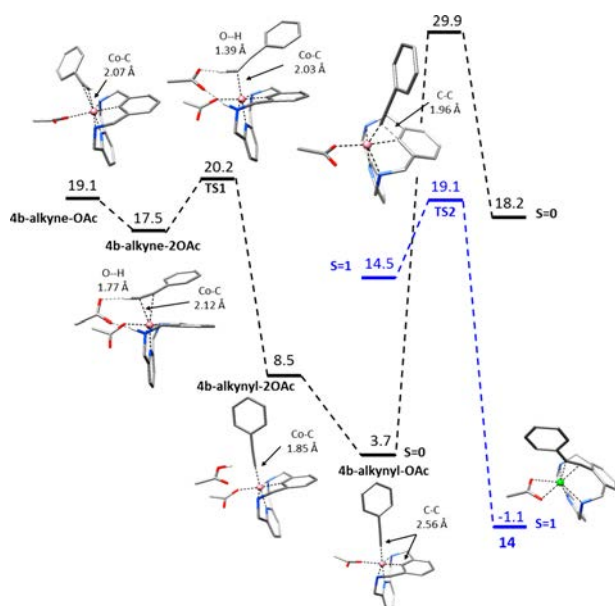


Figure 5. Gibbs energy profile of the formation of the acetylide pathway. Relative Gibbs energy values are given in kcal mol⁻¹ and selected bond distances in Å. Hydrogens not involved in reactivity are omitted for clarity (N, blue; O, red; Co, pink; Co(III), orange; Co(I), green; C, gray; H, white).

singlet form of **4b-alkynyl-OAc**, which after a spin-crossing to the *S* = 1 state overcomes an overall barrier of 19.1 kcal mol⁻¹. Thereafter, a Co-assisted intramolecular cyclization furnishes

either the dihydroisoquinoline (6-membered ring, **10a**) or dihydroisoindoline (5-membered ring, **10b**) product depending on both the reaction temperature and the electronic properties of the alkyne.

In the “ β -migratory insertion pathway” (Figure 6), no deprotonation occurs and **4b-alkyne-OAc** undergoes β -migratory insertion toward the commonly proposed 7-membered cyclic intermediate (**15a**, Scheme 3), with a barrier of ($\Delta G^\ddagger = 29.4$ kcal mol⁻¹). Thereafter, reductive elimination from **15a** furnishes the 6-membered ring **10a**, whereas the 5-membered product **10b** cannot be obtained through this mechanism.

Our experimental observations of the formation of **10a** and **10b** when **4b-OAc** is reacted with phenylacetylene and the higher energy barrier to form **15a** ($\Delta\Delta G^\ddagger = 9.2$ kcal mol⁻¹) indicate that the key intermediate is likely to be an organometallic aryl-Co(III)-alkynyl species (**4b-alkynyl-OAc**, Figure 5 and Scheme 2). Thus, our proposal involves the deprotonation of the terminal acetylene by an acetate anion and the subsequent formation of an organometallic aryl-Co(III)-alkynyl intermediate, **4b-alkynyl-OAc**, which furnishes the linear intermediate **14** after a reductive elimination (upper green highlighted route in Scheme 3). Then, it is proposed that 6-membered ring (**9a** and **10a**) or 5-membered ring (**9b** and **10b**) products are obtained through a nucleophilic attack of one of the lateral amines through a Co-assisted intramolecular cyclization. Taking into account the DFT calculations, we propose that the mechanism exclusively operates through an “acetylide pathway”, whereas the commonly proposed “migratory insertion pathway” is excluded for terminal alkynes.

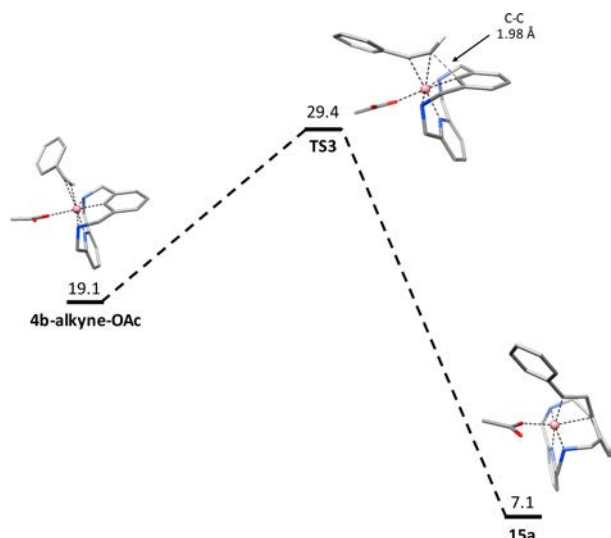


Figure 6. Gibbs energy profile of the formation of the β -migratory insertion pathway. Relative Gibbs energy values are given in kcal mol⁻¹ and selected bond distances in Å. Hydrogens not involved in reactivity are omitted for clarity (N, blue; O, red; Co(III), orange; C, gray; H, white).

Furthermore, the fact that no other 6-membered ring regioisomers are detected under any experimental conditions further supports the “acetylide pathway” operating for terminal acetylenes.

Our proposed mechanism also provides potential reasoning for experimental observations reported by Song,^{11f,k} Glorius,^{11h} and Ackermann^{11j} for other Co(III)-catalyzed annulation protocols displaying different selectivity, but starting from identical substrates. Furthermore, formation of **4b-alkynyl-OAc** is consistent with both the previously described organometallic Co(III) acetylide complexes²³ and the organometallic aryl-Co(III)-alkynyl species proposed by Zhang,^{11a} Song,^{11f,k} and Balaraman²⁴ in alkyne annulation reactions. Additionally, formation of two regioisomers (**10a** and **10b**) from a common starting material (**14**, Scheme 3, upper green highlighted route) can be explained by a nucleophilic attack of a lateral amine to one of the C(sp) centers. The kinetically and thermodynamically favored products depend on the substituents attached to the phenyl group.²⁵ On the other hand, when using internal alkynes (e.g., 1-phenyl-1-propyne) the organometallic aryl-Co(III)-alkynyl intermediate species are not accessible. However, DFT calculations show that the migratory insertion pathway is a plausible mechanism (see Figure S23). Therefore, we propose formation of **11a** and **11aa** via the β -migratory insertion and reductive elimination from a 7-membered ring intermediate analogous to **15a**. Recently, Zhang and co-workers have provided MALDI-TOF evidence of the formation of these intermediates.²⁶

CONCLUSIONS

In summary, we have prepared a number of organometallic aryl-Co(III) complexes using model macrocyclic arene substrates which enable the isolation and complete spectroscopic characterization of these key intermediates in Co-catalyzed C–H activation protocols. The design of the model arene substrates **2b-H** and **2c-H** is key for the stabilization of the organometallic aryl-Co(III) in a preferred-octahedral environment. Additionally, we provide definitive crystallo-

graphic proof of a sought-after organometallic aryl-Co(III) intermediate proposed in 8-aminoquinoline directed Co-catalyzed C–H activation processes. Reaction of organometallic aryl-Co(III) intermediates has been proven to follow different reaction pathways depending on the nature of the alkyne coupling partners. Terminal alkynes furnished 5- and 6-membered ring products depending on both the electronic properties of the alkynes and the reaction temperature. Clear evidence arising from the regioselectivity of the annulation reactions, in combination with a DFT study, indicates that the “acetylide pathway” is preferred for terminal alkynes, in contrast to the usually proposed “ β -migratory insertion pathway”. These findings strongly suggest that the “acetylide pathway” is general for terminal alkynes, representing the first solid experimental evidence of an organometallic aryl-Co(III)-alkynyl intermediate in alkyne C–H annulation reactions. This work constitutes a unique fundamental basis for the understanding of Co-catalyzed C–H activation protocols.

METHODS

XAS Data Acquisition and processing. Samples were prepared as solids diluted in boron nitride, loaded into holders with Kapton windows and stored at liquid nitrogen temperatures until run. All data was collected in transmission mode. Complexes **3c-Br** and **3c-OAc** were run under vacuum at 77 K using a liquid nitrogen finger dewar available from the XAFS beamline at Elettra Sincrotrone Trieste (2.0 GeV, 300 mA storage ring) equipped with a Si(111) double crystal monochromator. Data on the **4c-OAc** complex were collected at 77 K using a liquid nitrogen cryostat and a Si(111) double-crystal monochromator available at Diamond Light Source (3.0 GeV, 300 mA storage ring) beamline B18. Lastly data on the **4b-OAc** species was collected at SOLEIL synchrotron (2.75 GeV, 400 mA storage ring) at 20 K using a liquid helium cryostat and Si(220) double crystal monochromator. Data calibration and normalization were carried out using the Athena software package. Energies were calibrated to the first inflection point of Co foil spectra set at 7709.5 eV. A linear pre-edge function and a quadratic polynomial for the postedge were used for background subtraction and normalization of the edge jump. EXAFS data was extracted using the AUTOBK algorithm with a spline between $k = 1$ and 15 \AA^{-1} having a R_{bkg} value of 1.0 \AA . EXAFS analysis was carried out with the Artemis software program running the IFEFFIT engine and the FEFF6 code.²⁷ Unless otherwise specified k^3 -weighted data was fit in r -space using a Hannings window ($dk = 2$) over a k -range of $2\text{--}12.5 \text{ \AA}^{-1}$, and an r -range of $1\text{--}3 \text{ \AA}$. The S_0^2 value was set to 0.9, and a global ΔE_0 was employed with the initial E_0 value set to the inflection point of the rising edge. Single and multiple scattering paths were fit in terms of a Δr_{eff} and σ^2 as previously described.²⁸ To assess the goodness of the fits the R_{factor} (%R) was minimized. Overfitting the data was controlled by minimizing the number of adjustable parameters and ensuring that the reduced χ^2 (χ^2_{v}) decreases with increasing number of adjustable parameters.

Density Functional Theoretical Calculations. Theoretical calculations were carried out using the ORCA package.²⁹ Geometry optimizations were carried out using the spin-unrestricted Kohn–Sham formalism employing a BP86 functional³⁰ with a def2-TZVP(-f) basis set on the metal, nitrogens and oxygens, a SVP basis set on the hydrogens and def2-SVP on carbons, as well as a def2-TZVP/J auxiliary basis set on all atoms.³¹ A dense integration grid (ORCA Grid 5 = Lebedev 434 points) was used for all atoms. Furthermore, dispersion corrections were included using the Grimme and co-workers DFT-D3BJ approach³² and solvent effects were incorporated using a conductor like screening model (COSMO) using 2,2,2-trifluoroethanol as solvent ($\epsilon = 27$). Subsequent frequency calculations were done to evaluate enthalpy and entropy corrections at 298.15 K (G_{corr}) and ensured that all local minima had only real frequencies while a single imaginary frequency confirmed the presence of transition states. Single-point calculations on the equilibrium geo-

metries, including the solvent effects and D3BJ dispersion corrections were computed using the B3LYP functional and def2-TZVPP basis set for all the atoms (E_{B3LYP}). The density fitting and chain of spheres (RIJCOSX) approximations³³ were employed together with the def2-QZVP/JK auxiliary basis set.³¹ The free energy change associated with moving from a standard-state gas phase pressure of 1 atm to a standard state gas phase concentration of 0.046 M for solutes ($\Delta G^{\circ}/^*$) was also included in the final free energies. The value of $\Delta G^{\circ}/^*$ at 298.15 K is 0.079 kcal mol⁻¹ for 0.046 M standard state solutes. Then, the final total Gibbs free energy (G) was given by

$$G = E_{\text{B3LYP}} + G_{\text{corr}} + \Delta G^{\circ}/^* \quad (1)$$

Representative C–H Cobaltation of 2b-H and 2c-H. In a 10 mL vial, 2b-H or 2c-H (0.41 mmol) and Co(OAc)₂ (0.41 mmol) were mixed in TFE (2.5 mL). The vial was then sealed with a septum, and the mixture was heated at 100 °C for 36 h. Thereafter, the solvent was removed, and the crude was dissolved in CHCl₃ and layered with pentane. After 24 h at 4 °C, the resulting oil was dried under vacuum for 6 h, giving the product as a gray-red foam (58–70%).

Representative Stoichiometric Reaction of 4b-OAc with Alkynes. In a 2 mL vial, 4b-OAc (40 mg, 0.077 mmol) and alkyne (0.077 mmol) were mixed in TFE (1.5 mL). The vial was then sealed with a septum, and the mixture was stirred for 16 h at different temperatures. After removal of TFE, NH₄OH (2 mL) was added, and the solution was extracted using CH₂Cl₂ (2 × 5 mL). Products were purified by column chromatography on silica gel (CH₂Cl₂ then CH₂Cl₂/MeOH 95:5) and characterized by NMR techniques and HRMS (see Supporting Information for full details).

Representative Catalytic Reaction of 4b-OAc with Alkynes. In a 2 mL vial, 2b-H (0.077 mmol) and alkyne (0.154 mmol) were mixed in TFE (1.5 mL) with 10–20 mol% of 4b-OAc. The vial was then sealed with a septum, and the mixture was stirred for 16 h at 80 °C. After removal of the solvent, NH₄OH (2 mL) was added, and the solution was extracted using CH₂Cl₂ (2 × 5 mL). The products were then purified by column chromatography on silica gel (CH₂Cl₂, then CH₂Cl₂/MeOH 95:5) and characterized by NMR techniques. 1,3,5-Trimethoxybenzene was used as internal standard in selected cases (see Supporting Information for full details).

■ ASSOCIATED CONTENT

● Supporting Information

The Supporting Information is available free of charge on the ACS Publications website at DOI: 10.1021/jacs.6b08593.

General considerations, experimental details for the preparation and characterization of ligands 2b-H and 2c-H, and compounds 4b-OAc, 4c-OAc, 4b-CH₃CN, 4c-CH₃CN, 5c-Cl, 7 and 8; optimization details; experimental details of stoichiometric reactions of 4b-OAc with alkynes; experimental details of catalytic reactions of 4b-OAc with alkynes; XYZ coordinates for DFT structures; full XAS analysis; full characterization of compounds; X-ray parameters and original NMR spectra [including Schemes S1–S24, Tables S1–S41, and Figures S1–S85] (PDF)

X-ray crystallographic data for 3b-OAc (CIF)

X-ray crystallographic data for 3c-Br (CIF)

X-ray crystallographic data for 4b-CH₃CN (CIF)

X-ray crystallographic data for 4c-CH₃CN (CIF)

X-ray crystallographic data for 5c-Cl (CIF)

X-ray crystallographic data for 8 (CIF)

■ AUTHOR INFORMATION

Corresponding Author

*xavi.ribas@udg.edu

Notes

The authors declare no competing financial interest.

Crystallographic data for compounds 3b-OAc (CCDC-1493341), 3c-Br (CCDC-1493342), 4b-CH₃CN (CCDC-1493343), 4c-CH₃CN (CCDC-1493344), 5c-Cl (CCDC-1493345) and aryl-Co(III) species using nitro-aminoquinoline model substrate 8 (CCDC-1493346) can be obtained free of charge from the Cambridge Crystallographic Data Centre via www.ccdc.cam.ac.uk/data_request/cif.

■ ACKNOWLEDGMENTS

We acknowledge financial support from the European Research Council for the Starting Grant Project ERC-2011-StG-277801 to X.R. and from MINECO of Spain for project CTQ2013-43012-P to A.C. and X.R., CTQ2014-52525-P to J.M.L. and CTQ2015-64436-P to T.P. We also thank Generalitat de Catalunya for projects 2014SGR862 and 2014SGR931. We thank the MECED of Spain for a FPU PhD grant to O.P. and MINECO for a Ramón y Cajal contract to A.C. X.R. also thanks Generalitat de Catalunya for an ICREA-Acadèmia Award. In addition, the research leading to these results has received funding from the European Community's Seventh Framework Programme (FP7/2007-2013) under grant agreement no. 312284. XAS data was collected at Elettra and SOLEIL synchrotron facilities. We thank Dr. Luca Olivi from Elettra and Dr. Landrot Gautier from SOLEIL for their help with experimental setup. XRD (Xavi Fontrodona) and HRMS (Dr. Laura Gómez) data was collected at STR-UdG.

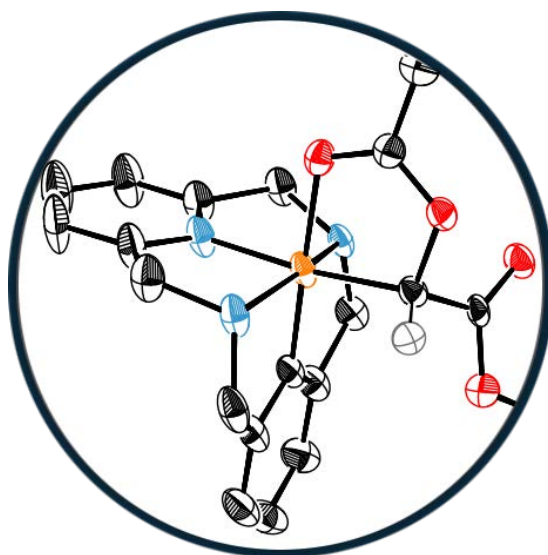
■ REFERENCES

- (1) Yamaguchi, J.; Yamaguchi, A. D.; Itami, K. *Angew. Chem., Int. Ed.* **2012**, *51*, 8960.
- (2) Chen, X.; Engle, K. M.; Wang, D.-H.; Yu, J.-Q. *Angew. Chem., Int. Ed.* **2009**, *48*, 5094.
- (3) (a) Bolm, C.; Legros, J.; Le Pailh, J.; Zani, L. *Chem. Rev.* **2004**, *104*, 6217. (b) Ambhaikar, N. *C-H Bond Activation in Organic Synthesis*; CRC Press: Boca Raton, FL, 2015; p 145.
- (4) (a) Guo, X.-X.; Gu, D.-W.; Wu, Z.; Zhang, W. *Chem. Rev.* **2015**, *115*, 1622. (b) Ahmad, N. *C-H Bond Activation in Organic Synthesis*; CRC Press: Boca Raton, FL, 2015; p 175.
- (5) (a) Moselage, M.; Li, J.; Ackermann, L. *ACS Catal.* **2016**, *6*, 498. (b) Wei, D.; Zhu, X.; Niu, J.-L.; Song, M.-P. *ChemCatChem* **2016**, *8*, 1242. (c) Gao, K.; Yoshikai, N. *Acc. Chem. Res.* **2014**, *47*, 1208.
- (6) (a) Tasker, S. Z.; Standley, E. A.; Jamison, T. F. *Nature* **2014**, *509*, 299. (b) Williams, A. *C-H Bond Activation in Organic Synthesis*; CRC Press: Boca Raton, FL, 2015; p 113.
- (7) Gensch, T.; Klauk, F. J. R.; Glorius, F. *Angew. Chem., Int. Ed.* **2016**, *55*, 11287.
- (8) (a) Colby, D. A.; Tsai, A. S.; Bergman, R. G.; Ellman, J. A. *Acc. Chem. Res.* **2012**, *45*, 814. (b) Song, G.; Wang, F.; Li, X. *Chem. Soc. Rev.* **2012**, *41*, 3651. (c) Satoh, T.; Miura, M. *Chem. - Eur. J.* **2010**, *16*, 11212.
- (9) Yamakawa, T.; Yoshikai, N. *Org. Lett.* **2013**, *15*, 196.
- (10) (a) Wu, X.; Yang, K.; Zhao, Y.; Sun, H.; Li, G.; Ge, H. *Nat. Commun.* **2015**, *6*, 6462. (b) Grigorjeva, L.; Daugulis, O. *Org. Lett.* **2014**, *16*, 4684. (c) Grigorjeva, L.; Daugulis, O. *Org. Lett.* **2014**, *16*, 4688. (d) Hummel, J. R.; Ellman, J. A. *J. Am. Chem. Soc.* **2015**, *137*, 490. (e) Zhao, D.; Kim, J. H.; Stegemann, L.; Strassert, C. A.; Glorius, F. *Angew. Chem., Int. Ed.* **2015**, *54*, 4508. (f) Gandeepan, P.; Rajamalli, P.; Cheng, C.-H. *Angew. Chem., Int. Ed.* **2016**, *55*, 4308. (g) Li, J.; Tang, M.; Zang, L.; Zhang, X.; Zhang, Z.; Ackermann, L. *Org. Lett.* **2016**, *18*, 2742. (h) Li, L.; Wang, H.; Yu, S.; Yang, X.; Li, X. *Org. Lett.* **2016**, *18*, 3662. (i) Ma, W.; Ackermann, L. *ACS Catal.* **2015**, *5*, 2822. (j) Wang, H.; Lorion, M. M.; Ackermann, L. *Angew. Chem., Int. Ed.* **2016**, *55*, 10386.

- (11) (a) Zhang, J.; Chen, H.; Lin, C.; Liu, Z.; Wang, C.; Zhang, Y. *J. Am. Chem. Soc.* **2015**, *137*, 12990. (b) Grigorjeva, L.; Daugulis, O. *Angew. Chem., Int. Ed.* **2014**, *53*, 10209. (c) Nguyen, T. T.; Grigorjeva, L.; Daugulis, O. *ACS Catal.* **2016**, *6*, 551. (d) Planas, O.; Whiteoak, C. J.; Company, A.; Ribas, X. *Adv. Synth. Catal.* **2015**, *357*, 4003. (e) Kalsi, D.; Sundararaju, B. *Org. Lett.* **2015**, *17*, 6118. (f) Zhang, L.-B.; Hao, X.-Q.; Liu, Z.-J.; Zheng, X.-X.; Zhang, S.-K.; Niu, J.-L.; Song, M.-P. *Angew. Chem., Int. Ed.* **2015**, *54*, 10012. (g) Ikemoto, H.; Yoshino, T.; Sakata, K.; Matsunaga, S.; Kanai, M. *J. Am. Chem. Soc.* **2014**, *136*, 5424. (h) Lu, Q.; Vásquez-Céspedes, S.; Gensch, T.; Glorius, F. *ACS Catal.* **2016**, *6*, 2352. (i) Kim, J. H.; Greßies, S.; Glorius, F. *Angew. Chem., Int. Ed.* **2016**, *55*, 5577. (j) Mei, R.; Wang, H.; Warratz, S.; Macgregor, S. A.; Ackermann, L. *Chem. - Eur. J.* **2016**, *22*, 6759. (k) Hao, X.-Q.; Du, C.; Zhu, X.; Li, P.-X.; Zhang, J.-H.; Niu, J.-L.; Song, M.-P. *Org. Lett.* **2016**, *18*, 3610.
- (12) (a) Robitzer, M.; Bouamaied, I.; Sirlin, C.; Chase, P. A.; van Koten, G.; Pfeffer, M. *Organometallics* **2005**, *24*, 1756. (b) Meneghetti, M. R.; Grellier, M.; Pfeffer, M.; Cian, A. D.; Fischer, J. *Eur. J. Inorg. Chem.* **2000**, *2000*, 1539.
- (13) (a) Harvey, J. D.; Ziegler, C. J. *Chem. Commun.* **2004**, *14*, 1666. (b) Çetin, A.; Sripothongnak, S.; Kawa, M.; Durfee, W. S.; Ziegler, C. J. *Chem. Commun.* **2007**, *41*, 4289.
- (14) Wang, Y.-C.; Chen, J.-H.; Wang, S.-S.; Tung, J.-Y. *Inorg. Chem.* **2013**, *52*, 10711.
- (15) Maity, S.; Kancherla, R.; Dhawa, U.; Hoque, E.; Pimparkar, S.; Maiti, D. *ACS Catal.* **2016**, *6*, 5493.
- (16) Ribas, X.; Calle, C.; Poater, A.; Casitas, A.; Gómez, L.; Xifra, R. I.; Parella, T.; Benet-Buchholz, J.; Schweiger, A.; Mitrikas, G.; Solà, M.; Llobet, A.; Stack, T. D. P. *J. Am. Chem. Soc.* **2010**, *132*, 12299.
- (17) (a) Casitas, A.; King, A. E.; Parella, T.; Costas, M.; Stahl, S. S.; Ribas, X. *Chem. Sci.* **2010**, *1*, 326. (b) Huffman, L. M.; Casitas, A.; Font, M.; Canta, M.; Costas, M.; Ribas, X.; Stahl, S. S. *Chem. - Eur. J.* **2011**, *17*, 10643. (c) King, A. E.; Huffman, L. M.; Casitas, A.; Costas, M.; Ribas, X.; Stahl, S. S. *J. Am. Chem. Soc.* **2010**, *132*, 12068.
- (18) (a) Zhou, W.; Schultz, J. W.; Rath, N. P.; Mirica, L. M. *J. Am. Chem. Soc.* **2015**, *137*, 7604. (b) Zhou, W.; Zheng, S.; Schultz, J. W.; Rath, N. P.; Mirica, L. M. *J. Am. Chem. Soc.* **2016**, *138*, 5777. (c) Zhou, W.; Rath, N. P.; Mirica, L. M. *Dalton Trans.* **2016**, *45*, 8693. (d) Zhou, W.; Watson, M. B.; Zheng, S.; Rath, N. P.; Mirica, L. M. *Dalton Trans.* **2016**, *45*, 15886.
- (19) Goswami, M.; Lyaskovskyy, V.; Domingos, S. R.; Buma, W. J.; Woutersen, S.; Troeppner, O.; Ivanović-Burmazović, I.; Lu, H.; Cui, X.; Zhang, X. P.; Reijerse, E. J.; DeBeer, S.; van Schooneveld, M. M.; Pfaff, F. F.; Ray, K.; de Bruin, B. *J. Am. Chem. Soc.* **2015**, *137*, 5468.
- (20) For examples of reactions where the use of fluorinated alcohols has proved highly beneficial, see: (a) Shuklov, I. A.; Dubrovina, N. V.; Börner, A. *Synthesis* **2007**, *2007*, 2925. (b) Wencel-Delord, J.; Colobert, F. *Org. Chem. Front.* **2016**, *3*, 394.
- (21) During the preparation of this manuscript, Maiti and co-workers reported a related XRD structure; see ref 15.
- (22) Whiteoak, C. J.; Planas, O.; Company, A.; Ribas, X. *Adv. Synth. Catal.* **2016**, *358*, 1679.
- (23) Cummins, D.; McKenzie, E. D.; Segnitz, A. *J. Organomet. Chem.* **1975**, *87*, C19.
- (24) Landge, V. G.; Jaiswal, G.; Balaraman, E. *Org. Lett.* **2016**, *18*, 812.
- (25) Rovira, M.; Font, M.; Acuña-Parés, F.; Parella, T.; Luis, J. M.; Lloret-Fillol, J.; Ribas, X. *Chem. - Eur. J.* **2014**, *20*, 10005.
- (26) Yu, W.; Zhang, W.; Liu, Z.; Zhang, Y. *Chem. Commun.* **2016**, *52*, 6837.
- (27) (a) Ravel, B.; Newville, M. *J. Synchrotron Radiat.* **2005**, *12*, 537. (b) Newville, M. *J. Synchrotron Radiat.* **2001**, *8*, 96. (c) Rehr, J. J.; Albers, R. C. *Rev. Mod. Phys.* **2000**, *72*, 621.
- (28) (a) Martin-Diaconescu, V.; Bellucci, M.; Musiani, F.; Ciurli, S.; Maroney, M. J. *JBIC, J. Biol. Inorg. Chem.* **2012**, *17*, 353. (b) Zambelli, B.; Berardi, A.; Martin-Diaconescu, V.; Mazzei, L.; Musiani, F.; Maroney, M. J.; Ciurli, S. *JBIC, J. Biol. Inorg. Chem.* **2014**, *19*, 319.
- (29) Becke, A. D. *Phys. Rev. A: At., Mol., Opt. Phys.* **1988**, *38*, 3098.
- (30) Neese, F. *Wiley Interdiscip. Rev. Comput. Mol. Sci.* **2012**, *2*, 73.
- (31) (a) Schäfer, A.; Horn, H.; Ahlrichs, R. *J. Chem. Phys.* **1992**, *97*, 2571. (b) Weigend, F.; Ahlrichs, R. *Phys. Chem. Chem. Phys.* **2005**, *7*, 3297.
- (32) (a) Grimme, S.; Antony, J.; Ehrlich, S.; Krieg, H. *J. Chem. Phys.* **2010**, *132*, 154104. (b) Grimme, S.; Ehrlich, S.; Goerigk, L. *J. Comput. Chem.* **2011**, *32*, 1456.
- (33) Neese, F.; Wennmohs, F.; Hansen, A.; Becker, U. *Chem. Phys.* **2009**, *356*, 98.

Chapter IV

Carboxylate-Assisted Formation of Aryl-Co(III) Masked-Carbenes in Cobalt-Catalyzed C-H Functionalization with Diazo Esters



This chapter corresponds to the following publication:

Oriol Planas, Steven Roldán-Gómez, Vlad Martin-Diaconescu, Teodor Parella, Josep M. Luis,
Anna Company and Xavi Ribas.

J. Am. Chem. Soc. **2017**, *139*, 14649-14655.

For this publication O.P. synthesized and characterized the organometallic complexes and performed both stoichiometric and catalytic experiments. T.P. supervised the NMR experiments. S. R.-G. performed the theoretical calculations. V. M.-D. collected and analyzed the XAS data. J.M.L. supervised the DFT studies. A.C. and X.R. designed the project. Besides, O.P. contributed in writing the manuscript and was involved in argumentations and discussions.

Reproduced with permission from:

Diazo Esters, Oriol Planas, Steven Roldan-Gomez, Vlad Martin-Diaconescu, Teodor Parella, Josep M. Luis, Anna Company and Xavi Ribas. "Carboxylate-Assisted Formation of Aryl-Co(III) Masked-Carbenes in Cobalt-Catalyzed C-H Functionalization". *Journal of the American Chemical Society*. Vol. 139, Issue 41 (2017) : 14649-14655.

<http://dx.doi.org/10.1021/jacs.7b07880>

Copyright © 2017 American Chemical Society

Carboxylate-Assisted Formation of Aryl-Co(III) Masked-Carbenes in Cobalt-Catalyzed C–H Functionalization with Diazo Esters

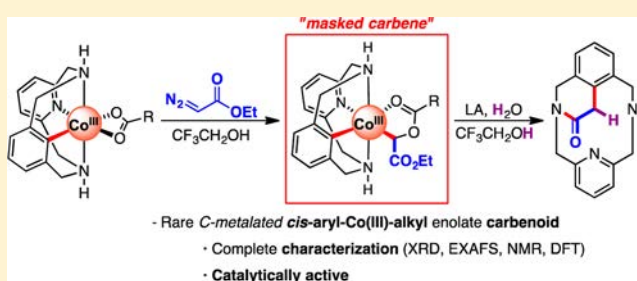
Oriol Planas,[†] Steven Roldán-Gómez,[†] Vlad Martin-Diaconescu,[†] Teodor Parella,[‡] Josep M. Luis,[†] Anna Company,[†] and Xavi Ribas^{*,†}

[†]Institut de Química Computacional i Catàlisi (IQCC) and Departament de Química, Universitat de Girona, Campus Montilivi, Girona, E-17003 Catalonia, Spain

[‡]Servei de RMN, Facultat de Ciències, Universitat Autònoma de Barcelona, Campus UAB, Bellaterra, E-08193 Catalonia, Spain

S Supporting Information

ABSTRACT: Herein we describe the synthesis of a family of aryl-Co(III)-carboxylate complexes and their reactivity with ethyl diazoacetate. Crystallographic, full spectroscopic characterization, and theoretical evidence of unique C-metalated aryl-Co(III) enolate intermediates is provided, unraveling a carboxylate-assisted formation of aryl-Co(III) *masked-carbenes*. Moreover, additional evidence for an unprecedented Co(III)-mediated intramolecular S_N2-type C–C bond formation in which the carboxylate moiety acts as a relay is disclosed. This novel strategy is key to tame the hot reactivity of a metastable Co(III)-carbene and elicit C–C coupling products in a productive manner.



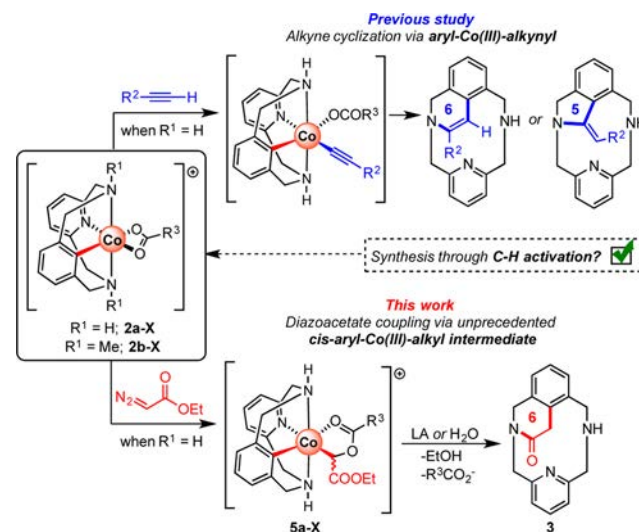
INTRODUCTION

Directed C–H functionalization methodologies using nonprecious earth-abundant 3d transition metal catalysts are currently attracting increasing attention.¹ In particular, high-valent cobalt catalysis has emerged as a valuable approach for the construction of a wide variety of organic molecules, mainly due to the highly polarized character of C–Co bonds when compared to the other group 9 neighbors.² Among the vast array of possible transformations, the use of diazocarbonyl compounds as coupling partners constitutes a particularly attractive method due to their wide application as precursors for several metal-catalyzed processes,³ including cyclopropanation⁴ and functionalization of inert C–H bonds.⁵ Although Co-carbenes have been extensively studied,⁶ directed C–H functionalization involving high-valent aryl-Co-carbene intermediates is still in its infancy and their mechanistic understanding is based on limited experimental evidence as well as computational studies.⁷

The synthesis of organometallic Co(III) species through C–H activation is challenging and still remains underdeveloped.⁸ Legg and co-workers made the first contribution to the field, being able to isolate an organometallic alkyl-Co(III) complex through C–H activation starting from Co(II) salts and characterizing several intermediates in a stepwise manner.^{8c,d} In our commitment to unravel key intermediates,⁹ our group has recently published the synthesis and characterization of a family of aryl-Co(III) complexes through C–H activation,¹⁰ taking advantage of the enhanced stability offered by a macrocyclic model substrate which has proven to stabilize other organometallic high-valent aryl/alkyl-metal intermediate species.¹¹ These complexes proved to be catalytically

competent during alkyne annulation reactions, furnishing either five- or six-membered-ring products (Scheme 1, blue). Taking into account the increasing attention to the use of carbene surrogates for C–C bond formation reactions, we became interested in the reactivity of our previously reported aryl-

Scheme 1. Previous Work with Alkynes as Coupling Partners (Top, Blue) and Current Study Disclosing the Reactivity of Aryl-Co(III) Complexes toward Diazo Esters (Bottom, Red)



Received: July 27, 2017

Published: September 18, 2017

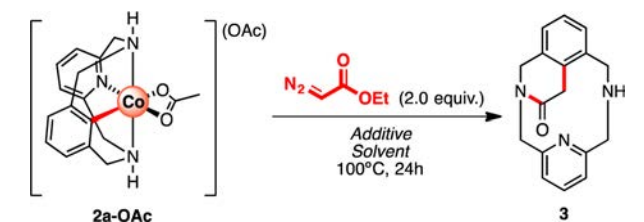
Co(III) complexes toward diazo esters to elucidate the operative mechanism as well as the nature of the key intermediates (Scheme 1, red).

Herein we describe the reactivity of organometallic aryl-Co(III) species (2a-X) with ethyl diazoacetate (EDA). Crystallographic, spectroscopic, and theoretical evidence of a unique C-metalated *cis*-aryl-Co(III)-alkyl enolate intermediate is provided, unveiling a novel strategy to tame the hot reactivity of cobalt-carbenes and construct C–C bonds through an unusual intramolecular S_N2-like pathway. Theoretical studies show the feasibility of this transformation, in which Lewis acids play an important role turning the carboxylate moiety into a better leaving group.

RESULTS

Stoichiometric Annulation Reaction with EDA. Initially, we attempted to perform the stoichiometric annulation reaction of the previously reported aryl-Co(III) complex 2a-OAc with 2.0 equiv of EDA.¹⁰ When the reaction was performed in ethanol, no reaction was observed (Table 1, entry 1). However,

Table 1. Evaluation of Stoichiometric Reaction Conditions¹²



entry	additives (equiv)	solvent	yield of 3 (%) ^a
1	none	EtOH	0%
2	none	TFE ^b	10%
3	none	HFIP ^c	31%
4	AcOH (1.0)	TFE	15% ^d
5	H ₂ O (1.0)	TFE	57%
6	H ₂ O (2.0)	TFE	82%
7	H ₂ O (4.0)	TFE	96% (91%) ^e
8	Mg(OTf) ₂ (1.0)	TFE	67%
9	H ₂ O (1.0) + Mg(OTf) ₂ (1.0)	TFE	92% (87%) ^e
10	Li(OTf) (1.0)	TFE	95% (88%) ^e
11	H ₂ O (4.0)	EtOH	88%
12	Li(OTf) (1.0)	EtOH	91%

^aNMR yield determined using 1,3,5-trimethoxybenzene as internal standard. ^b2,2,2-Trifluoroethanol (TFE). ^c1,1,1,3,3,3-Hexafluoro-2-propanol (HFIP). ^dProto-demetalation of 2a-OAc was observed. ^eIsolated yield.

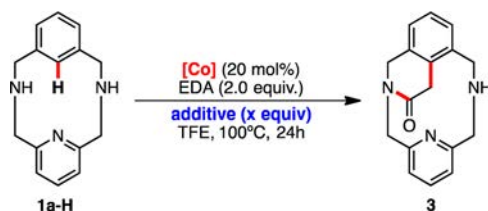
the use of fluorinated alcohols was beneficial for the formation of macrocyclic amide 3 (Table 1, entries 2 and 3). In addition, reaction with the aryl-Co(III) complex bearing methylated tertiary amines, 2b-OAc, was not successful, and only trace amounts of product 4 were detected by HRMS (4 corresponds to the C–C coupling product with no intramolecular reorganization; see Scheme S5).

A variety of commonly used proton sources were investigated as additives. Unfortunately, acetic acid was not successful (Table 1, entry 4), mainly showing proto-demetalation of the starting 2a-OAc complex. However, water as additive proved to be effective, and 3 was obtained in 91% isolated yield when 4.0 equiv of H₂O was added (Table 1, entry 7). To gain more insight into the reaction mechanism,

a variety of Lewis acids (LA) were tested as additives (Table 1, entries 8–10), as they proved to be beneficial in other methodologies using cobalt as catalysts.^{7c} Interestingly, the addition of 1.0 equiv of Mg(OTf)₂ allowed the formation of 3 in 67% yield. Furthermore, when 1.0 equiv of both Mg(OTf)₂ and H₂O were added, 3 was obtained in 92% yield. Finally, when a stronger Lewis acid such as Li(OTf) was used in the absence of water, 3 was obtained in 95% yield. If H₂O or Li(OTf) was used as additive, 3 was also obtained with EtOH as solvent (Table 1, entries 11 and 12).

Catalytic Annulation Reaction with EDA. The annulation reaction was also studied in a catalytic fashion (Table 2).

Table 2. Evaluation of Catalytic Reaction Conditions¹³



entry	[Co]	additive (equiv)	yield of 3 (%) ^a
1	none	H ₂ O (4.0)	n.r.
2	2a-OAc	H ₂ O (4.0)	93% (87%) ^b
3 ^c	2a-OAc	H ₂ O (4.0)	95% (84%) ^b
4	Co(OAc) ₂	H ₂ O (4.0)	96% (89%) ^b
5 ^c	Co(OAc) ₂	H ₂ O (4.0)	traces
6	Co(OAc) ₂	none	15%
7	Co(OAc) ₂	Mg(OTf) ₂ (1.0)	42%
8	Co(OAc) ₂	Mg(OTf) ₂ (1.0) + H ₂ O (1.0)	93% (84%) ^b
9	Co(OAc) ₂	Li(OTf) (1.0)	96% (88%) ^b

^aNMR yield determined using 1,3,5-trimethoxybenzene as internal standard. ^bIsolated yield. ^cReaction performed under nitrogen.

EDA was successfully coupled with 1a-H using 2a-OAc as catalyst (20 mol %), under air in 2,2,2-trifluoroethanol (TFE) with 4.0 equiv of H₂O, forming 3 in 93% yield (Table 2, entry 2). Product 3 was also obtained in excellent yield (Table 2, entry 3) under an inert atmosphere (N₂) using 2a-OAc as catalyst, indicating a redox neutral mechanism where Co(III) does not change its oxidation state. The role of external oxidants was evaluated performing the catalysis with readily available Co(II) salts. When 20 mol % of Co(OAc)₂ was used under air (Table 2, entry 4), 3 was obtained in 96% yield. On the other hand, under an inert atmosphere the reactivity was completely inhibited (Table 2, entry 5), thus indicating that Co(III) species are required to effect the C–H activation to form 2a-OAc.¹¹ Moreover, additives have also proven to be essential in catalysis (Table 2, entries 6–9). Thus, when 1a-H was reacted with EDA using Co(OAc)₂ as catalyst without water, only a 15% yield was obtained. However, as it was previously observed in the stoichiometric reaction, when 1a-H was reacted with EDA in the presence of 1.0 equiv of Mg(OTf)₂ using Co(OAc)₂ as catalyst, a 42% yield of 3 was obtained (Table 2, entry 7). Interestingly, a cooperative effect between Mg(OTf)₂ and H₂O is observed when 1.0 equiv of each of them is added, obtaining 3 in a 93% yield (Table 2, entry 8). Furthermore, when 1.0 equiv of Li(OTf) was added as additive in the absence of water, 3 was obtained in 96% yield, which indicated the key role of Lewis acids.

Isolation of Reaction Intermediates. A detailed study of the reaction of 2a-OAc with EDA under anhydrous conditions

was performed. When **2a-OAc** was reacted with 2.0 equiv of EDA at 100 °C for 15 min, HRMS analysis showed a single peak at $m/z = 442.1183$ (Figure S48), corresponding to the molecular formula $[C_{21}H_{25}CoN_3O_4]^+$, suggesting the formation of a putative aryl-Co(III)-carbene intermediate. Encouraged by this result, this compound (**5a-OAc**) was analyzed by NMR spectroscopy. A diamagnetic NMR spectrum was obtained, which is consistent with an octahedral Co(III) low-spin species. Moreover, a singlet at a chemical shift of 5.81 ppm excludes the presence of a Co(III)-carbene species (Figure S41), as the α proton of the carbene moiety is known to be strongly deshielded.³ Attempts to unravel the nature of **5a-OAc** have been pursued by crystallographic analysis without success. Nevertheless, suitable crystals for XRD analysis were obtained by replacement of the acetate anion with *p*-substituted benzoate. Reaction of **2a-OBz-R** (R = OMe, Cl; for their synthesis see Scheme S1) with EDA caused a rapid color change from red to orange, and recrystallization in $CHCl_3$ /pentane afforded a 85–97% yield of orange crystals corresponding to **5a-X** (X = OBz-Cl, OBz-OMe, Figure 1).

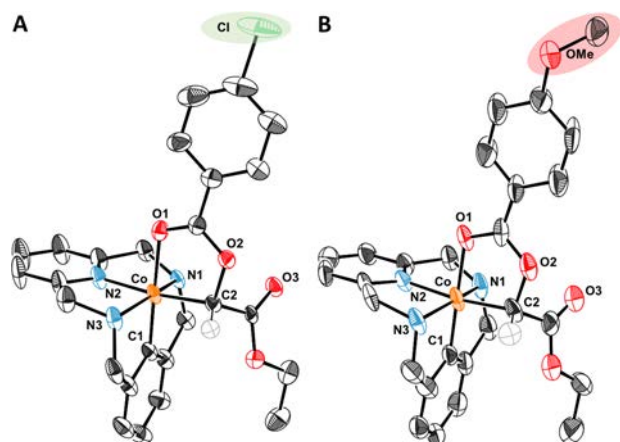


Figure 1. Crystal structures of **5a-OBz-R** complexes. (A) **5a-OBz-Cl**. Selected bond distances [Å] and angles [deg]: Co–C(1) 1.846(3), Co–C(2) 1.972(5), Co–N(2) 1.891(4), Co–O(1) 2.008(3); C(1)–Co–C(2) 95.71(2). (B) **5a-OBz-OMe**. Selected bond distances [Å] and angles [deg]: Co–C(1) 1.84(1), Co–C(2) 1.97(1), Co–N(2) 1.878(8), Co–O(1) 2.004(7); C(1)–Co–C(2) 96.3(4). Hydrogen atoms, anions, and solvent molecules have been omitted, and only one of the enantiomers is depicted for clarity; ellipsoids are displayed at 50% (**5a-OBz-Cl**) and 30% (**5a-OBz-OMe**) probability.

Strikingly, the solid-state structures showed an O_h aryl-Co(III) center bearing a carbonyl and a chiral alkyl group as ligands (**5a-OBz-R**). The formation of **5a-X** (X = carboxylate) species is rationalized by the entrapment of the electron-demanding Co(III)-carbene through the nucleophilic intramolecular attack of the carboxylate to C2. Both **5a-OBz-OMe** and **5a-OBz-Cl**¹⁴ compounds show spectroscopic features analogous to **5a-OAc**, indicating the same structure. In addition, EXAFS analysis of **5a-OAc** agrees with the structures in Figure 1 and the DFT-derived model (see below), showing a metal center having two N/O/C scattering paths at 1.93 Å and four N/O/C scattering paths at 2.05 Å (Figure 2 and Table S9). In addition, the metal *K*-pre-edge and rising edge of **5a-OAc** occur at 7711.2 and 7720.2 eV, respectively, consistent with the presence of a Co(III) center.¹⁰ An analogous Rh intermediate (**7b-OBz-Cl**, Figures S67–74) was obtained when the aryl-Rh(III)(Cl)₂ complex **6b-Cl**¹⁰ was reacted with 4.0

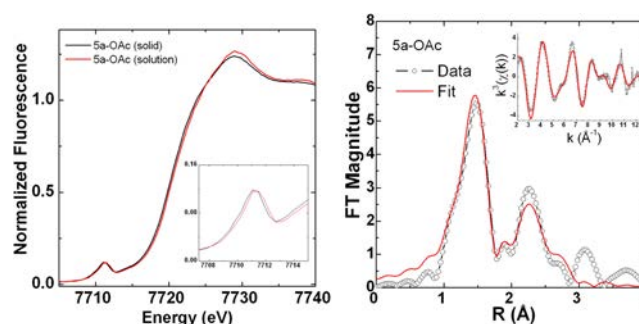
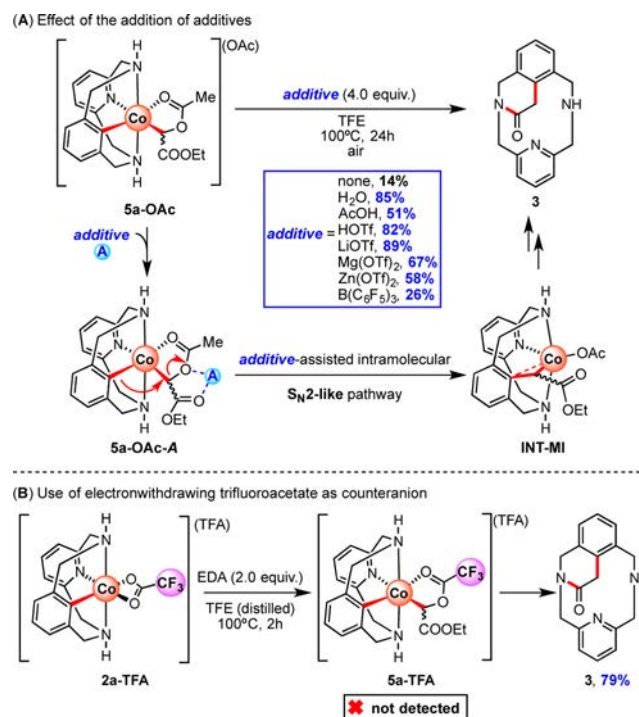


Figure 2. XAS of **5a-OAc**. Left: XANES region showing the pelleted sample diluted in boron nitride and the 15 mM solution sample. Right: Fourier-transformed EXAFS spectra fit (inset: k^3 -weighted unfiltered EXAFS spectra).

equiv of EDA and Ag(OBz-Cl) (Scheme S14). Although the formation of organometallic Rh(III)-alkyl species from carbenes is rare, a similar nucleophilic attack to carbenes using half-sandwich Rh-carbene complexes has been recently described.¹⁵

Mechanistic Insight. To better understand the role of additives in the formation of cyclic amide **3**, a variety of control experiments were performed starting from **5a-OAc**. Surprisingly, the isolated aryl-Co(III)-alkyl enolate evolves to product **3** in good yields by addition of water, organic acids, and Lewis acids, involving the cleavage of a C–O bond and the formation of a new C–C bond (Scheme 2A and Table S5). As expected, when the same reaction was carried out in the absence of additives, poor yields (14%) were obtained. The enhanced reactivity observed in the presence of additives (for instance, with Li(OTf), 89% yield of **3** is obtained, Scheme 2A) suggests

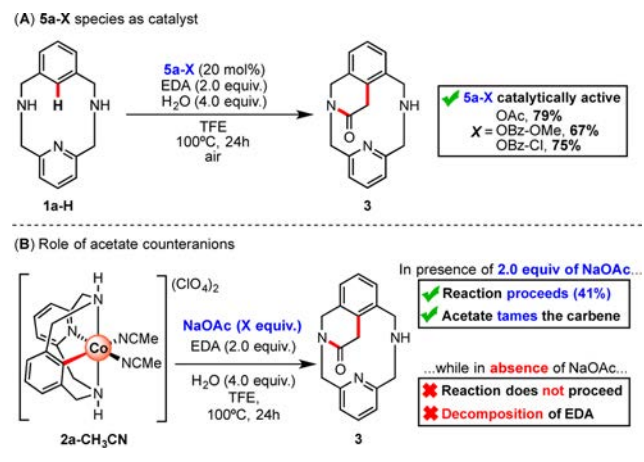
Scheme 2. (A) Evolution of **5a-OAc** to **3** with Additives and Rationalization of the Observed Reactivity and (B) Reactivity of Intermediate Bearing Electron-Poor Carboxylate **5a-TFA**



an activation of the carboxylate group through hydrogen bonding or coordination to Lewis acids, which converts it to a better leaving group. Indeed, when the organometallic aryl-Co(III) complex **2a-TFA**, which is bearing an electron-poor carboxylate group such as trifluoroacetate, was reacted with EDA (Scheme 2B), neither isolation nor detection of **5a-TFA** by HRMS was achieved and **3** was obtained in 79% yield in the absence of any external additive.

Furthermore, **5a-X** complexes can be used as catalysts (20 mol %), affording **3** in good yields (Scheme 3A), indicating that

Scheme 3. (A) Catalysis with **5a-X** and (B) Role of Acetate



organometallic **5a-X** complexes are catalytically active species. In order to test the role of carboxylate anions, the dicationic complex **2a-CH₃CN** was reacted with 2.0 equiv of EDA in TFE at 100 °C over 24 h (Scheme 3B and Table S3, entry 5). A complex mixture of decomposition products of EDA was obtained, suggesting the formation of a very reactive, unstable Co(III)-carbene intermediate. However, when 2.0 equiv of NaOAc was added (Table S3, entry 6), **3** was obtained in 41% yield. We hypothesize that when the Co(III) center is bearing a carboxylate moiety, carboxylate-masked aryl-Co(III) carbenoids species (**5a-X**) are formed, which highlights the key role of carboxylate anions in taming the reactivity of a putative highly electrophilic aryl-Co(III)-carbene intermediate.

Interestingly, **INT-MI** (Scheme 2A) could be detected by high-resolution mass spectrometry (HRMS) studies when MS/MS analysis was performed at the mass peak corresponding to **5a-X** (X = OBz-Cl, green; OBz-OMe, red; Figure 3). A single peak, which corresponds to a fragment involving the loss of carboxylic acid ($[\text{INT-MI-RCOOH}]^+ = \text{C}_{19}\text{H}_{21}\text{CoN}_3\text{O}_2^+$; $m/z = 382.0970$), was observed, regardless of the carboxylate moiety present in the isolated compounds (see also Scheme S11 and Figures S7–9). The relative intensity of **INT-MI'** at the same collision energy (15 eV) is higher when an electron-poor *p*-substituted benzoate is present in the molecule, supporting the *better-leaving-group* hypothesis presented above.

Further insight into the subsequent proto-demetalation of **INT-MI** was obtained by D-labeling experiments (Table 3). When **2a-OAc** was treated with EDA and 4.0 equiv of D₂O was added in TFE at 100 °C (Table 3, entry 1), a 36% D-incorporation was observed by NMR and HRMS analysis at the α position of the carbonyl group in **3**, in a stereoselective manner (Figures S10 and S11). Increasing D-incorporation was observed when H₂O (65%; Table 3, entry 2) and D₂O (86%;

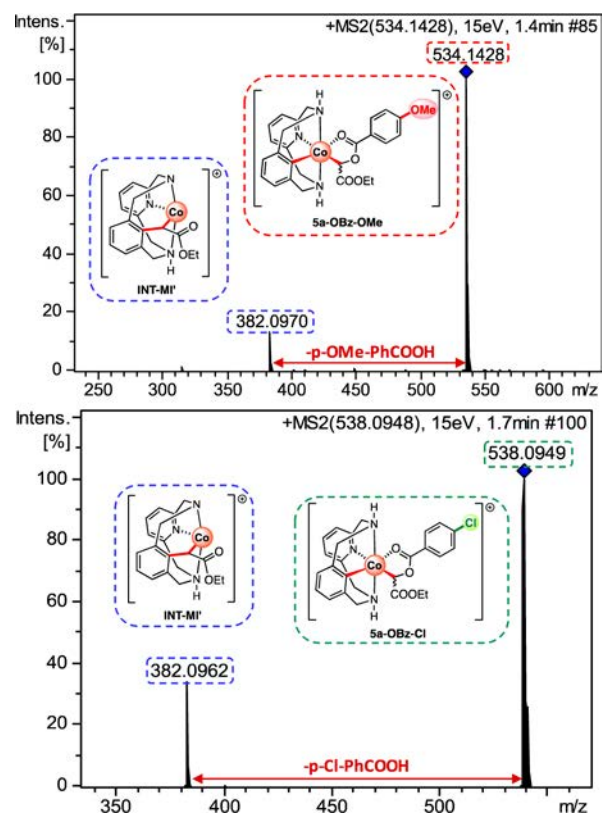
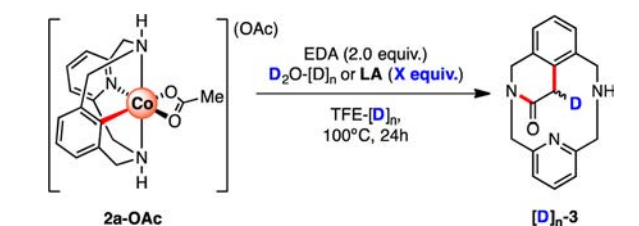


Figure 3. Detection of **INT-MI'** (experimentally obtained $m/z = 382.0970$; simulated $m/z = 382.0960$) by MS/MS studies of **5a-OBz-OMe** ($m/z = 534.1428$, top) and **5a-OBz-Cl** ($m/z = 538.0949$, bottom) organometallic intermediates.

Table 3. Deuterium-Labeling Experiments¹⁶



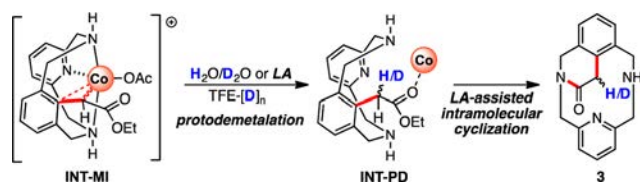
entry	additive (equiv)	solvent	D-incorporation (%) ^a
1	D ₂ O (4.0)	TFE	36%
2	H ₂ O (4.0)	TFE- <i>d</i> ₃	65%
3	D ₂ O (4.0)	TFE- <i>d</i> ₃	86%
4	Li(OTf) (1.0)	TFE- <i>d</i> ₃	91%
5	Li(OTf) (1.0)	MeOD- <i>d</i> ₄	93%

^aD-incorporation determined by ¹H NMR integration and HRMS analysis.

Table 3, entry 3) were added as additives in TFE-*d*₃ (Figures S12–S19).

These results suggest **INT-MI** is involved in a deuterio-demetalation step to furnish **INT-PD** in a stereoselective manner (Scheme 4), which is a strong evidence of the previous existence of a C_{sp³}-Co(III) bond. Interestingly, 91% (Table 3, entry 4) and 93% (Table 3, entry 5) D-labeled **3** were obtained when the reaction was performed in the absence of water but using 1.0 equiv of Li(OTf) in TFE-*d*₃ (Figures S16 and S17) and in MeOD-*d*₄ (Figure S18 and S19), respectively. These results suggest that Lewis acids may cooperate with the solvent, increasing its acidity as proton source and favoring a plausible

Scheme 4. Proposed Evolution of INT-MI to Product 3



proto-demetalation of INT-MI. After this step, as it was described in previously reported studies, INT-PD will evolve to 3 through a LA-assisted cyclization reaction in which Co(III) or the additive can act as catalyst (Scheme 4).⁷

Theoretical Studies. DFT studies (see Supporting Information for computational details) of the reaction profile in Figure 4 show that 2a-OAc reacts with EDA to form an

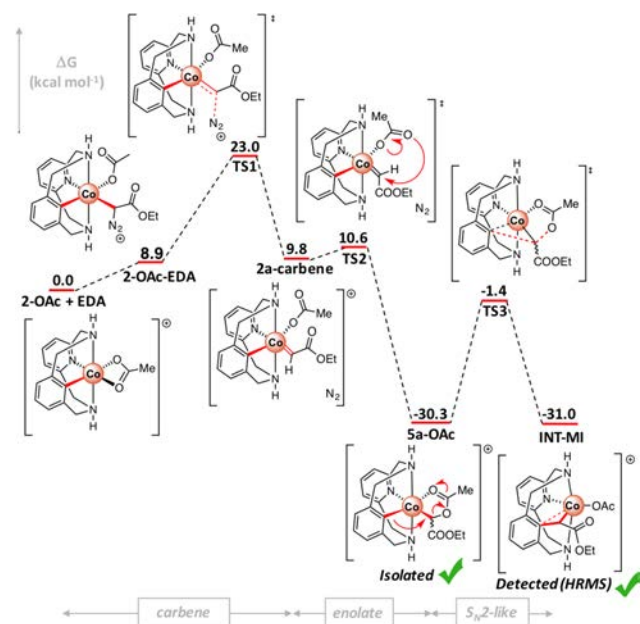


Figure 4. Gibbs energy profile of the reaction. Relative Gibbs energy values are given in kcal·mol⁻¹.

adduct (2a-OAc-EDA), in which the carboxylate ligand is now coordinated in a monodentate fashion. Then, 2a-carbene is obtained after a first transition state, TS1 ($\Delta G^\ddagger = 23$ kcal·mol⁻¹), with the concomitant liberation of N₂. However, the transient aryl-Co(III)-carbene falls to the isolated 5a-OAc organometallic species in an almost barrierless manner (TS2, $\Delta G^\ddagger = 0.8$ kcal·mol⁻¹). Indeed, depending on the DFT method, 2a-carbene cannot be optimized and TS1 directly evolves to the experimentally isolated 5a-OAc (Figure S23). Therefore, TS1 can be understood as a concerted asynchronous transition state that leads to the formation of the new C–Co and C–O bonds of 5a-OAc species. Then, in the absence of additives, 5a-OAc evolves to INT-MI, overcoming a barrier of $\Delta G^\ddagger = 28.9$ kcal·mol⁻¹ (TS3). Indeed, TS3 shows the cleavage of the C–O bond and formation of the new aryl–C bond in an S_N2-type transition state, in which the aryl–Co bond acts as a nucleophile and the acetate acts as a leaving group. Thus, this energetic profile supports the accumulation of 5a-OAc in the absence of water ($\Delta\Delta G^\ddagger(\text{TS3} - \text{TS1}) = 5.9$ kcal·mol⁻¹).

Water turned out to be tremendously beneficial for the reaction outcome, and therefore we considered the explicit

inclusion of a water molecule in the calculations (Figure 5). We hypothesized that the nucleophilic character of water could

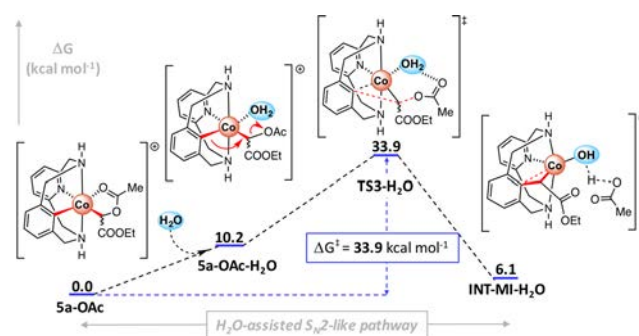


Figure 5. Gibbs energy profile of the S_N2-type step in the presence of H₂O. Relative Gibbs energy values are given in kcal·mol⁻¹ (see Figure S24 for details).

promote its coordination to the Co(III) center and enhance its Lewis acid character, favoring the S_N2-type event. However, when H₂O is coordinated to 5a-OAc, the carboxylate group is displaced and the overall energy of the resulting complex increases by 10.2 kcal·mol⁻¹ (5a-OAc-H₂O). Then, 5a-OAc-H₂O evolves into INT-MI-H₂O through the S_N2-like pathway with an activation barrier of $\Delta G^\ddagger = 33.9$ kcal·mol⁻¹ (TS3-H₂O), 5.0 kcal·mol⁻¹ higher than in the absence of water (TS3).

As the effect of an explicit water molecule coordinated to Co(III) on TS3 was not consistent with the experimental results, the addition of Lewis acids to 5a-X to obtain 3 was also investigated by DFT (Figure 6). Indeed, in the presence of 1.0

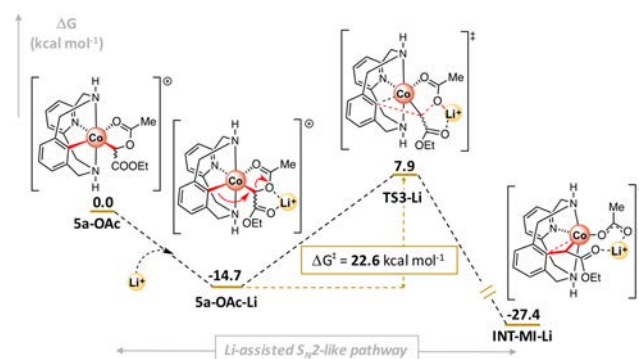


Figure 6. Gibbs energy profile of the S_N2-like step in the presence of Li⁺. Relative Gibbs energy values are given in kcal·mol⁻¹ (see Figure S25 for details).

equiv of Li(OTf) in anhydrous conditions, the reaction proceeded in excellent yields (see Table 1, entry 10). Thus, we considered the explicit inclusion of a lithium cation in the computational analysis of the C–O cleavage/C–C bond formation event. Strikingly, when a Li⁺ ion interacts with O2 and O3 (see Figure 1), the activation barrier for the S_N2-like pathway decreases by 6.3 kcal·mol⁻¹ ($\Delta\Delta G^\ddagger = 28.9$ (TS3, Figure 4) to 22.6 kcal·mol⁻¹ (TS3-Li, Figure 6)). Thus, when Lewis acids are added to the reaction media, they coordinate to the ester moieties in 5a-OAc, turning them into better leaving groups through an LA-mediated carboxylate activation.

This result suggests that the interaction of a Lewis acid with 5a-OAc triggers the concomitant C–O cleavage/C–C

formation event, probably by turning the carboxylate moiety into a better leaving group. Actually, when a weak base such as trifluoroacetate was used as counteranion (Figure 7), **5a-TFA**



Figure 7. Gibbs energy profile of the S_N2 -type step for **5a-TFA**. Relative Gibbs energy values are given in $\text{kcal}\cdot\text{mol}^{-1}$ (see Figure S26 for details).

evolved to **INT-MI-TFA**, overcoming a small activation barrier of $\Delta G^\ddagger = 19.7 \text{ kcal}\cdot\text{mol}^{-1}$ (**TS3-TFA**), which is similar to the barrier obtained when **5a-OAc** interacts with Li^+ (Figure 6). Thus, this result supports the beneficial effect of having a better carboxylate leaving group at the S_N2 -type step, as well as the *carboxylate-activation* observed when Lewis acids such as Li^+ are present in the reaction media.

Then, after the unprecedented Co(III)-mediated intramolecular S_N2 -type C–C bond formation in which the carboxylate moiety acts as a relay, **INT-MI** evolves to **3** through a protodemetalation step and a subsequent LA-assisted cyclization, as it has been observed experimentally. Furthermore, these results are supported by previously reported Co(III)-catalyzed protocols.⁷

CONCLUSIONS

In conclusion, unique C-metalated *cis*-aryl-Co(III)-alkyl enolate species (**5a-X**), which can be considered carbenoids, have been synthesized using EDA. Crystallographic, full spectroscopic characterization, and theoretical evidence show that masked-carbenes **5a-X** are necessary intermediates to deliver the alkyl fragment and elicit the new C–C bond, finally furnishing a six-membered cyclic amide product. To the best of our knowledge, this is the first example of a C-metalated aryl-Co(III)-alkyl enolate engaging in C–H functionalization reactions. Moreover, these species are proven to be catalytically active in the synthesis of final product **3**. DFT studies indicate that this transformation occurs through a unique intramolecular S_N2 -like pathway in which the carboxylate acts as a relay. The experimental key role of Lewis acids, particularly $\text{Li}(\text{OTf})$, is reflected in the theoretical studies, unveiling a Li-mediated carboxylate activation that triggers the C–O bond cleavage/C–C bond formation event. Efforts on transferring this reactivity to other catalytic systems are currently being performed in our laboratory.

ASSOCIATED CONTENT

Supporting Information

The Supporting Information is available free of charge on the ACS Publications website at DOI: 10.1021/jacs.7b07880.

Spectroscopic characterization of all compounds and computational details (PDF)

Crystallographic data for **5a-OBz-Cl** (CCDC 1545619) (CIF)

Crystallographic data for **5a-OBz-OMe** (CCDC 1545620) (CIF)

AUTHOR INFORMATION

Corresponding Author

*xavi.ribas@udg.edu

ORCID

Vlad Martin-Diaconescu: 0000-0002-7575-2237

Teodor Parella: 0000-0002-1914-2709

Xavi Ribas: 0000-0002-2850-4409

Notes

The authors declare no competing financial interest.

Crystallographic data for compounds **5a-OBz-Cl** (CCDC 1545619) and **5a-OBz-OMe** (CCDC 1545620) can be obtained free of charge from the Cambridge Crystallographic Data Center via www.ccdc.cam.ac.uk/data_request/cif.

ACKNOWLEDGMENTS

We acknowledge financial support from the European Research Council for the Starting Grant Project ERC-2011-StG-277801 to X.R. and from MINECO of Spain for project CTQ2016-77989-P to A.C. and X.R., project CTQ2014-52525-P to J.M.L., and project CTQ2015-64436-P to T.P. We also thank Generalitat de Catalunya for projects 2014SGR862 and 2014SGR931. We thank the MECED and MINECO of Spain for an FPU grant to O.P. and FPI grant to S.R. X.R. also thanks ICREA for an ICREA Acadèmia Award. We acknowledge SOLEIL for provision of synchrotron radiation facilities, and we would like to thank Dr. Landrot Gautier for assistance in using beamline SAMBA. We also thank STR from UdG for technical support.

REFERENCES

- (1) (a) Su, B.; Cao, Z.-C.; Shi, Z.-J. *Acc. Chem. Res.* **2015**, *48*, 886. (b) Pototshnig, G.; Maulide, N.; Schnürch, M. *Chem. - Eur. J.* **2017**, *23*, 9206.
- (2) For recent reviews on high-valent cobalt-catalyzed C–H activation, see: (a) Yoshino, T.; Matsunaga, S. *Adv. Synth. Catal.* **2017**, *359*, 1245. (b) Chirila, P. G.; Whiteoak, C. *J. Dalton Trans.* **2017**, *46*, 9721. (c) Wang, S.; Chen, S.-Y.; Yu, X.-Q. *Chem. Commun.* **2017**, *53*, 3165. (d) Moselage, M.; Li, J.; Ackermann, L. *ACS Catal.* **2016**, *6*, 498.
- (3) Jia, M.; Ma, S. *Angew. Chem., Int. Ed.* **2016**, *55*, 9134.
- (4) (a) Liu, J.; Hu, L.; Wang, L.; Chen, H.; Deng, L. *J. Am. Chem. Soc.* **2017**, *139*, 3876. (b) Wang, Y.; Wen, X.; Cui, X.; Wojtas, L.; Zhang, X. *J. Am. Chem. Soc.* **2017**, *139*, 1049. (c) Das, B. G.; Chirila, A.; Tromp, M.; Reek, J. N. H.; Bruin, B. d. *J. Am. Chem. Soc.* **2016**, *138*, 8968. (d) Lu, H.; Dzik, W. I.; Xu, X.; Wojtas, L.; de Bruin, B.; Zhang, X. *J. Am. Chem. Soc.* **2011**, *133*, 8518. (e) Ikeno, T.; Iwakura, I.; Yamada, T. *J. Am. Chem. Soc.* **2002**, *124*, 15152. (f) Brookhart, M.; Studabaker, W. B. *Chem. Rev.* **1987**, *87*, 411.
- (5) (a) Fructos, M. R.; Besora, M.; Braga, A. A. C.; Díaz-Requejo, M. M.; Maseras, F.; Pérez, P. *J. Organometallics* **2017**, *36*, 172. (b) Xia, Y.; Liu, Z.; Feng, S.; Zhang, Y.; Wang, J. *J. Org. Chem.* **2015**, *80*, 223. (c) Hu, F.; Xia, Y.; Ma, C.; Zhang, Y.; Wang, J. *Chem. Commun.* **2015**, *51*, 7986. (d) Hu, F.; Xia, Y.; Ye, F.; Liu, Z.; Ma, C.; Zhang, Y.; Wang, J. *Angew. Chem., Int. Ed.* **2014**, *53*, 1364. (e) Dötz, K. H.; Stendel, J. *Chem. Rev.* **2009**, *109*, 3227. (f) Davies, H. M. L.; Manning, J. R. *Nature* **2008**, *451*, 417.
- (6) For characterized cobalt–carbene species, see: (a) Bellow, J. A.; Stoian, S. A.; van Tol, J.; Ozarowski, A.; Lord, R. L.; Groysman, S. *J. Am. Chem. Soc.* **2016**, *138*, 5531. (b) Mondal, K. C.; Samuel, P. P.; Roesky, H. W.; Carl, E.; Herbst-Irmer, R.; Stalke, D.; Schwederski, B.; Kaim, W.; Ungur, L.; Chibotaru, L. F.; Hermann, M.; Frenking, G. *J.*

Am. Chem. Soc. **2014**, *136*, 1770. (c) Harrison, D. J.; Lee, G. M.; Leclerc, M. C.; Korobkov, I.; Baker, R. T. *J. Am. Chem. Soc.* **2013**, *135*, 18296. (d) Marquard, S. L.; Bezpalko, M. W.; Foxman, B. M.; Thomas, C. M. *J. Am. Chem. Soc.* **2013**, *135*, 6018. (e) Harrison, D. J.; Gorelsky, S. I.; Lee, G. M.; Korobkov, I.; Baker, R. T. *Organometallics* **2013**, *32*, 12 and references therein.

(7) (a) Yao, T.; Hirano, K.; Satoh, T.; Miura, M. *Angew. Chem., Int. Ed.* **2012**, *51*, 775. (b) Zhao, D.; Kim, J. H.; Stegemann, L.; Strassert, C. A.; Glorius, F. *Angew. Chem., Int. Ed.* **2015**, *54*, 4508. (c) Liu, X.-G.; Zhang, S.-S.; Wu, J.-Q.; Li, Q.; Wang, H. *Tetrahedron Lett.* **2015**, *56*, 4093. (d) Li, J.; Tang, M.; Zang, L.; Zhang, X.; Zhang, Z.; Ackermann, L. *Org. Lett.* **2016**, *18*, 2742. (e) Kim, J. H.; Greßies, S.; Glorius, F. *Angew. Chem., Int. Ed.* **2016**, *55*, 5577. (f) Baek, Y.; Kim, S.; Jeon, B.; Lee, P. H. *Org. Lett.* **2016**, *18*, 104. (g) Qu, S.; Cramer, C. J. *J. Org. Chem.* **2017**, *82*, 1195.

(8) For relevant examples of isolated alkyl- and aryl-Co(III) intermediates through organometallic C–H activation, see: (a) Maity, S.; Kancherla, R.; Dhawa, U.; Hoque, E.; Pimparkar, S.; Maiti, D. *ACS Catal.* **2016**, *6*, 5493. (b) Avilés, T.; Dinis, A.; Calhorda, M. J.; Pinto, P. c.; Félix, V.; Drew, M. G. B. *J. Organomet. Chem.* **2001**, *625*, 186. (c) Kanamori, K.; Broderick, W. E.; Jordan, R. F.; Willett, R. D.; Legg, J. I. *J. Am. Chem. Soc.* **1986**, *108*, 7122. (d) Broderick, W. E.; Kanamori, K.; Willet, R. D.; Legg, J. I. *Inorg. Chem.* **1991**, *30*, 3875.

(9) For examples of macrocyclic organometallic aryl–M compounds isolated and characterized in our group, see: (a) Font, M.; Acuña-Parés, F.; Parella, T.; Serra, J.; Luis, J. M.; Lloret-Fillol, J.; Costas, M.; Ribas, X. *Nat. Commun.* **2014**, *5*, 4373. (b) Casitas, A.; King, A. E.; Parella, T.; Costas, M.; Stahl, S. S.; Ribas, X. *Chem. Sci.* **2010**, *1*, 326.

(10) Planas, O.; Whiteoak, C. J.; Martin-Diaconescu, V.; Gamba, L.; Luis, J. M.; Parella, T.; Company, A.; Ribas, X. *J. Am. Chem. Soc.* **2016**, *138*, 14388.

(11) (a) Zhou, W.; Watson, M. B.; Zheng, S.; Rath, N. P.; Mirica, L. M. *Dalton Trans.* **2016**, *45*, 15886. (b) Zhou, W.; Rath, N. P.; Mirica, L. M. *Dalton Trans.* **2016**, *45*, 8693. (c) Zhou, W.; Zheng, S.; Schultz, J. W.; Rath, N. P.; Mirica, L. M. *J. Am. Chem. Soc.* **2016**, *138*, 5777. (d) Zhou, W.; Schultz, J. W.; Rath, N. P.; Mirica, L. M. *J. Am. Chem. Soc.* **2015**, *137*, 7604.

(12) For full evaluation of the stoichiometric reaction see [Table S1](#).

(13) For full evaluation of catalytic conditions see [Table S4](#).

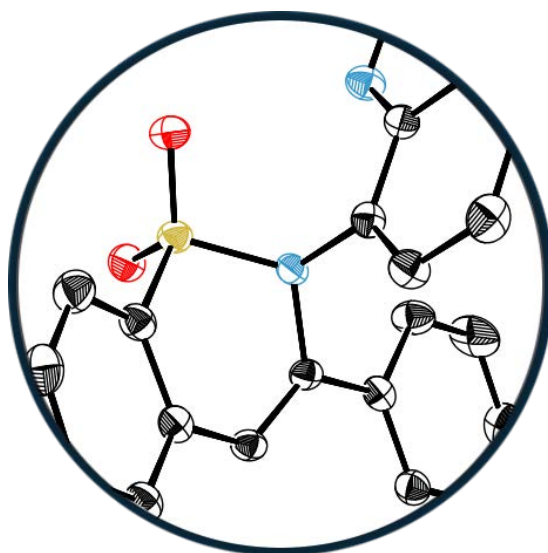
(14) **5a-OBz-Cl** presents a minor conformer in equilibrium with the major species (ratio major/minor = 4:1) in DMSO-*d*₆ ([Scheme S8](#)). However, the major conformer is favored in the presence of water and heat, as well as when mixed with 1.0 equiv of Zn(OTf)₂ ([Figures S4–6](#)).

(15) Werlé, C.; Goddard, R.; Philipps, P.; Farès, C.; Fürstner, A. *J. Am. Chem. Soc.* **2016**, *138*, 3797.

(16) For full spectroscopic and spectrometric data, see [Schemes S12 and S13](#) and [Figures S10–S19](#).

Chapter V

Regioselective Access to Sultam Motifs through Cobalt-Catalyzed Annulation of Aryl Sulfonamides and Alkynes using an 8- Aminoquinoline Directing Group



This chapter corresponds to the following publication:

Oriol Planas, Christopher J. Whiteoak, Anna Company and Xavi Ribas.

Adv. Synth. Catal. **2015**, *357*, 4003-4012.

For this publication O.P. synthesized and characterized starting materials and products and performed mechanistic experiments. C.W., A.C. and X.R. designed the project. Besides, O.P. contributed in writing the manuscript and was involved in argumentations and discussions.

Reproduced with permission from:

Oriol Planas, Christopher J. Whiteoak, Anna Company and Xavi Ribas . “Regioselective Access to Sultam Motifs through Cobalt-Catalyzed Annulation of Aryl Sulfonamides and Alkynes using an *c*-Aminoquinoline Directing Group”. *Advanced Synthesis & Catalysis*. Vol. 357 (2015) : 4003-4012.

<https://doi.org/10.1002/adsc.201500690>

© 2015 WILEY-VCH Verlag GmbH & Co. KGaA, Weinheim

Regioselective Access to Sultam Motifs through Cobalt-Catalyzed Annulation of Aryl Sulfonamides and Alkynes using an 8-Aminoquinoline Directing Group

Oriol Planas,^a Christopher J. Whiteoak,^{a,*} Anna Company,^a and Xavi Ribas^{a,*}

^a QBIS-CAT Research Group, Institut de Química Computacional i Catàlisi (IQCC) and Departament de Química, Universitat de Girona, Campus Montilivi, E-17071 Girona, Catalonia, Spain
E-mail: christopher.whiteoak@udg.edu or xavi.ribas@udg.edu

Received: July 20, 2015; Revised: September 25, 2015; Published online: November 25, 2015

Supporting information for this article is available on the WWW under <http://dx.doi.org/10.1002/adsc.201500690>.

Abstract: The use of cobalt as catalyst in direct C–H activation protocols as a replacement for more expensive second row transition metals is currently attracting significant attention. Herein we disclose a facile cobalt-catalyzed C–H functionalization route towards sultam motifs through annulation of easily prepared aryl sulfonamides and alkynes using 8-aminoquinoline as a directing group. The reaction shows broad substrate scope with products obtained in

a highly regioselective manner in good to excellent isolated yields. Mechanistic insights suggest the formation of a Co(III)-aryl key species *via* a rate-determining arene C–H activation during the annulation reaction.

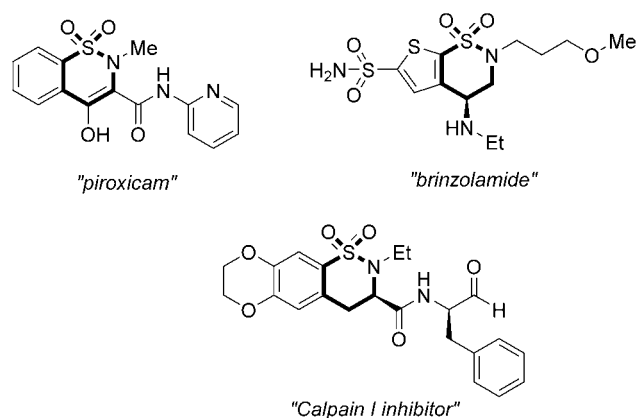
Keywords: alkynes; annulation; C–H activation; cobalt; regioselectivity; sulfonamides; sultams

Introduction

Direct C–H bond functionalization has revolutionized synthetic methodology providing new facile synthetic routes to access molecules which would otherwise require preparation through complex, time-consuming synthetic procedures.^[1] Sulfonamides have become an important motif in pharmaceutical drugs.^[2] In particular, cyclic sulfonamide motifs (sultams) have found use as anti-inflammatory drugs (piroxicam), carbonic anhydrase inhibitors used to lower intraocular pressure in patients with open-angle glaucoma or ocular hypertension (brinzolamide) and calpain I inhibitors in cell signalling dysfunctions (Scheme 1).^[3] A number of synthetic protocols towards sultams have been reported, although to date the majority of these methodologies start from elaborated precursors.^[4] The development of a simple metal-mediated C–H bond functionalization protocol starting from easily synthesized starting materials would provide a very appealing route towards the realization of sultam motifs.

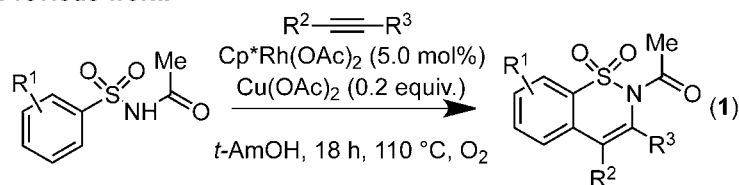
Historically, most C–H coupling protocols have been based on relatively expensive precious transition metals, for example Ru, Rh, Pd and Ir. More recently, attention has turned to the use of more abundant, cheaper first row transition metals, such as Fe,^[5] Co,^[6] Cu^[7] and Ni.^[8]

The use of alkynes in annulation reactions has become a very powerful tool for the construction of cyclic compounds. In particular, protocols using Rh,^[9] Ru,^[10] Cu,^[11] Pd^[12] and Ni^[13] have been reported for the preparation of a variety of heterocyclic compounds. In terms of the use of these annulation reactions for the realization of sultams, in 2012 Cramer and co-workers reported on a Rh-catalyzed protocol starting from aryl sulfonamides incorporating an acyl



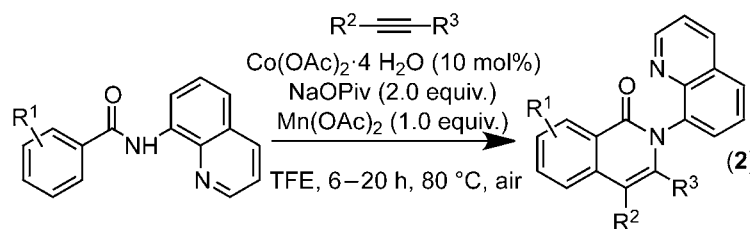
Scheme 1. Examples of pharmaceutical drugs containing cyclic sulfonamide (sultam) motifs.

Previous work:



- moderate to good regioselectivities with unsymmetrical alkynes

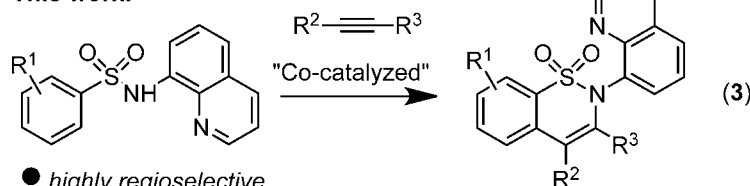
Cramer, 2012



- good to excellent regioselectivities with unsymmetrical alkynes

Daugulis, 2014

This work:



- highly regioselective

Scheme 2. (1) Previously reported Rh-catalyzed annulation of alkynes to aryl sulfonamides forming functionalized sultam motifs. (2) Co-catalyzed annulation of alkynes to aryl carboxamides. (3) Co-catalyzed annulation of aryl sulfonamides and alkynes forming functionalized sultam motifs reported herein.

directing group (Scheme 2.1).^[14] The catalyst system displayed a broad substrate scope, furnishing a range of sultam products in good to excellent yields. The limitation of this protocol was that when unsymmetrical alkynes were employed as coupling partners, both possible regioisomers were formed, with only moderate regioselectivities in some cases.

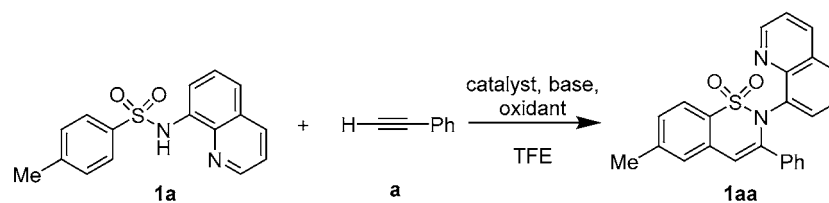
More recently, Daugulis and co-workers have shown that using Co-catalysis, alkynes can be annulated with aryl carboxamides containing an 8-aminoquinoline directing group (Scheme 2.2).^[61] The 8-aminoquinoline moiety has been shown to be a privileged directing group for a number of metal-catalyzed conversions.^[15] In this example the regioselectivities obtained using comparable unsymmetrical alkynes were considerably higher than for the Rh-catalyzed formation of sultams. For example, when 1-propynylbenzene was employed as coupling partner using the Rh-catalyzed protocol, both possible regioisomers were obtained in a 2:1 ratio, whereas in the Co-catalyzed example the regioselectivity is significantly enhanced at 14:1. With these precedents in mind we decided to investigate the possibility of realizing a Co-catalyzed aryl sulfonamide annulation with alkynes (Scheme 2.3), seeking improved regioselective control

compared with the previously described Rh-catalyzed protocol and to showcase the potential of using Co in annulation reactions.

Results and Discussion

Initially, we attempted the annulation of the aryl sulfonamide derived from *p*-toluenesulfonyl chloride and 8-aminoquinoline, **1a**, with phenylacetylene, **a**, in a variety of solvents using a catalytic system comprising of Co(OAc)₂ (20 mol%), KOAc (2 equiv.) and Mn(OAc)₂ (1 equiv.) at 100 °C for 24 h under an atmosphere of air. The observation of 22% of the desired aryl sultam product, **1aa**, using trifluoroethanol (TFE; found to be the optimal solvent, see the Supporting Information for solvent optimization) (Table 1, entry 1) prompted us to further optimize the synthetic protocol in terms of Co source, oxidant and base using this solvent.^[16]

A number of commonly used oxidants for cross-coupling protocols were investigated using Co(OAc)₂ and KOAc (Table 1, entries 1–7). It was found that the optimal oxidant among those tested was Mn(OAc)₃·2H₂O, which furnished a 62% yield of **1aa**

Table 1. Optimization of the reaction conditions,^[a]


Entry	Catalyst	Oxidant	Base	1aa [%] ^[b]
1	Co(OAc) ₂	Mn(OAc) ₂	KOAc	22
2	Co(OAc) ₂	benzoquinone	KOAc	< 1
3	Co(OAc) ₂	Ag ₂ O	KOAc	6
4	Co(OAc) ₂	AgNO ₃	KOAc	50
5	Co(OAc) ₂	PhI(OAc) ₂	KOAc	12
6	Co(OAc) ₂	Mn(OAc) ₃ ·2H ₂ O	KOAc	62
7	Co(OAc) ₂	O ₂	KOAc	3
8 ^[c]	Co(OAc) ₂	–	KOAc	< 1
9	Co(OAc) ₂	Mn(OAc) ₃ ·2H ₂ O	Na ₂ CO ₃	22
10	Co(OAc) ₂	Mn(OAc) ₃ ·2H ₂ O	K ₂ CO ₃	7
11	Co(OAc) ₂	Mn(OAc) ₃ ·2H ₂ O	Cs ₂ CO ₃	4
12	Co(OAc)₂	Mn(OAc)₃·2H₂O	NaOPiv·H₂O	91(90^[d])
13	Co(OAc) ₂	Mn(OAc) ₃ ·2H ₂ O	CsOPiv	78
14	Co(OAc) ₂	Mn(OAc) ₃ ·2H ₂ O	NaOAc·H ₂ O	67
15	Co(OAc) ₂	Mn(OAc) ₃ ·2H ₂ O	CsOAc	69
16	–	Mn(OAc) ₃ ·2H ₂ O	NaOPiv·H ₂ O	0
17	CoCl ₂	Mn(OAc) ₃ ·2H ₂ O	NaOPiv·H ₂ O	90
18	CoBr ₂	Mn(OAc) ₃ ·2H ₂ O	NaOPiv·H ₂ O	88
19	Co(NO ₃) ₂ ·6H ₂ O	Mn(OAc) ₃ ·2H ₂ O	NaOPiv·H ₂ O	81
20	Co(Cp) ₂	Mn(OAc) ₃ ·2H ₂ O	NaOPiv·H ₂ O	< 1
21	Co(acac) ₂	Mn(OAc) ₃ ·2H ₂ O	NaOPiv·H ₂ O	28
22	Co(acac) ₃	Mn(OAc) ₃ ·2H ₂ O	NaOPiv·H ₂ O	17
23	Co(OTf) ₂ (MeCN) ₂	Mn(OAc) ₃ ·2H ₂ O	NaOPiv·H ₂ O	31
24	Co(OAc) ₂ ·4H ₂ O	Mn(OAc) ₃ ·2H ₂ O	NaOPiv·H ₂ O	90
25	CoCl ₂ ·6H ₂ O	Mn(OAc) ₃ ·2H ₂ O	NaOPiv·H ₂ O	87

^[a] Reaction conditions: aryl sulfonamide (**1a**) (0.17 mmol), ethynylbenzene (**a**) (2.0 equiv.), Co source (20 mol%), oxidant (1.0 equiv.), base (2.0 equiv.), 2.0 mL TFE (trifluoroethanol) at 100 °C, under air for 24 h.

^[b] Yield calculated by ¹H NMR analysis of crude reaction mixture using mesitylene as internal standard.

^[c] Reaction prepared and performed under a N₂ atmosphere.

^[d] At 100 °C for 16 h.

(Table 1, entry 6). Importantly it was found that the addition of an oxidant is of significant importance as in its absence and under a nitrogen atmosphere, no product formation was observed (Table 1, entry 8). Thereafter, optimization of the base was studied (Table 1, entries 9–15), whereby it was found that a yield of 91% of product **1aa** could be obtained when using NaOPiv·H₂O (Table 1, entry 12). Finally the Co source was optimized (Table 1, entries 17–22), where it was found that Co(OAc)₂ was the optimal Co source (Table 1, entry 12). It was also observed that there is little difference between the use of anhydrous and hydrated Co sources [see, for example, Table 1, entries 17 and 25; CoCl₂ and CoCl₂·4H₂O or Table 1, entries 12 and 24; Co(OAc)₂ and Co(OAc)₂·6H₂O], indicating tolerance of the catalyst system to the presence of water. In the absence of Co

the reaction did not proceed at all and the starting aryl sulfonamide, **1a**, could be fully recovered (Table 1, entry 16). Final optimization of the reaction time and temperature set the preferred experimental conditions at 100 °C and 16 h for further substrate scoping (see the Supporting Information). These reaction conditions are similar to those identified by Daulgis and co-workers for the Co-catalyzed conversion of aryl carboxamide substrates,^[61] except for the clear beneficial use of Mn(OAc)₃ instead of Mn(OAc)₂ with our sulfonamide substrates. Detailed inspection of the ¹H NMR of the final product confirmed the presence of a single regioisomer. The absolute configuration of **1aa** was established from the structure obtained from X-ray crystallography studies (Figure 1).

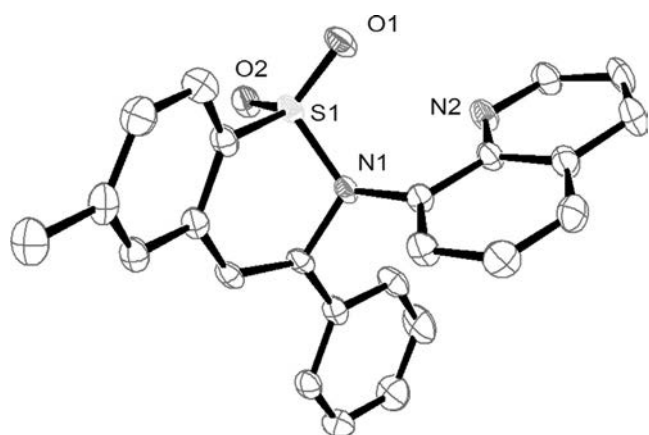
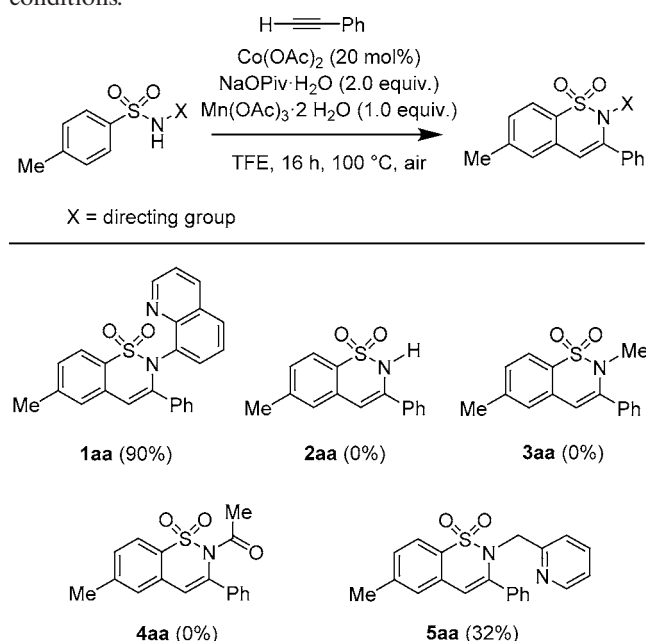


Figure 1. X-ray structure obtained for compound **1aa**, hydrogen atoms omitted for clarity. For full details see the Supporting Information.

With these optimal reaction conditions in hand, we investigated the importance of the 8-aminoquinoline directing group. The results obtained (Table 2) show that the 8-aminoquinoline directing group gives superior yields compared to when no directing group is used (0%) or when acetyl (0%) and pyridyl (32%);

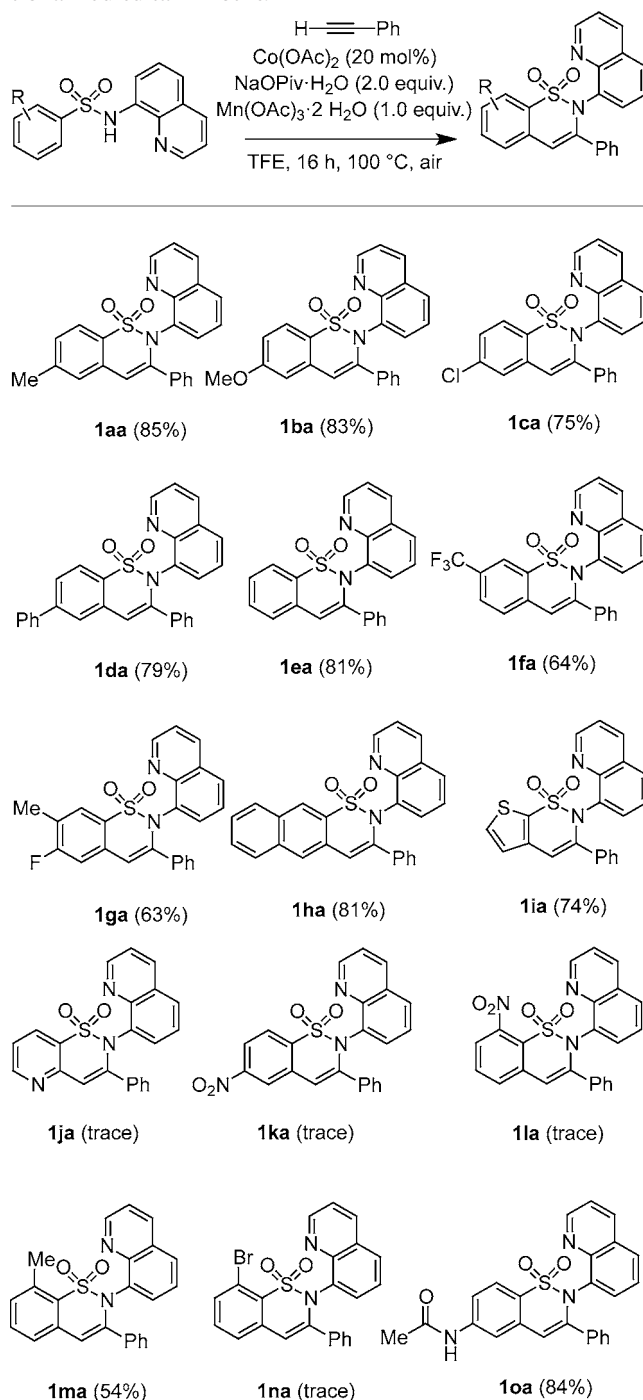
Table 2. Screening of aryl sulfonamides (**1a–5a**) with/without different directing groups (X) using the optimized reaction conditions.^[a,b]



^[a] Reaction conditions: aryl sulfonamide (**1a–5a**) (0.17 mmol), alkyne (**a**) (2.0 equiv.), Co(OAc)₂ (20 mol%), Mn(OAc)₃·2H₂O (1.0 equiv.), NaOPiv·H₂O (2.0 equiv.), 2.0 mL TFE (trifluoroethanol) at 100 °C, under air for 16 h.

^[b] Yield calculated by ¹H NMR analysis of crude reaction mixture using mesitylene as internal standard.

Table 3. Scope of Co-catalyzed coupling of phenylacetylene (**a**) to aryl sulfonamide derivatives (**1a–1o**) forming functionalized sultam motifs.^[a,b]



^[a] Reaction conditions: aryl sulfonamide (**1a–1o**) (0.35 mmol), alkyne (**a**) (2.0 equiv.), Co(OAc)₂ (20 mol%), Mn(OAc)₃·2H₂O (1.0 equiv.), NaOPiv·H₂O (2.0 equiv.), 2.0 mL TFE (trifluoroethanol) at 100 °C, under air for 16 h.

^[b] Isolated yields obtained after purification by column chromatography.

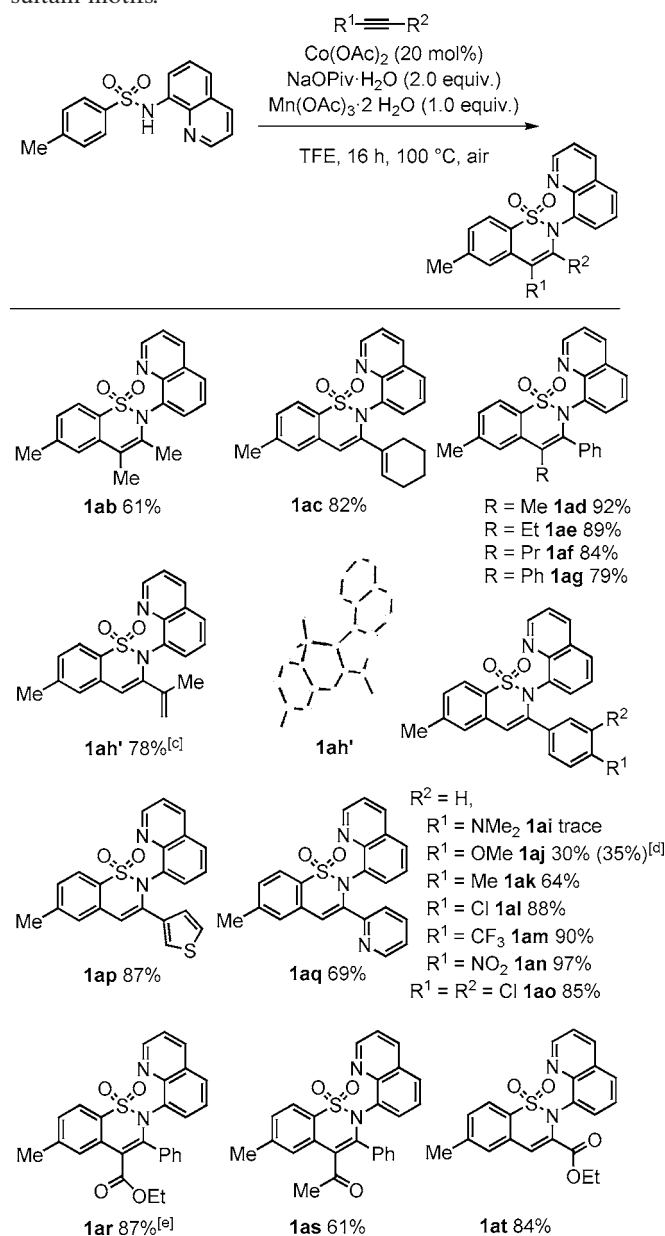
single regioisomer) directing groups are present under these conditions. The absence of activity when using the acetyl directing group is in sharp contrast to the Rh-catalyzed protocol reported by Cramer and co-workers.^[14]

Next, the scope of the newly optimized protocol was probed using different aryl sulfonamide derivatives, which were easily prepared from 8-aminoquinoline and the requisite sulfonyl chloride. These studies furnished functionalized sultam motifs in good to excellent yields (Table 3). In all cases the crude reaction mixtures displayed three well defined species when analyzed by TLC, corresponding to starting aryl sulfonamide, residual alkyne and sultam product. The product isolated after column chromatography was found to contain only a single regioisomer. Trace amounts of other regioisomers were only observed in the formation of **1da** and **1ga** (see the Supporting Information). The highest yields were obtained with derivatives containing electron-donating groups (up to 85% isolated yield), whilst those containing electron-withdrawing substituents furnished lower yields (e.g., **1fa** was obtained in only 64% yield and **1ka**, **1la**, **1na** were obtained in only trace amounts). We were also able to obtain the sultam containing a thiophene moiety (**1ia**), although only traces of sultam product were obtained when the pyridine derivative was employed (**1ja**), demonstrating some limitations to the substrate scope. When the substituents are present in the *ortho*-position to the sulfonamide reduced yields are obtained, likely as a result of the blocking of one of the C–H bonds to activation (for example, see **1aa** and **1ma**, whereby changing the position of the methyl group decreases the isolated yield from 85% to 54%, respectively, Table 3).

Substrates that failed to give satisfactory product yields were then included in poisoning experiments in order to see if the substrate was inhibiting the reaction or if the reaction rate was comparatively slower with these substrates. One equivalent of **1j**, **1k**, **1l** or **1n** was included in reactions respectively for the conversion of **1a** to **1aa** (see the Supporting Information for details). It was found that indeed in all cases these substrates are poisoning the catalyst system, resulting in decreased yields of **1aa**. This type of poisoning has recently been described by Glorius and co-workers.^[17] We propose that the poisoning observed in our studies arises from poorly reversible coordination of the Co to the substrate.

Following screening with substituted aryl sulfonamides, we turned our attention to the use of differently substituted alkynes (Table 4). Again the catalyst system displayed broad substrate tolerance for a variety of functional groups and again high regioselectivities were observed as confirmed by the presence of only one species in the ¹H NMR in most cases. When an ester substituent was present in the alkyne (**1ar**)

Table 4. Scope of Co-catalyzed coupling of substituted alkynes (**b–t**) to aryl sulfonamide (**1a**) forming functionalized sultam motifs.^[a,b]



^[a] Reaction conditions: aryl sulfonamide **1a** (0.35 mmol), acetylene derivatives (**b–t**) (2.0 equiv.), $Co(OAc)_2$ (20 mol%), $Mn(OAc)_3 \cdot 2H_2O$ (1.0 equiv.), $NaOPiv \cdot H_2O$ (2.0 equiv.), 2.0 mL TFE (trifluoroethanol) at 100 °C, under air for 16 h.

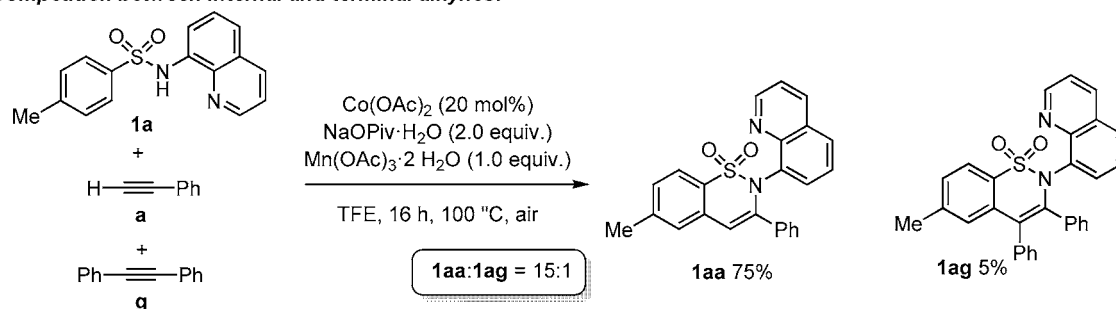
^[b] Isolated yields obtained after purification by column chromatography.

^[c] Product derived from 3-chloro-3-methylbut-1-yne.

^[d] Reaction at 100 °C for 40 h.

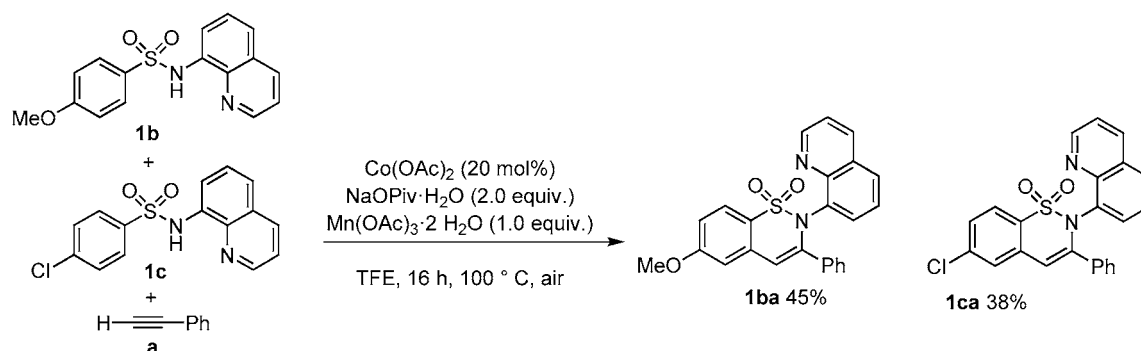
^[e] Combined yield of both regioisomers. Regioisomers obtained in a ratio of 3:1; major regioisomer depicted (see the Supporting Information for X-ray crystal structure obtained).

(1) Competition between internal and terminal alkynes:^[a,b]



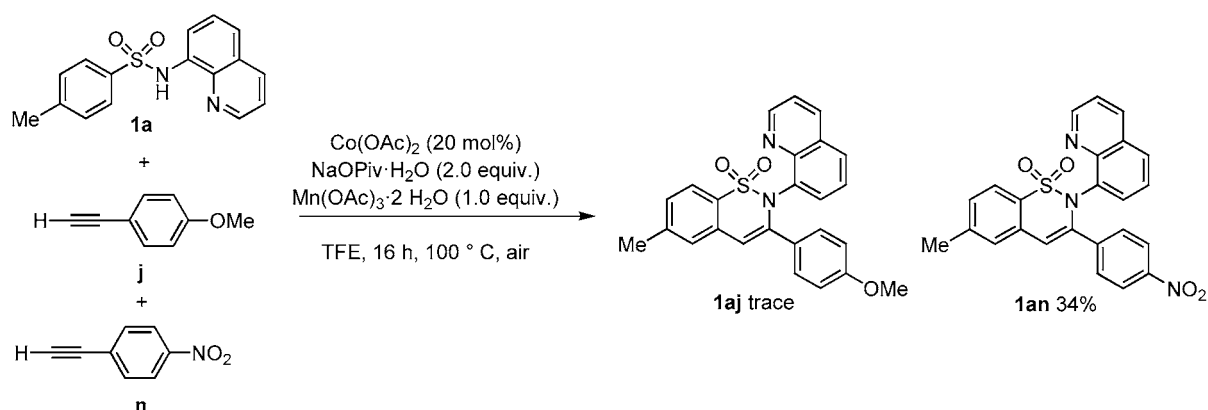
(2.0 equiv. of each alkyne with respect to aryl sulfonamide)

(2) Competition between differently substituted aryl sulfonamides:^[c,d]



(2.0 equiv. of each aryl sulfonamide with respect to alkyne)

(3) Competition between differently substituted alkynes:^[e,f]



(2.0 equiv. of each alkyne with respect to aryl sulfonamide)

[a] Aryl sulfonamide **1a** (0.35 mmol), phenylacetylene derivatives (2.0 equiv. of **a** and 2.0 equiv. of **g**), 2.0 mL TFE.

[b] Yields based on **1a**.

[c] Aryl sulfonamide **1b** and **1c** (0.70 mmol of each), phenylacetylene derivatives (0.35 mmol, 0.25 equiv. of **a** with respect to combined aryl sulfonamide), 2.0 mL TFE.

[d] Yields based on **a**.

[e] Aryl sulfonamide **1a** (0.35 mmol), phenylacetylene derivatives (2.0 equiv. of **j** and 2.0 equiv. of **n**), 2.0 mL TFE.

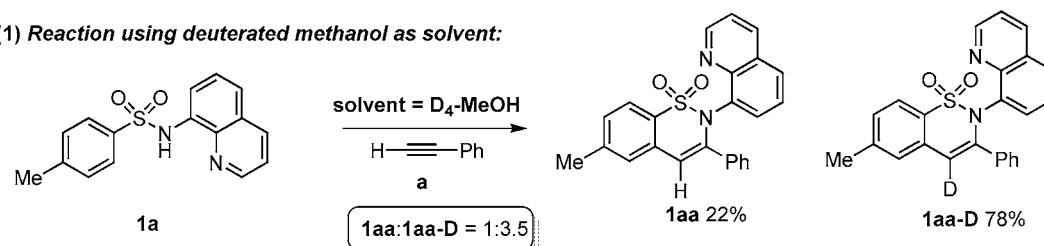
[f] Yields based on **1a**.

Scheme 3. Intermolecular competition reactions under optimized reaction conditions; yields calculated by ¹H NMR analysis of crude reaction mixture using mesitylene as internal standard.

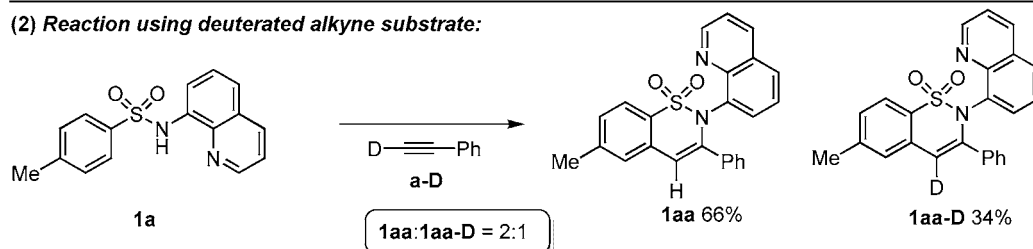
both possible regioisomers were identified (the TLC displayed a single spot for a combination of the two regioisomers). The major regioisomer could be separated from the minor regioisomer by recrystallization

and was fully characterized (see the Supporting Information). Unexpectedly, when using 3-chloro-3-methylbut-1-yne as substrate (**h**), the product was obtained (**1ah'**) whereby hydrogen chloride had been eliminat-

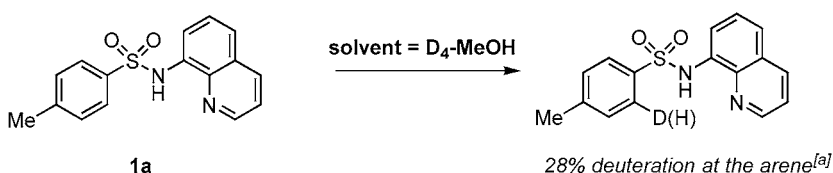
(1) Reaction using deuterated methanol as solvent:



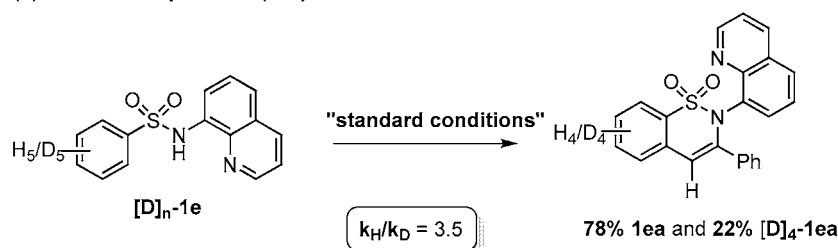
(2) Reaction using deuterated alkyne substrate:



(3) Reaction using deuterated methanol as solvent, without alkyne substrate:



(4) Kinetic isotope effect (KIE):



^[a] See the Supporting Information for full details.

Scheme 4. Deuterium labelling experiments: *Reaction conditions:* aryl sulfonamide **1a** (0.35 mmol), phenylacetylene (**a**) (2.0 equiv.), $\text{Co}(\text{OAc})_2$ (20 mol%), $\text{Mn}(\text{OAc})_3 \cdot 2\text{H}_2\text{O}$ (1.0 equiv.), $\text{NaOPiv} \cdot \text{H}_2\text{O}$ (2.0 equiv.), 2.0 mL solvent at 100 °C, under air for 16 h. KIE experiment: 0.17 mmol of both **1e** and **D₅-1e**, phenylacetylene (**a**) (2.0 equiv.), $\text{Co}(\text{OAc})_2$ (20 mol%), $\text{Mn}(\text{OAc})_3 \cdot 2\text{H}_2\text{O}$ (1.0 equiv.), $\text{NaOPiv} \cdot \text{H}_2\text{O}$ (2.0 equiv.), 2.0 mL solvent at 100 °C, under air for 16 h. Yields reported are percentage of isolated compounds obtained after purification by column chromatography.

ed. When electron-donating substituents are present on the aryl group of phenylacetylene the reaction resulted in low or trace yields (trace amounts and 30% for **1ai** and **1aj**, respectively). In the case of **1aj**, even after an extended reaction time the yield was not significantly improved.

The effectiveness of this transformation was further checked by performing a gram-scale reaction to obtain **1aa** and **1al**, furnishing 64% (0.87 g) and 61% (0.89 g), respectively (see the Supporting Information).

In order to further compare the reactivities of the substrates under the optimized protocol, we performed intermolecular competition reactions

(Scheme 3). When two equivalents of both a terminal (**a**) and an internal (**g**) alkyne were included it was found that insertion of the terminal alkyne was significantly favored, resulting in a product ratio of 15:1 for terminal and internal alkyne insertion, respectively (Scheme 3.1). Thereafter we also ran competition reactions using differently substituted aryl sulfonamide and phenylacetylene substrates (Scheme 3.2 and Scheme 3.3, respectively). As expected, in agreement with the results obtained from the substrate screening, reaction with electron-donating aryl sulfonamides (methoxy, **1b**) was found to be slightly favored over electron-withdrawing (chloro, **1c**) aryl sulfonamides. Likewise, insertion of the *p*-nitrophenylacetylene (**n**)

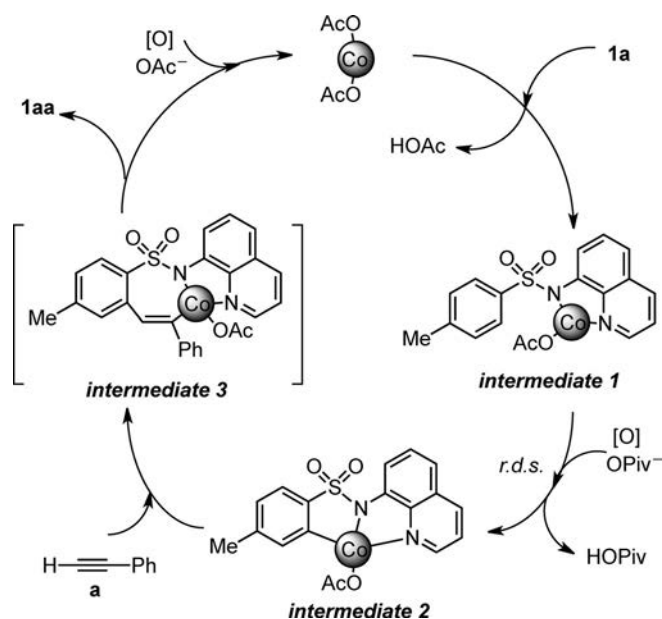
was favored over *p*-methoxyphenylacetylene (**j**). The latter competition reaction only yielded 34% of the *p*-nitro product (**1an**), whereas in the absence of the competing *p*-methoxyphenylacetylene during substrate screening we obtained 97% isolated yield. This result suggests that the *p*-methoxyphenylacetylene is inhibiting the reaction to some extent. This inhibition is similar to the result obtained by Ackermann and co-workers during their intermolecular competition reactions.^[6r]

We also performed a range of deuterium exchange reactions (Scheme 4). We found that when the reaction was performed in D₄-methanol the final sultam product was 78% deuterated on the sultam motif (Scheme 4.1). Likewise, when deuterated phenylacetylene was used as substrate we observed 66% of ¹H incorporation into the sultam product (Scheme 4.2). These results indicate that the proton/deuterium of the terminal alkyne likely exchanges with the solvent under the basic reaction conditions.

Additionally, we performed a reaction in the absence of alkyne in D₄-methanol (Scheme 4.3). At the end of the reaction we observed a low inclusion of deuterium in the starting sulfonamide, suggesting the deuterio-demetalation of a putative aryl-Co intermediate species (see the Supporting Information). This is further supported by the kinetic isotope effect (KIE) of 3.5 calculated when including both **1e** and **D₅-1e** in the reaction (Scheme 4.4). The value obtained is consistent with C–H activation being the rate-determining step in the reaction.

The exact mechanisms of Co-catalyzed C–H activation protocols are still not fully understood. Recently, Niu, Song and co-workers identified the presence of radicals using EPR spectroscopy in their Co-catalyzed alcohol coupling protocol.^[6m] This was further evidenced by the lack of activity when the radical scavenger 2,2,6,6-tetramethylpiperidine 1-oxyl (TEMPO) was included (see the Supporting Information). We therefore included several different radical scavengers [BHT, AIBN and P(OEt)₃] in our reactions and found that activity was almost completely inhibited in agreement with this previous work, suggesting that our reaction likely proceeds through radical intermediates in some steps of the mechanism.

We propose a mechanism (Scheme 5) in which initially the Co(OAc)₂ chelates to the quinoline directing group and to the sulfonamide of the substrate, **1a**, (intermediate 1) releasing one equivalent of acetic acid. The aminoquinoline coordination environment favors the stabilization of high-valent Co species; we therefore propose that once coordinated to the aryl sulfonamide substrate the Co(II) undergoes oxidation to Co(III) using oxygen as the terminal oxidant. Indeed our studies show that the presence of oxygen is highly beneficial for the process to proceed (see the Supporting Information). Subsequently, this Co(III) inter-



Scheme 5. Proposed mechanistic cycle (**1a** substrate is shown as example).

mediate can activate the aryl C–H bond through a concerted metallation deprotonation (CMD) type process as a result of its higher electrophilicity of Co(III) compared with Co(II), giving rise to intermediate 2, although at this point other activation processes cannot be completely discarded.^[18] An analogous Co(III) species was isolated and characterized by Daugulis and co-workers using Co(II) precursors for their analogous aryl carboxamide substrates.^[6l] KIE experiments indicate that this challenging C–H activation event is the rate-determining step of the reaction (Scheme 4.4). Subsequently, insertion of the alkyne, **a**, into the Co(III)-aryl bond results in the transient intermediate 3. Finally, elimination of Co(I) which is then reoxidized to Co(OAc)₂, provides the desired sultam product, **1aa**. As suggested by the radical scavenger experiments described above, some steps of the catalytic cycle may involve radical intermediates. We propose that the improved regioselectivity when using Co catalysts compared with the Rh catalyst reported by Cramer for sultam formation probably arises from the fact that there is poor interference of the Cp* ligand in the alkyne insertion into the Rh(III)-aryl bond.^[14]

Finally, we attempted to upgrade the products obtained by removing the 8-aminoquinoline directing group (see the Supporting Information for details), although to date we have not been successful. The removal of 8-aminoquinoline directing groups has been reported to be possible using ammonia if the annulated product contains carbonyl functionalities at either side of the 8-aminoquinoline, in similarity to the final step of the Gabriel synthesis of amines.^[6n,19] If two ad-

jacent carbonyl functionalities are not present, the directing group can be removed using cerium(IV) ammonium nitrate (CAN) only if the 5-methoxy-8-aminoquinoline is used.^[20] However, the CAN strategy does not always work using this elaborated directing group^[21] as well as in our compounds. We also attempted a H₂:Pd(0)/C reduction, but only the pyridinic moiety of the 8-aminoquinoline was reduced to afford **1aaH₄** (see the Supporting Information). We also tried reduction with a stronger reducing agent such as SmI₂, but a complex mixture of products was obtained. Our next goal is to develop a facile methodology for the 8-aminoquinoline directing group removal or extrapolate the reported reactivity to more easily removable directing groups.

Conclusions

In summary, we have reported on a new Co-catalyzed protocol for the synthesis of sultam motifs starting from easily prepared aryl sulfonamides and alkynes. The protocol permits the use of a broad range of substituted aryl sulfonamides and alkynes, as well as displaying excellent regioselectivities compared with the previously reported Rh-catalyzed protocol, where moderate regioselectivity was found.^[14] This protocol demonstrates the increasing potential of Co to replace more expensive second row transition metals as a result of favorable reactivities and selectivities.^[22]

Experimental Section

General Considerations

All reagents and solvents were purchased from Sigma Aldrich, Fisher Scientific or Fluorochem and used without further purification. Aryl sulfonamide (**2a**) was purchased from Sigma Aldrich, all other substrates were synthesized as described in the Supporting Information. ¹H and ¹³C {¹H} NMR spectra were recorded on Bruker AV-300 or Bruker DPX 400 MHz spectrometers and referenced to the residual deuterated solvent signals. High resolution mass spectra (HR-MS) were recorded by the Serveis Tècnics of the University of Girona on a Bruker MicroTOF-Q IITM instrument using an ESI ionization source. IR spectra (FT-IR) were recorded on an FT-IR Alpha spectrometer from Bruker with a PLATINUM-ATR attachment using OPUS software to process the data

Typical Optimized Procedure for Synthesis of Sultam Compounds

Aryl sulfonamide (0.35 mmol), Co(OAc)₂ (12.4 mg, 20 mol%, 0.07 mmol), NaOPiv·H₂O (86.8 mg, 2.0 equiv., 0.70 mmol), Mn(OAc)₃·2H₂O (94.0 mg, 1.0 equiv., 0.35 mmol), alkyne substrate (2.0 equiv., 0.70 mmol) and 2 mL of trifluoroethanol were added to a glass vial under air

and the vial was subsequently sealed. The resulting mixture was stirred at 100 °C for 16 h and thereafter cooled to room temperature. The solvent was removed and the product purified using column chromatography (silica gel: dichloromethane). After purification the product was dried under reduced pressure.

Full characterization data obtained (including original ¹H, ¹³C {¹H} and COSY NMR spectra for all sultam products) can be found in the Supporting Information. CCDC 1407285 (**1aa**), CCDC 1407286 (**1ah'**), CCDC 1411541 (**1ar**) and CCDC 1407287 (**1aaH₄**) contains the supplementary crystallographic data for this paper. These data can be obtained free of charge from The Cambridge Crystallographic Data Centre via www.ccdc.cam.ac.uk/data_request/cif.

Acknowledgements

We acknowledge financial support from the ERC for the Starting Grant Project ERC-2011-StG-277801 to X.R. and MINECO of Spain for CTQ2013-43012-P to X.R. and A.C. and a RyC contract to A.C. We thank the MECED for a FPU PhD grant to O.P. X.R. also thanks ICREA for an ICREA-Acadèmia award. We are also grateful to X. Fontrodona (X-ray crystallography), Dr. L. Gómez (HR-MS) and STR-UdG.

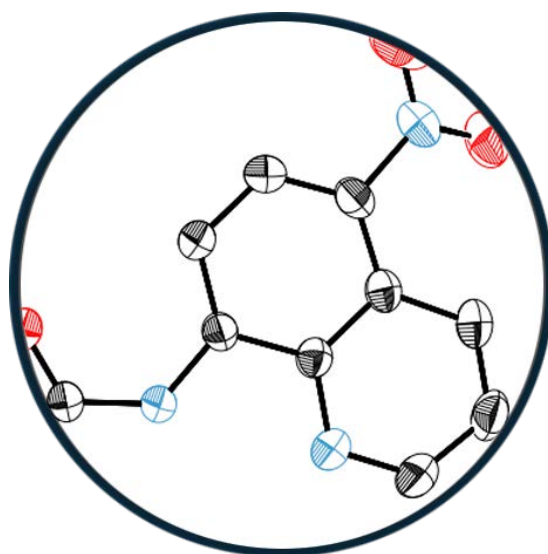
References

- [1] a) *C–H Activation*, (Eds.: J.-Q. Yu, Z. Shi), Vol. 292, Springer-Verlag, Berlin, **2010**; b) J. Yamaguchi, A. D. Yamaguchi, K. Itami, *Angew. Chem.* **2012**, *124*, 9092; *Angew. Chem. Int. Ed.* **2012**, *51*, 8960; c) J. Wencel-Delord, F. Glorius, *Nature Chem.* **2013**, *5*, 369; d) T. W. Lyons, M. S. Sanford, *Chem. Rev.* **2010**, *110*, 1147; e) K. Godula, D. Sames, *Science* **2006**, *312*, 67; f) J. J. Mousseau, A. B. Charette, *Acc. Chem. Res.* **2013**, *46*, 412; g) X. Chen, K. M. Engle, D.-H. Wang, J.-Q. Yu, *Angew. Chem.* **2009**, *121*, 5196; *Angew. Chem. Int. Ed.* **2009**, *48*, 5094; h) A. E. Shilov, G. B. Shul'pin, *Chem. Rev.* **1997**, *97*, 2879; i) C. Jia, T. Kitamura, Y. Fujiwara, *Acc. Chem. Res.* **2001**, *34*, 633; j) C. S. Yeung, V. M. Dong, *Chem. Rev.* **2011**, *111*, 1215; k) *C–H and C–X Bond Functionalization*, in: *Transition Metal Mediation*, (Ed.: X. Ribas), RSC Catalysis, Series No. 11, **2013**.
- [2] S. S. Shah, G. Rivera, M. Ashfaq, *Mini. Rev. Med. Chem.* **2013**, *13*, 70.
- [3] a) J. G. Lombardino, E. H. Wiseman, W. Mclamore, *J. Med. Chem.* **1971**, *14*, 1171; b) L. De Santis, *Surv. Ophthalmol.* **2000**, *44*, S119; c) G. J. Wells, M. Tao, K. A. Josef, R. J. Bihovsky, *J. Med. Chem.* **2001**, *44*, 3488.
- [4] For some examples of current methods for the synthesis of sultams, see: a) V. A. Rassadin, D. S. Grosheva, A. A. Tomashevskii, V. V. Sokolov, *Chem. Heterocycl. Compd.* **2013**, *49*, 39; b) K. C. Majumdar, *RSC Adv.* **2011**, *1*, 1152; c) S. Merten, R. Fröhlich, O. Kataeva, P. Metz, *Adv. Synth. Catal.* **2005**, *347*, 754; d) X.-Y. Liu, C.-H. Li, C.-M. Che, *Org. Lett.* **2006**, *8*, 2707; e) M. Jiménez-Hopkins, P. R. Hanson, *Org. Lett.* **2008**, *10*,

- 2223; f) K. Kaneko, T. Yoshino, S. Matsunaga, M. Kanai, *Org. Lett.* **2013**, *15*, 2502.
- [5] For examples, see: X. Sun, J. Li, X. Huang, C. Sun, *Curr. Inorg. Chem.* **2012**, *2*, 64.
- [6] For recent examples, see: a) Z. Ding, N. Yoshikai, *Angew. Chem.* **2013**, *125*, 8736; *Angew. Chem. Int. Ed.* **2013**, *52*, 8574; b) P.-S. Lee, N. Yoshikai, *Angew. Chem.* **2013**, *125*, 1278; *Angew. Chem. Int. Ed.* **2013**, *52*, 1240; c) B. Wu, M. Santra, N. Yoshikai, *Angew. Chem.* **2014**, *126*, 7673; *Angew. Chem. Int. Ed.* **2014**, *53*, 7543; d) T. Andou, Y. Saga, H. Komai, S. Matsunaga, M. Kanai, *Angew. Chem.* **2013**, *125*, 3295; *Angew. Chem. Int. Ed.* **2013**, *52*, 3213; e) H. Ikemoto, T. Yoshino, K. Sakata, S. Matsunaga, M. Kanai, *J. Am. Chem. Soc.* **2014**, *136*, 5424; f) B. Sun, T. Yoshino, S. Matsunaga, M. Kanai, *Adv. Synth. Catal.* **2014**, *356*, 1491; g) T. Yoshino, H. Ikemoto, S. Matsunaga, M. Kanai, *Angew. Chem.* **2013**, *125*, 2263; *Angew. Chem. Int. Ed.* **2013**, *52*, 2207; h) W. Song, L. Ackermann, *Angew. Chem.* **2012**, *124*, 8376; *Angew. Chem. Int. Ed.* **2012**, *51*, 8251; i) J. Li, L. Ackermann, *Chem. Eur. J.* **2015**, *21*, 5718; j) J. Li, L. Ackermann, *Angew. Chem.* **2015**, *127*, 3706; *Angew. Chem. Int. Ed.* **2015**, *54*, 3635; k) W. Ma, L. Ackermann, *ACS Catal.* **2015**, *5*, 2822; l) L. Ackermann, *J. Org. Chem.* **2014**, *79*, 8948; m) B. Punji, W. Song, G. A. Shevchenko, L. Ackermann, *Chem. Eur. J.* **2013**, *19*, 10605; n) A. B. Pawar, S. Chang, *Org. Lett.* **2015**, *17*, 660; o) D. Zhao, J. H. Kim, L. Stegemann, C. A. Strassert, F. Glorius, *Angew. Chem.* **2015**, *127*, 4591; *Angew. Chem. Int. Ed.* **2015**, *54*, 4508; p) T. Gensch, S. Vásquez-Céspedes, D.-G. Yu, F. Glorius, *Org. Lett.* **2015**, *17*, 3714; q) D.-G. Yu, T. Gensch, F. de Azambuja, S. Vásquez-Céspedes, F. Glorius, *J. Am. Chem. Soc.* **2014**, *136*, 17722; r) L.-B. Zhang, X.-Q. Hao, S.-K. Zhang, Z.-J. Liu, X.-X. Zheng, J.-F. Gong, J.-L. Niu, M.-P. Song, *Angew. Chem.* **2015**, *127*, 274; *Angew. Chem. Int. Ed.* **2015**, *54*, 272; s) L. Grigorjeva, O. Daugulis, *Org. Lett.* **2014**, *16*, 4688; t) L. Grigorjeva, O. Daugulis, *Angew. Chem.* **2014**, *126*, 10373; *Angew. Chem. Int. Ed.* **2014**, *53*, 10209; u) X. Wu, K. Yang, Y. Zhao, H. Sun, G. Li, H. Ge, *Nat. Commun.* **2015**, *6*, 6462; v) L.-B. Zhang, X.-Q. Hao, Z.-J. Liu, X.-X. Zheng, S.-K. Zhang, J.-L. Niu, M.-P. Song, *Angew. Chem.* **2015**, *127*, 10150; *Angew. Chem. Int. Ed.* **2015**, *54*, 10012; w) J. R. Hummel, J. A. Ellman, *J. Am. Chem. Soc.* **2015**, *137*, 490.
- [7] For an overview see: a) A. Casitas, X. Ribas, *Chem. Sci.* **2013**, *4*, 2301; b) C. Zhang, C. Tang, N. Jiao, *Chem. Soc. Rev.* **2012**, *41*, 3464; c) A. E. Wendlandt, A. M. Suess, S. S. Stahl, *Angew. Chem.* **2011**, *123*, 11256; *Angew. Chem. Int. Ed.* **2011**, *50*, 11062; d) I. P. Beletskaya, A. V. Cheprakov, *Coord. Chem. Rev.* **2004**, *248*, 2337.
- [8] For an overview, see: S. Z. Tasker, E. A. Standley, T. F. Jamison, *Nature* **2014**, *509*, 299.
- [9] See, for example: a) N. Umeda, H. Tsurugi, T. Satoh, M. Miura, *Angew. Chem.* **2008**, *120*, 4083; *Angew. Chem. Int. Ed.* **2008**, *47*, 4019; b) K. Ueura, T. Satoh, M. Miura, *J. Org. Chem.* **2007**, *72*, 5362; c) D. R. Stuart, P. Alsabeh, M. Kuhn, K. Fagnou, *J. Am. Chem. Soc.* **2010**, *132*, 18326; d) K. Ueura, T. Satoh, M. Miura, *Org. Lett.* **2007**, *9*, 1407; e) D. R. Stuart, M. Bertrand-Laperle, K. M. N. Burgess, K. Fagnou, *J. Am. Chem. Soc.* **2008**, *130*, 16474; f) M. P. Huestis, L. Chan, D. R. Stuart, K. Fagnou, *Angew. Chem.* **2011**, *123*, 1374; *Angew. Chem. Int. Ed.* **2011**, *50*, 1338; g) K. Morimoto, K. Hirano, T. Satoh, M. Miura, *Org. Lett.* **2010**, *12*, 2068; h) N. Guimond, K. Fagnou, *J. Am. Chem. Soc.* **2009**, *131*, 12050; i) S. Rakshit, F. W. Patureau, F. Glorius, *J. Am. Chem. Soc.* **2010**, *132*, 9585; j) T. K. Hyster, T. Rovis, *J. Am. Chem. Soc.* **2010**, *132*, 10565; k) G. Song, D. Chen, C.-L. Pan, R. H. Crabtree, X. Li, *J. Org. Chem.* **2010**, *75*, 7487.
- [10] See, for example: a) C.-Y. Wu, M. Hu, Y. Liu, R.-J. Song, Y. Lei, B.-X. Tang, R.-J. Li, J.-H. Li, *Chem. Commun.* **2012**, *48*, 3197; b) L. Ackermann, A. V. Lygin, N. Hofmann, *Angew. Chem.* **2011**, *123*, 6503; *Angew. Chem. Int. Ed.* **2011**, *50*, 6379; c) L. Ackermann, *Acc. Chem. Res.* **2014**, *47*, 281; d) B. Li, N. Wang, Y. Liang, S. Xu, B. Wang, *Org. Lett.* **2013**, *15*, 136.
- [11] See, for example: R. Bernini, G. Fabrizi, A. Sferrazza, S. Cacchi, *Angew. Chem.* **2009**, *121*, 8222; *Angew. Chem. Int. Ed.* **2009**, *48*, 8078.
- [12] See, for example: a) J. Wu, X. Cui, X. Mi, Y. Li, Y. Wu, *Chem. Commun.* **2010**, *46*, 6771; b) Z. Shi, S. Ding, Y. Cui, N. Jiao, *Angew. Chem.* **2009**, *121*, 8035; *Angew. Chem. Int. Ed.* **2009**, *48*, 7895; c) R. C. Larock, *Top. Organomet. Chem.* **2005**, *14*, 147.
- [13] See, for example: a) Y. Kajita, S. Matsubara, T. Kurahashi, *J. Am. Chem. Soc.* **2008**, *130*, 6058; b) C.-C. Liu, K. Parthasarathy, C.-H. Cheng, *Org. Lett.* **2010**, *12*, 3518.
- [14] M. V. Pham, B. Ye, N. Cramer, *Angew. Chem.* **2012**, *124*, 10762; *Angew. Chem. Int. Ed.* **2012**, *51*, 10610.
- [15] For an overview of conversions utilizing 8-aminoquinoline directing groups see: a) M. Corbet, F. De Campo, *Angew. Chem.* **2013**, *125*, 10080; *Angew. Chem. Int. Ed.* **2013**, *52*, 9896; b) O. Daugulis, J. Roane, L. D. Tran, *Acc. Chem. Res.* **2015**, *48*, 1053.
- [16] For examples of the benefits of using fluorinated solvents see: I. A. Shuklov, N. V. Dubrovina, A. Börner, *Synthesis* **2007**, 2925.
- [17] K. D. Collins, F. Glorius, *Acc. Chem. Res.* **2015**, *48*, 619.
- [18] *Organometallic Mechanisms and Catalysis*, (Ed.: J. K. Kochi), Academic Press, London, **1978**.
- [19] X. Wu, Y. Zhao, H. Ge, *J. Am. Chem. Soc.* **2015**, *137*, 4924.
- [20] a) L. Grigorjeva, O. Daugulis, *Org. Lett.* **2014**, *16*, 4684; b) G. He, S.-Y. Zhang, W. A. Nack, Q. Li, G. Chen, *Angew. Chem.* **2013**, *125*, 11330; *Angew. Chem. Int. Ed.* **2013**, *52*, 11124.
- [21] J. Dong, F. Wang, J. You, *Org. Lett.* **2014**, *16*, 2884.
- [22] For example, Kanai and co-workers have recently described the unique reactivity of [Cp*Co(III)] over [Cp*Rh(III)] for the direct dehydrative C–H allylation with non-activated allyl alcohols, thus providing an excellent example the potential advantages of the use of Co over Rh; Y. Suzuki, B. Sun, K. Sakata, T. Yoshino, S. Matsunaga, M. Kanai, *Angew. Chem.* **2015**, *127*, 10082; *Angew. Chem. Int. Ed.* **2015**, *54*, 9944.

Chapter VI

A First Example of Cobalt-Catalyzed Remote C-H Functionalization of 8-Aminoquinolines Operating through a Single Electron Transfer Mechanism



This chapter corresponds to the following publication:

Christopher J. Whiteoak,* **Oriol Planas**,* Anna Company and Xavi Ribas.

Adv. Synth. Catal. **2016**, 358, 1679-1688. (*equal contribution)

For this publication O.P. synthesized and characterized several substrates and products and performed mechanistic studies and product upgrading reactions. C.J.W. synthesized and characterized several substrates and products and performed mechanistic experiments. A.C. and X.R. designed the project. Besides, O.P. contributed in writing the manuscript and was involved in argumentations and discussions.

Reproduced with permission from:

Christopher J. Whiteoak,* Oriol Planas,* Anna Company and Xavi Ribas. "A First Example of Cobalt-Catalyzed Remote C-H Functionalization of c-Aminoquinolines Operating through a Single Electron Transfer Mechanism". *Advanced Synthesis & Catalysis*. Vol. 358 (2016) : 1679-1688.

<https://doi.org/10.1002/adsc.201600161>

© 2016 WILEY-VCH Verlag GmbH & Co. KGaA, Weinheim

A First Example of Cobalt-Catalyzed Remote C–H Functionalization of 8-Aminoquinolines Operating through a Single Electron Transfer Mechanism

Christopher J. Whiteoak,^{+a,b,*} Oriol Planas,^{+a} Anna Company,^a and Xavi Ribas^{a,*}

^a Grup de Química Bioinspirada, Supramolecular i Catalisi (QBIS-CAT), Institut de Química Computacional i Catalisi (IQCC) and Departament de Química, Universitat de Girona, Campus de Montilivi, 17071 Girona, Catalonia, Spain
E-mail: xavi.ribas@udg.edu

^b Current address: Bimolecular Sciences Research Centre, Faculty of Health and Wellbeing, City Campus, Sheffield Hallam University, Sheffield, S1 1WB, U.K.
E-mail: C.Whiteoak@shu.ac.uk

⁺ These authors contributed equally to this work.

Received: February 6, 2016; Revised: March 2, 2016; Published online: April 15, 2016



Supporting information for this article is available on the WWW under <http://dx.doi.org/10.1002/adsc.201600161>.

Abstract: The development of new C–H functionalization protocols based on inexpensive cobalt catalysts is currently attracting significant interest. Functionalized 8-aminoquinoline compounds are high-potential building blocks in organic chemistry and pharmaceutical compounds and new facile routes for their preparation would be highly valuable. Recently, copper has been applied as catalyst for the functionalization of 8-aminoquinoline compounds and found to operate through a single electron transfer (SET) mechanism, although requiring elevated reaction temperatures. Herein, we described the first example of a cobalt-catalyzed remote C–H functionalization

of 8-aminoquinoline compounds operating through a SET mechanism, exemplified using a practical and mild nitration protocol. The reaction uses inexpensive cobalt nitrate hexahydrate [Co(NO₃)₂·6H₂O] as catalyst and *tert*-butyl nitrite (TBN) as nitro source. This methodology offers the basis for the facile preparation of many new functionalized 8-aminoquinoline derivatives.

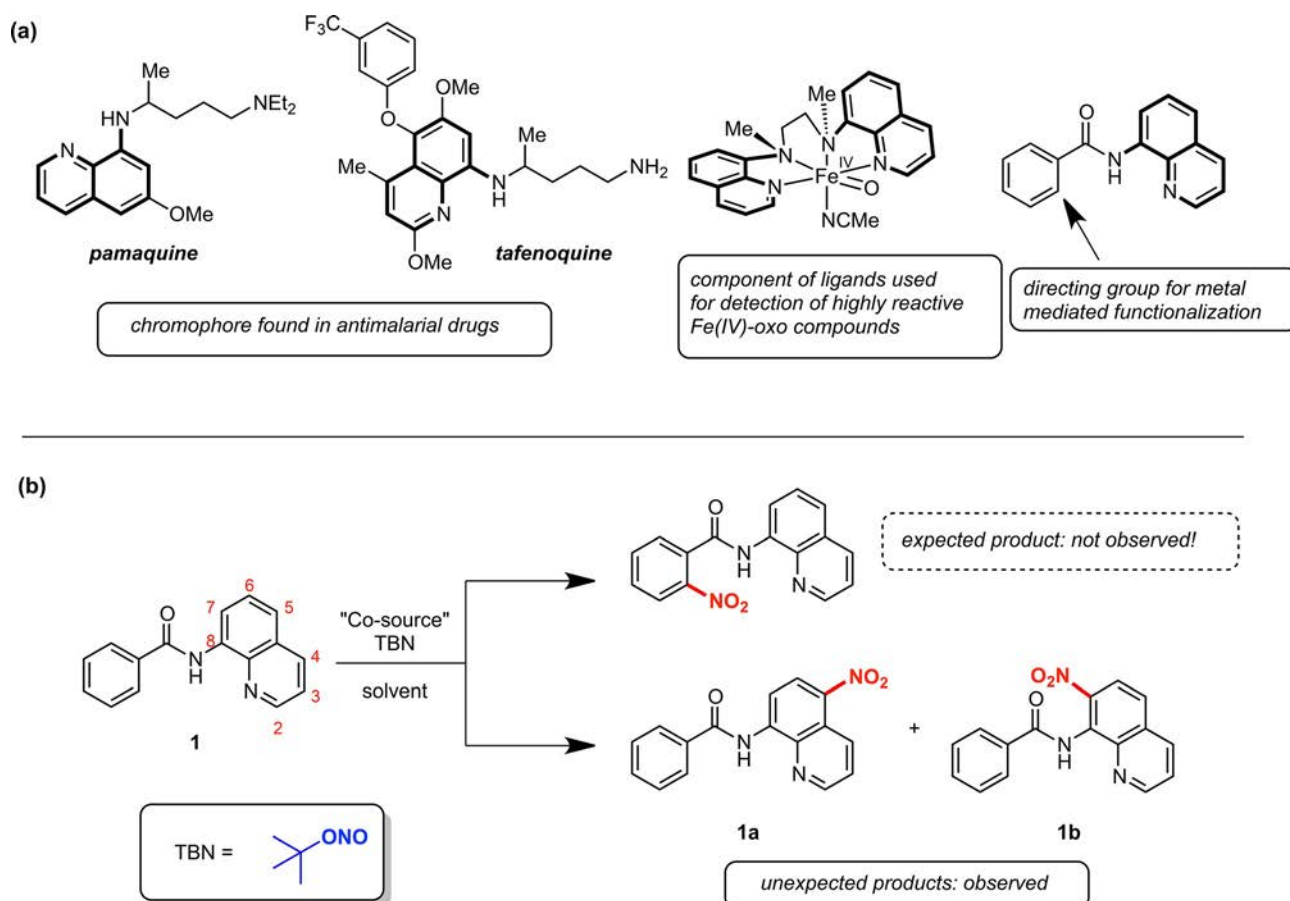
Keywords: 8-aminoquinolines; C–H functionalization; cobalt; homogeneous catalysis; nitration; nitrogen oxides

Introduction

The 8-aminoquinoline scaffold is an important motif found in a variety of compounds (Scheme 1a), including pharmaceutical drugs (e.g., the antimalarial drugs pamaquine and tafenoquine),^[1] ligands for coordination chemistry^[2] and more recently as a successful directing group for a number of metal-catalyzed transformations.^[3] As a result, new methodologies for further functionalization of readily accessible 8-aminoquinoline compounds are potentially very important developments in organic synthesis. There are many reports of metal-catalyzed C–H functionalization of simple quinolines,^[4] whilst in comparison, there are very few concerning C–H functionalization reactions of 8-aminoquinolines. The first reports of C–H functionalization protocols using 8-aminoquinoline as substrate came from Stahl and co-workers, who reported

on a single electron transfer (SET) based remote Cu-catalyzed C-5 chlorination.^[5,6] Since this initial report other Cu-catalyzed functionalizations have been described; remote C-5 sulfonylation,^[7] C-2 alkylation^[8] and more recently remote C-5 chalcogenation^[9,10] and C-5 amination.^[11] Besides Cu-catalyzed protocols, Fe-catalyzed C-4 and C-5 allylation,^[12] Rh-catalyzed C-7 alkenylation^[13] and Pd-catalyzed C-5/C-7 chlorination^[6] have also been described, thus expanding the toolbox for the preparation of novel 8-aminoquinoline derivatives. Unfortunately though, all of these reports suffer from the requirement of elevated temperatures and/or high catalyst loadings and as a result the development of catalytic protocols which are operative under milder conditions still remains a challenge.

In this work we demonstrate a new methodology for the functionalization of 8-aminoquinolines using nitration as an example, providing potentially valua-



Scheme 1. (a) Examples of compounds containing the 8-aminoquinoline scaffold; arrow indicating the C–H bond selectively activated when using the 8-aminoquinoline directing group. (b) Expected and observed nitration products from this work.

ble products for further elaboration (*vide infra*) or application. Nitro compounds are key synthons in organic synthesis as a result of their high-potential for further transformation^[14] and therefore nitrated derivatives of 8-aminoquinoline compounds may be of significant interest. The classical methodology for nitration is based on a mixed acid H₂SO₄/HNO₃ protocol. Albeit a simple and successful procedure, it suffers from many drawbacks including the use of harsh reaction conditions, poor functional group compatibility, regioselectivity problems and possible over-nitration.^[15] As a result of these issues, efforts have been directed towards the development of new nitration protocols.^[16] Nitration using mixtures of Cu(NO₃)₂ and acetic anhydride has long been known, although the requirement for stoichiometric amounts of Cu has limited the application of this procedure.^[17] In the search for more favorable protocols, one of the most promising routes that has emerged is the transition metal-catalyzed transformation of aryl halides, triflates and nonaflates reported by Saito and co-workers (Cu-catalyzed)^[18] and later Buchwald's methodology (Pd-catalyzed)^[19] using nitrite salts as the nitro source. Although solving many of the drawbacks of

previous nitration protocols, the main disadvantage of these methodologies is the necessity for a pre-functionalized substrate. Since these early developments and with the advent of directing groups, a number of metal-catalyzed direct C–H nitration protocols have been reported, particularly based on Pd^[20] and Cu.^[21] Although the field is rapidly developing, selective nitration of C–H bonds still remains a significant challenge.

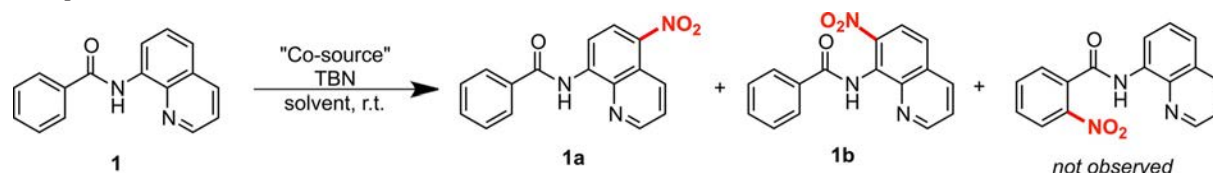
Nitrogen dioxide (NO₂) is an atom economic and therefore highly attractive nitrating agent, but its extreme reactivity (due to its open-shell nature) and toxicity have restricted its use to date. One way of overcoming the issues associated with the handling of NO₂ is to generate it *in situ*, in a stoichiometric manner. This can be achieved through the use of cheap, commercially available *tert*-butyl nitrite (TBN), which can convert into the *tert*-butoxy radical and NO₂ in the presence of air at room temperature.^[22,23] Recently there have been a number of reports pertaining to the use of TBN in nitration protocols, although examples using metal catalysts are still rare.^[24,25]

The field of Co-catalyzed C–H activation has recently started to receive significant attention as interest in replacing second and third row transition metals with cheaper, more abundant first row transition metals gathers pace.^[26] To this end, we have recently become interested in exploiting the potential of Co for the development of new C–H functionalization protocols.^[27] We surmised that the use of TBN and Co-catalysis may permit the nitration of the aromatic moiety of **1** (Scheme 1b), using directing group principals. This conversion has been previously successfully realized using Cu as catalyst.^[28] As will be described (*vide infra*), this was not the case and instead unexpected nitration of the aminoquinoline directing group was observed (Scheme 1b, products **1a** and **1b**), thus providing a new remote Co-catalyzed protocol for the functionalization of 8-aminoquinoline compounds, which we propose operates through an SET mechanism, similar to Cu-catalyzed 8-aminoquinoline C–H functionalizations.

Results and Discussion

Initially, nitration of **1** in 2,2,2-trifluoroethanol (TFE), using 20 mol% Co(OAc)₂ with TBN as nitro source at 100 °C was attempted (Table 1, entry 1). To our disappointment none of the expected aromatic nitration products from nitration of the quinoline directing group at the C-5 position (**1a**) were found. The same reaction at room temperature afforded increased yields to 12% of nitration product **1a** and a further unexpected 7-nitration product, **1b**, in 4% yield (Table 1, entry 2). Encouraged by these low but promising yields, the effect of changing the solvent was investigated (Table 1, entries 3–9), whereby it was found that the best results were obtained when acetic acid was used (Table 1, entry 4). Use of acetic acid as solvent furnished an overall yield of the two quinoline nitration products of 49%, in a similar ratio to that observed when using TFE as solvent. Thereafter, the Co source was opti-

Table 1. Optimization of reaction conditions.^[a]



Entry	Solvent	“Co-source”	Conversion [%] ^[b]	1a [%] ^[b]	1b [%] ^[b]
1 ^[c]	TFE	Co(OAc) ₂	> 99	trace	–
2	TFE	Co(OAc) ₂	55	12	4
3	CHCl ₃	Co(OAc) ₂	38	7	trace
4	acetic acid	Co(OAc) ₂	60	36	13
5	DMF	Co(OAc) ₂	45	–	–
6	toluene	Co(OAc) ₂	34	15	6
7	1,4-dioxane	Co(OAc) ₂	33	18	6
8	EtOAc	Co(OAc) ₂	44	11	3
9	THF	Co(OAc) ₂	33	6	2
10	acetic acid	Co(acac) ₃	25	13	5
11	acetic acid	CoCl ₂	29	19	5
12	acetic acid	Co(NO ₃) ₂ ·6H ₂ O	87	65	22
13	acetic acid	Co(BF ₄) ₂ ·6H ₂ O	61	44	17
14	acetic acid	Co(acac) ₂	40	21	10
15	acetic acid	Co(OAc) ₂ ·4H ₂ O	51	32	13
16	acetic acid	CoBr ₂	74	20	7
17	acetic acid	–	< 1	–	–
18^[d]	acetic acid	Co(NO₃)₂·6H₂O	> 99	74	25
19 ^[e]	acetic acid	Co(NO ₃) ₂ ·6H ₂ O	14	9	2
20 ^[f]	acetic acid	Co(NO ₃) ₂ ·6H ₂ O	71	46	17

^[a] Reaction conditions: **1** (50 mg, 0.2 mmol), Co source (0.04 mmol, 20 mol%), TBN (53 μL, 90%, 2.0 equiv., 0.4 mmol), solvent (1.5 mL), room temperature, 18 h.

^[b] Conversions and yields calculated from ¹H NMR spectra of the crude reaction mixture using 1,3,5-trimethoxybenzene as internal standard.

^[c] At 100 °C.

^[d] 4.0 equiv, TBN.

^[e] No TBN used.

^[f] 10 mol% Co(NO₃)₂·6H₂O.

mized (Table 1, entries 10–16), where it was found that $\text{Co}(\text{NO}_3)_2 \cdot 6\text{H}_2\text{O}$ was the optimal catalyst (Table 1, entry 12), furnishing a combined yield of 87% of both nitration products and also giving an excellent mass balance. The use of weakly coordinating anions such as tetrafluoroborate and nitrate appears to be beneficial as these Co sources provided significantly higher yields of the nitro products than Co sources with stronger coordinating anions (e.g., Cl, Br, acetate and acetylacetonate). In the absence of a Co source, no conversion was observed, highlighting the importance of Co to the conversion (Table 1, entry 17). In the absence of TBN, using $\text{Co}(\text{NO}_3)_2 \cdot 6\text{H}_2\text{O}$ as catalyst, 11% of nitrated products was observed, indicating that the nitrate ligand can also act as nitro source (Table 1, entry 19), which is likely as a result of the formation of HNO_3 *in situ*. Subsequently the effect of increasing the TBN loading to 4.0 equivalents was investigated, which resulted in quantitative conversion and yield of the nitro products (Table 1, entry 18).

To check if 20 mol% of $\text{Co}(\text{NO}_3)_2 \cdot 6\text{H}_2\text{O}$ was necessary, the catalyst loading was lowered to 10 mol% and it was found that the combined yield of the nitrated quinolines was reduced (Table 1, entries 12 vs. 20). It should be noted that throughout this study only mononitration products have been observed (either 5- or 7-nitro-8-aminoquinoline) and that elevated temperatures appear to be highly detrimental to the reaction outcome. After this optimization, it was decided that the optimal conditions for further substrate scoping would be 20 mol% $\text{Co}(\text{NO}_3)_2 \cdot 6\text{H}_2\text{O}$ and 4.0 equivalents of TBN in acetic acid at room temperature. This optimized protocol is adventitious over traditional nitration procedures as it avoids the use of highly corrosive H_2SO_4 and HNO_3 as reagents.

The optimized nitration protocol was then used with a number of other structurally related substrates (Figure 1, substrates 2–5). In all cases it was not possible to achieve the desired nitration products, thus indicating the necessity for the secondary amide and quinoline in the substrate. Importantly, it was not pos-

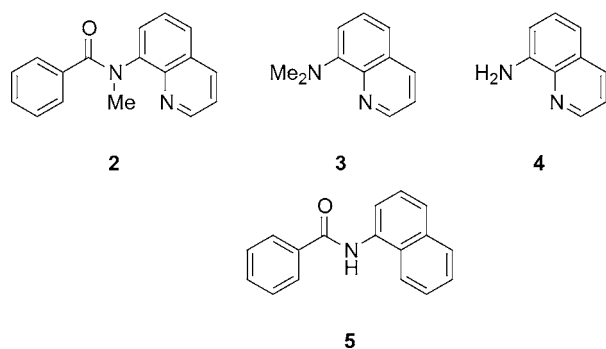


Figure 1. Unsuccessful substrates using the optimized reaction conditions.

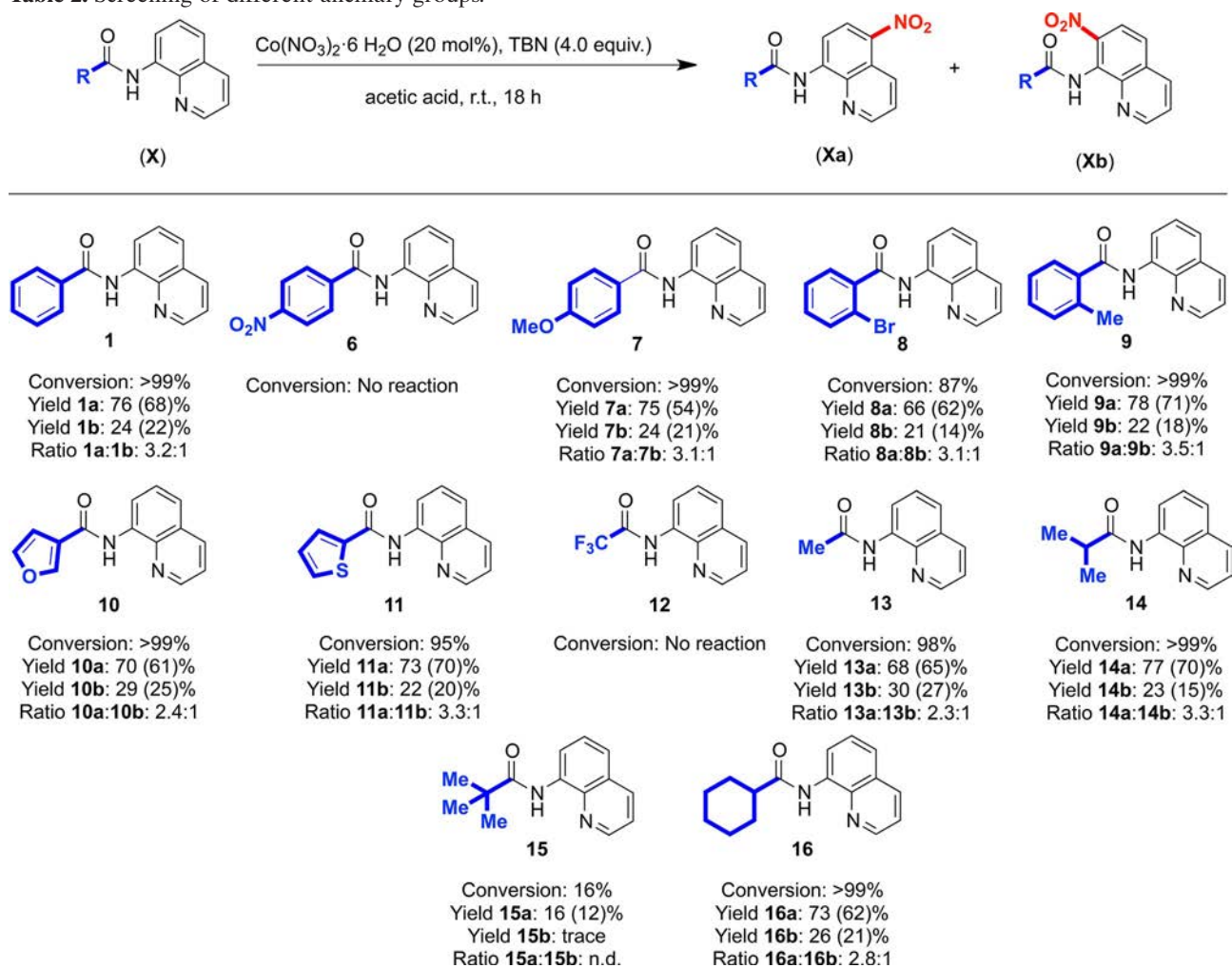
sible to obtain the nitration product from 8-aminoquinoline, **4**, indicating the importance of the ancillary benzoyl group. The lack of desired product from **4** could be a result of the formation of highly reactive diazonium compounds, which further react and result in a complex mixture of products.

Thereafter, a range of substrates bearing differently substituted ancillary groups were synthesized (Table 2, compounds 6–16). In most cases it was possible to obtain excellent to quantitative overall yields of the nitration products. Confirmation of the structures of the major 5- and minor 7-nitrated products was obtained from X-ray crystal structures of **11b** and **15a** (see the Supporting Information, Figures S140–S142). There are however several notable exceptions where the reaction was quenched; if a *p*-nitro group was included on the benzoyl ancillary (**6**) or if the ancillary group contained a trifluoromethyl group (**12**), no conversion was observed. These results suggest that ancillary groups containing strong electron-withdrawing moieties are unsuitable for use in the nitration reaction.

To investigate whether the strongly electron-withdrawing ancillary groups were unreactive or poisoning the catalyst, competitive reactions were performed (Scheme 2). In a single reaction vial, trifluoromethyl (**12**) and methyl (**13**) containing substrates were reacted at the same time and it was found that the conversion of **13** proceeded in similar yield to that in the absence of **12** (Scheme 2a). This result indicates that **12** did not convert due to it being unreactive rather than poisoning the catalyst.

In a similar manner, the reason why the substrate containing the *tert*-butyl group (**15**), which afforded significantly reduced nitration products, was investigated. Again, the related substrate bearing the methyl containing ancillary was used for the competition and little inhibition of the formation of the nitration products of **13** was observed (Scheme 2b). We therefore propose that the *tert*-butyl group is preventing the Co from coordinating to the amide through steric effects; indeed, the less sterically demanding isopropyl containing substrate (**14**) could be successfully converted (Table 2). From the results obtained in this study it was decided to continue using the benzoyl ancillary group for future studies as a result of the high yields, low cost and easy installation/cleavage (*vide infra*).

After ancillary group optimization, the potential for the reaction protocol to be transferred to a gram-scale and upgrading of the nitrated products was investigated (Scheme 3). We were pleased to find that when starting from 1.89 g of **1** it was possible to obtain attractive isolated yields of product **1a** (1.35 g, 61%) and also a sufficient amount of product **1b** (410 mg, 18%) to perform the upgrading experiments. The gram-scale experiments also led us to find a new facile route for isolation of the products, as it was

Table 2. Screening of different ancillary groups.^[a,b,c]


^[a] Reaction conditions: substrate (0.5 mmol), $\text{Co}(\text{NO}_3)_2 \cdot 6\text{H}_2\text{O}$ (29.1 mg, 0.1 mmol, 20 mol%), TBN (267 μL , 90%, 4.0 equiv., 2.0 mmol), acetic acid (3.5 mL), room temperature, 18 h.

^[b] Conversions and yields calculated from ^1H NMR spectra of the crude reaction mixture using 1,3,5-trimethoxybenzene as internal standard.

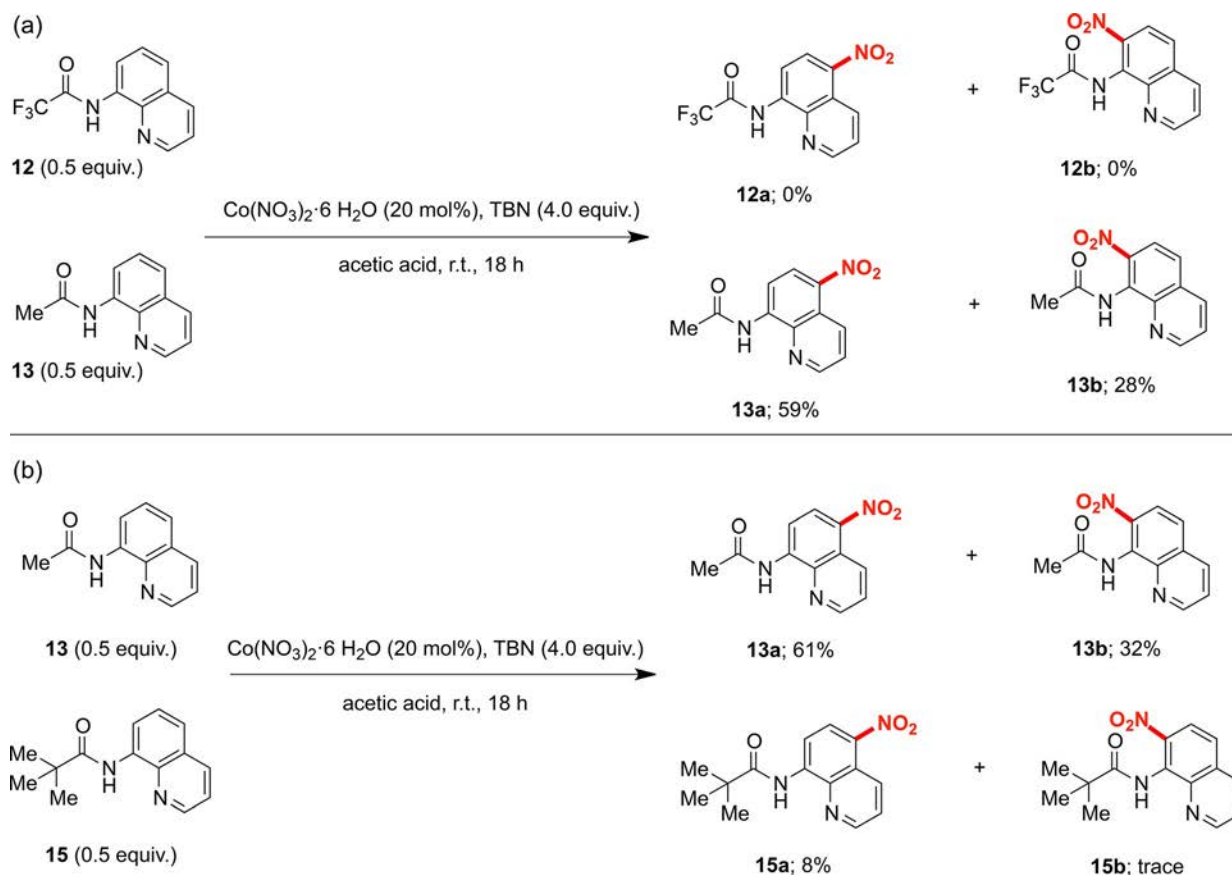
^[c] Isolated yields in parenthesis.

found that **1a** was significantly less soluble in ethanol than **1b**, permitting easy separation (see the Supporting Information for details).

With analytically pure samples in hand, reactions targeting the removal of the ancillary group and reduction of the nitro groups to amines were attempted (Scheme 3). Reduction of **1a** using Pd/C and H_2 (1 atm) results in selective formation of **1c** in 86% isolated yield, whereby the amide remains unaffected. The (benza)amide ancillary groups of both **1a** and **1b** can be easily removed by heating the compounds in boiling acidic ethanol to furnish the desired 5-nitro-8-aminoquinoline (**A**) and 7-nitro-8-aminoquinoline (**B**), respectively, in excellent yields. The nitro-8-aminoquinolines can then be easily converted into the corresponding diamines in excellent yield as exemplified by the conversion of **A** to 5,8-diaminoquinoline (**C**)

using Pd/C and H_2 (1 atm). These diamines may in the future find a wide range of applications, given that their ease of synthesis should make them relatively cheap synthetic precursors for increasing molecular complexity, compared with other substituted 8-aminoquinolines.

There are currently few inexpensive derivatives of the 8-aminoquinoline scaffold commercially available. To further study the versatility of our Co-catalyzed methodology, 5-substituted-8-nitroquinolines were prepared through Skraup reactions,^[29] and were subsequently reduced using Pd/C and H_2 , before addition of the ancillary benzoyl group (see the Supporting Information for details of the preparation of **17**, **18**, and **19**). Substrates **1a** and **1c** were prepared during this work (Scheme 3). Applying the optimized reaction conditions to these substrates furnished **17b**, **18b** and

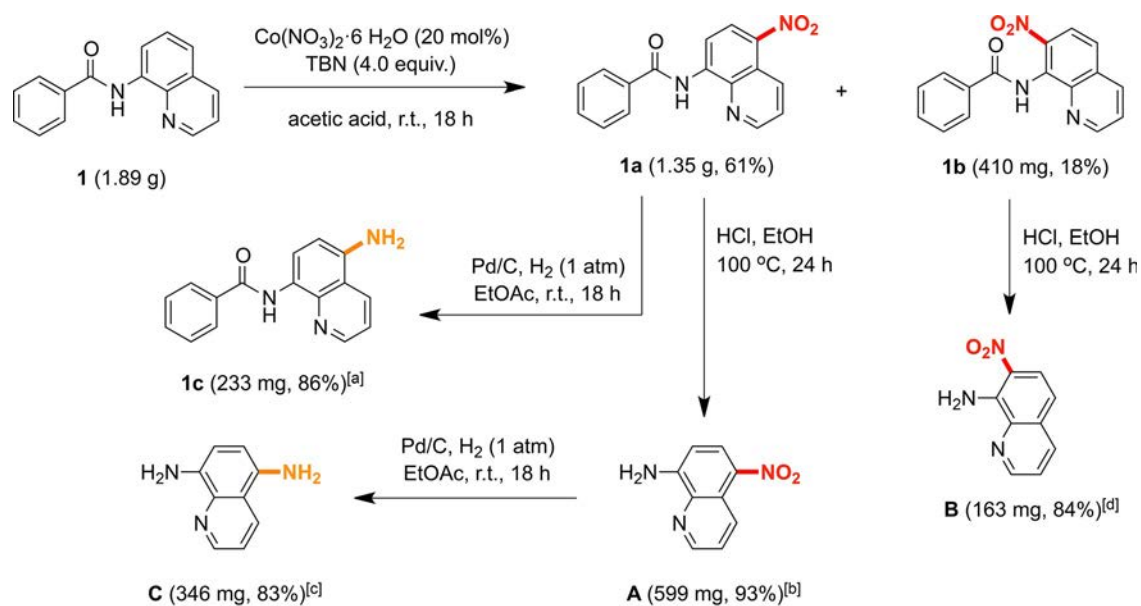


Scheme 2. Reactions performed to investigate the nature of the inactivity/poor activity of substrates **12** (a) and **15** (b). Yields calculated from ¹H NMR spectra of the crude reaction mixture using 1,3,5-trimethoxybenzene as internal standard and are based on conversion of the corresponding substrate. *Reaction conditions:* substrate (0.5 mmol; 0.25 mmol of each substrate), Co(NO₃)₂·6H₂O (29.1 mg, 0.1 mmol, 20 mol%), TBN (267 μL, 90%, 4.0 equiv., 2.0 mmol), acetic acid (3.5 mL), room temperature, 18 h.

19b in good to excellent isolated yields, with selective formation of the 7-nitro products (Table 3). In line with the exclusive mononitration observed previously (Table 2), when the substrate contained a nitro substituent, it was not possible to convert **1a**, with only trace amounts of product obtained. The amine containing substrate, **1c**, derived from **1a**, also failed to give the desired product, suggesting interference of the primary amine in the catalysis. When this substrate was dimethylated at the amine (**1d**), it was possible to obtain the nitrated product **1db** in an 80% isolated yield. This result indicates that the amine of **1c** should be pre-functionalized before further nitration is attempted. Compound **1db** contains amine, nitro and amide functionalities which can be derivatized independently making it an excellent candidate for further upgrading.

Taking into account all the observations during this study, the SET based mechanism depicted in Scheme 4 is proposed. Initially Co(II) coordinates to the substrate, and is oxidized to Co(III) by the *tert*-butoxy radical generated through the decomposition of TBN with O₂. The resulting Co(III) species is

a strong oxidizing species in acid media^[30,31] and as a result a SET from the quinoline occurs to yield a cationic quinoline radical and Co(II). Subsequently, NO₂, generated *in situ* from TBN, reacts with the quinoline radical and a concerted proton transfer/de-metallation step provides the nitration product and Co(II)X₂. This proposed mechanism is similar to the Cu(II)-catalyzed chlorination of 8-aminoquinolines reported by Stahl and co-workers, in that the key intermediate is a cationic quinoline radical species.^[5] To the best of our knowledge this work represents the first example of a SET remote functionalization of 8-aminoquinoline using Co. The absence of activity when strong electron-withdrawing groups are present in the substrate structure (**1a**, **6** and **12**) further indicates the plausibility of the proposed cationic quinoline radical species. To further highlight this effect a competitive reaction between **17** and **19** was performed (Scheme 5a), where it was observed that **19b** was obtained in >99% yield and **17b** in 41%, with respect to the individual starting substrates, confirming the preference for substrates containing electron-donating substituents as would be expected for the pro-



^[a] Isolated yield starting from 300 mg of 1a.

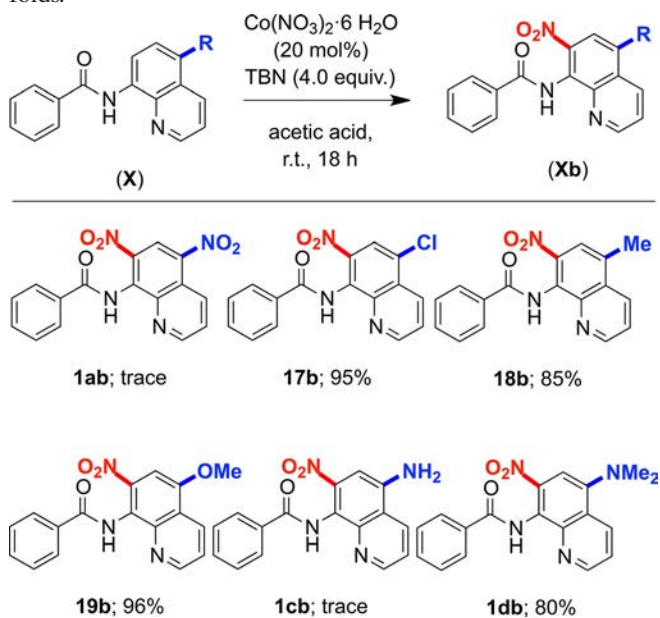
^[b] Isolated yield starting from 1.0 g of 1a.

^[c] Isolated yield starting from 500 mg of A.

^[d] Isolated yield starting from 320 mg of 1b.

Scheme 3. Gram-scale nitration reaction and subsequent upgrading of nitrated products obtained; Isolated yields reported. *Reaction conditions for gram-scale nitration reaction:* **1** (1.89 g, 7.6 mmol), $\text{Co(NO}_3)_2 \cdot 6\text{H}_2\text{O}$ (443 mg, 1.5 mmol, 20 mol%), TBN (4.1 mL, 90%, 4.0 equiv., 30.4 mmol), acetic acid (50 mL), room temperature, 18 h.

Table 3. Screening of different 8-aminoquinoline scaffolds.^[a,b,c]



^[a] *Reaction conditions:* substrate (0.5 mmol), $\text{Co(NO}_3)_2 \cdot 6\text{H}_2\text{O}$ (29.1 mg, 0.1 mmol, 20 mol%), TBN (267 μL , 90%, 4.0 equiv., 2.0 mmol), acetic acid (3.5 mL), room temperature, 18 h.

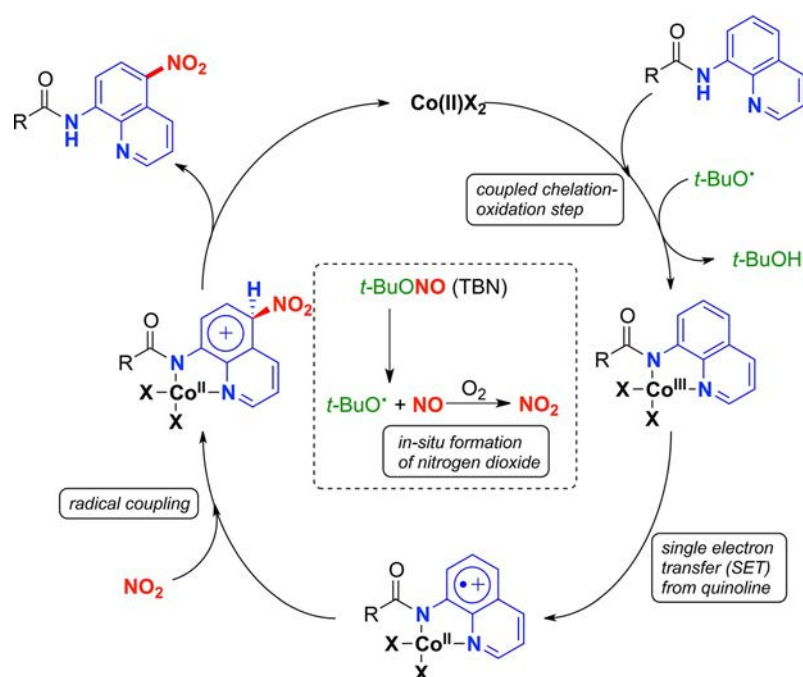
^[b] Isolated yields reported.

^[c] Selectivity > 99% in all cases.

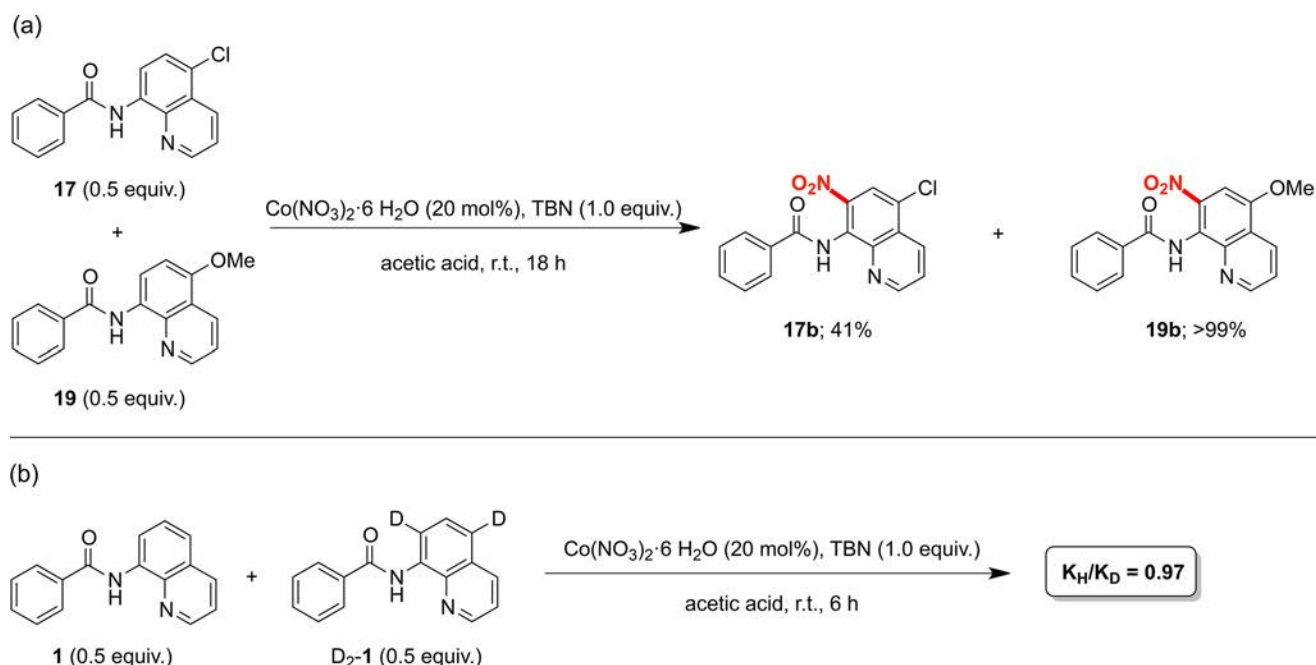
posed SET mechanism. Furthermore, a kinetic isotope experiment (KIE) revealed (Scheme 5b) a $k_{\text{H}}/k_{\text{D}}$ value of 0.97, indicating that the rate-limiting step is not a C–H activation and adding further evidence for the proposed mechanism.

Conclusions

In conclusion, a new practical room-temperature Co-catalyzed remote nitration protocol for the preparation of 5- and 7-nitro-8-aminoquinolines using easily installable and removable ancillary groups has been developed. The protocol is proposed to operate through a previously unreported remote C–H functionalization route based on a SET mechanism for the described 8-aminoquinoline substrates. This new methodology is intended to inspire further work into the development of new facile and mild catalytic routes for the preparation of newly functionalized 8-aminoquinoline compounds. Indeed, we are now working towards the installation of other functional groups using this radical-based protocol and also the application of the products obtained in this study, in particular the utilization of differently substituted 8-aminoquinolines as directing groups in C–H activation protocols.



Scheme 4. Proposed mechanism for the nitration reaction at C-5.



Scheme 5. (a) Competition reactions performed to investigate relative reactivity of substrates **17** and **19**. Yields calculated from ^1H NMR spectra of the crude reaction mixture using 1,3,5-trimethoxybenzene as internal standard and are based on conversion of corresponding substrate. *Reaction conditions:* substrate (0.5 mmol; 0.25 mmol of each substrate), $\text{Co}(\text{NO}_3)_2 \cdot 6\text{H}_2\text{O}$ (29.1 mg, 0.1 mmol, 20 mol%), TBN (267 μL , 90%, 4.0 equiv., 2.0 mmol), acetic acid (3.5 mL), room temperature, 18 h. (b) Summary of kinetic isotope experiment (KIE); for further details see the Supporting Information.

Experimental Section

General Procedure for Cobalt-Catalyzed Nitration Reactions

A 10-mL vial was charged with 0.5 mmol of substrate, $\text{Co}(\text{NO}_3)_2 \cdot 6\text{H}_2\text{O}$ (29.1 mg, 20 mol%, 0.1 mmol), *tert*-butyl nitrite (TBN) (267 μL , 90%, 4.0 equiv., 2.0 mmol) and 3.5 mL of acetic acid. The vial was sealed and the reaction stirred at room temperature for 18 h. After this period the reaction mixture was diluted with ethyl acetate (30 mL) and extracted using brine (20 mL). The aqueous layer was then extracted with ethyl acetate (2×30 mL), the organic layers combined, dried over magnesium sulfate and the solvent removed under reduced pressure. The crude reaction mixture was purified by column chromatography, using dichloromethane as eluent unless stated, providing analytically pure nitrated products.

Full characterization data obtained (including original ^1H , ^{13}C { ^1H } and COSY NMR spectra for all products and new compounds) can be found in the Supporting Information. CCDC 1438116 (**11b**), CCDC 1438117 (**13b**) and CCDC 1438118 (**15a**) contain the supplementary crystallographic data for this paper. These data can be obtained free of charge from The Cambridge Crystallographic Data Centre via www.ccdc.cam.ac.uk/data_request/cif.

Acknowledgements

We acknowledge financial support from the ERC for the Starting Grant Project ERC-2011-StG-277801 to X.R. and MINECO of Spain for CTQ2013-43012-P to X.R. and A.C., and a RyC contract to A.C. We thank the MECED for a FPU PhD grant to O.P. and Generalitat de Catalunya (2014 SGR 862). X.R. also thanks ICREA for ICREA-Acadèmia 2010 and 2015 awards. We are also grateful to X. Fontrodona (X-ray crystallography), Dr. L. Gómez (HR-MS) and STR-UdG.

References

- [1] J. Recht, E. Ashley, N. White, *Safety of 8-Aminoquinoline Antimalarial Medicines*, World Health Organization, 2014.
- [2] a) J. Yoon, S. A. Wilson, Y. K. Jang, M. S. Seo, K. Nehru, B. Hedman, K. O. Hodgson, E. Bill, E. I. Solomon, W. Nam, *Angew. Chem.* **2009**, *121*, 1283; *Angew. Chem. Int. Ed.* **2009**, *48*, 1257; b) S. Hong, Y.-M. Lee, K.-B. Cho, K. Sundaravel, J. Cho, M. J. Kim, W. Shin, W. Nam, *J. Am. Chem. Soc.* **2011**, *133*, 11876.
- [3] For examples, see: M. Corbet, F. De Campo, *Angew. Chem.* **2013**, *125*, 10080; *Angew. Chem. Int. Ed.* **2013**, *52*, 9896.
- [4] For a review of quinoline functionalization reactions, see: T. Iwai, M. Sawamura, *ACS Catal.* **2015**, *5*, 5031, and references cited therein.
- [5] A. M. Seuss, M. Z. Ertem, C. J. Cramer, S. S. Stahl, *J. Am. Chem. Soc.* **2013**, *135*, 9797.
- [6] For an expanded substrate scope see the more recent paper by Xie and co-workers: H. Guo, M. Chen, P. Jiang, J. Chen, L. Pan, M. Wang, C. Xie, Y. Zhang, *Tetrahedron* **2015**, *71*, 70.
- [7] See: a) H.-W. Liang, K. Jiang, W. Ding, Y. Yuan, L. Shuai, Y.-C. Chen, Y. Wei, *Chem. Commun.* **2015**, *51*, 16928; b) H. Qiao, S. Sun, F. Yang, Y. Zhu, W. Zhu, Y. Dong, Y. Wu, X. Kong, L. Jiang, Y. Wu, *Org. Lett.* **2015**, *17*, 6086; c) J. Wei, J. Jiang, X. Xiao, D. Lin, Y. Deng, Z. Ke, H. Jiang, W. Zeng, *J. Org. Chem.* **2016**, DOI: 10.1021/acs.joc.5b02509; d) J. Xu, C. Shen, X. Zhu, P. Zhang, M. J. Ajitha, K.-W. Huang, Z. An, X. Liu, *Chem. Asian J.* **2016**, DOI: 10.1002/asia.201501407.
- [8] X.-F. Xia, S.-L. Zhu, Z. Gu, H. Wang, *RSC Adv.* **2015**, *5*, 28892.
- [9] L. Zhu, R. Qiu, X. Cao, S. Xiao, X. Xu, C.-T. Au, S.-F. Yin, *Org. Lett.* **2015**, *17*, 5528.
- [10] Note that in ref.^[7d] other examples of couplings using a Cu SET methodology are described; $\text{N}(\text{SO}_2\text{Ph})_2$, OAc, Br, I and CF_3 ; therefore highlighting the future potential for SET C–H functionalization methodologies.
- [11] H. Sahoo, M. K. Reddy, I. Ramakrishna, M. Baiyda, *Chem. Eur. J.* **2016**, *22*, 1592.
- [12] X. Cong, X. Zeng, *Org. Lett.* **2014**, *16*, 3716.
- [13] J. Zhou, B. Li, F. Hu, B.-F. Shi, *Org. Lett.* **2013**, *15*, 3460.
- [14] N. Ono, *The Nitro Group in Organic Synthesis*, Wiley-VCH, New York, 2001.
- [15] G. A. Olah, R. Malhotra, S. C. Narang, *Nitration: Methods and Mechanisms*, Wiley-VCH, New York, 1989.
- [16] a) G. Yan, M. Yang, *Org. Biomol. Chem.* **2013**, *11*, 2554; b) G. Yan, A. J. Borah, L. Wang, *Org. Biomol. Chem.* **2014**, *12*, 6049.
- [17] For representative examples, see: a) K. I. H. Williams, S. E. Cremer, F. W. Kent, E. J. Sehm, D. S. Tarbell, *J. Am. Chem. Soc.* **1960**, *82*, 3982; b) M. Nakata, S. Wada, K. Tatsuta, M. Kinoshita, *Bull. Chem. Soc. Jpn.* **1985**, *58*, 1801; c) M. N. Gandy, M. J. Piggot, *J. Nat. Prod.* **2008**, *71*, 866.
- [18] S. Saito, Y. Koizumi, *Tetrahedron Lett.* **2005**, *46*, 4715.
- [19] B. P. Fors, S. L. Buchwald, *J. Am. Chem. Soc.* **2009**, *131*, 12898.
- [20] For examples of Pd-catalyzed nitration reactions, see: a) Y.-K. Liu, S.-J. Lou, D.-Q. Xu, Z.-Y. Xu, *Chem. Eur. J.* **2010**, *16*, 13590; b) W. Zhang, S. Lou, Y. Liu, Z. Xu, *J. Org. Chem.* **2013**, *78*, 5932; c) J. Dong, B. Jin, P. Sun, *Org. Lett.* **2014**, *16*, 4540; d) W. Zhang, S. Ren, J. Zhang, Y. Liu, *J. Org. Chem.* **2015**, *80*, 5973.
- [21] For examples of Cu-catalyzed nitration reactions, see: a) L. Zhang, Z. Liu, H. Li, G. Fang, B.-D. Barry, T. A. Belay, X. Bi, Q. Liu, *Org. Lett.* **2011**, *13*, 6536; b) J. Liu, S. Zhuang, Q. Gui, X. Chen, Z. Yang, Z. Tan, *Adv. Synth. Catal.* **2015**, *357*, 732; c) D. Katayev, F. F. Pfister, T. Wendling, L. J. Gooßen, *Chem. Eur. J.* **2014**, *20*, 9902.
- [22] *tert*-Butyl nitrate is a known source of nitrogen monoxide, see: P. G. Wang, T. B. Cai, N. Taniguchi, in: *Nitric Oxide Donors: for Pharmaceutical and Biological Application*, (Eds.: P. G. Wang, T. B. Cai, N. Taniguchi), Wiley-VCH, Weinheim, 2005.

- [23] In the presence of oxygen the autoxidation of nitrogen monoxide results in nitrogen dioxide: a) S. Goldstein, G. Czapski, *J. Am. Chem. Soc.* **1995**, *117*, 12078; b) L. Grossi, S. Strazzari, *J. Org. Chem.* **1999**, *64*, 8076; c) B. Galliker, R. Kissner, T. Nauser, W. H. Koppenol, *Chem. Eur. J.* **2009**, *15*, 6161.
- [24] For examples of transition metal free nitration reactions using *tert*-butyl nitrate see: a) T. Taniguchi, A. Yajima, H. Ishibashi, *Adv. Synth. Catal.* **2011**, *353*, 2643; b) M. Hu, B. Liu, X.-H. Ouyang, R.-J. Song, J.-H. Li, *Adv. Synth. Catal.* **2015**, *357*, 3332; c) S. Maity, T. Naveen, U. Sharma, D. Maiti, *Org. Lett.* **2013**, *15*, 3384; d) B. Kilpatrick, M. Heller, S. Arns, *Chem. Commun.* **2013**, *49*, 514; e) J. Zhao, P. Li, C. Xia, F. Li, *RSC Adv.* **2015**, *5*, 32835; f) D. Koley, O. C. Colón, S. N. Savinov, *Org. Lett.* **2009**, *11*, 4172.
- [25] For an example of a metal-catalyzed nitration protocol using *tert*-butyl nitrate, see ref.^[20d]
- [26] For an overview of cobalt-catalyzed C–H activation protocols, see: a) L. Ackermann, *J. Org. Chem.* **2014**, *79*, 8948; b) M. Moselage, J. Li, L. Ackermann, *ACS Catal.* **2016**, *6*, 498; c) D. Wei, X. Zhu, J.-L. Niu, M.-P. Song, *ChemCatChem.* **2016**, DOI: 10.1002/cctc.201600040.
- [27] O. Planas, C. J. Whiteoak, A. Company, X. Ribas, *Adv. Synth. Catal.* **2015**, *357*, 4003.
- [28] See refs.^[21b,21c]
- [29] For a general procedure, see: G. He, S.-Y. Zhang, W. A. Nack, Q. Li, G. Chen, *Angew. Chem.* **2013**, *125*, 11330; *Angew. Chem. Int. Ed.* **2013**, *52*, 11124.
- [30] Co(III) acetate compounds are strong one-electron oxidizing species, see: J. D. Donaldson, D. Beyersmann, *Cobalt and Cobalt Compounds*, in: *Ullmann's Encyclopedia of Industrial Chemistry*, Wiley-VCH, **2005**.
- [31] Cobalt-catalyzed SET C–H activation mechanisms have been previously implicated, see, for example: a) J. K. Kochi, R. T. Tang, T. Bernath, *J. Am. Chem. Soc.* **1973**, *95*, 7114; b) X.-K. Guo, L.-B. Zhang, D. Wei, J.-L. Niu, *Chem. Sci.* **2015**, *6*, 7059.

Chapter VII

Results and Discussion

Since the renaissance of the high-valent approach for C-H bond activation and functionalization with cobalt, the development of new methodologies mimicking and improving the reactivity and selectivity of rhodium and iridium catalysts has been a topic of interest. Indeed, cobalt presents unique reactivity modes with respect to its group neighbours, probably because its higher electronegativity gives an enhanced nucleophilic character to the organometallic intermediates. The key of success of synthetic methodologies generally is the detailed mechanistic understanding of some fundamental steps, including the key C-H activation and functionalization modes. However, albeit this exponential increase in methodology-based publications, just a few groups focused their research on the isolation and characterization of reaction intermediates such as aryl-Co(III) compounds. Our group is specialized in the isolation and characterization of catalytically relevant intermediates with macrocyclic model substrates, which have proven to be tremendously efficient to stabilize high-valent organometallic aryl-metal species. Therefore, this thesis focuses on the investigation of the fundamental mechanistic features that govern high-valent cobalt C-H activation and functionalization using arene model substrates. Moreover, the knowledge acquired from these studies is applied to substrates bearing a N,N-bidentate chelating group, thus developing catalytic methodologies for the synthesis of biologically active products.

In section VII.1 we will describe the synthesis and characterization of bench-top stable organometallic aryl-Co(III) compounds obtained through C(sp²)-H activation, in a clear stepwise manner, using a 12-membered macrocyclic model substrate especially designed to stabilize octahedral metal geometries. Subsequent insights obtained from the application of these intermediates in alkyne annulation reactions, in which they are proposed as key reaction intermediates, will be disclosed, including theoretical evidence for a novel ‘acetylide pathway’ for terminal alkynes in annulation reactions. Putting this work into context, we also report crystallographic evidence of the sought-after organometallic aryl-Co(III) intermediate proposed in 8-aminoquinoline directed Co(II)-catalyzed C-H functionalization processes.

In section VII.2 we describe the synthesis of a new family of bench-top stable aryl-Co(III)-carboxylate complexes and their reactivity with ethyl diazoacetate (EDA). Crystallographic, spectroscopic and theoretical evidence of a unique C-metalated *cis*-aryl-Co(III) enolate intermediate is provided, unveiling a novel strategy to tame the hot reactivity of Co(III)-carbenes and construct C-C bonds through an unusual intramolecular S_N2-type pathway. DFT studies show the feasibility of this transformation, in which Lewis acids play a crucial role turning the carboxylate moiety into a better leaving group.

Section VII.3 describes a facile cobalt-catalyzed C-H functionalization route towards sultam motifs through annulation of easily prepared aryl sulfonamides and alkynes using a directing group approach. The reaction shows broad substrate scope with products obtained in a highly regioselective manner in good to excellent isolated yields. Mechanistic insights suggest the formation of aryl-Co(III) key species *via* C-H activation during the annulation reaction.

Finally, section VII.4 describes the first example of a cobalt-catalyzed remote C-H functionalization of 8-aminoquinoline compounds operating through a SET mechanism, exemplified using a practical and mild nitration protocol. The reaction uses inexpensive $\text{Co}(\text{NO}_3)_2 \cdot 6\text{H}_2\text{O}$ as catalyst and *tert*-butyl nitrite (TBN) as nitro source. This methodology offers the basis for the facile preparation of many new functionalized 8-aminoquinoline derivatives.

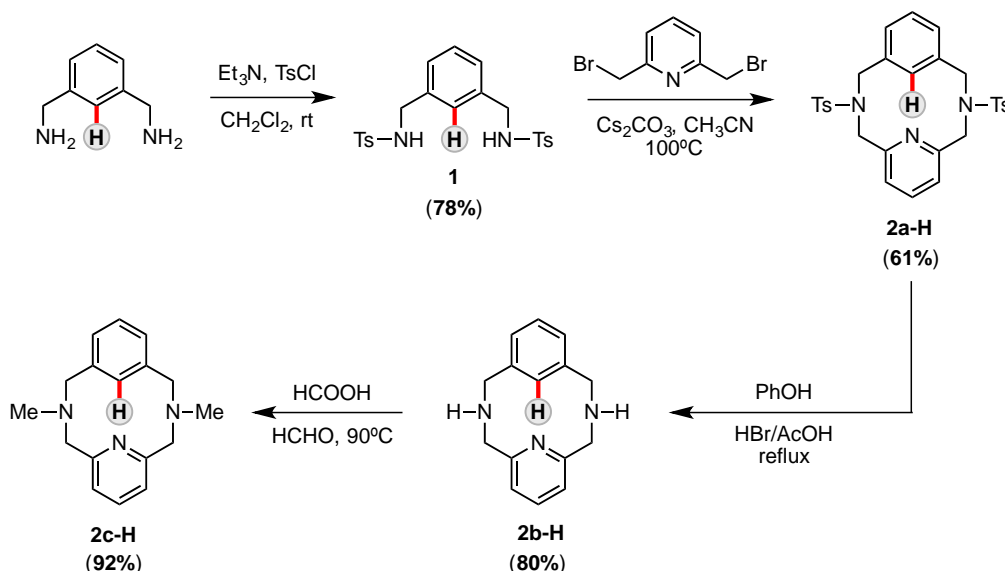
Note: the numbering of metal complexes and organic compounds is consistent within each chapter (VII.1 to VII.4) and refers to the numbering used in the corresponding publications.

VII.1 Isolation of Key Organometallic Aryl-Co(III) Intermediates in Cobalt-Catalyzed C(sp²)-H Functionalization and New Insights into Alkyne Annulation Reaction Mechanisms

This section corresponds to the contents of the manuscript by Oriol Planas, Christopher J. Whiteoak, Vlad Martin-Diaconescu, Ilaria Gamba, Josep M. Luis, Teodor Parella, Anna Company and Xavi Ribas. *J. Am. Chem. Soc.* **2016**, *138*, 14388-14397, which can be found in Chapter III of this thesis.

VII.1.1 Synthesis of macrocyclic model substrates and Co(II) precursors

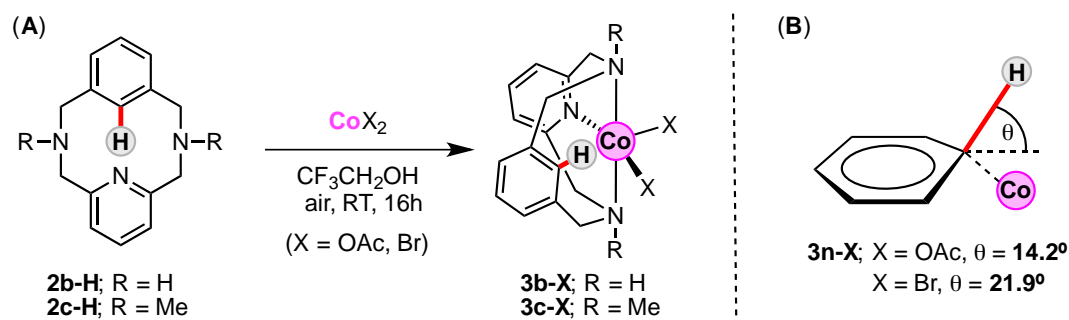
This project started with the synthesis of macrocyclic model substrates **2b-H** and **2c-H**. As explained in Section II, these ligands were selected due to their bent structure, which favors coordination to octahedral metal centers such as Co(II) and Co(III). Thus, the synthesis of the macrocyclic model substrates starts from the commercially available 1,3-phenylenedimethanamine. First, tosylation with TsCl and triethylamine yields tosylated amine **1**. Then, **1** is combined with 1.0 equivalents of 2,6-bis(bromomethyl)pyridine in CH₃CN to furnish the protected N-tosyl macrocyclic model substrate **2a-H**. Deprotection of tosyl amides was achieved through a protocol widely used in our group,¹⁻³ which consists in the phenol-assisted cleavage of the S-N bond in acidic media. This reaction furnishes the free-amine macrocyclic substrate **2b-H**, which can be further methylated with formaldehyde/formic acid to obtain **2c-H**. The sequence for the synthesis of ligands **2b-H** and **2c-H** is depicted in Scheme VII.1.



Scheme VII.1. Synthesis of building blocks **1**, **2a-H** and ligands **2b-H** and **2c-H**.

With the macrocyclic model substrates in our hands, the next goal was the synthesis and characterization of the corresponding Co(II) complexes to study the

interaction of the metal center with the corresponding C-H bond (Scheme VII.2, A). In this line, $\text{Co}(\text{OAc})_2$ was mixed with **2b-H** and **2c-H** in TFE at 25 °C to yield $[(\mathbf{2b-H})\text{Co}(\text{II})(\text{OAc})_2]$ (**3b-OAc**, 72%) and $[(\mathbf{2c-H})\text{Co}(\text{II})(\text{OAc})_2]$ (**3c-OAc**, 58%). The structure of **3b-OAc** was initially confirmed by NMR, HRMS ($[\text{M-OAc}]^+$; calcd. $m/z = 357.0882$; found: 357.0874) as well as XRD analysis (Figure VII.1A). The Co center was coordinated to one secondary amine, one pyridine and two bidentate acetates.



Scheme VII.2. (A) Synthesis of Co(II) precursors **3b-X** (X = OAc) and **3c-X** (X = OAc, Br). (B) Bending of the targeted C-H bond through interaction with the Co(II) centre.

On the contrary, when CoBr_2 was used as the cobalt source, secondary amine complex $[(\mathbf{2b-H})\text{Co}(\text{II})\text{Br}_2]$ **3b-Br** could not be obtained and only the synthesis of $[(\mathbf{2c-H})\text{Co}(\text{II})\text{Br}_2]$ (**3c-Br**, 99%) was achieved, which has been also characterized by XRD analysis (see Figure VII.1B). An important feature observed in the solid-state structures of the Co(II) coordination complex **3c-Br** (Figure VII.1) is the out-of-plane targeted C-H bond, which indicates an interaction with the Co(II) centre.

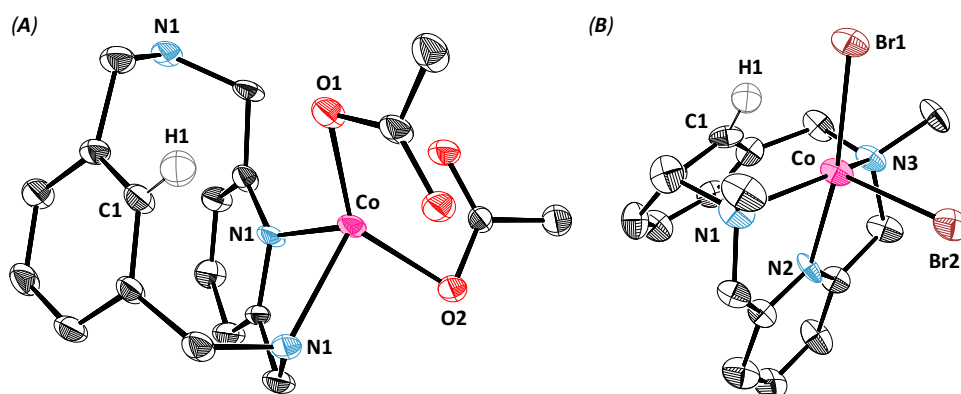


Figure VII.1 Solid state structures of Co(II) coordination complexes. H-atoms and solvent molecules have been omitted for clarity; ellipsoids are set at 50% probability level. (A) Crystal data for **3b-OAc**. Selected bond distances [\AA] and angles [$^\circ$]: Co-C(1) 3.321(5), Co-H(1) 2.945(5), Co-N(1) 2.159(4), Co-N(2) 2.112(6), Co-N(3) 4.614(6), Co-O(1) 2.085(5), Co-O(2) 2.136(4); C(1)-Co-H(1) 58.90(1). (B) Crystal data for **3c-Br**. Selected bond distances [\AA] and angles [$^\circ$]: Co-C(1) 2.599(1), Co-H(1) 2.368(9), Co-N(1) 2.267(1), Co-N(2) 2.067(8), Co-N(3) 2.271(6), Co-Br(1) 2.476(2), Co-Br(2) 2.491(3); C(1)-Co-H(1) 65.49(5).

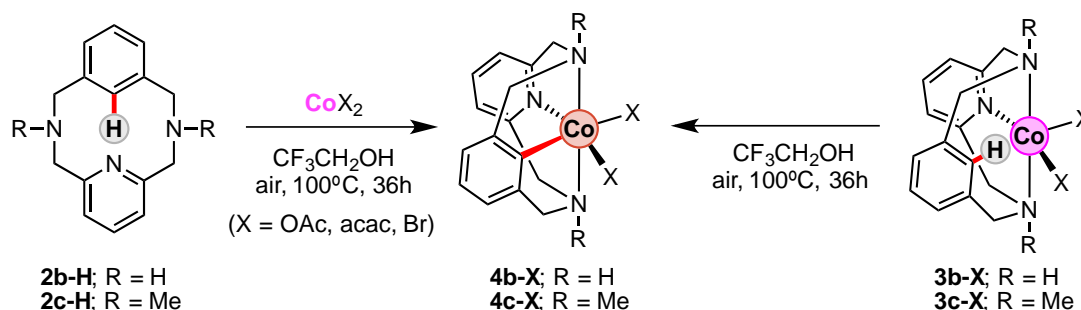
As depicted in Scheme VII.2B and in Figure VII.1, in **3b-OAc** the Co(II) center is coordinated to the pyridine motif, to one of the secondary amines and to the acetate anions in a bidentate fashion. In this crystal structure, the C1-H1 bond (see structure A in Figure VII.1) has a torsion angle of $\theta = 14.2^\circ$ out-of-plane of the arene ring, indicating a weak interaction with the metal centre. In the case of **3c-Br** (see structure B in Figure VII.2), which is fully coordinated to the macrocyclic ligand, the C-H is bent with an angle of $\theta = 21.9^\circ$, suggesting a stronger interaction compared to **3b-OAc**.

VII.1.2 Synthesis and characterization of aryl-Co(III) complexes

Once we had the Co(II) coordination complexes in our hands we focused our efforts in the synthesis of organometallic aryl-Co(III) complexes. Indeed, the incipient interaction between the Co(II) centre and the targeted C-H bond, especially in **3c-Br**, suggested that C-H activation with a more electropositive metal center such as Co(III) would be possible.

VII.1.2.1 Synthesis of Aryl-Co(III) complexes

When Co(II) salts such as $\text{Co}(\text{OAc})_2$ were reacted with arene macrocyclic substrates **2b-H** and **2c-H** in TFE at 100°C , the corresponding organometallic complexes $[(\mathbf{2b})\text{Co(III)}(\eta^2\text{-OAc})](\text{OAc})$ (**4b-OAc**, 82%) and $[(\mathbf{2c})\text{Co(III)}(\eta^2\text{-OAc})](\text{OAc})$ (**4c-OAc**, 58%) were achieved (Scheme VII.3, left). Interestingly, the same red-colored intermediates could be furnished starting from the previously synthesized bright-purple Co(II) complexes **3b-OAc** and **3c-OAc** in TFE at 100°C in the presence of an oxidant atmosphere (Scheme VII.3, right). When starting from **3c-Br**, the bromide analogue **4c-Br** was observed by NMR and HRMS techniques (Figure SI, Annex I), but it was not possible to isolate it. This result indicates the importance of the internal base, which is probably playing a role in the C-H cleavage and Co-C formation event through a base-assisted mechanism such as a Concerted Metalation-Deprotonation pathway.



Scheme VII.3. Synthesis of aryl-Co(III) intermediates **4b-X** and **4c-X**.

The isolated organometallic aryl-Co(III) complexes are stable at room temperature under an air atmosphere, and due to this fact, it was possible to characterize them by

NMR and HRMS (Figure S14-23, Annex I). NMR analysis of **4b-OAc** and **4c-OAc** provided spectra consistent with low spin diamagnetic Co(III) species. Furthermore, two non-equivalent acetate signals can be observed, indicating that only one acetate is likely to be coordinated to the Co(III) centre, while the second acetate remains as an outer-sphere counteranion. The proposed structure was further supported by HRMS studies, which afforded clean spectra with main signals corresponding to the $[(4x)Co(III)(OAc)]^+$ ions (**4b-OAc**, $[M-OAc]^+$; calcd. $m/z = 356.0804$; expt. $m/z = 356.0802$; **4c-OAc**, $[M-OAc]^+$; calcd. $m/z = 384.1117$; expt. $m/z = 384.1122$). Unfortunately, crystallographic analysis of these intermediates was unsuccessful, as we were not able to obtain suitable crystals for XRD. As result we turned to X-ray Absorption Spectroscopy (XAS), in order to understand the electronic structure (XANES) and coordination environment (EXAFS) of the metal complexes. The results of these studies, which were performed by Dr. Vlad Martin-Diaconescu and include geometry optimized structures for **4b-OAc** and **4c-OAc**, are summarized in Figure VII.2. Thus, as shown in Figure VII.2, the proposed structures for the organometallic complexes are in agreement with the NMR and HRMS data. Furthermore, the corresponding geometry optimized structures explain the intense pre-edge features from XAS analysis, whereby a trigonal bipyramidal local metal geometry facilitates p-mixing into the d-manifold resulting in a more intense pre-edge.⁴ In addition, XAS and EXAFS studies also support the presence of a monocoordinated acetate, as proposed above.

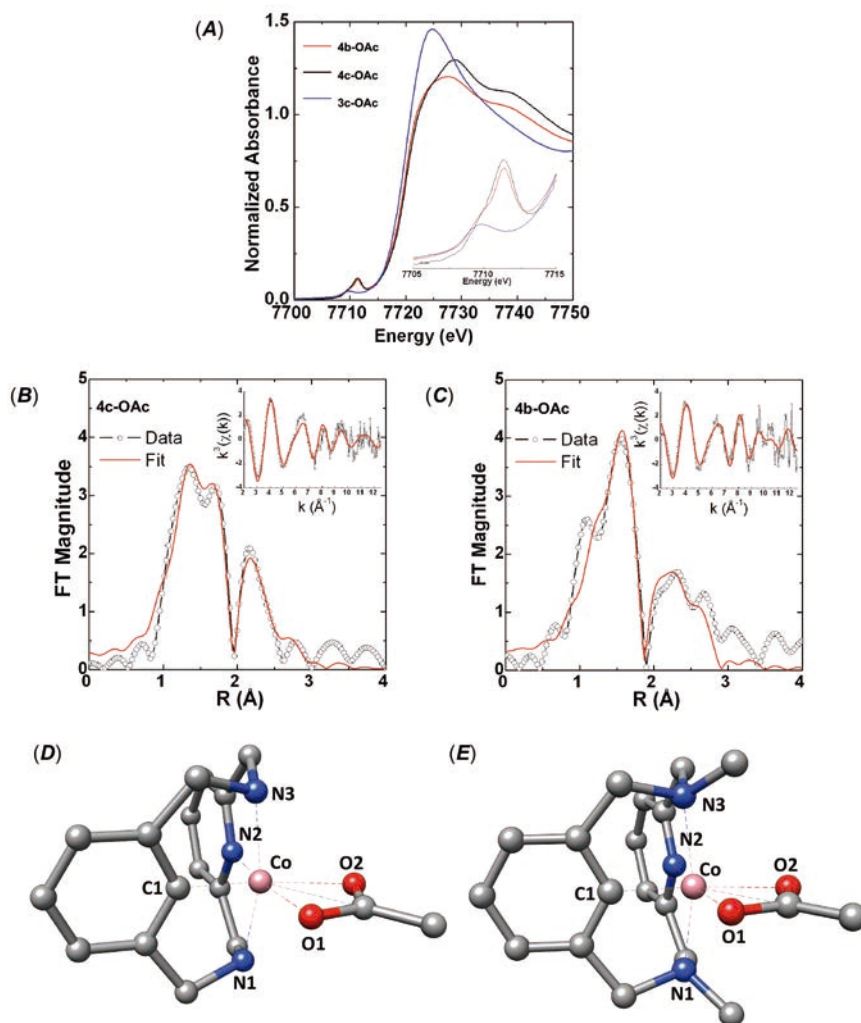


Figure VII.2. Characterization of aryl-Co(III) compounds through XAS spectroscopy. (A) XAS spectra at the Co K-edge highlighting the XANES region of the spectrum, and the $1s \rightarrow 3d$ pre-edge transitions (inset). (B) EXAFS analysis of **4b-OAc**. Shown are Fourier-transformed EXAFS spectra (no phase correction, k -window = 2 -12.5 \AA^{-1}), as well as the k^3 -weighted unfiltered EXAFS spectra (inset). (C) EXAFS analysis of **4c-OAc**. Shown are Fourier-transformed EXAFS spectra (no phase correction, k -window = 2 -12.5 \AA^{-1}) as well as the k^3 -weighted unfiltered EXAFS spectra (inset). (D) Geometry optimized structure for **4b-OAc**. Selected bond distances [\AA] and angles [$^\circ$]: Co-C(1) 1.85, Co-N(1) 1.85, Co-N(2) 2.00, Co-N(3) 2.00, Co-O(1) 1.96, Co-O(2) 2.11; C(1)-Co-N(1) 89.8, C(1)-Co-N(2) 84.5, C(1)-Co-N(3) 84.4, C(1)-Co-O(1) 99.6, C(1)-Co-O(2) 164.9. (E) Geometry optimized structure for **4c-OAc**. Selected bond distances [\AA] and angles [$^\circ$]: Co-C(1) 1.85, Co-N(1) 1.85, Co-N(2) 2.05, Co-N(3) 2.05, Co-O(1) 1.96, Co-O(2) 2.11; C(1)-Co-N(1) 86.5, C(1)-Co-N(2) 84.6, C(1)-Co-N(3) 84.6, C(1)-Co-O(1) 101.0, C(1)-Co-O(2) 166.3.

Formation of the organometallic aryl-Co(III) compounds was further studied by performing several control experiments (Scheme VII.4). The solvent and the counteranion resulted to be key in the formation of the organometallic complexes, as shown in Tables S1 and Table S2 (Annex I). In this line, the addition of 2.0 equiv of KOAc to a mixture of **2c-H** and CoBr_2 in CH_3CN was found to be tremendously

mixture at 100 °C, whereby the corresponding organometallic complex [(**4x**)-Co(III)(CH₃CN)₂](ClO₄)₂ (**4x-CH₃CN**) was obtained. Subsequently, crystals of **4b-CH₃CN**, as well as **4c-CH₃CN** were obtained and fully characterized by XRD techniques (Figure VII.3). Interestingly, the experimentally determined EXAFS Cl-Co(III) bond distances of 1.88 Å for **4b-OAc** and 1.90 Å for **4c-OAc** (Figure VII.2) are consistent with the Cl-Co(III) distance of 1.86 Å determined for both **4b-CH₃CN** and **4c-CH₃CN** from their crystal structures (Figure VII.3).

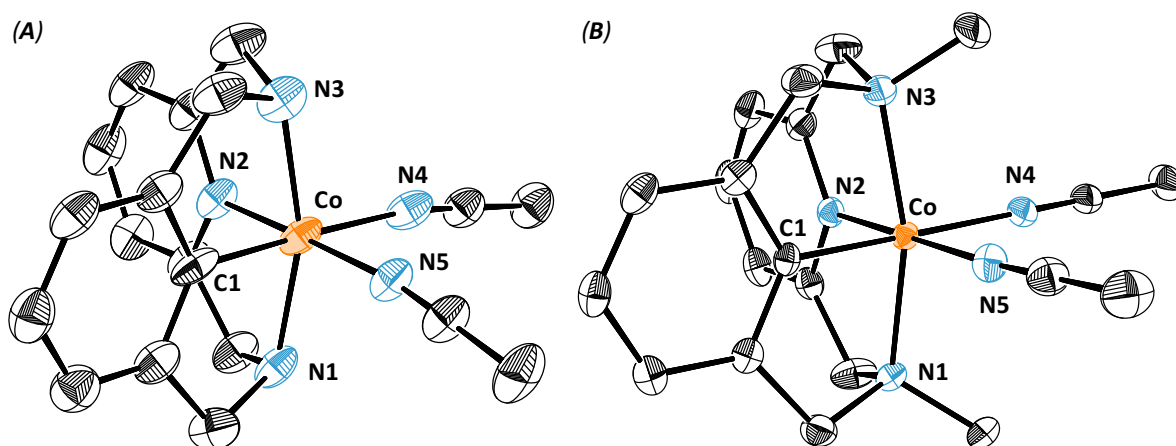
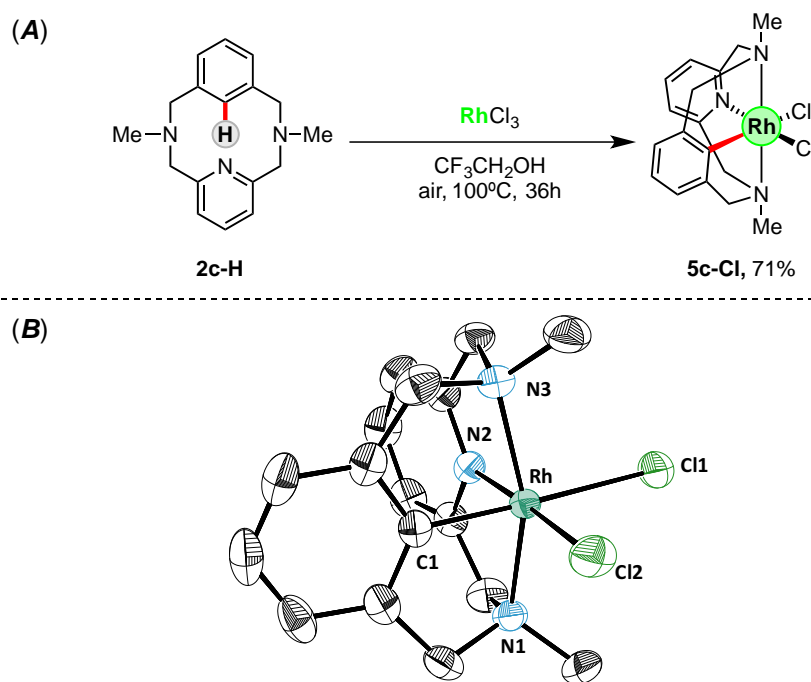


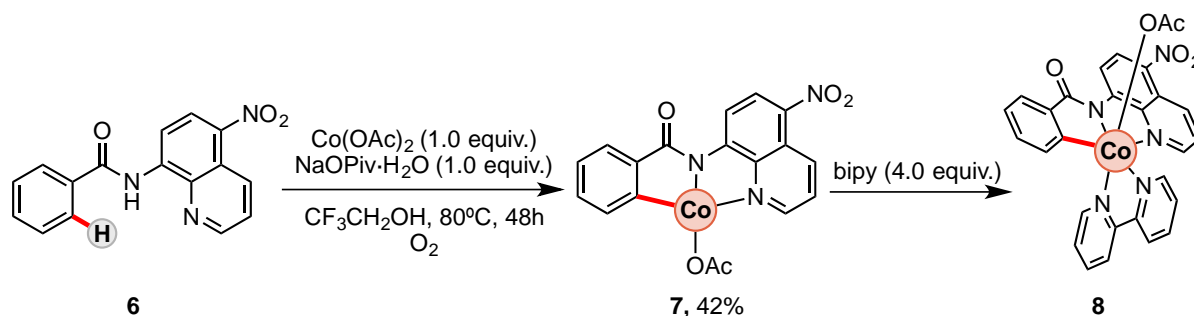
Figure VII.3. Solid state structures of aryl-Co(III) complexes **4b-CH₃CN** and **4c-CH₃CN**. Hydrogen atoms, perchlorate anions and solvent molecules have been omitted for clarity; ellipsoids are set at 50% probability. (A) Crystal data for **4b-CH₃CN**. Selected bond distances [Å] and angles [°]: Co-C(1) 1.876(7), Co-N(1) 1.853(4), Co-N(2) 1.997(6), Co-N(3) 2.008(5), Co-N(4) 2.025(6), Co-N(5) 1.897(4); C(1)-Co-N(1) 90.55(2), C(1)-Co-N(2) 83.68(2), C(1)-Co-N(3) 83.66(2), C(1)-Co-N(4) 177.87 (2), C(1)-Co-N(5) 88.40(2). (B) Crystal data for **4c-CH₃CN**. Selected bond distances [Å] and angles [°]: Co-C(1) 1.865(2), Co-N(1) 1.856(2), Co-N(2) 2.029(2), Co-N(3) 2.027(2), Co-N(4) 1.999(2), Co-N(5) 1.927(2); C(1)-Co-N(1) 88.16(9), C(1)-Co-N(2) 84.13(9), C(1)-Co-N(3) 84.26(9), C(1)-Co-N(4) 178.30(9), C(1)-Co-N(5) 91.30(9).

An analogous organometallic aryl-Rh(III) complex was also prepared following a similar protocol. Despite the fact that coordination of RhCl₃ to **2b-H** was not successful, when the macrocyclic model substrate **2c-H** was mixed with RhCl₃ in TFE at 100 °C, the light-yellow aryl-Rh(III) complex [(**2c**)Rh(III)Cl₂] (**5c-Cl**) was obtained in 71% isolated yield (Scheme VII.5, A). Crystals suitable for XRD analysis were obtained by layering a 1:1 CH₃CN/CH₃OH mixture of **5c-Cl** with diethyl ether and storing it at 4 °C over 24 h (Scheme VII.5, B). Interestingly, Cl-Rh is significantly longer compared with aryl-Co(III) complexes, probably due to the larger Van der Waals radius of rhodium(III) compared to cobalt(III).



Scheme VII.5. (A) Synthesis of organometallic aryl-Rh(III)Cl₂ species. (B) Solid state structure of aryl-Rh(III) complex **5c-Cl**. Hydrogen atoms and solvent molecules have been omitted for clarity; ellipsoids are set at 50% probability. Selected bond distances [Å] and angles [°]: Rh-C(1) 1.929(2), Rh-N(1) 2.113(2), Rh-N(2) 1.953(2), Rh-N(3) 2.120(2), Rh-Cl(1) 2.525(7), Rh-Cl(2) 2.376(4); C(1)-Rh-N(1) 82.99(2), C(1)-Rh-Cl(1) 175.71(2), C(1)-Rh-Cl(2) 91.34(2).

We wanted to extrapolate the formation of aryl-Co(III) complexes with macrocyclic model platforms to other substrates used in high-valent cobalt C-H activation. To do so, we selected a benzamide substrate bearing an 8-amino-5-nitroquinoline directing group (**NO₂-AQ**). Thus, substrate **6** (Scheme VII.5) was reacted with 1.0 equiv of Co(OAc)₂ in presence of 1.0 equiv of NaOPiv·H₂O in TFE under an oxygenated atmosphere (Scheme VII.6). Through this protocol, an organometallic aryl-Co(III) was obtained (**7**), which was characterized by NMR spectroscopy (Figures S24-26, Annex I). Indeed, a diamagnetic ¹H NMR spectrum was obtained consistent with a low spin Co(III) species similarly to the previously synthesized **4x-OAc** intermediates.



Scheme VII.6. Synthesis of aryl-Co(III) complexes **7** and **8** containing benzamide **6** bearing an 8-aminoquinoline directing group.

Although suitable crystals of **7** for XRD analysis could not be obtained, when ether was slowly diffused to a solution containing **7** and 4.0 equiv of 2,2-bipyridine in CH₃CN, crystals of the octahedral complex **8** were obtained and analyzed by XRD (Figure VII.4). This compound represents a rare example of an organometallic aryl-Co(III) complex synthesized through *N,N*-bidentate directing-group-assisted C-H activation.

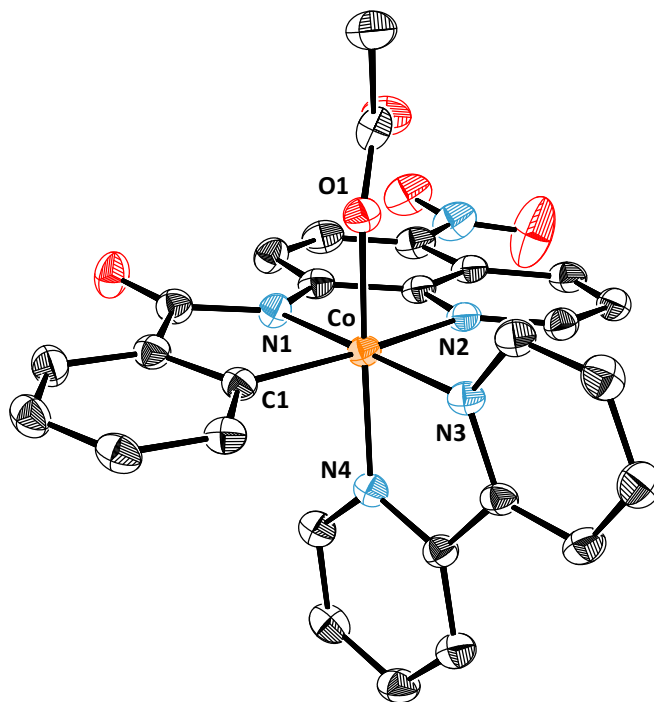


Figure VII.4. Solid state structure of aryl-Co(III) species **8**. Selected bond distances [Å] and angles [°]: Co-C(1) 1.919(2), Co-N(1) 1.889(2), Co-N(2) 2.007(2), Co-N(3) 1.934(2), Co-N(4) 1.931(2), Co-O(1) 1.932(2); C(1)-Co-N(1) 84.24(9), C(1)-Co-N(2) 166.33(9), C(1)-Co-N(3) 97.67(9), C(1)-Co-N(4) 88.88(9), C(1)-Co-O(1) 87.48(8).

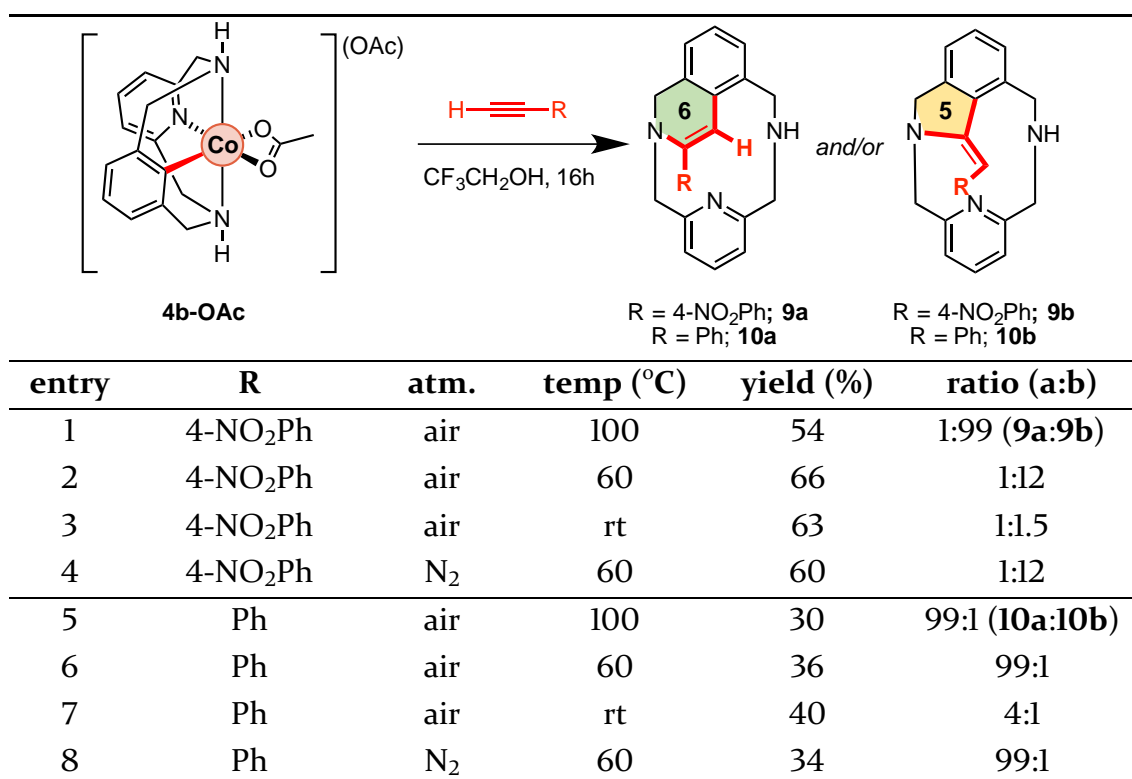
VII.1.3 Reactivity of aryl-Co(III) complexes with terminal alkynes

Once we had been able to synthesize, isolate and characterize the above disclosed organometallic aryl-Co(III) compounds, the next goal was to evaluate their reactivity towards alkynes. In fact, alkynes were selected due to their importance in Co(III)-catalyzed annulation reactions, providing a facile route towards a variety of biologically and pharmaceutically relevant heterocycles, as it has been exposed in Chapter I. Unfortunately, the mechanisms of these reactions are still poorly understood, although organometallic intermediates are generally implicated. Thus, in this section we evaluated the reactivity of **4b-OAc** towards terminal alkynes. Important mechanistic implications were obtained from the stoichiometric and catalytic reactions, as well as some insight in the reaction mechanism was achieved through theoretical calculations performed in collaboration with Dr. Vlad Martin-Diaconescu and Dr. Josep Maria Luis.

VII.1.3.1 Stoichiometric reaction

We envisioned that **4b-OAc** may provide similar products to the previously reported Co(III)-catalyzed annulation reactions with alkynes,⁸ which are believed to proceed via β -migratory insertion of the alkyne into the carbon-Co(III) bond, furnishing dihydroisoquinoline cyclic compounds (6-membered ring) after reductive elimination of the Co(III) centre with our macrocyclic ligand. However, reaction of **4b-OAc** with 1-ethynyl-4-nitrobenzene at 100 °C in TFE unexpectedly resulted in the regioselective formation of the 5-membered ring dihydroisoindoline product **9b** in good yields (Table VII.1, entry 1). The unexpected formation of **9b** led us to explore this reactivity further, changing the reaction conditions, such as temperature and electronic properties of the alkyne coupling partner. Thus, reactions with 1-ethynyl-4-nitrobenzene were carried out at lower temperatures (Table VII.1, entries 2 and 3) and interestingly, mixtures of **9a** (6-membered ring) and **9b** were obtained, with increasing ratio of **9a** with decreasing temperature. This result suggests that **9b** is the thermodynamic product, whilst **9a** is the kinetic product. Interestingly, the reaction can be carried out under an inert atmosphere (Table VII.1, entry 4), which indicates that no oxidant is required.

Table VII.1. Stoichiometric reaction of **4b-OAc** with terminal alkynes for the synthesis of dihydroisoquinoline (**9a** and **10a**) or dihydroisoindoline (**9b** and **10b**) products.



^a Reaction conditions: **4b-OAc** (40 mg, 0.077 mmol) and alkyne (2.0 equiv.) were mixed in TFE and stirred at different temperatures and atmospheres over 16 h. ^b Products were isolated using silica-gel chromatography. ^c Ratios were determined by NMR spectrometry.

Thereafter, reaction of **4b-OAc** with phenylacetylene was tested at 100 °C in TFE, which resulted in the selective formation of the 6-membered ring product **10a** (Table 1, entry 5). Surprisingly, other isomers were never observed, showing that the reaction is regioselective towards the dihydroisoquinoline product **10a**. The same results were obtained when reactions were carried out at 60 °C in TFE, under air or N₂ atmospheres. However, when reactions were carried out at room temperature, a mixture of **10a** and **10b** was obtained (Table 1, entries 6 and 7), similarly to the reactivity observed with 1-ethynyl-4-nitrobenzene. In contrast, in the reaction with phenylacetylene the thermodynamic product is **10a**, while **10b** is the kinetic product.

VII.1.3.2 Catalytic transformation

The annulation reaction was also studied in a catalytic fashion starting from **2b-H** and terminal alkynes. Catalytic quantities of Co(OAc)₂, **3b-OAc** and **4b-OAc** were used, together with 1-ethynyl-4-nitrobenzene and **2b-H** (Table VII.2).

Table VII.2. Catalytic transformation of **2b-H** with terminal alkynes for the synthesis of dihydroisoquinoline (**9a**) or dihydroisoindoline (**9b**) products.

entry ^a	[Co] (x mol%)	atm.	yield ^b (%)	ratio ^c (9a:9b)
1	Co(OAc) ₂ (20)	air	66	1:99
2	Co(OAc) ₂ (20)	N ₂	5 ^d	n.d.
3	4b-OAc (20)	air	69	1:99
4	4b-OAc (20)	N ₂	13 ^d	1:99
5	4b-OAc (10)	air	43	1:99
6	4b-OAc (10)	N ₂	trace ^d	n.d.
7	3b-OAc (20)	air	58	1:99
8	3b-OAc (20)	N ₂	7 ^d	n.d.

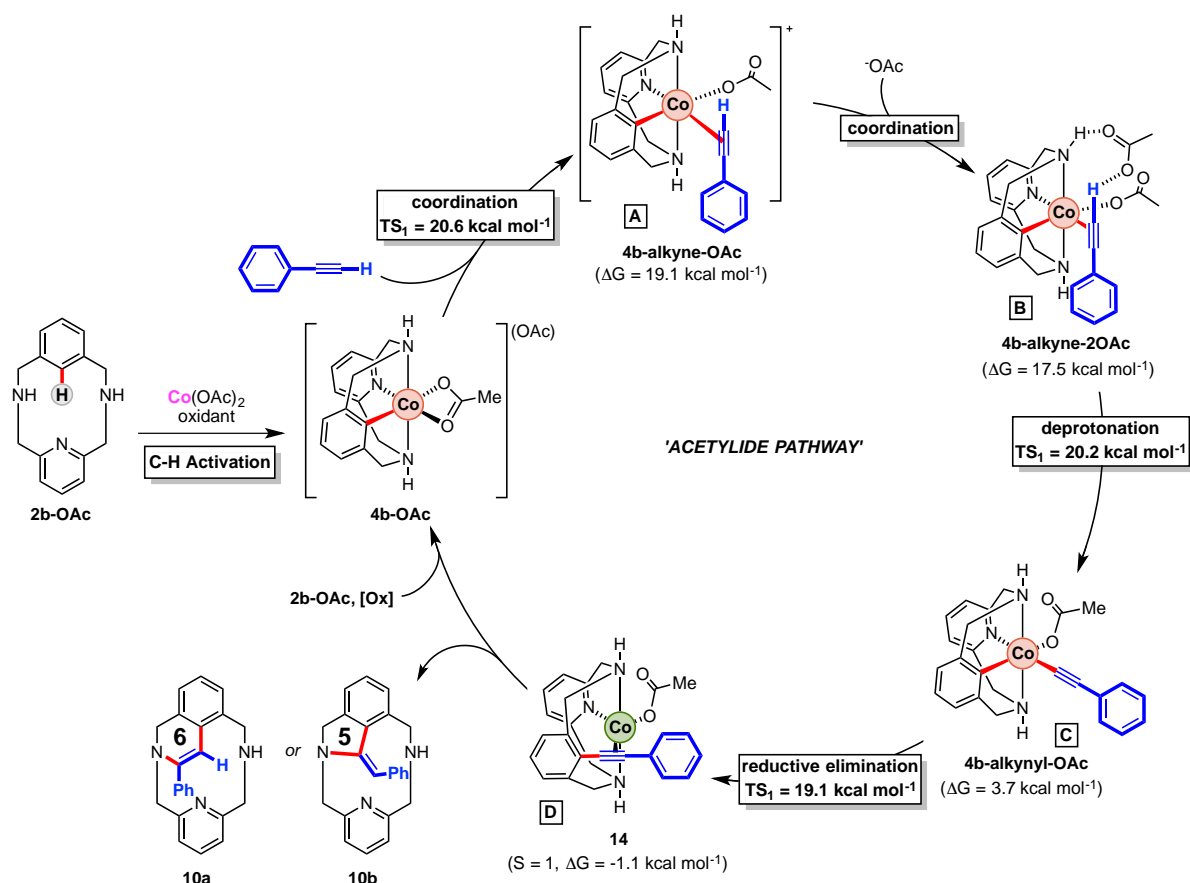
^a Reaction conditions: **2b-H** (0.077 mmol) and 1-phenyl-1-propyne (2.0 equiv.) were mixed in TFE with 10-20 mol% of **4b-OAc** and stirred at 100 °C under different atmospheres over 16 h. ^b Products were isolated using silica-gel chromatography. ^c Ratios were determined by ¹H NMR. ^d Yield determined using 1,3,5-trimethoxybenzene (TMB) as internal standard.

While the stoichiometric reactions proceed at room temperature (Table VII.1, entries 3 and 7), when the catalytic transformation was performed starting from $\text{Co}(\text{OAc})_2$ at room temperature no product was furnished. These results suggests that C-H activation is the rate determining step for these transformations, similarly to what is suggested for most studies in this field. 1-ethynyl-4-nitrobenzene was successfully coupled to **2b-H** at 80 °C using TFE as solvent, under air, with 20 mol% $\text{Co}(\text{OAc})_2$, **3b-OAc** or **4b-OAc** (Table VII.2, entries 1, 3 and 7). Under nitrogen, the reaction was quenched when starting from both Co(II) precursors or **4b-OAc** (Table VII.3 entries 2, 4 and 8), suggesting that a plausible reductive elimination takes place at some point of the mechanism, yielding a low-valent cobalt species that needs to be regenerated in the presence of external oxidant.

VII.1.4 Theoretical studies and reaction mechanism

To rationalize the formation of two different products (**10a** and **10b**) from the same starting materials (**4b-OAc** and phenyl acetylene) we propose the mechanism depicted in Scheme VII.6, which is supported by theoretical calculations and indicates that an aryl-Co(III)-alkynyl organometallic species is the key intermediate.

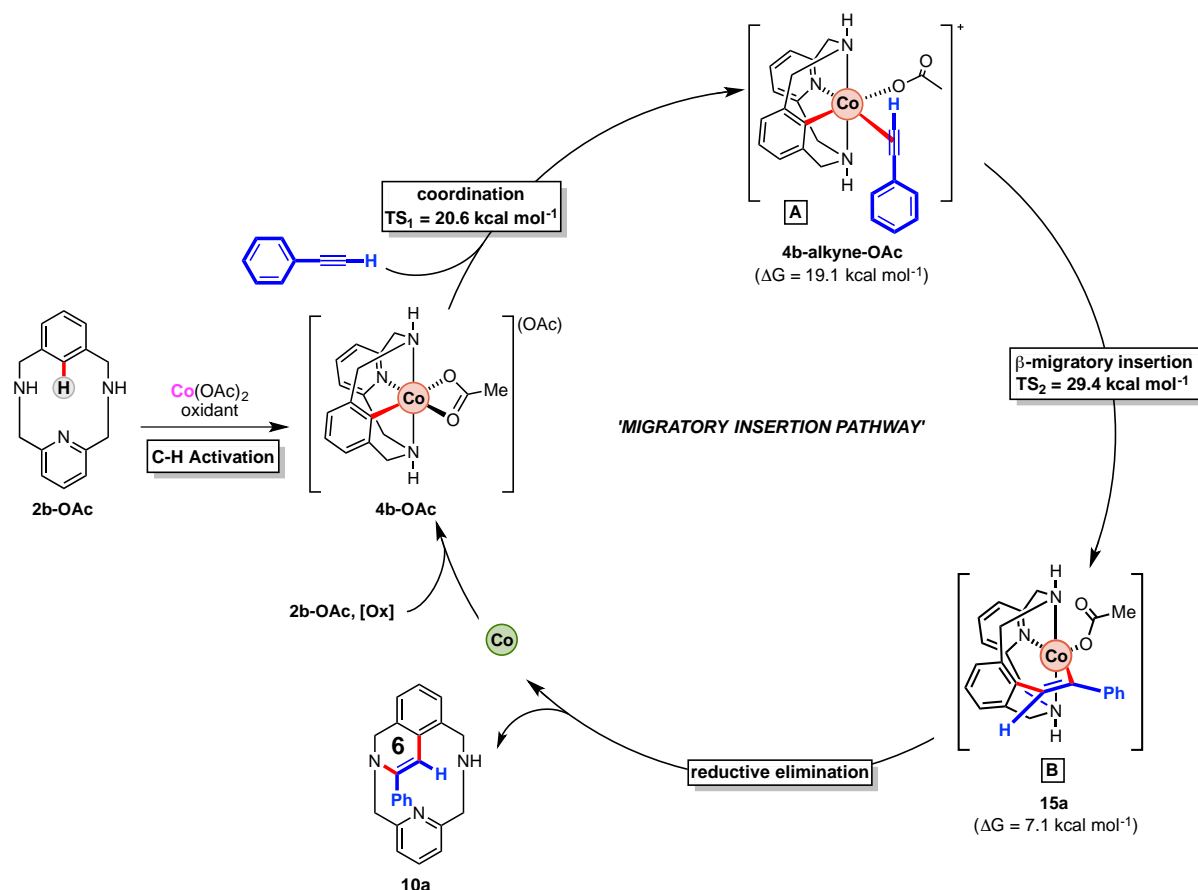
The proposed mechanistic pathway starts with the coordination of $\text{Co}(\text{OAc})_2$ to the model substrate **2b-H**, followed by oxidation and C-H activation through an electrophilic pathway such as CMD to yield **4b-OAc**. Starting from this intermediate, DFT calculations reveal that reaction with terminal alkynes proceeds through the detachment of the η^2 -OAc followed by coordination of the incoming alkyne, furnishing a cationic π -complex (**4b-alkyne-OAc**, $\Delta G = 19.1 \text{ kcal mol}^{-1}$, Scheme VII.7, A). Then, acetate-assisted deprotonation of the alkyne occurs *via* **4b-alkyne-2OAc** ($\Delta G = 17.5 \text{ kcal mol}^{-1}$, Scheme VII.7, B), which presents a hydrogen-bond between the alkyne and an acetate anion. Subsequent proton transfer and coordination of the alkyne furnishes the low spin aryl-Co(III)-alkynyl intermediate **4b-alkynyl-OAc** ($\Delta G = 3.7 \text{ kcal mol}^{-1}$, Scheme VII.7, C) through an energy barrier of $20.2 \text{ kcal mol}^{-1}$. **4b-alkynyl-OAc** is the characteristic intermediate of this cycle, which coins the name of this proposed mechanism as the “acetylide pathway”. Then, reductive elimination from **4b-alkynyl-OAc** produces the high spin $[(\mathbf{2b}\text{-CCPh})\text{Co}(\text{I})](\text{OAc})$ complex **14** ($\Delta G = -1.1 \text{ kcal mol}^{-1}$, Scheme VII.7, D). Thus, the C-C coupling proceeds from the singlet state of **4b-alkynyl-OAc**, which after a spin-crossing to the $S=1$ state overcomes a barrier of $\Delta G^\ddagger = 19.1 \text{ kcal mol}^{-1}$. Thereafter, an intramolecular cyclization assisted by the resulting Co(I) center furnishes either the 6-membered ring dihydroisoquinoline (**10a**) or the 5-membered ring dihydroisoinsoline (**10b**), depending on both the reaction temperature and the electronic properties of the alkyne.



Scheme VII.7. Mechanistic proposal for the formation of 5- and 6-membered ring products through the “acetylide pathway”. This mechanism was supported by DFT calculations.

For the synthesis of 6-membered ring products we can also think about a mechanism in which a β -migratory insertion takes place to furnish the commonly proposed 7-membered cobaltacycle. This process is referred as “migratory insertion pathway” (Scheme VII.8). In this alternative route, no deprotonation occurs and **4b-alkyne-OAc** undergoes a β -migratory insertion to yield the 7-membered cyclic intermediate **15a** ($\Delta G = 7.1 \text{ kcal mol}^{-1}$, Scheme VII.8, B), with a barrier of $\Delta G^\ddagger = 29.4 \text{ kcal mol}^{-1}$. Thereafter, reductive elimination from **15a** furnishes the 6-membered ring **10a**, whereas the 5-membered product **10b** cannot be obtained through this mechanism.

Our experimental observations of the formation of **10a** and **10b** when **4b-OAc** is reacted with phenylacetylene and the higher energy barrier to form **15a** compared to the barrier obtained for the “acetylide pathway” ($\Delta\Delta G^\ddagger = 9.2 \text{ kcal mol}^{-1}$) indicate that the key intermediate is likely to be an organometallic aryl-Co(III)-alkynyl species (**4b-alkynyl-OAc**, Scheme VII.7, C). Taking into account the DFT calculations, we propose that the mechanism exclusively operates through the ‘acetylide pathway’, whereas the commonly proposed ‘migratory insertion pathway’ is excluded for terminal alkynes (for results with internal alkynes, see Figure S13, Annex I).



Scheme VII.8. Mechanistic proposal for the formation of 5- and 6-membered ring products through the “migratory insertion pathway”. This mechanism was supported by DFT calculations.

The “acetylide pathway” provides potential reasoning for the reactivity reported by Song,⁹ Glorius¹⁰ and Ackermann¹¹ for Co(III)-catalyzed annulation protocols displaying different selectivity, but starting from the same substrates. Furthermore, formation of **4b-alkynyl-OAc** is consistent with the previously described aryl-Co(III)-alkynyl species proposed by Zhang,¹² Song⁹ and Balaraman¹³ in alkyne annulation reactions, albeit some of these authors propose a Co(II)/Co(IV) system.

In summary, a number of bench-top stable organometallic aryl-Co(III) complexes using model macrocyclic arene substrates have been prepared *via* C-H activation. Reaction of organometallic aryl-Co(III) intermediates has been proven to follow different reaction pathways depending on the nature of the alkyne coupling partners. Particularly, terminal alkynes furnished 5- and 6-membered ring products depending on both the electronic properties of the alkynes and the reaction temperature. The regioselectivity of the reactions as well as theoretical studies indicate that the ‘acetylide pathway’ is preferred for terminal alkynes, in contrast to the usually proposed ‘ β -migratory insertion pathway’. This work constitutes a unique fundamental basis for the understanding of Co-catalyzed C-H functionalization protocols.

VII.2 Carboxylate-Assisted Formation of Aryl-Co(III) Masked-Carbenes in Cobalt-Catalyzed C-H Functionalization with Diazo Esters

This section corresponds to the contents of the manuscript by Oriol Planas, Steven Roldan-Gomez, Vlad Martin-Diaconescu, Teodor Parella, Josep M. Luis, Anna Company and Xavi Ribas. *J. Am. Chem. Soc.* **2017**, *139*, 114649-14655, which can be found in Chapter IV of this thesis.

VII.2.1 Reactivity with ethyl diazo acetate (EDA)

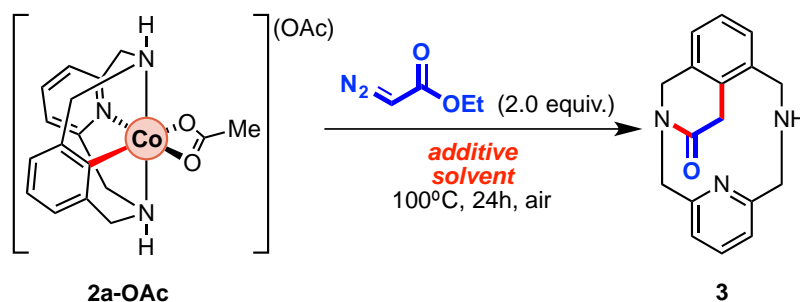
Among the variety of transformations catalyzed by Co(III) complexes, the use of diazo carbonyl compounds as carbene precursors has become a particularly attractive method. The interest on these coupling partners relies in their wide application in metal catalysis,¹⁴ including cyclopropanation¹⁵⁻¹⁸ as well as C-H functionalization.¹⁹⁻²¹ Several cobalt-carbene species are known with a variety of formal oxidation states,²²⁻²⁶ but their implication in C-H functionalization is barely known.²⁷⁻³² For this reason, we studied the reactivity of the isolated aryl-Co(III) complexes, reported in Chapter III towards ethyl diazo acetate (EDA). Thus, the main goal of this project was to elucidate the operative mechanism as well as the nature of the key reaction intermediates of this transformation.

VII.2.1.1 Stoichiometric reaction with EDA

This project started with the evaluation of the stoichiometric annulation reaction of the previously reported aryl-Co(III) complex **2a-OAc** (synthesized from macrocyclic model substrate **1a-H** and Co(OAc)₂) and ethyl diazo acetate (EDA). Solvents demonstrated to be key in this transformation (Table VII.3), and fluorinated alcohols such as TFE (Table VII.3, entry 2) and HFIP (Table VII.3, entry 3) were more beneficial for the formation of macrocyclic amide **3** compared to ethanol (Table VII.3, entry 1). Different commonly used proton sources were investigated as additives. Acetic acid, despite being an excellent proton source, was not successful for the formation of **3** (Table VII.3, entry 4), and protodemetalation of **2a-OAc** was observed. Then, softer proton sources were tried, and we were surprised to see that water was an excellent additive for this transformation, yielding up to 96% of macrocyclic amide **3** (Table VII.3, entries 7-9). Interestingly, the addition of 4.0 equiv water allowed to use ethanol as solvent, obtaining 88% NMR yield (Table VII.3, entry 10). Lewis acids, which have demonstrated to be excellent additives in other Co(III)-catalyzed C-H functionalization with diazo compounds,²⁸ were also evaluated. Indeed, 1.0 equiv of LiOTf was enough to obtain 88% isolated yield of **3**, even in absence of water (Table VII.3, entry 11) or using ethanol as solvent (91% NMR yield, Table VII.3, entry 12). The latter result indicates a cooperative effect between the solvent and the Lewis acids, probably by acidification of

ethanol converting it into a better proton source. The addition of other Lewis acids such as $\text{Mg}(\text{OTf})_2$ was also beneficial for the reaction (Table VII.3, entries 13 and 14) albeit the best results were obtained with higher acidic Lewis acids such as LiOTf . However, when both 1.0 equiv of $\text{Mg}(\text{OTf})_2$ and 1.0 equiv of H_2O were used as additives, **3** was obtained in a 92% yield, which suggest a cooperative effect between both additives.

Table VII.3. Optimization of stoichiometric reaction (see Table S13, Annex II).



entry	additive	solvent	yield of 3 (%) ^a
1	none	EtOH	traces
2	none	TFE ^b	10%
3	none	HFIP ^c	31%
4	AcOH (1.0 equiv.)	TFE	15% ^d
7	H_2O (1.0 equiv.)	TFE	57%
8	H_2O (2.0 equiv.)	TFE	82%
9	H_2O (4.0 equiv.)	TFE	96% (91%)^f
10	H_2O (4.0 equiv.)	EtOH	88%
11	LiOTf (1.0 equiv.)	TFE	95% (88%)^f
12	LiOTf (1.0 equiv.)	EtOH	91%
13	$\text{Mg}(\text{OTf})_2$ (1.0 equiv.)	TFE	67%
14	$\text{Mg}(\text{OTf})_2$ (4.0 equiv.)	TFE	52%
15	H_2O (1.0 equiv.) + $\text{Mg}(\text{OTf})_2$ (1.0 equiv)	TFE	92% (87%)^f

^aYield determined using 1,3,5-trimethoxybenzene as internal standard. ^b2,2,2-trifluoroethanol. ^c1,1,1,3,3,3-hexafluoro-2-propanol. ^dProtodemetalation of **2a-OAc** was observed. ^eTrifluoroacetic acid. ^fIsolated yield after silica gel chromatography in parenthesis.

In addition, reaction with the aryl-Co(III) complex bearing methylated tertiary amines (**2b-OAc**) was not successful and only trace amounts of product **4** were detected by HRMS ($[\text{M}+\text{H}]^+$; calcd. $m/z = 354.2176$; expt. $m/z = 354.2188$; Figure VII.5) together with starting **2b-OAc** and other products that will be disclosed and rationalized later (**5b-OAc**, see below).

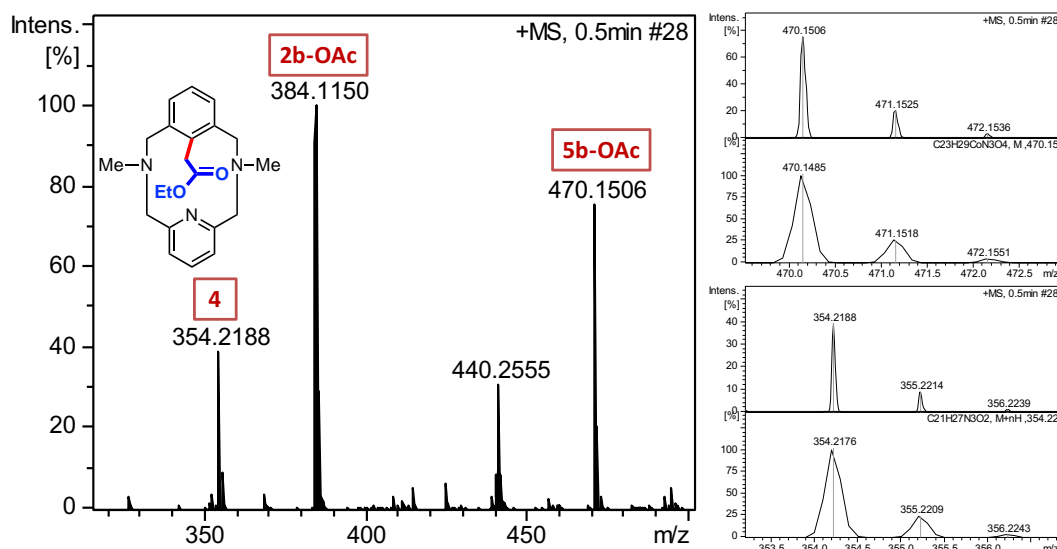


Figure VII.5. HRMS analysis of the crude reaction of **2b-OAc** and EDA in presence of water after 24h in TFE (main peaks). Peak at $m/z = 384.1150$ corresponds to **2b-OAc**; peak at $m/z = 354.2188$ corresponds to **4** and peak at $m/z = 470.1506$ corresponds to **5b-OAc**.

VII.2.1.2 Catalytic transformation with EDA

Catalytic conditions have also been evaluated, using either **2a-OAc** complexes or commercially available Co(II) salts as catalysts (Table VII.4). Not surprisingly, the reaction did not work in the absence of cobalt (Table VII.4, entry 1). When **2a-OAc** (20 mol%) was added, EDA (4.0 equiv) was successfully coupled with **1a-H** under air with TFE, yielding **3** in 87% isolated yield (Table VII.4, entry 2). When the same reaction was performed under an inert atmosphere (N_2), a similar result was obtained (Table VII.4, entry 3), which indicates that Co(III) does not undergoes reductive elimination generating a low-valent species that needs to be reoxidized. Co(II) salts were also tested as catalysts, and indeed **1a-H** and EDA were successfully coupled using $Co(OAc)_2$ (20 mol%) under an oxygenated atmosphere (89% isolated, Table VII.4, entry 5). When the reaction starting with Co(II) was run under an inert atmosphere **3** was obtained in trace amounts (Table VII.4, entry 6) indicating that an oxidant is essential in this transformation. Furthermore, additives proved to be key in the catalytic reaction as well, as in their absence **3** was obtained in 15% NMR yield (Table VII.4, entry 7). The relevance of oxidants was further tested with Ag(I) and $CoBr_2$ as catalyst (20 mol%). Interestingly, when 40 mol% $AgOAc$ was added (Table VII.4, entry 8), $AgBr$ precipitates, which excludes Ag(I) as a possible oxidant, an only trace amounts of product are obtained. However, when 1.0 equiv $AgOAc$ is added **3** is obtained in 67% NMR yield (Table VII.4, entry 9) indicating that the remaining $AgOAc$ acts as oxidant and allows reactivity. Addition of Lewis acids such as $Mg(OTf)_2$ (1-4 equiv, Table VII.4, entries 10 and 11) worked well, as well as when 1.0 equiv of $Mg(OTf)_2$ is mixed with 1.0

equiv of H₂O (Table VII.4, entry 12) However, the best result was obtained when 1.0 equiv LiOTf was added, furnishing **3** in 88% isolated yield.

Table VII.4. Optimization of catalytic reaction using a variety of cobalt salts as catalysts and water or Lewis acids as additives (see Table SI6, Annex II).

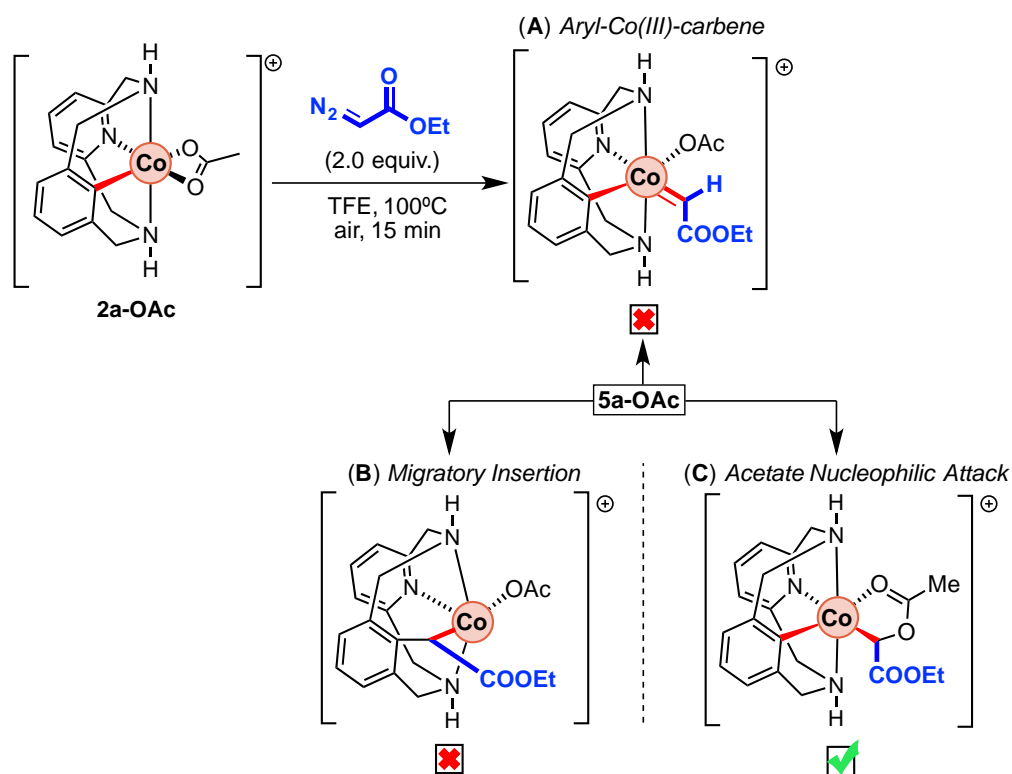
entry	[Co] (x mol%)	additives (equiv.)	yield of 3 (%) ^b
1	-	H ₂ O (4.0)	n.r.
2	2a-OAc (20)	H ₂ O (4.0)	93% (87%) ^c
3 ^d	2a-OAc (20)	H ₂ O (4.0)	95% (84%)^c
4	2a-OAc (10)	H ₂ O (4.0)	47%
5	Co(OAc) ₂ (20)	H ₂ O (4.0)	96% (89%)^c
6 ^d	Co(OAc) ₂ (20)	H ₂ O (4.0)	traces
7	Co(OAc) ₂ (20)	none	15%
8 ^d	CoBr ₂ (20)	H ₂ O (4.0) + Ag(OAc) (0.4)	traces
9 ^d	CoBr ₂ (20)	H ₂ O (4.0) + Ag(OAc) (1.0)	67%
10	Co(OAc) ₂ (20)	Mg(OTf) ₂ (1.0)	42%
11	Co(OAc) ₂ (20)	Mg(OTf) ₂ (4.0)	73%
12	Co(OAc) ₂ (20)	Mg(OTf) ₂ (1.0) + H ₂ O (1.0)	93% (84%) ^c
13	Co(OAc) ₂ (20)	Li(OTf)	96% (88%)^c

^aRatio determined by NMR. ^bYield using 1,3,5-trimethoxybenzene as internal standard. ^cIsolated yields after silica gel chromatography. ^dReaction performed under inert atmosphere (N₂). ^eNMR with presence of multiple byproducts was obtained.

VII.2.2 Mechanistic Insight

To understand the key mechanistic features of this transformation we initially focused on the possibility of isolating the corresponding reaction intermediates. When **2a-OAc** was reacted with 2.0 equivalents of EDA at 100 °C over 15 minutes, HRMS analysis showed the formation of a single species with a peak at $m/z = 442.1183$ (Figure S54, Annex II), which corresponds to the molecular formula [C₂₁H₂₅CoN₃O₄]⁺ and suggests the formation of the aryl-Co(III)-carbene intermediate **A** depicted in Scheme VII.9. To gain more information about this intermediate (**5a-OAc**), it was analyzed by

ID and 2D NMR spectroscopy. A diamagnetic ^1H NMR spectrum was obtained (Figure S49, Annex II), which is consistent with an octahedral Co(III) low spin species. Interestingly, a singlet at a chemical shift of 5.81 ppm discarded the presence of a putative aryl-Co(III)-carbene species, as the α -proton of the carbene moiety is known to be highly deshielded.³³ Moreover, the presence of two double quadruplets at 3.21 and 3.75 ppm corresponding to the diastereotopic protons of the methylene group of the ester confirms the existence of an intermediate containing a chiral center, which further discards an aryl-Co(III)-carbene intermediate. Further spectroscopic evidence for the absence of this intermediate was obtained from the ^{13}C NMR spectra (Figure S51, Annex II), as no signal was detected in the typical metal-carbene region.³⁴ The presence of signal at a chemical shift of 76.5 ppm HSQC-correlated to the singlet at a chemical shift of 5.81 ppm (Figure S52, Annex II) suggests a possible intermediate in which the carbene migratory insertion into the aryl-Co(III) bond has already taken place (Scheme VII.9, species B). However, further characterization by 2D NMR revealed that the actual intermediate is obtained after a nucleophilic attack of the carboxylate moiety to the electrophilic carbon atom from a putative aryl-Co(III)-carbene. This nucleophilic attack allows the formation of an unprecedented C-metalated aryl-Co(III) enolate, **5a-OAc** (Scheme VII.9, species C), which could be formally described as a carbenoid species (carbon atom attached to both a metal centre and a leaving group).



Scheme VII.9. Reactivity of bench-top stable aryl-Co(III) organometallic compounds with diazoacetates and formation of hypothesized intermediates **A** (aryl-Co(III)-carbene) and **B** (Aryl-EDA-Co(III)), or the actual intermediate, **C** (Aryl-Co(III)-alkyl).

Attempts to unravel the nature of **5a-OAc** have been pursued by crystallographic analysis without success. Nevertheless, suitable crystals for XRD analysis were obtained by reaction of *p*-substituted benzoate complexes **2a-OBz-R** (R = OMe, Cl) with EDA. Reaction of **2a-OBz-R** with 2.0 equiv of EDA in TFE at 100 °C resulted in a rapid color change from red to orange, and after recrystallization in CH₃Cl/pentane, **5a-OBz-R** were obtained in good yields (85-97%). The solid-state structures of the corresponding intermediates supported the initial NMR characterization (Figure VII.6), showing an octahedral aryl-Co(III) center bearing a carbonyl and a chiral alkyl group as ligands (**5a-OBz-R**). Subsequently, the formation of **5a-OBz-R** species is rationalized by trapping of the highly electrophilic Co(III)-carbene through a nucleophilic intramolecular attack of the carboxylate moiety to C2. Both **5a-OBz-OMe** and **5a-OBz-Cl** compounds show spectroscopic features analogous to **5a-OAc**, indicating the same structure, although **5a-OBz-Cl** presented a minor conformer in solution (See Figures S57, Annex II). In addition, EXAFS analysis of **5a-OAc** agrees with the structures depicted in Figure VII.6 (see Supplementary Digital Material).

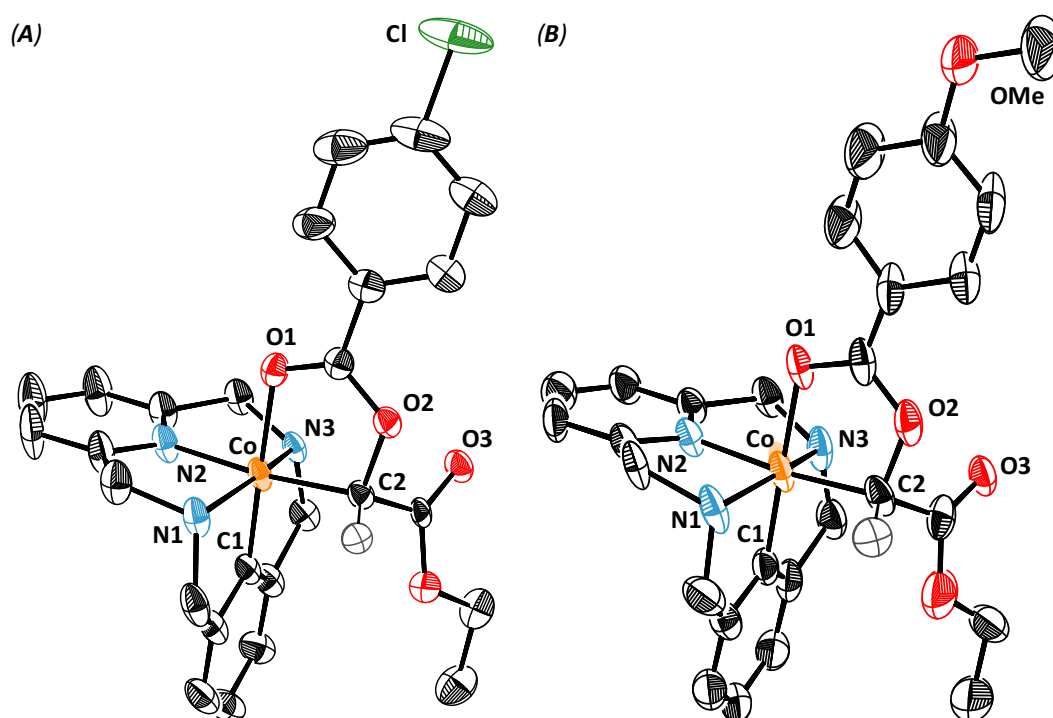


Figure VII.6. Solid state structures of **5a-OBz-R**. Hydrogen-atoms, anions and solvent molecules have been omitted and only one of the enantiomers is depicted for clarity; ellipsoids displayed at 50% (**5a-OBz-Cl**) and 30% (**5a-OBz-OMe**) probability. (A) **5a-OBz-OMe**. Selected bond distances [Å] and angles [°]: Co-C(1) 1.82(2), Co-C2 1.97(4), Co-N(1) 2.02(4), Co-N(2) 1.88(3), Co-N(3) 1.99(4), Co-O(1) 2.01(4), C(2)-O(2) 1.50(7); C(1)-Co-C(2) 95.6(1), C(1)-Co-O(1) 179.2(2). (B) **5a-OBz-Cl**. Selected bond distances [Å] and angles [°]: Co-C(1) 1.82(2), Co-C2 1.97(4), Co-N(1) 2.02(4), Co-N(2) 1.88(3), Co-N(3) 1.99(4), Co-O(1) 2.01(4), C(2)-O(2) 1.50(7); C(1)-Co-C(2) 95.6(1), C(1)-Co-O(1) 179.2(2).

To better understand the role of additives in the formation of cyclic amide **3**, a variety of control experiments were performed starting from **5a-OAc** (Table VII.5). While without additives poor yields were obtained (Table VII.5, entry 1), even with longer reaction times (Table VII.5, entry 2), when water (Table VII.5, entry 3), organic acids (Table VII.5, entries 4 and 5) or Lewis acids (Table VII.5, entries 6-9) were added to **5a-OAc**, **3** was obtained in 26-89% yield. The transformation of **5a-OAc** into **3** involves the cleavage of a C-O bond and the formation of a new C-C bond. Furthermore, the increase in yield obtained when LiOTf or organic acids are added suggests an activation of the carboxylate group through hydrogen bonding or coordination to Lewis acids, which converts it in a better leaving group. Indeed, when the aryl-Co(III) complex **2a-TFA**, which is bearing a weak base as anion such as trifluoroacetate, was reacted with EDA neither isolation nor detection of **5a-TFA** by HRMS was achieved and **3** was obtained in 79% yield in absence of any external additive.

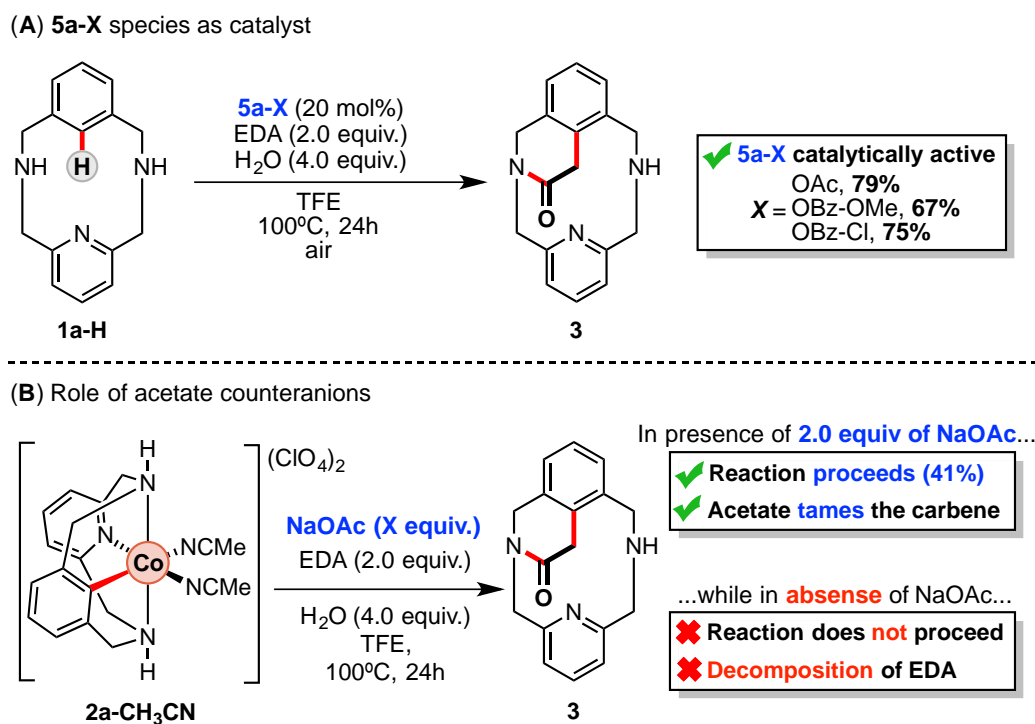
Table VII.5. Use of a variety of additives in the formation of **3** from **5a-OAc** species.

entry	additive	yield of 3 (%) ^a
1	none	14%
2 ^b	none	52%
3	H ₂ O	85%
4	AcOH	51%
5	CF ₃ SO ₃ H	82%
6	Li(OTf)	89%
7	Mg(OTf) ₂	67%
8	Zn(OTf) ₂	58%
9	B(C ₆ F ₅) ₃	26%

^aYield determined using TMB as internal standard. ^bReaction was carried out over 48h.

The catalytic competence of **5a-X** (X = OAc, OBz-OMe and OBz-Cl) was tested in a reaction with **1a-H**, 2.0 equiv of EDA and 4.0 equiv of H₂O in TFE at 100 °C (Scheme VII.10, A). Regardless of the carboxylate anion, **3** was obtained in good yields (67-79%) which indicates that organometallic **5a-X** complexes are catalytically active and might be actual on-cycle intermediates. Furthermore, in order to know which is the role of the

acetate anions, the previously reported dicationic complex **2a-CH₃CN** was reacted with 2.0 equiv of EDA and 4.0 equiv of H₂O in TFE at 100 °C over 24h (Scheme VII.10, B). Interestingly, EDA was fully decomposed, which suggest the formation of a very reactive and unstable Co(III)-carbene intermediate. Indeed, when 2.0 equiv of NaOAc were added, **3** was obtained in 41% yield. This result suggests that when the Co(III) center contains a carboxylate moiety, carboxylate-masked aryl-Co(III) carbenoids (**5a-X**) are formed. Therefore, carboxylate anions may be involved in taming the reactivity of a highly electrophilic aryl-Co(III)-carbene intermediate.



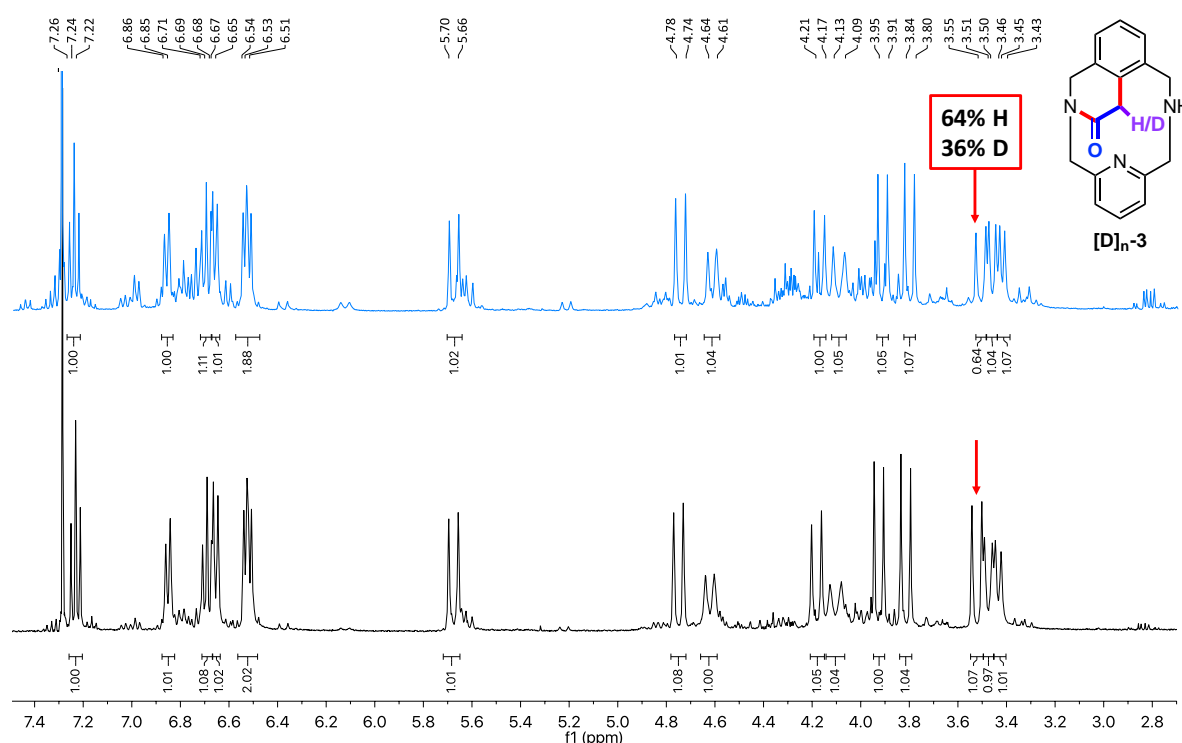
Scheme VII.10. (A) Use of **5a-X** as catalysts for the construction of macrocyclic amide **3** and (B) role of acetate anions in this transformation.

Further insight into the reaction mechanism was obtained by D-labeling experiments (Table VII.6). When **2a-OAc** was treated with EDA and 4.0 equiv of D₂O were added in TFE at 100 °C (Table VII.6, entry 1), a 36% D-incorporation was observed by NMR and HRMS analysis at the α position of the carbonyl group in **3**, in a stereoselective manner (Figure VII.7). Increasing D-incorporation was observed when H₂O (65%; Table VII.6, entry 2) and D₂O (86%; Table VII.6, entry 3) were added as additives in TFE-d₃ (Figures S34-39, Annex II). Interestingly, 91% (Table VII.6, entry 4) and 93% (Table VII.6, entry 4) D-labeled **3** was obtained when the reaction was performed using 1.0 equiv of Li(OTf) in TFE-d₃ (Figures S40-41, Annex II) and in MeOD-d₄ (Figures S42-43, Annex II), respectively, in absence of water. These results suggest that 1) there is a protodemetalation event of a plausible alkyl-Co(III) species and 2) Lewis acids may cooperate with the solvent, increasing its acidity as proton source.

Table VII.6. Deuterium-labeling experiments with deuterated TFE as solvent or labeled D₂O and Lewis acids as additives.

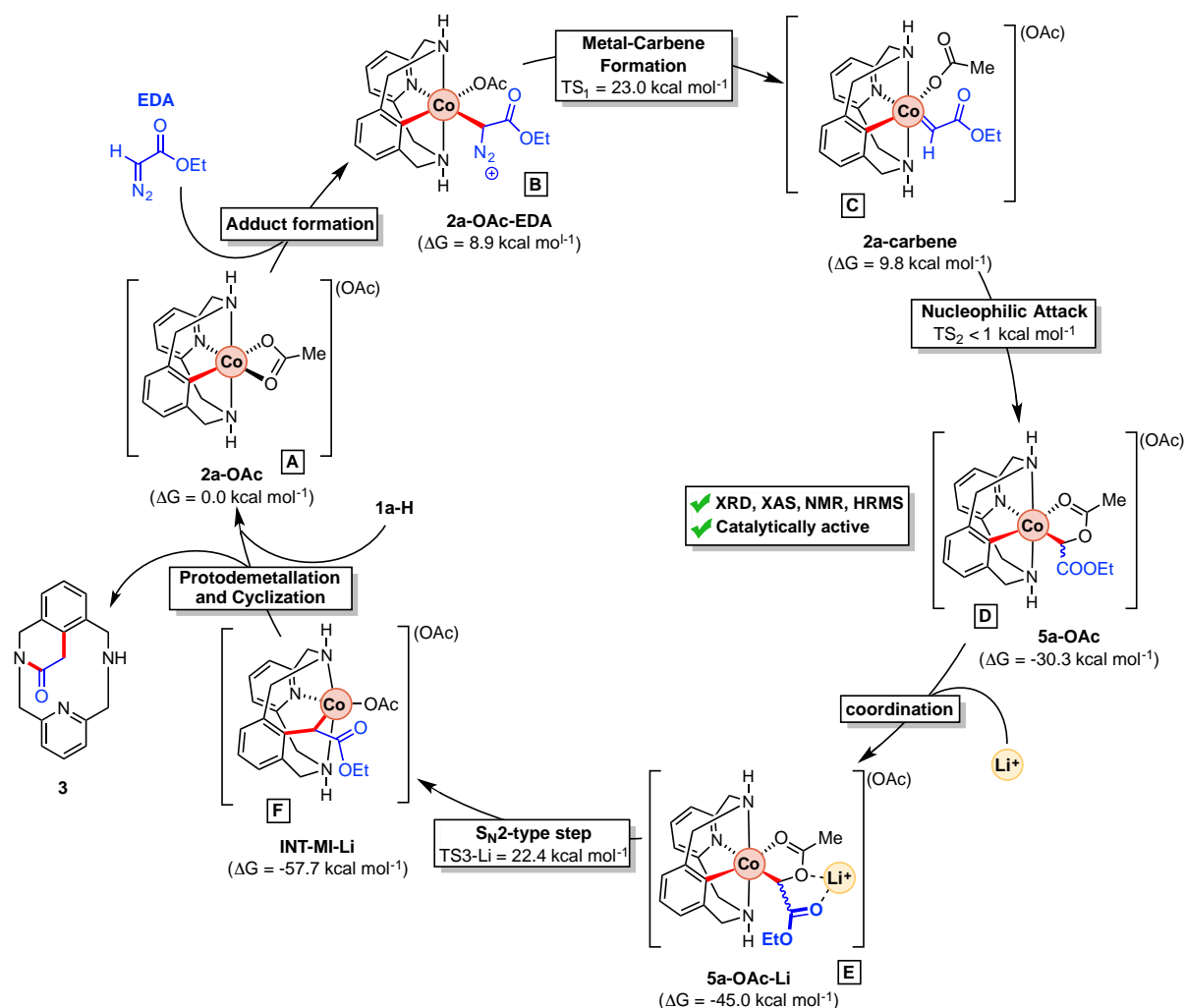
entry	additive (equiv.)	solvent	D-incorporation (%)
1	D ₂ O (4.0)	TFE	36%
2	H ₂ O (4.0)	TFE-d ₃	65%
3	D ₂ O (4.0)	TFE-d ₃	86%
4	Li(OTf) (1.0)	TFE-d ₃	91%
5	Li(OTf) (1.0)	MeOD-d ₄	93%

^aD-incorporation determined by ¹H NMR integration and HRMS analysis (see Annex I).

**Figure VII.7.** ¹H NMR spectrum of [D]_n-3 (up, blue) and 3 (down, black) recorded at 298K using CDCl₃ as solvent. 36% of D-incorporation was observed (Table VII.6, entry 1).

With all the exposed experimental evidences, we propose the catalytic cycle depicted in Scheme VII.11, which is supported by DFT calculations performed in collaboration with Steven Roldán and Josep M. Luis from Universitat de Girona. The

cycle starts from the organometallic aryl-Co(III) species **2a-OAc** (**A**), which mixed with EDA furnishes the C-metalated adduct **2a-OAc-EDA** ($\Delta G = 8.9 \text{ kcal mol}^{-1}$, **B**). Afterwards, **2a-OAc-EDA** evolves to **2a-carbene** ($\Delta G = 9.8 \text{ kcal mol}^{-1}$, **C**) overcoming a $23.0 \text{ kcal mol}^{-1}$ transition state (TS_1). This putative Co-carbene species reacts with the adjacent acetate, giving the isolated C-metalated aryl-Co(III) enolate **5a-OAc** ($\Delta G = -30.3 \text{ kcal mol}^{-1}$, **D**) in a barrierless manner. Indeed, depending on the DFT method, **2a-carbene** cannot be optimized and TS_1 directly evolves to the isolated **5a-OAc** (Figure S45, Annex II). Therefore, TS_1 can be understood as a *concerted asynchronous* transition state that leads to the formation of the new C-Co and C-O bonds in **5a-OAc**.



Scheme VII.11. Mechanistic proposal for the formation 6-membered ring cyclic amide **3** by reaction of **2a-OAc** with EDA as coupling partner. This mechanism was supported by DFT calculations.

At this point, a Li^+ ion coordinates **5a-OAc**, furnishing the intermediate **5a-OAc-Li** ($\Delta G = -45.0 \text{ kcal mol}^{-1}$, **E**), which evolves through an unprecedented intramolecular $\text{S}_{\text{N}}2$ -type C-O cleavage/C-C formation event ($\text{TS}_{3\text{-Li}} = 22.4 \text{ kcal mol}^{-1}$). This low barrier

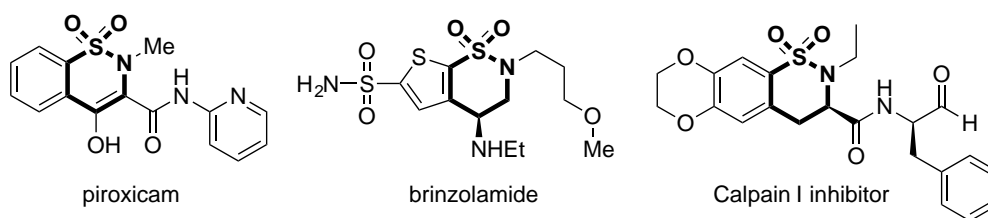
explains the experimental results obtained when Lewis acids such as LiOTf are added, promoting the formation of the macrocyclic amide **3**. Indeed, DFT calculations in absence of Li⁺ provide a higher barrier (TS3 = 29.4 kcal mol⁻¹, see Chapter IV) which indeed explains the accumulation of **5a-OAc**. Then, after overcoming this barrier, **INT-MI-Li** ($\Delta G = -57.7$ kcal mol⁻¹, **F**), which can be indirectly detected by HRMS (See Figure S33, Annex II), undergoes protodemetalation, as we observed by the deuterium incorporation experiments. Finally, after a Lewis acid promoted intramolecular cyclization, compound **3** is obtained and the cycle starts again. It should be noted that in this mechanistic proposal the oxidation state of cobalt remains unaltered. Thus, Co(III) promotes the C-H activation step, as well as the S_N2-type C-O cleavage/C-C formation event and the final Lewis acid intramolecular condensation of one of the lateral amines and the ester.

To summarize, in this section unique C-metalated aryl-Co(III) enolate species (**5a-X**) have been synthesized and fully characterized. Indeed, crystallographic, full spectroscopic characterization and theoretical evidences show that masked carbenes **5a-X**, which have proved to be catalytically active intermediates, are necessary to construct the new C-C bond and finally furnish the cyclic amide **3**. Moreover, theoretical studies indicate that this transformation occurs through a unique intramolecular S_N2-type C-C bond formation event in which the carboxylate acts as a relay. The experimental key role of Lewis acids, particularly LiOTf, is reflected in the theoretical studies, unveiling a Li-mediated carboxylate activation that triggers the S_N2-like pathway.

VII.3 Regioselective Access to Sultam Motifs through Cobalt-Catalyzed Annulation of Aryl Sulfonamides and Alkynes using an 8-Aminoquinoline Directing Group

This section corresponds to the contents of the manuscript by Oriol Planas, Christopher J. Whiteoak, Anna Company and Xavi Ribas. *Adv. Synth. Catal.* **2015**, 357, 4003-4012, which can be found in Chapter V of this thesis.

The fundamental knowledge derived from sections VII.1 and VII.2 with macrocyclic model substrates is a feedback for the development of methodologies for the synthesis of cyclic sulfonamide motifs (sultams). Indeed, sultams have found application as anti-inflammatory drugs (piroxicam), carbonic anhydrase inhibitors (brinzolamide) as well as calpain I inhibitors in cell signaling dysfunctions (Scheme VII.12).



Scheme VII.12. Drugs containing cyclic sulfonamide motifs.

Although the typical methodologies for their synthesis involve elaborated precursors and precious transition metals,³⁵⁻³⁷ new methodologies using cobalt as catalysts have proven to be promising alternatives for their synthesis.³⁸ With these precedents in mind, we decided to investigate the possibility of performing a Co(II)-catalyzed aryl sulfonamide annulation with alkynes (see below), seeking improved regioselective control compared with the previously described Rh-catalyzed protocol and to showcase the potential of using Co in annulation reactions.

VII.3.1 Optimization of reaction conditions

The first steps of this project were directed towards the optimization of reaction conditions starting from the benzenesulfonamide **1a** towards the formation of sultam **1aa**. Thus, we attempted the coupling of sulfonamide **1a** with phenylacetylene using a catalytic system comprising Co(OAc)₂ (20 mol%) as catalyst, Mn(OAc)₂ as oxidant and KOAc as base, in TFE at 100 °C. With these conditions, which are similar to the catalytic system reported by Daugulis,⁸ **1aa** was obtained in 22% NMR yield. Encouraged by this result, the reaction conditions were further optimized in terms of cobalt source, oxidant and base using 2,2,2-trifluoroethanol (TFE) as solvent (Table VII.7).

A variety of oxidants were investigated using $\text{Co}(\text{OAc})_2$ and KOAc (Table VII.7, entries 1-7). From these experiments, $\text{Mn}(\text{OAc})_3 \cdot 2\text{H}_2\text{O}$ was found to be the best oxidant among those tested and **1aa** was obtained in 62% NMR yield. It should be noted that the presence of oxidants is crucial, and when the reaction is carried out under inert atmosphere, **1aa** is obtained in only trace amounts (Table VII.7, entry 7). Afterwards, a variety of bases were tested (Table VII.7, entries 8-12), whereby the best result was obtained with $\text{NaOPiv} \cdot \text{H}_2\text{O}$, with a 91% NMR yield of **1aa**. In addition, no improvement was obtained with other cobalt sources (Table VII.7, 13-17).

Table VII.7. Optimization of the reaction conditions for the synthesis of sultam motifs.^a

entry	catalyst	oxidant	base	Yield of 1aa [%] ^b
1	$\text{Co}(\text{OAc})_2$	$\text{Mn}(\text{OAc})_2$	KOAc	22
2	$\text{Co}(\text{OAc})_2$	Benzoquinone	KOAc	<1
3	$\text{Co}(\text{OAc})_2$	Ag_2O	KOAc	6
4	$\text{Co}(\text{OAc})_2$	$\text{PhI}(\text{OAc})_2$	KOAc	12
5	$\text{Co}(\text{OAc})_2$	$\text{Mn}(\text{OAc})_3 \cdot 2\text{H}_2\text{O}$	KOAc	62
6	$\text{Co}(\text{OAc})_2$	O_2	KOAc	3
7 ^c	$\text{Co}(\text{OAc})_2$	-	KOAc	<1
8	$\text{Co}(\text{OAc})_2$	$\text{Mn}(\text{OAc})_3 \cdot 2\text{H}_2\text{O}$	Na_2CO_3	22
9	$\text{Co}(\text{OAc})_2$	$\text{Mn}(\text{OAc})_3 \cdot 2\text{H}_2\text{O}$	$\text{NaOPiv} \cdot \text{H}_2\text{O}$	91(90)^d
10	$\text{Co}(\text{OAc})_2$	$\text{Mn}(\text{OAc})_3 \cdot 2\text{H}_2\text{O}$	CsOPiv	78
11	$\text{Co}(\text{OAc})_2$	$\text{Mn}(\text{OAc})_3 \cdot 2\text{H}_2\text{O}$	$\text{NaOAc} \cdot \text{H}_2\text{O}$	67
12	$\text{Co}(\text{OAc})_2$	$\text{Mn}(\text{OAc})_3 \cdot 2\text{H}_2\text{O}$	CsOAc	69
13	-	$\text{Mn}(\text{OAc})_3 \cdot 2\text{H}_2\text{O}$	$\text{NaOPiv} \cdot \text{H}_2\text{O}$	0
14	CoCl_2	$\text{Mn}(\text{OAc})_3 \cdot 2\text{H}_2\text{O}$	$\text{NaOPiv} \cdot \text{H}_2\text{O}$	90
16	$\text{Co}(\text{acac})_2$	$\text{Mn}(\text{OAc})_3 \cdot 2\text{H}_2\text{O}$	$\text{NaOPiv} \cdot \text{H}_2\text{O}$	28
17	$\text{Co}(\text{acac})_3$	$\text{Mn}(\text{OAc})_3 \cdot 2\text{H}_2\text{O}$	$\text{NaOPiv} \cdot \text{H}_2\text{O}$	17

^aReaction conditions: aryl sulfonamide (**1a**) (0.17 mmol), ethynylbenzene (2.0 equiv.), Co source (20 mol%), oxidant (1.0 equiv.), base (2.0 equiv.), 2.0 mL TFE at 100 °C, under air for 24 h.

^bYield calculated by ¹H NMR analysis of crude reaction mixture using mesitylene as internal standard. ^cReaction prepared and performed under a N_2 atmosphere. ^dAt 100 °C for 16 h.

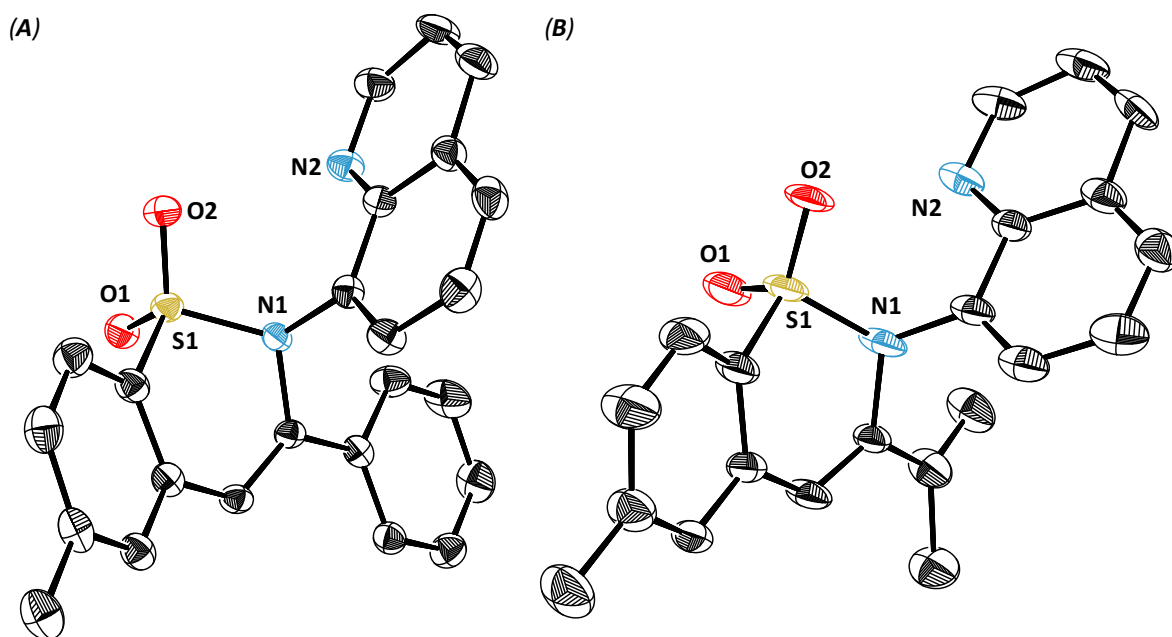
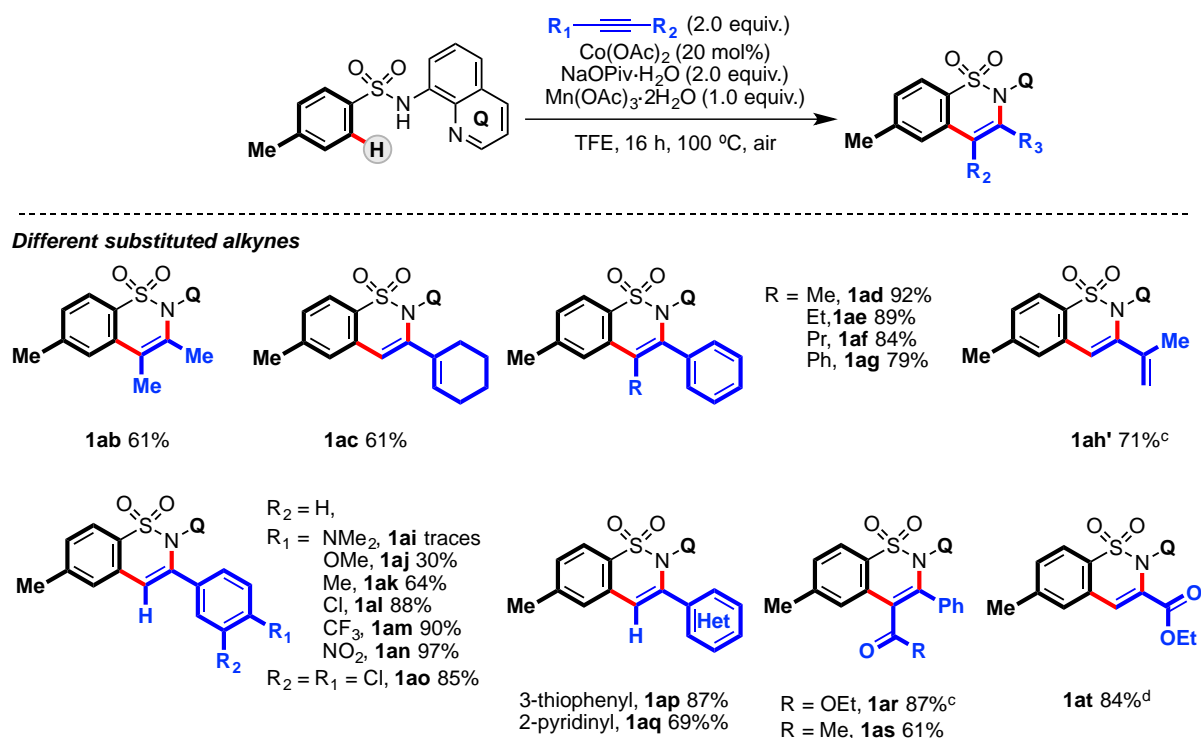


Figure VII.8. Solid state structures of synthesized sultam motifs. Hydrogen-atoms and solvent molecules have been omitted for clarity; ellipsoids displayed at 50% probability. **(A) 1aa.** Selected bond distances [\AA] and angles [$^\circ$]: S-O(1) 1.428(1), S-O(2) 1.429(1), S-N(1) 1.658(1); O(1)-S-O(2) 119.1(2). **(B) 1ah'.** Selected bond distances [\AA] and angles [$^\circ$]: S-O(1) 1.415(5), S-O(2) 1.434(4), S-N(1) 1.647(5); O(1)-S-O(2) 119.5(2).

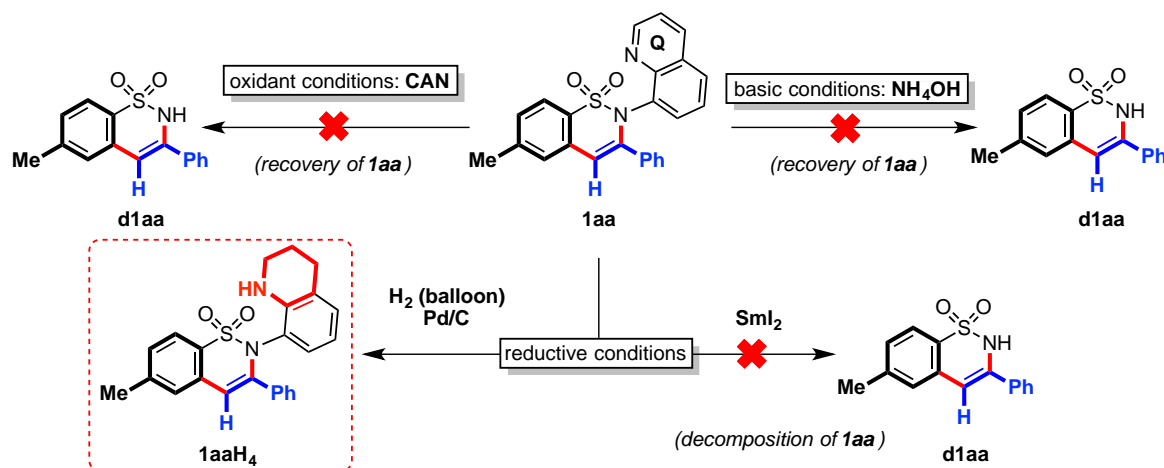
Then, we turned our attention to differently substituted alkynes (Table VII.9). To do so, we used the same catalytic system that was applied in table VII.8, which showed wide tolerance for a variety of functional groups, high regioselectivities as well as high efficiency for the synthesis of sultam motifs (up to 97% isolated yield). Indeed, the reaction achieved good to excellent yields when alkyl and vinyl substituted alkynes were used (**1aa-1ag**). Unexpectedly, when using 3-chloro-3-methylbut-1-yne as substrate (**h**), the product whereby hydrogen chloride had been eliminated was obtained (**1ah'**, see XRD in Figure VII.8). Furthermore, when an ester substituent was present in the alkyne coupling partner, both possible isomers were identified (**1ar**). Despite the mixture of products, the major regioisomer could be separated from the minor regioisomer by recrystallization in CH_3Cl /pentane, and subsequently it was fully characterized by XRD analysis (see Supplementary Digital Material). Interestingly, when electron-donating substituents are present on the aryl group of phenylacetylene the reaction resulted in low or trace yields (trace amounts and 30% for **1ai** and **1aj** respectively). In the case of **1aj**, even after an extended reaction time the yield was not significantly improved.

Furthermore, to prove the practicality of this transformation a gram-scale reaction with sulfonamide **1a** and alkynes **a** and **I** was performed, furnishing **1aa** and **1a** sultam motifs in 64 % (0.87 g) and 61% (0.89 g) yield, respectively (see Scheme S23, Annex III).

Table VII.9. Scope of Co(II)-catalyzed coupling of a variety of alkynes (blue) to tosyl sulfonamide forming functionalized sultams (**1ab-1at**).^{a,b}

^aReaction conditions: see Table VII.8. ^bIsolated yields after silica chromatography. ^cProduct derived from 3-chloro-3-methylbut-1-yne. ^dCombined yield of both regioisomers.; major regioisomer depicted.

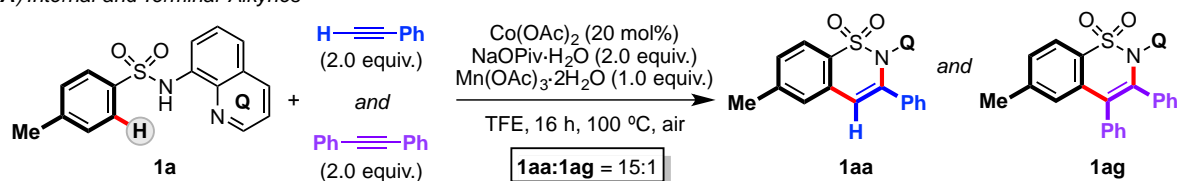
After being able to synthesize a vast array of sultam motifs, even at gram-scale, we attempted to upgrade them by removing the 8-aminoquinoline group (Scheme VII.13).^{39,40} Unfortunately, basic and oxidant conditions could not successfully cleave the AQ group. When reductive conditions were used, only possible the hydrogenated quinoline product **1aaH₄** (see Supplementary Digital Material). Thus, the development of a methodology for the AQ-directing group removal would be tremendously useful.

**Scheme VII.13.** Attempted upgrading of sultam **1aa**.

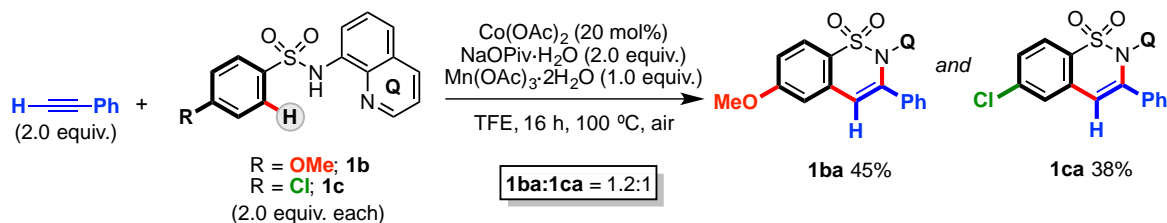
VII.3.3 Mechanistic experiments and possible reaction pathway

In order to understand how the reaction works, a variety of control experiments were performed, including intramolecular competition reactions (Scheme VII.14) and deuterium labeling experiments (Scheme VII.15). When two equivalents of both a terminal and internal alkyne were mixed together with **1a**, insertion of terminal alkynes was tremendously favored, resulting in a 15:1 ratio for terminal and internal alkynes insertion respectively (Scheme VII.14, **A**). Furthermore, in agreement with the results obtained in the substrate scope, reaction with electron-rich aryl sulfonamides (**1b**) was slightly favored over electron-poor aryl sulfonamides (**1c**) with a ratio of 1.2:1 respectively (Scheme VII.14, **B**). Likewise, insertion of the *p*-nitro phenylacetylene (**n**) was favored over *p*-methoxy phenylacetylene (**j**) (Scheme VII.14, **C**). The latter competition reaction only yielded 34% of the *p*-nitro product (**1an**), whereas in the absence of the competing *p*-methoxy phenylacetylene **1an** was obtained 97% isolated yield. This result suggests that the *p*-methoxy phenylacetylene is inhibiting the reaction to some extent.

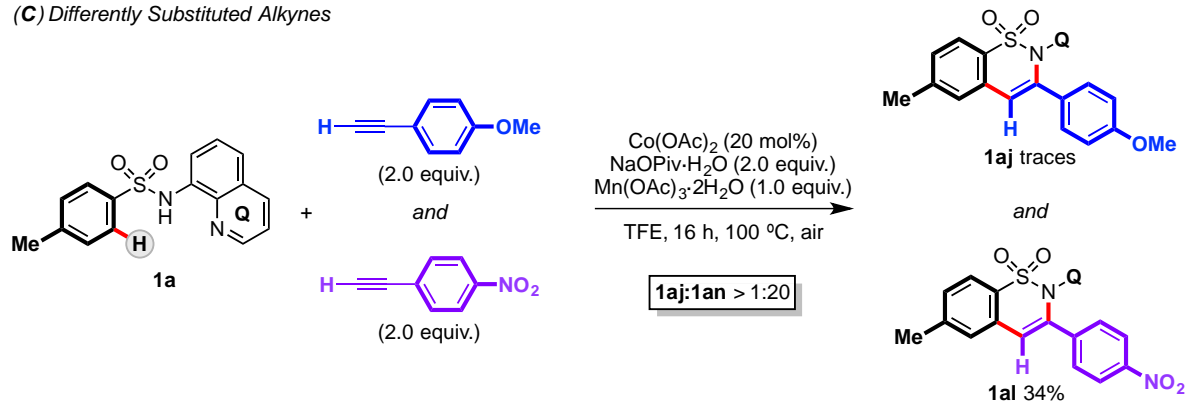
(A) Internal and Terminal Alkynes



(B) Differently Substituted Aryl Sulfonamides

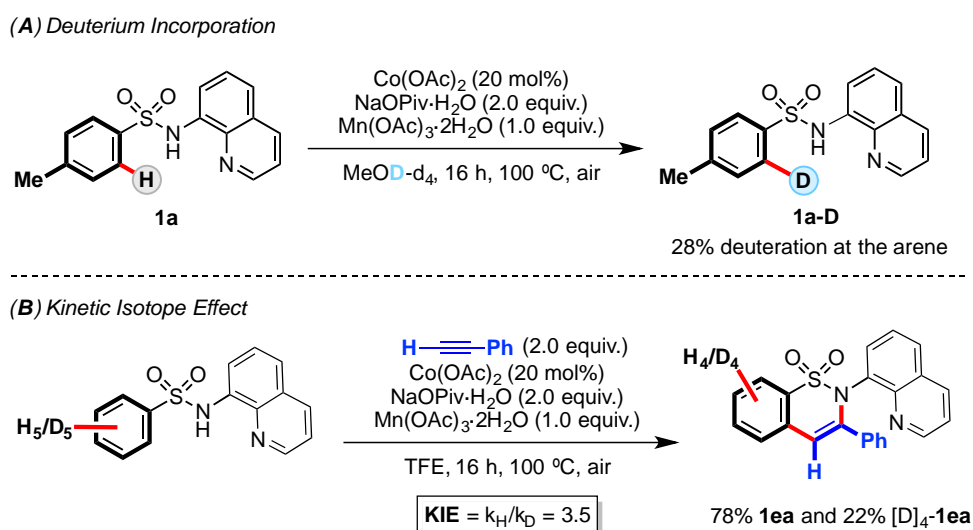


(C) Differently Substituted Alkynes



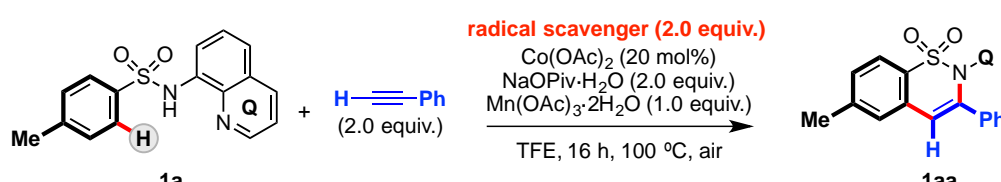
Scheme VII.14. Intermolecular competition experiments using standard conditions. Yields were calculated by ¹H NMR analysis using mesitylene as internal standard.

A range of deuterium incorporation reactions were also performed (Scheme VII.12). First, **1a** was reacted with $\text{Co}(\text{OAc})_2$ (20 mol%) in presence of $\text{NaOPiv}\cdot\text{H}_2\text{O}$ and $\text{Mn}(\text{OAc})_3\cdot 2\text{H}_2\text{O}$, but in the absence of alkyne (Scheme VII.15, **A**). The reaction was run in d_4 -methanol, and at the end of the reaction a low D-incorporation was observed in the starting sulfonamide **1a** (28% D-incorporation, **1a-D**). This result suggests the deuterium-demetalation of a putative aryl-Co(III) intermediate species, which formation is proposed to be reversible. On the other hand, an intermolecular competition experiment between **1e** and **D₅-1e** revealed a Kinetic Isotope Effect (KIE) value of 3.5 (Scheme VII.15, **B**). The experimental KIE value obtained is consistent with C-H activation being the rate-determining step in the reactions.



Scheme VII.15. Deuterium labeling experiments using standard conditions. Deuterium incorporation was obtained from ^1H NMR integration of signals.

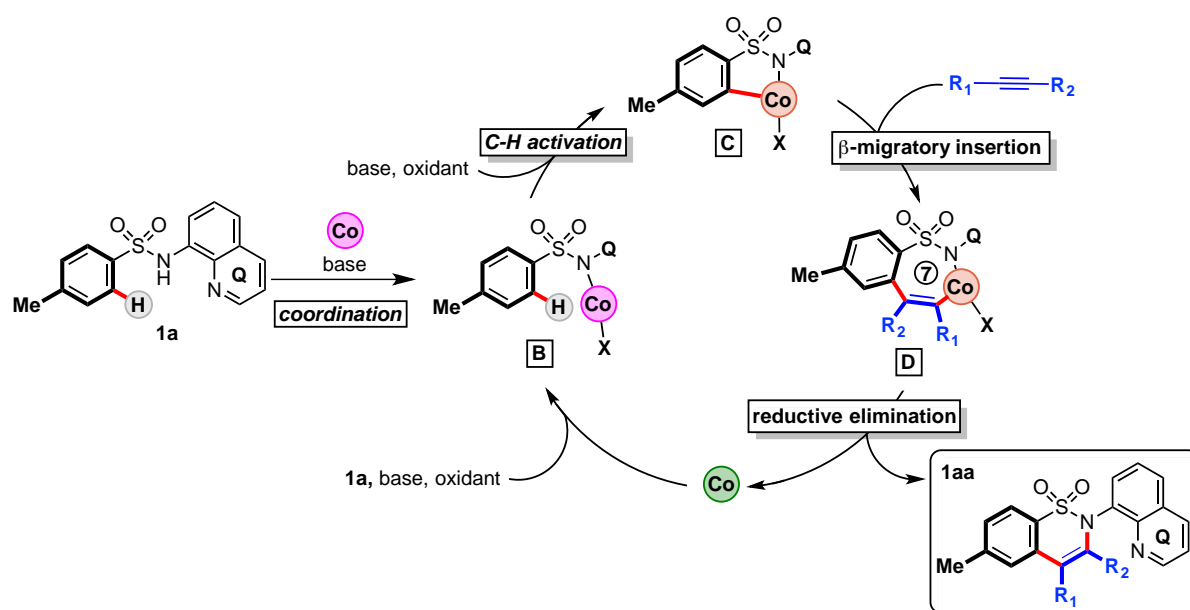
As exposed in *Chapter I*, recent Co(II)-catalyzed C-H functionalization methodologies identified the presence of radicals through radical quenchers or EPR spectroscopy.⁴¹⁻⁴⁵ We also considered the possibility of radical intermediates in our reaction, and to have an insight on this question several radical scavengers were tested. Indeed, when the annulation of **1a** was performed in the presence of the radical scavenger 2,2,6,6-tetramethylpiperidine 1-oxyl (TEMPO), **1aa** was obtained in only 8% yield (Table VII.10, entry 1). We therefore included a variety of radical scavengers such as 2,6-bis(1,1-dimethylethyl)-4-methylphenol (BHT, Table VII.10, entry 2), triethyl phosphite ($\text{P}(\text{OEt})_3$, Table VII.10, entry 3) and 2,2'-azobis(2-methylpropionitrile) (AIBN, Table VII.10, entry 4) in our reactions and found that the activity was almost completely inhibited in agreement with this previous work, suggesting that our reaction likely proceeds through radical intermediates in some steps of the mechanism. However, an inhibition of reactivity by catalyst chelation cannot be discarded.

Table VII.10. Reaction in the presence of radical scavengers.


entry	radical scavenger	yield of 1aa (%) ^a
1	(2,2,6,6-Tetramethyl-piperidin-1-yl)oxyl (TEMPO)	8
2	2,6-Bis(1,1-dimethylethyl)-4-methylphenol (BHT)	6
3	Triethyl phosphite (P(OEt) ₃)	0
4	2,2'-Azobis(2-methylpropionitrile) (AIBN)	3

^a ¹H NMR yield using mesitylene as internal standard.

With all the described experimental evidences, we proposed the catalytic cycle depicted in Scheme VII.16. Initially, Co(OAc)₂ chelates the AQ directing group furnishing the Co(II) coordination complex A. Then, Mn(OAc)₃·2H₂O oxidized Co(II) to Co(III), which performs the C-H cleavage to yield the corresponding aryl-Co(III) complex C. Albeit we propose C-H activation occurs through a CMD mechanism, the involvement of radicals cannot be fully discarded. Furthermore, the use of other acronyms such as BIES (base-assisted intramolecular electrophilic substitution) to describe the formation of C could be more appropriate. The slightly higher yields obtained when using electron-rich sulfonamide motifs (Scheme VII.14) can be explained by an acetate-assisted internal electrophilic substitution-type mechanism.^{46,47}



Scheme VII.16. Proposed reaction mechanism for the Co(II)-catalyzed synthesis of sultam motifs from sulfonamides and alkynes. Color code: Co(I), green; Co(II), pink; Co(III), orange.

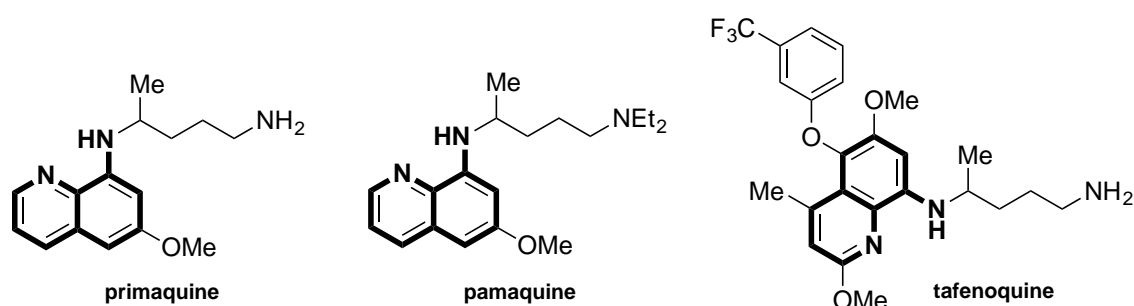
Subsequently, insertion of the alkyne into the aryl-Co(III) bond generates the transient 7-membered ring **D**. Finally, reductive elimination provides the desired sultam product, **1aa**, together with Co(I), which is oxidized to Co(II) and enters again the catalytic cycle. As suggested by the radical trap experiments described above, some steps of the cycle may involve radical intermediates.

In summary, in this section we have been able to develop a new Co(II)-catalyzed protocol for the synthesis of sultam motifs starting from easily prepared aryl sulfonamide and alkynes. Furthermore, the protocol permits the use of a broad range of substituted aryl sulfonamides and alkynes and displays excellent regioselectivities, demonstrating that cobalt can become a catalytic alternative to precious transition metals.

VII.4 A First Example of Cobalt-Catalyzed Remote C-H Functionalization of 8-Aminoquinolines Operating through a Single Electron Transfer Mechanism

This section corresponds to the contents of the manuscript by Christopher J. Whiteoak,* Oriol Planas,* Anna Company and Xavi Ribas. *Adv. Synth. Catal.* **2016**, *358*, 1679-1688 (*equal contribution), which can be found in Chapter VI of this thesis.

While working with 8-aminoquinoline (AQ) as directing group, we realized that this scaffold is an important motif found in a variety of drugs, including anti-malarial drugs such as primaquine, pamaquine and tafenoquine (Scheme VII.17).⁴⁸



Scheme VII.17. Antimalarial drugs containing the 8-aminoquinoline scaffold.

For this reason, we considered that the development of new methodologies for the functionalization of commercially available AQ compounds are potentially important for organic synthesis. Indeed, we were inspired by Stahl work, who reported on a Single Electron Transfer (SET) based remote Cu-catalyzed C5-chlorination.⁴⁹ As it is exposed in *Chapter I*, since this report several AQ functionalization protocols have been described, thus expanding the toolbox for preparation of novel AQ derivatives. In this work, we wondered if cobalt could imitate other metals in such transformations and promote remote C-H functionalization reactions under mild conditions. To do so, we selected *tert*-butyl nitrate (tBuONO, TBN) as coupling partner, which may elicit the formation of new C-N bonds. Indeed, TBN is known to be a NO₂ surrogate in presence of air at room temperature⁵⁰ and NO₂ is an open-shell molecule capable of reacting as a radical compound. This reactivity, combined with the oxidant properties of Co(III), led us to develop a new remote cobalt-catalyzed protocol for the functionalization of C-H bonds in AQ compounds.

VII.4.1 Optimization of reaction conditions

Initially, we attempted the remote nitration of N-(quinolin-8-yl)benzamide (**1**) using Co(OAc)₂ (20 mol%) as catalyst and 4.0 equiv of TBN in several solvents (Table VII.11, entries 1-9). Interestingly, we observed that when the reaction was run in TFE at

100 °C all the starting material was consumed but no desired product was obtained (Table VII.11, entry 1). However, when the reaction was run at room temperature, two different products were identified by ¹H NMR (**1a** and **1b**), which combined yield reached 16%. From this screening, the best solvent among those tested was acetic acid, which yielded 49% combined NMR yield (Table VII.11, entry 4) in a similar ratio to that observed when using TFE as solvent. Afterwards, we optimized the cobalt source (Table VII.11, entries 16), where it was found that Co(NO₃)₂·6H₂O was the optimal to promote the nitration reaction of **1** (Table VII.11, entry 12), furnishing a combined yield of 87%.

Table VII.11. Optimization of the reaction conditions for the nitration of 8-aminoquinoline.^a

entry	solvent	[Co] source	conv (%) ^b	1a (%) ^b	1b (%) ^b
1 ^c	TFE	Co(OAc) ₂	>99	trace	-
2	TFE	Co(OAc) ₂	55	12	4
3	CHCl ₃	Co(OAc) ₂	38	7	trace
4	Acetic acid	Co(OAc) ₂	60	36	13
5	DMF	Co(OAc) ₂	45	-	-
6	Toluene	Co(OAc) ₂	34	15	6
7	1,4-dioxane	Co(OAc) ₂	33	18	6
8	EtOAc	Co(OAc) ₂	44	11	3
9	THF	Co(OAc) ₂	33	6	2
10	Acetic acid	Co(acac) ₃	25	13	5
11	Acetic acid	CoCl ₂	29	19	5
12	Acetic acid	Co(NO ₃) ₂ ·6H ₂ O	87	65	22
13	Acetic acid	Co(BF ₄) ₂ ·6H ₂ O	61	44	17
14	Acetic acid	Co(acac) ₂	40	21	10
15	Acetic acid	Co(OAc) ₂ ·4H ₂ O	51	32	13
16	Acetic acid	CoBr ₂	74	20	7
17	Acetic acid	-	<1	-	-
18^d	Acetic acid	Co(NO₃)₂·6H₂O	>99	74	25
19 ^e	Acetic acid	Co(NO ₃) ₂ ·6H ₂ O	14	9	2
20 ^f	Acetic acid	Co(NO ₃) ₂ ·6H ₂ O	71	46	17

^aReaction conditions: **1** (50 mg, 0.2 mmol), cobalt source (0.04 mmol, 20 mol%), TBN (53 μL, 90 %, 2.0 equiv., 0.4 mmol), solvent (1.5 mL), RT, 18 h. ^bConversions and yields calculated from ¹H NMR of crude reaction mixture using 1,3,5-trimethoxy benzene as internal standard. ^cAt 100 °C. ^d4.0 equiv of TBN. ^eNo TBN used. ^f10 mol% Co(NO₃)₂·6H₂O.

As can be observed in entries 12 and 13 (Table VII.11), the use of weakly coordinating anions appears to be very beneficial for the reaction as these cobalt sources

provided significant higher yields compared to cobalt halides (Table VII.11, entry 11 and 16), acetyl acetonates (Table VII.11 entry 10 and 14) and acetate (Table VII.11, entry 15). Furthermore, as expected, in the absence of cobalt, no conversion was observed. (Table VII.11, entry 17). Interestingly, when $\text{Co}(\text{NO}_3)_2 \cdot 6\text{H}_2\text{O}$ (20 mol%) was used in the absence of TBN, 11% nitrated products were obtained (9% **1a**, 2% **1b**; Table VII.11, entry 19), which suggests that the nitrate group can also act as nitro source. When 4.0 equiv of TBN were used, nitration was achieved almost quantitatively (Table VII.11, entry 18), and when the catalyst loading was decreased to 10 mol%, the reaction yield was also reduced (Table VII.11, entry 20). This optimized protocol is advantageous over traditional nitration procedures, since it avoids the use of corrosive H_2SO_4 and HNO_3 as reagents.

VII.4.2 Substrate scope and upgrading

With the optimized conditions in our hands, we applied this protocol to a number of other structurally related substrates (Figure VII.9, substrates 2-5). Unfortunately, in all cases it was not possible to achieve the desired nitration products, which indicates the key role of the secondary amide and quinoline motifs in the substrate.

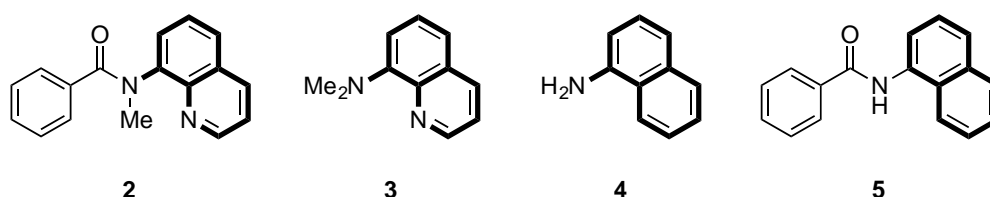
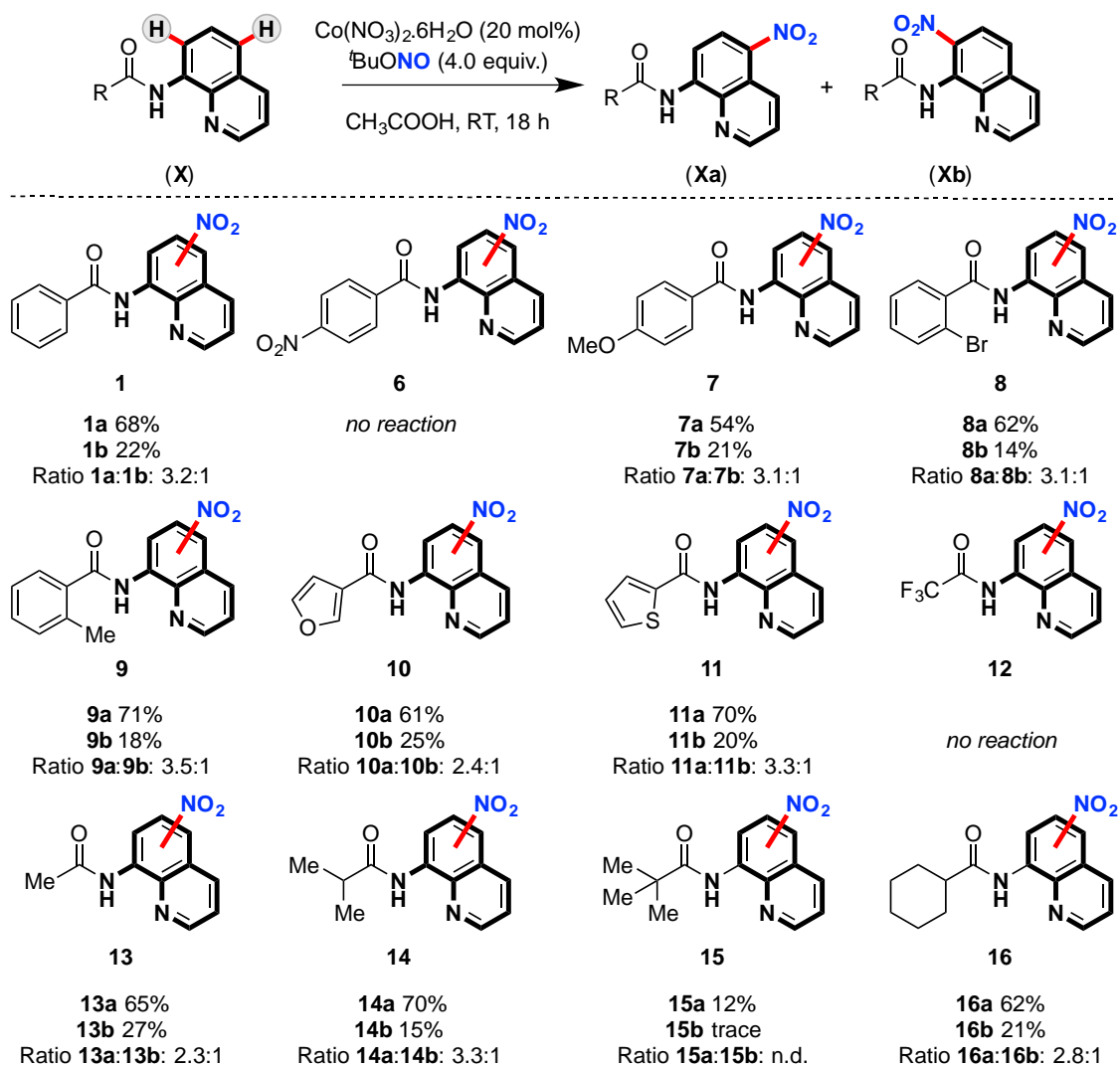


Figure VII.9. Unsuccessful substrates using the optimized reaction conditions.

Then, we turned our attention to the applicability of this protocol to a range of substrates bearing differently substituted ancillary groups (Table VII.12, products 6-16). In most substrates, it was possible to obtain excellent to quantitative overall combined yields of nitration products. Furthermore, we confirmed the structure of both C5- and C7-nitro regioisomers from XRD analysis of products **15a** and **13b** (Figure VII.10). However, there are several exceptions where the reaction was not successful, for instance, when a *p*-nitro group was included to the benzoyl ancillary (Table VII.12, substrate 6). A similar result was obtained when the electron-withdrawing trifluoromethyl ancillary group was used (Table VII.12, substrate 12). Thus, ancillary groups containing strong electron-withdrawing groups are not suitable for this transformation. However, poisoning experiments in which trifluoromethyl- (**12**) and methyl- (**13**) containing substrates were mixed demonstrated that **12** was not nitrated due to being unreactive rather than poisoning the catalysts. Furthermore, low yield is obtained with **15**, which indicate that Co cannot coordinate to the amide due to steric effects.

Table VII.12. Screening of different ancillary groups (1y-16y).^a

^aReaction conditions: substrate (0.5 mmol), Co(NO₃)₂·6H₂O (29.1 mg, 0.1 mmol, 20 mol%), TBN (267 μL, 90%, 4.0 equiv., 2.0 mmol), acetic acid (3.5 mL), RT, 18 h. ^bIsolated yields in parenthesis.

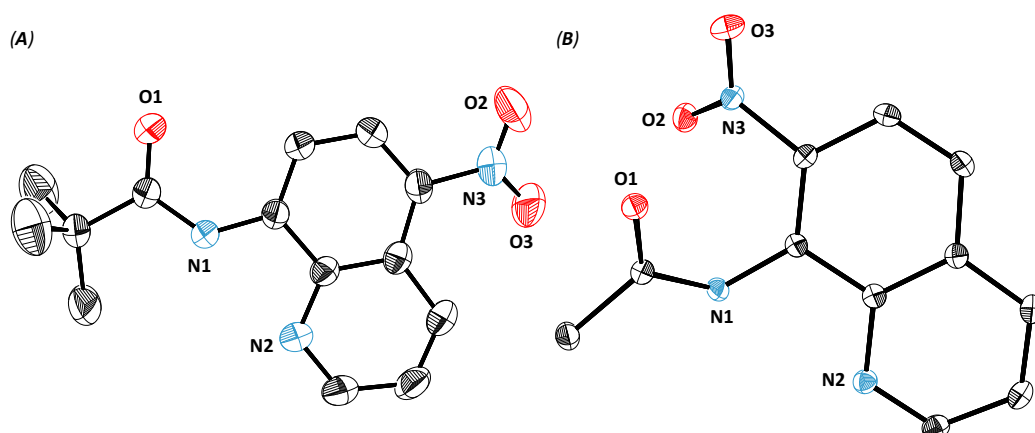
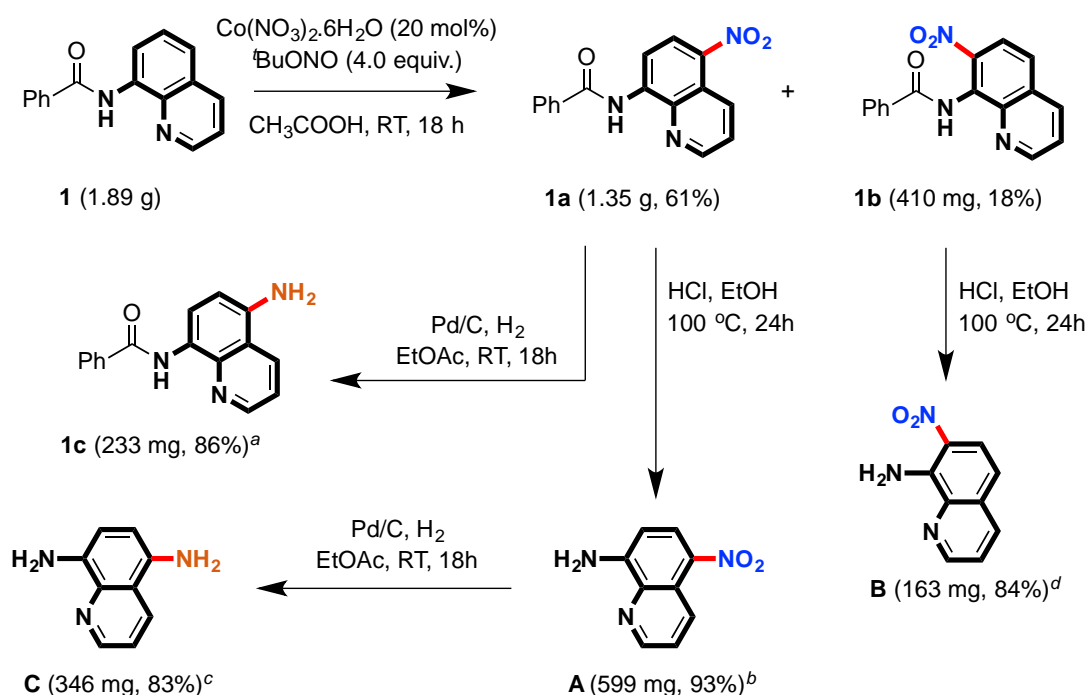


Figure VII.10. Solid state structures of C5- (A, 15a) and C7- (B, 13b) nitration products. Hydrogen-atoms have been omitted for clarity; ellipsoids displayed at 50% probability.

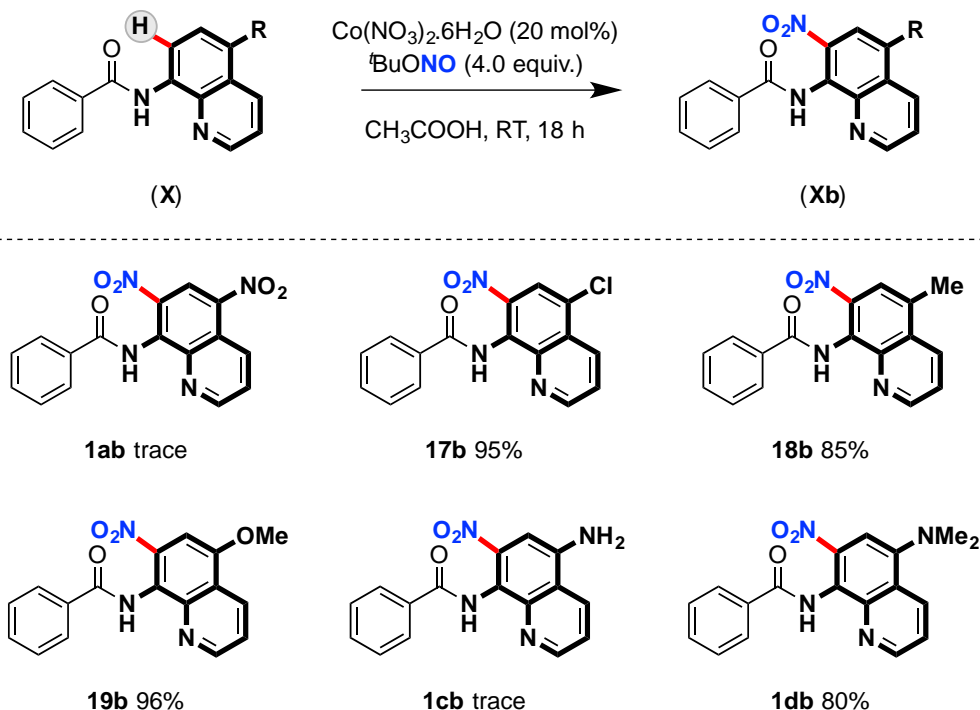
Once we optimized the ancillary group and selected benzoyl as a suitable motif, we investigated the potential for the reaction protocol to be transferred to gram-scale (Scheme VII.18). Indeed, we found that when starting from 1.89 g of **1** it was possible to obtain 1.35 g of 5-nitro-quinoline product **1a** (61%) and also 0.410 g of 7-nitro-quinoline product **1b** (18%). These amounts of nitrated products were enough to perform and investigate their upgrading. With analytically pure samples in-hand, reactions targeting the removal of the ancillary group and reduction of the nitro groups to amines were attempted (Scheme VII.18). Thus, reduction of **1a** was performed using Pd/C and H₂ (1 atm), and it resulted in the selective formation of **1c** in 86% isolated yield. The benzoyl ancillary groups of both **1a** and **1b** can be easily removed by acid hydrolysis to furnish the desired 5-nitro-8-aminoquinoline (**A**) and 7-nitro-8-aminoquinoline (**B**), respectively, in excellent yields. Moreover, the nitro-8-aminoquinolines can then be easily converted into the corresponding diamines in excellent yield using Pd/C and H₂ (1 atm) (conversion of **A** to **C** in Scheme VII.18). These diamines, which are not commercially available, may find a wide range of applications in the future as a result of this new nitration protocol, which allows their synthesis in high yields, low cost and facile installation and cleavage.



Scheme VII.18. Gram-scale nitration reaction and product upgrading (isolated yields reported). Reaction conditions for gram-scale nitration reaction: **1** (1.89 g, 7.6 mmol), $\text{Co}(\text{NO}_3)_2 \cdot 6\text{H}_2\text{O}$ (443 mg, 1.5 mmol, 20 mol%), TBN (4.1 mL, 90%, 4.0 equiv., 30.4 mmol), acetic acid (50 mL), RT, 18 h. ^aIsolated yield starting from 300 mg of **1a**. ^bIsolated yield starting from 1.0 g of **1a**. ^cIsolated yield starting from 500 mg of **A**. ^dIsolated yield starting from 320 mg of **1b**.

Thereafter, we wanted to apply the nitration protocol to previously substituted quinoline motifs. However, there are currently few inexpensive commercially available derivatives of AQ scaffolds. Thus, to further study the practicality we synthesized several 5-substituted-8-aminoquinoline motifs through Skraup reactions⁵¹ and further reduction of the corresponding nitro compounds through Pd/C (Table VII.13, substrates **17**, **18** and **19**). After applying the standard conditions to these new substrates **17b**, **18b** and **19b** were obtained in excellent isolated yields, with selective formation of 7-nitro products (Table VII.13). When the quinoline motif contained a nitro- (**1a**) or an amine- (**1c**) substituent group the reaction failed to synthesize **1ab** and **1cb**, respectively (Table VII.13, trace amounts). The inhibition of reactivity in presence of a nitro group is in line with the quenching observed when the benzoyl ancillary group bears an electron-withdrawing group (Table VII.12, entries 6 and 12). In the case of the free amine, we suggest a possible interference of the amine with the catalyst, which may quench its reactivity. Despite these negative results with free-amine substituted quinoline motifs, when **1c** was dimethylated at the amine (**1d**), it was possible to obtain the nitrated product (**1db**) in 80% isolated yield. The latter compound is interesting from a point of view of applicability, as it contains amine, nitro and amide functionalities which can be derivatized independently making it an excellent candidate for further upgrading.

Table VII.13. Screening of different 8-aminoquinoline scaffolds.^{a,b}

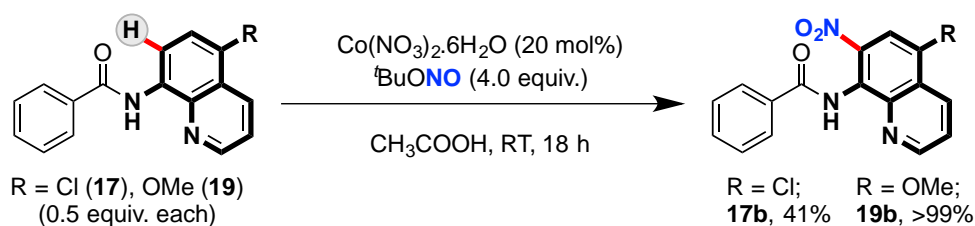


^aReaction conditions: substrate (0.5 mmol), $\text{Co(NO}_3)_2 \cdot 6\text{H}_2\text{O}$ (29.1 mg, 0.1 mmol, 20 mol%), TBN (267 μL , 90%, 4.0 equiv., 2.0 mmol), acetic acid (3.5 mL), RT, 18 h. ^bIsolated yields reported. ^cSelectivity >99% in all cases.

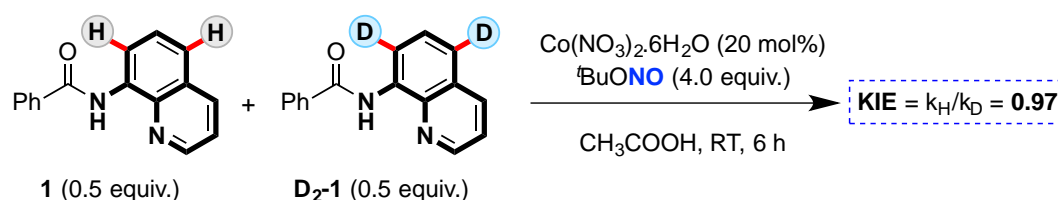
VII.4.3 Mechanistic experiments and possible reaction pathway

The absence of reactivity when electron-withdrawing groups are present in the amide moiety (Table VII.12, products **6** and **12**) as well as in the quinoline motif (Table VII.13, product **lab**) suggests that the formation of nitration products is governed by a SET mechanism. Further evidence to support this mechanism was obtained from competition experiments between **17** and **19** (Scheme VII.19, **A**) as well as deuterium incorporation experiments (Scheme VII.19, **B**). With the former experiment, it was observed that electron-rich quinoline motifs (**19**, >99% NMR yield) react faster compared to electron-poor quinolines (**17**, 41% NMR yield). This preference for electron-donating substituents is the expected one for the formation of a transient radical cation intermediate through a SET pathway. Furthermore, a Kinetic Isotope Experiment (KIE) revealed a k_H/k_D value of 0.97 (Scheme VII.19, **B**), indicating that the rate limiting step is not a C-H activation and adding further support for the proposed Single Electron Transfer (SET) pathway depicted in Scheme VII.20.

(A) Competition experiments with electronically different quinolines



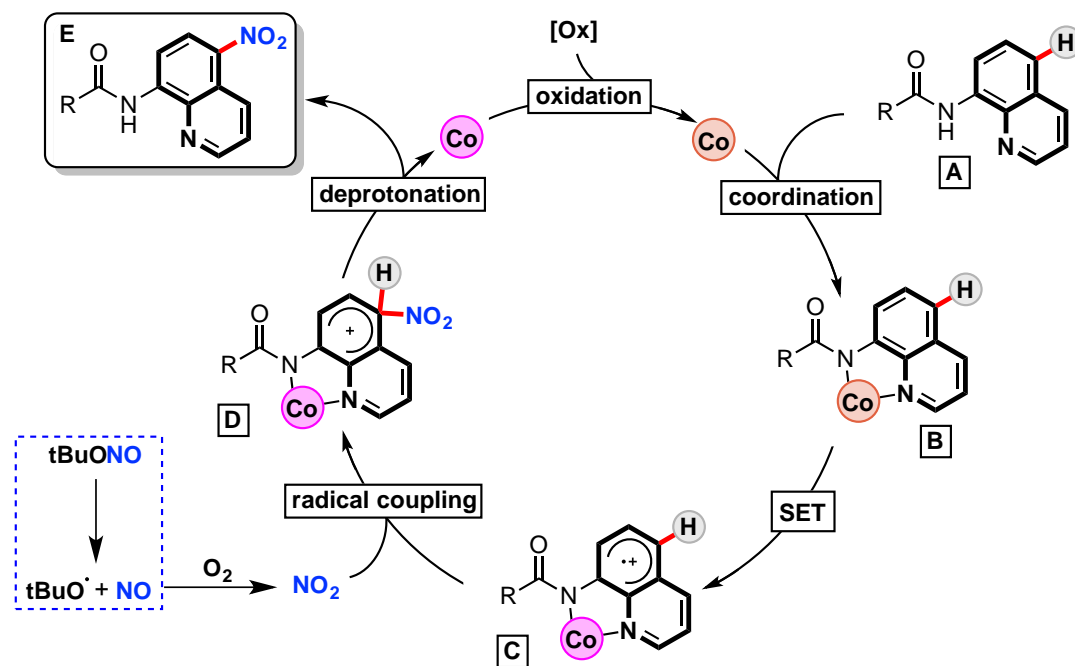
(B) Kinetic isotope effect



Scheme VII.19. (A) Competition reactions performed to investigate relative reactivity of substrates **17** and **19**. Yields calculated from ^1H NMR of crude reaction mixture using 1,3,5-trimethoxy benzene as internal standard and are based on conversion of corresponding substrate. Reaction conditions: substrate (0.5 mmol; 0.25 mmol of each substrate), $\text{Co}(\text{NO}_3)_2 \cdot 6\text{H}_2\text{O}$ (29.1 mg, 0.1 mmol, 20 mol%), TBN (267 μL , 90%, 4.0 equiv., 2.0 mmol), acetic acid (3.5 mL), RT, 18 h. (B) Summary of Kinetic Isotope Experiment (KIE); for further details see Supporting Information.

Taking into account all the observations obtained during this study, we proposed a Single Electron Transfer (SET) based mechanism to explain the nitration on the 5- and 7-positions of the quinoline motif (Scheme VII.20). Initially, Co(II) is oxidized to Co(III) by the *tert*-butoxy radical generated through decomposition of TBN with oxygen. Then,

the metal center coordinates to substrate **A** to furnish the Co(III) complex **B**. Afterwards, Co(III), which is a strong oxidant in acidic media,⁵² drags an electron from the quinoline moiety and generates a cationic quinoline radical and Co(II) (Scheme VII.20, species **C**). Subsequently, NO₂, generated in situ from TBN reacts with the quinoline radical (Scheme VII.20, species **D**), and a concerted proton-transfer/demetalation step provides the nitration product **E** and Co(II). Indeed, this mechanistic cycle is reminiscent to the pioneer work from Stahl and co-workers, in which Cu(II) promotes the functionalization of remote C-H bonds.⁴⁹



Scheme VII.20. Proposed mechanism for the C5-H nitration of substrate **A**.

To summarize this section, a new mild Co-catalyzed remote nitration protocol for the preparation of 5- and 7-nitro-8-aminoquinoline motifs was developed. As far as we know, this constitutes the first example of remote Single Electron Transfer mechanism promoted by cobalt-catalysis.

VII.5 References

- (1) Ribas, X.; Jackson, D. A.; Donnadiou, B.; Mahía, J.; Parella, T.; Xifra, R.; Hedman, B.; Hodgson, K. O.; Llobet, A.; Stack, T. D. P. *Angew. Chem. Int. Ed.* **2002**, *41*, 2991.
- (2) Casitas, A.; King, A. E.; Parella, T.; Costas, M.; Stahl, S. S.; Ribas, X. *Chem. Sci.* **2010**, *1*, 326.
- (3) Casitas, A.; Canta, M.; Solà, M.; Costas, M.; Ribas, X. *J. Am. Chem. Soc.* **2011**, *133*, 19386.
- (4) Goswami, M.; Lyaskovskyy, V.; Domingos, S. R.; Buma, W. J.; Woutersen, S.; Troeppner, O.; Ivanović-Burmazović, I.; Lu, H.; Cui, X.; Zhang, X. P.; Reijerse, E. J.; DeBeer, S.; van Schooneveld, M. M.; Pfaff, F. F.; Ray, K.; de Bruin, B. *J. Am. Chem. Soc.* **2015**, *137*, 5468.
- (5) Wencel-Delord, J.; Colobert, F. *Org. Chem. Front.* **2016**, *3*, 394.
- (6) Kanamori, K.; Broderick, W. E.; Jordan, R. F.; Willett, R. D.; Legg, J. I. *J. Am. Chem. Soc.* **1986**, *108*, 7122.
- (7) Broderick, W. E.; Kanamori, K.; Willett, R. D.; Legg, J. I. *Inorg. Chem.* **1991**, *30*, 3875.
- (8) Grigorjeva, L.; Daugulis, O. *Angew. Chem. Int. Ed.* **2014**, *53*, 10209.
- (9) Hao, X.-Q.; Du, C.; Zhu, X.; Li, P.-X.; Zhang, J.-H.; Niu, J.-L.; Song, M.-P. *Org. Lett.* **2016**, *18*, 3610.
- (10) Lu, Q.; Vásquez-Céspedes, S.; Gensch, T.; Glorius, F. *ACS Catal.* **2016**, *6*, 2352.
- (11) Mei, R.; Wang, H.; Warratz, S.; Macgregor, S. A.; Ackermann, L. *Chem. Eur. J.* **2016**, *22*, 6759.
- (12) Zhang, J.; Chen, H.; Lin, C.; Liu, Z.; Wang, C.; Zhang, Y. *J. Am. Chem. Soc.* **2015**, *137*, 12990.
- (13) Landge, V. G.; Jaiswal, G.; Balaraman, E. *Org. Lett.* **2016**, *18*, 812.
- (14) Hu, F.; Xia, Y.; Ma, C.; Zhang, Y.; Wang, J. *Chem. Commun.* **2015**, *51*, 7986.
- (15) Liu, J.; Hu, L.; Wang, L.; Chen, H.; Deng, L. *J. Am. Chem. Soc.* **2017**, *139*, 3876.
- (16) Wang, Y.; Wen, X.; Cui, X.; Wojtas, L.; Zhang, X. P. *J. Am. Chem. Soc.* **2017**, *139*, 1049.
- (17) Das, B. G.; Chirila, A.; Tromp, M.; Reek, J. N. H.; Bruin, B. de. *J. Am. Chem. Soc.* **2016**, *138*, 8968.
- (18) Brookhart, M.; Studabaker, W. B. *Chem. Rev.* **1987**, *87*, 411.
- (19) Dötz, K. H.; Stendel, J. *Chem. Rev.* **2009**, *109*, 3227.
- (20) Davies, H. M. L.; Manning, J. R. *Nature* **2008**, *451*, 417.
- (21) Hao, W.-J.; Gao, Q.; Jiang, B.; Liu, F.; Wang, S.-L.; Tu, S.-J.; Li, G. *J. Org. Chem.* **2016**, *81*, 11276.
- (22) Bellow, J. A.; Stoian, S. A.; van Tol, J.; Ozarowski, A.; Lord, R. L.; Groysman, S. *J. Am. Chem. Soc.* **2016**, *138*, 5531.
- (23) Mondal, K. C.; Samuel, P. P.; Roesky, H. W.; Carl, E.; Herbst-Irmer, R.; Stalke, D.; Schwederski, B.; Kaim, W.; Ungur, L.; Chibotaru, L. F.; Hermann, M.; Frenking, G. *J. Am. Chem. Soc.* **2014**, *136*, 1770.
- (24) Harrison, D. J.; Lee, G. M.; Leclerc, M. C.; Korobkov, I.; Baker, R. T. *J. Am. Chem. Soc.* **2013**, *135*, 18296.
- (25) Harrison, D. J.; Gorelsky, S. I.; Lee, G. M.; Korobkov, I.; Baker, R. T. *Organometallics* **2013**, *32*, 12.
- (26) Marquard, S. L.; Bezpalko, M. W.; Foxman, B. M.; Thomas, C. M. *J. Am. Chem. Soc.* **2013**, *135*, 6018.

- (27) Zhao, D.; Kim, J. H.; Stegemann, L.; Strassert, C. A.; Glorius, F. *Angew. Chem. Int. Ed.* **2015**, *54*, 4508.
- (28) Kim, J. H.; Grefies, S.; Glorius, F. *Angew. Chem. Int. Ed.* **2016**, *55*, 5577.
- (29) Li, J.; Tang, M.; Zang, L.; Zhang, X.; Zhang, Z.; Ackermann, L. *Org. Lett.* **2016**, *18*, 2742.
- (30) Qu, S.; Cramer, C. J. *J. Org. Chem.* **2017**, *82*, 1195.
- (31) Baek, Y.; Kim, S.; Jeon, B.; Lee, P. H. *Org. Lett.* **2016**, *18*, 104.
- (32) Liu, X.-G.; Zhang, S.-S.; Wu, J.-Q.; Li, Q.; Wang, H. *Tetrahedron Lett.* **2015**, *56*, 4093.
- (33) Jia, M.; Ma, S. *Angew. Chem. Int. Ed.* **2016**, *55*, 9134.
- (34) Werlé, C.; Goddard, R.; Philipps, P.; Farès, C.; Fürstner, A. *J. Am. Chem. Soc.* **2016**, *138*, 3797.
- (35) Lombardino, J. G.; Wiseman, E. H.; McLamore, W. M. *J. Med. Chem.* **1971**, *14*, 1171.
- (36) Pham, M. V.; Ye, B.; Cramer, N. *Angew. Chem. Int. Ed.* **2012**, *51*, 10610.
- (37) Ackermann, L. *Acc. Chem. Res.* **2014**, *47*, 281.
- (38) Moselage, M.; Li, J.; Ackermann, L. *ACS Catal.* **2016**, *6*, 498.
- (39) Zhang, F.; Spring, D. R. *Chem. Soc. Rev.* **2014**, *43*, 6906.
- (40) Berger, M.; Chauhan, R.; Rodrigues, C. A. B.; Maulide, N. *Chem. Eur. J.* **2016**, *22*, 16805.
- (41) Zhang, L.-B.; Hao, X.-Q.; Zhang, S.-K.; Liu, Z.-J.; Zheng, X.-X.; Gong, J.-F.; Niu, J.-L.; Song, M.-P. *Angew. Chem. Int. Ed.* **2015**, *54*, 272.
- (42) Suo, J. F.; Zhao, X. M.; Zhang, K. X.; Zhou, S. L.; Niu, J. L.; Song, M. P. *Synth.* **2017**, *49*, 3916.
- (43) Nageswar Rao, D.; Rasheed, S.; Raina, G.; Ahmed, Q. N.; Jaladanki, C. K.; Bharatam, P. V.; Das, P. *J. Org. Chem.* **2017**, *82*, 7234.
- (44) Nguyen, T. T.; Grigorjeva, L.; Daugulis, O. *Chem. Commun.* **2017**, *53*, 5136.
- (45) Zhou, Y.; Tang, Z.; Song, Q. *Chem. Commun.* **2017**, *53*, 8972.
- (46) Ma, W.; Mei, R.; Tenti, G.; Ackermann, L. *Chem. Eur. J.* **2014**, *20*, 15248.
- (47) Oxgaard, J.; Tenn, W. J.; Nielsen, R. J.; Periana, R. A.; Goddard, W. A. *Organometallics* **2007**, *26*, 1565.
- (48) Recht, J.; Ashley, E.; White, N. *Safety of 8-aminoquinoline Antimalarial Medicines*; World Health Organization, 2014.
- (49) Suess, A. M.; Ertem, M. Z.; Cramer, C. J.; Stahl, S. S. *J. Am. Chem. Soc.* **2013**, *135*, 9797.
- (50) Bill Cai, T.; Wang, P. G.; Holder, A. A. In *Nitric Oxide Donors*; Wiley-VCH, Weinheim, Germany, 2005; 1-31.
- (51) He, G.; Zhang, S.-Y.; Nack, W. A.; Li, Q.; Chen, G. *Angew. Chem. Int. Ed.* **2013**, *52*, 11124.
- (52) Tang, R.; Kochi, J. K. *J. Inorg. Nucl. Chem.* **1973**, *35*, 3845.

Chapter VIII

General Conclusions

Recently, the field of high-valent cobalt-catalyzed C-H activation and functionalization field has exponentially grown, demonstrating a tremendous potential for a sustainable and cost-efficient synthesis of biologically active compounds and material with unique properties. Despite this increasing interest in Co(III)-catalysis, the field can be further explored in terms of methodology development and mechanistic understanding. In this thesis, several organometallic aryl-Co(III) complexes have been synthesized and characterized. Furthermore, their reactivity towards alkynes (Chapter III) and ethyl diazo acetate (Chapter IV) has been described, including the isolation of a variety of reaction intermediates. The knowledge acquired from these studies, together with the development of cobalt-catalyzed C-H functionalization methodologies for the synthesis of cyclic sulfonamide motifs (Chapter V) and the nitration of remote C-H bonds of 8-aminoquinoline-containing substrates (Chapter VII), confers to this thesis a global perspective on cobalt-catalyzed C-H functionalizations.

Particularly, in **Chapter III**, we have prepared and characterized several organometallic aryl-Co(III) complexes using model macrocyclic arene substrates. The design of substrates **2b-H** and **2c-H** (See Chapter VII, section VII.1) is key for the stabilization of the organometallic aryl-Co(III) in a preferred-octahedral environment. Additionally, we provide definitive crystallographic proof of an organometallic aryl-Co(III) intermediate often proposed in 8-aminoquinoline directed Co(III)-catalyzed C-H activation processes. Reaction of organometallic aryl-Co(III) intermediates follows different reaction pathways depending on the nature of the alkyne coupling partners. Terminal alkynes furnish 5- and 6-membered ring products depending on both the electronic properties of the alkynes and the reaction temperature, while internal alkynes only give 6-membered ring products. DFT studies together with experimental evidence indicates that a newly proposed ‘acetylide pathway’ is preferred for terminal alkynes, in contrast to the usually proposed ‘ β -migratory insertion pathway’.

In **Chapter IV**, the previously synthesized aryl-Co(III) intermediates are reacted with ethyl diazo acetate to furnish unique C-metalated *cis*-aryl-Co(III)-alkyl enolate species (**5a-X**; see Chapter VII, section VII.2), which can be considered carbenoids. Crystallographic, full spectroscopic characterization and theoretical evidences show that the isolated intermediates **5a-X** are necessary to deliver the alkyl fragment and give a 6-membered cyclic amide product. This is the first example of a C-metalated aryl-Co(III) enolate engaging in C-H functionalization reactions. Moreover, these species are proven to be catalytically active in the synthesis of final macrocyclic amide (**3**). DFT studies indicate that this transformation occurs through a rare intramolecular S_N2 -type step in which the carboxylate acts as relay. The experimental key role of Lewis acids, particularly LiOTf, is reflected in the theoretical studies, unveiling a Li-mediated

carboxylate activation that triggers the C-O bond cleavage/C-C bond formation event. These results open the door to investigate the scope of this reactivity in other catalytic systems.

In **Chapter V**, we have reported on a new high valent cobalt-catalyzed protocol for the construction of cyclic sulfonamide (sultam) motifs starting from easily prepared aryl sulfonamides and alkynes. The protocol displays excellent regioselectivities compared with the previously reported Rh-catalyzed protocol, where moderate regioselectivity was found. Furthermore, this protocol demonstrates the increasing potential of cobalt to substitute more expensive second-row transition metals such as rhodium and iridium, as a result of favorable reactivities and selectivities.

In **Chapter VI**, a new mild cobalt-catalyzed nitration of remote C-H bonds for the preparation of 5- and 7-nitro-8-aminoquinolines using easily installable and removable ancillary groups has been developed. The protocol is proposed to operate through a previously unreported remote C-H functionalization route based on a Single Electron Transfer (SET) mechanism for the described 8-aminoquinoline substrates. This new methodology is intended to inspire further work directed towards the development of new facile and mild catalytic routes for the preparation of functionalized 8-aminoquinoline compounds.

Annex

Supporting Information

Supporting Information for Chapter III

Isolation of Key Organometallic Aryl-Co(III) Intermediates in Co-Catalyzed C(sp²)-H Functionalizations and New Insights into Alkyne Annulation Reaction Mechanisms

Oriol Planas,¹ Christopher J. Whiteoak,^{1,2} Vlad Martin-Diaconescu,¹ Ilaria Gamba,¹
Josep M. Luis,¹ Teodor Parella,³ Anna Company,¹ Xavi Ribas^{1,*}

Table of Contents

1. GENERAL CONSIDERATIONS.....	S3
2. SYNTHESIS OF LIGANDS 2b-H AND 2c-H.....	S5
3. SYNTHESIS OF COMPLEXES	S7
3.1 Synthesis of Co(II) coordination complexes.....	S7
3.2 Synthesis of organometallic aryl-Co(III) complexes	S8
3.3 Synthesis of Aryl-Co(III) species AQ directing group (7 and 8)	S11
4. OPTIMIZATION STUDIES OF ARYL-Co(III) SYNTHESIS.....	S12
4.1 Evaluation of different Cobalt Salts	S12
4.2. Effect of an External Base and Evaluation of Solvents.....	S15
4.3. Evaluation of different oxidants	S16
5. STOICHIOMETRIC STUDIES WITH ALKYNES.....	S20
5.1 Organometallic 4b-OAc Complex Reactivity towards Internal Alkynes	S20
5.2 Organometallic 4b-OAc Complex Reactivity towards Internal Alkynes.....	S21
5.3 Reaction of Organometallic 4c-OAc Complex towards Alkynes	S23
6. CATALYTIC STUDIES WITH ALKYNES.....	S25
6.1 Reactivity of 2b-H towards Terminal Alkynes.....	S25
6.2 Reactivity of 2b-H towards Internal Alkynes	S20
7. CRYSTALLOGRAPHIC DATA INFORMATION	S26
8. DFT MIGRATORY INSERTION PATHWAY	S31
9. REFERENCES.....	S32
10. SELECTED ORIGINAL NMR SPECTRA.....	S33

1. General considerations

All reagents and solvents were purchased from Sigma Aldrich, Fisher Scientific or Fluorochem and used without further purification. *N*-(5-nitroquinolin-8-yl)benzamide was synthesized as reported in the literature.¹ NMR data concerning product identity were collected with a Bruker 400 AVANCE (Serveis Tècnics, University of Girona) or a 600 AVANCE (Servei de RMN, Autonomous University of Barcelona) spectrometers in the corresponding deuterated solvent (CDCl₃ and CD₃CN) and calibrated relative the residual protons of the solvent. All NMR experiments (¹H, ¹³C{¹H}, COSY, HSQC, HMBC and NOESY) were recorded and processed using standard parameters and no more details are given. Quantification of reaction yields through integration of peaks was performed using an internal reference (1,3,5-trimethoxybenzene). Preparation and handling of air-sensitive materials were carried out in a N₂ drybox with O₂ and H₂O concentrations < 1 ppm. High resolution mass spectra (HRMS) were recorded on a Bruker MicrOTOF-Q IITM instrument using ESI or Cryospray ionization sources at Serveis Tècnics University of Girona. C, H, N elemental analyses were performed on a ThermoFinnigan Flash-EA1112 analyzer.

XAS Data Acquisition and processing

Samples were prepared as solids diluted in boron nitride, loaded into holders with Kapton windows and stored at liquid nitrogen temperatures until run. All data was collected in transmission mode. Complexes **3c-Br** and **3c-OAc** were run under vacuum at 77 K using a liquid nitrogen finger dewar available from the XAFS beamline at Elettra Sincrotrone Trieste (2.0 GeV, 300 mA storage ring) equipped with a Si(III) double crystal monochromator. Data on the **4c-OAc** complex was collected at 77K using a liquid nitrogen cryostat and a Si(III) double crystal monochromator available at Diamond Light Source (3.0GeV, 300mA storage ring) beamline B18. Lastly data on the **4b-OAc** species was collected at SOLEIL synchrotron (2.75 GeV, 400mA storage ring) at 20 K using a liquid helium cryostat and Si(220) double crystal monochromator.

Data calibration and normalization was carried out using the Athena software package.¹ Energies were calibrated to the first inflection point of Co foil spectra set at 7709.5 eV. A linear pre-edge function and a quadratic polynomial for the post-edge were used for background subtraction and normalization of the edge jump. EXAFS data was extracted using the AUTOBK algorithm with a spline between a *k* of 1 and 15 Å⁻¹ having a R_{bk} value of 1.0 Å. EXAFS analysis was carried out with the Artemis software program running the IFEFFIT engine and the FEFF6 code.¹⁻³ Unless otherwise specified *k*³-

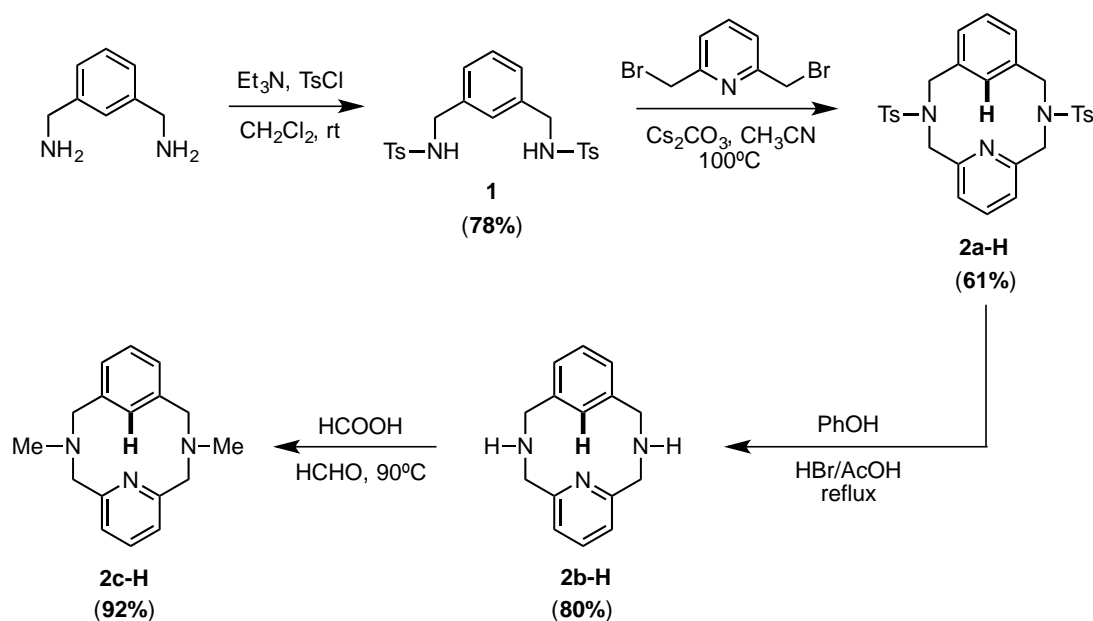
weighted data was fit in r-space using a Hannings window ($dk=2$) over a k-range of 2 to 12.5 \AA^{-1} , and an r-range of 1 to 3 \AA . The S_0^2 value was set to 0.9, and a global ΔE_0 was employed with the initial E_0 value set to the inflection point of the rising edge. Single and multiple scattering paths were fit in terms of a Δr_{eff} and σ^2 as previously described.^{4,5} To assess the goodness of the fits the R_{factor} (%R) was minimized. Over-fitting the data was controlled by minimizing the number of adjustable parameters and ensuring that the reduced χ^2 (χ_v^2) decreases with increasing number of adjustable parameters.

Theoretical Calculations

Theoretical calculations were carried out using the ORCA package.⁶ Geometry optimizations were carried out using the spin-unrestricted Kohn-Sham formalism employing a BP86 functional⁷ with a def2-TZVP(-f) basis set on the metal, nitrogens and oxygens, a SVP basis set on the hydrogens and def2-SVP on carbons, as well as a def2-TZVP/J auxiliary basis set on all atoms.^{8,9} A dense integration grid (ORCA Grid 5 = Lebedev 434 points) was used for all atoms. Furthermore, dispersion corrections were included using the Grimme and coworkers DFT-D3BJ approach^{10,11} and solvent effects were incorporated using a conductor like screening model (COSMO) using 2,2,2 trifluoroethanol as solvent ($\epsilon = 27$). Subsequent frequency calculations were done to evaluate enthalpy and entropy corrections at 298.15 K ($G_{\text{corr.}}$) and ensured that all local minima had only real frequencies while a single imaginary frequency confirmed the presence of transition states. Single point calculations on the equilibrium geometries, including the solvent effects and D3BJ dispersion corrections were computed using the B3LYP functional and def2-TZVPP basis set for all the atoms (E_{B3LYP}). The density fitting and chain of spheres (RIJCOSX) approximations¹² were employed together with the def2-QZVP/JK auxiliary basis set.^{8,9} The free energy change associated with moving from a standard-state gas phase pressure of 1 atm to a standard state gas phase concentration of 0.046 M for solutes ($\Delta G^{o/*}$) was also included in the final free energies. The value of $\Delta G^{o/*}$ at 298.15 K is $0.079 \text{ kcal}\cdot\text{mol}^{-1}$ for 0.046 M standard state solutes. Then, the final total Gibbs free energy (G) was given by:

$$G = E_{\text{B3LYP}} + G_{\text{corr.}} + \Delta G^{o/*} \quad (\text{Equation 1})$$

2. Synthesis of ligands 2b-H and 2c-H

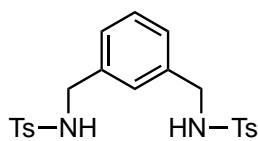


Scheme S1. Synthesis protocol for **2b-H** and **2c-H** macrocyclic ligands.

2.1 Synthesis of protected diamine **1**

3-(aminomethyl)benzylamine (6.81 g, 0.05 mols) and triethylamine (40 ml, 29.02 g, 0.29 mols) were mixed in CH₂Cl₂ and cooled to 0°C. A solution of tosyl chloride (21.9 g, 0.12 mol) was added dropwise (15-30 min) and the resulting mixture was left under stirring overnight at room temperature. The solution was then diluted with CHCl₃ and extracted with H₂O (3x100ml) and brine (3x100ml). The organic layer was then dried with Mg₂SO_{4(anh)} and the solvent was removed to yield an orange oil. Crude product was purified by silica gel using a mixture of CH₂Cl₂:AcOEt (90:10) to obtain tosyl-protected amine **1** as a white solid (17.45 gr, 0.039 mol, 78%).

¹H NMR (400 MHz, CDCl₃, ppm) δ 7.74 (d, ³J_H = 8.4 Hz, 4H), 7.32 (d, ³J_H = 8.4 Hz, 4H), 7.20 (t, ³J_H = 7.7 Hz, 1H), 7.11 (d, ³J_H = 7.7 Hz, 2H), 7.02 (s, 1H), 4.69 (s, 2H), 4.04 (s, 4H), 2.44 (s, 6H). ¹³C {¹H} NMR (100 MHz, CDCl₃, ppm) δ 143.7, 136.9, 129.8, 129.2, 127.5, 127.2, 47.01, 21.6. HRMS (ESI) calcd. for C₂₂H₂₄N₂O₄S₂ [M+H]⁺: 445.1250; found: 445.1249

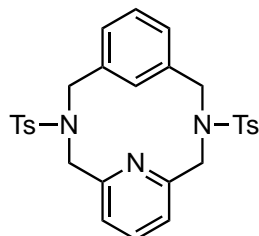


2.2 Synthesis of **2a-H**

Tosyl-protected amine **1** (3.9 g, 8.8 mmols) was dissolved in 70 mL of CH₃CN in a two-necked round bottom-flask. Then, Cs₂CO₃ (7.11 g, 22.2 mmols, excess) was added as a solid to the reaction mixture, and the solution was refluxed at 90°C. After reflux is initiated, 2,6-Bis(bromomethyl)pyridine (2.9 g, 8.8 mmols) in 40 mL of CH₃CN was added drop wise to the reaction mixture. After heating for 24h under reflux, the crude was cooled down to room temperature and filtered. The solvent of the filtrate was

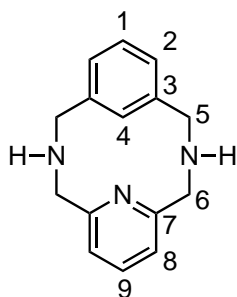
evaporated under vacuum and the resulting pale-brown solid was purified by recrystallization in CHCl_3 :EtOH (1:3). White crystals of **2a-H** were obtained in a 61% (5.4 mmol, 2.9 g) yield after leaving the solution cooling down in a freezer overnight.

^1H NMR (400 MHz, CDCl_3 , ppm) δ 7.78 (d, $^3J_{\text{H}} = 8.4$ Hz, 4H), 7.38 (d, $^3J_{\text{H}} = 8.4$ Hz, 4H), 7.30 (t, $^3J_{\text{H}} = 7.7$ Hz, 1H), 7.19 (s, 1H), 7.05 (d, $^3J_{\text{H}} = 8.2$ Hz, 2H), 7.01 (d, $^3J_{\text{H}} = 7.4$ Hz, 2H), 6.91 (t, $^3J_{\text{H}} = 7.3$ Hz, 1H), 4.44 (s, 2H), 4.30 (s, 4H), 2.44 (s, 6H). **^{13}C $\{^1\text{H}\}$ NMR (100 MHz, CDCl_3 , ppm)** δ 155.1, 143.5, 136.5, 134.2, 127.0, 122.8, 56.6, 55.1, 21.5. **HRMS (ESI)** calcd. for $\text{C}_{29}\text{H}_{29}\text{N}_3\text{O}_4\text{S}_2$ $[\text{M}+\text{H}]^+$: 548.1672; found: 548.1677.



2.3 Synthesis of **2b-H**

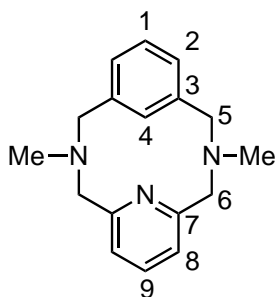
Tosyl-protected macrocyclic ligand **2a-H** (1.75 g, 3.2 mmol) and phenol (7.75 g, 82.4 mmol) were added as solids into a flask. Then, 140 mL of HBr/AcOH 30 % were added to the flask and the resulting mixture was vigorously stirred and heated at 90°C for 24 h. The crude was concentrated until the initial volume was reduced to the half part. Then, 20 mL of H_2O were added to the crude and the aqueous phase is extracted using CHCl_3 (3 x 40 mL). The aqueous phase was basified with NaOH until pH 14, and the resulting mixture was extracted with CHCl_3 (3 x 40 mL). The organic phase was then separated, dried with MgSO_4 and the solvent removed. Pure unprotected macrocyclic ligand **2b-H** was obtained as a white solid (620 mg, 2.6 mmol, 81%).



^1H NMR (400 MHz, CDCl_3 , ppm) δ 7.56 (s, 1H, H_4), 7.19 (t, $^3J_{\text{H}} = 7.6$ Hz, 1H, H_9), 6.78 (t, $^3J_{\text{H}} = 7.6$ Hz, 1H, H_1), 6.66 (d, $^3J_{\text{H}} = 7.4$ Hz, 2H, H_2), 6.62 (d, $^3J_{\text{H}} = 7.5$ Hz, 2H, H_8), 4.05 (s, 4H, H_6), 3.97 (s, 4H, H_5), 2.33 (s, 2H, NH). **^{13}C $\{^1\text{H}\}$ NMR (100 MHz, CDCl_3 , ppm)** δ 159.4, 139.2, 136.2, 132.9, 127.3, 126.4, 120.6, 56.5, 55.2. **HRMS (ESI)** calcd. for $\text{C}_{15}\text{H}_{17}\text{N}_3$ $[\text{M}+\text{H}]^+$: 240.1495; found: 240.1496.

2.4 Synthesis of **2c-H**

Macrocyclic ligand **2b-H** (500 mg, 2.1 mmol), HCHO 37%w/w (51.2 mL, 0.68 mol), HCOOH (8.3 mL, 0.21 mmol) were mixed in a round-bottom flask and the resultant mixture was warmed to reflux at 105°C . After 24h, the crude mixture was cooled to room temperature and the solvent was removed under vacuum. Then, 20 mL of $\text{NaOH}_{(\text{aq})}$ 30%w/w were added to the crude and the aqueous phase was extracted using CHCl_3 (3 x 40 mL). The organic layer was washed with 50 mL $\text{NaOH}_{(\text{aq})}$ 30%w/w and the solvent removed to obtain **2b-H** in a pure form as a white solid (516.5 mg, 1.93 mmol, 92%).



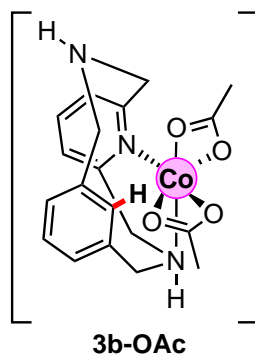
^1H NMR (400 MHz, CDCl_3 , ppm) δ 7.53 (s, 1H, H^4), 7.10 (t, $^3J_{\text{H}} = 7.6$ Hz, 1H, H^9), 6.75 (t, $^3J_{\text{H}} = 6.1$ Hz, 1H, H^1), 6.71 (d, $^3J_{\text{H}} = 7.4$ Hz, 2H, H^2), 6.69 (d, $^3J_{\text{H}} = 7.5$ Hz, 2H, H^8), 3.81 (s, 4H, H^6), 3.67 (s, 4H, H^5), 2.69 (s, 6H, N- CH_3). ^{13}C { ^1H } NMR (100 MHz, CDCl_3 , ppm) δ 157.5 (C_7), 136.6 (C_3), 136.1 (C_9), 135.8 (C_4), 127.5 (C_1), 126.7 (C_2), 122.4 (C_8), 66.5 (C_6), 64.8 (C_5), 48.8 (N- CH_3). HRMS (ESI) calcd. for $\text{C}_{15}\text{H}_{17}\text{N}_3$ $[\text{M}+\text{H}]^+$: 268.1808; found: 268.1811.

3. Synthesis of complexes

3.1 Synthesis of Co(II) coordination complexes

3.1.1 Synthesis of $[(\mathbf{2b-H})\text{Co}^{\text{II}}(\text{OAc})_2]$ ($\mathbf{3b-OAc}$)

In a 10 mL vial, macrocyclic ligand $\mathbf{2b-H}$ (100 mg, 0.41 mmol) and $\text{Co}(\text{OAc})_2$ (72.2mg, 0.41 mmol) were mixed in $\text{CF}_3\text{CH}_2\text{OH}$ (2.5 mL). The vial was then sealed with a septum and the mixture was stirred at RT over 16h. Solvent was removed and a purple foam corresponding to $\mathbf{3b-OAc}$ (121.7 mg, 0.29 mmol, 72%) was obtained. Suitable crystals for X-Ray spectrometry were grown by diethyl ether diffusion in a concentrated solution of $\mathbf{3b-OAc}$ in methanol (See Figure S11).

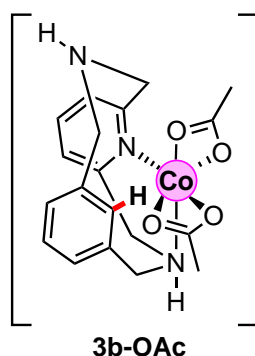


^1H NMR (400 MHz, CDCl_3 , ppm) δ 163.2, 67.8, 60.8, 38.5, 24.4, 11.3, -2.4, -17.8. HRMS (ESI) calcd. for $\text{C}_{17}\text{H}_{20}\text{CoN}_3\text{O}_2^+$ $[\text{M-OAc}]^+$: 357.0882; found: 357.0874.

EA: $\text{C}_{19}\text{H}_{23}\text{CoN}_3\text{O}_4 \cdot \text{H}_2\text{O}$ calcd. C 54.80, N 10.11, H 5.57 %; exp. C 54.76, N 10.05, H 5.62 %.

3.1.2 Synthesis of $[(\mathbf{2c-H})\text{Co}^{\text{II}}(\text{OAc})_2]$ ($\mathbf{3c-OAc}$)

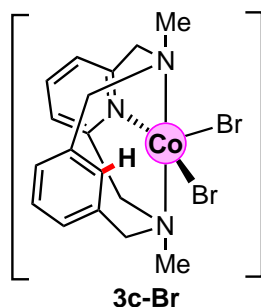
In a 10 mL vial, macrocyclic ligand $\mathbf{2c-H}$ (100 mg, 0.37 mmol) and $\text{Co}(\text{OAc})_2$ (65.5mg, 0.37 mmol) were mixed in CD_3Cl (2.5 mL). The vial was then sealed with a septum and the mixture was stirred at RT over 24h. The crude was layered with pentane. After 24h at 4°C , the resulting oil was dried under vacuum over 6h, obtaining a grey-purple foam corresponding to $\mathbf{3c-OAc}$ (95.2 mg, 0.21 mmol, 58%).



$^1\text{H NMR}$ (400 MHz, CDCl_3 , ppm) δ 129.4, 74.6, 72.0, 54.5, 31.7, -6.6, -7.3. **HRMS** (ESI) calcd. for $\text{C}_{19}\text{H}_{24}\text{CoN}_3\text{O}_2^+$ $[\text{M-OAc}]^+$: 385.1195; found: 385.1190. **EA**: $\text{C}_{21}\text{H}_{26}\text{CoN}_3\text{O}_4 \cdot \text{H}_2\text{O}$ calcd. C 55.14, N 9.12, H 6.12 %; exp. C 54.67, N 9.11, H 6.09 %.

3.1.3 Synthesis of $[(2\text{c-H})\text{Co}^{\text{II}}(\text{Br})_2]$ (**3c-Br**)

In a 10 mL vial, macrocyclic ligand **2c-H** (100 mg, 0.37 mmol) and CoBr_2 (80.9mg, 0.37 mmol) were mixed in $\text{CF}_3\text{CH}_2\text{OH}$ (2.5 mL). The vial was then sealed with a septum and the mixture was stirred at RT over 16h. Solvent was removed and a purple powder corresponding to **3c-Br** (175.1 mg, 0.36 mmol, 99%) was obtained. Suitable crystals for X-Ray spectrometry were grown by diethyl ether diffusion in a concentrated solution of **3c-Br** in methanol (see Figure S12).

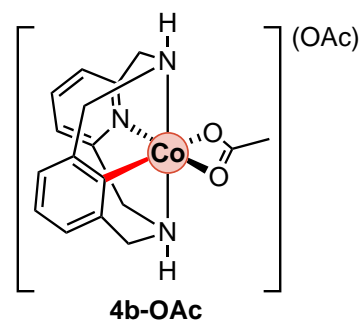


$^1\text{H NMR}$ (400 MHz, CDCl_3 , ppm) δ 126.4, 86.7, 61.3, 38.6, 32.7, 20.6, -5.1, -5.7. **HRMS** (ESI) calcd. for $\text{C}_{17}\text{H}_{21}\text{CoN}_3\text{Br}^+$ $[\text{M-Br}]^+$: 405.0245; found: 405.0240. **EA**: $\text{C}_{17}\text{H}_{21}\text{CoN}_3\text{Br}_2$ calcd. C 42.00, N 8.64, H 4.35 %; exp. C 42.09, N 8.44, H 4.81%.

3.2 Synthesis of organometallic aryl-Co(III) complexes

3.2.1 Synthesis of $[\text{2b-Co}^{\text{III}}(\text{OAc})](\text{OAc})$ (**4b-OAc**)

In a 10 mL vial, **2b-H** (100 mg, 0.41 mmol) and $\text{Co}(\text{OAc})_2$ (72.2mg, 0.41 mmol) were mixed in $\text{CF}_3\text{CH}_2\text{OH}$ (2.5 mL). The vial was then sealed with a septum and the mixture was warmed up to 100°C over 36h. Solvent was then removed, and the crude was dissolved in CHCl_3 and layered with pentane. After 24h at 4°C , the resulting oil was dried under vacuum over 6h, obtaining a grey-red foam corresponding to the organometallic complex **4b-OAc** (141 mg, 0.34 mmol, 82%).

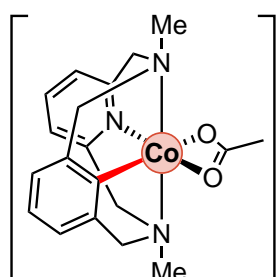


$^1\text{H NMR}$ (400 MHz, CDCl_3 , ppm) δ 7.46 (t, $^3J_{\text{H}} = 7.7$ Hz, 1H), 6.94 (t, $^3J_{\text{H}} = 7.6$ Hz, 1H), 6.90 (d, $^3J_{\text{H}} = 7.4$ Hz, 2H), 6.88 (d, $^3J_{\text{H}} = 7.5$ Hz, 2H), 6.71-5.16 (bs, 2H, N-H), 4.74 (m,

4H), 3.73 (d, $^2J_H = 15.0$ Hz, 2H), 3.69 (d, $^2J_H = 15.2$ Hz, 2H), 2.18 (s, 3H, ^-OAc), 1.72 (s, 3H, ^-OAc). ^{13}C { 1H } NMR (100 MHz, $CDCl_3$, ppm) 166.8, 161.6, 148.6, 137.0, 124.1, 120.2, 118.3, 62.2, 61.8, 24.6. HRMS (ESI) calcd. for $C_{17}H_{19}CoN_3O_2^+$ [M-OAc] $^+$: 356.0804; found: 356.0802. EA: $C_{19}H_{22}CoN_3O_4 \cdot CF_3CH_2OH \cdot H_2O$ calcd. C 47.29, N 7.88, H 5.10 %; exp. C 47.27, N 7.92, H 5.15 %.

3.2.2 Synthesis of [2c-Co^{III}(OAc)](OAc) (4c-OAc)

In a 10 mL vial, 2c-H (100 mg, 0.37 mmol) and $Co(OAc)_2$ (65.5mg, 0.37 mmol) were mixed in CF_3CH_2OH (2.5 mL). The vial was then sealed with a septum and the mixture was warmed up to 100°C over 36h. Solvent was then removed, and the crude was dissolved in $CHCl_3$ and layered with pentane. After 24h at 4°C, the resulting oil was dried under vacuum over 6h, obtaining a grey-red foam corresponding to the organometallic complex 4c-OAc (95.2 mg, 0.21 mmol, 58%).



4c-OAc

(OAc) 1H NMR (400 MHz, $CDCl_3$, ppm) δ 7.43 (t, $^3J_H = 7.7$ Hz, 1H), 6.98 (t, $^3J_H = 7.6$ Hz, 1H), 6.81 (d, $^3J_H = 7.4$ Hz, 2H), 6.77 (d, $^3J_H = 7.5$ Hz, 2H), 4.59 (d, $^2J_H = 15.1$ Hz, 2H), 4.45 (d, $^2J_H = 15.1$ Hz, 2H), 3.59 (d, $^2J_H = 15.1$ Hz, 2H), 3.57 (d, $^2J_H = 15.1$ Hz, 2H), 2.55 (s, 6H, N-CH $_3$), 2.41 (s, 3H, ^-OAc), 1.88 (s, 3H, ^-OAc). ^{13}C { 1H } NMR (100 MHz, $CDCl_3$, ppm) δ 169.3, 160.4, 146.0, 137.3, 124.0, 119.5, 117.5, 74.0, 72.4, 50.0, 25.5.

HRMS (ESI) calcd. for $C_{19}H_{23}CoN_3O_2^+$ [M-OAc] $^+$: 384.1117; found: 384.1122. EA: $C_{21}H_{26}CoN_3O_4 \cdot CF_3CH_2OH$ calcd. C 50.84, N 7.73, H 5.38 %; C 50.90, N 7.69, H 5.36 %.

3.2.3 Synthesis of [2b-Co^{III}(OAc)](OAc) (4b-OAc) from 3b-OAc

In a 4 mL vial, 3b-OAc (20 mg, 0.048 mmol) was dissolved in CF_3CH_2OH (2 mL). The vial was then sealed with a septum and the mixture was warmed up to 100°C over 16h. Solvent was then removed, and the crude was dissolved in $CHCl_3$ and layered with pentane. After 24h at 4°C, the resulting oil was dried under vacuum over 6h, obtaining a grey-red foam corresponding to the organometallic complex 4b-OAc (13.4 mg, 0.032 mmol, 67%). Spectroscopic characterization of the resulting complex matches with values obtained in page S11.

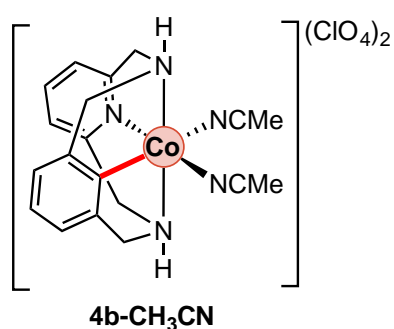
3.2.4 Synthesis of [2c-Co^{III}(OAc)](OAc) (4c-OAc) from 3c-OAc

In a 10 mL vial, 3c-OAc (20 mg, 0.045 mmol) was dissolved in CF_3CH_2OH (2.5 mL). The vial was then sealed with a septum and the mixture was warmed up to 100°C over 16h. Solvent was then removed, and the crude was dissolved in $CHCl_3$ and layered with pentane. After 24h at 4°C, the resulting oil was dried under vacuum over 6h, obtaining a grey-red foam corresponding to the organometallic complex 4c-OAc (15.4 mg, 0.035

mmol, 77%). Spectroscopic characterization of the resulting complex matches with values obtained in page S12.

3.2.5 Synthesis of [2b-Co^{III}(CH₃CN)₂](ClO₄) (4b-CH₃CN)

In a 2 mL vial, 2b-H (9.6 mg, 0.04 mmol), CoBr₂ (8.9 mg, 0.04 mmol) and AgClO₄ (24.6 mg, 0.12 mmol) were mixed in 1 mL of a mixture CH₃CN/CF₃CH₂OH (10:1). The vial was then sealed with a septum and the mixture was warmed up to 100°C over 36h under air. The resulting crude was filtered through a celite pad and suitable crystals for X-Ray spectrometry were obtained by slow ether diffusion into the crude solution of 4 (see Figure S13) (9.0 mg, 0.016 mmol, 39%).

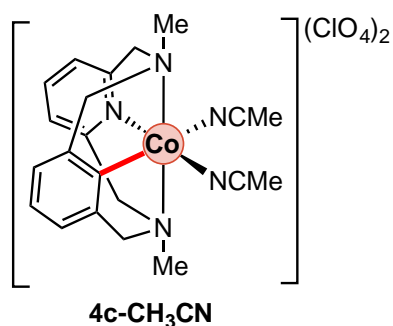


¹H NMR (400 MHz, CD₃CN, ppm) δ 7.81 (t, ³J_H = 7.9 Hz, 1H), 7.24 (d, ³J_H = 8.6 Hz, 2H), 7.16 (t, ³J_H = 7.6 Hz, 1H), 7.05 (d, ³J_H = 7.6 Hz, 2H), 5.20 (b, 1H), 4.69 (m, 4H), 4.13 (d, ²J_H = 17.4 Hz, 2H), 3.99 (d, ²J_H = 16.3 Hz, 2H), 2.31 (s, 3H, CH₃CN). **¹³C {¹H} NMR (100 MHz, CD₃CN, ppm)** 160.8, 146.7, 139.8, 131.2, 125.9, 122.1, 120.6, 100.0, 63.2, 63.1, 3.6. **HRMS (ESI)** calcd. for C₁₇H₂₀CoClN₃O₄⁺ [M-2CH₃CN-ClO₄]⁺: 396.0161; found: 396.0154. **EA:**

C₁₉H₂₂CoCl₂N₅O₈·3CH₃CN calcd. C 42.81, N 15.98, H 4.46 %; exp. C 42.61, N 15.82, H 4.53 %.

3.2.6 Synthesis of [2c-Co^{III}(CH₃CN)₂](ClO₄) (4c-CH₃CN)

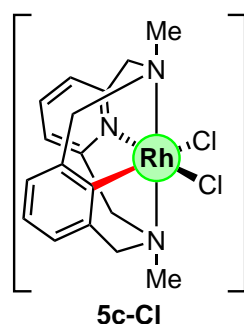
In a 2 mL vial, 3c-Br (20 mg, 0.04 mmol) and AgClO₄ (24.6 mg, 0.12 mmol) were mixed in 1 mL of a mixture CH₃CN/CF₃CH₂OH (10:1). The vial was then sealed with a septum and the mixture was warmed up to 100°C over 36h under air. The resulting crude was filtered through a celite pad and suitable crystals for X-Ray crystallography were obtained by slow ether diffusion (see Figure S14) (20.1 mg, 0.031 mmol, 79%).



¹H NMR (400 MHz, CD₃CN, ppm) δ 7.85 (t, ³J_H = 7.9 Hz, 1H), 7.24 (d, ³J_H = 8.6 Hz, 2H), 7.19 (t, ³J_H = 7.6 Hz, 1H), 7.04 (d, ³J_H = 7.6 Hz, 2H), 4.51 (d, ²J_H = 17.1 Hz, 2H), 4.46 (d, ²J_H = 16.2 Hz, 2H), 4.27 (d, ²J_H = 17.4 Hz, 2H), 4.16 (d, ²J_H = 16.3 Hz, 2H), 2.71 (s, 6H, N-CH₃), 2.41 (s, 3H, CH₃CN). **¹³C {¹H} NMR (100 MHz, CD₃CN, ppm)** 159.9, 145.5, 140.4, 131.4, 126.3, 122.1, 120.7, 73.1, 72.1, 52.3, 4.2. **HRMS (ESI)** calcd. for C₁₇H₂₀CoClN₃O₄⁺ [M-2CH₃CN-ClO₄]⁺: 424.0474; found: 424.0474. **EA:** C₁₇H₂₀CoCl₂N₃O₈·3CH₃CN calcd. C 42.47, N 12.78, H 4.32 %; exp. C 42.41, N 12.82, H 4.33 %.

3.2.7 Synthesis of [2c-Rh^{III}Cl₂] (5c-Cl)

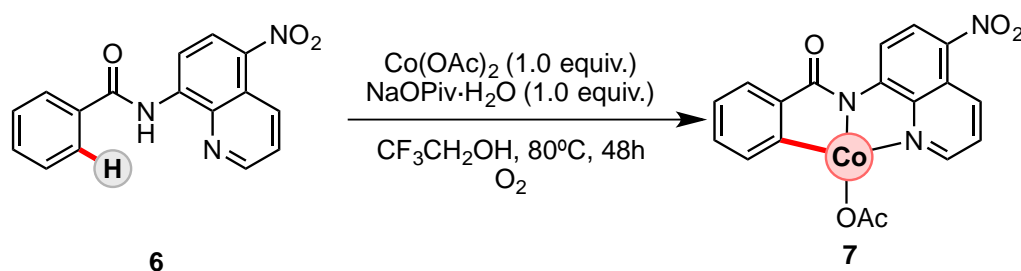
In a 10 mL round-bottom flask, 2c-H (100 mg, 0.37 mmol) and RhCl₃ (77.4 mg, 0.37 mmol) were mixed in CF₃CH₂OH (2.5 mL). The mixture was then warmed up to 100°C and refluxed over 36h. Then, solvent was removed and the crude was dissolved in a mixture 1:1 CH₃CN/CH₃OH and layered with ether. After 24h at 4°C, yellow crystals of 5c-Cl were obtained (124.9 mg, 0.264 mmol, 71%).



¹H NMR (400 MHz, CDCl₃, ppm) δ 7.55 (t, ³J_H = 7.1 Hz, 1H), 7.05 (d, ³J_H = 7.6 Hz, 1H), 6.75 (m, 3H), 4.88 (d, ²J_H = 15.0 Hz, 2H), 4.76 (d, ²J_H = 15.1 Hz, 2H), 4.10 (d, ²J_H = 15.1 Hz, 2H), 3.97 (d, ²J_H = 15.1 Hz, 2H), 3.32 (s, 6H, N-CH₃). **¹³C {¹H} NMR (100 MHz, CDCl₃, ppm)** δ 158.4, 141.1, 137.3, 123.3, 120.5, 119.2, 77.2, 75.5, 74.3, 53.5. **HRMS (ESI)** calcd. for C₁₇H₂₀RhN₃Cl⁺ [M-Cl]⁺: 404.0395; found: 404.0394.

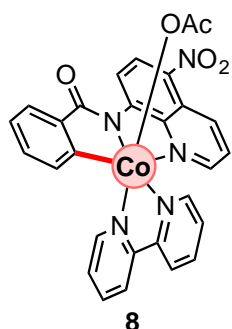
3.3 Synthesis of Aryl-Co(III) species AQ directing group (7 and 8).¹⁴

To a 10 mL round bottom flask was added model substrate 6 (147 mg, 0.5 mmol), Co(OAc)₂ (89 mg, 0.5 mmol), NaOPiv·H₂O (142 mg, 1 equiv.) and 3 mL of 2,2,2-trifluoroethanol. The flask was then sealed with a septum and O₂ was bubbled for 15 minutes until the solution was saturated. The reaction was then heated at 80 °C for 48 hours, after which time the solvent was removed. The crude reaction mixture was then purified by column chromatography (Hexane/EtOAc 1:2) and the isolated product 7 was further washed with dichloromethane providing analytically pure compound as a brown solid (85 mg, 42%). ¹H and {¹H} ¹³C data are consistent with the proposed organometallic Co^{III} species.



Scheme S2. Synthesis of aryl-Co(III) complex 7.

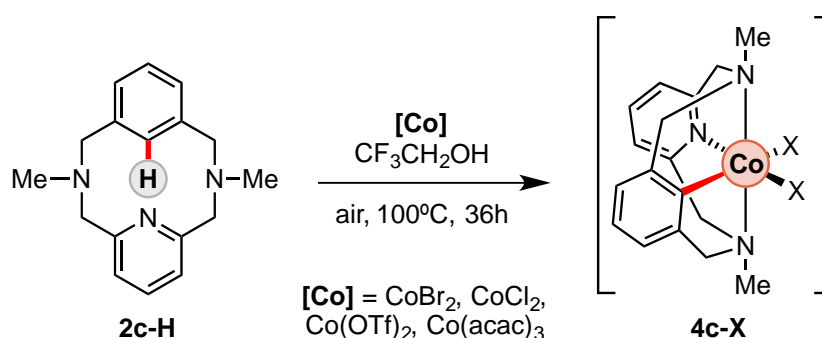
¹H NMR (400 MHz, CDCl₃, ppm) δ 9.71 (dd, ³J_H = 8.7 Hz, ⁴J_H = 1.4 Hz, 1H), 8.88 (dd, ³J_H = 4.9 Hz, ⁴J_H = 1.3 Hz, 1H), 8.50 (d, ³J_H = 9.5 Hz, 1H), 8.17 (d, ³J_H = 9.5 Hz, 1H), 7.99 (dd, ³J_H = 8.8 Hz, ³J_H = 4.8 Hz, 1H), 6.65 (m, 2H), 6.57 (dq, ³J_H = 7.6 Hz, ⁴J_H = 0.9 Hz, 1H), 6.47 (dt, ³J_H = 7.5 Hz, ⁴J_H = 1.4 Hz, 1H), 0.6 (s, 3H). **¹³C {¹H} NMR (100 MHz, CDCl₃, ppm)** δ 202.2, 178.7, 156.5, 150.8, 146.4, 141.1, 137.1, 136.8, 133.9, 131.0, 129.3, 127.7, 126.2, 125.1, 124.9, 123.8, 39.6, 25.3.



Crystals of the organometallic compound suitable for X-Ray crystallography studied were grown by slow evaporation of a concentrated solution of **7** in acetonitrile containing 4 equivalents of bipyridine (Figure S14). We have been unable to characterize complex **8** further due to their insolubility in common laboratory deuterated solvents.

4. Optimization studies of aryl-Co(III) synthesis

4.1 Evaluation of different Cobalt Salts



Scheme S3. Synthesis of aryl-Co(III) complexes **4c-X** using different cobalt salts.

In a 2 mL vial, macrocyclic ligand **2c-H** (0.11 mmol) and CoX_2 (0.11 mmol) were mixed in $\text{CF}_3\text{CH}_2\text{OH}$ (1 mL). The vial was then sealed with a septum and the mixture was warmed up to 100°C over 36h. Solvent was then removed and the mixture was analyzed through ^1H NMR techniques and/or ESI-HRMS-QTOF. Resulting complexes were not isolated and fully characterized. Result are summarized in Table S1, where it can be seen that reaction of CoX_2 salts proceed when using labile and weakly basic anions.

Table S1. Reaction of **2c-H** with different cobalt salts. ^1H NMR and/or HRMS were used to detect organometallic **4c-X** species. See Fig. S1-S4.

entry	[Co] source	aryl-Co(III) detection
1	CoBr ₂	detected (mixture)
1b	CoBr ₂ with 2b-H	n.r.
2	CoCl ₂	n.r.
3	Co(OTf) ₂ ·2CH ₃ CN	n.r.
4	Co(acac) ₃	detected

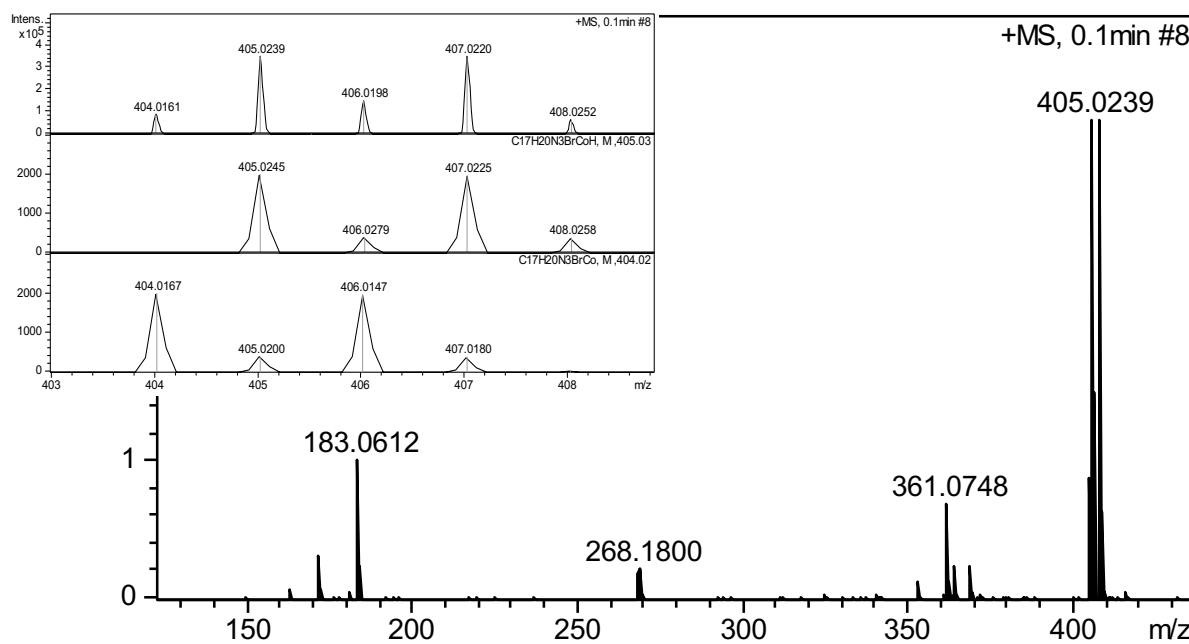


Figure S1. HRMS of crude mixture obtained after reaction of **2c-H** with CoBr₂ in CF₃CH₂OH at 100°C. **4c-Br** peak appears at m/z = 404.0161 (M-Br⁻). Peak with m/z = 405.0239 corresponds to Co(II) complex **3c-Br**. Inset: Up, experimental spectrum; down, simulated spectrum.

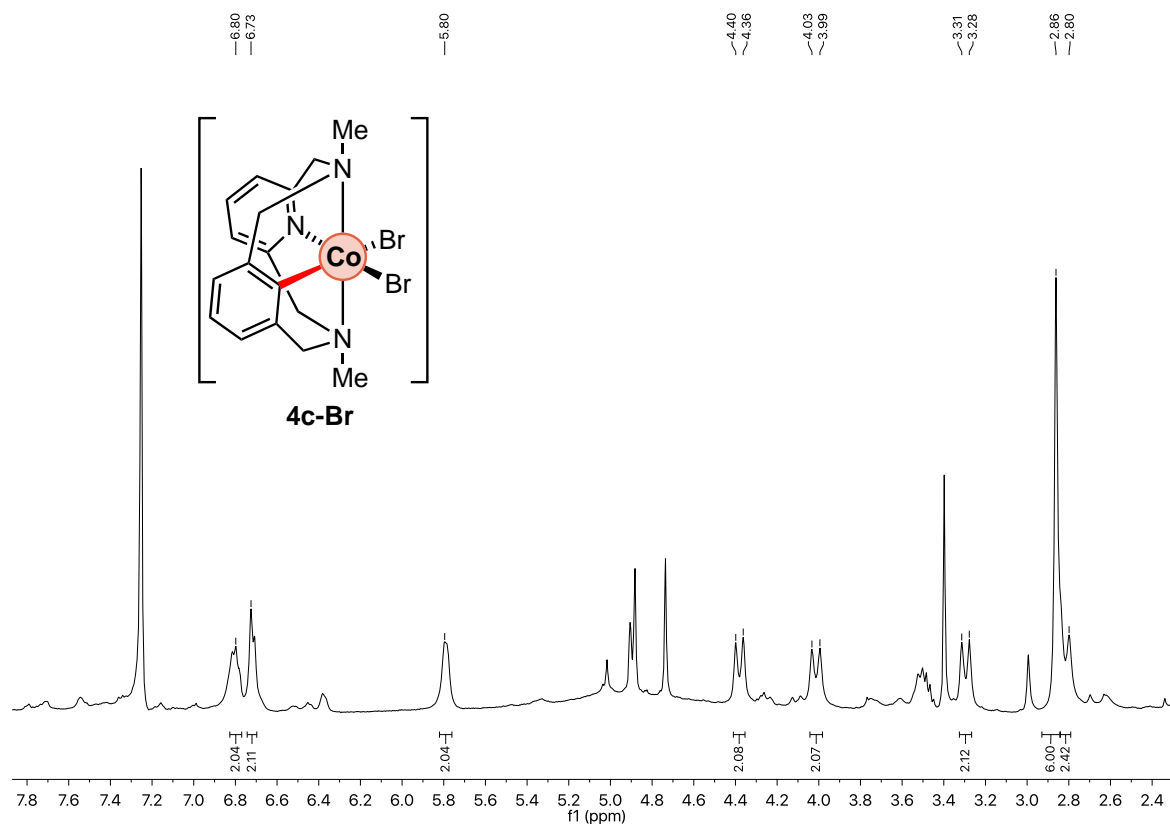


Figure S2. ¹H NMR spectrum of crude mixture obtained after reaction of **2c-H** with CoBr₂ in CF₃CH₂OH at 100°C. Formation of **4c-Br** intermediate (CD₃Cl, 400MHz, 298K).

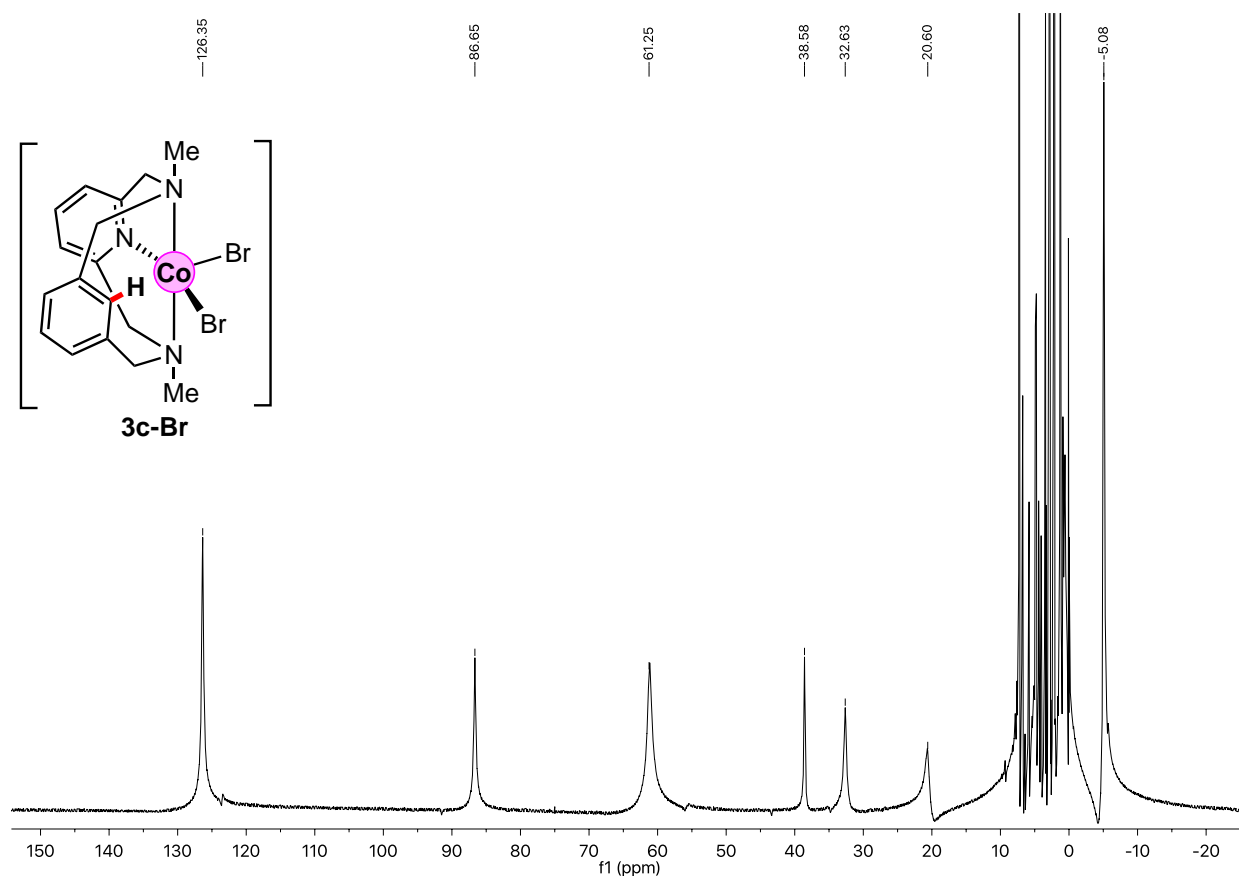


Figure S3. Paramagnetic ^1H NMR spectrum of **3c-Br** (crude mixture) obtained after reaction of **2c-H** with CoBr_2 in $\text{CF}_3\text{CH}_2\text{OH}$ at 100°C (CD_3Cl , 400MHz, 298K).

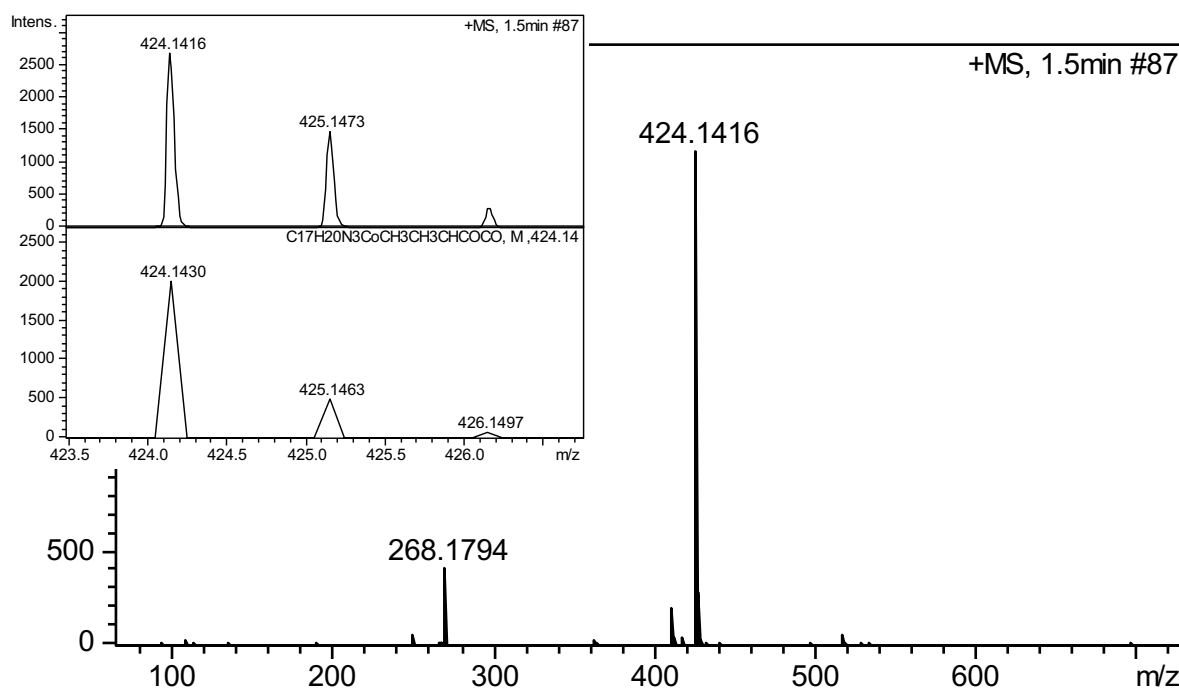
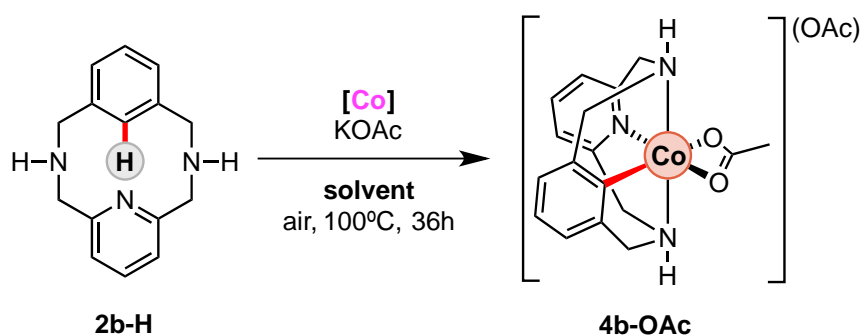


Figure S4. HRMS of crude mixture obtained after reaction of **2c-H** with $\text{Co}(\text{acac})_3$ in $\text{CF}_3\text{CH}_2\text{OH}$ at 100°C . **4c-acac** peak appears at $m/z = 424.1416$ (M-acac^-) Inset: Up, experimental spectrum; down, simulated spectrum.

4.2. Effect of an External Base and Evaluation of Solvents



Scheme S4. Synthesis of aryl-Co(III) complex **4b-OAc** under different reaction conditions.

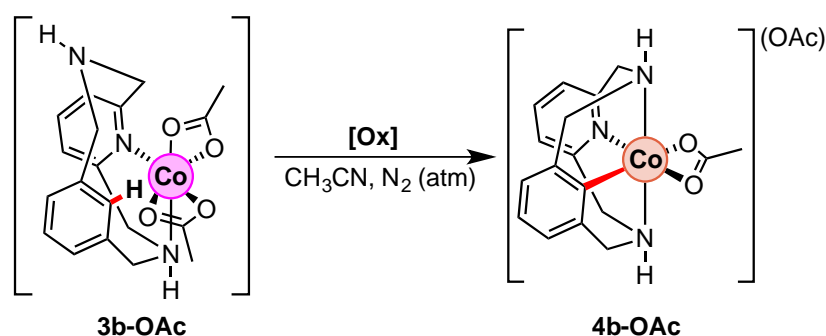
In Table S1 it has been seen that reaction of CoX_2 salts proceed when using labile and weakly basic anions (Br, OAc) and 2,2,2-trifluoroethanol as a solvent. In this section, different solvents have been evaluated in combination of an external base, such as KOAc. On one hand, if CoBr_2 is mixed with **2c-H** (1.0 equiv.) in TFE, mixture of Co(II) and aryl-Co(III) intermediates are observed by NMR as well as HRMS (Table S2, entry 1). However, when CoBr_2 (1.0 equiv.) is used as cobalt source and KOAc (2.0 equiv.) is added (Entries 2 and 3), **4b-OAc** and **4c-OAc** were obtained. On the other hand, the influence of the solvent was also evaluated and it has been seen that reaction only takes place without addition of an external base when a polar protic solvent is used (Entries 6, 8, 10, 11 and 12). However, when adding an additional equivalent of acetate (KOAc) to the reaction media, **4b-OAc** can be obtained quantitatively, no matter the solvent that is used (Entries 5, 7 and 9). These experimental observations suggest that C-H activation is likely to proceed through a base-assisted mechanism, such as a CMD pathway. Furthermore, these experiments suggest that fluorinated solvents are very beneficial in these transformations, somehow assisting the C-H activation step.

Table S2. Reaction of **4b-OAc** with different cobalt sources in different solvents at 100°C. Evaluation of the presence of a base (KOAc).

entry	solvent	[Co] source	KOAc (eq)	yield 4b-OAc ^c
1 ^a	TFE	CoBr_2	-	NMR and MS detection (Fig. S2-S4)
2	TFE	CoBr_2	2.0	99%
3 ^a	TFE	CoBr_2	2.0	99%
4	CH_3CN	CoBr_2	-	traces
5	CH_3CN	$\text{Co}(\text{OAc})_2$	1.0	99%
6	CH_3CN	$\text{Co}(\text{OAc})_2$	-	traces
7	EtOH	$\text{Co}(\text{OAc})_2$	1.0	99%
8	EtOH	$\text{Co}(\text{OAc})_2$	-	45%
9	MeOH	$\text{Co}(\text{OAc})_2$	1.0	99%
10	MeOH	$\text{Co}(\text{OAc})_2$	-	21%
11	TFE	$\text{Co}(\text{OAc})_2$	-	99%
12	HFIP ^b	$\text{Co}(\text{OAc})_2$	-	99%

^aReaction of CoBr_2 with **2c-H** instead of **2b-H**. ^b1,1,1,3,3,3-hexafluoroisopropanol. ^cIsolated yield after crystallization of residual Co(II).

4.3. Evaluation of different oxidants



Scheme S5. Synthesis of aryl-Co(III) complex **4b-OAc** using different oxidants under N_2 atmosphere.

In this section, different oxidants have been evaluated under inert atmosphere to gain some insights in its role in the reaction mechanism.

In a 2 mL vial, complex **3b-OAc** (5 mg, 0.012 mmol) and **OXIDANT** (1.0 equiv.) were mixed in CD_3CN (1 mL) under a N_2 atmosphere. The vial was then sealed with a septum and the mixture stirred at RT-100°C over 16h. Crude was then analyzed by HRMS to confirm the presence of Co(III) organometallic species. Reaction proceed only at high temperatures and using TEMPO or silver salts as oxidants, (Entry 4-10, Table S3). Interestingly, reaction also proceeds under inert atmosphere when starting from a Co(III) precursor, such as $Co(acac)_3$ (Entry 1, Table S3). This results suggest that oxidation from Co(II) to Co(III) takes places previously to the C-H activation event. This oxidation is likely to construct a highly electrophilic Co(III) center that allows C-H metalation.

Table S3. Reaction of **3b-OAc** with different oxidants. 1H NMR and/or HRMS were used to detected organometallic **4b-OAc** species.

entry	oxidant	temperature (°C)	4b-OAc
1^a	-	100	Detected
2	$NOSbF_6$	100	n.r.
3		RT	n.r.
4	TEMPO	100	Detected^b
5		RT	n.r.
6^c	$AgClO_4$	100	Detected^d
7^e		100	Detected^d
8^c	$AgOTf$	100	Detected^d
9^{c,f}	$AgOPiv$	100	Detected^d
10^g		100	Detected^d
11^c	$AgOAc$	100	Detected^d

^a Reaction performed starting from $Co(acac)_3$ and **2c-H** under an inert atmosphere. ^b Organometallic cobalt complex **4b-OAc** detected by NMR and HRMS together with decomposition products of TEMPO. See Fig. S5. ^c **3c-Br** was used as starting material. ^d Organometallic aryl-Co(III) complexes detected by ESI-HRMS-TOF. ^e **2c-H** and 1.0 equiv of $CoCl_2$ were used as starting materials. ^f Reaction time of 2h. ^g Reaction performed starting from $CoBr_2$ and $AgOPiv$ and **2b-H** under an inert atmosphere.

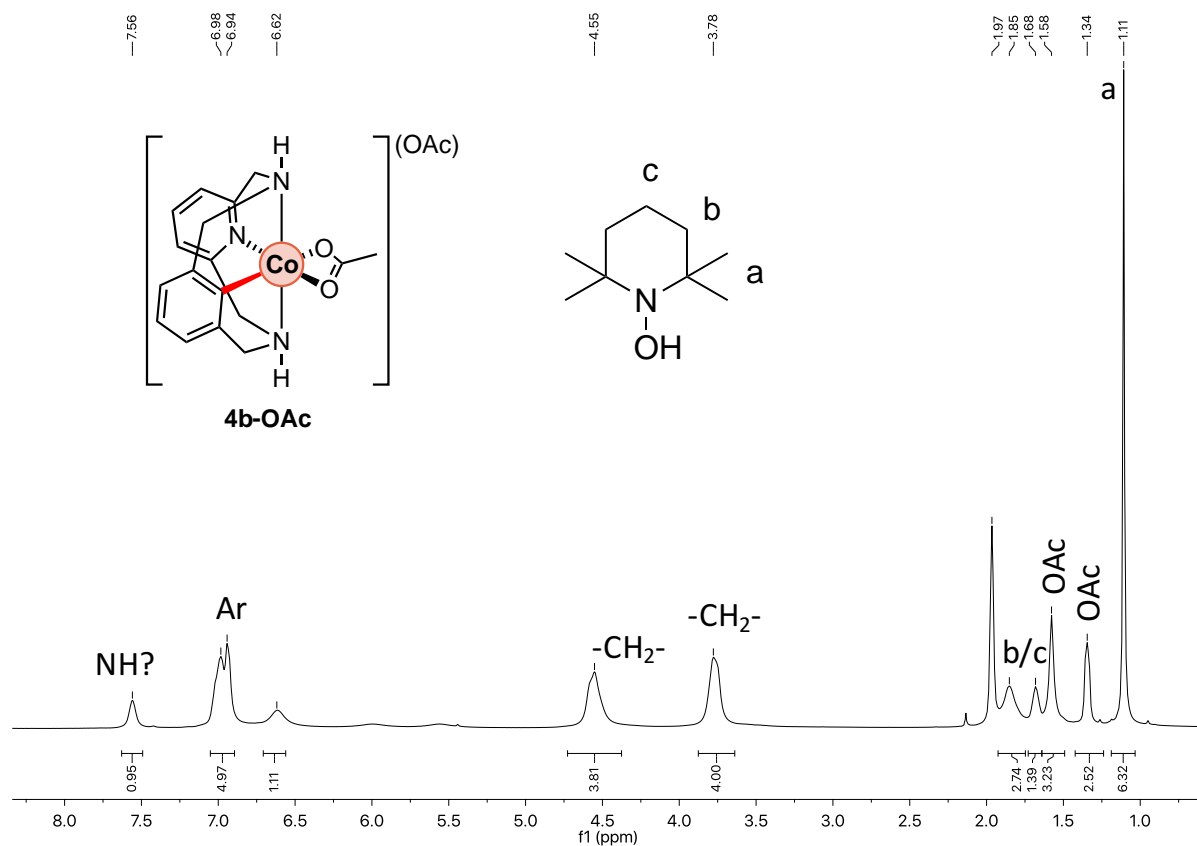


Figure S5. ^1H NMR spectrum of crude mixture obtained after reaction of **3b-OAc** with TEMPO in CD_3CN at 100°C . Peaks of **4b-OAc** and TEMPO-H appear as broad bands due to the presence of paramagnetic species TEMPO and **3b-OAc** in solution (CD_3Cl , 400MHz, 298K).

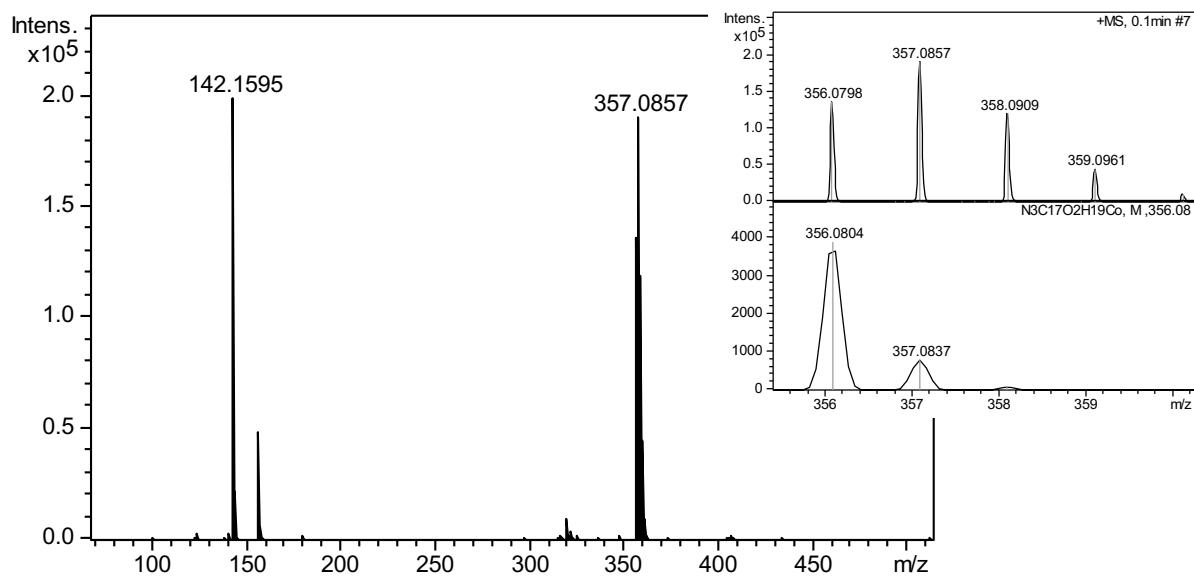


Figure S6. HRMS of crude mixture obtained after reaction of **3b-OAc** with TEMPO in CD_3CN at 100°C . **4b-OAc** peak appears at $m/z = 356.0798$ ($M\text{-OAc}^-$) mixed with **3b-OAc** ($m/z = 357.0857$ ($M\text{-OAc}$)) and 2,2,6,6-tetramethylpiperidine peak appears at 142.1595 ($M+\text{H}^+$). Inset: Up, experimental spectrum; down, simulated spectrum.

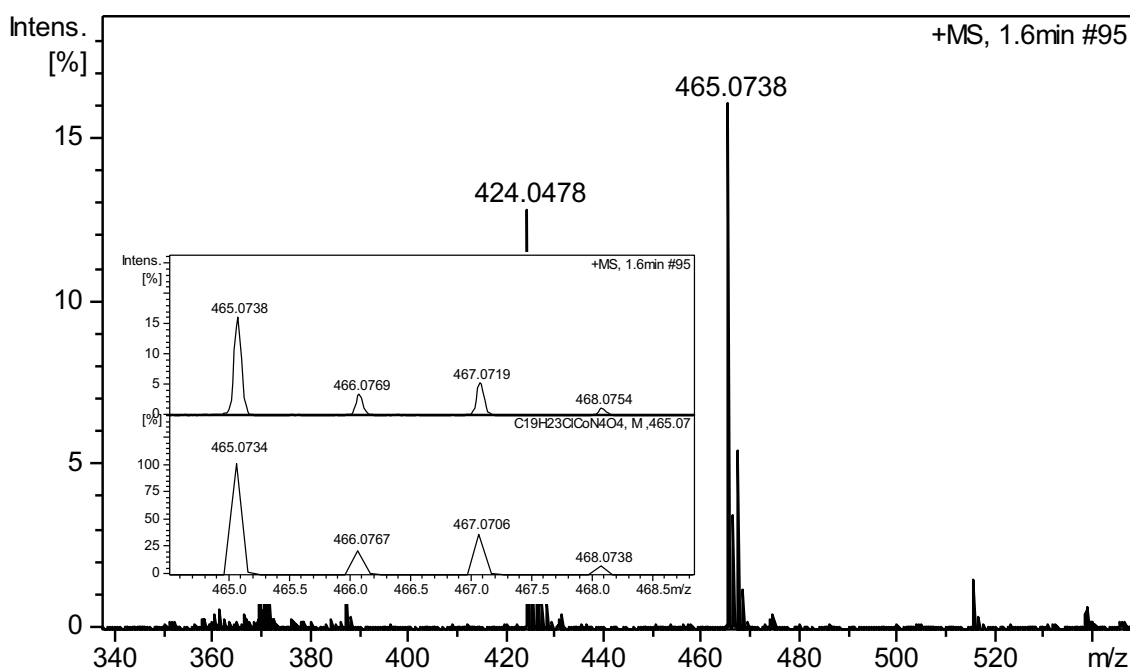


Figure S7. HRMS of crude mixture obtained after reaction of **3c-Br** with AgClO_4 in CH_3CN at 100°C . **4c-CH₃CN** peak appears at $m/z = 465.0738$ ($\text{M-ClO}_4 + \text{CH}_3\text{CN}$) and at $m/z = 424.0478$ ($-\text{ClO}_4$). Inset: Up, experimental spectrum; down, simulated spectrum.

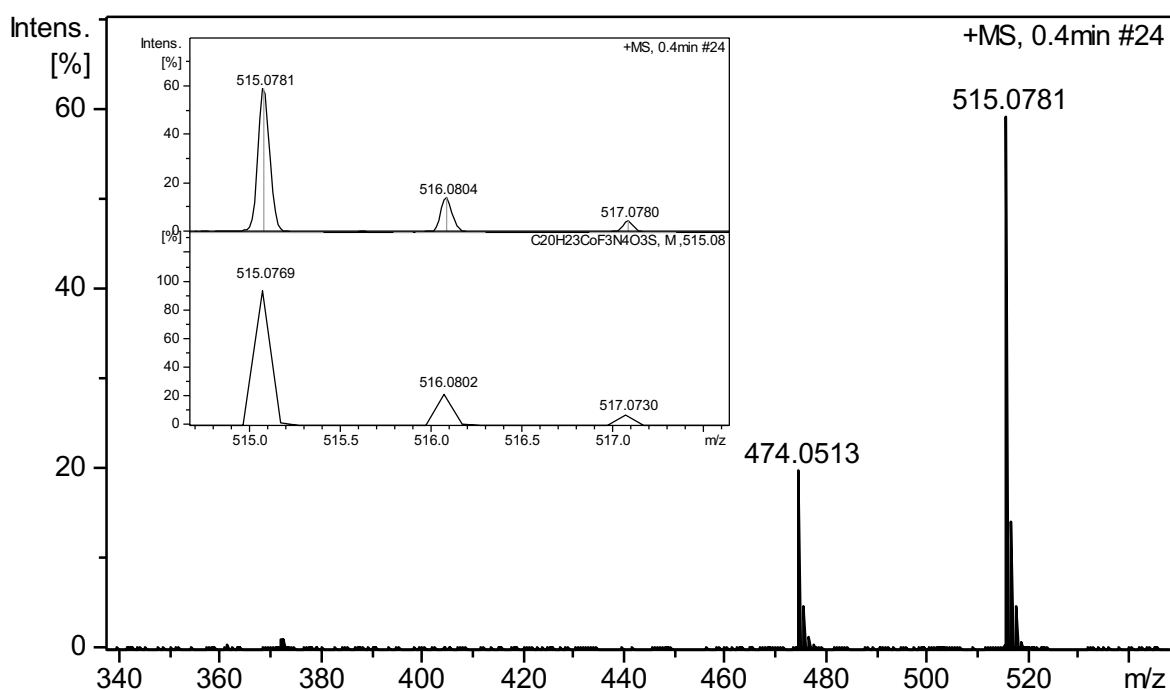


Figure S8. HRMS of crude mixture obtained after reaction of **3c-Br** with AgOTf in CH_3CN at 100°C . **4c-OTf** peak appears at $m/z = 515.0781$ ($\text{M-OTf} + \text{CH}_3\text{CN}$) and at $m/z = 474.0513$ (M-OTf). Inset: Up, experimental spectrum; down, simulated spectrum.

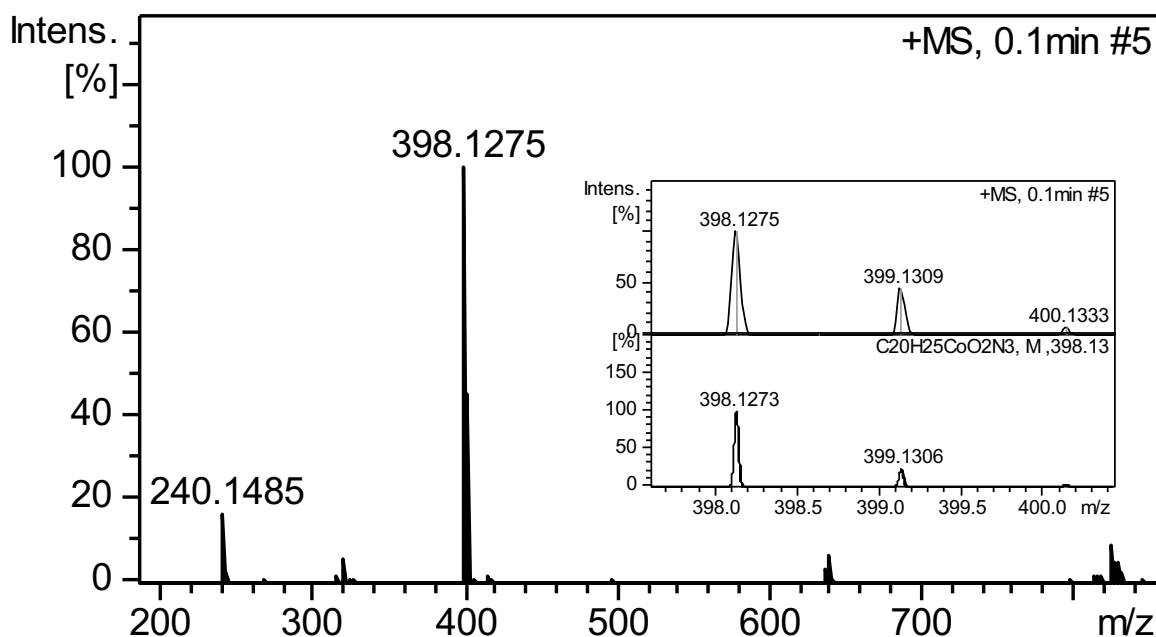


Figure S9. HRMS of crude mixture obtained after reaction of **CoBr**₂ with **2b-H** in presence of AgOPiv in CH₃CN at 100°C. **4b-OPiv** peak appears at m/z = 398.1275 (M-OPiv). Inset: Up, experimental spectrum; down, simulated spectrum.

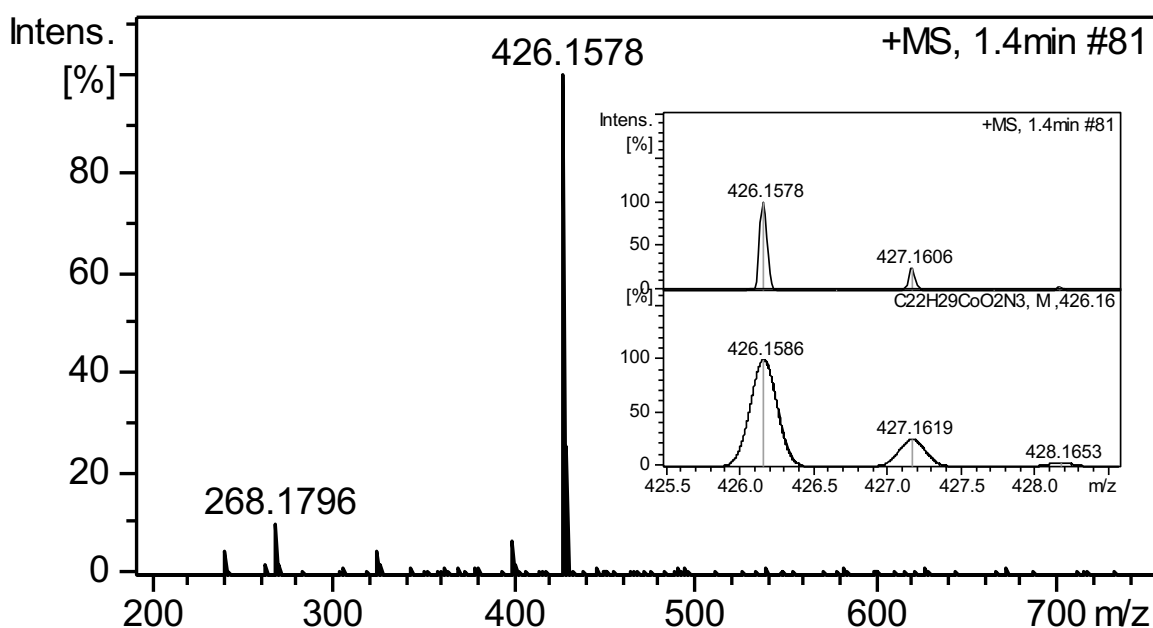


Figure S10. HRMS of crude mixture obtained after reaction of **3c-Br** with AgOPiv in CH₃CN at 100°C. **4c-OPiv** peak appears at m/z = 426.1578 (M-OPiv). Inset: Up, experimental spectrum; down, simulated spectrum.

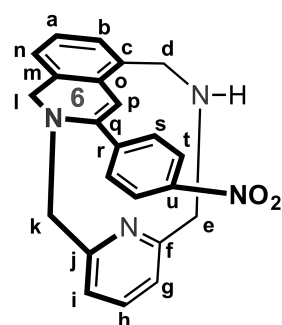
5. Stoichiometric studies with alkynes

5.1 Organometallic **4b-OAc** Complex Reactivity towards Internal Alkynes

In a 2 mL vial, **4b-OAc** (40mg, 0.077 mmol) and **terminal alkyne** (0.077 mmol) were mixed in TFE (1.5 mL). The vial was then sealed with a septum and the mixture was stirred over 16h at different temperatures. Then, after removal of the solvent, NH_4OH (2 mL) was added and the solution was extracted using CH_2Cl_2 (2x5mL). Then, products were purified using silica gel chromatography (CH_2Cl_2 , then $\text{CH}_2\text{Cl}_2/\text{MeOH}$ 95:5) and characterized by NMR techniques.

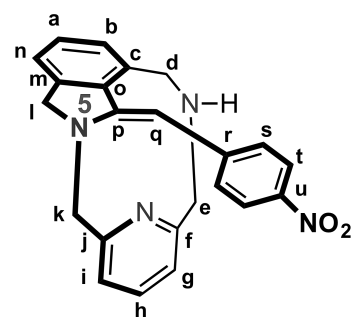
5.1.1 Description of terminal alkyne products

5.1.1.1 4-Ethynyl-1-nitrobenzene – Isoquinoline product (**9a**)

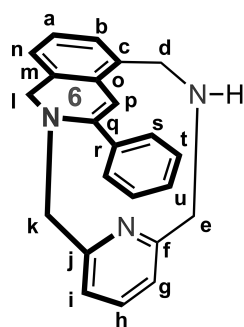


^1H NMR (600 MHz, CDCl_3 , ppm) δ 8.34 (d, $^3J_{\text{H}} = 7.6$ Hz, 2H, **Ht**), 8.16 (d, $^3J_{\text{H}} = 7.7$ Hz, 2H, **Hs**), 7.21 (s, 1H, **Hp**), 7.19 (t, $^3J_{\text{H}} = 6.9$ Hz 1H, **Hh**), 6.76 (d, $^3J_{\text{H}} = 7.6$ Hz, 1H, **Hb**), 6.72 (t, $^3J_{\text{H}} = 7.8$ Hz 1H, **Ha**), 6.71 (s, 1H, **Hi**), 6.44-6.40 (m, 2H, **Hn**, **Hg**), 4.71 (d, $^2J_{\text{H}} = 15.3$ Hz, 1H, **Hd**), 4.27 (s, 1H, **Hi**), 4.18 (d, $^2J_{\text{H}} = 15.7$ Hz, 1H, **He**), 4.06 (d, $^2J_{\text{H}} = 15.7$ Hz, 1H, **Hi'**), 3.99 (s, 1H, **Hk**), 3.77 (d, $^2J_{\text{H}} = 15.3$ Hz, 1H, **Hk'**), 3.59 (d, $^2J_{\text{H}} = 16.3$ Hz, 1H, **Hd'**), 3.41 (d, $^2J_{\text{H}} = 15.3$ Hz, 1H, **He'**). ^{13}C $\{^1\text{H}\}$ NMR (150 MHz, CDCl_3 , ppm) δ 157.6 (**Cf**), 156.5 (**Cj**), 147.9 (**Cq**), 147.5 (**Cu**), 143.0 (**Cr**), 136.3 (**Ch**), 133.7 (**Co**), 133.4 (**Cc**), 133.3 (**Cm**), 128.3 (**Cb**, **Cs**), 126.3 (**Ca**), 124.1 (**Cn**, **Ct**), 120.7 (**Ci**), 120.6 (**Cg**), 116.1 (**Cp**), 57.7 (**Ck**), 53.4 (**Cl**), 53.1 (**Cd**), 51.7 (**Ce**). HRMS (ESI) calcd. for $\text{C}_{23}\text{H}_{21}\text{N}_4\text{O}_2^+$ $[\text{M}+\text{H}]^+$: 385.1659; found: 385.1651. (mixture of **9a** and **9b**)

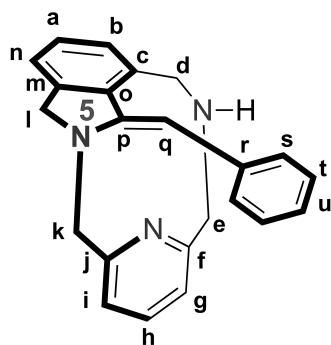
5.1.1.2 4-Ethynyl-1-nitrobenzene – Isoindoline product (**9b**)



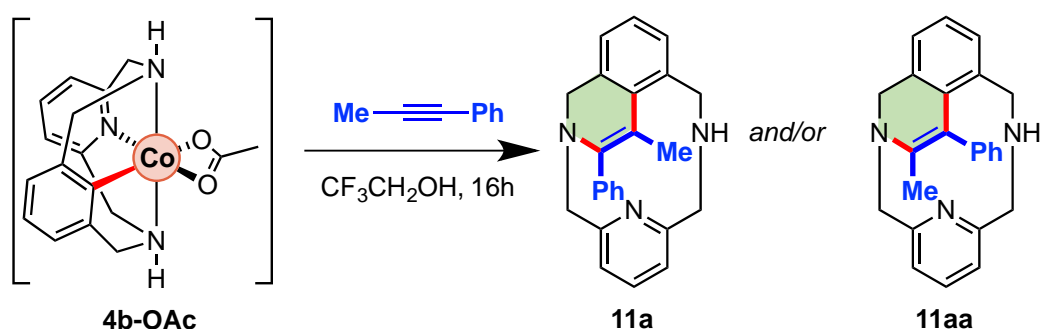
^1H NMR (600 MHz, CDCl_3 , ppm) δ 8.26 (d, $^3J_{\text{H}} = 7.7$ Hz, 2H, **Ht**), 8.20 (d, $^3J_{\text{H}} = 7.7$ Hz, 2H, **Hs**), 7.20 (t, $^3J_{\text{H}} = 7.7$ Hz, 1H, **Hh**), 6.87-6.86 (m, 2H, **Ha**, **Hb**), 6.82 (d, $^3J_{\text{H}} = 7.6$ Hz, 1H, **Hi**), 6.77 (s, 1H, **Hn**), 6.65 (s, 1H, **Hq**), 6.53 (d, $^3J_{\text{H}} = 7.8$ Hz, 1H, **Hg**), 5.06 (d, $^2J_{\text{H}} = 15.3$ Hz, 1H, **Hd**), 4.50 (m, 2H, **Hi**, **Hk**), 4.23 (d, $^2J_{\text{H}} = 15.9$ Hz, 1H, **He**), 3.99 (d, $^2J_{\text{H}} = 15.5$ Hz, 1H, **Hk'**), 3.72 (d, $^2J_{\text{H}} = 15.2$ Hz, 1H, **Hd'**), 3.65 (d, $^2J_{\text{H}} = 16.3$ Hz, 1H, **Hi'**), 3.40 (d, $^2J_{\text{H}} = 15.3$ Hz, 1H, **He'**). ^{13}C $\{^1\text{H}\}$ NMR (150 MHz, CDCl_3 , ppm) δ 157.8 (**Cf**), 157.7 (**Cj**), 157.2 (**Cp**), 145.1 (**Cu**), 144.1 (**Cr**), 141.4 (**Cm**), 139.9 (**Co**), 136.4 (**Ch**), 132.3 (**Cc**), 130.0 (**Cb**), 129.0 (**Ca**), 128.4 (**Cs**), 123.5 (**Ct**), 121.3 (**Cn**), 120.8 (**Ci**), 119.4 (**Cg**), 111.1 (**Cq**), 59.8 (**Ck**), 57.7 (**Cl**), 53.1 (**Cd**), 51.7 (**Ce**). HRMS (ESI) calcd. for $\text{C}_{23}\text{H}_{21}\text{N}_4\text{O}_2^+$ $[\text{M}+\text{H}]^+$: 385.1659; found: 385.1663.

5.1.1.3 Phenylacetylene – Isoquinoline (**10a**)

^1H NMR (600 MHz, CDCl_3 , ppm) δ 8.00 (d, $^3J_{\text{H}} = 7.8$ Hz, 2H, **Hs**), 7.52 (d, $^3J_{\text{H}} = 7.6$ Hz, 2H, **Ht**), 7.46 (t, $^3J_{\text{H}} = 7.5$ Hz, 1H, **Hu**), 7.20 (t, $^3J_{\text{H}} = 7.7$ Hz, 1H, **Hh**), 7.02 (s, 1H, **Hp**), 6.78 (d, $^3J_{\text{H}} = 7.3$ Hz, 1H, **Hb**), 6.73-6.68 (m, 2H, **Ha**, **Hi**), 6.46-6.43 (m, 2H, **Hn**, **Hg**), 4.86 (d, $^2J_{\text{H}} = 15.3$ Hz, 1H, **Hd**), 4.31 (d, $^2J_{\text{H}} = 15.2$ Hz, 1H, **He**), 4.27 (d, $^2J_{\text{H}} = 15.5$ Hz, 1H, **Hi**), 4.17 (d, $^2J_{\text{H}} = 15.8$ Hz, 1H, **Hk**), 4.10 (d, $^2J_{\text{H}} = 15.2$ Hz, 1H, **Hi'**), 3.74 (d, $^2J_{\text{H}} = 15.2$ Hz, 1H, **Hk'**), 3.67 (d, $^2J_{\text{H}} = 15.8$ Hz, 1H, **Hd'**), 3.43 (d, $^2J_{\text{H}} = 15.3$ Hz, 1H, **He'**). ^{13}C $\{^1\text{H}\}$ NMR (150 MHz, CDCl_3 , ppm) δ 157.6 (**Cj**), 155.9 (**Cf**), 151.1 (**Cq**), 136.3 (**Ch**), 136.2 (**Cr**), 134.7 (**Co**), 133.0 (**Cm**), 131.4 (**Cc**), 129.0 (**Cu**), 128.8 (**Ct**), 128.0 (**Cs**, **Cb**), 125.2 (**Ca**), 124.1 (**Cn**), 120.6 (**Ci**), 120.0 (**Cg**), 111.6 (**Cp**), 57.3 (**Ck**), 53.5 (**Cd**), 53.4 (**Cl**), 52.8 (**Ce**). HRMS (ESI) calcd. for $\text{C}_{23}\text{H}_{22}\text{N}_3^+$ $[\text{M}+\text{H}]^+$: 340.1808; found: 340.1811.

5.1.1.4 Phenylacetylene – Indoline (**10b**)

When we attempted to characterize **10b**, we found that it was unstable towards temperature. Reaction was not always reproducible and when **10b** was detected, we were not able to fully characterize it.

5.2 Organometallic **4b-OAc** Complex Reactivity towards Internal Alkynes

Scheme S6. Reaction of **4b-OAc** with internal alkynes.

In a 2 mL vial, **4b-OAc** (40mg, 0.077 mmol) and **1-methyl-1-propyne** (0.077 mmol) were mixed in TFE (1.5 mL). The vial was then sealed with a septum and the mixture was stirred over 16h at different temperatures. Then, after removal of the solvent, NH_4OH (2 mL) was added and the solution was extracted using CH_2Cl_2 (2x5mL). Then, products were purified using silica gel chromatography (CH_2Cl_2 , then $\text{CH}_2\text{Cl}_2/\text{MeOH}$ 95:5) and characterized by NMR techniques.

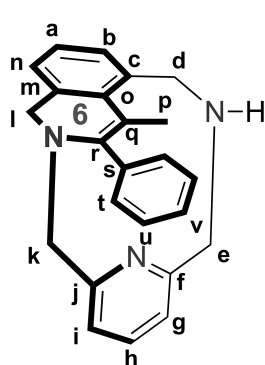
Table S4. Yields and ratios obtained using 1-methyl-1-propyne at different temperatures.

entry	atm.	temp (°C)	yield (%)	ratio (IIa:IIaa)
1	air	100	72	99:1
2	air	60	70	4:1
3	air	rt	54	2:1
4	N ₂	60	65	4:1

5.2.1 Description of internal alkyne products

5.2.1.1 1-Pheny-1-propyne (11)

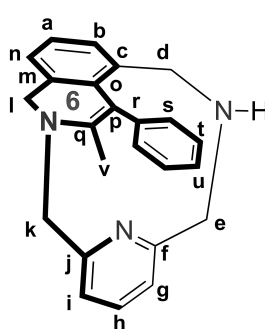
Major Regioisomer (IIa). ¹H NMR (500 MHz, CDCl₃, ppm) δ 7.86 (d, ³J_H = 7.8 Hz,



2H, **Ht**), 7.50 (t, ³J_H = 7.8 Hz, 2H, **Hu**), 7.46 (t, ³J_H = 7.5 Hz, 1H, **Hv**), 7.16 (t, ³J_H = 7.8 Hz, 1H, **Hh**), 6.71 (d, ³J_H = 7.3 Hz, 1H, **Hb**), 6.68-6.63 (m, 2H, **Ha**, **Hi**), 6.41 (d, ³J_H = 7.3 Hz, 2H, **Hn**, **Hg**), 4.90 (d, ²J_H = 15.3 Hz, 1H, **Hd**), 4.26 (d, ²J_H = 15.8 Hz, 1H, **Hi**), 4.22 (d, ²J_H = 15.2 Hz, 1H, **He**), 3.99 (d, ²J_H = 15.4 Hz, 1H, **Hi'**), 3.90 (d, ²J_H = 15.7 Hz, 1H, **Hk**), 3.59 (d, ²J_H = 15.1 Hz, 1H, **Hk'**), 3.48 (d, ²J_H = 15.3 Hz, 1H, **Hd'**), 3.43 (d, ²J_H = 15.4 Hz, 1H, **He'**), 2.32 (s, 3H, **Hp**). ¹³C

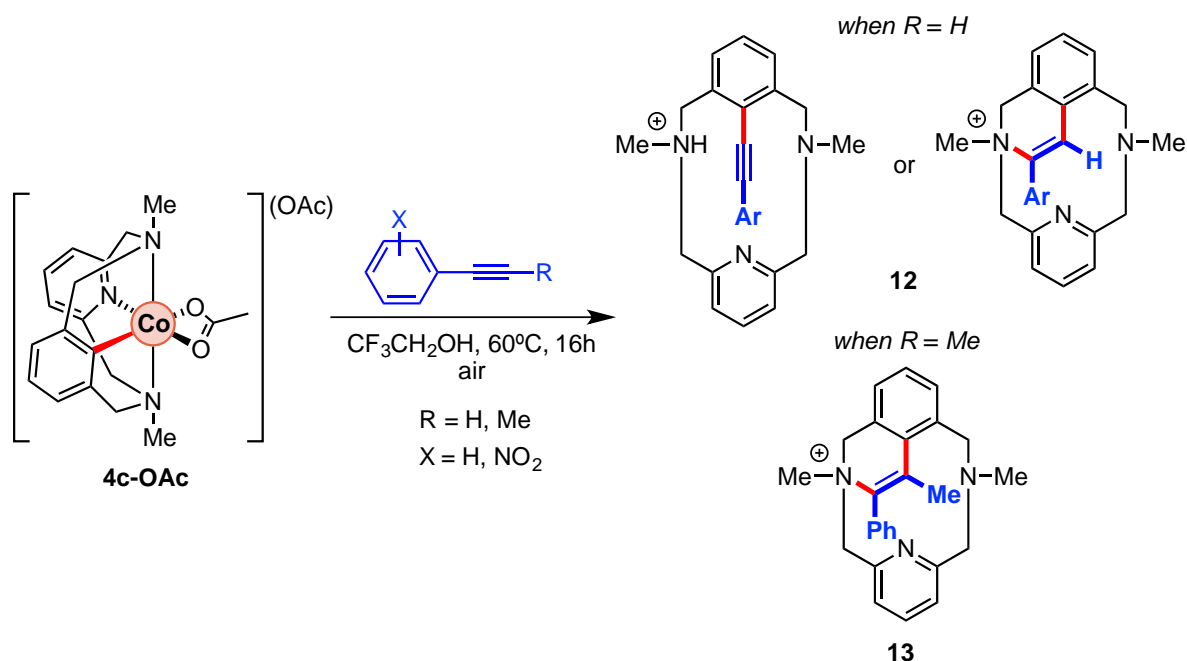
{¹H} NMR (125 MHz, CDCl₃, ppm) δ 157.9 (**Cf**), 157.5 (**Cj**), 148.2 (**Cr**), 137.7 (**Co**), 137.0 (**Cs**), 136.2 (**Ch**), 135.1 (**Cm**), 133.9 (**Cc**), 131.9 (**Ct**), 129.3 (**Cb**), 128.3 (**Cv**), 128.1 (**Cu**), 124.5 (**Ca**), 123.3 (**Cn**), 120.1 (**Cq**), 120.0 (**Ci**), 119.9 (**Cg**), 56.8 (**Ck**), 55.9 (**Cd**), 54.4 (**Ce**), 54.0 (**Cl**), 18.2 (**Cp**). HRMS (ESI) calcd. for C₂₄H₂₄N₃⁺ [M+H]⁺: 354.1965; found: 354.1970.

Minor Regioisomer (IIaa). ¹H NMR (500 MHz, CDCl₃, ppm) δ 7.40 (d, ³J_H = 7.8 Hz,



2H, **Hs**), 7.39 (d, ³J_H = 7.6 Hz, 2H, **Ht**), 7.31 (t, ³J_H = 7.2 Hz, 1H, **Hu**), 7.21 (t, ³J_H = 7.3 Hz, 1H, **Hh**), 6.73-6.40 (m, 5H, **Ha**, **Hi**, **Hn**, **Hb**, **Hg**), 4.46 (d, ²J_H = 15.3 Hz, 1H, **Hk**), 4.26 (d, ²J_H = 15.2 Hz, 1H, **Hi**), 4.18 (d, ²J_H = 15.5 Hz, 1H, **He**), 3.87 (d, ²J_H = 15.8 Hz, 1H, **Hi'**), 3.77 (d, ²J_H = 15.2 Hz, 1H, **Hk'**), 3.31 (d, ²J_H = 15.2 Hz, 1H, **He**), 3.27 (d, ²J_H = 15.8 Hz, 1H, **Hd**), 2.98 (d, ²J_H = 15.3 Hz, 1H, **Hd'**). ¹³C {¹H}

NMR (125 MHz, CDCl₃, ppm) δ 157.8 (**Cf**), 157.3 (**Cj**), 144.2 (**Cq**), 136.9 (**Co**), 136.2 (**Ch**), 135.1 (**Cm**), 133.4 (**Cc**), 129.5 (**Cb**), 128.3 (**Cu**), 128.1 (**Cs**), 126.5 (**Ct**), 126.2 (**Cp**), 123.4 (**Cn**), 120.2 (**Ci**), 120.0 (**Cg**), 56.4 (**Ck**), 54.2 (**Cd**), 53.4 (**Ce**), 53.1 (**Cl**), 17.9 (**Cv**). (Ca and Cr were not assigned). HRMS (ESI) calcd. for C₂₄H₂₄N₃⁺ [M+H]⁺: 354.1965; found: 354.1972. (minor + major regioisomer)

5.3 Reaction of Organometallic **4c-OAc** Complex towards Alkynes

Scheme S7. Reaction of **4c-OAc** with alkynes.

To have further evidence of a lineal insertion of terminal alkynes through a reductive elimination of Co(III) to Co(I), the reaction of the methylated derivative **4c-OAc** with 4-ethynyl-1-nitrobenzene was carried out. In a similar way, 1-methyl-propyne was also tested toward the **4c-OAc** to further prove a possible formation of the cationic quaternary amine through β -migratory insertion of the alkyne.

Thus, in a 2 mL vial, **4c-OAc** (40mg, 0.075 mmol) and **alkyne** (0.075 mmol) were mixed in TFE (1.5 mL). The vial was then sealed with a septum and the mixture was stirred over 16h at 60°C. Then, after removal of the solvent, NH_4OH (2 mL) was added and the solution was extracted using DCM (2x5mL). Then, products were purified using silica gel chromatography (CH_2Cl_2 , then $CH_2Cl_2/MeOH$ 95:5). Isolation of products **12** and **13** resulted unachievable, but products were detected by HRMS (Figure S11 and S12).

- When R = H,

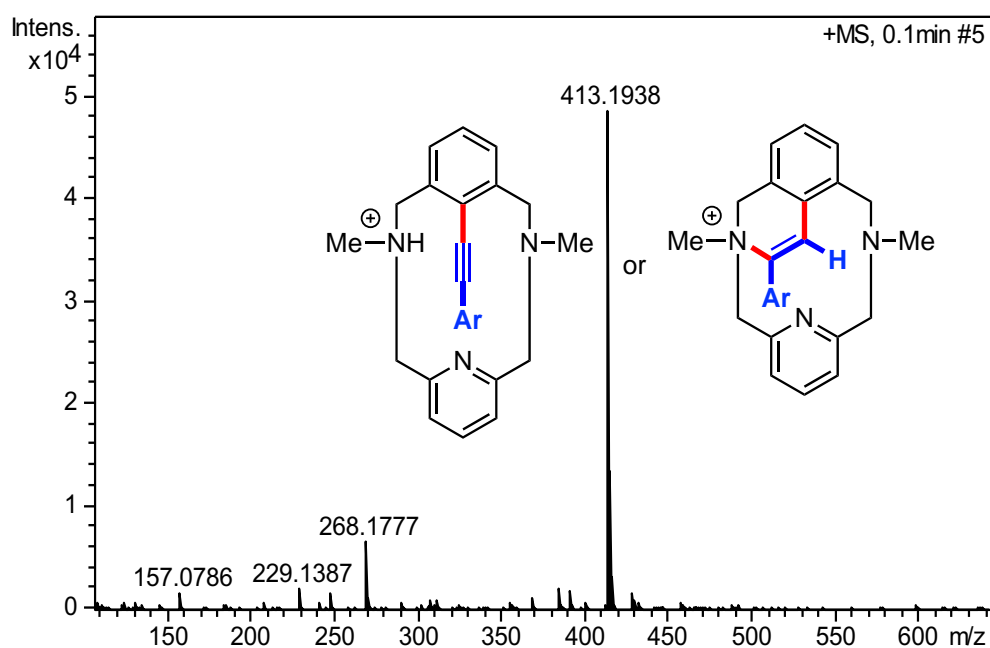


Figure S11. Product **12** obtained from reaction of **4c-OAc** with 4-ethynyl-1-nitrobenzene (Ar = 4-nitrobenzene). HRMS (ESI) calcd. for $C_{25}H_{26}N_4O_2^+$ [M] $^+$: 413.1947; found: 413.1938.

- When R = Me,

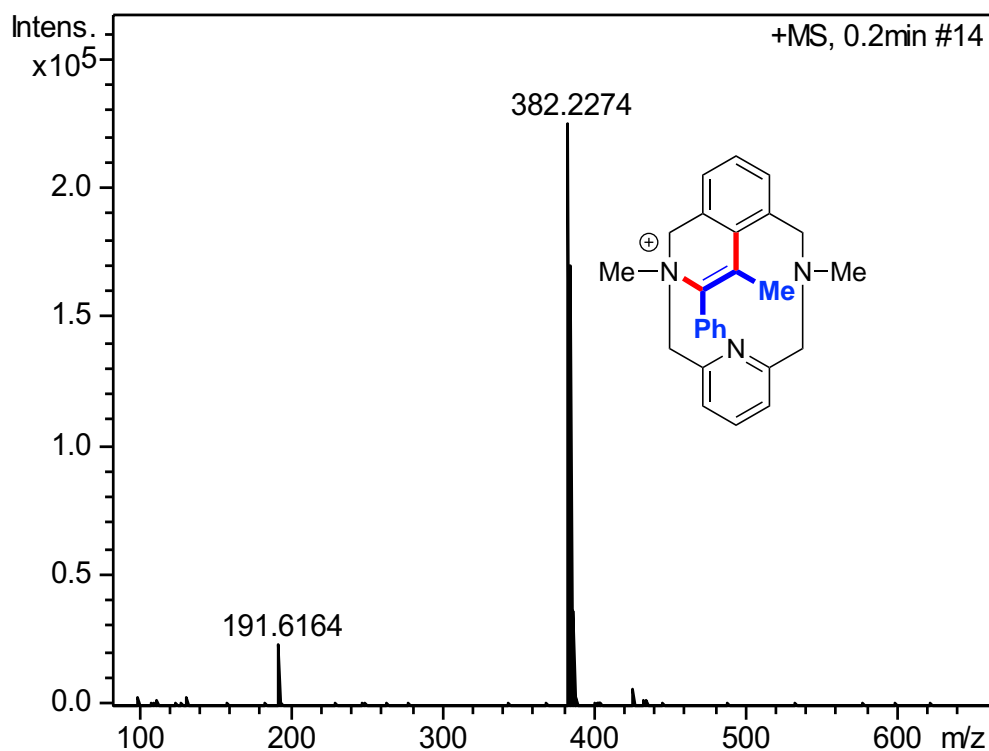


Figure S12. Product **13** obtained from reaction of **4c-OAc** with 1-methyl-propyne. HRMS (ESI) calcd. for $C_{26}H_{28}N_3^+$ [M] $^+$: 382.2278; found: 382.2274.

7. Crystallographic data information

Crystallographic data for compounds **3b-OAc** (CCDC-1493341), **3c-Br** (CCDC-1493342), **4b-CH₃CN** (CCDC-1493343), **4c-CH₃CN** (CCDC-1493344), **5c-Cl** (CCDC-1493345) and aryl-Co(III) species using nitro-aminoquinoline model substrate **8** (CCDC-1493346) can be obtained free of charge from the Cambridge Crystallographic Data Centre via www.ccdc.cam.ac.uk/data_request/cif. Furthermore, the corresponding CIF files have been included in the Supplementary Digital Material included in the attached CD.

7.1 X-Ray structure of **4b-CH₃CN**

Orange crystals of C₁₉H₂₂CoN₅, 2(ClO₄), 2(C₂H₃N), H₂O, were grown from slow diffusion of ethyl ether in a CH₃CN solution of the compound, and used for low temperature (100(2) K) X-ray structure determination. The measurement was carried out on a *BRUKER SMART APEX CCD* diffractometer using graphite-monochromated Mo K α radiation ($\lambda = 0.71073$ Å) from an x-Ray Tube. The measurements were made in the range 1.80 to 27.70° for θ . Full-sphere data collection was carried out with ω and ϕ scans. A total of 8983 reflections were collected of which 6178 [R(int) = 0.033] were unique. Programs used: data collection, Smart¹⁵; data reduction, Saint+¹⁶; absorption correction, SADABS¹⁷. Structure solution and refinement was done using SHELXTL¹⁸. The structure was solved by direct methods and refined by full-matrix least-squares methods on F². The non-hydrogen atoms were refined anisotropically. The H-atoms were placed in geometrically optimized positions and forced to ride on the atom to which they are attached except the OH2 hydrogens, which were located in a different Fourier map.

Table S6. Crystallographic parameters for **4b-CH₃CN**.

Chemical formula	C ₁₉ H ₂₂ CoN ₅ , 2(ClO ₄), 2(C ₂ H ₃ N), H ₂ O
fw (g mol⁻¹)	678.37
T (K)	100(2)
Space group	P-1, triclinic
a (Å)	11.6313(9)
b (Å)	11.6947(9)
c (Å)	12.0054(1)
α (deg.)	115.424(1)
β (deg.)	92.168(1)
γ (deg.)	97.853(1)
V (Å³)	1452(2)
$\rho_{\text{calcd.}}$ (g cm⁻³)	1.551
λ (Å)	0.71073
R₁ [I > 2σ(I)]	0.0926
wR₂ [I > 2σ(I)]	0.2364

7.2 X-Ray structure of **4c-CH₃CN**

Orange crystals of C₂₁H₂₆CoN₅, 2(ClO₄), C₂H₃N, were grown from slow diffusion of ethyl ether in a CH₃CN solution of the compound, and used for low temperature (100(2) K) X-ray structure determination. The measurement was carried out on a *BRUKER SMART APEX CCD* diffractometer using graphite-monochromated Mo *K*α radiation ($\lambda = 0.71073 \text{ \AA}$) from an x-Ray Tube. The measurements were made in the range 2.00 to 28.28° for θ . Full-sphere data collection was carried out with ω and ϕ scans. A total of 42221 reflections were collected of which 6672 [R(int) = 0.0383] were unique. Programs used: data collection, Smart¹⁵; data reduction, Saint+¹⁶; absorption correction, SADABS¹⁷. Structure solution and refinement was done using SHELXTL¹⁸. The structure was solved by direct methods and refined by full-matrix least-squares methods on F². The non-hydrogen atoms were refined anisotropically. The H-atoms were placed in geometrically optimized positions and forced to ride on the atom to which they are attached.

Table S7. Crystallographic parameters for **4c-CH₃CN**.

Chemical formula	C ₂₃ H ₂₉ Cl ₂ CoN ₆ O ₈
fw (g mol⁻¹)	674.35
T (K)	100(2)
Space group	Not defined
<i>a</i> (Å)	11.9362(8)
<i>b</i> (Å)	20.3758(13)
<i>c</i> (Å)	12.2543(8)
α (deg.)	90
β (deg.)	114.52
γ (deg.)	90
<i>V</i> (Å³)	2711.7 (3)
$\rho_{\text{calcd.}}$ (g cm⁻³)	1.586
λ (Å)	0.71073
R₁ [<i>I</i>>2sigma(<i>I</i>)]	0.0466
wR₂ [<i>I</i>>2sigma(<i>I</i>)]	0.1129

7.3 X-Ray structure of **3b-OAc**

Violet crystals of C₁₉H₂₃CoN₃O₄, were grown from slow diffusion of ethyl ether in a MeOH solution of the compound, and used for low temperature (100(2) K) X-ray structure determination. The measurement was carried out on a *BRUKER SMART APEX CCD* diffractometer using graphite-monochromated Mo *K*α radiation ($\lambda = 0.71073 \text{ \AA}$) from an x-Ray Tube. The measurements were made in the range 1.841 to 27.914° for θ . Hemi-sphere data collection was carried out with ω and ϕ scans. A total of 4397 reflections were collected of which 3511 [R(int) = 0.0329] were unique. Programs used: data collection, Smart¹⁵; data reduction, Saint+¹⁶; absorption correction, SADABS¹⁷. Structure solution and refinement was done using SHELXTL¹⁸. The structure was solved

by direct methods and refined by full-matrix least-squares methods on F^2 . The non-hydrogen atoms were refined anisotropically. The H-atoms were placed in geometrically optimized positions and forced to ride on the atom to which they are attached.

Table S10. Crystallographic parameters for **3b-OAc**.

Chemical formula	$C_{19}H_{23}CoN_3O_4$
fw (g mol⁻¹)	416.34
T (K)	100(2)
Space group	Triclinic, P-1
a (Å)	8.766(5)
b (Å)	10.310(6)
c (Å)	11.915(7)
α (deg.)	69.5
β (deg.)	76.7
γ (deg.)	71.5
V (Å³)	948.03 (1)
ρ_{calcd.} (g cm⁻³)	1.458
λ (Å)	0.71073
R₁ [I>2σ(I)]	0.0782
wR₂ [I>2σ(I)]	0.1997

7.4 X-Ray structure of **3c-Br**

Violet crystals of $(C_{17}H_{21}CoN_3Br_2)_2(CHCl_3)_2$, were grown from slow diffusion of ethyl ether in a $CHCl_3$ solution of the compound, and used for low temperature (130(2) K) X-ray structure determination. The measurement was carried out on a *BRUKER SMART APEX CCD* diffractometer using graphite-monochromated Mo $K\alpha$ radiation ($\lambda = 0.71073$ Å) from an x-Ray Tube. The measurements were made in the range 1.490 to 27.648° for θ . Hemi-sphere data collection was carried out with ω and ϕ scans. A total of 14172 reflections were collected of which 10439 [$R(\text{int}) = 0.0692$] were unique. Programs used: data collection, Smart¹⁵; data reduction, Saint+¹⁶; absorption correction, SADABS¹⁷. Structure solution and refinement was done using SHELXTL¹⁸. The structure was solved by direct methods and refined by full-matrix least-squares methods on F^2 . The non-hydrogen atoms were refined anisotropically. The H-atoms were placed in geometrically optimized positions and forced to ride on the atom to which they are attached.

Table S11. Crystallographic parameters for **3c-Br**.

Chemical formula	$C_{37}H_{45}Br_4Cl_9N_6Co_2$
fw (g mol⁻¹)	1330.4
T (K)	130 (2)
Space group	Triclinic, P-1
a (Å)	8.791(7)
b (Å)	14.498(11)
c (Å)	20.353(20)
α (deg.)	96.829(14)
β (deg.)	97.972(13)
γ (deg.)	106.988(12)
V (Å³)	2421(3)
ρ_{calcd.} (g cm⁻³)	1.825
λ (Å)	0.71073
R₁ [I>2σ(I)]	0.1092
wR₂ [I>2σ(I)]	0.2556

7.5 X-Ray structure of **5c-Cl**

Yellow crystals of $C_{17}H_{20}Cl_2N_3Rh(CH_3O)$ were grown from slow diffusion of ethyl ether in a $CH_3CN/MeOH$ solution of the compound, and used for low temperature (173(2) K) X-ray structure determination. The measurement was carried out on a *BRUKER SMART APEX CCD* diffractometer using graphite-monochromated Mo $K\alpha$ radiation ($\lambda = 0.71073$ Å) from an x-Ray Tube. The measurements were made in the range 2.108 to 28.289° for θ . Full-sphere data collection was carried out with ω and ϕ scans. A total of 29546 reflections were collected of which 4689 [$R(\text{int}) = 0.0303$] were unique. Programs used: data collection, Smart¹⁵; data reduction, Saint+¹⁶; absorption correction, SADABS¹⁷. Structure solution and refinement was done using SHELXTL¹⁸. The structure was solved by direct methods and refined by full-matrix least-squares methods on F^2 . The non-hydrogen atoms were refined anisotropically. The H-atoms were placed in optimized positions and forced to ride on the atom to which they are attached.

Table S12. Crystallographic parameters for **5c-Cl**.

Chemical formula	$C_{18}H_{24}Cl_2N_3ORh$
fw (g mol⁻¹)	472.21
T (K)	173(2)
Space group	Monoclinic, P21/n
a (Å)	9.6236(9)
b (Å)	16.6150(16)
c (Å)	11.8767(11)
α (deg.)	90(0)
β (deg.)	91.405(2)
γ (deg.)	90(0)
V (Å³)	1898.5(3)
ρ_{calcd.} (g cm⁻³)	1.652
λ (Å)	0.71073
R₁ [I>2σ(I)]	0.0267
wR₂ [I>2σ(I)]	0.0643

7.6 X-Ray structure of **8**

Red crystals of $C_{28}H_{20}CoN_5O_5 \cdot 2(C_2H_3N)$, were grown from CH_3CN , and used for low temperature (100(2) K) X-ray structure determination. The measurement was carried out on a *BRUKER SMART APEX CCD* diffractometer using graphite-monochromated Mo $K\alpha$ radiation ($\lambda = 0.71073 \text{ \AA}$) from an x-Ray Tube. The measurements were made in the range 2.081 to 28.295° for θ . Full-sphere data collection was carried out with ω and ϕ scans. A total of 45267 reflections were collected of which 7190 [$R(\text{int}) = 0.0726$] were unique. Programs used: data collection, Smart¹⁵; data reduction, Saint+¹⁶; absorption correction, SADABS¹⁷. Structure solution and refinement was done using SHELXTL¹⁸. The structure was solved by direct methods and refined by full-matrix least-squares methods on F^2 . The non-hydrogen atoms were refined anisotropically. The H-atoms were placed in geometrically optimized positions and forced to ride on the atom to which they are attached.

Table S13. Crystallographic parameters for **8**.

Chemical formula	$C_{32}H_{26}O_5N_7Co$
fw (g mol⁻¹)	647.53
T (K)	100(2)
Space group	Monoclinic, P21/n
a (Å)	12.740(2)
b (Å)	15.430(3)
c (Å)	14.863(3)
α (deg.)	90(0)
β (deg.)	96.496(4)
γ (deg.)	90(0)
V (Å³)	2903.1(9)
$\rho_{\text{calcd.}}$ (g cm⁻³)	1.482
λ (Å)	0.71073
R₁ [$I > 2\sigma(I)$]	0.0466
wR₂ [$I > 2\sigma(I)$]	0.0998

8. DFT β -migratory insertion pathway free energy profile for internal alkynes

Reaction of aryl-Co(III) intermediates with internal alkynes cannot proceed through the ‘acetylide pathway’, as lineal coordination is not allowed. Thus, DFT calculations were performed to study the ‘ β -migratory insertion pathway’ (Figure S23) for 1-phenyl-1-propyne. Our calculations show that **4b-alkyne-OAc** (both regioisomers) undergo migratory insertion towards the commonly proposed 7-membered cyclic intermediate (**15_{int}a** and **15_{int}aa**, Figure S23), with a barrier of $\Delta G^\ddagger = 29.5$ kcal mol⁻¹ for **15_{int}a** and $\Delta G^\ddagger = 28.7$ kcal mol⁻¹ for **15_{int}aa**. Thereafter, reductive elimination from **15_{int}a** or **15_{int}aa** furnishes the 6-membered ring **IIa/IIaa** (Scheme 3, main text) depending on the reaction conditions.

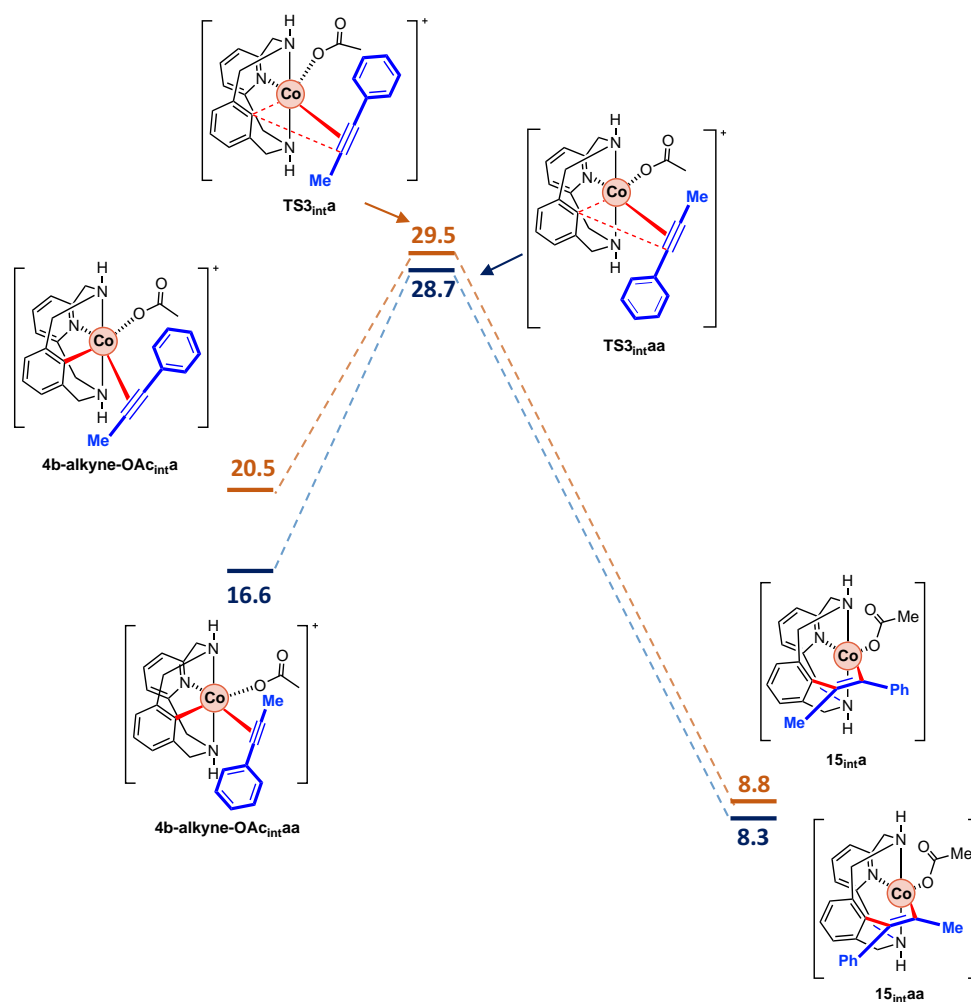
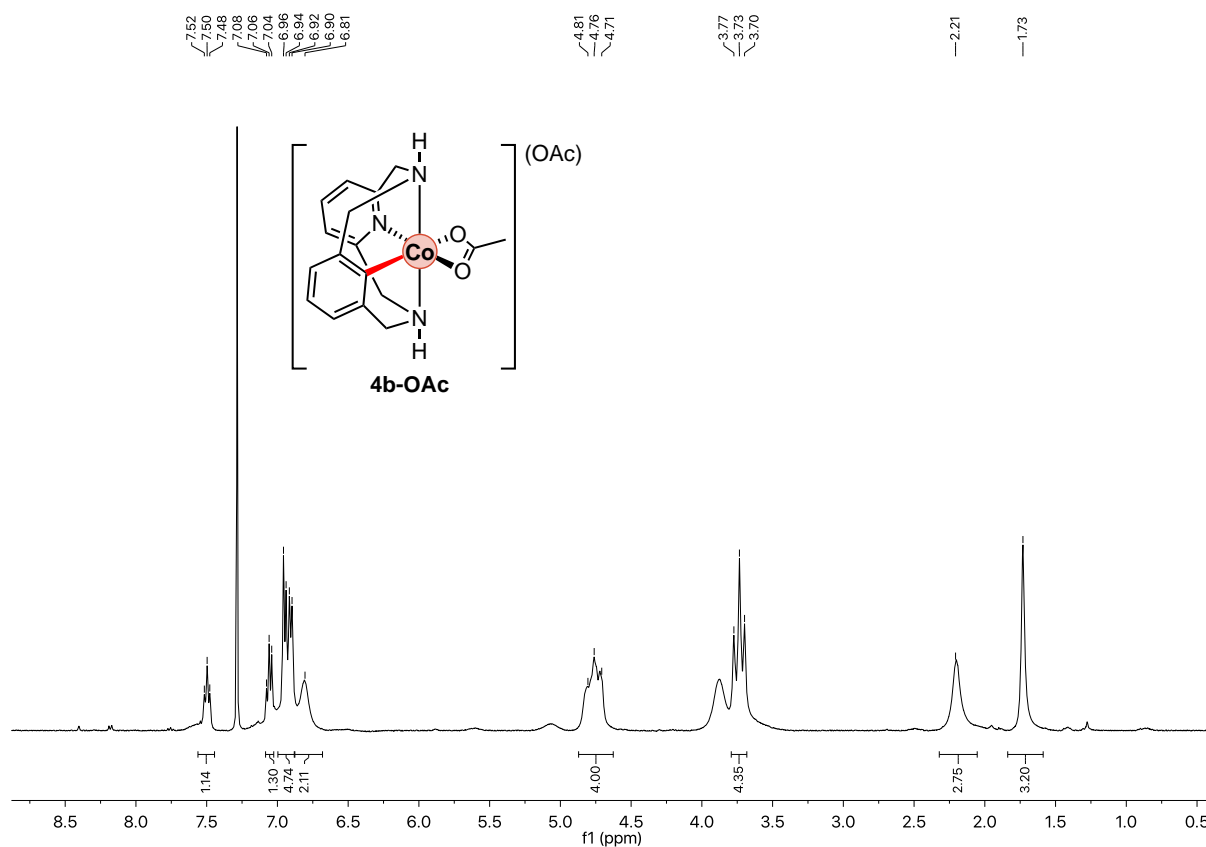
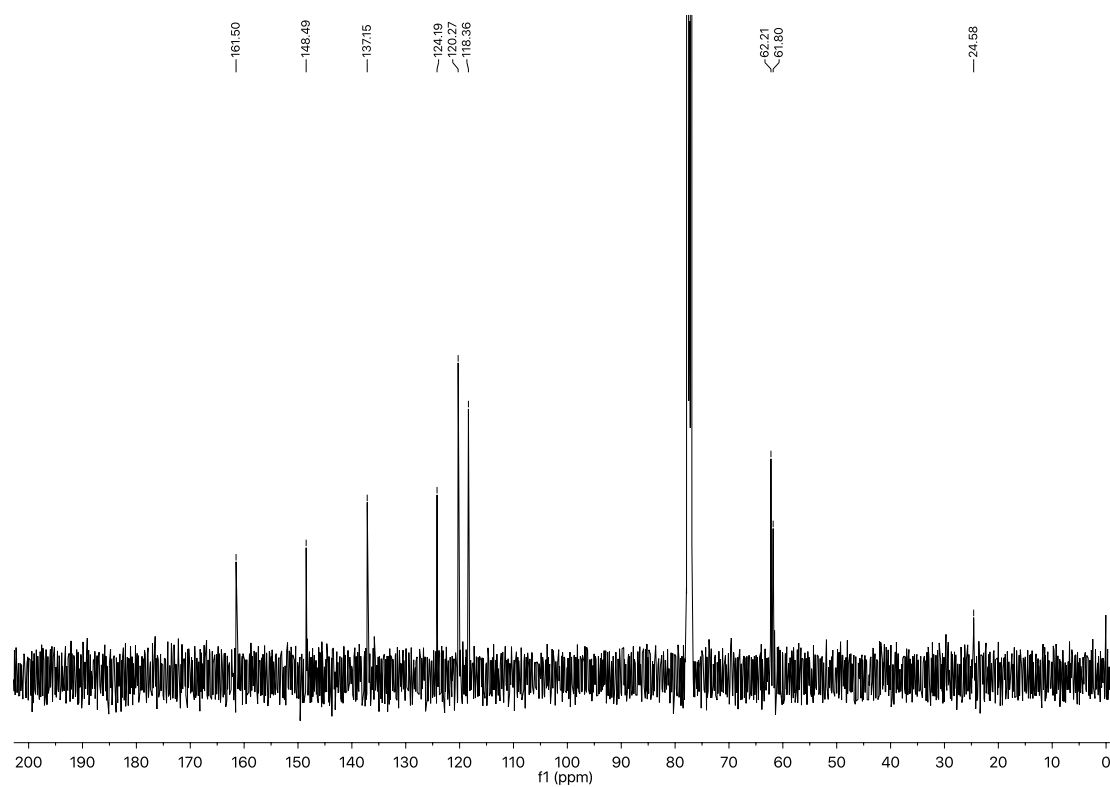


Figure S13. Gibbs energy profile of the formation of the β -migratory insertion pathway with 1-phenyl-1-propyne (internal alkyne). Relative Gibbs energy values are given in kcal·mol⁻¹.

9. References

- (1) Whiteoak, C. J; Planas, O.; Company, A.; Ribas, X. *Adv. Synth. Catal.* **2016**, *358*, 1679.
- (2) Ravel, B.; Newville, M. *J. Synchrotron Rad.* **2005**, *12*, 537.
- (3) Newville, M. *J. Synchrotron Rad.* **2001**, *8*, 96.
- (4) Rehr, J. J; Albers, R. C. *Rev. Mod. Phys.* **2000**, *72*, 621.
- (5) Martin-Diaconescu, V.; Bellucci, M.; Musiani, F.; Ciurli, S.; Maroney, M. J. *J. Biol. Inorg. Chem.* **2012**, *17*, 353.
- (6) Zambelli, B.; Berardi, A.; Martin-Diaconescu, V.; Mazzei, L.; Musiani, F.; Maroney, M. J.; Ciurli, S. *J. Biol. Inorg. Chem.* **2014**, *19*, 319.
- (7) Becke, A. D. *Phys. Rev. A. Gen. Phys* **1988**, *38*, 3098.
- (8) Neese, F. T. *Wiley Interdiscip. Rev. Comp. Mol. Sci.* **2012**, *2*, 73.
- (9) Schäfer, A.; Horn, H.; Ahlrichs, R. *J. Chem. Phys.* **1992**, *97*, 2571.
- (10) Weigend, F.; Ahlrichs, R. *Phys. Chem. Chem. Phys.* **2005**, *7*, 3297.
- (11) Grimme, S.; Antony, J.; Ehrlich, S.; Krieg, H. *J. Chem. Phys.* **2010**, *132*, 154104.
- (12) Grimme, S.; Ehrlich, S.; Goerigk, L. *J. Comput. Chem.* **2011**, *32*, 1456.
- (13) Neese, F.; Wennmohs, F.; Hansen, A.; Becker, U. *J. Chem. Phys.* **2009**, *356*, 98.
- (14) Grigorjeva, L.; Daugulis, O. *Angew. Chem. Int. Ed.* **2014**, *53*, 10209.
- (15) Bruker Advanced X-ray Solutions. SMART: Version 5.631, **1997-2002**.
- (16) Bruker Advanced X-ray Solutions. SAINT +, Version 6.36A, **2001**.
- (17) Sheldrick, G. M. *Empirical Absorption Correction Program*, Universität Göttingen, **1996**. Bruker Advanced X-ray Solutions. SADABS Version 2.10, **2001**.
- (18) Sheldrick, G. M. *Program for Crystal Structure Refinement*, Universität Göttingen, **1997**. Bruker Advanced X-ray Solutions. SHELXTL Version 6.14, **2000-2003**. SHELXL-2013 (Sheldrick, **2013**).

10. Selected Original NMR spectra

Figure S14. 400 MHz ^1H NMR spectrum of **4b-OAc** in CDCl_3 , 400 MHz, 298 K.Figure S15. 100 MHz ^{13}C $\{^1\text{H}\}$ NMR spectrum of **4b-OAc** in CDCl_3 , 298 K.

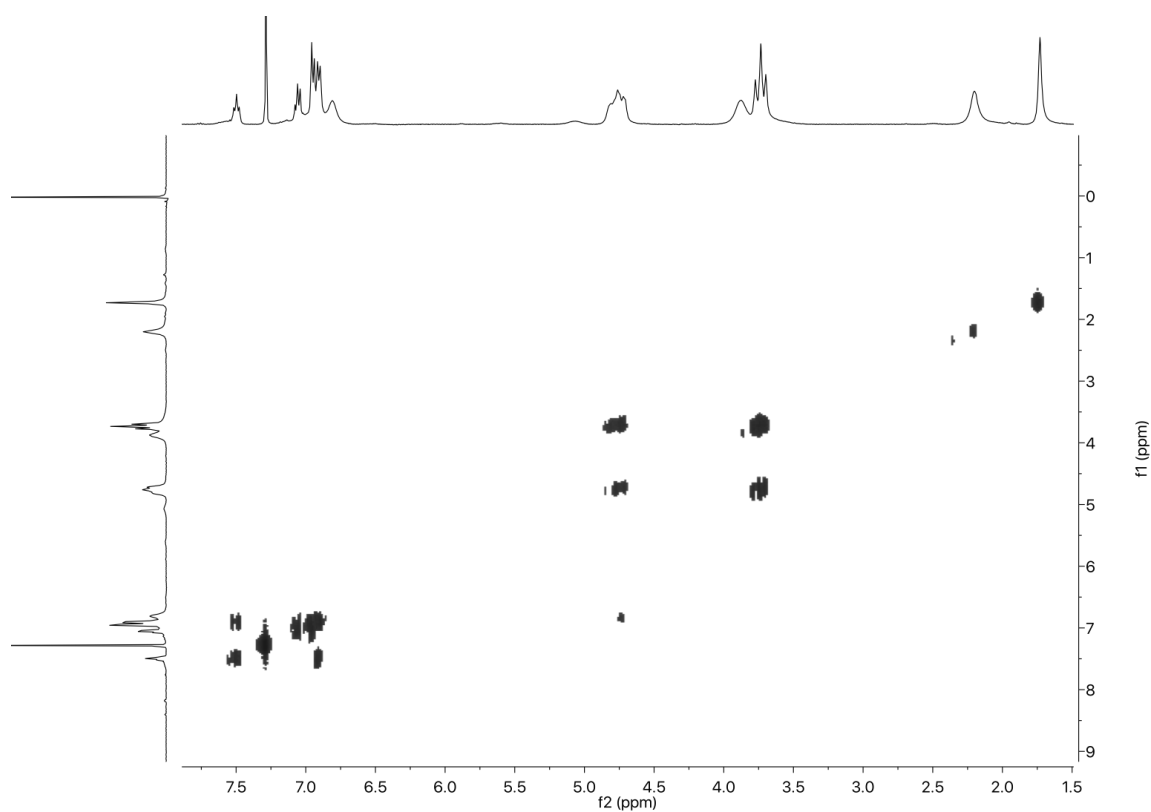


Figure S16. 400 MHz ^1H - ^1H COSY spectrum of **4b-OAc** in CDCl_3 , 298 K.

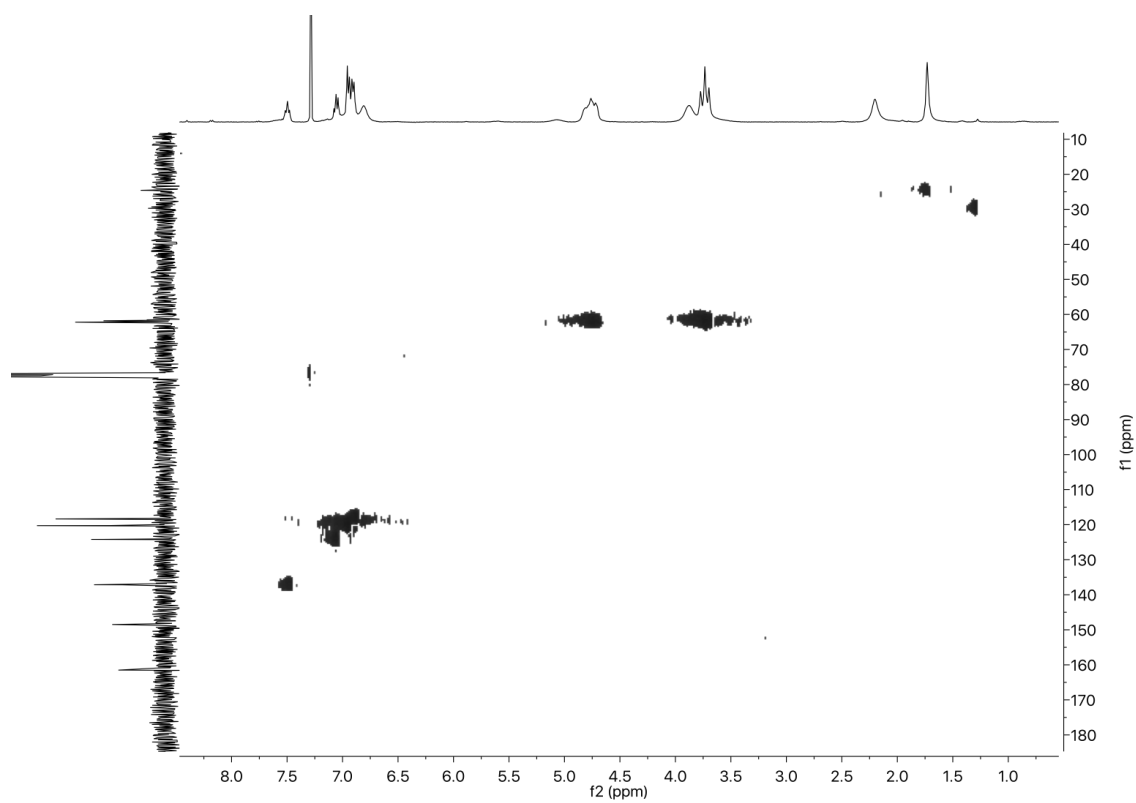


Figure S17. 400 MHz ^1H - ^{13}C HSQC spectrum of **4b-OAc** in CDCl_3 , 298 K.

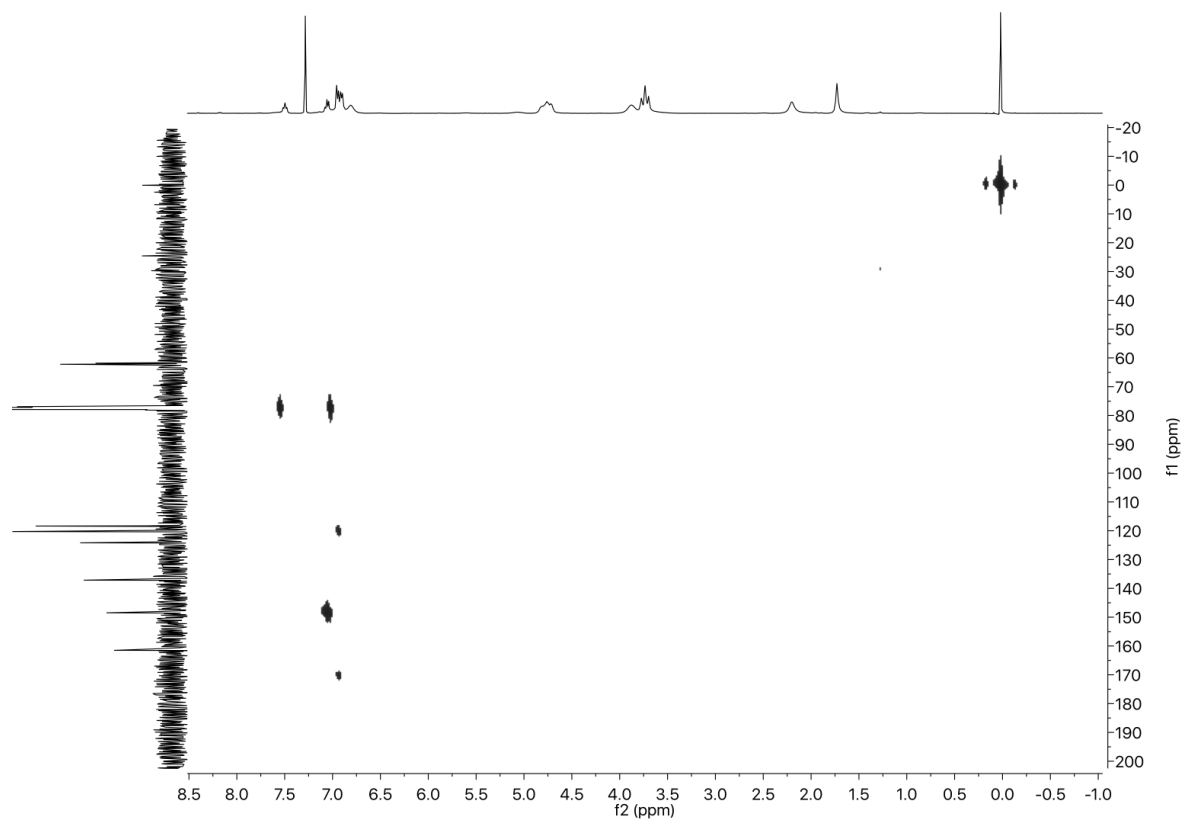


Figure S18. 400 MHz ^1H - ^{13}C HMBC spectrum of **4b-OAc** in CDCl_3 , 298 K.

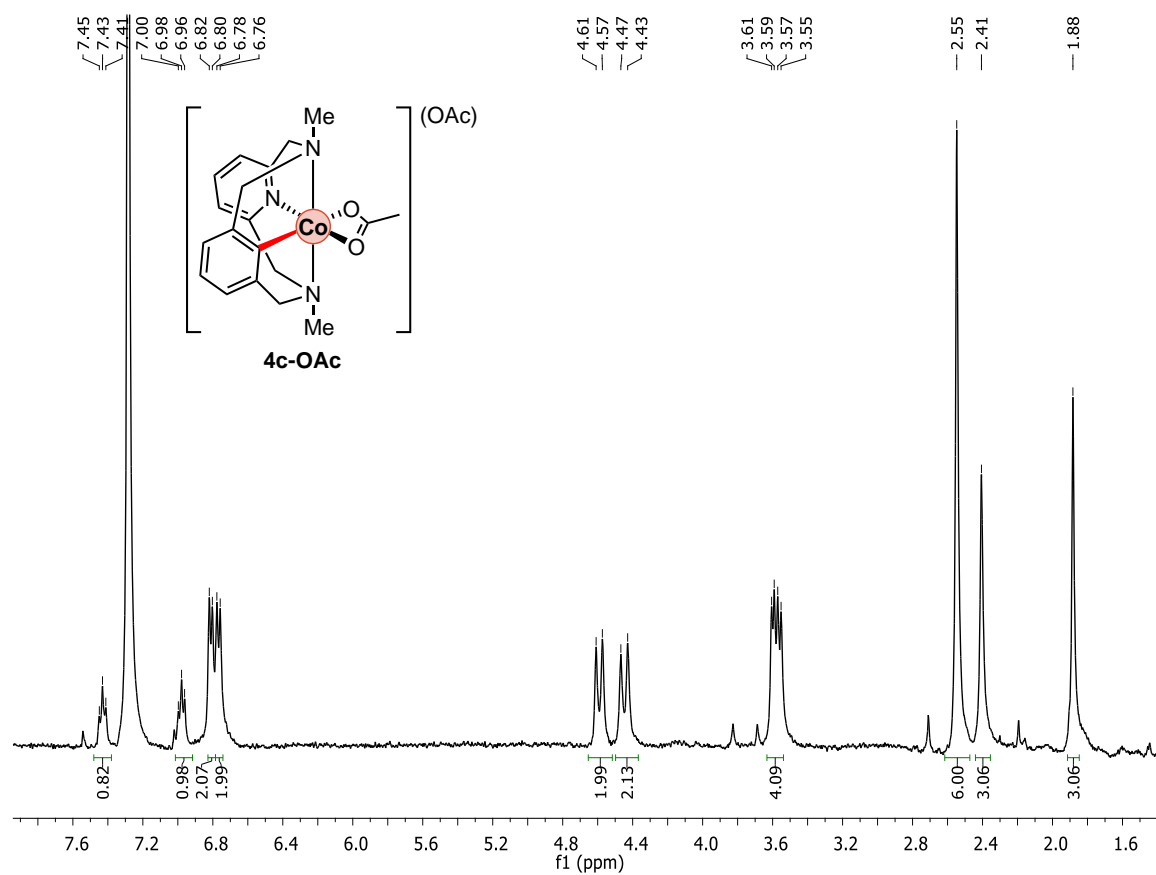


Figure S19. 400 MHz ^1H NMR spectrum of **4c-OAc** in CDCl_3 , 298 K.

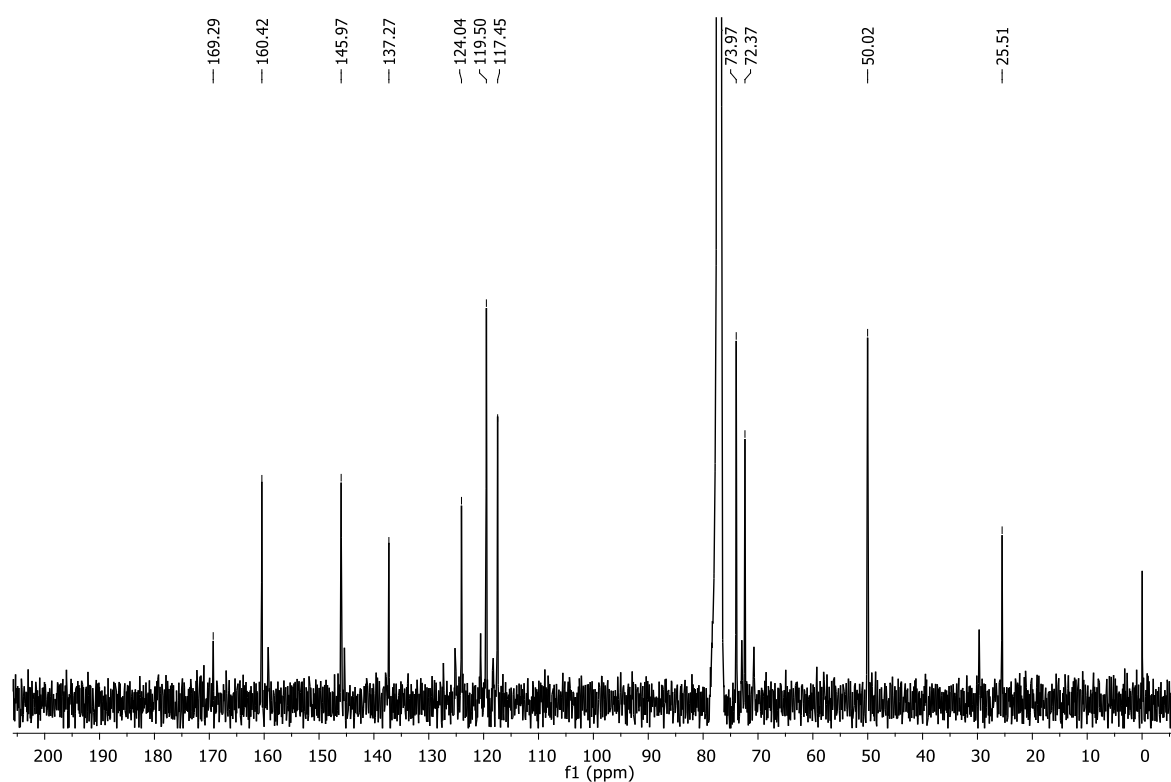


Figure S20. 100 MHz ^{13}C $\{^1\text{H}\}$ NMR spectrum of **4c-OAc** in CDCl_3 , 298 K.

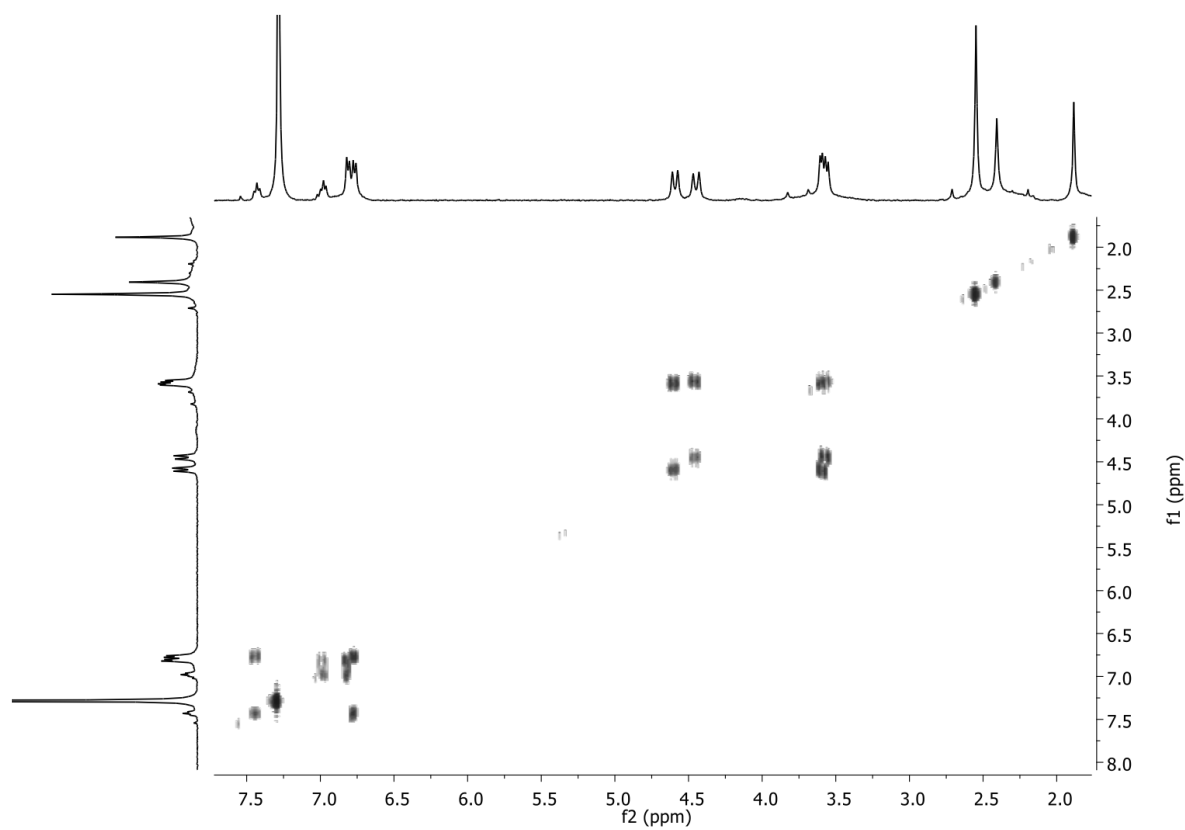


Figure S21. 400 MHz ^1H - ^1H COSY spectrum of **4c-OAc** in CDCl_3 , 298 K.

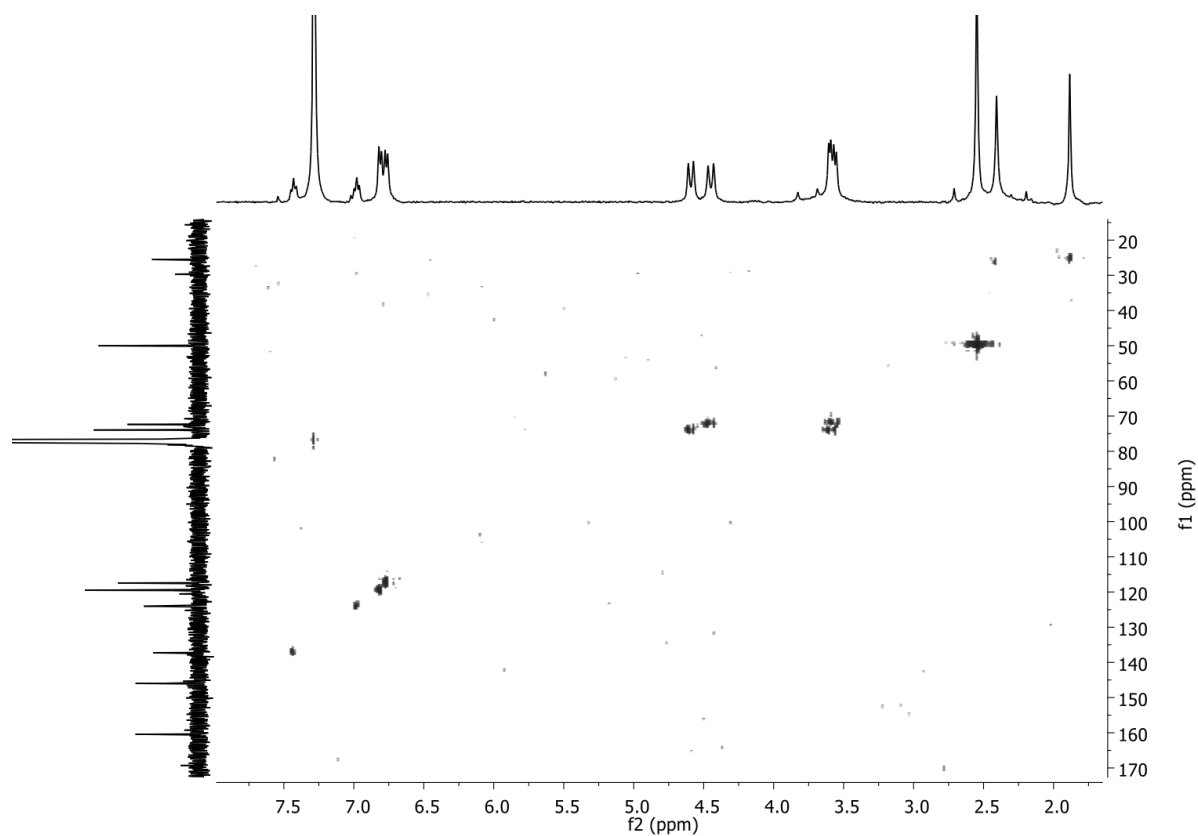


Figure S22. 400 MHz ^1H - ^{13}C HSQC spectrum of **4c-OAc** in CDCl_3 , 298 K.

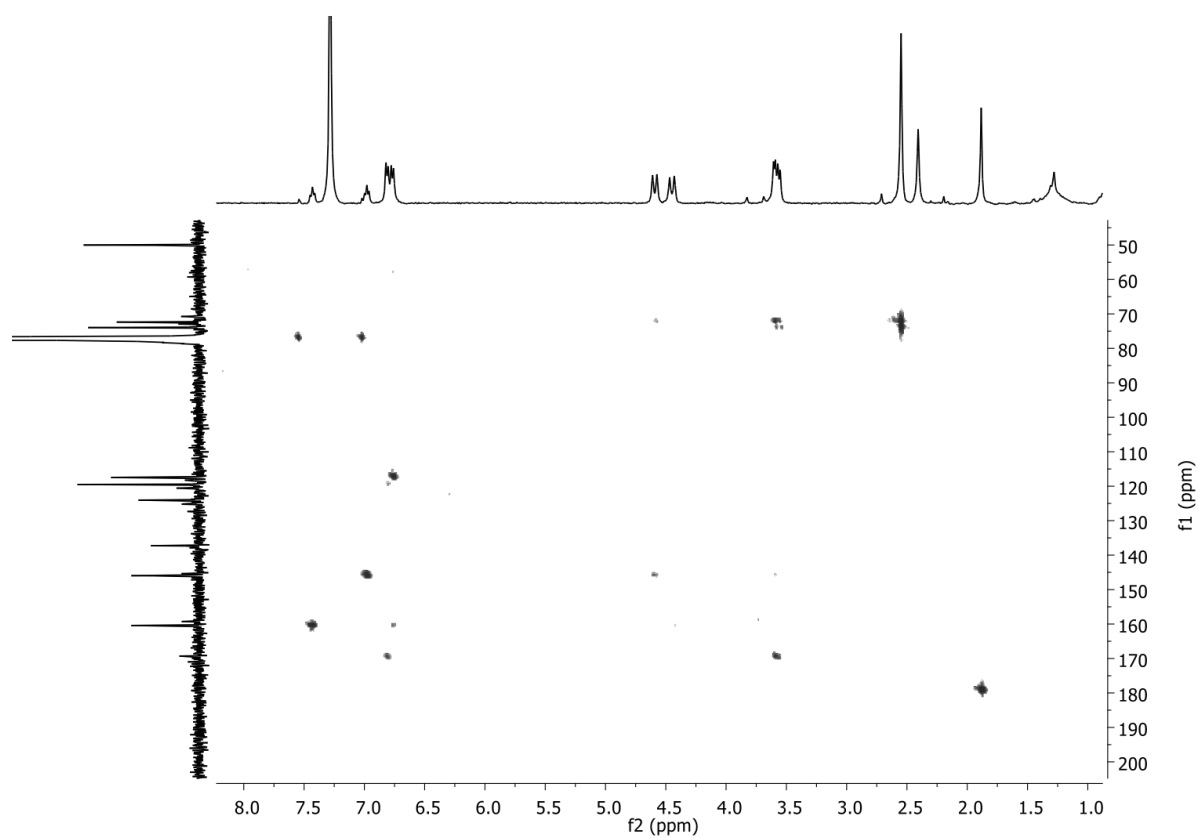


Figure S23. 400 MHz ^1H - ^{13}C HMBC spectrum of **4c-OAc** in CDCl_3 , 298 K.

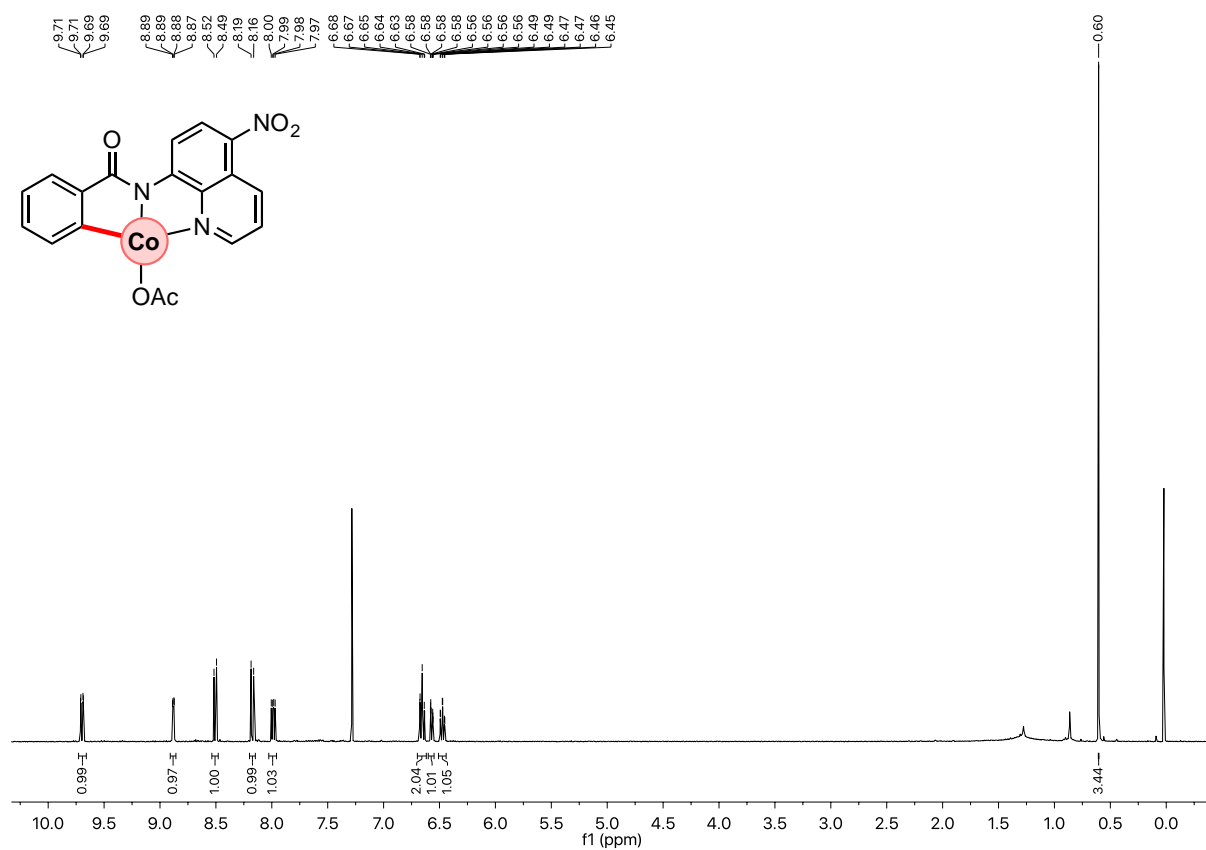


Figure S24. 400 MHz ¹H NMR spectrum of **7** in CDCl₃, 298 K.

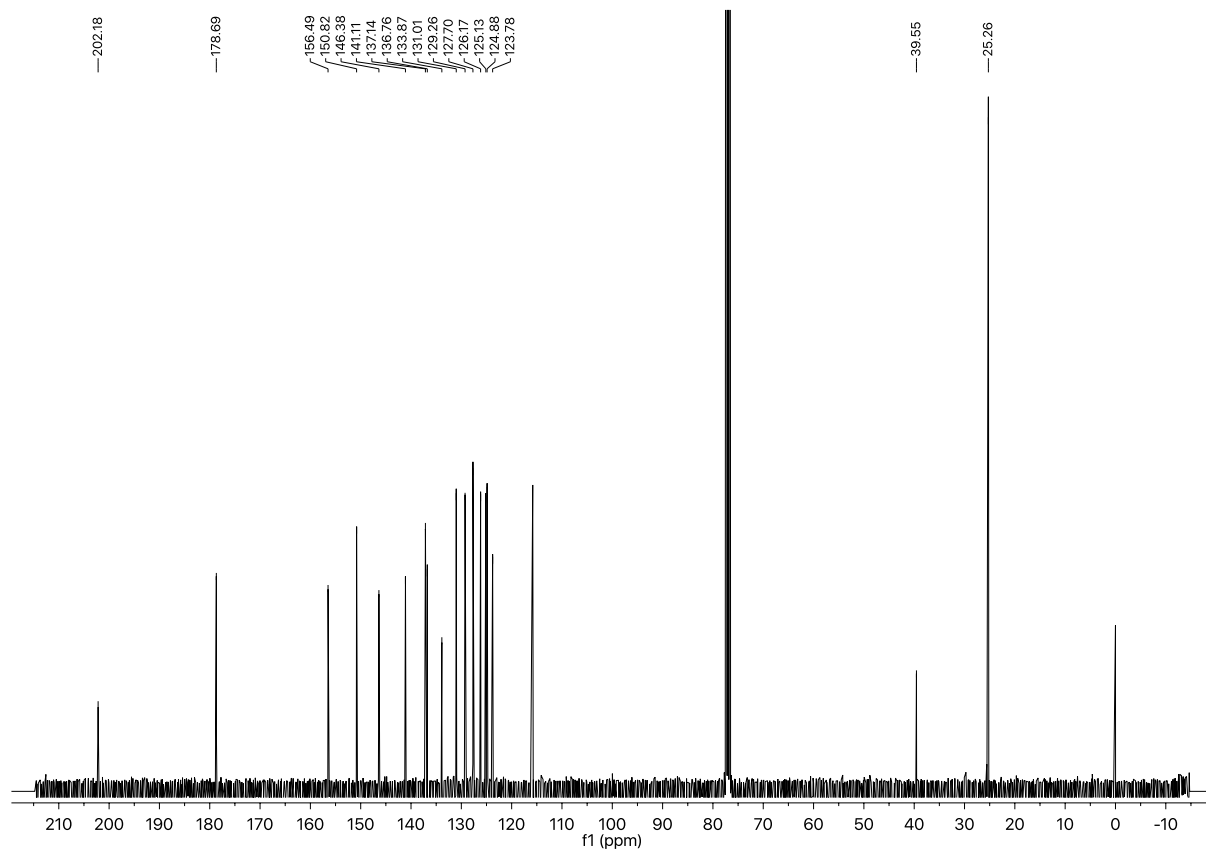


Figure S25. 100 MHz ¹³C {¹H} NMR spectrum of **7** in CDCl₃, 298 K.

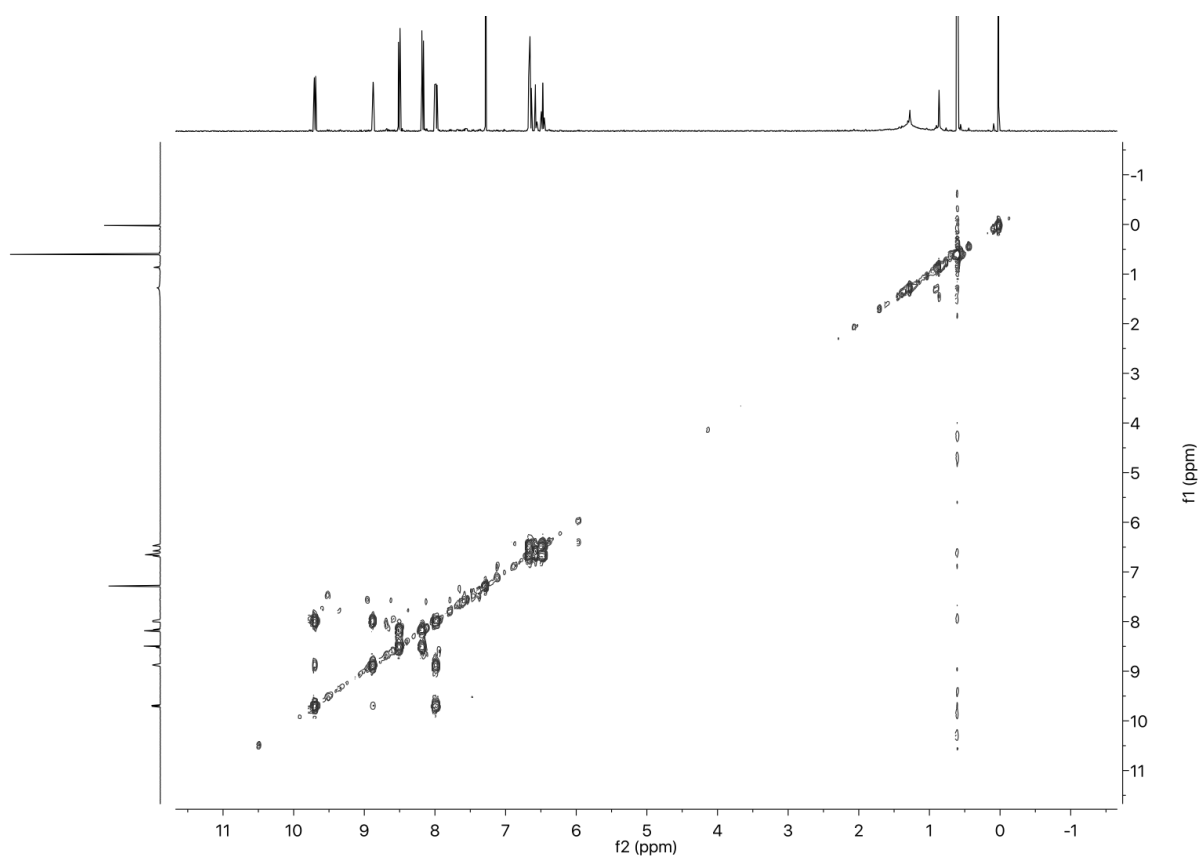


Figure S26. 400 MHz ^1H - ^1H COSY spectrum of **7** in CDCl_3 , 298.

Supporting Information for Chapter IV

Carboxylate-Assisted Formation of Aryl-Co(III) Masked-Carbenes in Cobalt-Catalyzed C-H Functionalization with Diazo Esters

Oriol Planas,¹ Steven Roldán-Gómez,² Vlad Martin-Diaconescu,¹ Teodor Parella,² Josep M. Luis,¹ Anna Company,¹ Xavi Ribas^{1*}

Table of Contents

1. GENERAL CONSIDERATIONS.....	S43
2. SYNTHESIS OF ARYL-Co(III)-CARBOXYLATE COMPLEXES	S45
3. OPTIMIZATION OF STOICHIOMETRIC REACTION CONDITIONS	S47
3.1 Additives.....	S47
3.2 Equivalents of starting EDA.....	S48
3.3 Carboxylate anions.....	S48
4. REACTION WITH TERTIARY AMINE ARYL-Co(III) COMPLEX.....	S50
5. EVALUATION OF CATALYTIC REACTION CONDITIONS	S51
6. ISOLATION OF REACTION INTERMEDIATES.....	S52
7. REACTIVITY OF 5a-X INTERMEDIATES	S57
7.1 Evolution of organometallic 5a-OAc complexes to cyclic amide 3 – Effect of additives	S57
7.2 Evaluation of organometallic 5a-X complexes as catalysts	S58
7.3 MS/MS experiments of 5a-X complexes (X = OAc)	S59
8. DEUTERIUM LABELING EXPERIMENTS	S60
8.1 D-incorporation starting from 2a-OAc	S60
8.2 D-incorporation starting from 5a-OAc.....	S66
9. REACTIVITY OF Rh ANALOGUE WITH EDA	S67
10. CRYSTALLOGRAPHIC DATA INFORMATION	S68
10.1 X-Ray structure of 5a-OBz-Cl	S68
10.2 X-Ray structure of 5a-OBz-OMe	S69
12. ADDITIONAL DFT INFORMATION	S70
13. REFERENCES.....	S73
14. SELECTED ORIGINAL NMR SPECTRA	S74

1. General considerations

Materials and methods

All reagents and solvents were purchased from Sigma Aldrich, Fisher Scientific or Fluorochem and used without further purification. Silver carboxylates were synthesized according to a previously described protocol.¹ NMR data concerning product identity were collected with a Bruker 400 AVANCE (Serveis Tècnics, Universitat de Girona) or a 600 AVANCE (Servei de RMN, Autonomous University of Barcelona) spectrometers (CDCl_3 and DMSO-d_6) and calibrated relative the residual protons of the solvent. All NMR experiments (^1H , $^{13}\text{C}\{^1\text{H}\}$, COSY, HSQC, HMBC and NOESY) were recorded and processed using standard parameters and no more details are given. Quantification of reaction yields through integration of peaks was performed using an internal reference (1,3,5-trimethoxybenzene). Preparation and handling of air-sensitive materials were carried out in a N_2 drybox with O_2 and H_2O concentrations < 1 ppm. High resolution mass spectra (HRMS) were recorded on a Bruker MicrOTOF-Q IITM instrument using ESI or Cryospray ionization sources at Serveis Tècnics University of Girona. C, H, N elemental analyses were performed on a ThermoFinnigan Flash-EA1112 analyzer. IR Spectra (FTIR) were recorded on a FT-IR Alpha spectrometer from Bruker with a PLATINUM-ATR attachment using OPUS software to process the data.

XAS Data Acquisition and processing

Samples of **5a-OAc** were prepared both as boron nitride diluted solid pellets and 15 mM solutions in trifluoroethanol. Samples were loaded into holders with Kapton windows and data was collected at SOLEIL synchrotron, SAMBA beamline, under vacuum at 20 K using a liquid helium cryostat and Si(220) double crystal monochromator. Transmission mode was used for solid samples and fluorescence mode was used for solution samples employing a 36-channel Ge fluorescence detector. Data calibration and normalization was carried out using the Athena software package.² The first inflection point of Co foil spectra taken as 7709.5 eV was used for energy calibration. A linear pre-edge function, followed by a quadratic polynomial for the post-edge, were used for background subtraction and normalization of the edge jump to unity. The AUTOBK algorithm with a spline between a k of 1 and 15 \AA^{-1} having a R_{bkg} value of 1.0 \AA was used for EXAFS extraction. EXAFS analysis was carried out using the IFEFFIT engine and the FEFF6 code available in the Artemis software package.²⁻⁴ The k^3 -weighted data was fit in r -space over a r -range of 1 to 3 \AA and a k -range of 2 to 13 \AA^{-1} using a Hannings window ($dk=2$). The S_0^2 value was set to 0.9, and a global ΔE_0 was employed with the initial E_0 value set to the inflection point of the rising edge. Scattering paths were fit in

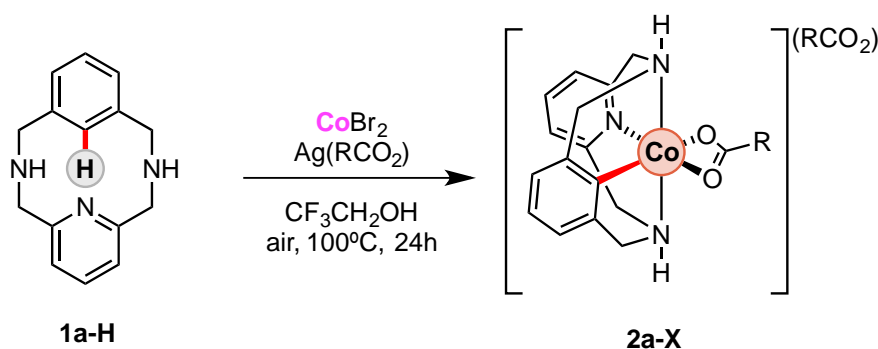
terms of a Δr_{eff} and σ^2 as previously described.^{5,6} To assess the goodness of the fits the R_{factor} (%R) was minimized. Over-fitting the data was controlled by minimizing the number of adjustable parameters and ensuring that the reduced χ^2 (χ^2_{v}) decreases with increasing number of adjustable parameters.

Theoretical Calculations

Theoretical calculations were carried out using the Gaussian 09 package.⁷ Geometry optimizations were performed using BP86 functional^{8,9} along with the def2-TZVP basis set developed by Ahlrichs.^{10,11} The empirical dispersion were included using Grimme's DFT-D3 approach¹² and solvation effects in 2,2,2-TriFluoroEthanol (TFE) were simulated using the PCM-SMD method developed by Truhlar *et al.*¹³ Subsequent frequency calculations were done to evaluate enthalpy and entropy corrections at 298.15 K ($G_{\text{corr.}}$) and ensured that all local minima have only real frequencies while a single imaginary frequency confirms the presence of transition states. All the transition states are connected to the corresponding reactants and products with IRC calculations. Single Point Energy calculations on the equilibrium geometries, including the solvent effects and D3 dispersion corrections were computed using the B3LYP¹⁴⁻¹⁷ functional and def2-TZVP basis set for all the atoms (E_{B3LYP}). The free energy change associated with moving from a standard-state gas concentration of 1 atm to a standard state gas phase concentration of 1 M for solutes ($\Delta G^{o/*}$) was also included in the final free energies. The value of $\Delta G^{o/*}$ at 298.15 K is 1.89 kcal·mol⁻¹ for 1 M standard state solutes. Then, the final total Gibbs free energy (G) was given by:

$$G = E_{\text{B3LYP}} + G_{\text{corr.}} + \Delta G^{o/*} \text{ (Equation 1)}$$

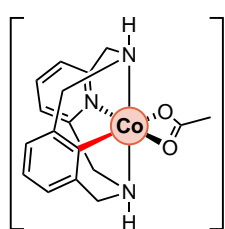
2. Synthesis of aryl-Co(III)-carboxylate complexes



Scheme S9. Synthesis of aryl-Co(III) carboxylate complexes **2a-X**.

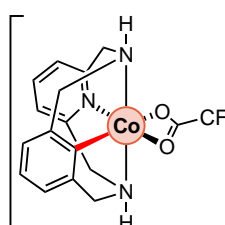
In a 10 mL vial, **1a-H** (50 mg, 0.21 mmol), Ag(RCOO₂) (0.63 mmol) and CoBr₂ (45.9 mg, 0.21 mmol) were mixed in CF₃CH₂OH (2.5 mL). The vial was then sealed with a septum and the mixture was warmed up to 100°C over 24h. Solvent was then removed, and the crude was dissolved in CHCl₃ and layered with pentane or diethyl ether. After 24h at 4°C, the resulting oil was dried under vacuum over 6h, obtaining a grey-red foam corresponding to the Co^{III} organometallic complex.

[**1a-Co^{III}**(OAc)](OAc) – (**2a-OAc**)¹⁸

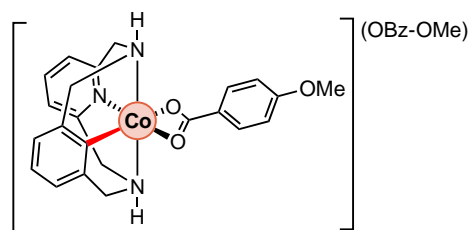


Red foam (76% yield, 66 mg, 0.16 mmol). ¹H NMR (400 MHz, CDCl₃, ppm) δ 7.46 (t, ³J_H = 7.7 Hz, 1H), 6.94 (t, ³J_H = 7.6 Hz, 1H), 6.90 (d, ³J_H = 7.4 Hz, 2H), 6.88 (d, ³J_H = 7.5 Hz, 2H), 6.71-5.16 (bs, 2H, N-H), 4.74 (m, 4H), 3.73 (d, ²J_H = 15.0 Hz, 2H), 3.69 (d, ²J_H = 15.2 Hz, 2H), 2.18 (s, 3H, ⁻OAc), 1.72 (s, 3H, ⁻OAc). ¹³C {¹H} NMR (100 MHz, CDCl₃, ppm) 166.8, 161.6, 148.6, 137.0, 124.1, 120.2, 118.3, 62.2, 61.8, 24.6. **HRMS** (ESI) calcd. for C₁₇H₁₉CoN₃O₂⁺ [M-OAc]⁺: 356.0804; found: 356.0802. **EA**: C₁₉H₂₂CoN₃O₄·(H₂O)(CF₃CH₂OH) calcd. C 47.29, N 7.88, H 5.10 %; exp. C 47.48, N 8.02, H 5.09 %.

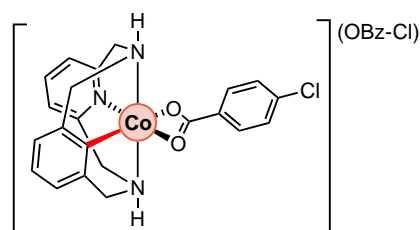
[**1a-Co^{III}**(TFA)](TFA) – (**2a-TFA**)



Red-purple solid (83% yield, 91.2 mg, 0.17 mmol). ¹H NMR (400 MHz, DMSO-d₆, ppm) δ 7.73 (t, ³J_H = 7.3 Hz, 1H), 7.17 (d, ³J_H = 7.4 Hz, 2H), 6.98 (t, ³J_H = 7.3 Hz, 1H), 6.89 (d, ³J_H = 7.2 Hz, 2H), 6.08 (m, 4H), 4.50 (m, 4H). ¹⁹F {¹H} NMR (375 MHz, DMSO-d₆, ppm) δ -74.27, -75.24. ¹³C {¹H} NMR (100 MHz, DMSO-d₆, ppm) δ 162.1 (d), 149.2, 139.1, 129.9, 127.1, 124.9, 124.3, 121.5, 120.9, 119.9, 62.3, 62.1, 59.6 (q). **HRMS** (ESI) calcd. for C₁₇H₁₆CoF₃N₃O₂⁺ [M-TFA]⁺: 410.0527; found: 410.0517. **EA**: C₁₉H₁₆CoF₆N₃O₄·(CF₃CH₂OH)₂ calcd. C 38.19, N 5.81, H 3.07 %; exp. C 38.26, N 5.91, H 2.97 %.

2.3 [1a-Co^{III}(OBz)](OBz) – (2a-OBz-OMe)

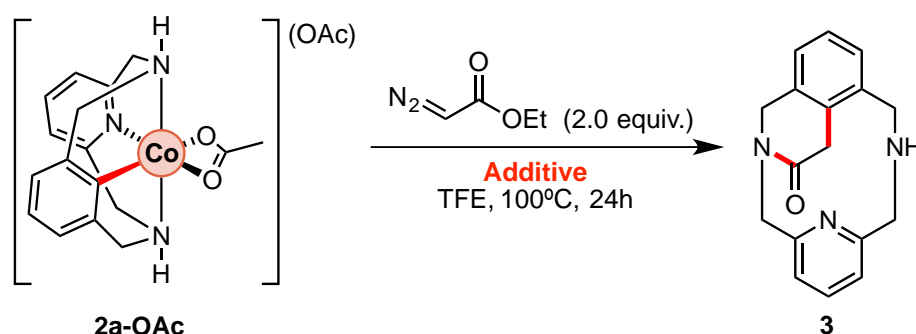
Red foam (85% yield, 107 mg, 0.18 mmol). ¹H NMR (400 MHz, CDCl₃, ppm) δ 8.14 (b, 2H), 7.66 (d, ³J_H = 7.9 Hz, 2H), 7.47 (t, ³J_H = 7.5 Hz, 1H), 7.26 (b, 2H), 7.06 (m, 4H), 6.95 (d, ³J_H = 7.5 Hz, 2H), 6.89 (d, ³J_H = 8.1 Hz, 2H), 5.04 (dd, ²J_H = 14.5 Hz, ³J_H = 7.0 Hz, 2H), 4.93 (dd, ²J_H = 14.1 Hz, ³J_H = 6.8 Hz, 2H), 3.84 (m, 2H), 3.81 (b, 3H), 3.72 (s, 3H). ¹³C {¹H} NMR (100 MHz, CDCl₃, ppm) δ 157.0, 156.4, 143.8, 132.2, 125.9, 124.4, 119.4, 115.6, 113.5, 107.7, 57.5, 57.2, 50.3. HRMS (ESI) calcd. for C₂₃H₂₃CoN₃O₃⁺[M-(OBz-OMe)]⁺: 448.1065; found: 448.1051. EA: C₁₉H₁₆CoF₆N₃O₄·(H₂O)(CF₃CH₂OH) calcd. C 55.24, N 5.86, H 4.92 %; exp. C 55.08, N 5.89, H 4.79 %.

[1a-Co^{III}(OBz-Cl)](OBz-Cl) – (2a-OBz-Cl)

Red foam (98% yield, 125.2 mg, 0.205 mmol). ¹H NMR (400 MHz, CDCl₃, ppm) δ 8.05 (b, 2H), 7.56 (d, ³J_H = 7.1 Hz, 2H), 7.47 (t, ³J_H = 7.4 Hz, 1H), 7.04 (t, ³J_H = 7.1 Hz, 2H), 6.96 (d, ³J_H = 6.7 Hz, 2H), 6.92 (d, ³J_H = 6.9 Hz, 2H), 6.82 (b, 2H), 6.64 (d, ³J_H = 6.9 Hz, 2H), 4.97 (dd, ²J_H = 15.1 Hz, ³J_H = 7.6 Hz, 2H), 4.86 (dd, ²J_H = 15.1 Hz, ³J_H = 7.3 Hz, 2H), 3.84 (m, 4H). ¹³C {¹H} NMR (100 MHz, CDCl₃, ppm) δ 161.5, 148.4, 137.4, 136.2, 134.3, 130.3, 127.5, 124.5, 120.6, 118.6, 62.3, 61.9, 60.6 (q, TFE). HRMS (ESI) calcd. for C₂₂H₂₀CoClN₃O₂⁺[M-(OBz-Cl)]⁺: 452.0575; found: 452.0586. EA: C₃₁H₃₁CoCl₂N₃O₄·(H₂O)(CF₃CH₂OH) calcd. C 51.26, N 5.78, H 4.02 %; exp. C 51.16, N 5.91, H 3.98 %.

3. Optimization of stoichiometric reaction conditions

3.1 Additives



Scheme S10. Stoichiometric reaction of **2a-OAc** with EDA to furnish cyclic amide **3**.

In a 2 mL vial, **2a-OAc** (30mg, 0.058 mmol), ethyl diazoacetate (14μl, 0.115 mmol) and **additives** (1.0-4.0 equiv.) were mixed in TFE (1.5 mL). The vial was then sealed with a septum and the mixture was stirred under air over 24h at 100°C. Then, after removal of the solvent, NH₄OH (2 mL) was added and the solution was extracted using CH₂Cl₂ (2x5mL). Then, products were purified using silica gel chromatography (CH₂Cl₂, then CH₂Cl₂/MeOH 95:5) and characterized by NMR techniques.

Table S13. Reaction of **2a-OAc** with EDA and different additives to furnish cyclic amide **3**.

entry	additive	solvent	yield of 3 (%) ^a
1	none	EtOH	traces
2	none	TFE ^b	10%
3	none	HFIP ^c	31%
4	AcOH (1.0 equiv.)	TFE	15% ^d
5	PivOH (1.0 equiv.)	TFE	12% ^d
6	TFA ^e (1.0 equiv.)	TFE	n.r. ^d
7	NaOPiv-H ₂ O (1.0 equiv.)	TFE	26%
8	H ₂ O (1.0 equiv.)	TFE	57%
9	H ₂ O (2.0 equiv.)	TFE	82%
10	H ₂ O (4.0 equiv.)	TFE	96% (91%) ^f
11	H ₂ O (4.0 equiv.)	EtOH	88%
12	AcOH (1.0 equiv.) + H ₂ O (1.0 equiv)	TFE	23%
13	(C ₆ F ₅) ₃ B (1.0 equiv.)	TFE	21%
14	Sc(OTf) ₃ (1.0 equiv)	TFE	traces
15	LiOTf (1.0 equiv.)	TFE	95% (88%) ^f
16	LiOTf (1.0 equiv.)	EtOH	91%
17	Zn(OTf) ₂ (1.0 equiv.)	TFE	37%
18	Mg(OTf) ₂ (1.0 equiv.)	TFE	67%
19	Mg(OTf) ₂ (4.0 equiv.)	TFE	52%
20	H ₂ O (1.0 equiv.) + Mg(OTf) ₂ (1.0 equiv)	TFE	92% (87%) ^f

^aYield determined using 1,3,5-trimethoxybenzene as internal standard. ^b2,2,2-trifluoroethanol. ^c1,1,1,3,3,3-hexafluoro-2-propanol. ^dProtodemetalation of **2a-OAc** was observed. ^eTrifluoroacetic acid. ^fIsolated yield after silica gel chromatography.

3.2 Equivalents of starting EDA

In a 2 mL vial, **2a-OAc** (30mg, 0.058 mmol), ethyl diazoacetate (EDA, 1.0-10.0 equiv) and H₂O (4.2 μ l, 4.0 equiv.) were mixed in TFE (1.5 mL). The vial was then sealed with a septum and the mixture was stirred under air over 24h at 100°C. Then, after removal of the solvent, NH₄OH (2 mL) was added and the solution was extracted using CH₂Cl₂ (2x5mL). Then, products were purified using silica gel chromatography (CH₂Cl₂, then CH₂Cl₂/MeOH 95:5) and characterized by NMR techniques.

Table S14. Reaction of **2a-OAc** with EDA (x equiv.) and water as additive (4.0 equiv.) to furnish cyclic amide **3**.

entry	Ethyl diazo acetate (equiv.)	Yield of 3 (%) ^a
1	1.0	53%
2	1.5	67%
3	2.0	96% (91%)^b
4	5.0	11% ^c
5	10.0	Traces ^c

^aYield determined using 1,3,5-trimethoxybenzene as internal standard. ^bIsolated yield. ^cComplex NMR spectrum with generation of undetermined products.

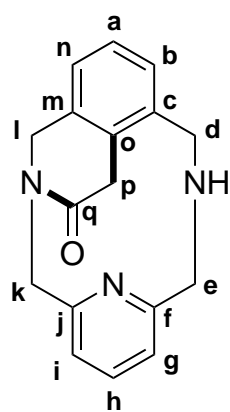
3.3 Carboxylate anions

In a 2 mL vial, **2a-X** (0.058 mmol), ethyl diazoacetate (14 μ l, 0.115 mmol) and H₂O (4.2 μ l, 4.0 equiv.) were mixed in TFE (1.5 mL). The vial was then sealed with a septum and the mixture was stirred under air over 24h at 100°C. Then, after removal of the solvent, NH₄OH (2 mL) was added and the solution was extracted using CH₂Cl₂ (2x5mL). Then, products were purified using silica gel chromatography (CH₂Cl₂, then CH₂Cl₂/MeOH 95:5) and characterized by NMR techniques.

Table S15. Reaction of **2a-X** with EDA to furnish cyclic amide **3**.

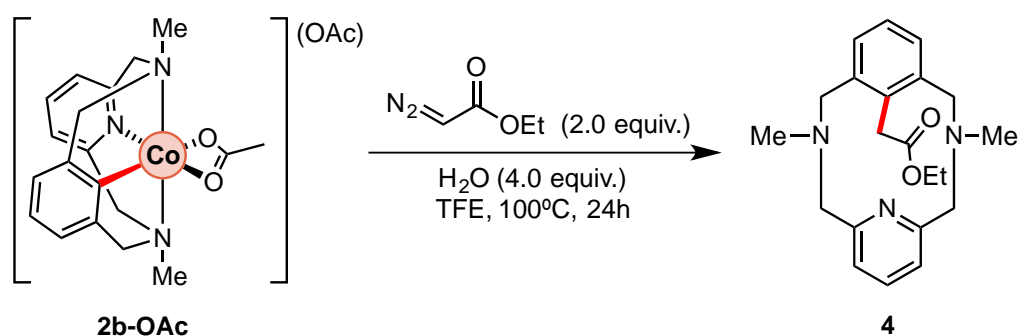
entry	R (RCO ₂)	yield of 3 (%) ^a
1	Me (OAc)	96%
2	CF ₃ (TFA)	75%
3	p-OMe-Ph (OBz-OMe)	71%
4	p-Cl-Ph (OBz-Cl)	81%
5 ^b	-- (starting from 2a-CH₃CN)	0%
6 ^b	-- (starting from 2a-CH₃CN + 2.0 equiv. NaOAc)	41%

^aYield determined using 1,3,5-trimethoxybenzene as internal standard. ^bReaction starting from **2a-CH₃CN** ([**1a-Co(III)(CH₃CN)₂**](ClO₄)₂).



^1H NMR (400 MHz, CDCl_3 , ppm) δ 7.23 (t, $^3J_H = 6.0$ Hz, 1H, **Hh**), 6.85 (d, $^3J_H = 7.2$ Hz, 1H, **Hb**), 6.69 (t, $^3J_H = 7.5$ Hz, 1H, **Ha**), 6.66 (t, $^3J_H = 7.6$ Hz, 1H, **Hi**), 6.53-6.52 (m, 2H, **Hn**, **Hg**), 5.67 (d, $^2J_H = 15.8$ Hz, 1H, **Hk**), 4.75 (d, $^2J_H = 15.4$ Hz, 1H, **Hl**), 4.61 (d, $^2J_H = 14.3$ Hz, 1H, **Hd**), 4.19 (d, $^2J_H = 15.8$ Hz, 1H, **Hp**), 4.10 (d, $^2J_H = 15.9$ Hz, 1H, **He**), 3.92 (d, $^2J_H = 15.9$ Hz, 1H, **Hk'**), 3.82 (d, $^2J_H = 15.5$ Hz, 1H, **HI'**), 3.53 (d, $^2J_H = 16.1$ Hz, 1H, **Hp'**), 3.48 (d, $^2J_H = 14.8$ Hz, 1H, **He'**), 3.44 (d, $^2J_H = 15.1$ Hz, 1H, **Hd'**). ^{13}C $\{^1\text{H}\}$ NMR (100 MHz, CDCl_3 , ppm) δ 180.5 (**Cq**), 158.2 (**Cj**), 152.6 (**Cf**), 137.7 (**Cm**), 137.4 (**Co**), 136.3 (**Ch**), 135.2 (**Cc**), 128.5 (**Cb**), 124.5 (**Ca**), 123.8 (**Cn**), 119.0 (**Cg**), 118.6 (**Ci**), 58.8 (**Ck**), 54.3 (**Cl**), 52.9 (**Cd**), 51.3 (**Ce**), 39.5 (**Cp**). HRMS (ESI-QTOF) calcd. for $\text{C}_{17}\text{H}_{18}\text{N}_3\text{O}^+$ $[\text{M}+\text{H}]^+$: 280.1445; found: 280.1439. IR (ATR): $\bar{\nu}$ (C=O) = 1670 cm^{-1} .

4. Reaction with tertiary amine aryl-Co(III) complex



Scheme S11. Stoichiometric reaction of **2b-OAc** with EDA to furnish macrocyclic amine **4**.

In a 2 mL vial, **2b-OAc** (30mg, 0.058 mmol), EDA (14 μL , 0.115 mmol) and H_2O (4.2 μL , 4.0 equiv.) were mixed in TFE (1.5 mL, 0.04 M) (Standard reaction conditions). The vial was then sealed with a septum and the mixture was stirred under air over 24h at 100°C . Then, after removal of the solvent, NH_4OH (2 mL) was added and the solution was extracted using CH_2Cl_2 (2x5mL). Then, products were purified using silica gel chromatography (CH_2Cl_2 , then $\text{CH}_2\text{Cl}_2/\text{MeOH}$ 95:5). However, cyclic amine product **4** was only detected in trace amounts by HRMS techniques.

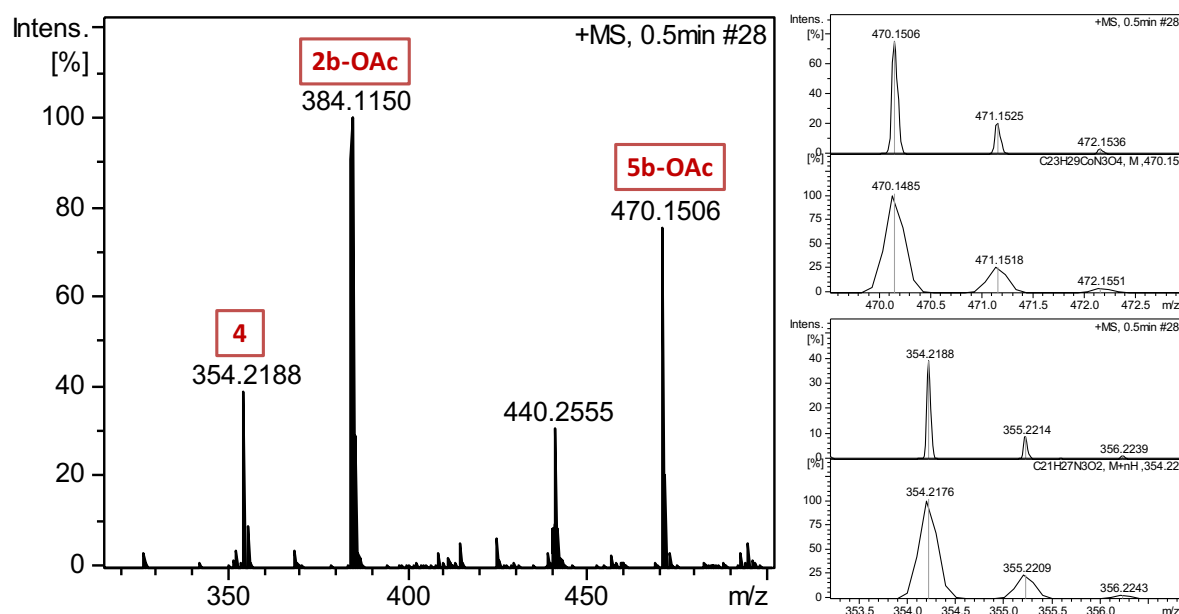
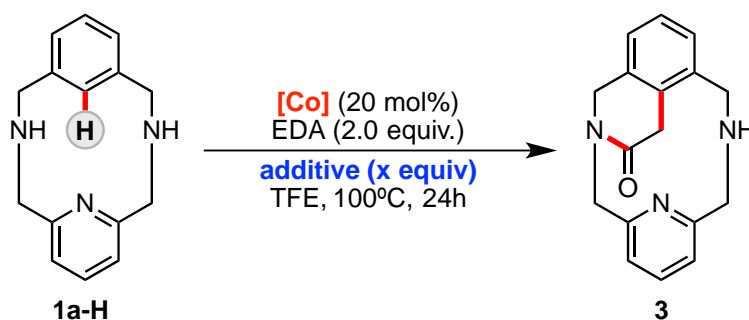


Figure S27. HRMS analysis of the crude reaction of **2b-OAc** and EDA in presence of water after 24h in TFE (main peaks). Peak at $m/z = 384.1150$ corresponds to **2b-OAc**; peak at $m/z = 354.2188$ corresponds to **4** and peak at $m/z = 470.1506$ corresponds to **5b-OAc**.

5. Evaluation of catalytic reaction conditions



Scheme S12. Cyclization of **1a-H** with EDA to furnish **3** using catalytic amounts of cobalt and a variety of additives.

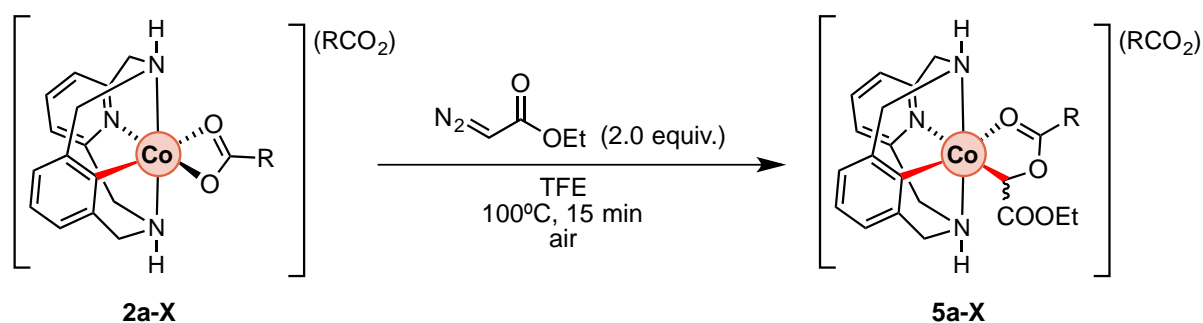
In a 2 mL vial, **1a-H** (28mg, 0.115 mmols), a cobalt source (x mol%), ethyl diazoacetate (28 μ l, 0.23 mmol) and additives (x equiv.) were mixed in TFE (1.5 mL). The vial was then sealed with a septum and the mixture was stirred under air over 24h at 100°C. Then, after removal of the solvent, NH₄OH (2 mL) was added and the solution was extracted using CH₂Cl₂ (2x5mL). Then, products were purified using silica gel chromatography (CH₂Cl₂, then CH₂Cl₂/MeOH 95:5) and characterized by NMR techniques.

Table S16. Reaction of **1a-H** with EDA (2.0 equiv.) and additives (4.0 equiv.) using different cobalt sources as catalyst to furnish cyclic amide **3**.

entry	[Co] (x mol%)	additives (equiv.)	ratio (3:1a-H) ^a	yield of 3 (%) ^b
1	-	H ₂ O (4.0)	-	n.r.
2	2a-OAc (20)	H ₂ O (4.0)	>20:1	93% (87%) ^c (4.4 TON)
3 ^d	2a-OAc (20)	H ₂ O (4.0)	>20:1	95% (84%) ^c (4.2 TON)
4	2a-OAc (10)	H ₂ O (4.0)	4:5	47% (4.7 TON)
5	Co(OAc) ₂ (20)	H ₂ O (4.0)	>20:1	96% (89%) ^c (4.5 TON)
6 ^d	Co(OAc) ₂ (20)	H ₂ O (4.0)	1:50	traces
7	Co(OAc) ₂ (20)	none	1:1	15% (0.8 TON)
8 ^d	CoBr ₂ (20)	H ₂ O (4.0) + Ag(OAc) (0.4)	-	traces
9 ^d	CoBr ₂ (20)	H ₂ O (4.0) + Ag(OAc) (1.0)	3:1	67% (3.4 TON)
10 ^d	CoBr ₂ (20)	H ₂ O (4.0) + Ag(OBz-Cl) (1.0)	4:1	71% (3.6 TON)
11 ^d	CoBr ₂ (20)	H ₂ O (4.0) + Ag(OBz-OMe) (1.0)	2:1	56% (2.8 TON)
12	Co(acac) ₃ (20)	H ₂ O (4.0)	4:1	traces ^e
13	Co(OAc) ₂ (20)	Mg(OTf) ₂ (1.0)	1:1	42% (2.1 TON)
14	Co(OAc) ₂ (20)	Mg(OTf) ₂ (4.0)	8:1	73% (3.7 TON)
15	Co(OAc) ₂ (20)	Mg(OTf) ₂ (1.0) + H ₂ O (1.0)	>20:1	93% (84%) ^c (4.2 TON)
16	Co(OAc) ₂ (20)	Li(OTf)	>20:1	96% (88%) ^c (4.4 TON)

^aRatio determined by NMR. ^bYield using 1,3,5-trimethoxybenzene as internal standard. ^cIsolated yields after silica gel chromatography. ^dReaction performed under inert atmosphere (N₂). ^eNMR with presence of multiple byproducts was obtained.

6. Isolation of Reaction Intermediates

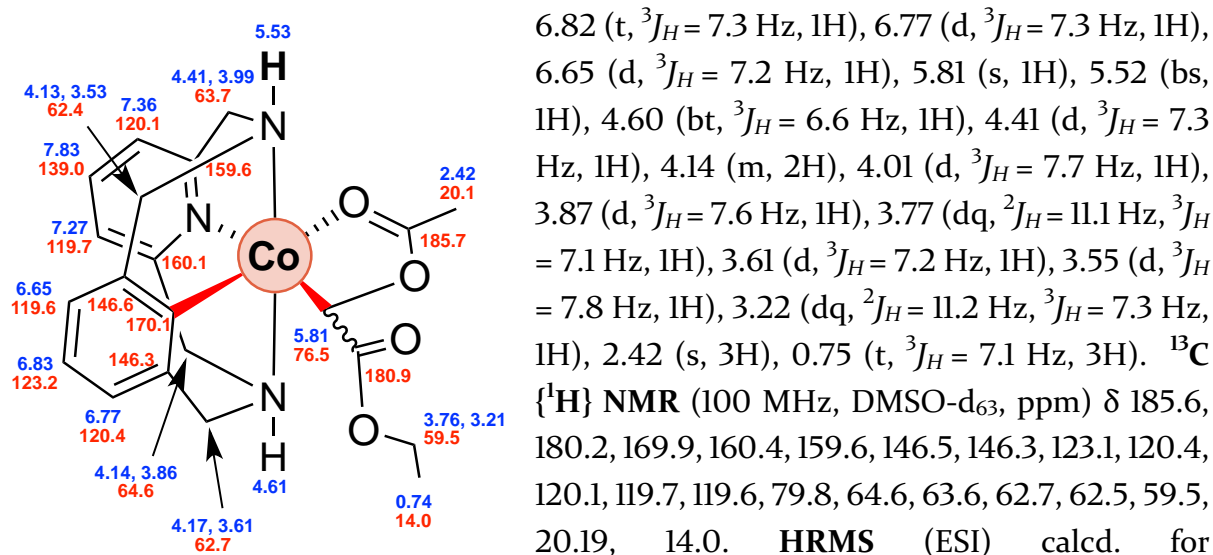


Scheme S13. Stoichiometric reaction of **2a-X** with EDA to furnish intermediate species **5a-X**.

In a 2 mL vial, **2a-X** (0.058 mmol) and EDA (2.0 equiv.) were mixed in freshly distilled TFE (1.5 mL) in anhydrous conditions. The vial was then sealed with a septum and the mixture was stirred under air over 15 min at 100°C. After reaction completion, crude mixture was analyzed by HRMS and reaction intermediates were detected as major products. Then, recrystallization with CHCl_3 layered with pentane yielded the corresponding organometallic complex **5a-X**, which was characterized by NMR and X-Ray spectroscopy. When R = strong EWG, intermediate **5a-X** (TFA) cannot be isolated.

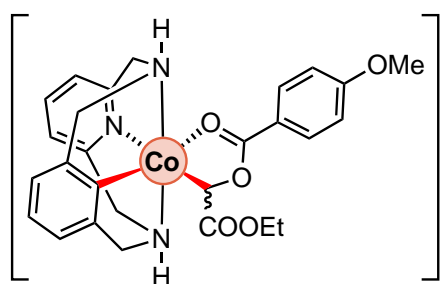
[1a-Co^{III}(EDA-OAc)](OAc) – (5a-OAc)

Orange-brown solid (74% yield, 21 mg, 0.04 mmol). ¹H NMR (400 MHz, DMSO-d₆, ppm) 6.01 7.83 (t, ³J_H = 7.3 Hz, 1H), 7.35 (d, ³J_H = 7.1 Hz, 1H), 7.27 (d, ³J_H = 7.2 Hz, 1H),



[1a-Co^{III}(EDA-OBz-OMe)](OBz-OMe) – (5a-OBz-OMe)

Orange crystalline solid (97% yield, 38.6 mg, 0.056 mmol). ¹H NMR (400 MHz, DMSO-



(OBz-OMe) d₆, ppm) δ 8.15 (d, ³J_H = 7.2 Hz, 1H), 7.92 (t, ³J_H = 7.4 Hz, 1H), 7.81 (b, 2H), 7.45 (d, ³J_H = 7.4 Hz, 1H), 7.37 (d, ³J_H = 7.3 Hz, 1H), 7.13 (d, ³J_H = 7.6 Hz, 2H), 6.90 (b, 2H), 6.83 (m, 2H), 6.67 (d, ³J_H = 7.1 Hz, 1H), 6.01 (s, 1H), 5.54 (t, ³J_H = 7.7 Hz, 1H), 4.68 (t, ³J_H = 7.8 Hz, 1H), 4.50 (dd, ²J_H = 16.4 Hz, ³J_H = 7.3 Hz, 1H), 4.24 (dd, ²J_H = 15.6 Hz, ³J_H = 7.3 Hz, 2H), 4.16 (dd, ²J_H = 15.2 Hz, ³J_H = 7.1 Hz, 1H), 4.04 (d, ²J_H = 15.8 Hz, 1H), 3.92 (d, ²J_H = 15.7 Hz, 1H), 3.83 (s, 3H), 3.80 (dq, ²J_H = 10.9 Hz, ³J_H = 7.3 Hz, 1H), 3.70 (d, ²J_H = 15.3 Hz, 1H), 3.67 (d, ²J_H = 14.4 Hz, 1H), 3.57 (d, ²J_H = 15.2 Hz, 1H), 3.26 (dq, ²J_H = 10.9 Hz, ³J_H = 7.3 Hz, 1H), 0.78 (t, ³J_H = 7.1 Hz, 3H). ¹³C {¹H} NMR (100 MHz, DMSO-d₆, ppm) δ 180.3, 179.3, 164.6, 160.5, 159.8, 146.6, 159.8, 146.6, 146.3, 139.0, 133.2, 131.2, 123.1, 120.4, 120.3, 120.1, 119.8, 119.6, 114.7, 76.7, 64.8, 63.7, 62.8, 62.5, 59.6, 56.2, 14.0. HRMS (ESI) calcd. for C₂₇H₂₉CoN₃O₃⁺ [M-(OBz-OMe)]⁺: 534.1434; found: 534.1421. IR (ATR): $\bar{\nu}$ = 2933, 1684, 1601, 1510, 1376, 1247, 1166, 1101, 1026, 849, 749, 607 cm⁻¹. EA: C₃₅H₃₆CoN₃O₈·(H₂O)₂ calcd. C 58.17, N 5.81, H 5.72 %; exp. C 58.44, N 5.82, H 5.82 %.

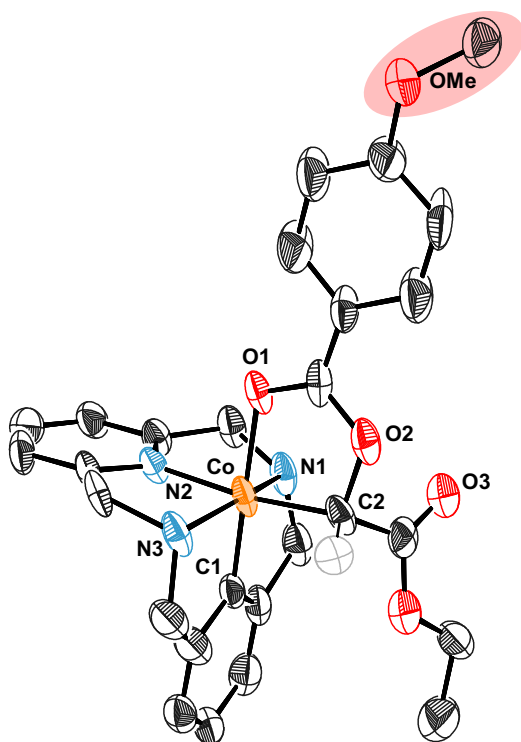
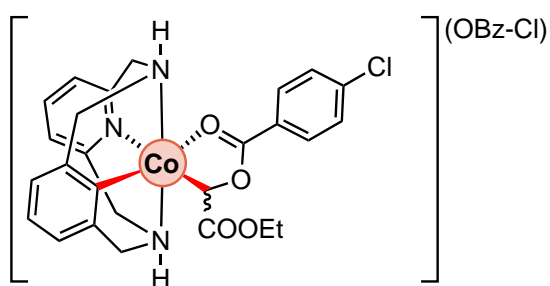


Figure S28. Solid state structure of **5a-OBz-OMe**. Hydrogen atoms, anions and solvent molecules have been omitted for clarity; ellipsoids are set at 33% probability. Selected bond distances [Å] and angles [°]: Co-C(1) 1.84(1), Co-C(2) 1.97(1), Co-N(1) 2.027(6), Co-N(2) 1.878(8), Co-N(3) 1.984(6), Co-O(1) 2.004(7); C(1)-Co-C(2) 96.3(4), C(2)-Co-O(1) 82.7(3), C(1)-Co-N(2) 91.0(4), C(1)-Co-O(1) 178.8(4).

[**1a**-Co^{III}(EDA-OBz-Cl)](OBz-Cl) – (**5a**-OBz-Cl)

Orange crystalline solid (85% yield, 38.6 mg, 0.056 mmol). ¹H NMR (400 MHz, DMSO-



d₆, ppm) δ 8.17 (d, ³J_H = 8.2 Hz, 2H), 7.91 (bt, 4H), 7.67 (d, ³J_H = 7.9 Hz, 2H), 7.50 (d, ³J_H = 7.8 Hz, 1H), 7.44 (d, ³J_H = 7.8 Hz, 1H), 7.37 (d, ³J_H = 7.9 Hz, 1H), 7.30 (d, ³J_H = 7.7 Hz, 1H), 6.85 (t, ³J_H = 7.6 Hz, 1H), 6.81 (d, ³J_H = 6.9 Hz, 1H), 6.68 (d, ³J_H = 7.1 Hz, 1H), 6.09 (s, 1H), 5.89 (t, ³J_H = 8.5 Hz, 1H), 4.75 (d, ³J_H = 7.9 Hz,

1H), 4.55 (dd, ²J_H = 17.4 Hz, ³J_H = 7.3 Hz, 1H), 4.26 (m, 2H), 4.16 (dd, ²J_H = 15.7 Hz, ³J_H = 7.3 Hz, 1H), 4.04 (d, ²J_H = 17.9 Hz, 1H), 3.95 (d, ²J_H = 16.3 Hz, 1H), 3.80 (dq, ²J_H = 12.1 Hz, ³J_H = 7.4 Hz, 1H), 3.68 (d, ²J_H = 17.2 Hz, 1H), 3.60 (d, ²J_H = 17.1 Hz, 1H), 3.28 (dq, ²J_H = 11.7 Hz, ³J_H = 7.3 Hz, 1H), 0.78 (t, ³J_H = 7.0 Hz, 3H). ¹³C {¹H} NMR (100 MHz, DMSO-d₆, ppm) δ 180.1, 178.8, 160.7, 159.8, 146.6, 146.4, 139.9, 132.8, 129.5, 126.9, 120.5, 120.2, 119.8, 119.7, 77.5, 64.8, 63.8, 62.7, 62.5, 59.6, 14.0. Minor conformer: ¹H NMR (400 MHz, DMSO-d₆, ppm) δ 7.90, 7.69, 7.50, 7.27, 7.23, 6.73, 6.61, 6.53, 4.97, 4.78, 4.45, 4.33, 4.32, 3.87, 3.84, 3.61, 3.50, 3.40, 3.15, 0.84. ¹³C {¹H} NMR (100 MHz, DMSO-d₆, ppm) δ 179.3, 176.0, 166.0, 160.4, 159.0, 147.7, 147.2, 137.4, 131.5, 128.7, 122.1, 119.4, 118.7, 64.0, 63.7, 63.1, 62.7, 58.5, 14.2. **HRMS** (ESI) calcd. for C₂₆H₂₆CoClN₃O₄⁺ [M-(OBz-Cl)]⁺: 538.0944; exp: 538.0946. **IR** (ATR): $\bar{\nu}$ = 3250, 3142, 1680, 1624, 1595, 1378, 1197, 1087, 752, 558 cm⁻¹. **EA**: C₃₃H₃₀CoN₃O₈Cl₂·(H₂O)₂ calcd. C 54.19, N 5.74, H 4.82 %; exp. C 54.31, N 5.68, H 5.01 %.

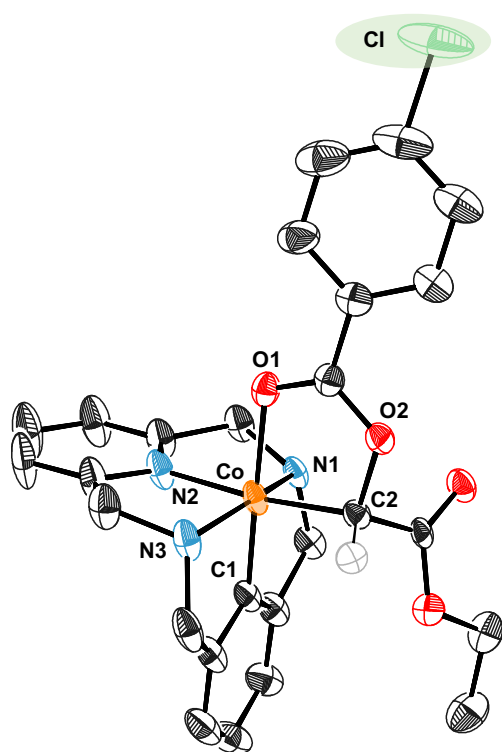
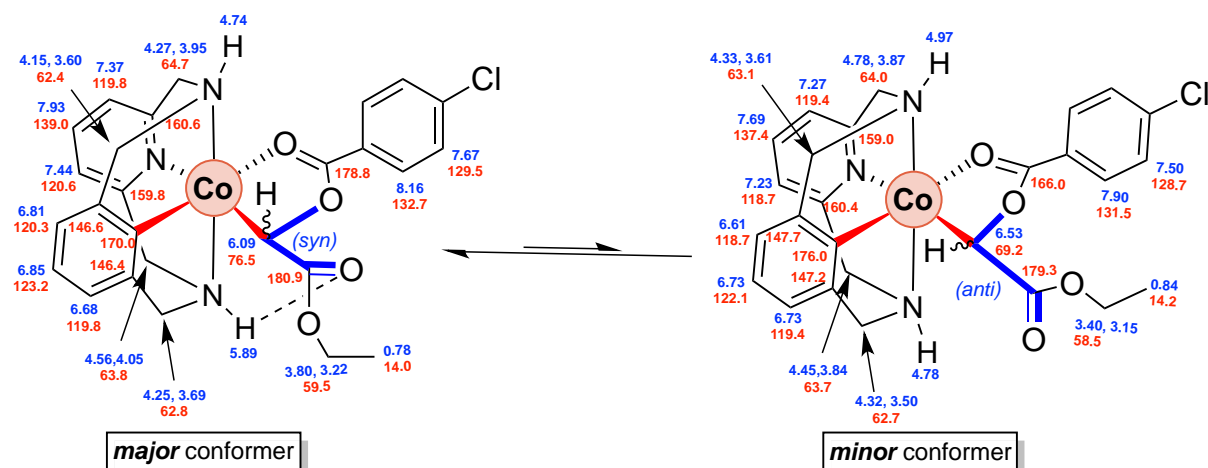


Figure S29. Solid state structure of **5a**-OBz-Cl. Hydrogen atoms, anions and solvent molecules have been omitted for clarity; ellipsoids are set at 50% probability. Selected bond distances [Å] and angles [°]: Co-C(1) 1.846(3), Co-C(2) 1.972(5), Co-N(1) 2.008(3), Co-N(2) 1.891(4), Co-N(3) 2.005(3), Co-O(1) 2.008(3); C(1)-Co-C(2) 95.71(2), C(2)-Co-O(1) 82.78(2), C(1)-Co-N(2) 91.78(2), C(1)-Co-O(1) 178.21(2).



Scheme S14. Proposed equilibrium of two different conformers of **5a-OBz-Cl** in solution at 298 K in DMSO- d_6 (ratio major/minor = 4:1). Taking into account the variation of chemical shifts in the enolate unit, as well as the ethyl group from the ester, our current hypothesis is depicted in this scheme.

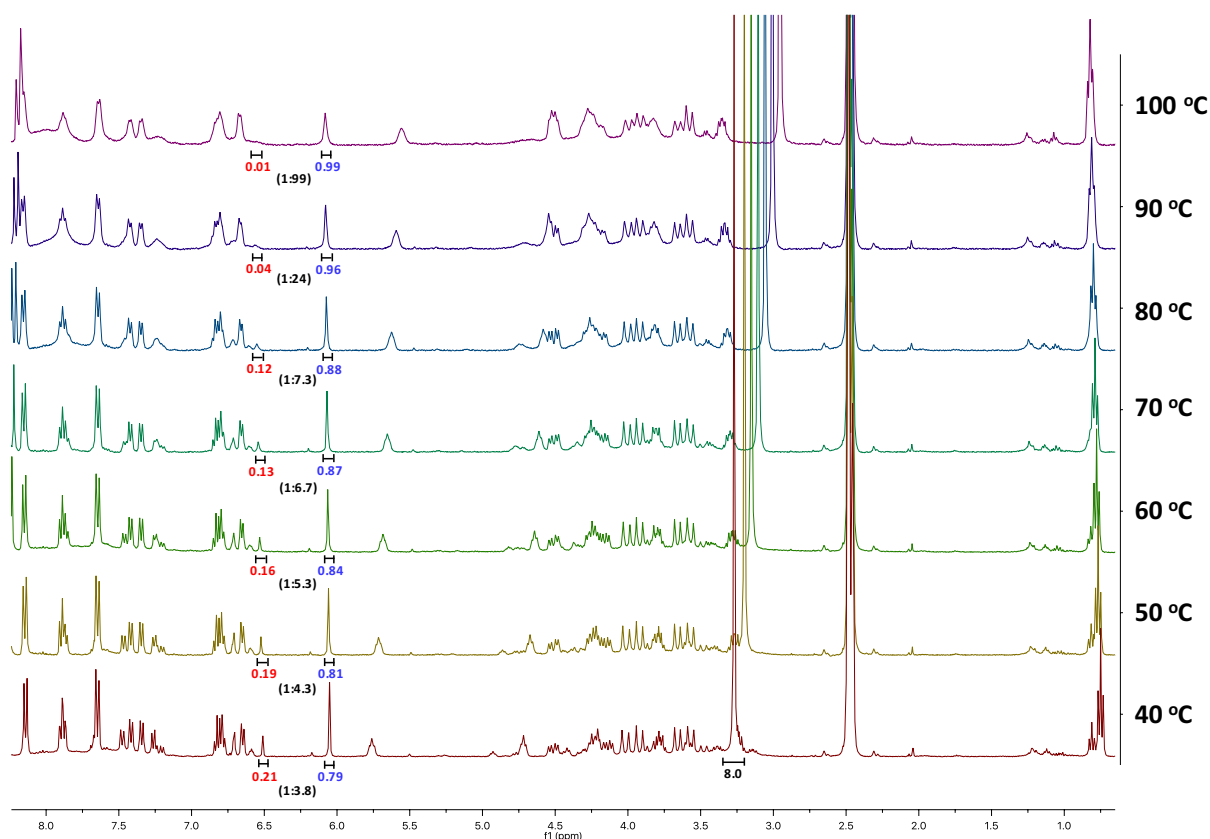


Figure S30. ^1H NMR spectra of **5a-OBz-Cl** mixed with 4.0 equiv. in DMSO- d_6 at variable temperatures (400 MHz). As it can be observed in this Figure, both conformers are present at 40°C. However, when the mixture is heated, the amount of major conformer is also increased, indicating its better stability in high temperatures by the effect of an external additive, in this case water.

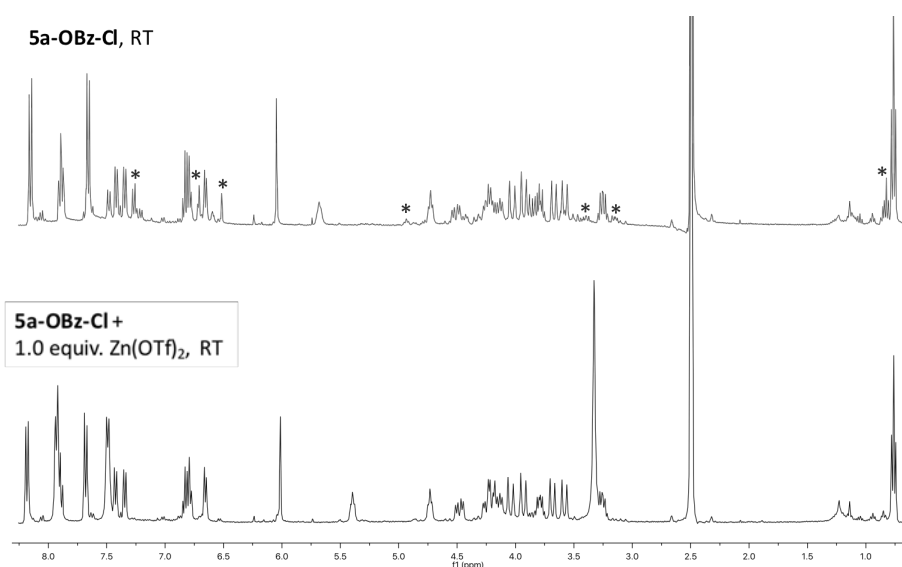


Figure S31. ^1H NMR spectra of **5a-OBz-Cl** in DMSO-d_6 without additives (top) and mixed with 1.0 equiv. of $\text{Zn}(\text{OTf})_2$ (bottom), 400 MHz, 298 K. Only the major conformer can be observed by ^1H NMR, which confirms its preference when additives are added.

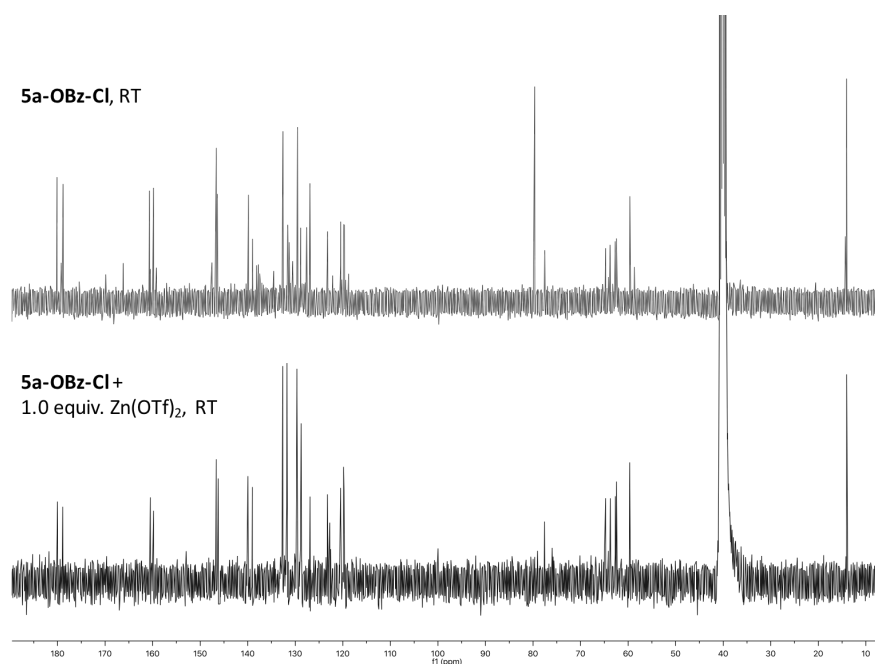
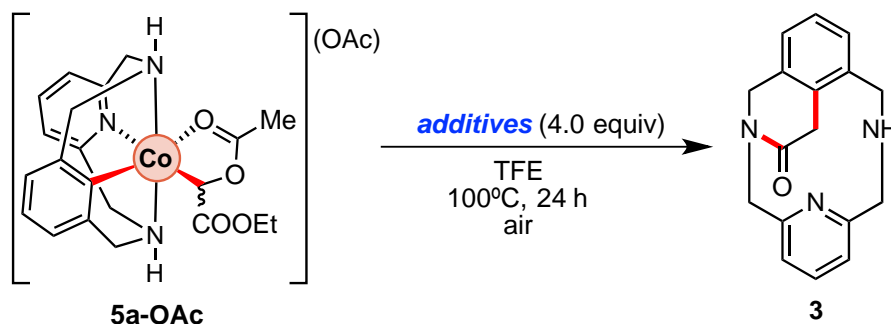


Figure S32. ^{13}C NMR spectra of **5a-OBz-Cl** in DMSO-d_6 without additives (top) and mixed with 1.0 equiv. of $\text{Zn}(\text{OTf})_2$ (bottom), 400 MHz, 298 K. Only the major conformer can be observed by ^{13}C NMR, which confirms its preference when additives are added.

These results suggest that the minor conformer does not participate in the evolution of **5a-X** complexes to the cyclic amide **3** and, indeed, the major conformer is the responsible of the $\text{S}_{\text{N}}2$ -like pathway to furnish **INT-MI** in presence of additives such as lewis acids or water.

7. Reactivity of 5a-X Intermediates

7.1 Evolution of organometallic 5a-OAc complexes to cyclic amide 3 – Effect of additives



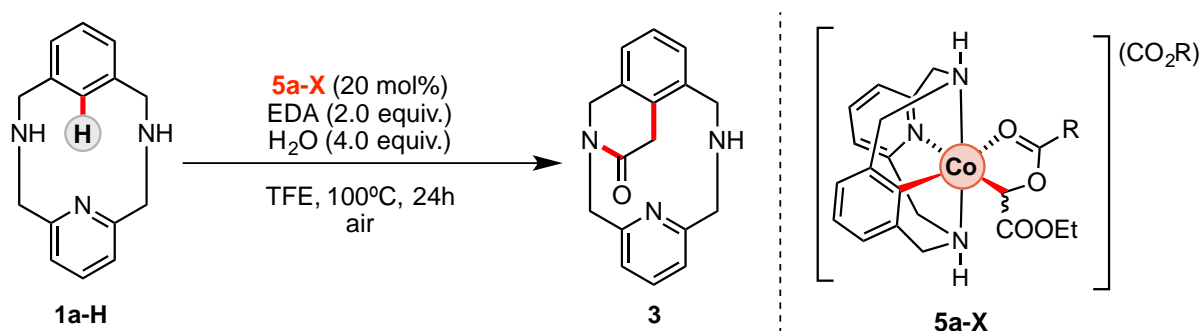
Scheme S15. Evolution of 5a-X to 3 in presence of a variety of additives.

In a 2 mL vial, 5a-OAc (0.029 mmol) and *additives* (4.0 equiv.) were mixed in freshly distilled TFE (1.5 mL). The vial was then sealed with a septum and the mixture was stirred under air over 24h at 100°C. Then, after removal of the solvent, NH₄OH (2 mL) was added and the solution was extracted using CH₂Cl₂ (2x5mL). Then, reactions crudes were analyzed by NMR techniques.

Table S17. Evolution of 5a-OAc to 3 in presence/absence of additives.

entry	additive	yield of 3 (%) ^a
1	-	14%
2	-	52% ^b
3	H ₂ O	85%
4	AcOH	51%
5	CF ₃ SO ₃ H	82%
6	Li(OTf)	89%
7	Mg(OTf) ₂	67%
8	Zn(OTf) ₂	58%
9	B(C ₆ F ₅) ₃	26%

^aYield determined using 1,3,5-trimethoxybenzene as internal standard. ^bReaction was carried out over 48h.

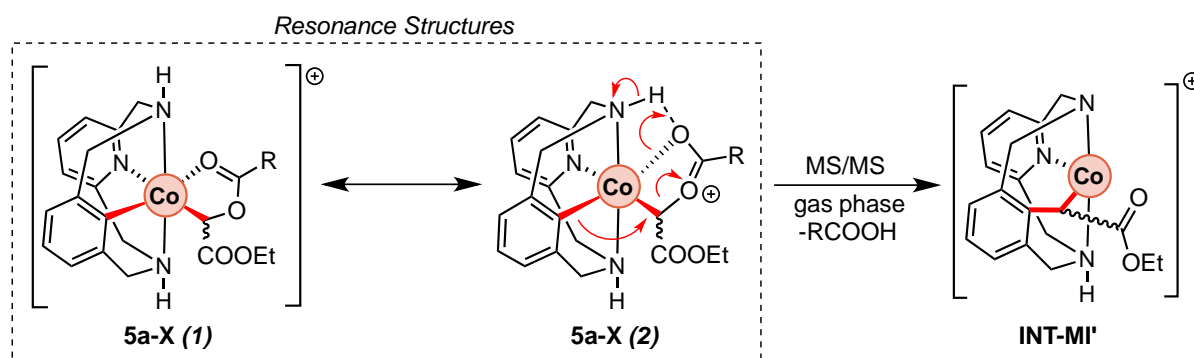
7.2 Evaluation of organometallic **5a-X** complexes as catalysts**Scheme S16.** Cyclization of **1a-H** with EDA to furnish **3** using catalytic amounts of **5a-X**.

In a 2 mL vial, **1a-H** (28mg, 0.115 mmols), **5a-X** (20 mol%), ethyl diazoacetate (28 μ l, 0.23 mmol) and H₂O (9 μ l, 4.0 equiv.) were mixed in TFE (1.5 mL). The vial was then sealed with a septum and the mixture was stirred under air over 24h at 100°C. Then, after removal of the solvent, NH₄OH (2 mL) was added and the solution was extracted using CH₂Cl₂ (2x5mL). Then, products were purified using silica gel chromatography (CH₂Cl₂, then CH₂Cl₂/MeOH 95:5) and characterized by NMR techniques.

Table S18. Reaction of **1a-H** with EDA (2.0 equiv.) and water as additive (4.0 equiv.) using **5a-X** as catalyst to furnish cyclic amide **3**.

entry	5a-X (x mol%)	Yield of 3 (%) ^a
1	5a-OAc (20)	79% (4.0 TON)
2	5a-OBz-OMe (20)	67% (3.4 TON)
3 ^c	5a-OBz-Cl (20)	75% (3.8 TON)

^aIsolated yields after silica gel chromatography.

7.3 MS/MS experiments of **5a-X** complexes (X = OAc)

Scheme S17. One of the possible resonance structures of **5a-X** proposed to be responsible of the evolution of **5a-X** to **3**. Reactivity observed through MS/MS analysis of **5a-X** intermediates.

5a-X complexes were analyzed by high-resolution ESI-MS-QTOF analysis, isolating the peak corresponding to $[(\mathbf{5a-X})\text{-X}]$ to subject it to tandem MS at different energies. As shown in Figures S7, S8 and S9, one peak corresponding to $[(\mathbf{INT-MI})\text{-RCOOH}]$ (R = Me, *p*-OMe-Ph, *p*-Cl-Ph) was observed (**INT-MI'**). As expected, the intensity of this peak increased with the energy applied. Significantly, when tandem MS experiments of **5a-OBz-OMe** and **5a-OBz-Cl** are compared when applying the same collision energy (20 eV), **5a-OBz-Cl** generates relative higher amounts of **INT-MI'** than **5a-OBz-OMe**, which suggests *p*-Cl-PhCOO⁻ is a better leaving group.

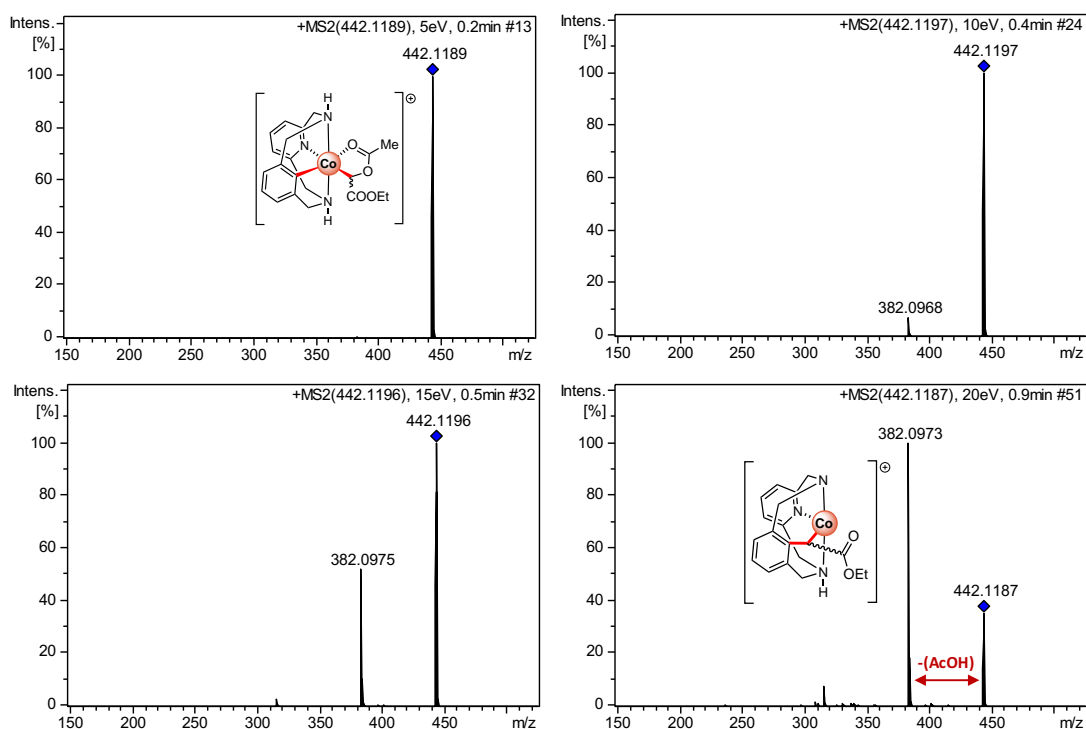
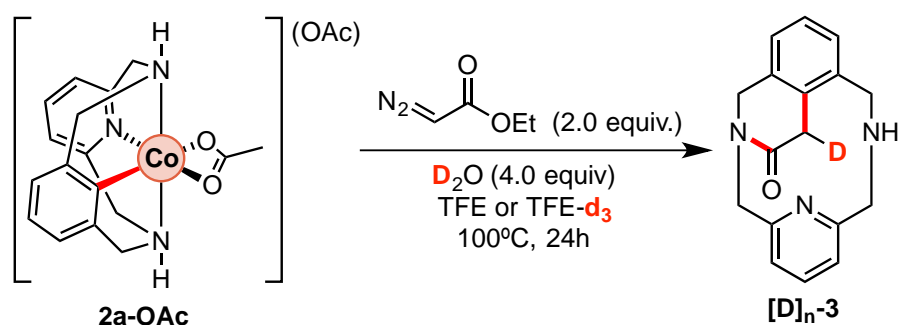


Figure S33. MS/MS spectrum of **5a-OAc** ($m/z = 442.1187$, 20 eV) showing a peak at $m/z = 382.0973$ (20 eV), which corresponds to **INT-MI'**.

8. Deuterium labeling experiments

8.1 D-incorporation starting from **2a-OAc**



Scheme S18. Reaction of **2a-X** with EDA to furnish deuterated cyclic amide **[D]_n-3**.

In a 2 mL vial, **2a-OAc** (0.058 mmol), ethyl diazoacetate (14 μ l, 0.115 mmol) and **D₂O** (4.2 μ l, 4.0 equiv.) were mixed in TFE or TFE-**d₃** (1.5 mL). The vial was then sealed with a septum and the mixture was stirred under air over 24h at 100°C. Then, after removal of the solvent, NH₄OH (2 mL) was added and the solution was extracted using CH₂Cl₂ (2x5mL). Then, products were purified using silica gel chromatography (CH₂Cl₂, then CH₂Cl₂/MeOH 90:10) and analyzed by NMR spectroscopy and MS spectrometry.

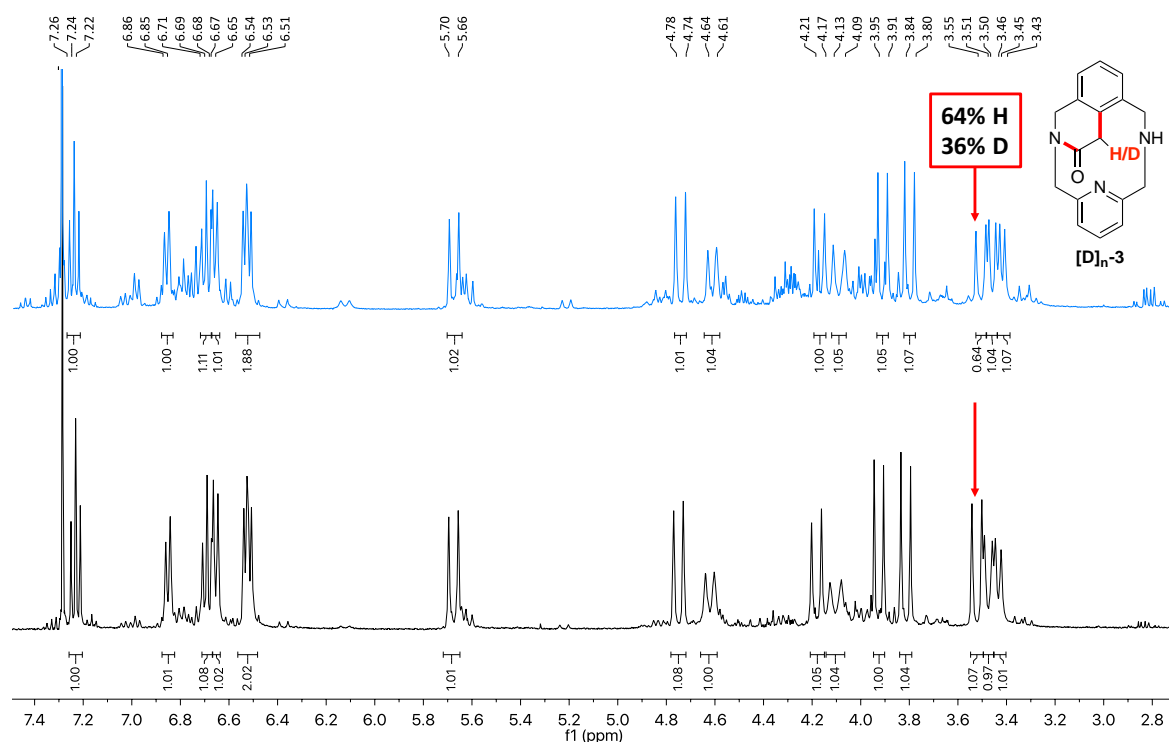


Figure S34. ^1H NMR spectrum of $[\text{D}]_n\text{-3}$ (up, blue) and $\mathbf{3}$ (down, black) recorded at 298K using CDCl_3 as solvent. 36% of deuterium incorporation from D_2O (4.0 equiv.) using TFE as solvent.

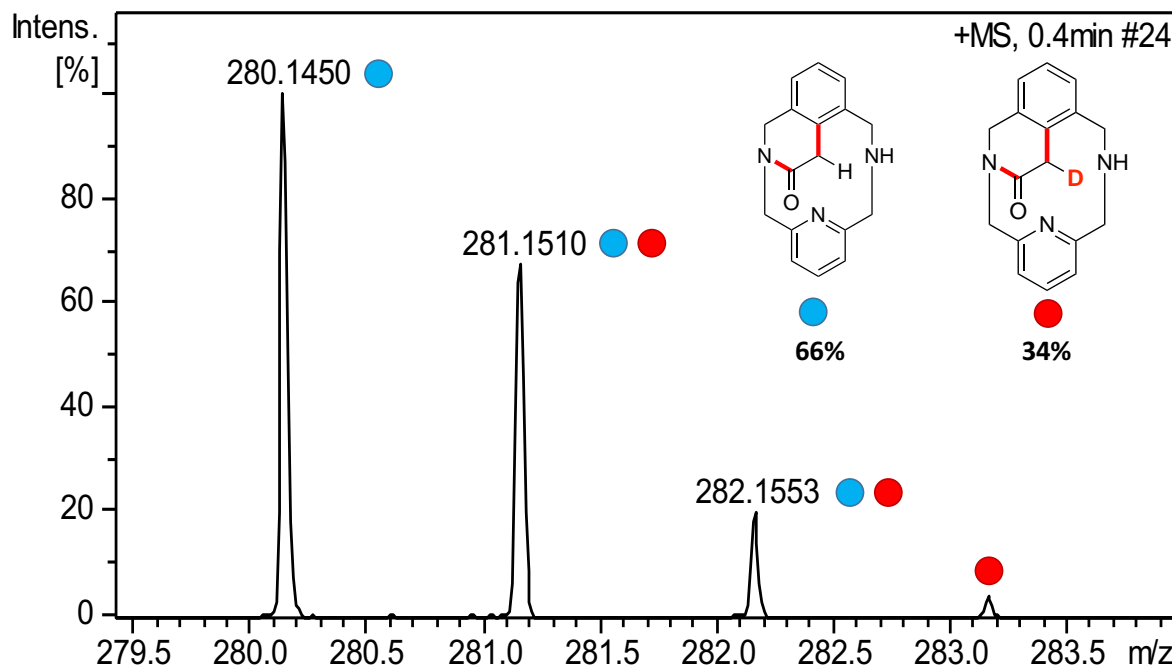


Figure S35. HRMS-ESI-QTOF of $[\text{D}]_n\text{-3}$ obtained after reaction of $\mathbf{2a-OAc}$ with EDA and D_2O (4.0 equiv.) in TFE. Mass analysis shows 34% D incorporation in agreement with ^1H -NMR (Figure S10). Deuterium incorporation was measured by the relative intensity of the peaks in the mass spectrum corresponding to the deuterated and non-deuterated products.

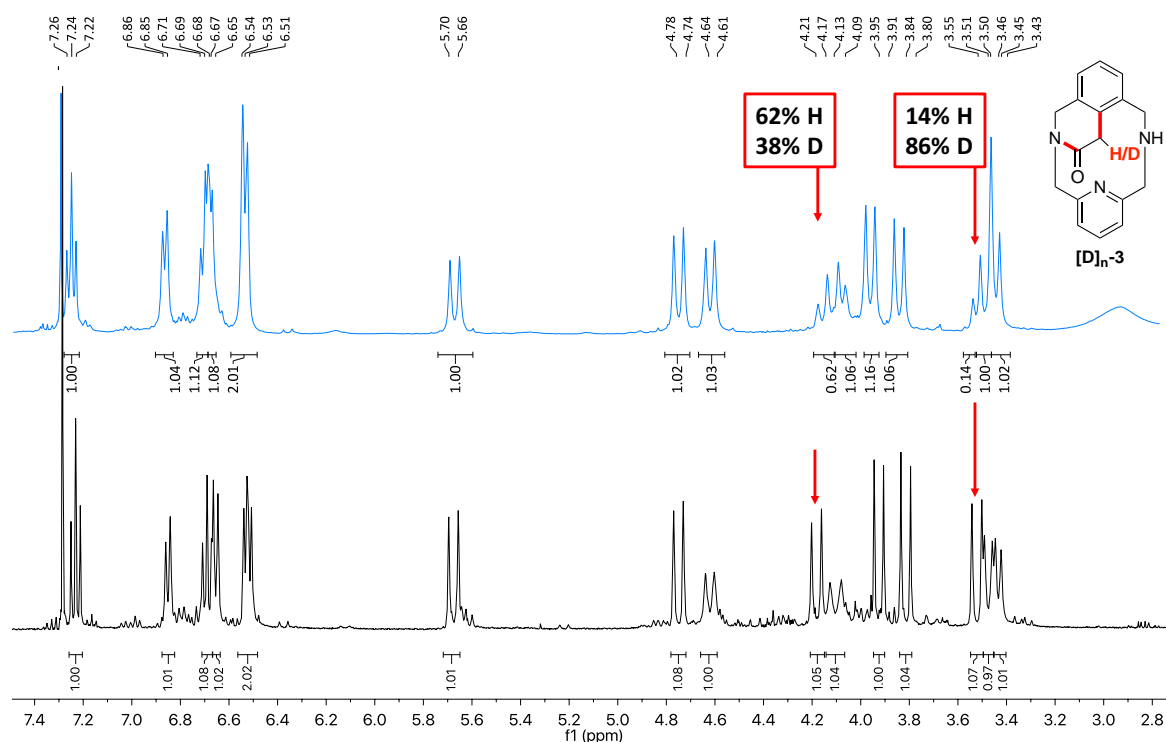


Figure S36. ^1H NMR spectrum of $[\text{D}]_n\text{-3}$ (up, blue) and 3 (down, black) recorded at 298K using CDCl_3 as solvent. 86% of deuterium incorporation from D_2O (4.0 equiv.) using TFE-d_3 as solvent. 38% of D incorporation due to D-exchange of the acidic proton of EDA.

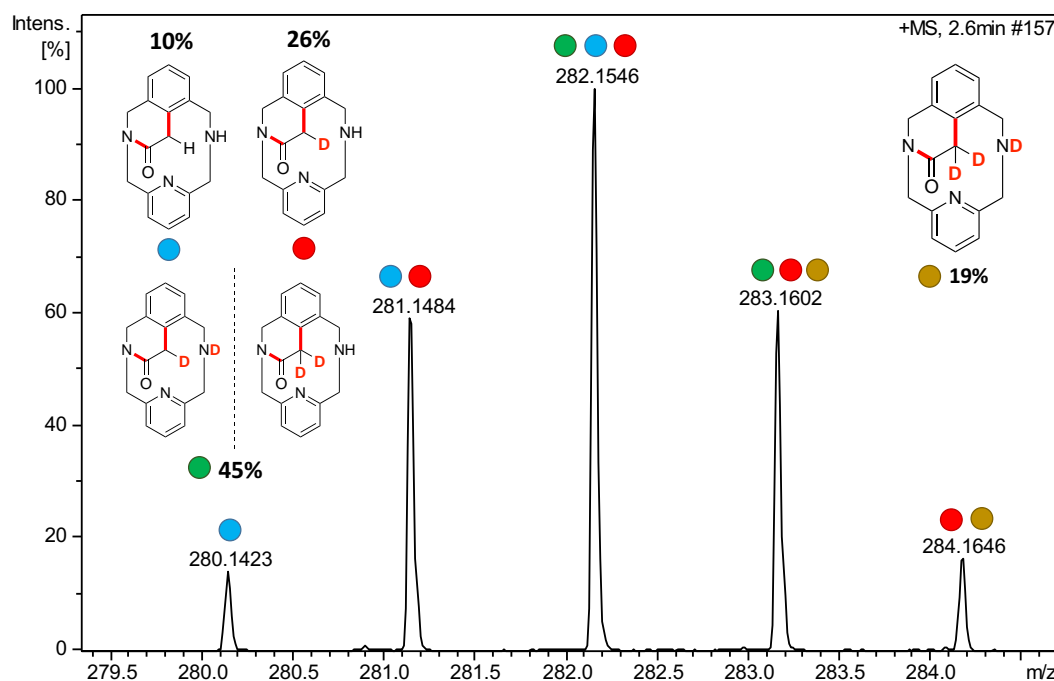


Figure S37. HRMS-ESI-QTOF of $[\text{D}]_n\text{-3}$ obtained after reaction of 2a-OAc with EDA and D_2O (4.0 equiv.) in TFE-d_3 . Mass analysis shows 90% D incorporation in agreement with ^1H -NMR (Figure S12). Deuterium incorporation was measured by the relative intensity of the peaks in the mass spectrum corresponding to the deuterated and non-deuterated products.

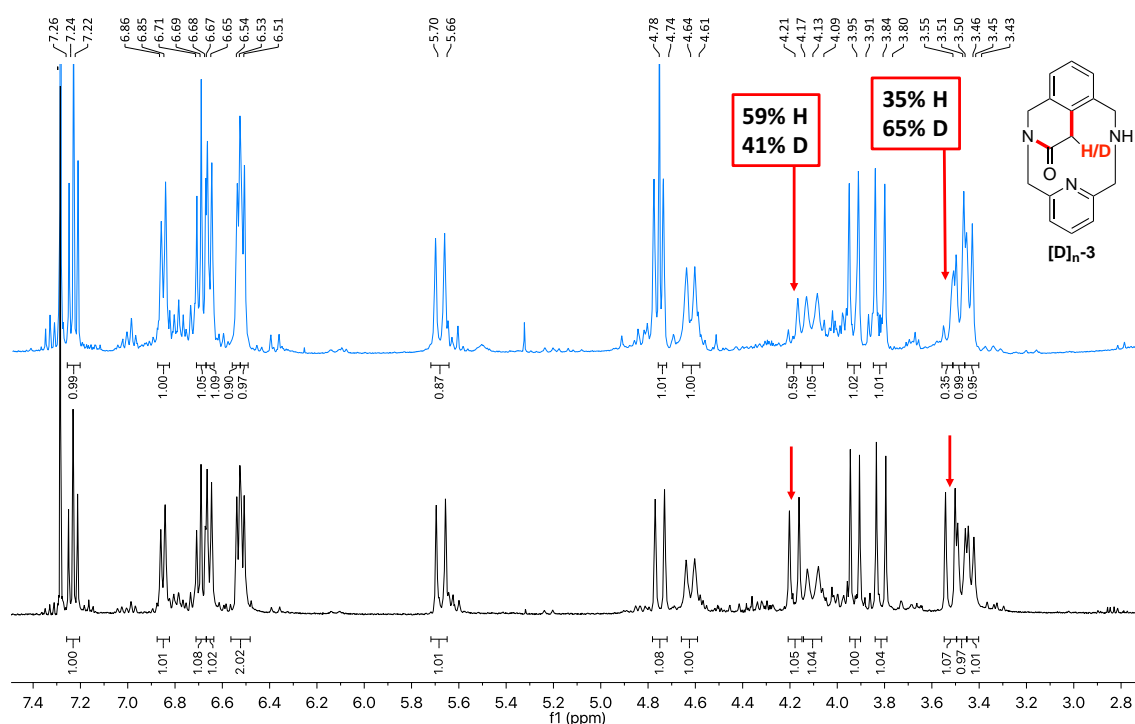


Figure S38. ^1H NMR spectrum of $[\text{D}]_n\text{-3}$ (up, blue) and $\mathbf{3}$ (down, black) recorded at 298K using CDCl_3 as solvent. 65% of deuterium incorporation from H_2O (4.0 equiv.) using TFE-d_3 as solvent. 41% of D incorporation due to D-exchange of the acidic proton of EDA can also be observed.

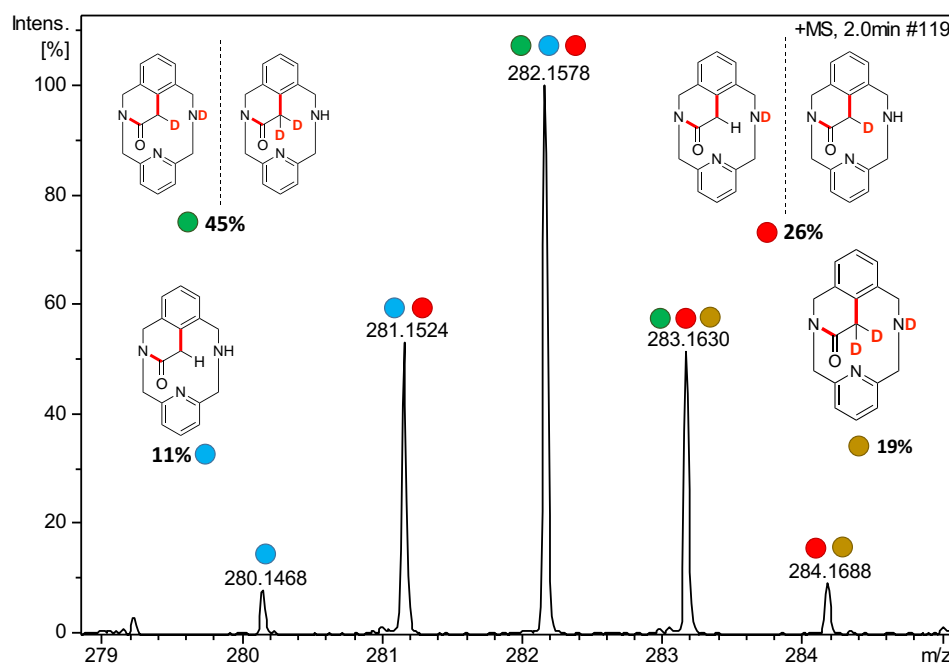


Figure S39. HRMS-ESI-QTOF of $[\text{D}]_n\text{-3}$ obtained after reaction of $\mathbf{2a-OAc}$ with EDA and D_2O (4.0 equiv.) in TFE-d_3 . Mass analysis shows 75% D incorporation in agreement with ^1H -NMR (Figure S14). Deuterium incorporation was measured by the relative intensity of the peaks in the mass spectrum corresponding to the deuterated and non-deuterated products.

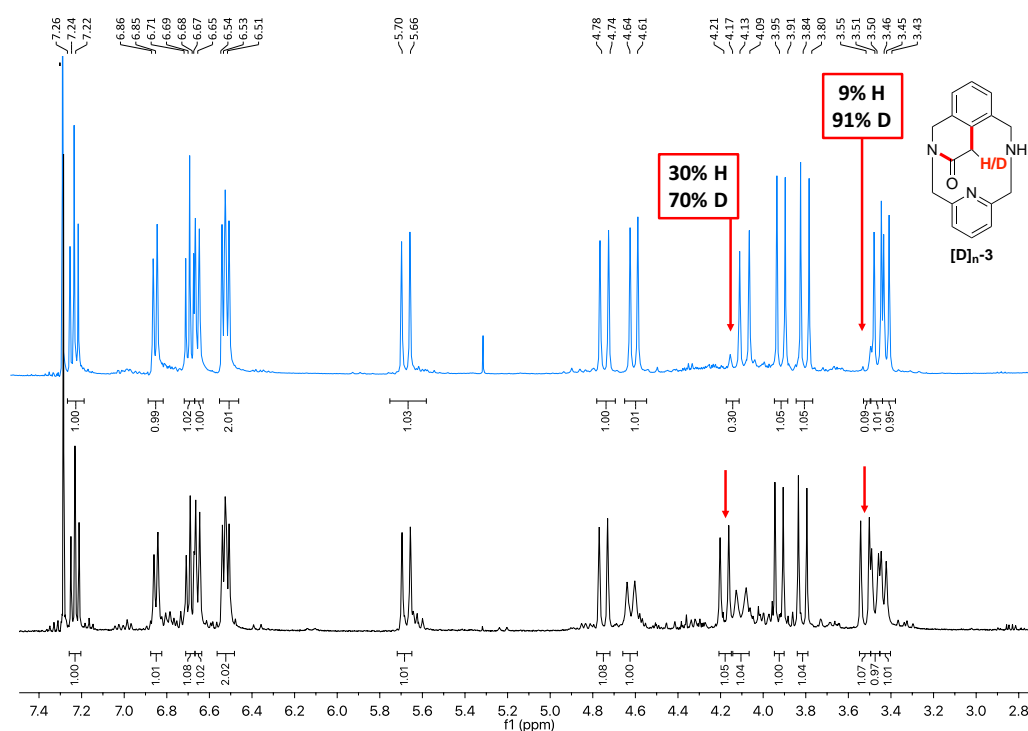


Figure S40. ^1H NMR spectrum of $[\text{D}]_n\text{-3}$ (up, blue) and **3** (down, black) recorded at 298 K using CDCl_3 as solvent. 91% of D-incorporation from TFE- d_3 (4.0 equiv.) using LiOTf as additive. 70% of D incorporation due to D-exchange of the acidic proton of EDA can also be observed.

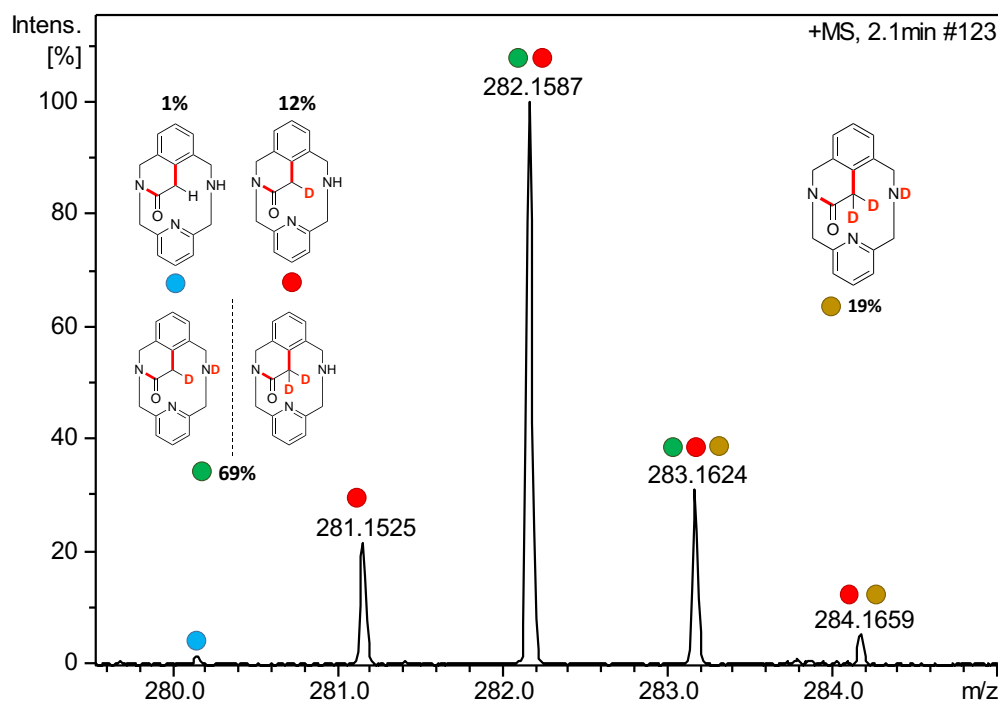


Figure S41. HRMS-ESI-QTOF of $[\text{D}]_n\text{-3}$ obtained after reaction of **2a-OAc** with EDA and Li(OTf) (1.0 equiv.) in TFE- d_3 . Mass analysis shows 99% D incorporation in agreement with ^1H -NMR (Figure S16). Deuterium incorporation was measured by the relative intensity of the peaks in the mass spectrum corresponding to the deuterated and non-deuterated products.

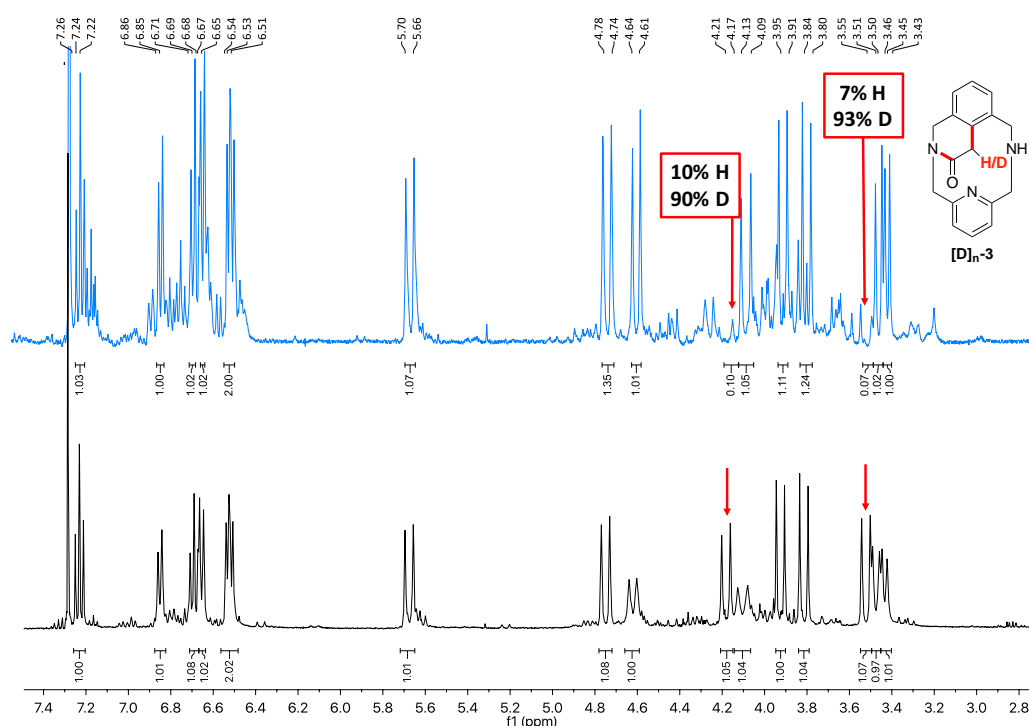


Figure S42. ^1H NMR spectrum of $[\text{D}]_n\text{-3}$ (up, blue) and 3 (down, black) recorded at 298K using CDCl_3 as solvent. 91% of D-incorporation from MeOD-d_4 using LiOTf (1.0 equiv.) as additive. 90% of D incorporation due to D-exchange of the acidic proton of EDA can also be observed.

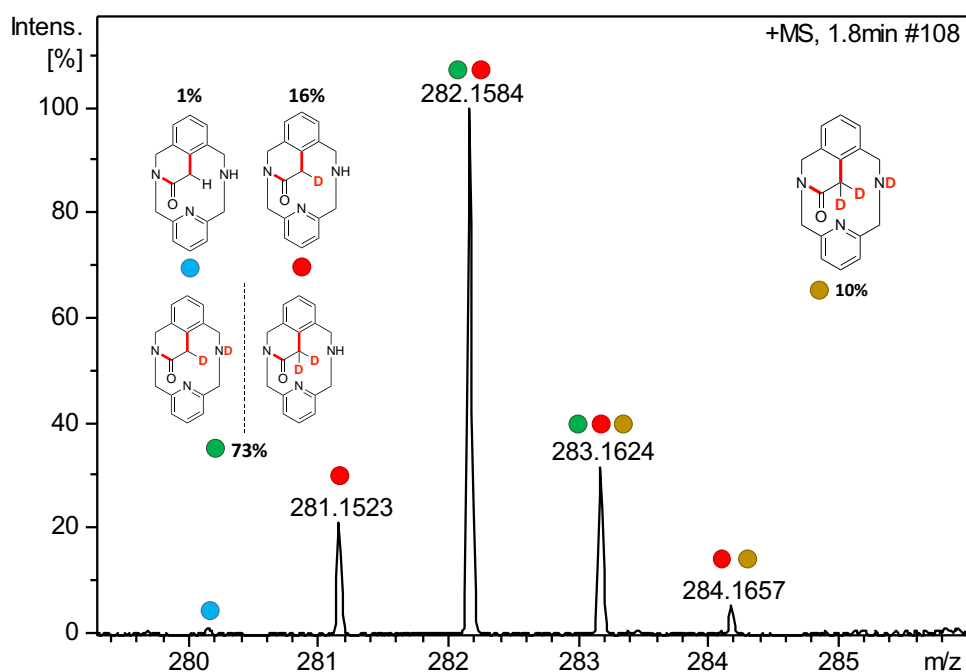
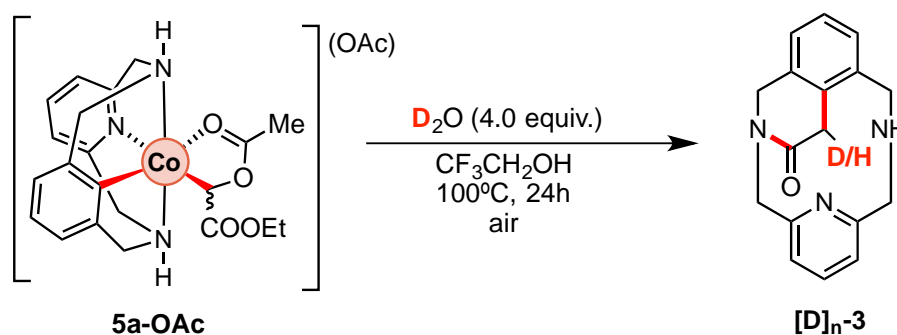


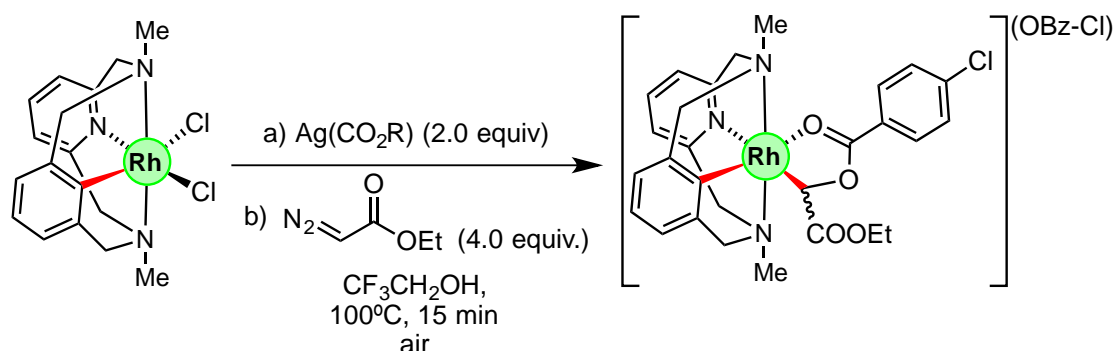
Figure S43. HRMS-ESI-QTOF of $[\text{D}]_n\text{-3}$ obtained after reaction of 2a-OAc with EDA and $\text{Li}(\text{OTf})$ (1.0 equiv.) in MeOD-d_4 . Mass analysis shows 99% D incorporation in agreement with ^1H -NMR (Figure S16). Deuterium incorporation was measured by the relative intensity of the peaks in the mass spectrum corresponding to the deuterated and non-deuterated products.

8.2 D-incorporation starting from **5a-OAc**

Scheme S19. D-incorporation reaction of **5a-OAc** to furnish **[D]_n-3** using D_2O as proton source.

In a 2 mL vial, **5a-OAc** (0.029 mmol), and D_2O (2.1 μ l, 4.0 equiv.) were mixed in TFE (1.5 mL). The vial was then sealed with a septum and the mixture was stirred under air over 24h at $100^\circ C$. Then, after removal of the solvent, NH_4OH (2 mL) was added and the solution was extracted using CH_2Cl_2 (2x5mL). Then, products were purified using silica gel chromatography (CH_2Cl_2 , then $CH_2Cl_2/MeOH$ 90:10) and analyzed by NMR spectroscopy. Cyclic amide was obtained in 87% yield with **33% D-incorporation** (67% H-3) in accordance with experiments starting from **2a-OAc** (Figures S3-4).

9. Reactivity of Rh-analogue complex with EDA

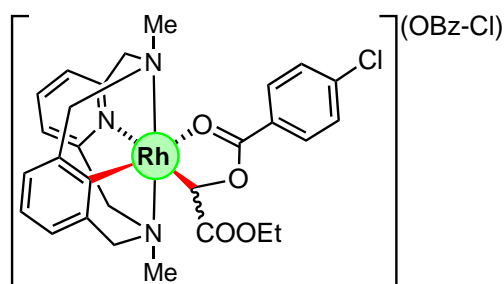


Scheme S20. Stoichiometric reaction of **6b-Cl** with EDA to furnish intermediate species **7b-OBz-Cl** in presence of $\text{Ag}(\text{OBz-Cl})$.

In a 2 mL vial, **6b-Cl** (0.058 mmol) and $\text{Ag}(\text{OBz-Cl})$ (2.0 equiv.) were mixed in TFE and heated over 15 min at 100°C . Then, the mixture was filtered and EDA (2.0 equiv.) was added. The vial was then sealed with a septum and the mixture was stirred under air over 15 min at 100°C . After reaction completion, crude mixture was analyzed by HRMS and reaction intermediates were detected as major products. Then, recrystallization with CHCl_3 layered with pentane yielded a white foam corresponding to the organometallic complex **7b-OBz-Cl**, which was characterized by NMR.

$[\mathbf{1b-Rh}^{\text{II}}(\text{EDA-OBz-Cl})](\text{OBz-Cl}) - (\mathbf{7b-OBz-Cl})$

White foam (97% yield, 38.6 mg, 0.056 mmol). $^1\text{H NMR}$ (400 MHz, CDCl_3 , ppm) δ 7.88



(d, $^3J_{\text{H}} = 8.2$ Hz, 2H), 7.81 (d, $^3J_{\text{H}} = 8.1$ Hz, 2H), 7.46 (t, $^3J_{\text{H}} = 7.8$ Hz, 1H), 7.25 (d, $^3J_{\text{H}} = 8.6$ Hz, 2H), 7.17 (d, $^3J_{\text{H}} = 8.5$ Hz, 1H), 6.98 (d, $^3J_{\text{H}} = 7.8$ Hz, 1H), 6.94 (d, $^3J_{\text{H}} = 7.8$ Hz, 1H), 6.75 (d, $^3J_{\text{H}} = 4.1$ Hz, 1H), 6.63 (d, $^3J_{\text{H}} = 7.0$ Hz, 1H), 6.59 (d, $^3J_{\text{H}} = 6.8$ Hz, 1H), 6.51 (d, $^3J_{\text{H}} = 6.9$ Hz, 1H), 5.46 (d, $^2J_{\text{H}} = 15.1$ Hz, 1H), 4.95 (d, $^2J_{\text{H}} = 14.8$ Hz, 1H), 4.82 (d, $^2J_{\text{H}} = 15.3$ Hz, 1H), 4.50 (d, $^2J_{\text{H}} = 14.9$ Hz, 1H), 3.83 (m, 3H), 3.70 (d, $^2J_{\text{H}} = 15.8$ Hz, 1H), 3.27 (s, 3H), 3.26 (s, 3H), 3.05 (m, 1H), 0.90 (t, $^3J_{\text{H}} = 7.4$ Hz, 3H). $^{13}\text{C} \{^1\text{H}\}$ NMR (100 MHz, CDCl_3 , ppm) δ 178.7, 171.4, 169.4 (d), 165.5, 157.4, 156.6, 141.9, 141.5, 138.0, 137.2, 136.5, 135.4, 130.8, 130.7, 128.2, 127.4, 121.4, 119.2, 119.0, 118.9, 118.7, 75.7, 75.2, 75.1, 67.9 (d), 58.8, 53.3, 52.3, 22.4, 14.0. **HRMS** (ESI) calcd. for $\text{C}_{28}\text{H}_{30}\text{RhClN}_3\text{O}_4^+$ $[\text{M}(\text{OBz-Cl})]^+$: 610.0980; found: 610.0988. **IR** (ATR): $\bar{\nu} = 2981, 1689, 1599, 1559, 1374, 1286, 1167, 1087, 1038, 844, 772, 750, 520$ cm^{-1} . **EA**: $\text{C}_{35}\text{H}_{35}\text{RhCl}_2\text{N}_3\text{O}_6 \cdot (\text{H}_2\text{O})_2$ calcd. C 52.32, N 5.23, H 4.89 %; exp. C 52.30, N 5.43, H 4.69 %.

10. Crystallographic Data Information

10.1 X-Ray structure of 5a-OBz-Cl

Orange crystals of $(C_{26}H_{26}CoN_3O_4)_2(C_7H_4O_2Cl)_2$, were grown from slow diffusion of pentane in a $CHCl_3$ solution of the compound, and used for low temperature (100(2) K) X-ray structure determination. The measurement was carried out on a *BRUKER SMART APEX CCD* diffractometer using graphite-monochromated Mo $K\alpha$ radiation ($\lambda = 0.71073 \text{ \AA}$) from an x-Ray Tube. The measurements were made in the range 1.484 to 27.497° for θ . Hemi-sphere data collection was carried out with ω and ϕ scans. A total of 14193 reflections were collected of which 8954 [$R(\text{int}) = 0.0434$] were unique. Programs used: data collection, Smart¹⁹; data reduction, Saint+²⁰; absorption correction, SADABS²¹. Structure solution and refinement was done using SHELXTL²². The structure was solved by direct methods and refined by full-matrix least-squares methods on F^2 . The non-hydrogen atoms were refined anisotropically. The H-atoms were placed in geometrically optimized positions and forced to ride on the atom to which they are attached. A considerable amount of electron density attributable to a disordered $CHCl_3$ solvent molecule per asymmetric unit was removed with the SQUEEZE option of PLATON.²³

Table S19. Crystallographic parameters for 5a-OBz-Cl.

Chemical formula	$C_{41}H_{35}Cl_6N_3CoO_8$
fw (g mol⁻¹)	969.4
T (K)	100 (2)
Space group	Triclinic, P-1
a (Å)	11.329(3)
b (Å)	13.762(3)
c (Å)	14.051(3)
α (deg.)	85.705(5)
β (deg.)	71.336(4)
γ (deg.)	88.624(4)
V (Å³)	2069.6(8)
$\rho_{\text{calcd.}}$ (g cm⁻³)	1.555
λ (Å)	0.71073
R₁ [$I > 2\sigma(I)$]	0.0640
wR₂ [$I > 2\sigma(I)$]	0.0.1340

10.2 X-Ray structure of **5a-OBz-OMe**

Orange crystals of $(C_{26}H_{28}CoN_3O_5)(C_8H_7O_3)_2$, were grown from slow diffusion of pentane in a $CHCl_3$ solution of the compound, and used for low temperature (100(2) K) X-ray structure determination. The measurement was carried out on a *BRUKER SMART APEX CCD* diffractometer using graphite-monochromated Mo $K\alpha$ radiation ($\lambda = 0.71073 \text{ \AA}$) from an x-Ray Tube. The measurements were made in the range 2.254 to 28.610° for θ . Hemi-sphere data collection was carried out with ω and ϕ scans. A total of 33374 reflections were collected of which 10459 [$R(\text{int}) = 0.1788$] were unique. Programs used: data collection, Smart¹⁹; data reduction, Saint+²⁰; absorption correction, SADABS²¹. Structure solution and refinement was done using SHELXTL²². The structure was solved by direct methods and refined by full-matrix least-squares methods on F^2 . The non-hydrogen atoms were refined anisotropically. The H-atoms were placed in geometrically optimized positions and forced to ride on the atom to which they are attached. A considerable amount of electron density attributable to disordered solvent molecules which could not be properly identified was removed with the SQUEEZE option of PLATON.²³

Table S20. Crystallographic parameters for **5a-OBz-OMe**.

Chemical formula	$C_{43}H_{43}CoN_3O_{11}$
fw (g mol⁻¹)	836.73
T (K)	100 (2)
Space group	Triclinic, P-1
a (Å)	11.440(8)
b (Å)	14.002(9)
c (Å)	14.246(10)
α (deg.)	87.644(14)
β (deg.)	83.554(12)
γ (deg.)	71.092(10)
V (Å³)	2145(2)
$\rho_{\text{calcd.}}$ (g cm⁻³)	1.295
λ (Å)	0.71073
R₁ [$I > 2\sigma(I)$]	0.1319
wR₂ [$I > 2\sigma(I)$]	0.3499

12. Additional DFT information

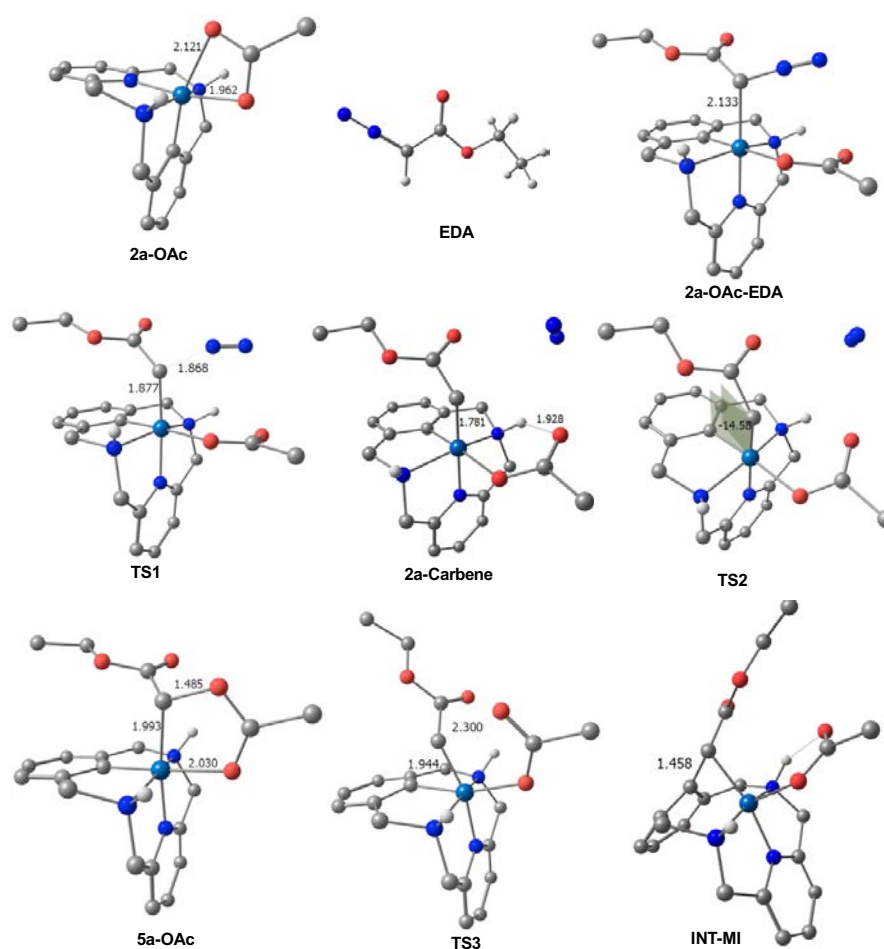


Figure S44. Geometry of the optimized structures for the profile of the reaction (Figure 4) computed at BP86/Def2TZVP level of theory. The following color code illustrates the kind of atoms in the figure: Carbon, Nitrogen, Oxygen, Hydrogen, Cobalt, Lithium. Most of hydrogens have been omitted for clarity.

We choose BP86 as the functional to optimize geometries because it describes better the Co(III)-C bond distances than B3LYP²⁴⁻²⁶, which overestimates those distances. However, to describe the energy values we performed single point energy (SPE) calculations at the B3LYP level. Furthermore, we optimized the geometries with another functional (M06-L) to compare the consistency of our results (See Figure S12). At the M06-L level, all our attempts to localize the carbene species end up in the species **5a-OAc**, which leads to conclude that at this level of theory the **2a-carbene** is not an intermediate. At this point it is important to remark that the fact that we were able to obtain the optimized **2a-carbene** with the BP86 functional is not in disagreement with the previously stated because the barrier to pass from carbene to **5a-OAc** (TS2) is very small (only 0.8 kcal mol⁻¹).

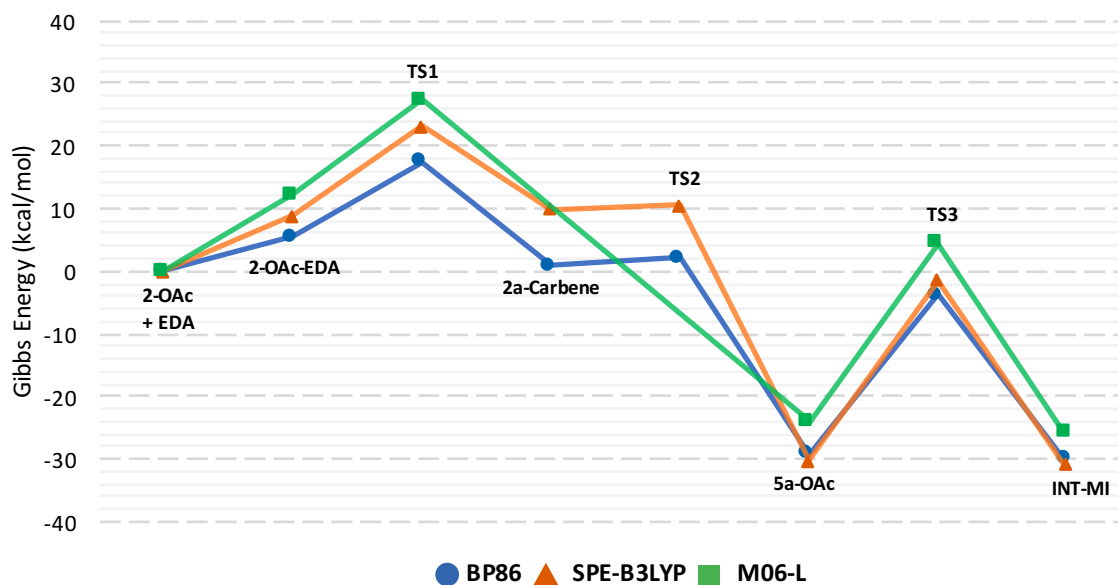


Figure S45. Gibbs Energy profiles described by DFT at three different level of theory (BP86, ML06-l, and B3LYP(SPE)//BP86). All the values are relative Gibbs energies referenced to their corresponding reactants' Gibbs energies at infinite distance (2a-OAc + EDA).

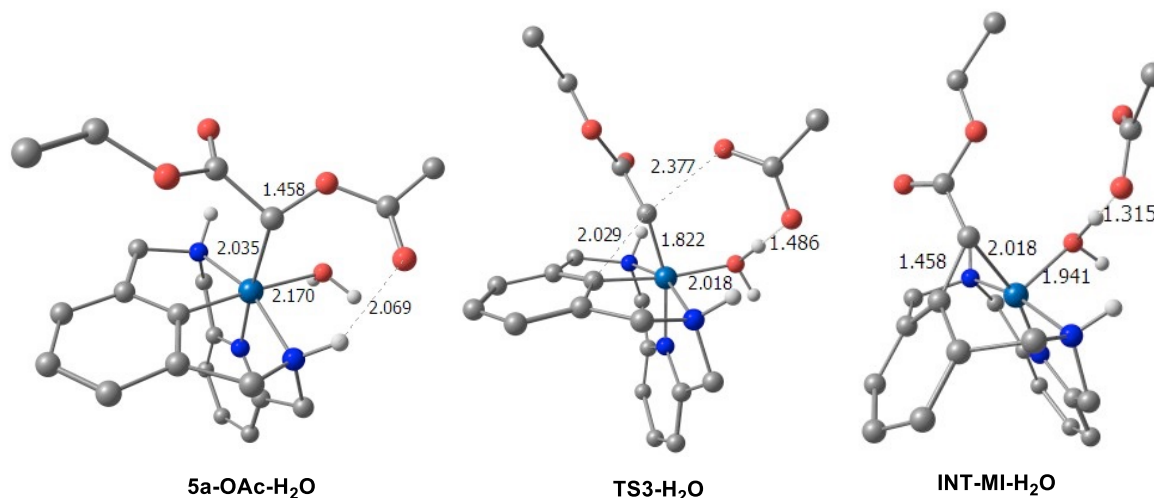


Figure S46. Geometry of the optimized water-coordinated structures computed at BP86/Def2TZVP level of theory. The following color code illustrates the kind of atoms in the figure: Carbon, Nitrogen, Oxygen, Hydrogen, Cobalt. Most of hydrogens have been omitted for clarity.

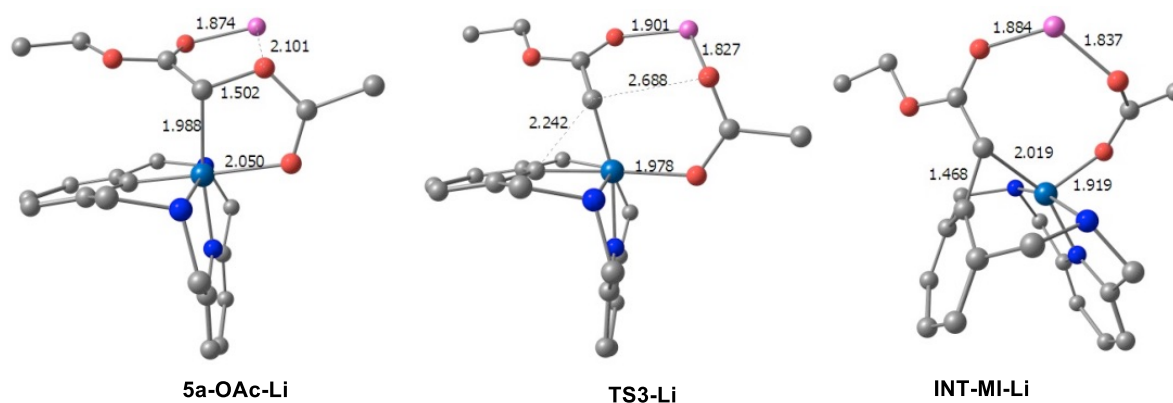


Figure S47. Geometry of the optimized structures coordinated to Lithium cation (Li^+) computed at BP86/Def2TZVP level of theory. The following color code illustrates the kind of atoms in the figure: Carbon, Nitrogen, Oxygen, Hydrogen, Cobalt, Lithium. Most of hydrogens have been omitted for clarity.

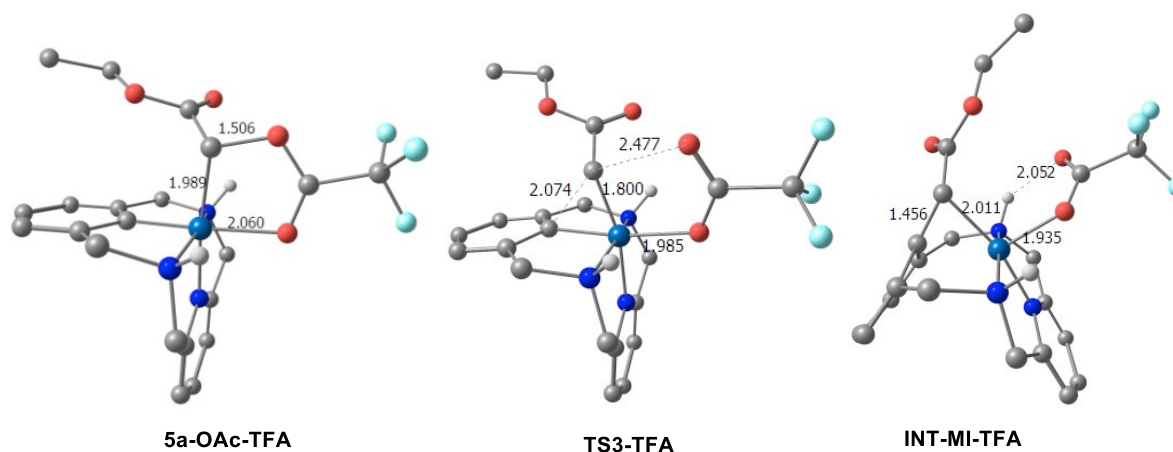
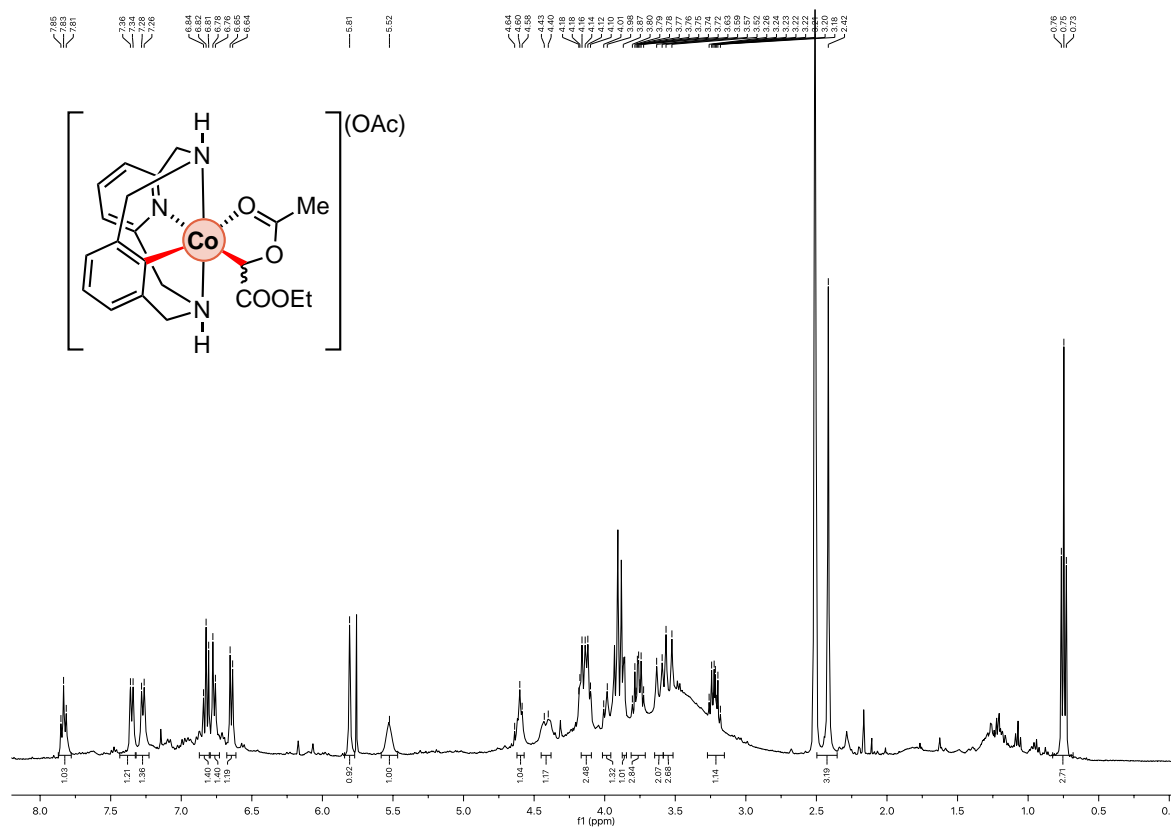
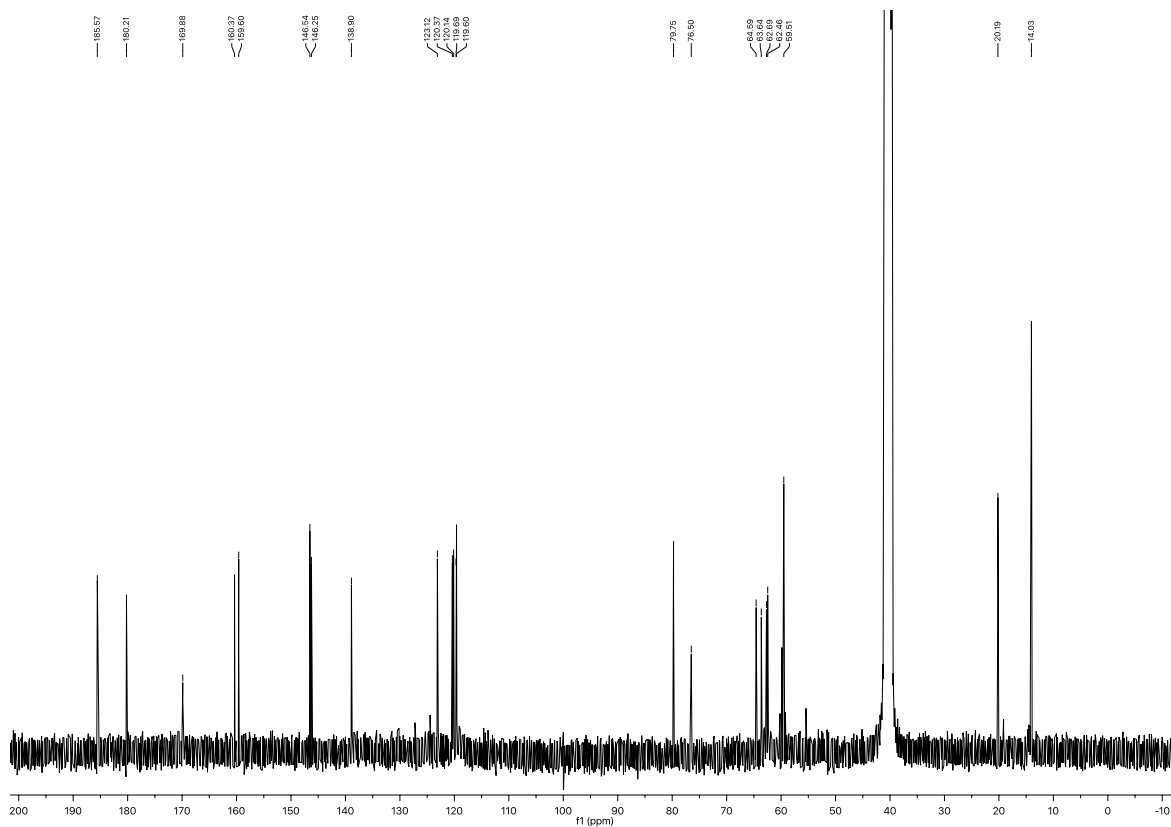


Figure S48. Geometry of the optimized TFA-complexes computed at BP86/Def2TZVP level of theory. The following color code illustrates the kind of atoms in the figure: Carbon, Nitrogen, Oxygen, Hydrogen, Cobalt, Fluorine. Most of hydrogens have been omitted for clarity.

13. References

- (1) Wong, V. H. L.; Vummaleti, S. V. C.; Cavallo, L.; White, A.; Nolan S. P.; Hii, K. K. *Chem. Eur. J.* **2016**, *22*, 13320.
- (2) Ravel, B.; Newville, M. *J. Synchrotron Rad.* **2005**, *12*, 537.
- (3) Newville, M. *J. Synchrotron Rad.* **2001**, *8*, 96.
- (4) Rehr, J. J.; Albers, R. C. *Rev. Mod. Phys.* **2000**, *72*, 621.
- (5) Martin-Diaconescu, V.; Bellucci, M.; Musiani, F.; Ciurli, S.; Maroney, M. J. *J. Biol. Inorg. Chem.* **2012**, *17*, 353.
- (6) Zambelli, B.; Berardi, A.; Martin-Diaconescu, V.; Mazzei, L.; Musiani, F.; Maroney M. J.; Ciurli, S. *J. Biol. Inorg. Chem.* **2014**, *19*, 319.
- (7) Gaussian 09, Revision D.01, Frisch, M. J.; Trucks, G. W.; Schlegel, H. B.; Scuseria, G. E.; Robb, M. A.; Cheeseman, J. R.; Scalmani, G.; Barone, V.; Mennucci, B.; Petersson, G. A.; Nakatsuji, H.; Caricato, M.; Li, X.; Hratchian, H. P.; Izmaylov, A. F.; Bloino, J.; Zheng, G.; Dapprich, S.; Daniels, A. D.; Farkas, Ö.; Foresman, J. B.; Ortiz, J. V.; Cioslowski, J.; Fox, D. J. et al. Gaussian, Inc., Wallingford CT, **2013**.
- (8) Becke, A. D. *Phys. Rev. A* **1988**, *38*, 3098.
- (9) Perdew, J. P. *Phys. Rev. B* **1986**, *33*, 8822.
- (10) Weigend, F.; Ahlrichs, R.; Peterson, K. A.; Dunning, T. H.; Pitzer, R. M.; Bergner, A. *Phys. Chem. Chem. Phys.* **2005**, *7*, 3297.
- (11) Weigend, F.; Hättig, C.; Patzelt, H.; Ahlrichs, R.; Spencer, S.; Willems, A. *Phys. Chem. Chem. Phys.* **2006**, *8*, 1057.
- (12) Grimme, S.; Antony, J.; Ehrlich, S.; Krieg, H. *J. Chem. Phys.* **2010**, *132*, 154104.
- (13) Marenich, A. V.; Cramer, C. J.; Truhlar, D. G. *J. Phys. Chem. B* **2009**, *113*, 6378.
- (14) Becke, A. D. *J. Chem. Phys.* **1993**, *98*, 1372.
- (15) Lee, C.; Yang, W.; Parr, R. G. *Phys. Rev. B* **1988**, *37*, 785.
- (16) Vosko, S. H.; Wilk, L.; Nusair, M. *Can. J. Phys.* **1980**, *58*, 1200.
- (17) Stephens, P. J.; Devlin, F. J.; Chabalowski, C. F.; Frisch, M. J. *J. Phys. Chem.* **1994**, *98*, 11623.
- (18) Planas, O.; Whiteoak, C. J.; Martin-Diaconescu, V.; Gamba, I.; Luis, J. M.; Parella, T.; Company, A.; Ribas, X. *J. Am. Chem. Soc.* **2016**, *138*, 14388.
- (19) Bruker Advanced X-ray Solutions. SMART: Version 5.631, **1997-2002**.
- (20) Bruker Advanced X-ray Solutions. SAINT +, Version 6.36A, **2001**.
- (21) Sheldrick, G. M. Empirical Absorption Correction Program, Universität Göttingen, 1996. Bruker Advanced X-ray Solutions. SADABS Version 2.10, **2001**.
- (22) Sheldrick, G. M. Program for Crystal Structure Refinement, Universität Göttingen, 1997. Bruker Advanced X-ray Solutions. SHELXTL Version 6.14, **2000-2003**. SHELXL-2014/7 (Sheldrick, 2014)
- (23) Spek, A. L. *Acta Cryst.* **2009**, *D65*, 148. PLATON, A Multipurpose Crystallographic Tool, Utrecht University, Utrecht, The Netherlands
- (24) Dzik, W. I.; Xu, X.; Zhang, X. P.; Reek, J. N. H.; Bruin, B. De. *J. Am. Chem. Soc.* **2010**, *132*, 10891.
- (25) Kuta, J.; Patchkovskii, S.; Zgierski, M. Z.; Kozłowski, P. M. *J. Comput. Chem.* **2006**, *27*, 1429.
- (26) Qi, X.-J.; Li, Z.; Fu, Y.; Guo, Q.-X.; Liu, L. *Organometallics* **2008**, *27*, 2688.

14. Selected Original NMR spectra

Figure S49. 400 MHz ^1H NMR spectrum of 5a-OAc in DMSO- d_6 , 298 K.Figure S50. 100 MHz ^{13}C $\{^1\text{H}\}$ NMR spectrum of 5a-OAc in DMSO- d_6 , 298 K.

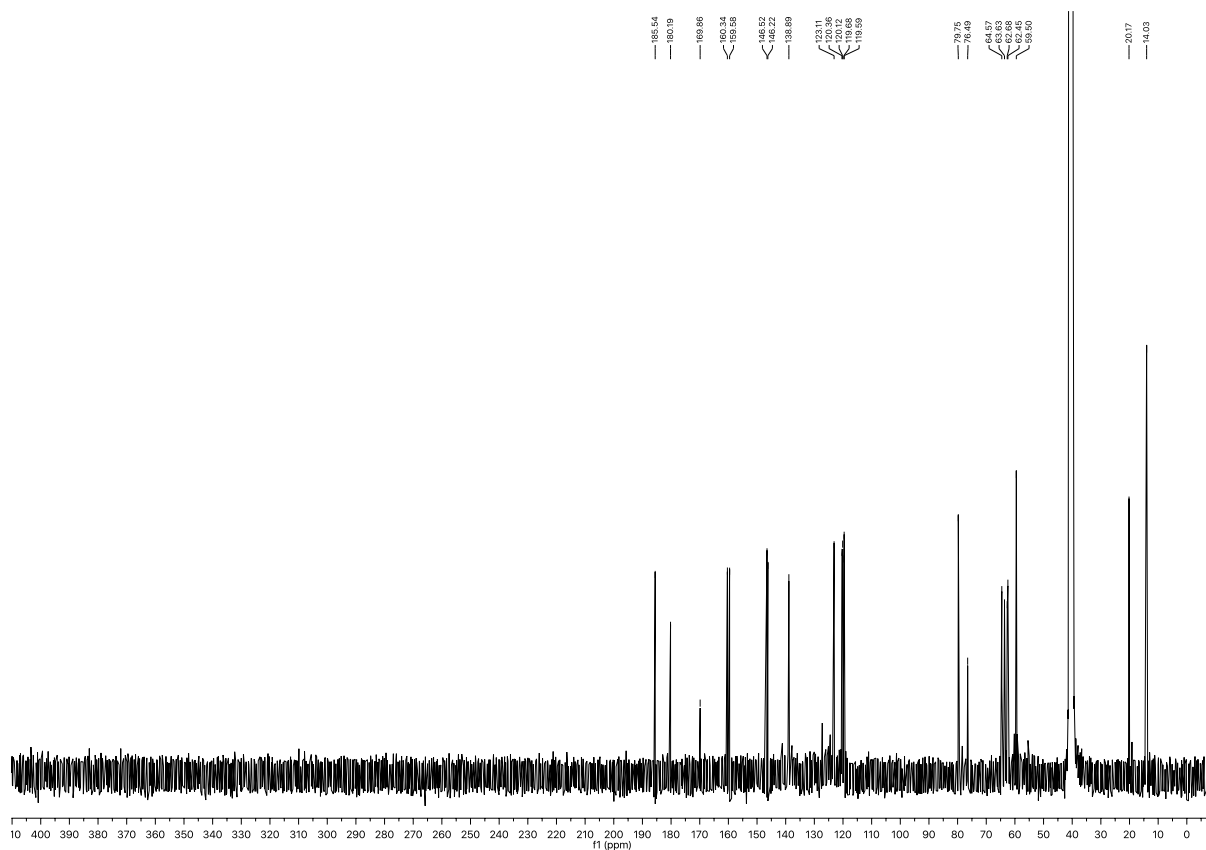


Figure S51. 100 MHz ^{13}C { ^1H } NMR spectrum (carbene region) of **5a-OAc** in DMSO- d_6 , 298 K.

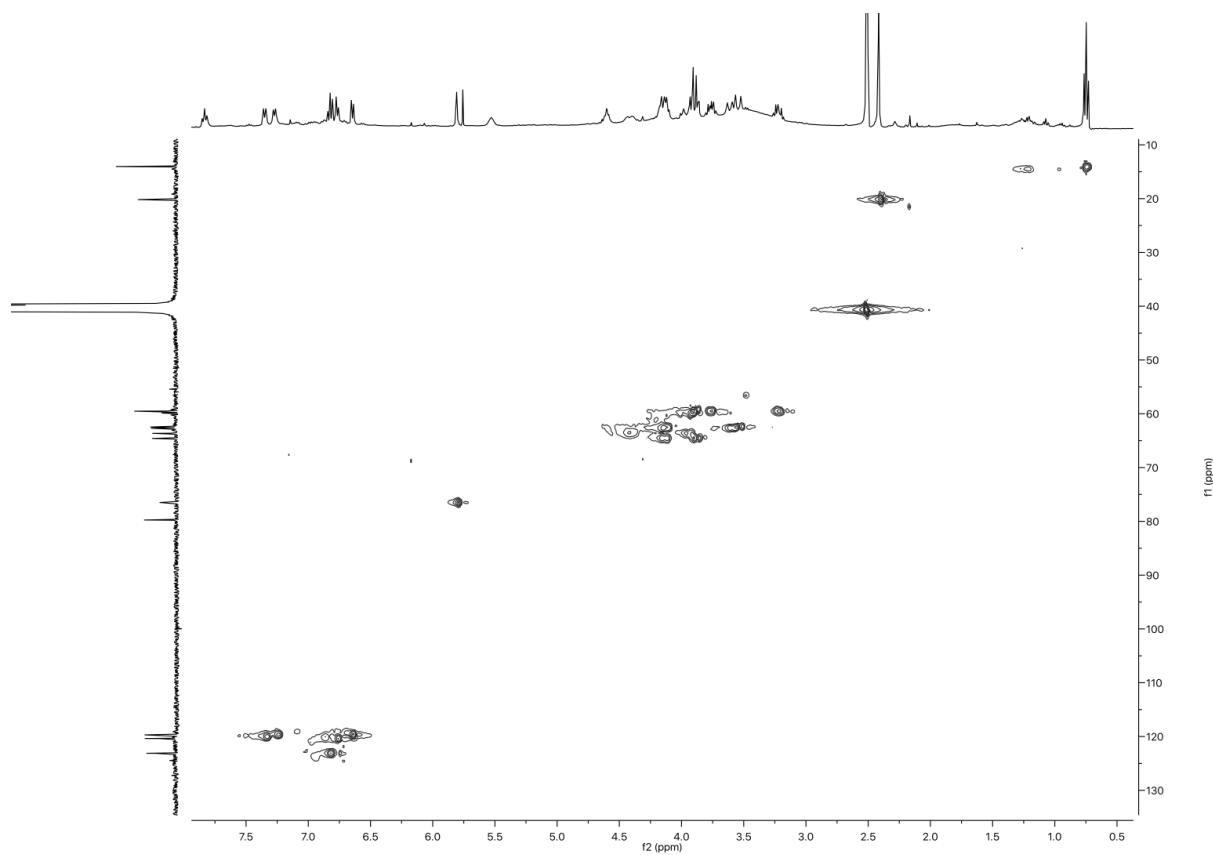


Figure S52. 400 MHz ^1H - ^{13}C HSQC spectrum of **5a-OAc** in DMSO- d_6 , 298 K.

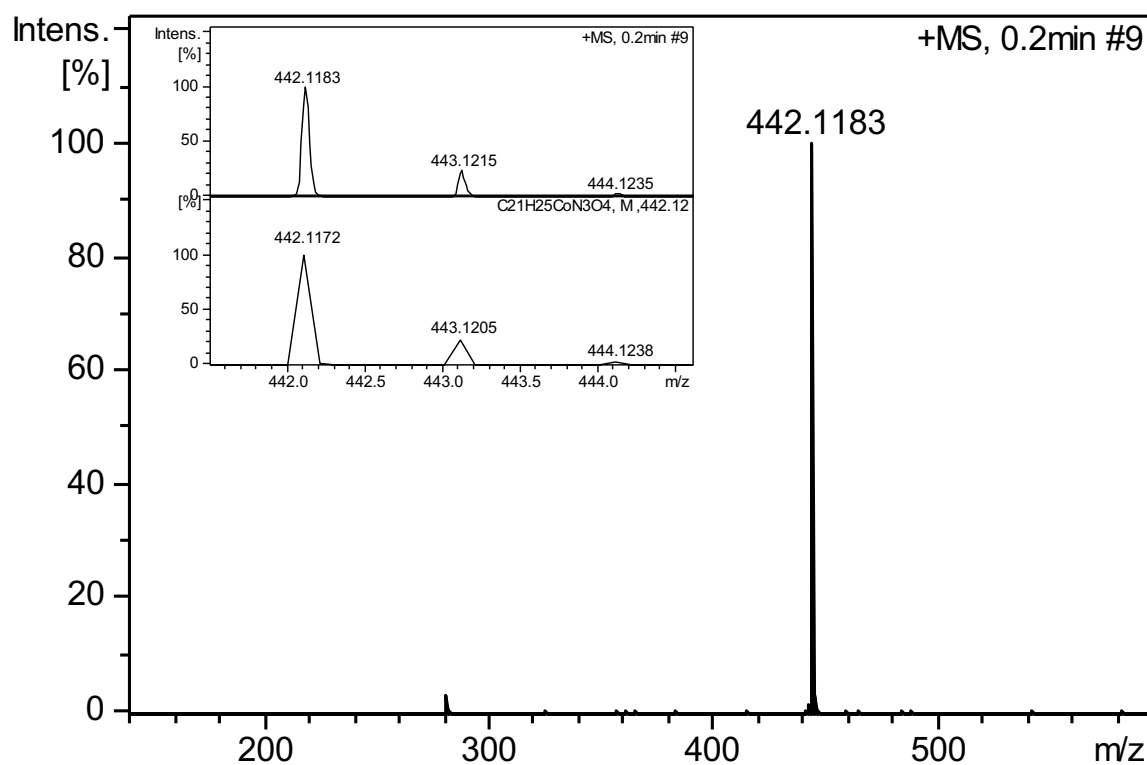


Figure S54. HRMS spectrum of **5a-OAc** showing a peak at $m/z = 442.1183$ Inset: up, experimental spectrum; down, simulated spectrum.

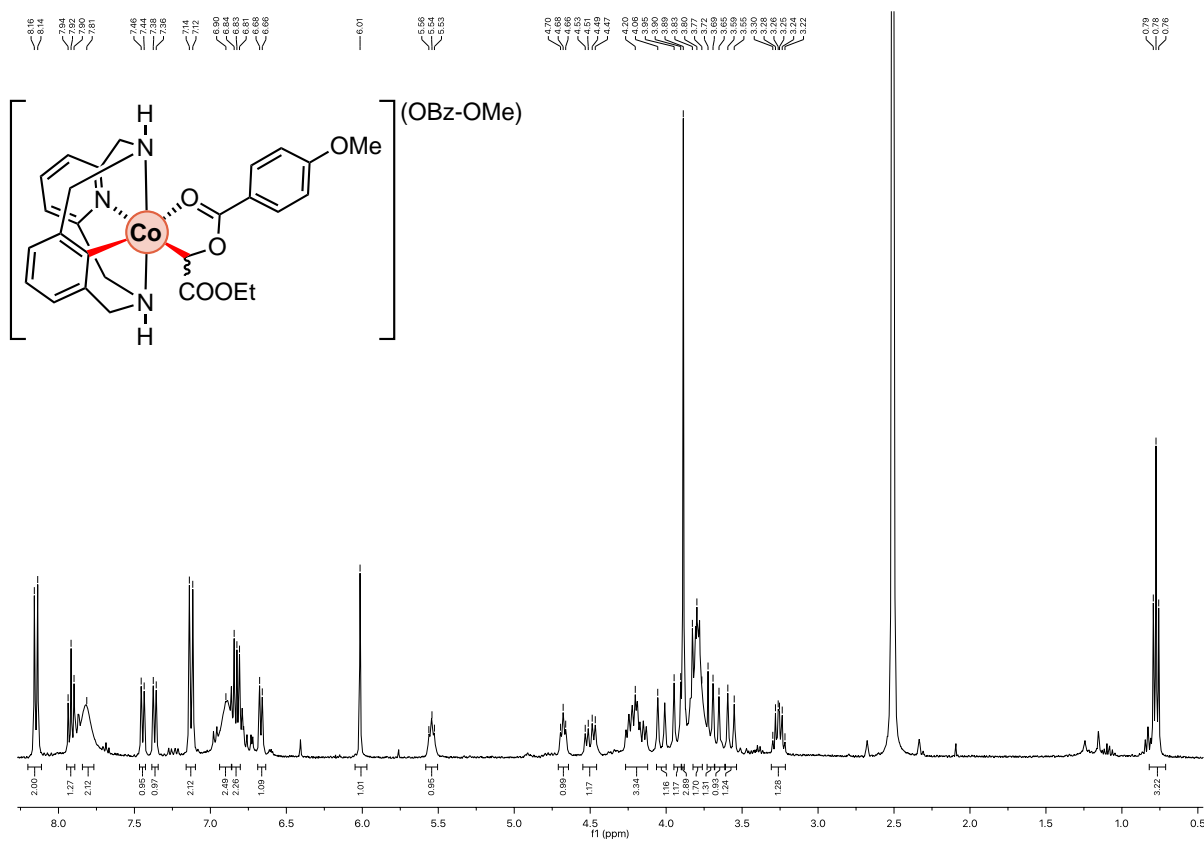


Figure S55. 400 MHz ^1H NMR spectrum of **5a-OBz-OMe** in DMSO-d_6 , 298 K.

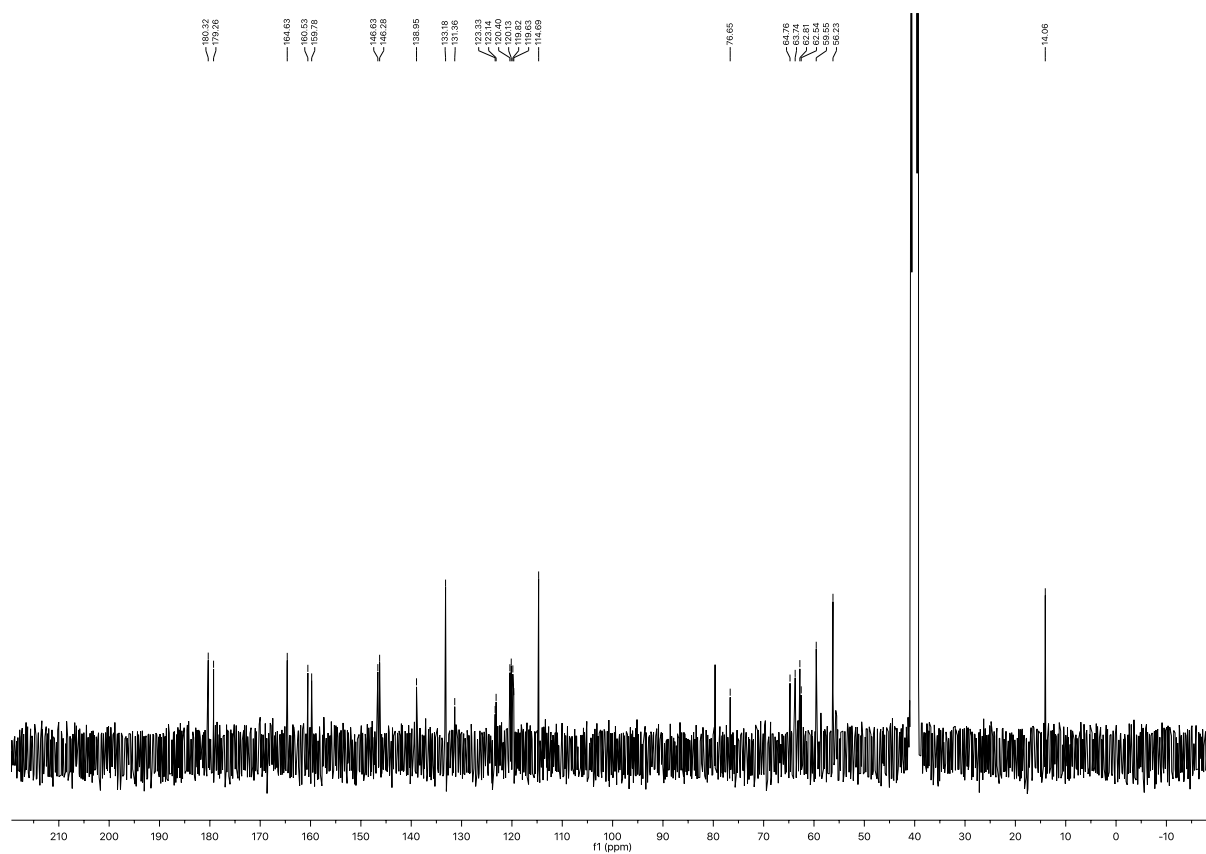


Figure S56. 100 MHz ^{13}C $\{^1\text{H}\}$ NMR spectrum of 5a-OBz-OMe in DMSO- d_6 , 298 K.

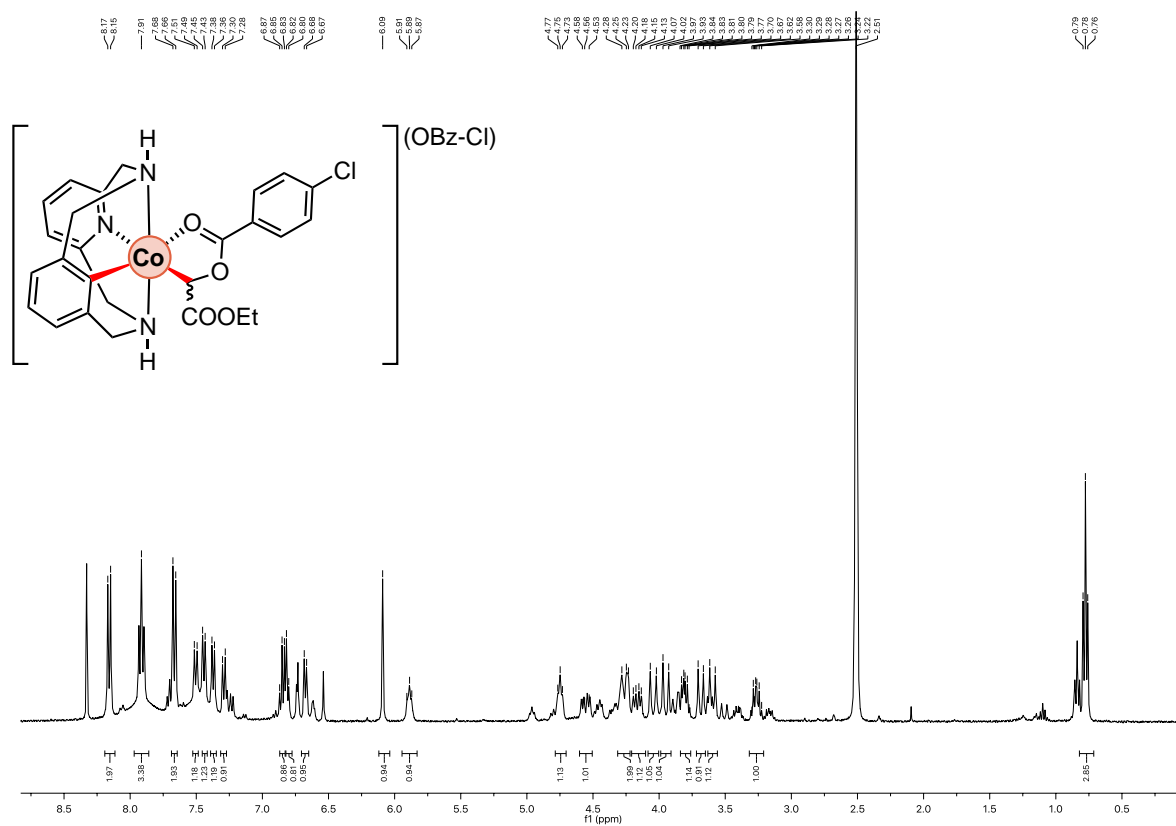


Figure S57. 600 MHz ^1H NMR spectrum of 5a-OBz-Cl in DMSO- d_6 , 298 K. Minor peaks correspond to a conformer in equilibrium with 5a-OBz-Cl.

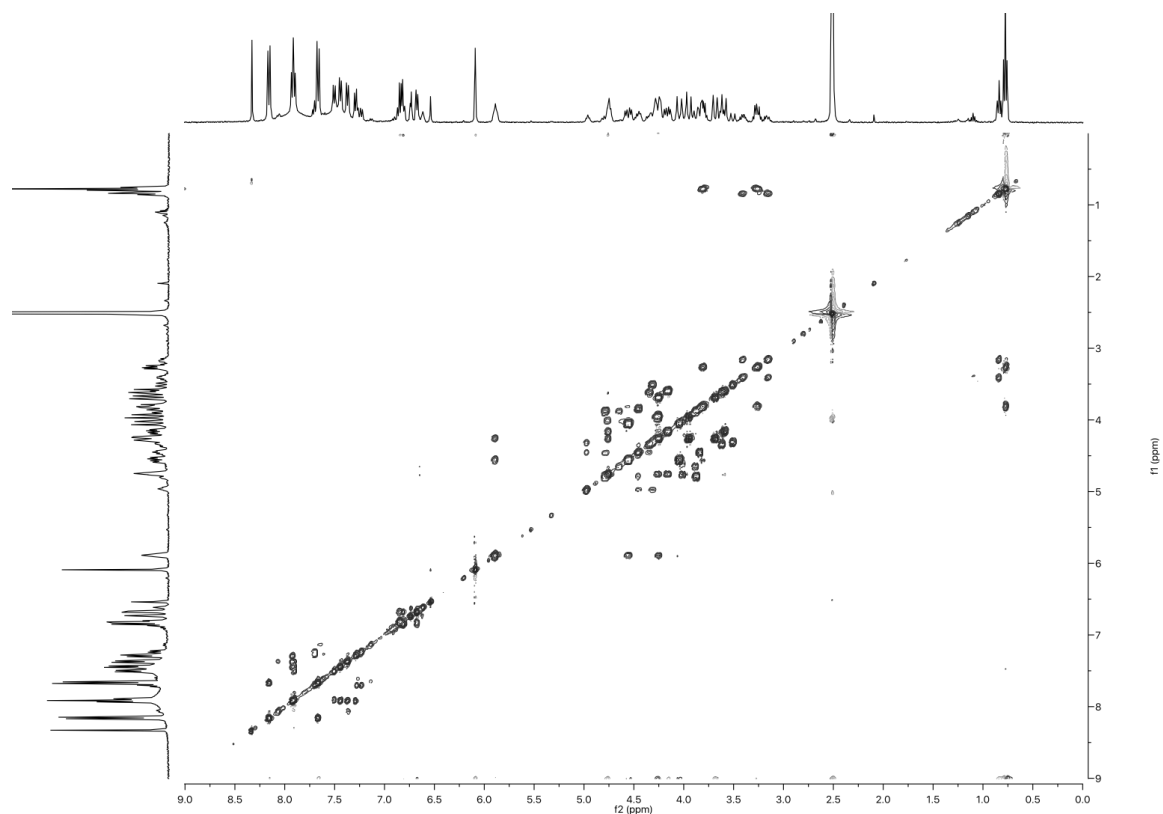


Figure S58. 600 MHz ^1H - ^1H COSY NMR spectrum of **5a-OBz-Cl** in DMSO-d_6 , 298 K. Exchange peaks show a conformer in equilibrium with **5a-OBz-Cl**.

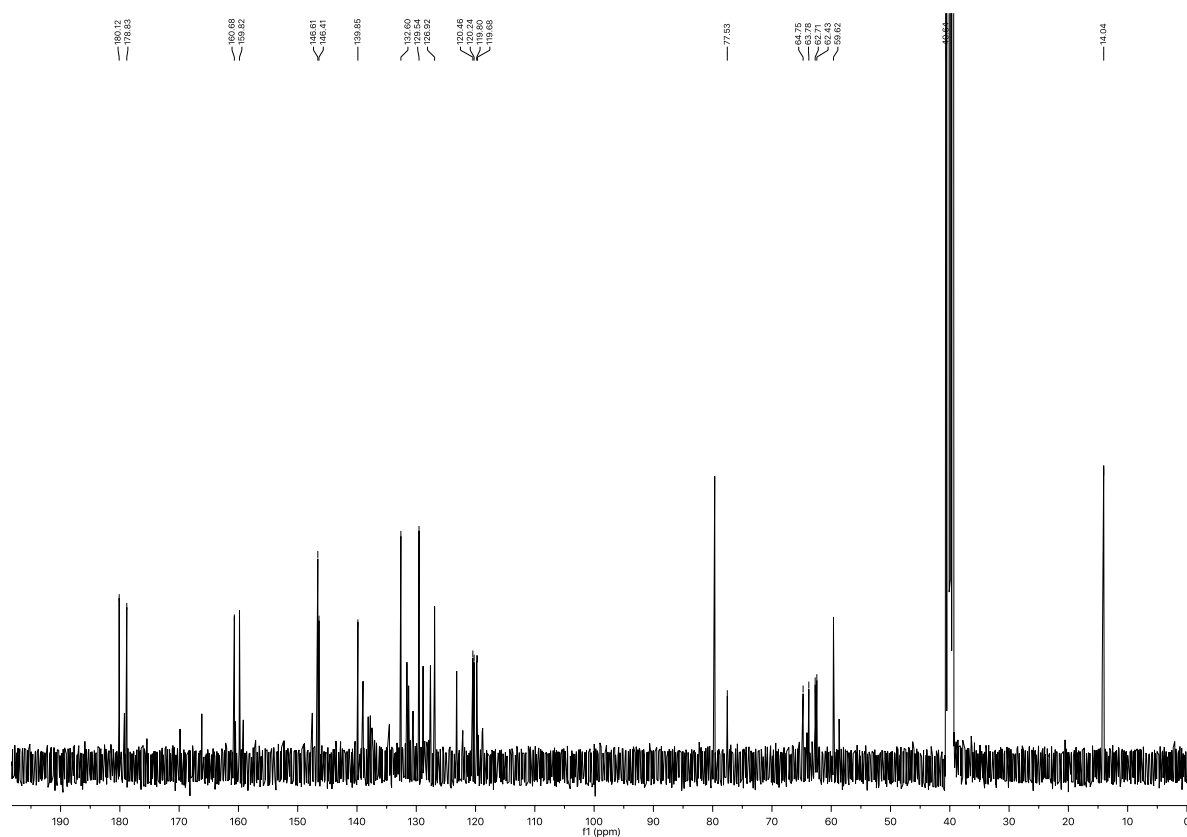


Figure S59. 150 MHz ^{13}C $\{^1\text{H}\}$ NMR spectrum of **5a-OBz-Cl** in DMSO-d_6 , 298 K.

Supporting Information for Chapter V

Regioselective Access to Functionalized Sultam Motifs through Cobalt-Catalyzed Annulation of Aryl Sulfonamides and Alkynes

Oriol Planas, Christopher J. Whiteoak,* Anna Company, Xavi Ribas*

Table of Contents

1. GENERAL CONSIDERATIONS.....	S81
2. COBALT-CATALYZED SULTAM SYNTHESIS	S82
2.1 Optimization of cobalt-catalyzed Sultam synthesis	S82
2.1.1 Solvent screening	S82
2.1.2 Oxidant screening	S82
2.1.3 Base screening.....	S83
2.1.4 Cobalt source screening.....	S83
2.2 Characterization Data for Sultam Products.....	S86
2.2.1 ¹ H and ¹³ C { ¹ H} NMR and mass spectrometry data.....	S86
2.3 Miscellaneous.....	S99
2.3.1 Reaction scale-up.....	S99
2.3.2 Attempted product upgrading.....	S99
2.3.3 Intermolecular competition experiments	101
2.3.4 Deuterium exchange experiments.....	S103
2.3.5 Intermolecular Kinetic Isotope Effect (Scheme VII.12b).....	S107
2.3.6 Reactions in the presence of radical scavengers.....	S107
2.3.7 Crystallographic data information.....	S108
3. REFERENCES.....	S112

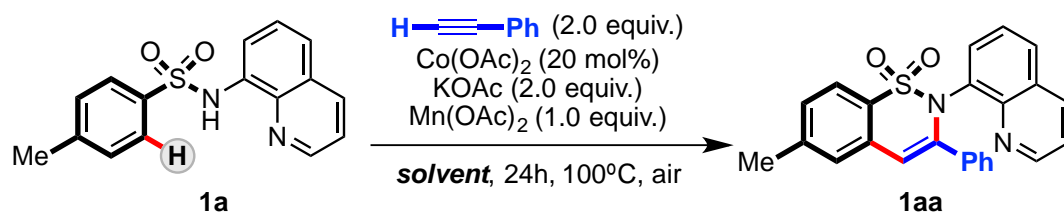
1. General Considerations

All reagents and solvents were purchased from Sigma Aldrich, Fisher Scientific or Fluorochem and used without further purification. Aryl sulfonamide (**2a**) was purchased from Sigma Aldrich. Phenyl Acetylene-D₁ (>95% D) and D₅-benzenesulfonylchloride were prepared according to the previously reported literature protocols.^{1,2} ¹H and ¹³C {¹H} NMR spectra were recorded on Bruker AV-300 or Bruker DPX 400 MHz spectrometers and referenced to the residual deuterated solvent signals. High Resolution Mass Spectra (HRMS) were recorded by the Serveis Tècnics of the University of Girona on a Bruker MicroTOF-Q IITM instrument using an ESI ionization source. IR Spectra (FTIR) were recorded on a FT-IR Alpha spectrometer from Bruker with a PLATINUM-ATR attachment using OPUS software to process the data. Starting aryl sulfonamide substrates were synthesized following reported protocols.³⁻¹¹

2. Cobalt-Catalyzed Sultam Synthesis

2.1 Optimization of cobalt-catalyzed Sultam synthesis

2.1.1 Solvent screening



Scheme S21. Optimization of conditions for the synthesis of cyclic sulfonamides.

General procedure: 50 mg of **1a** (0.17 mmol), Co(OAc)₂ (6.0 mg, 20mol%, 0.034 mmol), KOAc (33.4 mg, 2 equiv., 0.34 mmol), Mn(OAc)₂ (29.4 mg, 1 equiv., 0.17 mmol) and phenylacetylene (**a**) (34.7 mg, 2 equiv., 0.34 mmol) with 2mL solvent were added to a glass vial under air and the vial sealed. The resulting mixture was stirred at 100 °C for 24h and cooled to room temperature. The reaction crude was analysed by ¹H-NMR spectroscopy (CDCl₃) using mesitylene as internal standard.

Table S21. Optimization of solvent used for the synthesis of cyclic sulfonamides.

entry	solvent	yield (%) of 1aa ^[a]
1	DMF	trace
2	Trifluoroethanol (TFE)	22
3	Ethanol	12
4	MeCN	10
5	MeOH	11
6	Toluene	trace

^[a]Yield calculated from ¹H NMR of crude using mesitylene as internal standard

2.1.2 Oxidant screening

The same procedure was applied as described for the solvent screening, except 2 mL of trifluoroethanol was used as solvent and the oxidant was varied.

Table S22. Optimization of oxidant used for the synthesis of cyclic sulfonamides.

entry	oxidant	yield (%) of 1aa ^[a]
1	Mn(OAc) ₂	22
2	Benzoquinone	trace
3	Ag ₂ O	6
4	AgNO ₃	50
5	PhI(OAc) ₂	12
6	Mn(OAc)₃·2H₂O	62
7	O ₂ (atm)	3
8	N ₂ (No oxidant)	trace

^[a]Yield calculated from ¹H NMR of crude using mesitylene as internal standard

2.1.3 Base screening

The same procedure was applied as described for the solvent screening except 2 mL of trifluoroethanol was used as solvent, the oxidant was $\text{Mn}(\text{OAc})_3 \cdot 2\text{H}_2\text{O}$ and the base was varied.

Table S23. Optimization of base used for the synthesis of cyclic sulfonamides.

entry	base	yield (%) of 1aa ^[a]
1	KOAc	68
2	Na_2CO_3	22
3	K_2CO_3	7
4	Cs_2CO_3	4
5	NaOPiv.H₂O	91
6	CsOPiv	78
7	CsOAc	67
8	NaOAc.H ₂ O	69

^[a]Yield calculated from ¹H NMR of crude using mesitylene as internal standard.

2.1.4 Cobalt source screening

The same procedure was applied as described for the solvent screening except 2 mL of trifluoroethanol was used as solvent, the oxidant was $\text{Mn}(\text{OAc})_3 \cdot 2\text{H}_2\text{O}$, the base was NaOPiv.H₂O and the cobalt source was varied.

Table S24. Optimization of cobalt source used for the synthesis of cyclic sulfonamides.

entry	cobalt source	yield (%) of 1aa ^[a]
1	Co(OAc)₂	91
2	CoCl ₂	90
3	CoBr ₂	88
4	$\text{Co}(\text{NO}_3)_2 \cdot 6\text{H}_2\text{O}$	81
5	(Cp) ₂ Co	trace
6	Co(acac) ₂	28
7	Co(acac) ₃	17
8	$\text{Co}(\text{CF}_3\text{SO}_3)_2(\text{CH}_3\text{CN})_2$	31
9	Co(OAc) ₂ ·4H ₂ O	90
10	CoCl ₂ ·6H ₂ O	87

^[a]Yield calculated from ¹H NMR of crude using mesitylene as internal standard.

2.1.5 Catalyst loading and temperature screening

The effect of variation in catalyst loading and reaction temperature was studied using optimized reagents from 3.1.1-3.1.4.

50 mg of **1a** (0.17 mmol), Co(OAc)₂, NaOPiv.H₂O (42.2mg, 2 equiv., 0.34 mmol), Mn(OAc)₃·2H₂O (45.6 mg, 1 equiv., 0.17 mmol) and phenylacetylene (**a**) (34.7 mg, 2 equiv., 0.34 mmol) with 2mL trifluoroethanol were added to a glass vial under air and the vial sealed. The resulting mixture was stirred at the required temperature for 24h

and cooled to room temperature. The reaction crude was analysed by $^1\text{H-NMR}$ spectroscopy (CDCl_3) using mesitylene as internal standard.

Table S25. Optimization of temperature and catalyst loading used for the synthesis of cyclic sulfonamides.

entry	T (°C)	Co(OAc) ₂ (mol%)	yield (%) of 1aa ^[a]	TON
1	100	20	91	4.5
2	100	10	61	6.1
3	100	5	20	4.0
4	50	20	59	3.0
5	50	10	40	4.0
6	50	5	18	3.6
7	rt	20	15	0.8
8	rt	10	9	0.9
9	rt	5	4	0.8

^[a]Yield calculated from $^1\text{H NMR}$ of crude using mesitylene as internal standard.

2.1.6 Time studies

The effect of variation of time was studied using optimized reagents from 3.1.1-3.1.4.

50 mg of **1a** (0.17 mmol), Co(OAc)₂ (6.0 mg, 20 mol%, 0.034 mmol), NaOPiv.H₂O (42.2mg, 2 equiv., 0.34 mmol), Mn(OAc)₃.2H₂O (45.6 mg, 1 equiv., 0.17 mmol) and phenylacetylene (**a**) (34.7 mg, 2 equiv., 0.34 mmol) with 2mL trifluoroethanol were added to a glass vial under air and the vial sealed. The resulting mixture was stirred at 100 °C for the required time and cooled to room temperature. The reaction crude was analysed by $^1\text{H-NMR}$ spectroscopy (CDCl_3) using mesitylene as internal standard.

Table S26. Optimization of time employed for the synthesis of cyclic sulfonamides.

entry	time (h)	yield (%) of 1aa ^[a]
1	2	74
2	4	78
3	6	84
4	8	86
5	16	90
6	24	91

^[a]Yield calculated from $^1\text{H NMR}$ of crude using mesitylene as internal standard.

2.1.7 Effect of atmosphere and oxidant loading studies

The effect of the atmosphere was studied using optimized reagents from 3.1.1-3.1.4.

50 mg of **1a** (0.17 mmol), Co(OAc)₂ (6.0 mg, 20mol%, 0.034 mmol), NaOPiv.H₂O (42.2 mg, 2 equiv., 0.34 mmol), Mn(OAc)₃.2H₂O (45.6 mg, 1 equiv., 0.17 mmol) and 1,2-diphenylacetylene (**g**) (34.7 mg, 2 equiv., 0.34 mmol) with 2mL trifluoroethanol were added to a glass vial under air and the vial sealed. The resulting mixture was stirred at

100 °C for 16 h and cooled to room temperature. The reaction crude was analysed by ¹H-NMR spectroscopy (CDCl₃) using mesitylene as internal standard.

Table S27. Evaluation of the oxidants and their amount employed for the synthesis of

entry	atmosphere	Mn(OAc) ₃ ·2H ₂ O (equiv.)	yield (%) of laa ^[a]
1	air	1.0	79
2 ^[b]	O ₂	1.0	81
3 ^[b]	O ₂	0.5	62
4 ^[c]	N ₂	1.0	38
5 ^[c]	N ₂	2.0	44
6 ^[c]	N ₂	0.5	23
7 ^[c]	N ₂	5.0	66
8 ^[d]	N ₂ O	1.0	56
9 ^[d,e]	N ₂ O	1.0	54

^[a]Yield calculated from ¹H NMR of crude using mesitylene as internal standard ^[b]Trifluoroethanol saturated with O₂. ^[c]Degassed trifluoroethanol used. ^[d]Trifluoroethanol saturated with N₂O. ^[e]Phenylacetylene (a) used as substrate.

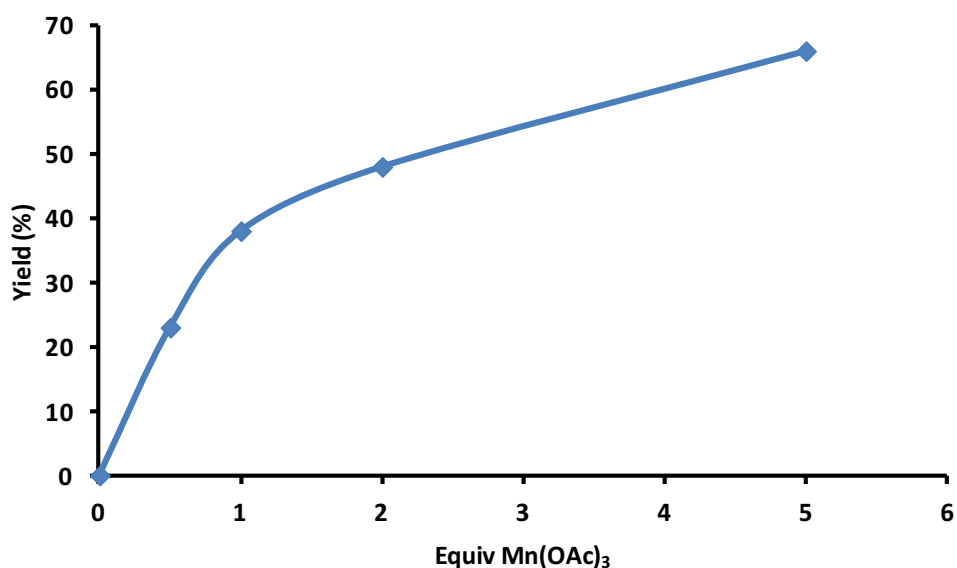
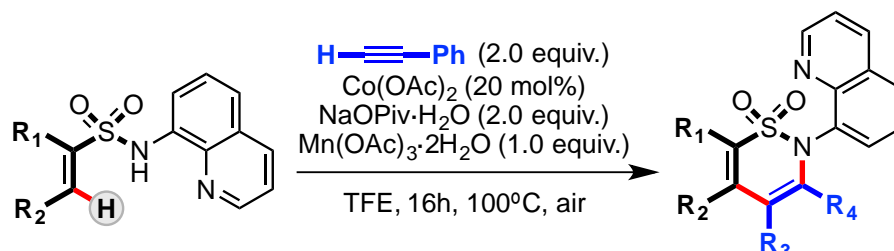


Figure S60. Effect of Mn(OAc)₃·2H₂O loading on yield of Sultam product using N₂ atmosphere.

2.2 Characterization Data for Sultam Products

2.2.1 ^1H and ^{13}C $\{^1\text{H}\}$ NMR and mass spectrometry data

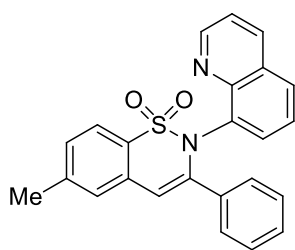
All the Sultam products were synthesized using the optimized reaction conditions from section 3.1:



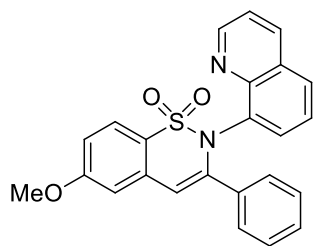
Scheme S22. Cobalt-catalyzed synthesis of cyclic sulfonamides (sultams) with alkynes.

Aryl sulfonamide (**1a-1k**) (0.35 mmol), $\text{Co}(\text{OAc})_2$ (12.4 mg, 20 mol%, 0.07 mmol), $\text{NaOPiv}\cdot\text{H}_2\text{O}$ (86.8 mg, 2 equiv., 0.70 mmol), $\text{Mn}(\text{OAc})_3\cdot 2\text{H}_2\text{O}$ (94.0 mg, 1 equiv., 0.35 mmol), alkyne substrate (**a-s**) (2 equiv., 0.70 mmol) and 2mL trifluoroethanol were added to a glass vial under air and the vial sealed. The resulting mixture was stirred at 100 °C for 16 h and cooled to room temperature. The solvent was removed and the product purified using column chromatography (Silica gel: dichloromethane). After purification the product was dried under reduced pressure.

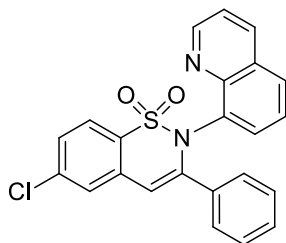
6-methyl-3-phenyl-2-(quinolin-8-yl)-2H-benzo[e][1,2]thiazine-1,1-dioxide (1aa)



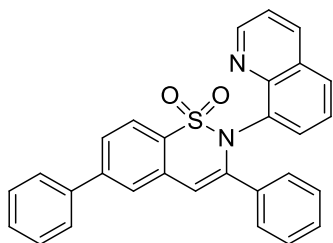
Prepared in accordance to the general synthesis described above: **1a** (104 mg, 0.35 mmol) was converted to **1aa**; 119 mg of a white powder (**85%**). ^1H NMR (300 MHz, CDCl_3 , ppm): δ 9.11 (dd, $^3J_{\text{HH}} = 4.2$ Hz, $^4J_{\text{HH}} = 1.7$ Hz, 1H), 8.08 (dd, $^3J_{\text{HH}} = 8.3$ Hz, $^4J_{\text{HH}} = 1.7$ Hz, 1H), 7.79 (d, $^3J_{\text{HH}} = 2.2$ Hz, 1H), 7.77 (m, 1H), 7.73 (d, $^3J_{\text{HH}} = 7.8$ Hz, 1H), 7.67 (dd, $^3J_{\text{HH}} = 7.4$ Hz, $^4J_{\text{HH}} = 2.1$ Hz, 1H), 7.45 (m, 2H), 7.30 (m, 3H), 7.17 (d, $^3J_{\text{HH}} = 2.5$ Hz, 2H), 7.15 (d, $^4J_{\text{HH}} = 1.1$ Hz, 1H), 6.96 (s, 1H), 2.51 (s, 3H). ^{13}C $\{^1\text{H}\}$ NMR (75 MHz, CDCl_3 , ppm): δ 151.2, 151.0, 145.7, 144.3, 142.7, 135.7, 135.6, 136.4, 133.2, 129.4, 129.1, 129.0, 128.7, 128.2, 127.9, 127.7, 125.6, 122.7, 121.7, 112.5, 112.4, 21.7. IR (ATR): $\bar{\nu} = 3058, 2930, 2840, 2247, 1709, 1591, 1468, 1342, 1314, 1251, 1167, 1109, 1081, 1025, 909, 828, 756, 728, 697, 530, 481$ cm^{-1} . HRMS (ESI) calcd. for $\text{C}_{24}\text{H}_{18}\text{N}_2\text{O}_2\text{S}[\text{M}+\text{H}]^+$: 399.1162; found: 399.1161. R_f : 0.51 (dichloromethane). **m.p.** 250-251°C.

6-methoxy-3-phenyl-2-(quinolin-8-yl)-2H-benzo[e][1,2]thiazine-1,1-dioxide (1ba)

Prepared in accordance to the general synthesis described above: **1b** (110 mg, 0.35 mmol) was converted to **1ba**; 120 mg of a white solid (**83%**). $^1\text{H NMR}$ (300 MHz, CDCl_3 , ppm): δ 9.07 (dd, $^3J_{\text{HH}} = 4.2$ Hz, $^4J_{\text{HH}} = 1.7$ Hz, 1H), 8.02 (dd, $^3J_{\text{HH}} = 8.3$ Hz, $^4J_{\text{HH}} = 1.7$ Hz, 1H), 7.75 (m, 2H), 7.73 (d, $^3J_{\text{HH}} = 8.2$ Hz, 1H), 7.64 (m, 1H), 7.37 (dd, $^3J_{\text{HH}} = 8.2$ Hz, $^4J_{\text{HH}} = 4.2$ Hz, 1H), 7.25 (s, 1H), 7.24 (d, $^3J_{\text{HH}} = 1.8$ Hz, 1H), 7.13 (d, $^3J_{\text{HH}} = 2.1$ Hz, 2H), 7.12 (d, $^3J_{\text{HH}} = 1.7$ Hz, 1H), 7.06 (d, $^3J_{\text{HH}} = 2.4$ Hz, 1H), 6.99 (dd, $^3J_{\text{HH}} = 8.2$ Hz, $^4J_{\text{HH}} = 2.4$ Hz, 1H), 6.90 (s, 1H), 3.91 (s, 3H). $^{13}\text{C}\{^1\text{H}\}$ NMR (75 MHz, CDCl_3 , ppm): δ 162.4, 151.2, 151.0, 145.7, 144.8, 135.8, 135.7, 135.3, 135.2, 129.3, 129.0, 128.7, 128.2, 127.9, 127.8, 125.6, 124.6, 124.5, 121.7, 114.7, 112.5, 112.4, 111.2, 55.7. IR (ATR): $\bar{\nu} = 3058, 2935, 2839, 2253, 1591, 1468, 1341, 1250, 1167, 1110, 1080, 1024, 908, 789, 755, 726, 696, 583, 530, 478$ cm^{-1} . HRMS (ESI) calcd. for $\text{C}_{24}\text{H}_{18}\text{N}_2\text{O}_3\text{S}$ $[\text{M}+\text{H}]^+$: 415.1111; found: 415.1113. R_f : 0.45 (dichloromethane). m.p. 226-228°C.

6-chloro-3-phenyl-2-(quinolin-8-yl)-2H-benzo[e][1,2]thiazine-1,1-dioxide (1ca)

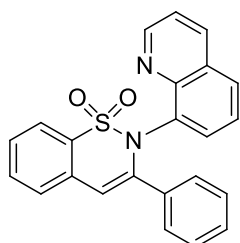
Prepared in accordance to the general synthesis described above: **1c** (112 mg, 0.35 mmol) was converted to **1ca**; 111 mg of a white solid (**75%**). $^1\text{H NMR}$ (300 MHz, CDCl_3 , ppm): δ 8.99 (dd, $^3J_{\text{HH}} = 4.2$ Hz, $^4J_{\text{HH}} = 1.7$ Hz, 1H), 8.05 (dd, $^3J_{\text{HH}} = 8.3$ Hz, $^4J_{\text{HH}} = 1.7$ Hz, 1H), 7.73 (d, $^3J_{\text{HH}} = 8.4$ Hz, 1H), 7.68 (m, 3H), 7.63 (d, $^3J_{\text{HH}} = 2.8$ Hz, 1H), 7.44 (dd, $^3J_{\text{HH}} = 8.4$ Hz, $^4J_{\text{HH}} = 2.2$ Hz, 1H), 7.40 (dd, $^3J_{\text{HH}} = 8.4$ Hz, $^4J_{\text{HH}} = 4.2$ Hz, 1H), 7.32 (m, 2H), 7.13 (m, 3H), 6.86 (s, 1H). $^{13}\text{C}\{^1\text{H}\}$ NMR (75 MHz, CDCl_3 , ppm): δ 151.2, 151.0, 145.8, 145.5, 138.2, 135.8, 135.2, 135.0, 134.9, 130.1, 129.5, 129.0, 128.3, 128.1, 127.9, 127.2, 127.0, 125.6, 124.3, 121.7, 111.2. IR (ATR): $\bar{\nu} = 3245, 3058, 2924, 2167, 1584, 1547, 1498, 1447, 1386, 1349, 1311, 1239, 1171, 1135, 1078, 1026, 861, 819, 760, 736, 696, 649, 592, 480, 427$ cm^{-1} . HRMS (ESI) calcd. for $\text{C}_{23}\text{H}_{15}\text{ClN}_2\text{O}_2\text{S}$ $[\text{M}+\text{H}]^+$: 419.0616; found: 419.0619. R_f : 0.58 (dichloromethane). m.p. 255-257°C.

3,6-diphenyl-2-(quinolin-8-yl)-2H-benzo[e][1,2]thiazine-1,1-dioxide (1da)

Prepared in accordance to the general synthesis described above: **1d** (126 mg, 0.35 mmol) was converted to **1da**; 131 mg of a white solid (**79% 1da** and <2% minor regioisomer (ratio of <20:1)). $^1\text{H NMR}$ (300 MHz, CDCl_3 , ppm): δ 9.07 (dd, $^3J_{\text{HH}} = 4.2$ Hz, $^4J_{\text{HH}} = 1.7$ Hz, 1H), 8.06 (dd, $^3J_{\text{HH}} = 8.4$ Hz, $^4J_{\text{HH}} = 1.7$ Hz, 1H), 7.86 (d, $^3J_{\text{HH}} = 8.2$ Hz, 1H), 7.81 (d, $^3J_{\text{HH}} = 18$ Hz, 1H), 7.76 (m, 2H), 7.67 (m, 4H), 7.65 (d, $^3J_{\text{HH}} = 2.2$ Hz, 2H), 7.56-7.37 (m, 4H), 7.30 (s, 1H), 7.28 (d, $^3J_{\text{HH}} = 1.8$ Hz, 1H), 7.15 (d, $^3J_{\text{HH}} = 1.8$ Hz, 1H), 7.14 (m, 3H), 7.03 (s, 1H). $^{13}\text{C}\{^1\text{H}\}$ NMR (75 MHz, CDCl_3 , ppm): δ 151.2, 151.0, 145.7, 145.2, 144.7, 144.4, 139.7, 135.7, 135.6, 135.5, 135.3, 133.7, 130.6, 129.3, 129.0, 128.9, 128.3, 127.9, 127.8, 127.5, 127.4, 126.8, 126.2,

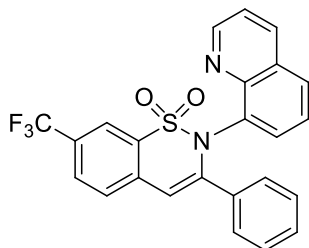
126.0, 125.6, 123.2, 121.7, 112.6, 112.5. **IR (ATR):** $\bar{\nu}$ = 3060, 2923, 2841, 2363, 1712, 1595, 1494, 1467, 1385, 1342, 1172, 1138, 1109, 1079, 1024, 906, 761, 696, 586, 535, 477 cm^{-1} . **HRMS (ESI)** calcd. for $\text{C}_{29}\text{H}_{20}\text{N}_2\text{O}_2\text{S}$ $[\text{M}+\text{H}]^+$: 461.1318; found: 461.1325. **R_f**: 0.57 (dichloromethane). **m.p.** 277-278°C (decomposes).

3-phenyl-2-(quinolin-8-yl)-2H-benzo[e][1,2]thiazine-1,1-dioxide (1ea)



Prepared in accordance to the general synthesis described above: **1e** (100 mg, 0.35 mmol) was converted to **1ea**; 109mg of a white solid (**81%**). **¹H NMR** (300 MHz, CDCl_3 , ppm): δ 9.08 (dd, $^3J_{\text{HH}} = 4.1$ Hz, $^4J_{\text{HH}} = 1.8$ Hz, 1H), 8.08 (dd, $^3J_{\text{HH}} = 8.4$ Hz, $^4J_{\text{HH}} = 1.7$ Hz, 1H), 7.83 (d, $^3J_{\text{HH}} = 8.1$ Hz, 1H), 7.78 (d, $^3J_{\text{HH}} = 2.1$ Hz, 1H), 7.76 (m, 1H), 7.67 (d, $^3J_{\text{HH}} = 2.2$ Hz, 1H), 7.65 (d, $^3J_{\text{HH}} = 2.2$ Hz, 2H), 7.51 (m, 1H), 7.42 (dd, $^3J_{\text{HH}} = 8.2$ Hz, $^3J_{\text{HH}} = 4.2$ Hz, 1H), 7.28 (m, 2H), 7.16 (d, $^3J_{\text{HH}} = 2.1$ Hz, 2H), 7.14 (d, $^3J_{\text{HH}} = 1.7$ Hz, 1H), 6.99 (s, 1H). **¹³C {¹H} NMR** (75 MHz, CDCl_3 , ppm): δ 151.2, 151.0, 145.7, 144.4, 135.8, 135.6, 135.5, 135.3, 133.2, 131.8, 129.2, 129.0, 128.9, 128.3, 127.9, 127.8, 125.6, 122.7, 121.8, 112.5, 112.4. **IR (ATR):** $\bar{\nu}$ = 3071, 3032, 1618, 1594, 1492, 1468, 1340, 1292, 1173, 1130, 790, 768, 760, 697, 646, 592, 583, 559, 527, 483 cm^{-1} . **HRMS (ESI)** calcd. for $\text{C}_{23}\text{H}_{16}\text{N}_2\text{O}_2\text{S}$ $[\text{M}+\text{H}]^+$: 385.1005; found: 385.1004. **R_f**: 0.53 (dichloromethane). **m.p.** 263-264°C.

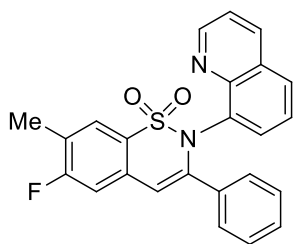
3-phenyl-2-(quinolin-8-yl)-7-(trifluoromethyl)-2H-benzo[e][1,2]thiazine-1,1-dioxide (1fa)



Prepared in accordance to the general synthesis described above: **1f** (123 mg, 0.35 mmol) was converted to **1fa**; 102 mg of a white solid (**64%**). **¹H NMR** (300 MHz, CDCl_3 , ppm): δ 8.97 (dd, $^3J_{\text{HH}} = 4.2$ Hz, $^4J_{\text{HH}} = 1.7$ Hz, 1H), 8.09 (s, 1H), 8.08 (dd, $^3J_{\text{HH}} = 8.2$ Hz, $^4J_{\text{HH}} = 1.8$ Hz, 1H), 7.91 (d, $^3J_{\text{HH}} = 8.2$ Hz, 1H), 7.73 (m, 4H), 7.40 (m, 3H), 7.17 (m, 3H), 6.98 (s, 1H). **¹³C {¹H} NMR** (75 MHz, CDCl_3 , ppm): 151.2, 151.0, 146.7, 145.4, 135.6, 135.8, 135.7, 135.1, 134.7, 131.8, 129.7, 129.0, 128.3, 128.2, 128.0, 125.6, 125.2, 121.8, 121.6, 120.2, 111.2, 111.1. **¹⁹F {¹H} NMR** (282 MHz, CDCl_3 , ppm): δ -62.4. **IR (ATR):** $\bar{\nu}$ = 3048, 2923, 2851, 1608, 1494, 1469, 1352, 1325, 1201, 1163, 1131, 1085, 884, 791, 760, 694, 559, 481 cm^{-1} . **HRMS (ESI)** calcd. for $\text{C}_{24}\text{H}_{15}\text{F}_3\text{N}_2\text{O}_2\text{S}$ $[\text{M}+\text{H}]^+$: 453.0885; found: 453.0883. **R_f**: 0.67 (dichloromethane). **m.p.** 199-201°C.

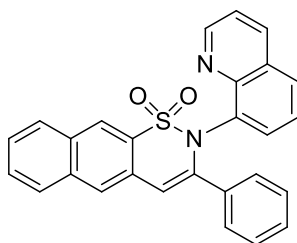
6-fluoro-7-methyl-3-phenyl-2-(quinolin-8-yl)-2H-benzo[e][1,2]thiazine-1,1-dioxide (1ga)

Prepared in accordance to the general synthesis described above: **lg** (110 mg, 0.35 mmol)



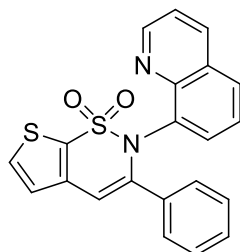
was converted to **1ga**; 94 mg of a white solid (63% and 2% minor regioisomer (ratio of 47:1)). $^1\text{H NMR}$ (300 MHz, CDCl_3 , ppm): δ 9.06 (dd, $^3J_{\text{HH}} = 4.2$ Hz, $^4J_{\text{HH}} = 1.7$ Hz, 1H), 8.08 (dd, $^3J_{\text{HH}} = 8.3$ Hz, $^4J_{\text{HH}} = 1.7$ Hz, 1H), 7.69 (m, 4H), 7.43 (dd, $^3J_{\text{HH}} = 8.4$ Hz, $^4J_{\text{HH}} = 4.2$ Hz, 1H), 7.32 (m, 2H), 7.26 (d, $^3J_{\text{HH}} = 8.4$ Hz, 1H), 7.15 (m, 3H), 6.89 (s, 1H). ^{13}C $\{^1\text{H}\}$ NMR (75 MHz, CDCl_3 , ppm): δ

165.0, 161.6, 151.2, 151.0, 145.6, 144.8, 135.8, 135.4, 135.1, 133.5, 129.3, 129.0, 128.3, 127.9, 127.8, 125.9, 125.6, 121.8, 113.5, 111.6, 111.5, 14.7. ^{19}F $\{^1\text{H}\}$ NMR (282 MHz, CDCl_3 , ppm): -110.8. IR (ATR): $\bar{\nu} = 3061, 2923, 2852, 1610, 1493, 1483, 1388, 1347, 1235, 1165, 1133, 1107, 1026, 877, 831, 789, 762, 688, 576, 506, 484$ cm^{-1} . HRMS (ESI) calcd. for $\text{C}_{24}\text{H}_{17}\text{FN}_2\text{O}_2\text{S}$ $[\text{M}+\text{H}]^+$: 417.1068; found: 417.1063. R_f : 0.69 (dichloromethane). **m.p.** 221-223°C.

3-phenyl-2-(quinolin-8-yl)-2H-naphtho[2,3-e][1,2]thiazine 1,1-dioxide (1ha)

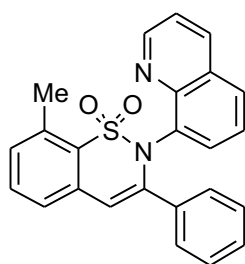
Prepared in accordance to the general synthesis described above: **lh** (117mg, 0.35 mmol) was converted to **1ha**; 126 mg of a white solid (81%). $^1\text{H NMR}$ (300 MHz, CDCl_3 , ppm): δ 9.06 (dd, $^3J_{\text{HH}} = 4.2$ Hz, $^4J_{\text{HH}} = 1.7$ Hz, 1H), 8.37 (s, 1H), 8.11 (s, 1H), 8.06 (dd, $^3J_{\text{HH}} = 7.4$ Hz, $^4J_{\text{HH}} = 1.7$ Hz, 1H), 8.01 (d, $^3J_{\text{HH}} = 7.7$ Hz, 1H), 7.96 (d, $^3J_{\text{HH}} = 7.7$ Hz, 1H), 7.84 (m, 2H), 7.66 (m, 2H), 7.57

(m, 1H), 7.42 (dd, $^3J_{\text{HH}} = 8.2$ Hz, $^4J_{\text{HH}} = 4.2$ Hz, 1H), 7.29 (s, 1H), 7.28 (d, $^3J_{\text{HH}} = 4.2$ Hz, 1H), 7.18 (m, 4H). ^{13}C $\{^1\text{H}\}$ NMR (75 MHz, CDCl_3 , ppm): δ 151.2, 150.9, 145.8, 143.9, 135.7, 135.6, 134.8, 132.1, 131.4, 130.3, 129.5, 129.3, 129.1, 128.6, 128.3, 128.1, 127.7, 127.5, 126.8, 126.7, 125.6, 123.5, 121.7, 113.7, 111.9. IR (ATR): $\bar{\nu} = 3053, 2918, 2867, 1722, 1614, 1571, 1492, 1349, 1262, 1165, 1105, 1051, 894, 787, 743, 694, 646, 540, 465$ cm^{-1} . HRMS (ESI) calcd. for $\text{C}_{27}\text{H}_{18}\text{N}_2\text{O}_2\text{S}$ $[\text{M}+\text{H}]^+$: 435.1162; found: 435.1159. R_f : 0.41 (DCM). **m.p.** 257-258°C.

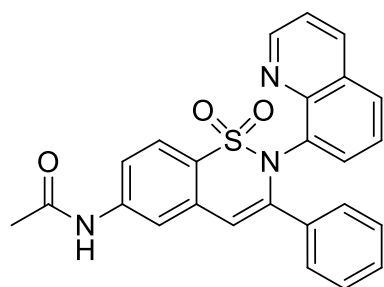
3-phenyl-2-(quinolin-8-yl)-2H-thieno[3,2-e][1,2]thiazine 1,1-dioxide (1ia)

Prepared in accordance to the general synthesis described above: **li** (101mg, 0.35mmol) was converted to **1ia**; 103 mg of a white solid (74%). $^1\text{H NMR}$ (300 MHz, CDCl_3 , ppm): δ 9.12 (dd, $^3J_{\text{HH}} = 4.2$ Hz, $^4J_{\text{HH}} = 1.7$ Hz, 1H), 8.09 (dd, $^3J_{\text{HH}} = 8.4$ Hz, $^4J_{\text{HH}} = 1.7$ Hz, 1H), 7.72 (m, 2H), 7.68 (dd, $^3J_{\text{HH}} = 7.8$ Hz, $^4J_{\text{HH}} = 1.7$ Hz, 1H), 7.61 (d, $^3J_{\text{HH}} = 4.2$ Hz, 1H), 7.45 (dd, $^3J_{\text{HH}} = 8.4$ Hz, $^4J_{\text{HH}} = 4.2$ Hz, 1H), 7.32 (t, $^3J_{\text{HH}} = 7.8$ Hz,

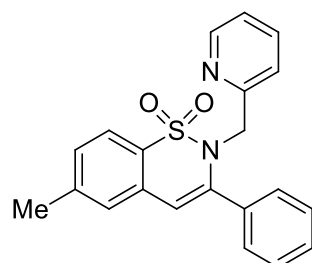
1H), 7.25 (m, 2H), 7.13 (m, 3H), 7.01 (s, 1H). ^{13}C $\{^1\text{H}\}$ NMR (75 MHz, CDCl_3 , ppm): δ 151.3, 151.1, 145.8, 144.6, 141.1, 135.8, 135.4, 135.0, 129.2, 129.0, 128.9, 128.2, 127.9, 127.8, 125.6, 121.8, 121.7, 108.7, 108.6. IR (ATR): $\bar{\nu} = 3096, 3073, 2923, 1592, 1575, 1494, 1387, 1339, 1167, 1103, 851, 819, 792, 759, 697, 614, 565, 525, 486, 458$ cm^{-1} . HRMS (ESI) calcd. for $\text{C}_{21}\text{H}_{14}\text{N}_2\text{O}_2\text{S}_2$ $[\text{M}+\text{H}]^+$: 391.0571; found: 391.0571. R_f : 0.53 (DCM). **m.p.** 263-265°C.

8-methyl-3-phenyl-2-(quinolin-8-yl)-2H-benzo[e][1,2]thiazine 1,1-dioxide (1ma)

Prepared in accordance to the general synthesis described above: **Im** (105mg, 0.35mmol) was converted to **1ma**; 75 mg of a white solid (**54%**). $^1\text{H NMR}$ (300 MHz, CDCl_3 , ppm): δ 9.14 (dd, $^3J_{\text{HH}} = 4.2$ Hz, $^4J_{\text{HH}} = 1.5$ Hz, 1H), 8.09 (dd, $^3J_{\text{HH}} = 8.4$ Hz, $^4J_{\text{HH}} = 1.2$ Hz, 1H), 7.76 (m, 2H), 7.68 (dt, $^3J_{\text{HH}} = 8.4$ Hz, $^4J_{\text{HH}} = 4.2$ Hz, 1H), 7.46 (m, 3H), 7.31 (d, $^3J_{\text{HH}} = 7.8$ Hz, 1H), 7.29 (s, 1H), 7.26 (d, $^3J_{\text{HH}} = 7.8$ Hz, 1H), 7.13 (m, 3H), 6.93 (s, 1H), 2.64 (s, 3H). $^{13}\text{C} \{^1\text{H}\}$ NMR (75 MHz, CDCl_3 , ppm): δ 151.1, 146.0, 143.4, 135.8, 135.6, 135.5, 134.0, 131.6, 131.5, 131.3, 129.1, 129.0, 128.9, 128.8, 128.2, 127.6, 126.1, 125.6, 121.7, 113.1, 20.5. **IR (ATR)**: $\bar{\nu} = 3062, 2929, 1623, 1567, 1493, 1463, 1341, 1253, 1165, 1111, 980, 939, 910, 857, 827, 810, 783, 755, 734, 694, 622, 590, 534, 510, 452, 419$ cm^{-1} . **HRMS (ESI)** calcd. for $\text{C}_{24}\text{H}_{18}\text{N}_2\text{O}_2\text{S}$ $[\text{M}+\text{H}]^+$: 399.1162; found: 399.1158. **R_f**: 0.42 (dichloromethane). **m.p.** 206-208°C.

N-(1,1-dioxido-3-phenyl-2-(quinolin-8-yl)-2H-benzo[e][1,2]thiazin-6-yl)acetamide (1oa)

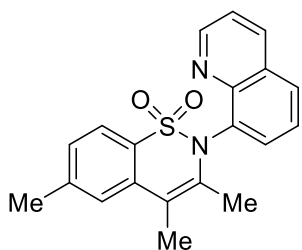
Prepared in accordance to the general synthesis described above: **Im** (120mg, 0.35mmol) was converted to **1oa**; 134 mg of a white solid (**87%**). $^1\text{H NMR}$ (300 MHz, CDCl_3 , ppm): δ 9.08 (dd, $^3J_{\text{HH}} = 4.2$ Hz, $^4J_{\text{HH}} = 1.5$ Hz, 1H), 8.08 (dd, $^3J_{\text{HH}} = 8.2$ Hz, $^4J_{\text{HH}} = 1.3$ Hz, 1H), 8.04 (s, 1H), 7.73 (m, 3H), 7.66 (m, 2H), 7.31 (dd, $^3J_{\text{HH}} = 8.2$ Hz, $^4J_{\text{HH}} = 4.2$ Hz, 1H), 7.32-7.25 (m, 3H), 7.14 (m, 3H), 6.92 (s, 1H), 2.19 (s, 3H). $^{13}\text{C} \{^1\text{H}\}$ NMR (75 MHz, CDCl_3 , ppm): δ 168.9, 151.1, 145.7, 144.7, 141.5, 135.7, 135.4, 135.1, 134.4, 130.4, 129.3, 129.0, 128.9, 128.8, 128.3, 127.8, 125.7, 123.6, 121.8, 118.7, 117.5, 112.6. **IR (ATR)**: $\bar{\nu} = 3359, 3043, 1698, 1530, 1494, 1475, 1392, 1332, 1229, 1163, 1130, 892, 854, 826, 782, 762, 730, 692, 651, 605, 528, 478, 419$ cm^{-1} . **HRMS (ESI)** calcd. for $\text{C}_{25}\text{H}_{19}\text{N}_3\text{O}_3\text{S}$ $[\text{M}+\text{H}]^+$: 442.1220; found: 442.1195. **R_f**: 0.51 (dichloromethane/AcOEt (4:1)). **m.p.** 211-212°C.

6-methyl-3-phenyl-2-(pyridin-2-ylmethyl)-2H-benzo[e][1,2]thiazine-1,1-dioxide (5aa)

Prepared in accordance to the general synthesis described above: **5a** (92 mg, 0.35 mmol) was converted to **5aa**; 12 mg of a white solid (Isolated: **9%**) ($^1\text{H NMR}$ yield: **32%**). $^1\text{H NMR}$ (300 MHz, CDCl_3 , ppm): δ 8.21 (dq, $^3J_{\text{HH}} = 4.9$ Hz, $^4J_{\text{HH}} = 1.2$ Hz, 1H), 7.75 (d, $^3J_{\text{HH}} = 8.2$ Hz, 1H), 7.57 (m, 2H), 7.41 (m, 3H), 7.31 (d, $^3J_{\text{HH}} = 8.2$ Hz, 2H), 7.20 (s, 1H), 6.98 (m, 1H), 6.91 (d, $^3J_{\text{HH}} = 7.5$ Hz, 1H), 6.60 (s, 1H), 4.87 (s, 2H), 2.46 (s, 3H). $^{13}\text{C} \{^1\text{H}\}$ NMR (75 MHz, CDCl_3 , ppm): δ 155.6, 148.8, 143.4, 142.5, 136.1, 134.7, 132.7, 130.3, 129.8, 129.0, 128.8, 128.0, 127.7, 122.2, 121.9, 121.7, 113.7, 53.4, 21.7. **IR (ATR)**: $\bar{\nu} = 3022, 2931, 2790, 2133, 1732, 1602, 1344, 1251, 1112, 1009, 909, 828, 756, 697, 530, 481$ cm^{-1} . **HRMS (ESI)**

calcd. for $C_{21}H_{18}N_2O_2S$ $[M+H]^+$: 363.1162; found: 363.1178. R_f : 0.49 (dichloromethane/EtOAc (2:1)). **m.p.** 155-157°C.

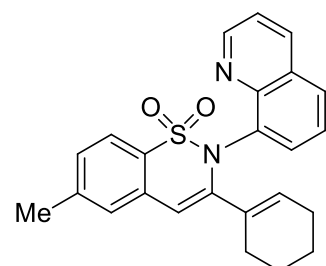
3,4,6-trimethyl-2-(quinolin-8-yl)-2H-benzo[e][1,2]thiazine 1,1-dioxide (1ab)

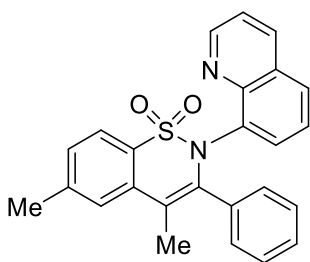


Prepared in accordance to the general synthesis described above: **1a** (104 mg, 0.35 mmol) was converted to **1ab**; 75 mg of a white solid (**61%**). 1H NMR (300 MHz, $CDCl_3$, ppm): δ 8.93 (dd, $^3J_{HH} = 4.2$ Hz, $^4J_{HH} = 1.7$ Hz, 1H), 8.15 (dd, $^3J_{HH} = 8.4$ Hz, $^4J_{HH} = 1.8$ Hz, 1H), 7.83 (dd, $^3J_{HH} = 7.2$ Hz, $^4J_{HH} = 2.4$ Hz, 1H), 7.69 (d, $^3J_{HH} = 8.2$ Hz, 1H), 7.47 (m, 3H), 7.40 (dd, $^3J_{HH} = 8.4$ Hz, $^4J_{HH} = 4.2$ Hz, 1H), 7.30 (m, 3H), 7.24 (dd, $^3J_{HH} = 7.8$ Hz, $^4J_{HH} = 1.0$ Hz, 1H), 2.50 (s, 3H), 2.31 (s, 3H), 1.95 (s, 3H). ^{13}C $\{^1H\}$ NMR (75 MHz, $CDCl_3$, ppm): δ 151.5, 151.2, 146.1, 142.1, 136.2, 136.0, 135.4, 134.5, 129.9, 129.2, 127.7, 125.9, 124.9, 124.8, 122.0, 121.8, 114.9, 22.1, 18.1, 15.0. **IR (ATR)**: $\bar{\nu} = 3033, 3005, 2920, 1700, 1619, 1594, 1495, 1467, 1382, 1336, 1262, 1182, 1145, 1128, 1057, 944, 832, 792, 677, 627, 598, 546, 487, 427$ cm^{-1} . **HRMS (ESI)** calcd. for $C_{30}H_{22}N_2O_2S$ $[M+H]^+$: 351.1162; found: 351.1158. R_f : 0.39 (DCM). **m.p.** 209-211°C.

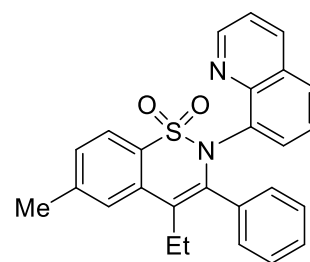
3-(cyclohex-1-en-1-yl)-6-methyl-2-(quinolin-8-yl)-2H-benzo[e][1,2]thiazine-1,1-dioxide (1ac)

Prepared in accordance to the general synthesis described above: **1a** (104 mg, 0.35 mmol) was converted to **1ac**; 116 mg of a white solid (**82%**). 1H NMR (400 MHz, $CDCl_3$, ppm): δ 9.09 (dd, $^3J_{HH} = 4.2$ Hz, $^4J_{HH} = 1.7$ Hz, 1H), 8.13 (dd, $^3J_{HH} = 8.4$ Hz, $^4J_{HH} = 1.8$ Hz, 1H), 7.74 (dd, $^3J_{HH} = 8.2$ Hz, $^4J_{HH} = 1.3$ Hz, 1H), 7.60 (d, $^3J_{HH} = 8.2$ Hz, 1H), 7.44 (dd, $^3J_{HH} = 8.4$ Hz, $^4J_{HH} = 4.2$ Hz, 1H), 7.34 (m, 2H), 7.30 (m, 3H), 7.22 (d, $^3J_{HH} = 8.1$ Hz, 1H), 7.07 (dd, $^3J_{HH} = 7.8$ Hz, $^4J_{HH} = 1.8$ Hz, 1H), 6.72 (s, 1H), 6.55 (dd, $^3J_{HH} = 3.9$ Hz, 1H), 2.47 (s, 3H), 2.21 (m, 2H), 1.93 (m, 2H), 1.39 (m, 4H). ^{13}C $\{^1H\}$ NMR (75 MHz, $CDCl_3$, ppm): δ 151.1, 150.9, 146.1, 142.5, 136.3, 135.6, 133.2, 132.5, 132.0, 129.3, 129.1, 128.7, 128.5, 127.8, 127.0, 125.6, 123.1, 121.5, 111.1, 26.1, 25.6, 22.3, 21.7. **IR (ATR)**: $\bar{\nu} = 3050, 2926, 2858, 1598, 1559, 1497, 1469, 1384, 1341, 1242, 1184, 1143, 1103, 1075, 1023, 907, 829, 789, 726, 652, 640, 555, 533, 499, 458$ cm^{-1} . **HRMS (ESI)** calcd. for $C_{24}H_{22}N_2O_2S$ $[M+H]^+$: 404.1469; found: 404.1475. R_f : 0.46 (dichloromethane). **m.p.** 199-201°C.

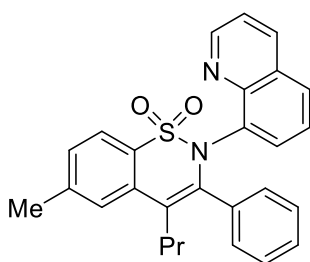


4,6-dimethyl-3-phenyl-2-(quinolin-8-yl)-2H-benzo[e][1,2]thiazine 1,1-dioxide (1ad)

Prepared in accordance to the general synthesis described above: **1a** (104 mg, 0.35 mmol) was converted to **1ad**; 133 mg of a white solid (**92%**). ¹H NMR (300 MHz, CDCl₃, ppm): δ 8.92 (dd, ³J_{HH} = 4.4 Hz, ⁴J_{HH} = 1.8 Hz, 1H), 7.94 (dd, ³J_{HH} = 8.2 Hz, ⁴J_{HH} = 2.4 Hz, 1H), 7.74 (d, ³J_{HH} = 8.2 Hz, 1H), 7.59 (s, 1H), 7.56 (m, 3H), 7.30 (dd, ³J_{HH} = 8.2 Hz, ⁴J_{HH} = 1.8 Hz, 3H), 7.23 (dd, ³J_{HH} = 8.2 Hz, ⁴J_{HH} = 0.9 Hz, 1H), 7.08 (m, 3H), 2.54 (s, 3H), 2.35 (s, 3H). ¹³C {¹H} NMR (75 MHz, CDCl₃, ppm): δ 150.8, 150.6, 145.5, 142.3, 139.7, 135.9, 135.4, 135.1, 130.5, 130.4, 129.4, 128.4, 127.5, 126.0, 125.8, 125.4, 122.1, 121.4, 117.1, 109.1, 22.1, 16.7. IR (ATR): $\bar{\nu}$ = 3055, 2942, 2918, 1592, 1497, 1468, 1358, 1342, 1265, 1241, 1187, 1170, 1138, 1051, 1015, 912, 860, 822, 789, 763, 703, 677, 603, 577, 546, 531, 498, 433 cm⁻¹. HRMS (ESI) calcd. for C₂₅H₂₀N₂O₂S [M+H]⁺: 413.1306; found: 467.1318. R_f: 0.54 (dichloromethane). m.p. 204-205°C.

4-ethyl-6-methyl-3-phenyl-2-(quinolin-8-yl)-2H-benzo[e][1,2]thiazine 1,1-dioxide (1ae)

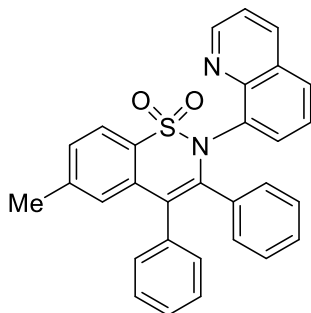
Prepared in accordance to the general synthesis described above: **1a** (104 mg, 0.35 mmol) was converted to **1ae**; 134 mg of a white solid (**89%**). ¹H NMR (300 MHz, CDCl₃, ppm): δ 8.88 (dd, ³J_{HH} = 4.3 Hz, ⁴J_{HH} = 1.6 Hz, 1H), 7.93 (dd, ³J_{HH} = 8.3 Hz, ⁴J_{HH} = 1.8 Hz, 1H), 7.76 (d, ³J_{HH} = 8.2 Hz, 1H), 7.64 (s, 1H), 7.54 (dd, ³J_{HH} = 8.2 Hz, ⁴J_{HH} = 1.8 Hz, 1H), 7.47 (m, 2H), 7.33 (m, 2H), 7.23 (d, ³J_{HH} = 8.2 Hz, 1H), 7.08 (m, 3H), 2.82 (m, 2H), 2.55 (s, 3H), 1.09 (d, ³J_{HH} = 7.8 Hz, 1H). ¹³C {¹H} NMR (75 MHz, CDCl₃, ppm): δ 150.7, 150.5, 145.5, 142.1, 139.2, 135.6, 135.0, 134.8, 134.3, 131.4, 130.3, 129.9, 128.8, 128.5, 128.3, 127.5, 126.0, 125.4, 123.5, 122.4, 121.4, 22.1, 14.4, 14.3. IR (ATR): $\bar{\nu}$ = 3057, 2965, 2930, 2872, 1595, 1497, 1469, 1386, 1337, 1260, 1172, 1147, 1074, 1025, 906, 790, 763, 700, 674, 605, 539, 435 cm⁻¹. HRMS (ESI) calcd. for C₂₅H₁₇F₃N₂O₂S [M+H]⁺: 427.1475; found: 427.1467. R_f: 0.49 (dichloromethane). m.p. 185-186°C.

6-methyl-3-phenyl-4-propyl-2-(quinolin-8-yl)-2H-benzo[e][1,2]thiazine-1,1-dioxide (1af)

Prepared in accordance to the general synthesis described above: **1a** (104 mg, 0.35 mmol) was converted to **1af**; 138 mg of a white solid (**84%**). ¹H NMR (300 MHz, CDCl₃, ppm): δ 8.90 (dd, ³J_{HH} = 4.3 Hz, ⁴J_{HH} = 1.7 Hz, 1H), 7.96 (dd, ³J_{HH} = 8.4 Hz, ⁴J_{HH} = 1.7 Hz, 1H), 7.75 (d, ³J_{HH} = 8.2 Hz, 1H), 7.63 (s, 1H), 7.56 (dd, ³J_{HH} = 7.7 Hz, ⁴J_{HH} = 1.7 Hz, 1H), 7.45 (m, 2H), 7.30 (m, 3H), 7.23 (d, ³J_{HH} = 7.4 Hz, 1H), 7.07 (m, 3H), 2.83 (t, ³J_{HH} = 7.2 Hz, 2H), 2.56 (s, 3H), 1.53 (m, 2H), 0.78 (t, ³J_{HH} = 7.3 Hz, 3H). ¹³C {¹H} NMR (75 MHz, CDCl₃, ppm): δ 150.7, 150.6, 145.5, 141.9, 139.8, 135.5, 135.1, 134.9, 134.4, 131.4, 130.5, 129.8, 128.7, 128.4, 128.2, 127.5,

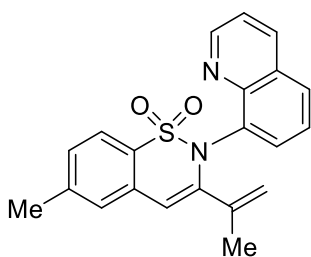
126.0, 125.9, 125.4, 124.0, 122.4, 121.9, 121.4, 30.2, 22.4, 22.1, 13.2. **IR (ATR):** $\bar{\nu}$ = 3000, 2964, 2931, 2870, 1596, 1498, 1471, 1336, 1295, 1268, 1168, 1112, 1057, 956, 919, 815, 767, 745, 699, 663, 608, 562, 539, 468, 440 cm^{-1} . **HRMS (ESI)** calcd. for $\text{C}_{25}\text{H}_{17}\text{F}_3\text{N}_2\text{O}_2\text{S}$ $[\text{M}+\text{H}]^+$: 441.1631; found: 441.1636. **R_f**: 0.44 (dichloromethane). **m.p.** 229-231°C.

6-methyl-3,4-diphenyl-2-(quinolin-8-yl)-2H-benzo[e][1,2]thiazine 1,1-dioxide (1ag)

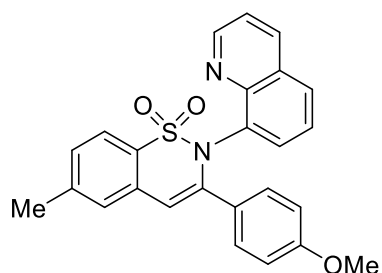


Prepared in accordance to the general synthesis described above: **1a** (104 mg, 0.35 mmol) was converted to **1ag**; 131 mg of a white solid (**79%**). **¹H NMR** (300 MHz, CDCl_3 , ppm): δ 8.97 (dd, $^3J_{\text{HH}} = 4.2$ Hz, $^4J_{\text{HH}} = 1.7$ Hz, 1H), 8.00 (dd, $^3J_{\text{HH}} = 8.3$ Hz, $^4J_{\text{HH}} = 1.7$ Hz, 1H), 7.82 (d, $^3J_{\text{HH}} = 7.9$ Hz, 1H), 7.61 (dd, $^3J_{\text{HH}} = 8.4$ Hz, $^4J_{\text{HH}} = 1.2$ Hz, 1H), 7.53 (dd, $^3J_{\text{HH}} = 7.5$ Hz, $^4J_{\text{HH}} = 1.3$ Hz, 1H) 7.32 (m, 8H), 7.26 (m, 3H), 6.80 (m, 3H), 2.41 (s, 3H). **¹³C {¹H} NMR** (75 MHz, CDCl_3 , ppm): δ 150.8, 150.6, 145.5, 142.2, 141.2, 136.5, 135.7, 135.0, 134.6, 134.6, 131.8, 130.5, 129.8, 128.8, 128.5, 128.0, 127.7, 127.5, 127.2, 126.8, 125.5, 124.2, 122.1, 122.0, 121.6, 22.0. **IR (ATR):** $\bar{\nu}$ = 3054, 2969, 2924, 1728, 1693, 1592, 1497, 1468, 1443, 1338, 1189, 1171, 1111, 1093, 1027, 901, 789, 719, 696, 677, 529, 489, 456 cm^{-1} . **HRMS (ESI)** calcd. for $\text{C}_{30}\text{H}_{22}\text{N}_2\text{O}_2\text{S}$ $[\text{M}+\text{H}]^+$: 475.1475; found: 475.1479. **R_f**: 0.59 (dichloromethane). **m.p.** 190-191°C.

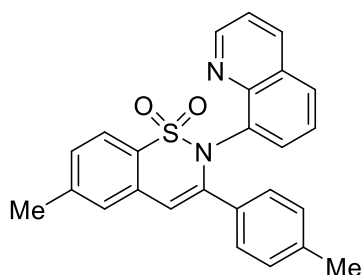
3-(2-chloropropan-2-yl)-6-methyl-2-(quinolin-8-yl)-2H-benzo[e][1,2]thiazine 1,1-dioxide (1ah')



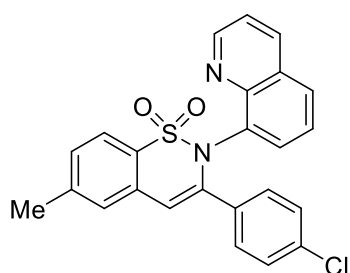
Prepared in accordance to the general synthesis described above: **1a** (104 mg, 0.35 mmol) was converted to **1ah'**; 99 mg of a white solid (**78%**). **¹H NMR** (300 MHz, CDCl_3 , ppm): δ 9.10 (dd, $^3J_{\text{HH}} = 4.2$ Hz, $^4J_{\text{HH}} = 1.7$ Hz, 1H), 8.14 (dd, $^3J_{\text{HH}} = 8.3$ Hz, $^4J_{\text{HH}} = 1.7$ Hz, 1H), 7.75 (dd, $^3J_{\text{HH}} = 8.2$ Hz, $^4J_{\text{HH}} = 1.8$ Hz, 1H), 7.64 (d, $^3J_{\text{HH}} = 8.2$ Hz, 1H), 7.44 (dd, $^3J_{\text{HH}} = 8.2$ Hz, $^4J_{\text{HH}} = 4.2$ Hz, 1H) 7.35 (m, 2H), 7.27 (d, $^3J_{\text{HH}} = 8.2$ Hz, 1H), 7.10 (dd, $^3J_{\text{HH}} = 7.8$ Hz, $^4J_{\text{HH}} = 1.4$ Hz, 1H) 6.84 (s, 1H), 5.75 (m, 1H), 4.95 (m, 1H) 2.49 (s, 3H), 1.96 (s, 3H). **¹³C {¹H} NMR** (75 MHz, CDCl_3 , ppm): δ 151.2, 151.0, 145.7, 145.1, 142.7, 138.1, 136.1, 135.8, 132.8, 129.5, 129.2, 128.5, 128.1, 127.0, 125.6, 123.1, 121.7, 119.7, 113.4, 21.7, 20.4. **IR (ATR):** $\bar{\nu}$ = 3067, 2923, 2860, 1598, 1560, 1496, 1469, 1382, 1313, 1247, 1186, 1162, 1126, 1095, 1030, 914, 891, 861, 828, 792, 739, 684, 638, 597, 560, 535, 516, 474, 443 cm^{-1} . **HRMS (ESI)** calcd. for $\text{C}_{21}\text{H}_{18}\text{N}_2\text{O}_2\text{S}$ $[\text{M}+\text{H}]^+$: 363.1162; found: 363.1162. **R_f**: 0.40 (dichloromethane). **m.p.** decomposes at 260°C.

3-(4-methoxyphenyl)-6-methyl-2-(quinolin-8-yl)-2H-benzo[e][1,2]thiazine 1,1-dioxide (1aj)

Prepared in accordance to the general synthesis described above: **1a** (104 mg, 0.35 mmol) was converted to **1aj**; 47mg of a white solid (**30%**). $^1\text{H NMR}$ (300 MHz, CDCl_3 , ppm): δ 9.11 (dd, $^3J_{\text{HH}} = 4.2$ Hz, $^4J_{\text{HH}} = 1.7$ Hz, 1H), 8.07 (dd, $^3J_{\text{HH}} = 8.3$ Hz, $^4J_{\text{HH}} = 1.8$ Hz, 1H), 7.71 (d, $^3J_{\text{HH}} = 8.2$ Hz, 1H), 7.69 (m, 4H), 7.42 (dd, $^3J_{\text{HH}} = 8.3$ Hz, $^4J_{\text{HH}} = 4.2$ Hz, 1H), 7.40 (s, 1H), 7.30 (m, 2H), 7.20 (dd, $^3J_{\text{HH}} = 7.7$ Hz, $^4J_{\text{HH}} = 1.6$ Hz, 1H), 6.87 d(s, 1H), 6.65 (dd, $^3J_{\text{HH}} = 8.4$ Hz, $^4J_{\text{HH}} = 1.8$ Hz, 1H), 3.67 (s, 3H), 2.50 (s, 3H). ^{13}C $\{^1\text{H}\}$ NMR (75 MHz, CDCl_3 , ppm): δ 160.3, 151.2, 151.0, 145.8, 144.2, 142.6, 135.7, 135.5, 133.4, 129.3, 129.1, 128.7, 128.6, 128.2, 127.7, 127.5, 125.6, 122.7, 121.6, 113.6, 111.2, 55.2, 21.7. IR (ATR): $\bar{\nu} = 3058, 3010, 2926, 2834, 1596, 1509, 1463, 1386, 1341, 1291, 1250, 1177, 1159, 1103, 1026, 892, 820, 790, 724, 689, 648, 592, 559, 528, 489$ cm^{-1} . HRMS (ESI) calcd. for $\text{C}_{25}\text{H}_{20}\text{N}_2\text{O}_3\text{S}$ $[\text{M}+\text{H}]^+$: 429.1267; found: 429.1273. *R*_f: 0.41 (dichloromethane). *m.p.* 99-100°C.

6-methyl-2-(quinolin-8-yl)-3-(p-tolyl)-2H-benzo[e][1,2]thiazine 1,1-dioxide (1ak)

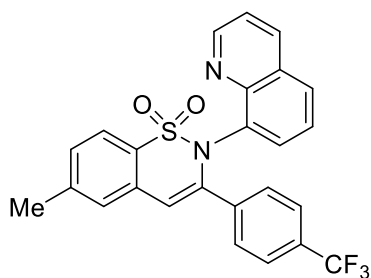
Prepared in accordance to the general synthesis described above: **1a** (104 mg, 0.35 mmol) was converted to **1ak**; 92mg of a white solid (**64%**). $^1\text{H NMR}$ (300 MHz, CDCl_3 , ppm): δ 9.11 (dd, $^3J_{\text{HH}} = 4.2$ Hz, $^4J_{\text{HH}} = 1.7$ Hz, 1H), 8.07 (dd, $^3J_{\text{HH}} = 8.3$ Hz, $^4J_{\text{HH}} = 1.8$ Hz, 1H), 7.71 (d, $^3J_{\text{HH}} = 8.2$ Hz, 1H), 7.64 (m, 3H), 7.43 (m, 2H), 7.67 (dd, $^3J_{\text{HH}} = 7.4$ Hz, $^4J_{\text{HH}} = 2.1$ Hz, 1H), 7.45 (m, 2H), 7.30 (m, 2H), 7.23 (dd, $^3J_{\text{HH}} = 7.8$ Hz, $^4J_{\text{HH}} = 1.8$ Hz, 1H), 6.98 (d, $^3J_{\text{HH}} = 7.9$ Hz, 1H), 6.93 (s, 1H), 2.52 (s, 3H), 2.21 (s, 3H). ^{13}C $\{^1\text{H}\}$ NMR (75 MHz, CDCl_3 , ppm): δ 151.2, 151.0, 145.8, 144.4, 142.6, 139.2, 135.7, 135.5, 133.3, 132.8, 129.3, 129.0, 128.8, 128.6, 127.7, 127.6, 125.6, 122.7, 121.6, 112.0, 111.9, 21.7, 21.2. IR (ATR): $\bar{\nu} = 3024, 2962, 2919, 2856, 1606, 1497, 1468, 1417, 1387, 1341, 1260, 1188, 1159, 1144, 1102, 1080, 1015, 907, 807, 788, 648, 559, 520, 482$ cm^{-1} . HRMS (ESI) calcd. for $\text{C}_{25}\text{H}_{20}\text{N}_2\text{O}_2\text{S}$ $[\text{M}+\text{H}]^+$: 413.1318; found: 413.1321. *R*_f: 0.51 (dichloromethane). *m.p.* decomposes at 265-266°C.

3-(4-chlorophenyl)-6-methyl-2-(quinolin-8-yl)-2H-benzo[e][1,2]thiazine 1,1-dioxide (1al)

Prepared in accordance to the general synthesis described above: **1a** (104 mg, 0.35 mmol) was converted to **1al**; 133 mg of a white solid (**88%**). $^1\text{H NMR}$ (300 MHz, CDCl_3 , ppm): δ 9.09 (dd, $^3J_{\text{HH}} = 4.2$ Hz, $^4J_{\text{HH}} = 1.7$ Hz, 1H), 8.10 (dd, $^3J_{\text{HH}} = 8.2$ Hz, $^4J_{\text{HH}} = 1.8$ Hz, 1H), 7.70 (m, 3H), 7.45 (d, $^3J_{\text{HH}} = 4.2$ Hz, 1H), 7.43 (m, 2H), 7.32 (m, 2H), 7.22 (dd, $^3J_{\text{HH}} = 7.8$ Hz, $^4J_{\text{HH}} = 1.8$ Hz, 1H), 7.11 (d, $^3J_{\text{HH}} = 8.4$ Hz, 2H) 6.92 (s, 1H), 2.52 (s, 3H). ^{13}C $\{^1\text{H}\}$ NMR (75 MHz, CDCl_3 , ppm): δ 151.3, 151.1, 145.7, 143.2, 142.8, 135.8, 135.1, 134.1, 133.0, 129.5, 129.1, 128.9, 128.5, 128.0, 127.9, 125.6, 122.7, 122.6, 121.9, 112.8, 112.7,

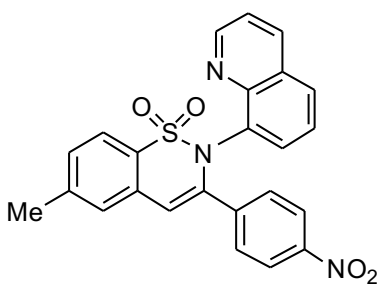
21.7. **IR (ATR)**: $\bar{\nu}$ = 3058, 2920, 2851, 1705, 1595, 1560, 1490, 1468, 1383, 1346, 1260, 1184, 1012, 905, 828, 788, 681, 640, 591, 537, 515, 485, 439 cm^{-1} . **HRMS (ESI)** calcd. for $\text{C}_{24}\text{H}_{17}\text{ClN}_2\text{O}_2\text{S}$ $[\text{M}+\text{H}]^+$: 433.0772; found: 433.0771. **R_f**: 0.48 (dichloromethane). **m.p.** 272-273°C.

6-methyl-2-(quinolin-8-yl)-3-(4-(trifluoromethyl)phenyl)-2H-benzo[e][1,2]thiazine 1,1-dioxide (1am)



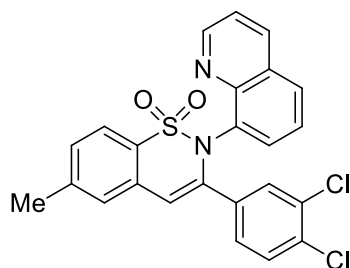
Prepared in accordance to the general synthesis described above: **1a** (104 mg, 0.35 mmol) was converted to **1am**; 147 mg of a white solid (**90%**). **¹H NMR** (300 MHz, d_6 -DMSO, ppm): δ 9.05 (dd, $^3J_{\text{HH}} = 4.4$ Hz, $^4J_{\text{HH}} = 1.8$ Hz, 1H), 8.36 (dd, $^3J_{\text{HH}} = 8.2$ Hz, $^4J_{\text{HH}} = 1.8$ Hz, 1H), 7.99 (d, $^3J_{\text{HH}} = 8.2$ Hz, 1H), 7.71 (s, 1H), 7.61 (m, 4H), 7.48 (s, 1H), 7.46 (d, $^3J_{\text{HH}} = 8.2$ Hz, 1H), 7.40 (d, $^3J_{\text{HH}} = 7.8$ Hz, 1H), 7.25 (dd, $^3J_{\text{HH}} = 7.8$ Hz, $^4J_{\text{HH}} = 1.6$ Hz, 1H), 6.60 (s, 1H), 2.50 (s, 3H). **¹³C {¹H} NMR** (75 MHz, d_6 -DMSO, ppm): δ 151.9, 151.7, 145.3, 143.4, 142.2, 139.5, 136.7, 134.8, 132.8, 130.3, 129.9, 129.6, 129.2, 128.9, 128.2, 126.5, 126.1, 125.8, 122.7, 122.5, 115.3, 115.1, 21.6. **¹⁹F {¹H} NMR** (282 MHz, d_6 -DMSO, ppm): -63.0. **IR (ATR)**: $\bar{\nu}$ = 3076, 2975, 2945, 1616, 1499, 1416, 1327, 1242, 1164, 1116, 1068, 1029, 1011, 843, 786, 742, 680, 651, 586, 573, 538, 530, 482 cm^{-1} . **HRMS (ESI)** calcd. for $\text{C}_{25}\text{H}_{17}\text{F}_3\text{N}_2\text{O}_2\text{S}$ $[\text{M}+\text{H}]^+$: 467.1036; found: 467.1034. **R_f**: 0.44 (dichloromethane). **m.p.** decomposes at 251-252°C.

6-methyl-3-(4-nitrophenyl)-2-(quinolin-8-yl)-2H-benzo[e][1,2]thiazine 1,1-dioxide (1an)



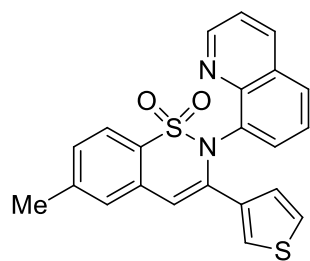
Prepared in accordance to the general synthesis described above: **1a** (104 mg, 0.35 mmol) was converted to **1an**; 150 mg of a white solid (**97%**). **¹H NMR** (300 MHz, d_6 -DMSO, ppm): δ 9.06 (dd, $^3J_{\text{HH}} = 4.4$ Hz, $^4J_{\text{HH}} = 1.8$ Hz, 1H), 8.37 (dd, $^3J_{\text{HH}} = 8.2$ Hz, $^4J_{\text{HH}} = 1.8$ Hz, 1H), 8.05 (s, 4H), 7.90 (dd, $^3J_{\text{HH}} = 8.4$ Hz, $^4J_{\text{HH}} = 1.8$ Hz, 1H), 7.74 (s, 1H), 7.63 (m, 2H), 7.57 (s, 1H), 7.49 (d, $^3J_{\text{HH}} = 8.2$ Hz, 1H), 7.41 (d, $^3J_{\text{HH}} = 7.7$ Hz, 1H), 7.27 (dd, $^3J_{\text{HH}} = 7.4$ Hz, $^4J_{\text{HH}} = 1.4$ Hz, 1H), 2.51 (s, 3H). **¹³C {¹H} NMR** (75 MHz, d_6 -DMSO, ppm): δ 152.0, 151.7, 148.0, 145.2, 143.5, 141.7, 136.7, 136.6, 132.7, 130.0, 129.7, 129.2, 128.9, 128.7, 126.5, 124.1, 122.6, 116.4, 116.2, 21.7. **IR (ATR)**: $\bar{\nu}$ = 3111, 3078, 3010, 1595, 1514, 1469, 1340, 1293, 1188, 1160, 1082, 946, 862, 828, 785, 750, 696, 677, 572, 534, 471, 429 cm^{-1} . **HRMS (ESI)** calcd. for $\text{C}_{25}\text{H}_{17}\text{F}_3\text{N}_2\text{O}_2\text{S}$ $[\text{M}+\text{H}]^+$: 444.1013; found: 444.1017. **R_f**: 0.67 (dichloromethane). **m.p.** >300°C.

3-(3,4-dichlorophenyl)-6-methyl-2-(quinolin-8-yl)-2H-benzo[e][1,2]thiazine-1,1-dioxide (1ao)



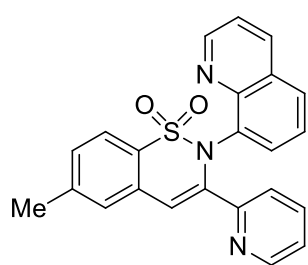
Prepared in accordance to the general synthesis described above: **1a** (104 mg, 0.35 mmol) was converted to **1ao**; 142 mg of a white solid (**85%**). $^1\text{H NMR}$ (300 MHz, d_6 -DMSO, ppm): δ 9.12 (dd, $^3J_{\text{HH}} = 4.2$ Hz, $^4J_{\text{HH}} = 1.7$ Hz, 1H), 8.40 (dd, $^3J_{\text{HH}} = 8.4$ Hz, $^4J_{\text{HH}} = 1.8$ Hz, 1H), 8.10 (d, $^4J_{\text{HH}} = 1.8$ Hz, 1H), 7.92 (d, $^3J_{\text{HH}} = 8.2$ Hz, 1H), 7.77 (dd, $^3J_{\text{HH}} = 8.2$ Hz, $^4J_{\text{HH}} = 1.8$ Hz, 1H), 7.65 (m, 3H), 7.45 (m, 4H), 7.15 (dd, $^3J_{\text{HH}} = 7.8$ Hz, $^4J_{\text{HH}} = 1.0$ Hz, 1H), 2.50 (s, 3H). ^{13}C $\{^1\text{H}\}$ NMR (75 MHz, d_6 -DMSO, ppm): δ 151.9, 151.7, 145.4, 143.5, 141.2, 136.8, 136.1, 134.8, 132.8, 132.4, 131.8, 130.0, 129.9, 129.6, 129.2, 129.0, 128.5, 127.5, 127.3, 122.8, 122.5, 115.2, 115.0, 21.7. IR (ATR): $\bar{\nu} = 3075, 3034, 1618, 1597, 1514, 1471, 1347, 1258, 1177, 1147, 1109, 1083, 1024, 898, 868, 815, 789, 761, 656, 572, 533, 483, 449\text{cm}^{-1}$. HRMS (ESI) calcd. for $\text{C}_{24}\text{H}_{16}\text{Cl}_2\text{N}_2\text{O}_2\text{S}$ $[\text{M}+\text{H}]^+$: 467.0366; found: 467.0371. R_f : 0.39 (95:5 dichloromethane/ethyl acetate). **m.p.** decomposes at 254-255°C.

6-methyl-2-(quinolin-8-yl)-3-(thiophen-3-yl)-2H-thiochromene 1,1-dioxide (1ap)



Following the general procedure above, **1a** (104.4 mg, 0.35 mmol) was converted to **1ap**; 115 mg of a white solid (**87%**). $^1\text{H NMR}$ (300 MHz, d_6 -DMSO, ppm) δ 9.07 (dd, $^3J_{\text{HH}} = 4.4$ Hz, $^4J_{\text{HH}} = 1.8$ Hz, 1H), 8.37 (dd, $^3J_{\text{HH}} = 8.2$ Hz, $^4J_{\text{HH}} = 1.8$ Hz, 1H), 7.90 (dd, $^3J_{\text{HH}} = 8.2$ Hz, $^4J_{\text{HH}} = 1.6$ Hz, 1H), 7.78 (dd, $^3J_{\text{HH}} = 2.8$ Hz, $^4J_{\text{HH}} = 1.4$ Hz, 1H), 7.59 (m, 3H), 7.40 (m, 5H), 7.16 (dd, $^3J_{\text{HH}} = 7.5$ Hz, $^4J_{\text{HH}} = 1.3$ Hz, 1H), 2.46 (s, 3H). ^{13}C $\{^1\text{H}\}$ NMR (75 MHz, d_6 -DMSO, ppm) δ 151.9, 151.6, 145.6, 143.3, 139.4, 137.8, 136.7, 135.5, 133.3, 129.7, 129.3, 128.8, 128.5, 128.3, 126.5, 125.6, 125.4, 122.7, 122.5, 112.9, 112.7, 21.7. IR (ATR): $\bar{\nu} = 3083, 2923, 1592, 1575, 1494, 1387, 1339, 1332, 1307, 1261, 1154, 1087, 1017, 925, 847, 784, 732, 661, 567, 514, 464, 424\text{cm}^{-1}$. HRMS (ESI) calcd. for $\text{C}_{22}\text{H}_{16}\text{N}_2\text{O}_2\text{S}_2$ $[\text{M}+\text{H}]^+$: 405.0731; found: 405.0729. R_f : 0.42 (95:5 dichloromethane/ethyl acetate). **m.p.** 272-274°C.

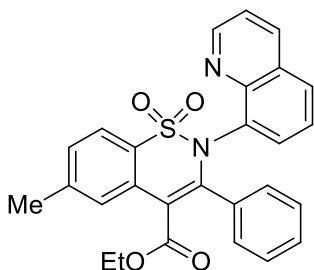
6-methyl-3-(pyridin-2-yl)-2-(quinolin-8-yl)-2H-benzo[e][1,2]thiazine 1,1-dioxide (1aq)



Prepared in accordance to the general synthesis described above: **1a** (104 mg, 0.35 mmol) was converted to **1aq**; 97mg of a white solid (**69%**). $^1\text{H NMR}$ (300 MHz, d_6 -DMSO, ppm) δ 9.05 (dd, $^3J_{\text{HH}} = 4.4$ Hz, $^4J_{\text{HH}} = 1.8$ Hz, 1H), 8.93 (s, 1H), 8.37 (dd, $^3J_{\text{HH}} = 4.2$ Hz, 1H), 8.34 (dd, $^3J_{\text{HH}} = 4.2$ Hz, 1H) 8.09 (m, 1H), 7.89 (dd, $^3J_{\text{HH}} = 8.2$ Hz, $^4J_{\text{HH}} = 1.4$ Hz, 1H), 7.68 (s, 1H), 7.59 (m, 2H), 7.43 (m, 3H), 7.30 (dd, $^3J_{\text{HH}} = 7.6$ Hz, $^4J_{\text{HH}} = 1.3$ Hz, 1H), 7.22 (dd, $^3J_{\text{HH}} = 7.8$ Hz, $^4J_{\text{HH}} = 1.3$ Hz, 1H) 2.50 (s, 3H). ^{13}C $\{^1\text{H}\}$ NMR (75 MHz, d_6 -DMSO, ppm) δ 151.9, 151.7, 150.5, 148.5, 145.2, 143.5, 141.0, 136.8, 134.9, 134.6, 133.0, 131.4, 129.9, 129.5,

129.2, 129.0, 128.8, 126.6, 126.5, 122.8, 114.3, 114.2, 21.7. **IR (ATR):** $\bar{\nu}$ = 3053, 1595, 1560, 1490, 1468, 1383, 1346, 1260, 1184, 1012, 905, 779, 725, 618, 596, 591, 576, 466 cm^{-1} . **HRMS (ESI)** calcd. for $\text{C}_{23}\text{H}_{17}\text{N}_3\text{O}_2\text{S}$ $[\text{M}+\text{H}]^+$: 400.1120; found: 400.1117. **R_f**: 0.48 (95:5 dichloromethane/ethyl acetate). **m.p.** 126-128°C.

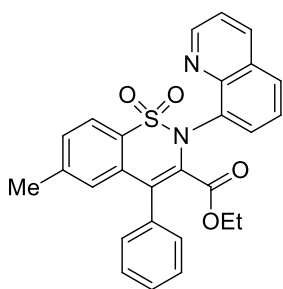
6-methyl-3-phenyl-2-(quinolin-8-yl)-2H-benzo[e][1,2]thiazine-4-carboxylate-1,1-dioxide (1ar)



Following the general procedure above, **1a** (104 mg, 0.35 mmol) was converted to **1ar**; both regioisomers were obtained in a combined yield of 133 mg of white solid (**87%**). **[1] Major product (65% ¹H NMR yield from initial isolated mixture. 69 mg (52%) isolated after recrystallization of the mixture by slow diffusion of pentane into a dichloromethane solution of the initial product mixture):**

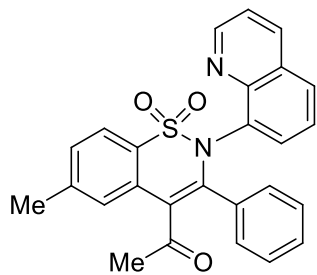
¹H NMR (300 MHz, CDCl_3 , ppm) δ 8.88 (dd, $^3J_{\text{HH}} = 4.2$ Hz, $^4J_{\text{HH}} = 1.8$ Hz, 1H), 8.20 (s, 1H), 7.99 (dd, $^3J_{\text{HH}} = 8.2$ Hz, $^4J_{\text{HH}} = 1.8$ Hz, 1H), 7.76 (d, $^3J_{\text{HH}} = 8.1$ Hz, 1H), 7.62 (dd, $^3J_{\text{HH}} = 8.4$ Hz, $^4J_{\text{HH}} = 1.8$ Hz, 1H), 7.52 (m, 3H), 7.33 (m, 3H), 7.03 (m, 3H), 3.91 (q, $^3J_{\text{HH}} = 7.4$ Hz, 2H), 2.50 (s, 3H), 0.72 (t, $^3J_{\text{HH}} = 7.3$ Hz, 3H). **¹³C {¹H} NMR** (75 MHz, CDCl_3 , ppm) δ 167.7, 151.0, 150.8, 146.9, 145.2, 142.9, 135.6, 135.4, 135.1, 134.1, 131.0, 130.6, 129.6, 129.4, 128.8, 127.6, 126.5, 126.2, 126.1, 125.5, 122.3, 121.7, 116.0, 61.2, 22.2, 13.3. **IR (ATR):** $\bar{\nu}$ = 3059, 2982, 2933, 1720, 1595, 1497, 1470, 1392, 1354, 1278, 1245, 1196, 1178, 1132, 1101, 1013, 944, 867, 815, 746, 704, 678, 652, 639, 571, 507, 489, 451 cm^{-1} . **HRMS (ESI)** calcd. for $\text{C}_{30}\text{H}_{22}\text{N}_2\text{O}_2\text{S}$ $[\text{M}+\text{H}]^+$: 471.1374; found: 471.1374. **R_f**: 0.65 (dichloromethane). **m.p.** 235-236°C.

[2] Minor product (22% ¹H NMR yield from initial isolated mixture – we were unable to fully purify this compound. The characterization data are taken from the minor product signals in the initial isolated product mixture.):



¹H NMR (300 MHz, CDCl_3 , ppm) δ 8.92 (dd, $^3J_{\text{HH}} = 4.2$ Hz, $^4J_{\text{HH}} = 1.8$ Hz, 1H), 8.12 (dd, $^3J_{\text{HH}} = 8.2$ Hz, $^4J_{\text{HH}} = 1.8$ Hz, 1H), 7.80 (dd, $^3J_{\text{HH}} = 8.4$ Hz, $^4J_{\text{HH}} = 1.8$ Hz, 1H), 7.77 (t, $^3J_{\text{HH}} = 8.1$ Hz, 2H), 7.42 (m, 3H), 7.30 (m, 3H), 7.10 (s, 1H), 7.03 (m, 3H), 3.61 (q, $^3J_{\text{HH}} = 7.4$ Hz, 2H), 2.36 (s, 3H), 0.36 (t, $^3J_{\text{HH}} = 7.3$ Hz, 3H). **¹³C {¹H} NMR** (75 MHz, CDCl_3 , ppm) δ 162.4, 151.0, 150.8, 146.9, 145.5, 142.4, 135.8, 135.7, 135.1, 133.8, 131.8, 131.2, 129.5, 129.1, 128.8, 128.0, 127.6, 126.2, 126.1, 125.5, 122.2, 121.7, 116.0, 61.0, 21.8, 12.8.

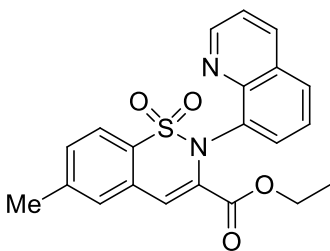
1-(6-methyl-1,1-dioxido-3-phenyl-2-(quinolin-8-yl)-2H-benzo[e][1,2]thiazin-4-yl)ethanone (1as)



Following the general procedure above, **1a** (104 mg, 0.35 mmol) was converted to **1as**; 99 mg of a white solid (**61%**). $^1\text{H NMR}$ (300 MHz, CDCl_3 , ppm) δ 8.97 (dd, $^3J_{\text{HH}} = 4.1$ Hz, $^4J_{\text{HH}} = 1.7$ Hz, 1H), 7.99 (dd, $^3J_{\text{HH}} = 8.2$ Hz, $^4J_{\text{HH}} = 1.8$ Hz, 1H), 7.98 (s, 1H), 7.76 (d, $^3J_{\text{HH}} = 8.1$ Hz, 1H), 7.62 (m, 3H), 7.35 (m, 4H), 7.15 (m, 3H), 7.03 (m, 3H), 2.53 (s, 3H), 1.93 (s, 3H). $^{13}\text{C} \{^1\text{H}\}$ NMR (75

MHz, CDCl_3 , ppm): δ 204.0, 151.1, 150.9, 145.3, 143.9, 143.0, 135.6, 135.7, 134.4, 130.4, 130.2, 129.1, 129.0, 128.8, 128.3, 126.0, 125.9, 125.6, 125.2, 122.5, 122.3, 121.8, 32.3, 22.1. **IR (ATR)**: $\bar{\nu} = 3033, 2971, 2325, 1959, 1725, 1665, 1597, 1497, 1449, 1341, 1285, 1144, 1083, 1026, 956, 882, 813, 764, 696, 550, 481, 457, 420$ cm^{-1} . **HRMS (ESI)** calcd. for $\text{C}_{26}\text{H}_{20}\text{N}_2\text{O}_3\text{S}$ $[\text{M}+\text{H}]^+$: 441.1273; found: 441.1277. **R_f**: 0.70 (dichloromethane). **m.p.** 95-97°C.

Ethyl 6-methyl-2-(quinolin-8-yl)-2H-benzo[e][1,2]thiazine-3-carboxylate 1,1-dioxide (1at)

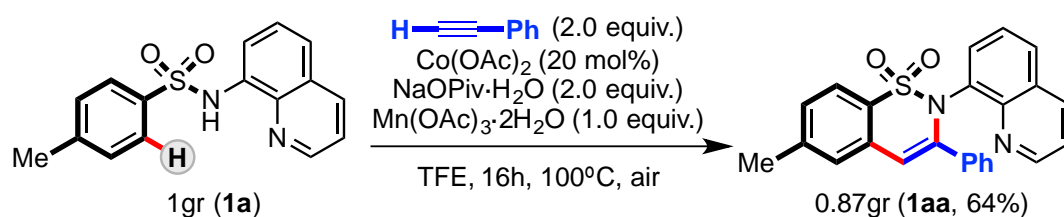


Following the general procedure above, **1a** (104 mg, 0.35 mmol) was converted to **1at**; An only regioisomer was obtained in a yield of 116 mg of white solid (**84%**). $^1\text{H NMR}$ (300 MHz, CDCl_3 , ppm): δ 8.85 (dd, $^3J_{\text{HH}} = 4.2$ Hz, $^4J_{\text{HH}} = 1.7$ Hz, 1H), 8.17 (dd, $^3J_{\text{HH}} = 8.3$ Hz, $^4J_{\text{HH}} = 1.7$ Hz, 1H), 7.82 (dd, $^3J_{\text{HH}} = 8.2$ Hz, $^4J_{\text{HH}} = 1.8$ Hz, 1H), 7.73 (d, $^3J_{\text{HH}} = 8.2$ Hz, 1H),

7.72 (s, 1H), 7.53 (dd, $^3J_{\text{HH}} = 8.2$ Hz, $^4J_{\text{HH}} = 4.2$ Hz, 1H) 7.51 (s, 1H), 7.49 (m, 1H), 7.40 (m, 2H), 3.96 (q, $^3J_{\text{HH}} = 6.7$ Hz, 2H), 2.54 (s, 3H), 0.73 (t, $^3J_{\text{HH}} = 7.8$ Hz, 3H). $^{13}\text{C} \{^1\text{H}\}$ NMR (75 MHz, CDCl_3 , ppm): δ 162.5, 150.8, 145.5, 142.8, 135.7, 135.6, 133.6, 131.5, 131.4, 131.2, 129.3, 128.9, 128.8, 128.7, 125.7, 122.5, 121.7, 120.6, 61.5, 21.7, 13.3. **IR (ATR)**: $\bar{\nu} = 3067, 2923, 2860, 1598, 1560, 1496, 1469, 1382, 1313, 1247, 1186, 1162, 1126, 1095, 1030, 914, 891, 861, 828, 792, 739, 684, 638, 597, 560, 535, 516, 474, 443$ cm^{-1} . **HRMS (ESI)** calcd. for $\text{C}_{21}\text{H}_{18}\text{N}_2\text{O}_4\text{S}$ $[\text{M}+\text{H}]^+$: 395.1060; found: 395.1053. **R_f**: 0.40 (dichloromethane). **m.p.** 202-204°C.

2.3 Miscellaneous

2.3.1 Reaction scale-up



Scheme S23. Synthesis of **1aa** starting from 1gr of substrate **1a**.

Aryl sulfonamide (**1a**) (1.0 g, 3.4 mmol), $\text{Co}(\text{OAc})_2$ (119 mg, 20mol%, 0.7 mmol), $\text{NaOPiv}\cdot\text{H}_2\text{O}$ (952 mg, 2 equiv., 6.7 mmol), $\text{Mn}(\text{OAc})_3\cdot 2\text{H}_2\text{O}$ (898 mg, 1 equiv., 3.4 mmol) and phenylacetylene (**a**) (684 mg, 2 equiv., 6.7 mmol) and 20mL trifluoroethanol were added to a 50 mL round bottom flask under air and attached to a reflux condenser. The resulting mixture was stirred at 100 °C for 16 h and cooled to room temperature. The solvent was removed and the product purified using column chromatography (Silica gel: dichloromethane). After purification product was dried under reduced pressure. 873 mg of a white powder (64%, **1aa**).

Same reaction was performed using 1-Chloro-4-Ethynylbenzene (**1**). 888mg of a white powder was obtained (61%, **1al**).

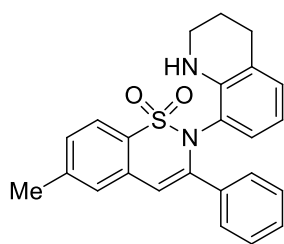
2.3.2 Attempted product upgrading

Several attempts were made to upgrade the sultam product **1aa**; reaction with (1) NaOH in water (RT), (2) cerium ammonium nitrate in water (RT), (3) reaction with sulfuric acid (140 °C), (4) ammonia in methanol and (5) Pd/C with hydrogen. The latter reaction resulted in a reduced quinoline product, leaving the sultam intact, demonstrating the robustness of the sultam motif. Attempts to develop a methodology for removing the quinoline directing group are continuing, but at this point remain elusive.

Methodolgy for Pd/C H_2 reduction of **1aa**:

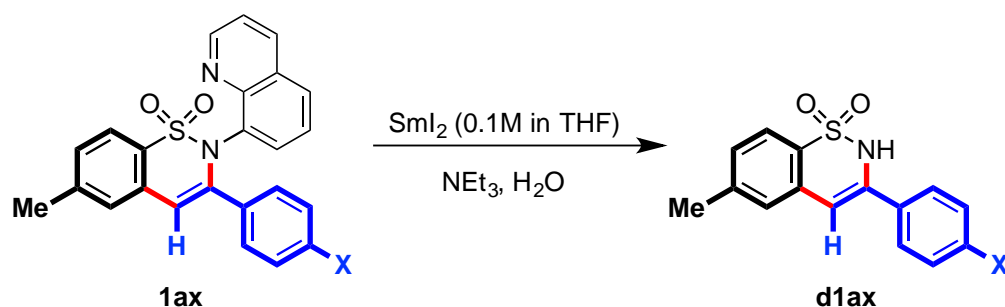
1aa (100mg, 0.34 mmol) was mixed with Pd/C (20mg, 20 wt%) and 5 ml of degassed ethyl acetate in a schlenk. The resulting mixture was stirred at RT for 24h under an atmosphere of hydrogen provided by a balloon. The reaction mixture was filtered through a pad of Celite® pad and the solvent was removed under vacuum. The product was purified using column chromatography (Silica gel: ethyl acetate: hexane 80:20). 75.3 mg of a pale yellow powder (55 %) were obtained. No other notable products were obtained from the purification process.

6-methyl-3-phenyl-2-(1,2,3,4-tetrahydroquinolin-8-yl)-2H-benzo[e][1,2]thiazine-1,1-dioxide (1aaH₄)



¹H-NMR (400 MHz, CDCl₃, ppm): δ 7.75 (d, ³J_{HH} = 7.9 Hz, 1H), 7.70 (m, 2H), 7.39 (s, 1H), 7.31 (m, 4H), 6.90 (s, 1H), 6.74 (m, 1H), 6.30 (dd, ³J_{HH} = 7.9 Hz, ⁴J_{HH} = 1.7 Hz, 1H), 6.23 (t, ³J_{HH} = 7.8 Hz, 1H), 4.93 (br s, 1H), 3.48 (m, 2H), 2.80 (m, 1H), 2.65 (m, 1H), 2.52 (s, 3H), 2.03 (m, 1H), 1.84 (m, 1H). ¹³C-NMR (100 MHz, CDCl₃, ppm): δ 145.1, 143.3, 143.2, 135.2, 133.1, 129.7, 129.5, 129.2, 128.4, 128.3, 127.8, 127.4, 125.2, 123.0, 122.9, 122.4, 115.5, 112.5, 41.9, 27.2, 21.8, 21.7. HRMS (ESI) calcd. for C₂₄H₂₂N₂O₂S [M+Na]⁺: 425.1294; found: 425.1296

Methodology for Samarium (II) Iodide reduction of **1aa**:



Scheme S24. Attempted cleavage of the 8-aminoquinoline directing group with SmI₂.

1ax (0.085mmol), SmI₂ (0.1M in THF), H₂O (7μL, 0.34mmol) and NEt₃ (25μL, 0.18mmol) were mixed in a 10mL vial under N₂. The resulting mixture was stirred at RT under a N₂ atmosphere. The mixture was then diluted with CH₂Cl₂ and washed with HCl_{dil} (3x10mL). The organic layer was dried over MgSO₄ and solvent was removed under reduced pressure. The crude was purified using column chromatography (Silica gel: dichloromethane).

Table S28. Optimization of time employed for the synthesis of cyclic sulfonamides

entry	benzosultam	SmI ₂ eq.	base	time (h)	yield	recovery of lax
1	laa	6	NEt ₃	24	nr ^[a]	Traces
2		3	NEt ₃	2	nr	94%
3		3	-	2	nr	98%
4	lac	6	NEt ₃	24	nr ^[a]	Traces

^[a]Starting material containing 8-aminoquinoline was observed in trace amounts using ¹H-NMR, however we were not able to isolate or identify the products.

2.3.3 Intermolecular competition experiments

a) Terminal versus internal alkynes (Scheme VII.11a)

Aryl sulfonamide (**1a**) (81 mg, 0.27 mmol), $\text{Co}(\text{OAc})_2$ (9.6 mg, 20mol%, 0.05 mmol), $\text{NaOPiv}\cdot\text{H}_2\text{O}$ (77 mg, 2 equiv., 0.54 mmol), $\text{Mn}(\text{OAc})_3\cdot 2\text{H}_2\text{O}$ (74 mg, 1 equiv., 0.27 mmol), phenylacetylene (**a**) (55 mg, 2 equiv., 0.54 mmol), 1,2-diphenylacetylene (**g**) (96 mg, 2 equiv., 0.54 mmol) and 2mL trifluoroethanol were added to a glass vial under air and the vial sealed. The resulting mixture was stirred at 100 °C for 16 h and cooled to room temperature. The reaction crude was analysed by ^1H -NMR spectroscopy (CDCl_3) using mesitylene as internal standard. A product ratio of 15:1 was observed (Yield: **1aa**, 75%; **1ag**, 5%, based on **1a**).

The reaction of phenylacetylene (**a**) and 1,2-diphenylacetylene (**g**) was also followed independently over time (separate reactions of (**a**) and (**b**)):

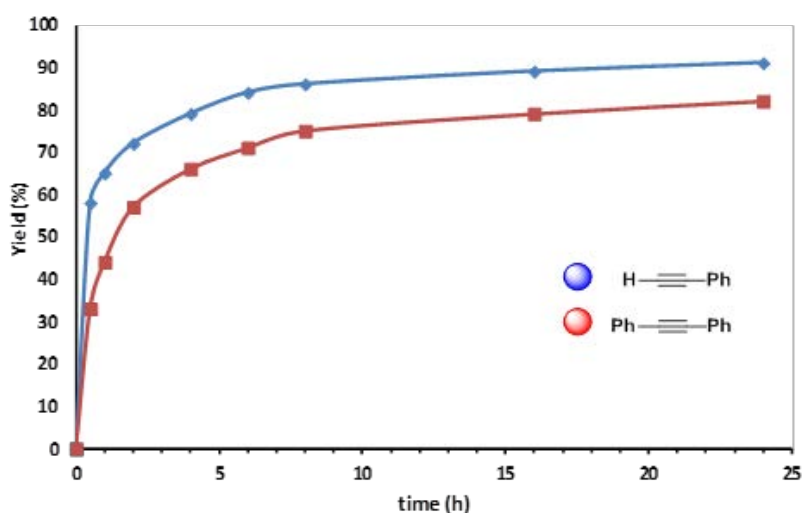


Figure S61. Reaction profiles of the evolution of products using internal and terminal alkynes.

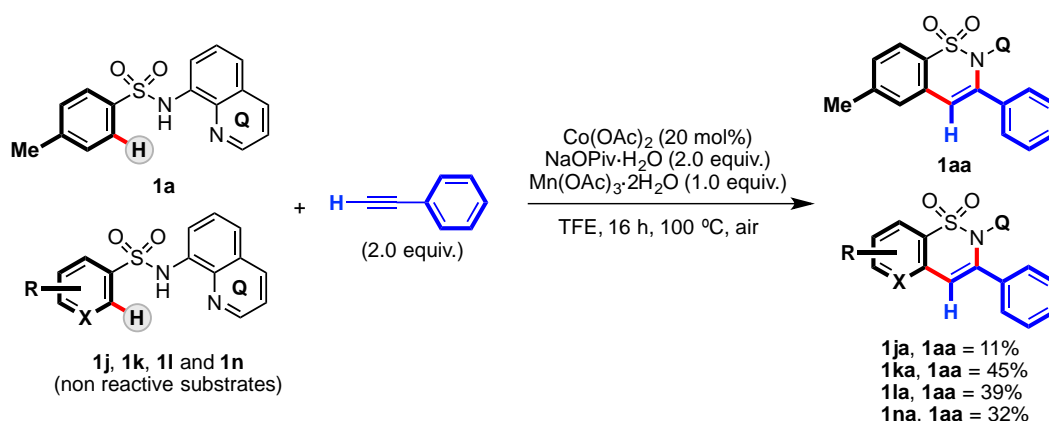
b) EDG versus EWG sulfonamides (Scheme VII.11b)

1b (85 mg, 0.27 mmol), **1c** (86 mg, 0.27 mmol), $\text{Co}(\text{OAc})_2$ (9.6 mg, 20mol%, 0.05 mmol), $\text{NaOPiv}\cdot\text{H}_2\text{O}$ (77 mg, 2 equiv., 0.54 mmol), $\text{Mn}(\text{OAc})_3\cdot 2\text{H}_2\text{O}$ (74 mg, 1 equiv., 0.27 mmol), phenylacetylene (**a**) (14.2 mg, 0.5 equiv., 0.14 mmol) and 2mL trifluoroethanol were added to a glass vial under air and the vial sealed. The resulting mixture was stirred at 100 °C for 16 h and cooled to room temperature. The reaction crude was analysed by ^1H -NMR spectroscopy (CDCl_3) using mesitylene as internal standard. **1ba** was obtained in 45% yield and **1ca** was obtained in 38% yield (Yield based on **a**).

c) EDG versus EWG para-substituted phenylacetylenes (Scheme VII.11c)

Aryl sulfonamide (**1a**) (81 mg, 0.27 mmol), Co(OAc)₂ (9.6 mg, 20mol%, 0.05 mmol), NaOPiv.H₂O (77 mg, 2 equiv., 0.54 mmol), Mn(OAc)₃.2H₂O (74 mg, 1 equiv., 0.27 mmol), p-methoxy-phenylacetylene (**j**) (71 mg, 2 equiv., 0.54 mmol), p-nitrophenylacetylene (**m**) (80 mg, 2 equiv., 0.54 mmol) and 2mL trifluoroethanol were added to a glass vial under air and the vial sealed. The resulting mixture was stirred at 100 °C for 16 h and cooled to room temperature. The reaction crude was analysed by ¹H-NMR spectroscopy (CDCl₃) using mesitylene as internal standard. **1an** was obtained in 34% yield and **1aj** was detected in trace amounts (<1%) (Yield based on **1a**).

d) Poisoning experiments – Presence of para-nitro/ortho-substituted benzenesulfonamides or pyridine sulfonamides



Scheme S25. Synthesis of **1aa** starting from lgr of substrate **1a**.

1a (50 mg, 0.17 mmol), **1j**, **1k** or **1l** (0.17 mmol), Co(OAc)₂ (6.4 mg, 20mol%, 0.034 mmol), NaOPiv.H₂O (42 mg, 2 equiv., 0.34 mmol), Mn(OAc)₃.2H₂O (46 mg, 1 equiv., 0.17 mmol), phenylacetylene (**a**) (68 mg, 2 equiv., 0.34 mmol) and 2 mL trifluoroethanol were added to a glass vial under air and the vial sealed. The resulting mixture was stirred at 100 °C for 16 h and cooled to room temperature. The reaction crude was analysed by ¹H NMR spectroscopy (CDCl₃) using mesitylene as internal standard. Results are summarized in the following table.

Table S29. Synthesis of **1aa** starting from lgr of substrate **1a**.

entry	poison	yield of 1aa ^a	yield of 1xa ^a
1	none	91%	-
2	1j	11%	x = j, 0%
3	1k	45%	x = k, traces
4	1l	39%	x = l, traces
5	1n	32%	x = n, 2%

^[a]Yield calculated from ¹H NMR of crude using mesitylene as internal standard

3.3.4 Deuterium exchange experiments

a) Using deuterated Methanol as solvent (Scheme VII.12a)

1a (0.35 mmol), Co(OAc)₂ (12.4 mg, 20 mol%, 0.07 mmol), NaOPiv.H₂O (86.8 mg, 2 equiv., 0.70 mmol), Mn(OAc)₃.2H₂O (94.0 mg, 1 equiv., 0.7 mmol), Phenylacetylene (**a**) (2 equiv., 0.70 mmol) and 2mL CD₃OD were added to a glass vial under air and the vial sealed. The resulting mixture was stirred at 100 °C for 16 h and cooled to room temperature. The solvent was removed and the product purified using column chromatography (Silica gel: dichloromethane). After purification the product was dried under reduced pressure. (Yield: 61%, 0.21mmol, 85.1mg; 22% H and 78% D, ¹H-NMR).

b) Deuterium exchange in substrate

1a (0.35 mmol), Co(OAc)₂ (12.4 mg, 20 mol%, 0.07 mmol), NaOPiv.H₂O (86.8 mg, 2 equiv., 0.70 mmol), Mn(OAc)₃.2H₂O (94.0 mg, 1 equiv., 0.35 mmol) and 2mL CD₃OD were added to a glass vial under air and the vial sealed. The resulting mixture was stirred at 100 °C for 16 h and cooled to room temperature. The solvent was removed and the product purified using flash-column chromatography (Silica gel: dichloromethane). After purification the product was dried under reduced pressure. (Recovery: 92%, 0.32 mmol, 96.3mg. 90% H and 10% D, ¹H-NMR).

b) Using Phenylacetylene-d₁ as substrate

1a (0.35 mmol), Co(OAc)₂ (12.4 mg, 20 mol%, 0.07 mmol), NaOPiv.H₂O (86.8 mg, 2 equiv., 0.70 mmol), Mn(OAc)₃.2H₂O (94.0 mg, 1 equiv., 0.7 mmol), **Phenylacetylene-d₁ (a-D)** (2 equiv., 0.70 mmol) and 2 mL CF₃CH₂OH were added to a glass vial under air and the vial sealed. The resulting mixture was stirred at 100 °C for 16 h and cooled to room temperature. The solvent was removed and the product purified using column chromatography (Silica gel: dichloromethane). After purification the product was dried under reduced pressure. (Yield: 82%, 0.29 mmol, 114.4 mg; 66% H and 34% D, ¹H-NMR).

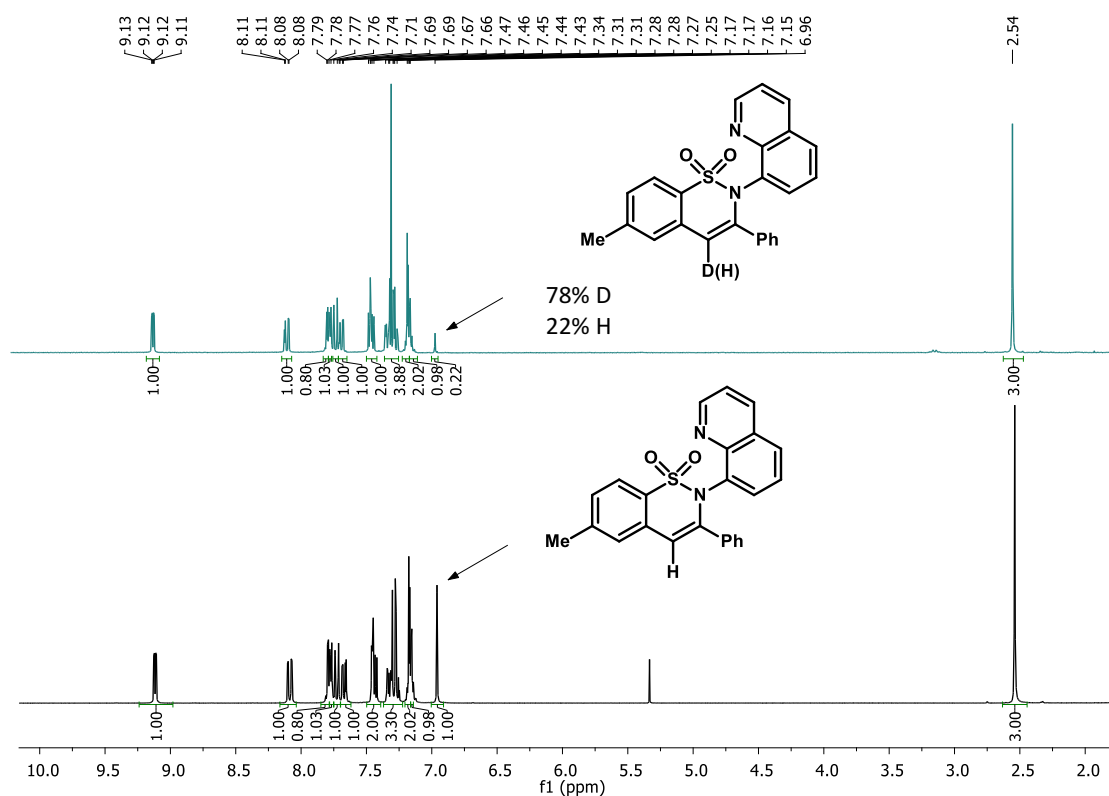


Figure S62. $^1\text{H-NMR}$ of **1aa-D** (blue, 78% D-incorporated) obtained after reaction with Phenylacetylene in CD_3OD .

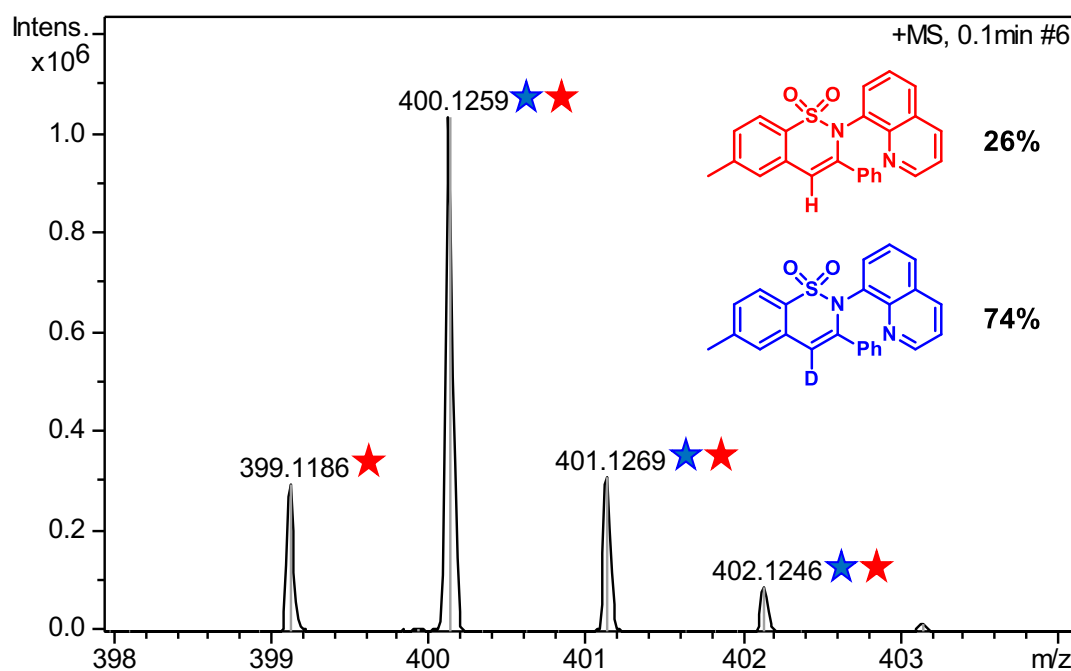


Figure S63. HRMS-ESI-QTOF of **1aa-D** obtained after reaction with Phenylacetylene in CD_3OD . Mass analysis shows 74% D incorporation in agreement with $^1\text{H-NMR}$ (Figure S62). Deuterium incorporation was measured by the relative intensity of the peaks in the mass spectrum corresponding to the deuterated and non-deuterated products.

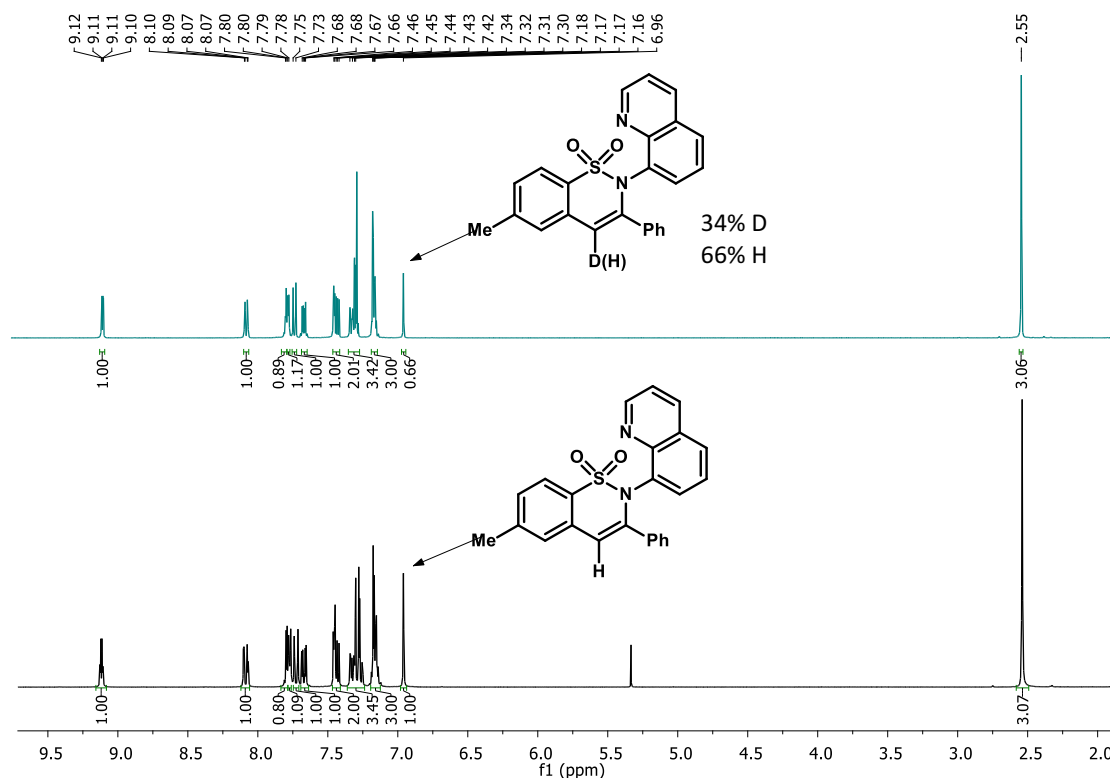


Figure S64. $^1\text{H-NMR}$ of **1aa-D** (blue, 34% D incorporated) obtained after reaction with Phenylacetylene- d_1 in $\text{CF}_3\text{CH}_2\text{OH}$.

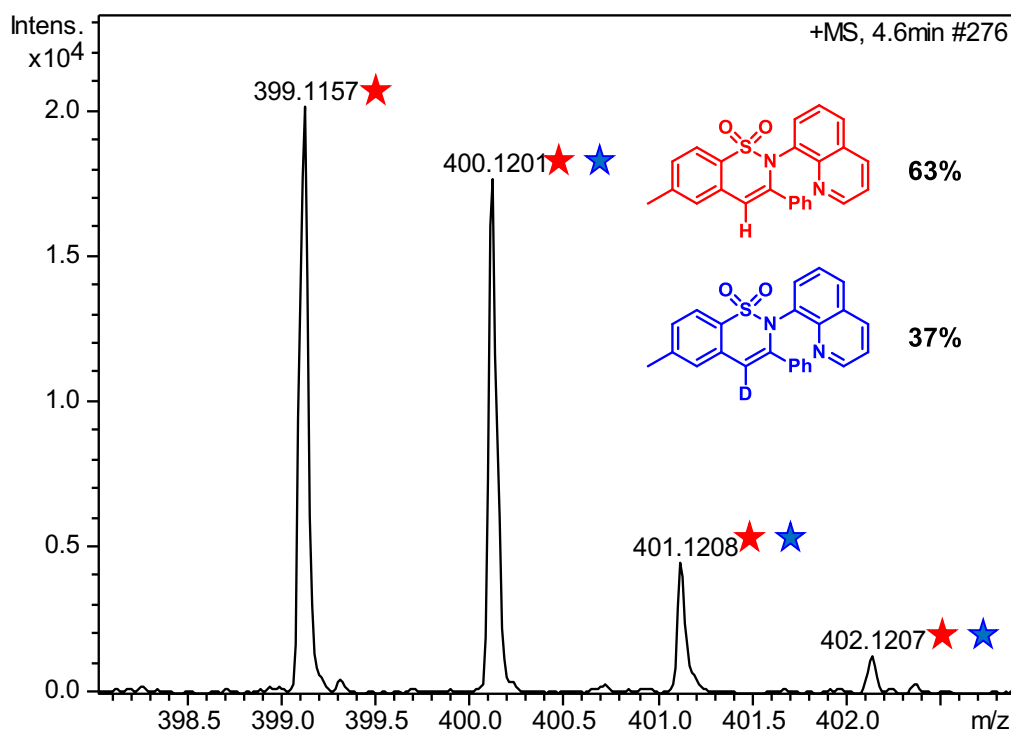


Figure S65. HRMS-ESI-QTOF of **1aa-D** obtained after reaction with Phenylacetylene- D_1 in $\text{CF}_3\text{CH}_2\text{OH}$. Mass analysis shows 37% D incorporation in agreement with $^1\text{H-NMR}$ (Figure S64). Deuterium incorporation was measured by the relative intensity of the peaks in the mass spectrum corresponding to the deuterated and non-deuterated products.

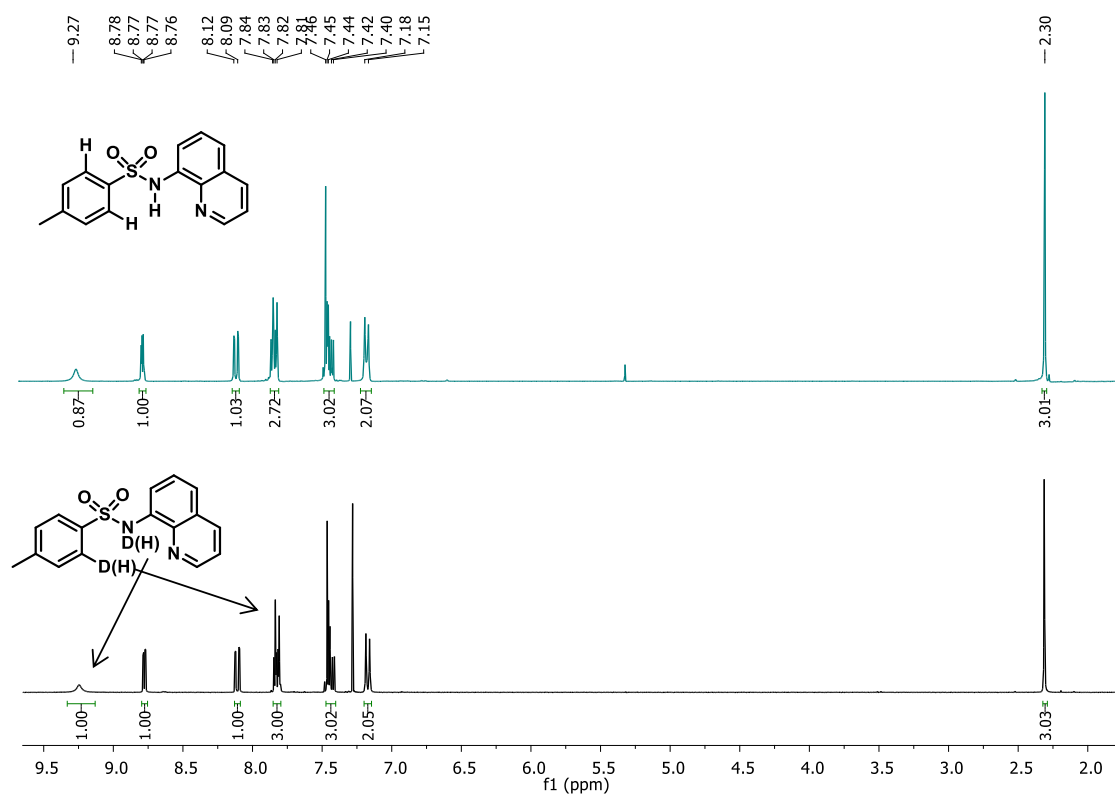


Figure S66. $^1\text{H-NMR}$ of **1a-D** (blue, 13% D incorporated in N-H and 28% D incorporated in the aryl ring) obtained after 16h under optimized conditions in CD_3OD , compared to the $^1\text{H-NMR}$ of **1a** (black).

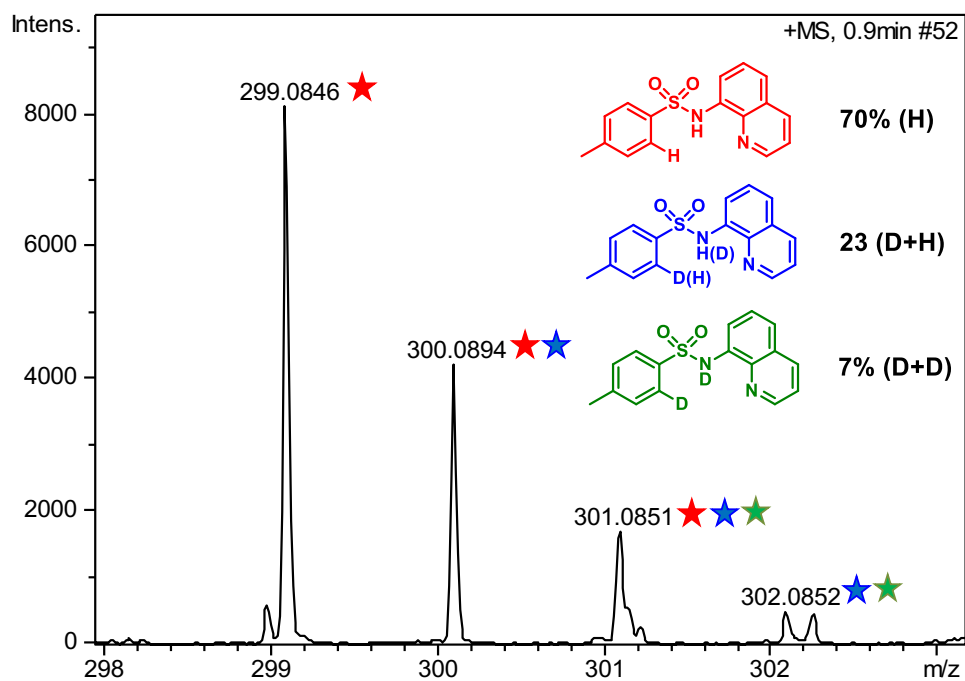


Figure S67. HRMS-ESI-QTOF of **1a-D** obtained after reaction with Phenylacetylene in CD_3OD . Deuterium incorporation was measured by the relative intensity of the peaks in the mass spectrum corresponding to the deuterated and non-deuterated products.

3.3.5 Intermolecular Kinetic Isotope Effect (Scheme VII.12b)

100 mg of **1e** (1 equiv., 0.35 mmol), 101 mg (1 equiv., 0.35 mmol) of $[D]_5\text{-1e}^{[a]}$, $\text{Co}(\text{OAc})_2$ (24 mg, 20mol%, 0.14 mmol), $\text{NaOPiv}\cdot\text{H}_2\text{O}$ (172 mg, 2 equiv., 1.40 mmol), $\text{Mn}(\text{OAc})_3\cdot 2\text{H}_2\text{O}$ (188 mg, 1 equiv., 0.7 mmol) and phenylacetylene (**a**) (35.7 mg, 1 equiv., 0.35 mmol) with 4 mL trifluoroethanol were added to a glass vial under air and the vial sealed. The resulting mixture was stirred at 100°C for 16h and cooled to room temperature. The solvent was removed and the product purified using column chromatography (Silica gel: dichloromethane). After purification the product was dried under reduced pressure (75.1 mg, 56% respect to **a**). The kinetic isotope effect was determined to be 3.5 as judged by $^1\text{H-NMR}$ spectroscopy:

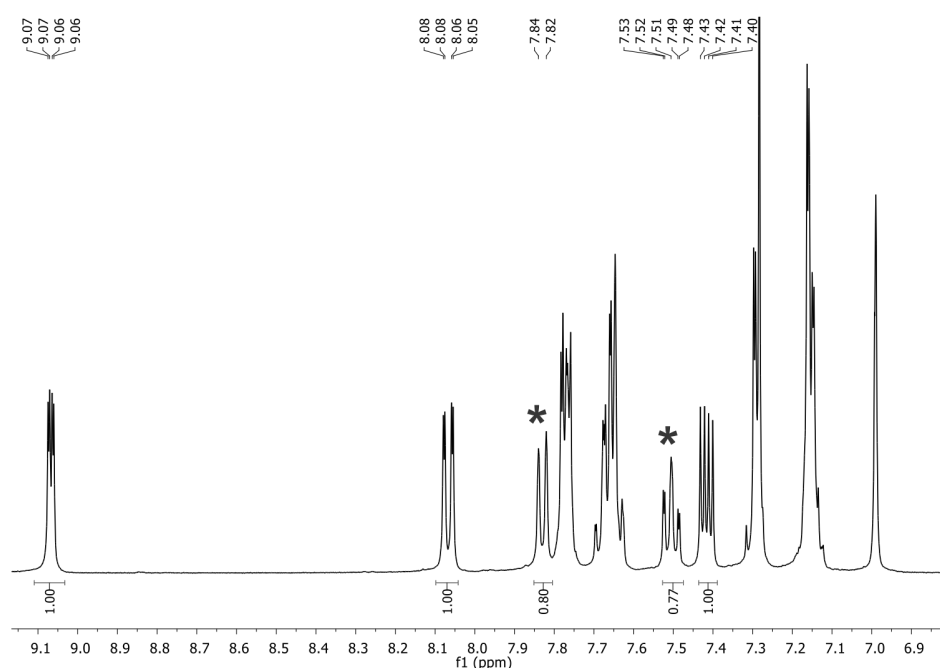


Figure S68. $^1\text{H NMR}$ of product from $[D/H]_5\text{-1e}$ intermolecular KIE experiment. Peaks marked in red were used to calculate the $k_{\text{H}}/k_{\text{D}}$ ratio. Integral value was taken as the average of two peaks.

3.3.6 Reactions in the presence of radical scavengers

1a (0.35 mmol), $\text{Co}(\text{OAc})_2$ (12.4 mg, 20 mol%, 0.07 mmol), $\text{NaOPiv}\cdot\text{H}_2\text{O}$ (86.8 mg, 2 equiv., 0.70 mmol), $\text{Mn}(\text{OAc})_3\cdot 2\text{H}_2\text{O}$ (94.0 mg, 1 equiv., 0.35 mmol), phenylacetylene (**a**) (2 equiv., 0.70 mmol), **Radical Scavenger** (2 equiv., 0.7 mmol) and 2mL $\text{CF}_3\text{CH}_2\text{OH}$ were added to a glass vial under air and the vial sealed. The resulting mixture was stirred at 100 °C for 16 h and cooled to room temperature. The reaction crude was analysed by $^1\text{H-NMR}$ spectroscopy (CDCl_3) using mesitylene as internal standard after a flash silica column (dichloromethane).

3.3.7 Crystallographic data information

Crystallographic data for compounds **1aa** (CCDC-1407285), **1ah** (CCDC-1407286), product derived from 1aa using Pd/C H₂ (**1aaH₄**) (CCDC-1407287) and **1ar** (major regioisomer) (CCDC-1411541) can be obtained free of charge from the Cambridge Crystallographic Data Centre via www.ccdc.cam.ac.uk/data_request/cif. Furthermore, the corresponding CIF files have been included in the Supplementary Digital Material included in the attached CD.

X-Ray structure of **1aa**:

Colorless crystals were grown by slow diffusion of pentane into a dichloromethane solution of the compound, and used for low temperature (143(2) K) X-ray structure determination. The measurement was carried out on a *BRUKER SMART APEX CCD* diffractometer using graphite-monochromated Mo *K* α radiation ($\lambda = 0.71073$ Å) from an x-Ray Tube. The measurements were made in the range 2.152 to 28.285° for θ . Full-sphere data collection was carried out with ω and ϕ scans. A total of 58854 reflections were collected of which 4882 [R(int) = 0.0648] were unique. Programs used: data collection, Smart^[2]; data reduction, Saint+^[13]; absorption correction, SADABS^[14]. Structure solution and refinement was done using SHELXTL^[15].

The structure was solved by direct methods and refined by full-matrix least-squares methods on F^2 . The non-hydrogen atoms were refined anisotropically. The H-atoms were placed in geometrically optimized positions and forced to ride on the atom to which they are attached.

Table S30. Crystallographic data of **1aa**.

Chemical formula	C ₂₄ H ₁₈ N ₂ O ₂ S
fw (g mol⁻¹)	398.46
T (K)	143(2)
Space group	Orthorhombic, <i>Pbca</i>
<i>a</i> (Å)	13.2726(13)
<i>b</i> (Å)	15.6962(16)
<i>c</i> (Å)	18.9250(19)
α (deg.)	90
β (deg.)	90
γ (deg.)	90
<i>V</i> (Å³)	3942.6(7)
$\rho_{\text{calcd.}}$ (g cm⁻³)	1.343
λ (Å)	0.71073
R₁ [<i>I</i> > 2σ(<i>I</i>)]	0.0491
wR₂ [<i>I</i> > 2σ(<i>I</i>)]	0.1136

X-Ray structure of **1ah'**:

Colorless crystals were grown by slow diffusion of hexane into a dichloromethane solution of the compound, and used for low temperature (143(2) K) X-ray structure determination. The measurement was carried out on a *BRUKER SMART APEX CCD* diffractometer using graphite-monochromated Mo $K\alpha$ radiation ($\lambda = 0.71073 \text{ \AA}$) from an x-Ray Tube. The measurements were made in the range 2.907 to 28.260° for θ . Full-sphere data collection was carried out with ω and ϕ scans. A total of 11179 reflections were collected of which 4375 [$R(\text{int}) = 0.0957$] were unique. Programs used: data collection, *Smart*^[12]; data reduction, *Saint+*^[13]; absorption correction, *SADABS*^[14]. Structure solution and refinement was done using *SHELXTL*^[15].

The structure was solved by direct methods and refined by full-matrix least-squares methods on F^2 . The non-hydrogen atoms were refined anisotropically. The H-atoms were placed in geometrically optimized positions and forced to ride on the atom to which they are attached.

Table S31. Crystallographic data of **1ah'**.

Chemical formula	$\text{C}_{21}\text{H}_{18}\text{N}_2\text{O}_2\text{S}$
fw (g mol⁻¹)	362.43
T (K)	143(2)
Space group	Triclinic, P-1
<i>a</i> (Å)	7.754(3)
<i>b</i> (Å)	11.381(4)
<i>c</i> (Å)	11.791(4)
α (deg.)	99.494(6)
β (deg.)	109.022(6)
γ (deg.)	102.707(6)
<i>V</i> (Å³)	927.6(5)
$\rho_{\text{calcd.}}$ (g cm⁻³)	1.298
λ (Å)	0.71073
R_1 [$I > 2\sigma(I)$]	0.1115
wR_2 [$I > 2\sigma(I)$]	0.2797

X-Ray structure of product derived from 1aa using Pd/C H₂: (**1aaH₄**)

Colorless crystals were grown by slow diffusion of Pentane into a chloroform solution of the compound, and used for low temperature (143(2) K) X-ray structure determination. The measurement was carried out on a *BRUKER SMART APEX CCD* diffractometer using graphite-monochromated Mo $K\alpha$ radiation ($\lambda = 0.71073 \text{ \AA}$) from an x-Ray Tube. The measurements were made in the range 1.986 to 28.213° for θ . Full-sphere data collection was carried out with ω and ϕ scans. A total of 7959 reflections were collected of which 3907 [R(int) = 0.0506] were unique. Programs used: data collection, Smart¹²; data reduction, Saint+^[13]; absorption correction, SADABS^[14]. Structure solution and refinement was done using SHELXTL^[15].

The structure was solved by direct methods and refined by full-matrix least-squares methods on F^2 . The non-hydrogen atoms were refined anisotropically. The H-atoms were placed in geometrically optimized positions and forced to ride on the atom to which they are attached, except N-H Hydrogen which was located in the difference Fourier Map and refined without constrains.

Table S32. Crystallographic data of **1aaH₄**.

Chemical formula	C ₂₄ H ₂₂ N ₂ O ₂ S
fw (g mol⁻¹)	402.49
T (K)	143(2)
Space group	Monoclinic, P 21/c
a (Å)	16.907(5)
b (Å)	13.192(4)
c (Å)	9.196(3)
α (deg.)	90
β (deg.)	105.281(6)
γ (deg.)	90
V (Å³)	1978.4(11)
$\rho_{\text{calcd.}}$ (g cm⁻³)	1.351
λ (Å)	0.71073
R₁ [I > 2sigma(I)]	0.0650
wR₂ [I > 2sigma(I)]	0.1402

X-Ray structure of **1ar** (major regioisomer):

Colorless crystals were grown by slow diffusion of Pentane into a chloroform solution of the compound, and used for low temperature (143(2) K) X-ray structure determination. The measurement was carried out on a *BRUKER SMART APEX CCD* diffractometer using graphite-monochromated Mo $K\alpha$ radiation ($\lambda = 0.71073 \text{ \AA}$) from an x-Ray Tube. The measurements were made in the range 2.215 to 28.372° for θ . Full-sphere data collection was carried out with ω and ϕ scans. A total of 35817 reflections were collected of which 5869 [R(int) = 0.0892] were unique. Programs used: data collection, Smart¹²; data reduction, Saint+^[13]; absorption correction, SADABS^[14]. Structure solution and refinement was done using SHELXTL^[15].

The structure was solved by direct methods and refined by full-matrix least-squares methods on F^2 . The non-hydrogen atoms were refined anisotropically. The H-atoms were placed in geometrically optimized positions and forced to ride on the atom to which they are attached, except N-H Hydrogen which was located in the difference Fourier Map and refined without constrains.

Table S33. Crystallographic data of **1ar**.

Chemical formula	C ₂₇ H ₂₂ N ₂ O ₄ S
fw (g mol⁻¹)	470.52
T (K)	173(2)
Space group	Monoclinic, P 21/c
a (Å)	9.639(2)
b (Å)	13.379(3)
c (Å)	18.394(4)
α (deg.)	90
β (deg.)	90.907(4)
γ (deg.)	90
V (Å³)	2371.9(9)
$\rho_{\text{calcd.}}$ (g cm⁻³)	1.318
λ (Å)	0.71073
R₁ [I > 2sigma(I)]	0.0991
wR₂ [I > 2sigma(I)]	0.2452

3. References

- (1) Bew, S.P.; Hiatt-Gipson, G.D.; Lovell, J. A.; Poullain, C. *Org. Lett.*, **2012**, *14*, 456.
- (2) Dong, X.; Sang, R.; Wang, Q.; Tang, X.-Y.; Shi, M.; *Chem. Eur. J.*, **2013**, *19*, 16910.
- (3) M. Rouffet, M.; de Oliveira, C. A. F.; Udi, Y.; Agrawal, A.; Sagi, I.; McCammon, J. A.; Cohen, S. M. *J. Am. Chem. Soc.*, 2010, **132**, 8232.
- (4) S. Dayan, S.; Kalaycioglu, N. O.; Daran, J.-C.; Labande, A.; Poli, R. *Eur. J. Inorg. Chem.*, **2013**, 3224.
- (5) Wang, Q.; Zhang, J.; Z Guo, Z. *Bioorg. Med. Chem.*, **2007**, *15*, 7561.
- (6) Buhr, W.; Burckhardt, S.; Dürrenberger, F.; Funk, F.; Geisser, P. O.; Corden, V. A.; Courtney, S. M.; Dawson, G.; Davenport, T.; Slack, M.; Ridgill, M. P.; Yarnold, C. J.; Boyce, S.; Ellenbroek, A. A.; Patent US2012214803A1, **2012**.
- (7) Xie, Y.; Gong, G.; Liu, Y.; Deng, S.; Rinderspacher, A.; Branden, L.; Landry, D. W.; *Tetrahedron Lett.*, **2008**, *49*, 2320.
- (8) Boyce, S.; Buhr, W.; Burckhardt, S.; Corden, V. A.; Courtney, S. M.; Davenport, T.; Dawson, G.; Dürrenberger, F.; Ellenbroek, A. A.; Funk, F.; Geisser, P. O.; Ridgill, M. P.; Slack, M.; Yarnold, C. J. Patent WO2012110603A1, **2012**.
- (9) Srinivas, K.; Saiprathima, P.; Balaswamy, K.; Rao, M. M. *J. Organomet. Chem.* **2013**, *741-742*, 162.
- (10) Reddy, C. R.; Mahipal, B.; Yaragorla, S. R. *Tetrahedron Lett.* **2007**, *48*, 7528.
- (11) Xu, C.; Xu, M.; Jia, Y.; Li, C. *Org. Lett.* **2011**, *13*, 1556.
- (12) Bruker Advanced X-ray Solutions. SMART: Version 5.631, **1997-2002**.
- (13) Bruker Advanced X-ray Solutions. SAINT +, Version 6.36A, **2001**.
- (14) Sheldrick, G. M. *Empirical Absorption Correction Program*, Universität Göttingen, 1996
Bruker Advanced X-ray Solutions. SADABS Version 2.10, **2001**.
- (15) Sheldrick, G. M. *Program for Crystal Structure Refinement*, Universität Göttingen, 1997
Bruker Advanced X-ray Solutions. SHELXTL Version 6.14, **2000-2003**. SHELXL-2013 (Sheldrick, 2013).

Supporting Information for Chapter VI

A First Example of Co-Catalyzed Remote C-H Functionalization of 8-aminoquinolines operating through a Single Electron Transfer Mechanism

Christopher J. Whiteoak,* Oriol Planas, Anna Company and Xavi Ribas*

Table of Contents

1. GENERAL EXPERIMENTAL CONSIDERATIONS	S115
2. GENERAL PROCEDURE FOR NITRATION REACTIONS.....	S115
3. POISONING STUDIES	S116
4. COMPETITION STUDIES.....	S116
5. SYNTHESIS AND CHARACTERIZATION DATA FOR PRODUCTS (Table VII.12).....	S117
6. SYNTHESIS AND CHARACTERIZATION DATA FOR PRODUCTS (Scheme VII.15) ..	S123
6.1 Gram-scale nitration of substrate 1	S123
6.2 Upgrading of products 1a and 1b.....	S123
7. SYNTHESIS AND CHARACTERIZATION DATA FOR 5-R-8-AMINOQUINOLINES....	S126
8. SYNTHESIS AND CHARACTERIZATION DATA FOR PRODUCTS (Table VII.13)	S130
9. X-RAY CRYSTALLOGRAPHIC DATA	S132
9.1 X-Ray structure of 11b	S132
9.2 X-Ray structure of 13b.....	S133
9.3 X-Ray structure of 15a.....	S134
10. KINETIC ISOTOPE EFFECT (KIE) EXPERIMENT.....	S135
11. REFERENCES	S136

1. General experimental considerations

All solvents and reagents were purchased from Sigma-Aldrich, Fisher Scientific or Fluorochem and used without further purification. ^1H , $^{13}\text{C}\{^1\text{H}\}$ and ^{19}F NMR spectra were recorded on Bruker AV-400 spectrometers in either CDCl_3 (99.8% D, containing 0.03% v/v TMS) or $\text{D}_6\text{-DMSO}$ (99.9% D) and referenced to the residual deuterated solvent signals. High Resolution Mass Spectra (HRMS) were recorded by the Serveis Tècnics of the University of Girona on a Bruker MicroTOF-Q IITM instrument using an ESI ionization source. Starting amides were synthesized according reported protocols.¹⁻¹¹

2. General procedure for nitration reactions

A 10 mL vial was charged with 0.5 mmol of substrate, $\text{Co}(\text{NO}_3)_2 \cdot 6\text{H}_2\text{O}$ (29.1 mg, 20 mol%, 0.1 mmol), *tert*-butyl nitrite (267 μL , 90%, 4.0 equiv., 2.0 mmol) and 3.5 mL of acetic acid. The vial was sealed and the reaction stirred at room temperature for 18 hours. After this period the reaction mixture was diluted with ethyl acetate (30 mL) and extracted using brine (20 mL). The aqueous layer was then further extracted with ethyl acetate (2 x 30 mL), the organic layers combined, dried over magnesium sulfate and the solvent removed under reduced pressure. The crude reaction mixture was purified by column chromatography, using dichloromethane as eluent unless stated, providing analytically pure nitrated products.

Note: For the ^1H NMR calculations of conversion and quantification of the two products, an aliquot of the reaction crude was analyzed using 1,3,5-trimethoxybenzene as internal standard (see Figure S1 for an example).

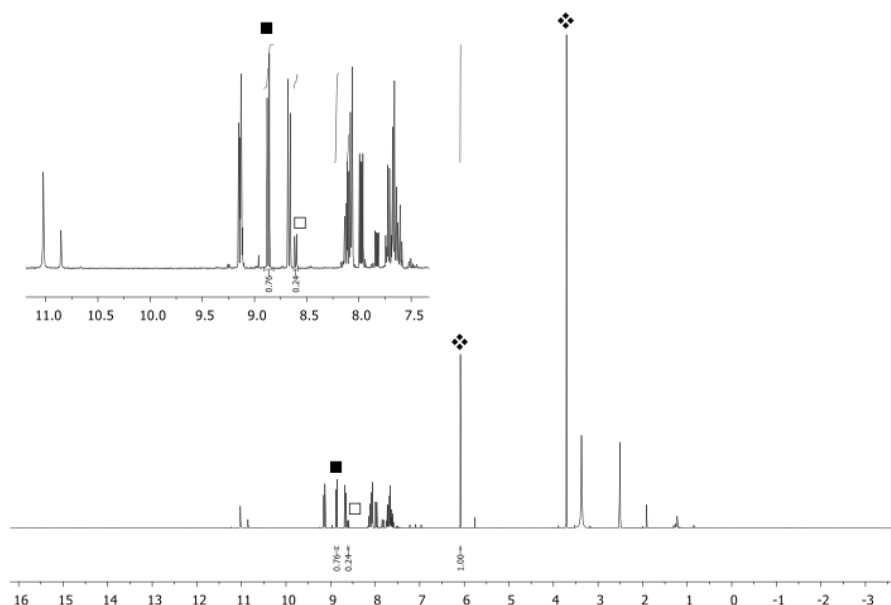
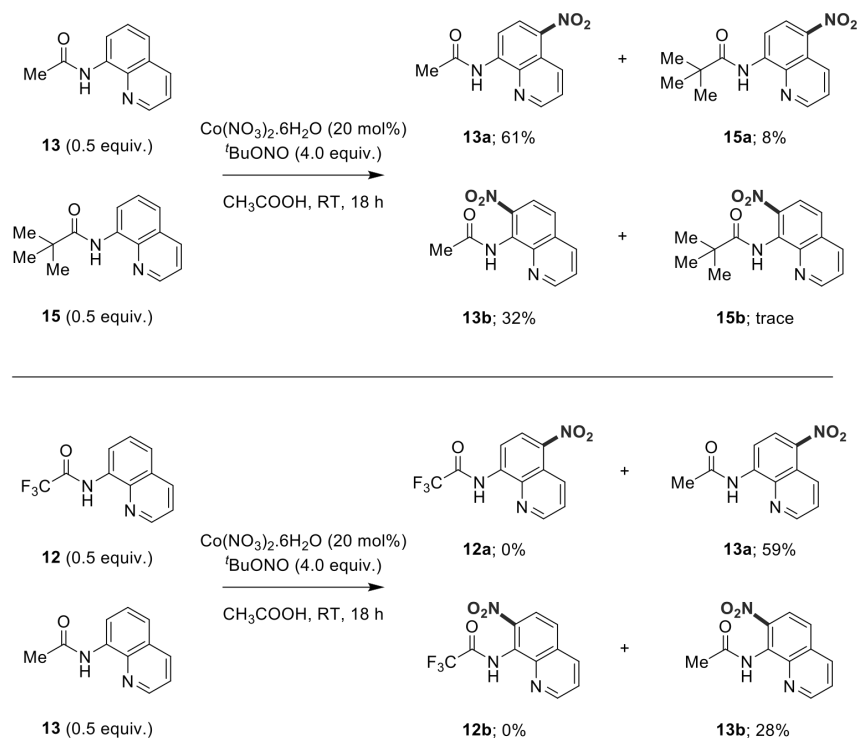


Figure S69. Example ^1H NMR of crude reaction mixture after extraction stage; from Table 2, entry 1 – 1,3,5-trimethoxy benzene as internal standard ($\text{D}_6\text{-DMSO}$, 298 K, 400 MHz). Peaks taken for calculation of: **1a** = ■; **1b** = □; internal standard = * (0.33 equiv.).

3. Poisoning studies

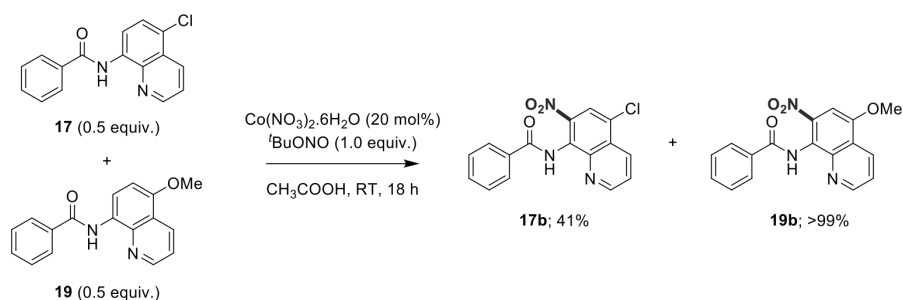
The general protocol described above was followed using the following conditions: substrate (0.5 mmol; 0.25 mmol of each substrate), $\text{Co}(\text{NO}_3)_2 \cdot 6\text{H}_2\text{O}$ (29.1 mg, 0.1 mmol, 20 mol%), $t\text{BuONO}$ (267 μL , 90%, 4.0 equiv., 2.0 mmol), acetic acid (3.5 mL), RT, 18 h. Yields calculated from ^1H NMR of crude reaction mixture using 1,3,5-trimethoxybenzene as internal standard and are based on conversion of corresponding substrate.



Scheme S26. Summary of results obtained from poisoning studies.

4. Competition study (17 and 19)

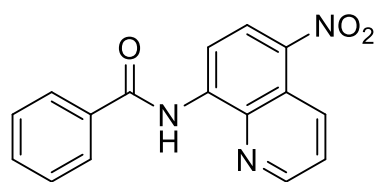
The general protocol described above was followed using the following conditions: substrate (0.5 mmol; 0.25 mmol of each substrate), $\text{Co}(\text{NO}_3)_2 \cdot 6\text{H}_2\text{O}$ (29.1 mg, 0.1 mmol, 20 mol%), $t\text{BuONO}$ (67 μL , 90%, 1.0 equiv., 0.5 mmol), acetic acid (3.5 mL), RT, 18 h. Yields calculated from ^1H NMR of crude reaction mixture using 1,3,5-trimethoxybenzene as internal standard and are based on conversion of corresponding substrate.



Scheme S27. Summary of results obtained from competition study (substrates **17** and **19**).

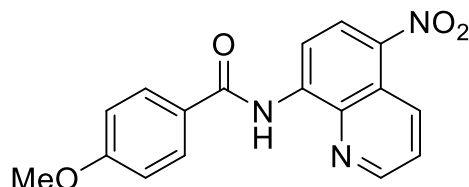
5. Synthesis and characterization data for products (Table VII.12)

N-(5-nitroquinolin-8-yl)benzamide (1a)



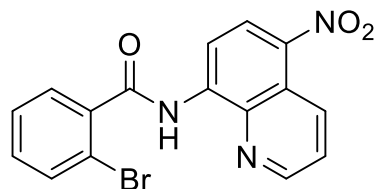
This compound was prepared by the general nitration protocol described above starting from substrate **1** (124 mg, 0.5 mmol) to yield a white powder (99 mg, 68 %). ^1H NMR (CDCl_3 , 400 MHz, 298 K); δ 11.09 (br s, 1H), 9.32 (dd, 1H, $^3J_{\text{HH}} = 8.8$, $^4J_{\text{HH}} = 1.5$), 9.02 (d, 1H, $^3J_{\text{HH}} = 8.8$), 8.98 (dd, 1H, $^3J_{\text{HH}} = 4.1$, $^4J_{\text{HH}} = 1.4$), 8.62 (d, 1H, $^3J_{\text{HH}} = 8.8$), 8.14-8.07 (m, 2H), 7.78 (dd, 1H, $^3J_{\text{HH}} = 8.8$, $^3J_{\text{HH}} = 4.2$), 7.70-7.55 (m, 3H). ^{13}C $\{^1\text{H}\}$ NMR (CDCl_3 , 100 MHz, 298 K); δ = 165.64, 149.07, 140.83, 138.67, 137.73, 134.11, 133.40, 132.64, 129.03, 127.86, 127.45, 124.72, 121.80, 113.69. HR-MS (ESI, m/z); calcd. for $\text{C}_{16}\text{H}_{11}\text{N}_3\text{O}_3 + \text{Na} = 316.0693$; obtained = 316.0696 $[\text{M} + \text{Na}]^+$. $R_f = 0.64$ (dichloromethane).

4-methoxy-*N*-(5-nitroquinolin-8-yl)benzamide (7a)

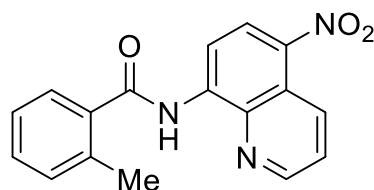


This compound was prepared by the general nitration protocol described above starting from substrate **7** (139 mg, 0.5 mmol) to yield a yellow powder (87 mg, 54 %). This compound was isolated as the precipitate obtained by suspending the crude reaction mixture in dichloromethane and the related product, **7b**, was isolated from the filtrate by column chromatography using dichloromethane as eluent. ^1H NMR ($\text{D}_6\text{-DMSO}$, 400 MHz, 353 K); δ 10.86 (br s, 1H), 9.14-9.06 (m, 2H), 8.82 (d, 1H, $^3J_{\text{HH}} = 8.8$), 8.59 (d, 1H, $^3J_{\text{HH}} = 8.8$), 8.01 (d, 2H, $^3J_{\text{HH}} = 8.8$), 7.92 (dd, 1H, $^3J_{\text{HH}} = 8.8$, $^3J_{\text{HH}} = 4.2$), 7.15 (d, 2H, $^3J_{\text{HH}} = 8.8$), 3.89 (s, 3H). ^{13}C $\{^1\text{H}\}$ NMR ($\text{D}_6\text{-DMSO}$, 100 MHz, 353 K); δ = 165.02, 163.53, 150.36, 141.06, 139.21, 137.90, 133.15, 129.70, 127.65, 126.71, 125.63, 121.68, 115.09, 113.94, 56.16. HR-MS (ESI, m/z); calcd. for $\text{C}_{17}\text{H}_{13}\text{N}_3\text{O}_4 + \text{Na} = 346.0798$; obtained = 346.0794 $[\text{M} + \text{Na}]^+$.

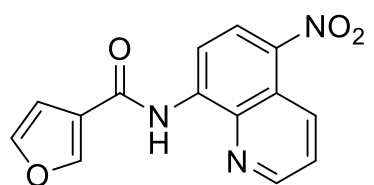
2-bromo-*N*-(5-nitroquinolin-8-yl)benzamide (8a)



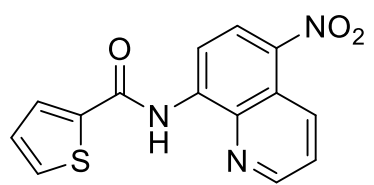
This compound was prepared by the general nitration protocol described above starting from substrate **8** (164 mg, 0.5 mmol) to yield a white powder (115 mg, 62 %). ^1H NMR (CDCl_3 , 400 MHz, 298 K); δ 10.71 (br s, 1H), 9.31 (dd, 1H, $^3J_{\text{HH}} = 8.9$, $^4J_{\text{HH}} = 1.5$), 9.05 (d, 1H, $^3J_{\text{HH}} = 8.8$), 8.93 (dd, 1H, $^3J_{\text{HH}} = 4.1$, $^4J_{\text{HH}} = 1.5$), 8.64 (d, 1H, $^3J_{\text{HH}} = 8.8$), 7.79-7.73 (m, 3H), 7.51 (ddd, 1H, $^3J_{\text{HH}} = 7.5$, 1H, $^3J_{\text{HH}} = 7.5$, $^4J_{\text{HH}} = 1.2$), 7.43 (ddd, 1H, $^3J_{\text{HH}} = 8.0$, 1H, $^3J_{\text{HH}} = 8.0$, $^4J_{\text{HH}} = 1.8$). ^{13}C $\{^1\text{H}\}$ NMR (CDCl_3 , 100 MHz, 298 K); δ = 166.23, 149.17, 140.43, 139.19, 137.72, 137.35, 133.94, 133.32, 132.18, 129.89, 127.86, 127.70, 124.73, 121.80, 119.63, 114.12. HR-MS (ESI, m/z); calcd. for $\text{C}_{16}\text{H}_{10}\text{BrN}_3\text{O}_3 + \text{Na} = 393.9798$; obtained = 393.9789 $[\text{M} + \text{Na}]^+$. $R_f = 0.70$ (dichloromethane).

2-methyl-*N*-(5-nitroquinolin-8-yl)benzamide (9a)

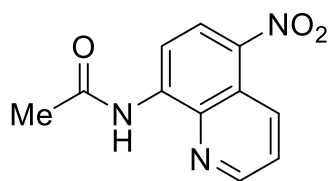
This compound was prepared by the general nitration protocol described above starting from substrate **9** (131 mg, 0.5 mmol) to yield a white powder (109 mg, 71 %). ^1H NMR (CDCl_3 , 400 MHz, 298 K); δ 10.60 (br s, 1H), 9.31 (dd, 1H, $^3J_{\text{HH}} = 8.9$, $^4J_{\text{HH}} = 1.6$), 9.04 (d, 1H, $^3J_{\text{HH}} = 8.8$), 8.91 (dd, 1H, $^3J_{\text{HH}} = 4.2$, $^4J_{\text{HH}} = 1.6$), 8.63 (d, 1H, $^3J_{\text{HH}} = 8.8$), 7.78-7.70 (m, 2H), 7.48 (ddd, 1H, $^3J_{\text{HH}} = 7.4$, 1H, $^3J_{\text{HH}} = 7.4$, $^4J_{\text{HH}} = 1.3$), 7.42-7.34 (m, 2H), 2.64 (s, 3H). ^{13}C $\{^1\text{H}\}$ NMR (CDCl_3 , 100 MHz, 298 K); δ = 168.32, 149.06, 140.98, 137.26, 133.36, 131.71, 131.09, 127.86, 127.32, 126.22, 124.70, 121.83, 113.66, 20.33. HR-MS (ESI, m/z); calcd. for $\text{C}_{17}\text{H}_{13}\text{N}_3\text{O}_3 + \text{Na} = 330.0849$; obtained = 330.0842 $[\text{M} + \text{Na}]^+$. $R_f = 0.75$ (dichloromethane).

***N*-(5-nitroquinolin-8-yl)furan-3-carboxamide (10a)**

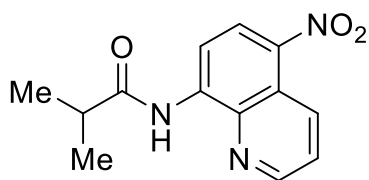
This compound was prepared by the general nitration protocol described above starting from substrate **10** (119 mg, 0.5 mmol) to yield a white powder (86 mg, 61 %). ^1H NMR ($\text{D}_6\text{-DMSO}$, 400 MHz, 298 K); δ 10.94 (br s, 1H), 9.13 (s, 1H), 9.12 (dd, 1H, $^3J_{\text{HH}} = 4.5$, $^4J_{\text{HH}} = 1.5$), 8.79 (d, 1H, $^3J_{\text{HH}} = 8.8$), 8.63 (d, 1H, $^3J_{\text{HH}} = 8.8$), 8.12 (dd, 1H, $^3J_{\text{HH}} = 1.7$, $^4J_{\text{HH}} = 0.8$), 7.99-7.94 (m, 1H), 7.47 (dd, 1H, $^3J_{\text{HH}} = 3.6$, $^4J_{\text{HH}} = 0.8$), 6.83 (dd, 1H, $^3J_{\text{HH}} = 3.6$, $^4J_{\text{HH}} = 1.7$). ^{13}C $\{^1\text{H}\}$ NMR ($\text{D}_6\text{-DMSO}$, 100 MHz, 298 K); δ = 156.08, 150.63, 147.35, 147.18, 140.16, 139.06, 137.23, 133.40, 128.07, 125.91, 121.54, 117.34, 113.69, 113.66. HR-MS (ESI, m/z); calcd. for $\text{C}_{14}\text{H}_9\text{N}_3\text{O}_4 + \text{Na} = 306.0485$; obtained = 306.0484 $[\text{M} + \text{Na}]^+$. $R_f = 0.55$ (dichloromethane).

***N*-(5-nitroquinolin-8-yl)thiophene-2-carboxamide (11a)**

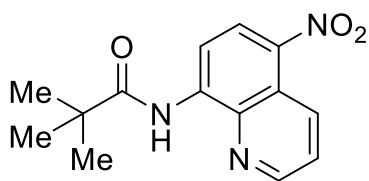
This compound was prepared by the general nitration protocol described above starting from substrate **11** (127 mg, 0.5 mmol) to yield a white powder (103 mg, 70 %). ^1H NMR (CDCl_3 , 400 MHz, 298 K); δ 10.92 (br s, 1H), 9.32 (dd, 1H, $^3J_{\text{HH}} = 8.8$, $^4J_{\text{HH}} = 1.6$), 8.98 (dd, 1H, $^3J_{\text{HH}} = 4.2$, $^4J_{\text{HH}} = 1.6$), 8.92 (d, 1H, $^3J_{\text{HH}} = 8.8$), 8.61 (d, 1H, $^3J_{\text{HH}} = 8.8$), 7.90 (dd, 1H, $^3J_{\text{HH}} = 3.8$, $^4J_{\text{HH}} = 1.2$), 7.78 (dd, 1H, $^3J_{\text{HH}} = 4.2$, $^4J_{\text{HH}} = 8.9$), 7.69 (dd, 1H, $^3J_{\text{HH}} = 5.0$, $^4J_{\text{HH}} = 1.2$), 7.25 (dd, 1H, $^3J_{\text{HH}} = 5.0$, $^3J_{\text{HH}} = 3.8$). ^{13}C $\{^1\text{H}\}$ NMR (CDCl_3 , 100 MHz, 298 K); δ = 160.18, 149.10, 140.60, 138.99, 138.67, 137.49, 133.45, 132.21, 129.38, 128.15, 127.87, 124.77, 121.84, 113.65. HR-MS (ESI, m/z); calcd. for $\text{C}_{14}\text{H}_9\text{N}_3\text{O}_3\text{S} + \text{Na} = 322.0257$; obtained = 322.0262 $[\text{M} + \text{Na}]^+$. $R_f = 0.66$ (dichloromethane).

***N*-(5-nitroquinolin-8-yl)acetamide (13a)**

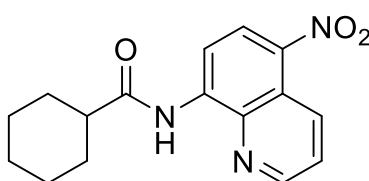
This compound was prepared by the general nitration protocol described above starting from substrate **13** (93 mg, 0.5 mmol) to yield a white powder (75 mg, 65 %). This product was purified using ethyl acetate: hexane (70:30). ^1H NMR (CDCl_3 , 400 MHz, 298 K); δ 10.13 (br s, 1H), 9.27 (dd, 1H, $^3J_{\text{HH}} = 8.6$, $^4J_{\text{HH}} = 1.6$), 8.98 (dd, 1H, $^3J_{\text{HH}} = 4.2$, $^4J_{\text{HH}} = 1.6$), 8.83 (d, 1H, $^3J_{\text{HH}} = 8.8$), 8.54 (d, 1H, $^3J_{\text{HH}} = 8.8$), 7.73 (dd, 1H, $^3J_{\text{HH}} = 4.2$, $^3J_{\text{HH}} = 8.6$), 2.42 (s, 3H). ^{13}C $\{^1\text{H}\}$ NMR (CDCl_3 , 100 MHz, 298 K); $\delta = 169.22, 148.89, 140.69, 138.53, 137.17, 133.30, 127.80, 124.62, 121.71, 113.51, 25.29$. HR-MS (ESI, m/z); calcd. for $\text{C}_{11}\text{H}_9\text{N}_3\text{O}_3 + \text{Na} = 254.0536$; obtained = 254.0527 $[\text{M} + \text{Na}]^+$. $R_f = 0.51$ (Ethyl acetate:hexane; 70:30).

***N*-(5-nitroquinolin-8-yl)isobutyramide (14a)**

This compound was prepared by the general nitration protocol described above starting from substrate **14** (107 mg, 0.5 mmol) to yield a white powder (90 mg, 70 %). ^1H NMR (CDCl_3 , 400 MHz, 298 K); δ 10.25 (br s, 1H), 9.29 (dd, 1H, $^3J_{\text{HH}} = 8.9$, $^4J_{\text{HH}} = 1.6$), 8.92 (dd, 1H, $^3J_{\text{HH}} = 4.2$, $^4J_{\text{HH}} = 1.6$), 8.87 (d, 1H, $^3J_{\text{HH}} = 8.9$), 8.56 (d, 1H, $^3J_{\text{HH}} = 8.9$), 7.74 (dd, 1H, $^3J_{\text{HH}} = 4.2$, $^3J_{\text{HH}} = 8.9$), 2.83 (h, 1H, $^3J_{\text{HH}} = 6.9$), 1.39 (d, 6H, $^3J_{\text{HH}} = 6.9$). ^{13}C $\{^1\text{H}\}$ NMR (CDCl_3 , 100 MHz, 298 K); $\delta = 176.22, 148.92, 140.93, 138.41, 137.43, 133.33, 127.91, 124.61, 121.77, 113.54, 37.29, 19.52$. HR-MS (ESI, m/z); calcd. for $\text{C}_{13}\text{H}_{13}\text{N}_3\text{O}_3 + \text{Na} = 282.0849$; obtained = 282.0855 $[\text{M} + \text{Na}]^+$. $R_f = 0.59$ (dichloromethane).

***N*-(5-nitroquinolin-8-yl)pivalamide (15a)**

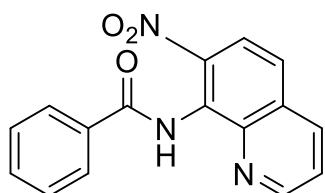
This compound was prepared by the general nitration protocol described above starting from substrate **15** (114 mg, 0.5 mmol) to yield a white powder (16 mg, 12 %). ^1H NMR (CDCl_3 , 400 MHz, 298 K); δ 10.61 (br s, 1H), 9.30 (dd, 1H, $^3J_{\text{HH}} = 8.9$, $^4J_{\text{HH}} = 1.6$), 8.94 (dd, 1H, $^3J_{\text{HH}} = 4.2$, $^4J_{\text{HH}} = 1.6$), 8.88 (d, 1H, $^3J_{\text{HH}} = 8.9$), 8.57 (d, 1H, $^3J_{\text{HH}} = 8.9$), 7.74 (dd, 1H, $^3J_{\text{HH}} = 4.2$, $^3J_{\text{HH}} = 8.9$), 1.46 (s, 9H). ^{13}C $\{^1\text{H}\}$ NMR (CDCl_3 , 100 MHz, 298 K); $\delta = 177.79, 149.00, 141.04, 138.47, 137.75, 133.34, 127.95, 124.58, 121.78, 113.40, 40.68, 27.57$. HR-MS (ESI, m/z); calcd. for $\text{C}_{14}\text{H}_{15}\text{N}_3\text{O}_3 + \text{Na} = 296.1006$; obtained = 296.1006 $[\text{M} + \text{Na}]^+$. $R_f = 0.60$ (dichloromethane).

***N*-(5-nitroquinolin-8-yl)cyclohexanecarboxamide (16a)**

This compound was prepared by the general nitration protocol described above starting from substrate **16** (127 mg, 0.5 mmol) to yield a white powder (93 mg, 62 %). ^1H NMR (CDCl_3 , 400 MHz, 298 K); δ 10.24 (br s, 1H), 9.29

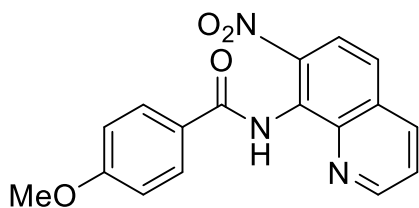
(dd, 1H, $^3J_{\text{HH}} = 8.8$, $^4J_{\text{HH}} = 1.6$), 8.93 (dd, 1H, $^3J_{\text{HH}} = 4.2$, $^4J_{\text{HH}} = 1.6$), 8.87 (d, 1H, $^3J_{\text{HH}} = 8.9$), 8.55 (d, 1H, $^3J_{\text{HH}} = 8.9$), 7.74 (dd, 1H, $^3J_{\text{HH}} = 4.2$, $^3J_{\text{HH}} = 8.9$), 2.59-2.49 (m, 1H), 2.14-2.08 (m, 2H), 1.95-1.88 (m, 2H), 1.81-1.74 (m, 1H), 1.69-1.60 (m, 2H), 1.48-1.26 (m, 3H). ^{13}C { ^1H } NMR (CDCl_3 , 100 MHz, 298 K); $\delta = 175.33$, 148.88, 140.97, 138.35, 137.44, 133.32, 127.93, 124.59, 121.78, 113.55, 46.91, 29.59, 25.68, 25.63. HR-MS (ESI, m/z); calcd. for $\text{C}_{16}\text{H}_{17}\text{N}_3\text{O}_3 + \text{Na} = 322.1162$; obtained = 322.1173 $[\text{M} + \text{Na}]^+$. $R_f = 0.54$ (dichloromethane).

***N*-(7-nitroquinolin-8-yl)benzamide (1b)**



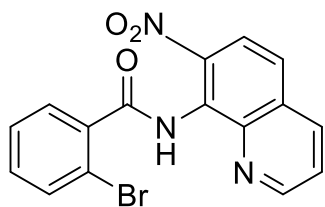
This compound was prepared by the general nitration protocol described above starting from substrate **1** (124 mg, 0.5 mmol) to yield a white powder (32 mg, 22 %). ^1H NMR (CDCl_3 , 400 MHz, 298 K); δ 10.43 (br s, 1H), 8.97 (dd, 1H, $^3J_{\text{HH}} = 4.2$, $^4J_{\text{HH}} = 1.7$), 8.29 (d, 1H, $^3J_{\text{HH}} = 8.4$, $^4J_{\text{HH}} = 1.6$), 8.16-8.10 (m, 2H), 8.07 (d, 1H, $^3J_{\text{HH}} = 9.1$), 7.70 (d, 1H, $^3J_{\text{HH}} = 9.1$), 7.68-7.62 (m, 2H), 7.61-7.54 (m, 2H). ^{13}C { ^1H } NMR (CDCl_3 , 100 MHz, 298 K); $\delta = 165.19$, 150.33, 140.67, 140.59, 136.48, 133.36, 132.76, 129.59, 128.91, 128.26, 128.03, 124.03, 122.84, 122.31. HR-MS (ESI, m/z); calcd. for $\text{C}_{16}\text{H}_{11}\text{N}_3\text{O}_3 + \text{Na} = 316.0693$; obtained = 316.0694 $[\text{M} + \text{Na}]^+$. $R_f = 0.43$ (dichloromethane).

4-methoxy-*N*-(7-nitroquinolin-8-yl)benzamide (7b)



This compound was prepared by the general nitration protocol described above starting from substrate **7** (139 mg, 0.5 mmol) to yield a yellow powder (34 mg, 21 %). ^1H NMR (CDCl_3 , 400 MHz, 298 K); δ 10.37 (br s, 1H), 8.96 (dd, 1H, $^3J_{\text{HH}} = 4.2$, $^4J_{\text{HH}} = 1.7$), 8.27 (d, 1H, $^3J_{\text{HH}} = 8.3$, $^4J_{\text{HH}} = 1.6$), 8.12-8.05 (m, 2H), 8.05 (d, 1H, $^3J_{\text{HH}} = 9.1$), 7.66 (d, 1H, $^3J_{\text{HH}} = 9.1$), 7.64 (d, 1H, $^3J_{\text{HH}} = 8.3$, $^3J_{\text{HH}} = 4.2$), 7.08-7.02 (m, 2H), 3.92 (s, 3H). ^{13}C { ^1H } NMR (CDCl_3 , 100 MHz, 298 K); $\delta = 164.70$, 163.27, 150.22, 140.58, 140.45, 136.47, 130.07, 129.57, 128.53, 125.62, 123.98, 122.49, 122.32, 114.12, 55.56. HR-MS (ESI, m/z); calcd. for $\text{C}_{17}\text{H}_{13}\text{N}_3\text{O}_4 + \text{Na} = 346.0798$; obtained = 346.0794 $[\text{M} + \text{Na}]^+$. $R_f = 0.42$ (dichloromethane).

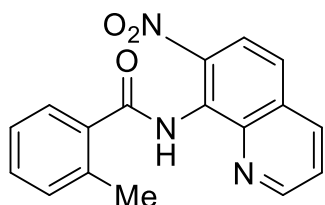
2-bromo-*N*-(7-nitroquinolin-8-yl)benzamide (8b)



This compound was prepared by the general nitration protocol described above starting from substrate **8** (164 mg, 0.5 mmol) to yield a white powder (26 mg, 14 %). ^1H NMR (CDCl_3 , 400 MHz, 298 K); δ 10.11 (br s, 1H), 8.96 (dd, 1H, $^3J_{\text{HH}} = 4.2$, $^4J_{\text{HH}} = 1.6$), 8.29 (dd, 1H, $^3J_{\text{HH}} = 8.4$, $^4J_{\text{HH}} = 1.6$), 8.07 (d, 1H, $^3J_{\text{HH}} = 9.1$), 7.83 (ddd, 1H, $^3J_{\text{HH}} = 7.6$, $^4J_{\text{HH}} = 1.8$, $^5J_{\text{HH}} = 0.3$), 7.73 (d, 1H, $^3J_{\text{HH}} = 9.3$), 7.74 (ddd, 1H, $^3J_{\text{HH}} = 7.9$, $^4J_{\text{HH}} = 1.2$, $^5J_{\text{HH}} = 0.3$), 7.65 (dd, 1H, $^3J_{\text{HH}} = 4.2$, $^3J_{\text{HH}} = 8.3$), 7.49 (ddd, 1H, $^3J_{\text{HH}} = 7.6$, $^3J_{\text{HH}} = 7.6$, $^4J_{\text{HH}} = 1.3$), 7.44-7.38 (m, 1H). ^{13}C { ^1H } NMR (CDCl_3 , 100 MHz, 298 K); $\delta = 165.18$, 151.50, 140.96, 140.58, 136.40, 136.38, 133.96, 133.25, 130.37,

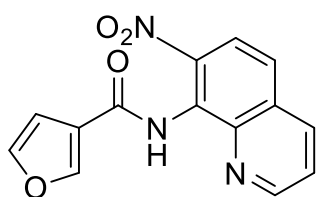
129.65, 127.69, 127.54, 124.06, 123.43, 122.25, 119.98. HR-MS (ESI, m/z); calcd. for $C_{16}H_{10}BrN_3O_3+Na = 393.9798$; obtained = 393.9778 $[M+Na]^+$. $R_f = 0.51$ (dichloromethane).

2-methyl-*N*-(7-nitroquinolin-8-yl)benzamide (9b)



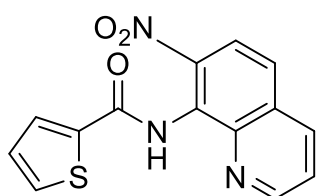
This compound was prepared by the general nitration protocol described above starting from substrate **9** (131 mg, 0.5 mmol) to yield a white powder (27 mg, 18 %). 1H NMR ($CDCl_3$, 400 MHz, 298 K); δ 9.95 (br s, 1H), 8.95 (dd, 1H, $^3J_{HH} = 4.2$, $^4J_{HH} = 1.6$), 8.29 (dd, 1H, $^3J_{HH} = 8.3$, $^4J_{HH} = 1.7$), 8.08 (d, 1H, $^3J_{HH} = 9.1$), 7.83 (dd, 1H, $^3J_{HH} = 7.6$, $^4J_{HH} = 1.4$), 7.72 (d, 1H, $^3J_{HH} = 9.1$), 7.65 (dd, 1H, $^3J_{HH} = 8.3$, $^3J_{HH} = 4.2$), 7.47 (ddd, 1H, $^3J_{HH} = 7.5$, $^3J_{HH} = 7.5$, $^4J_{HH} = 1.4$), 7.40-7.32 (m, 2H), 2.61 (s, 3H). ^{13}C $\{^1H\}$ NMR ($CDCl_3$, 100 MHz, 298 K); $\delta = 167.37, 150.36, 140.64, 140.37, 138.15, 136.42, 134.47, 131.60, 131.19, 129.66, 128.70, 127.98, 126.06, 123.99, 122.94, 122.31, 20.26$. HR-MS (ESI, m/z); calcd. for $C_{17}H_{13}N_3O_3+Na = 330.0849$; obtained = 330.0845 $[M+Na]^+$. $R_f = 0.55$ (dichloromethane).

N-(7-nitroquinolin-8-yl)furan-3-carboxamide (10b)

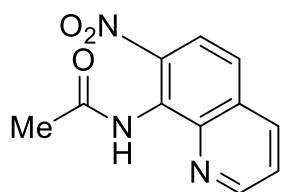


This compound was prepared by the general nitration protocol described above starting from substrate **10** (119 mg, 0.5 mmol) to yield a white powder (35 mg, 25 %). 1H NMR (D_6 -DMSO, 400 MHz, 298 K); δ 10.70 (br s, 1H), 9.14 (dd, 1H, $^3J_{HH} = 4.2$, $^4J_{HH} = 1.7$), 8.61 (dd, 1H, $^3J_{HH} = 8.4$, $^4J_{HH} = 1.7$), 8.10 (d, 1H, $^3J_{HH} = 9.0$), 8.09-8.05 (m, 2H), 7.85 (dd, 1H, $^3J_{HH} = 8.3$, $^3J_{HH} = 4.2$), 7.55 (dd, 1H, $^3J_{HH} = 3.5$, $^4J_{HH} = 0.8$), 6.80 (dd, 1H, $^3J_{HH} = 3.5$, $^4J_{HH} = 1.8$). ^{13}C $\{^1H\}$ NMR (D_6 -DMSO, 100 MHz, 298 K); $\delta = 156.04, 152.29, 147.25, 146.99, 142.70, 141.48, 137.37, 130.37, 127.42, 125.86, 125.03, 121.96, 117.10, 113.17$. HR-MS (ESI, m/z); calcd. for $C_{14}H_9N_3O_4+Na = 306.0485$; obtained = 306.0472 $[M+Na]^+$. $R_f = 0.41$ (dichloromethane).

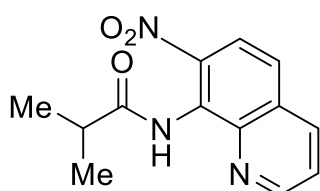
N-(7-nitroquinolin-8-yl)thiophene-2-carboxamide (11b)



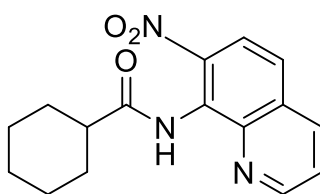
This compound was prepared by the general nitration protocol described above starting from substrate **11** (127 mg, 0.5 mmol) to yield a white powder (29 mg, 20 %). 1H NMR ($CDCl_3$, 400 MHz, 298 K); δ 10.35 (br s, 1H), 8.98 (dd, 1H, $^3J_{HH} = 4.2$, $^4J_{HH} = 1.6$), 8.29 (dd, 1H, $^3J_{HH} = 8.3$, $^4J_{HH} = 1.6$), 8.05 (d, 1H, $^3J_{HH} = 10.1$), 7.95 (dd, 1H, $^3J_{HH} = 3.8$, $^4J_{HH} = 1.2$), 7.71-7.63 (m, 3H), 7.23 (dd, 1H, $^3J_{HH} = 5.0$, $^3J_{HH} = 3.8$). ^{13}C $\{^1H\}$ NMR ($CDCl_3$, 100 MHz, 298 K); $\delta = 159.69, 150.38, 140.50, 140.44, 137.89, 136.50, 132.26, 130.51, 129.61, 128.06, 127.86, 124.06, 122.88, 122.29$. HR-MS (ESI, m/z); calcd. for $C_{14}H_9N_3O_3S+Na = 322.0257$; obtained = 322.0257 $[M+Na]^+$. $R_f = 0.40$ (dichloromethane).

***N*-(7-nitroquinolin-8-yl)acetamide (13b)**

This compound was prepared by the general nitration protocol described above starting from substrate **13** (93 mg, 0.5 mmol) to yield a white powder (31 mg, 27 %). This product was purified using ethyl acetate: hexane (70:30). ¹H NMR (CDCl₃, 400 MHz, 298 K); δ 9.58 (br s, 1H), 8.98 (dd, 1H, ³J_{HH} = 4.2, ⁴J_{HH} = 1.7), 8.27 (dd, 1H, ³J_{HH} = 8.2, ⁴J_{HH} = 1.6), 8.00 (d, 1H, ³J_{HH} = 9.1), 7.67 (d, 1H, ³J_{HH} = 9.1), 7.64 (dd, 1H, ³J_{HH} = 4.2, ³J_{HH} = 8.3), 2.40 (s, 3H). ¹³C {¹H} NMR (CDCl₃, 100 MHz, 298 K); δ = 168.14, 150.34, 140.38, 136.42, 129.59, 127.69, 123.93, 122.95, 122.22, 24.15. HR-MS (ESI, *m/z*); calcd. for C₁₁H₉N₃O₃+Na = 254.0536; obtained = 254.0539 [M+Na]⁺. *R_f* = 0.23 (Ethyl acetate:hexane; 70:30).

***N*-(7-nitroquinolin-8-yl)isobutyramide (14b)**

This compound was prepared by the general nitration protocol described above starting from substrate **14** (107 mg, 0.5 mmol) to yield a white powder (18 mg, 15 %). ¹H NMR (CDCl₃, 400 MHz, 298 K); δ 9.65 (br s, 1H), 8.97 (dd, 1H, ³J_{HH} = 4.2, ⁴J_{HH} = 1.7), 8.26 (dd, 1H, ³J_{HH} = 8.3, ⁴J_{HH} = 1.6), 7.98 (d, 1H, ³J_{HH} = 9.1), 7.65 (d, 1H, ³J_{HH} = 9.1), 7.64 (dd, 1H, ³J_{HH} = 4.2, ³J_{HH} = 8.3), 2.84 (h, 1H, ³J_{HH} = 6.9), 1.37 (d, 6H, ³J_{HH} = 6.9). ¹³C {¹H} NMR (CDCl₃, 100 MHz, 298 K); δ = 174.83, 150.30, 140.77, 140.52, 129.52, 127.88, 123.90, 122.67, 122.19, 36.39, 19.16. HR-MS (ESI, *m/z*); calcd. for C₁₃H₁₃N₃O₃+Na = 282.0849; obtained = 282.0854 [M+Na]⁺. *R_f* = 0.39 (dichloromethane).

***N*-(7-nitroquinolin-8-yl)cyclohexanecarboxamide (16b)**

This compound was prepared by the general nitration protocol described above starting from substrate **16** (127 mg, 0.5 mmol) to yield a white powder (31 mg, 21 %). ¹H NMR (CDCl₃, 400 MHz, 298 K); δ 9.64 (br s, 1H), 8.97 (dd, 1H, ³J_{HH} = 4.2, ⁴J_{HH} = 1.6), 8.25 (dd, 1H, ³J_{HH} = 8.2, ⁴J_{HH} = 1.6), 7.98 (d, 1H, ³J_{HH} = 9.1), 7.64 (d, 1H, ³J_{HH} = 9.1), 7.69 (dd, 1H, ³J_{HH} = 4.2, ³J_{HH} = 8.2), 2.59-2.52 (m, 1H), 2.14-2.07 (m, 2H), 1.94-1.86 (m, 2H), 1.77-1.60 (m, 3H), 1.47-1.28 (m, 3H). ¹³C {¹H} NMR (CDCl₃, 100 MHz, 298 K); δ = 173.92, 150.25, 140.81, 140.57, 136.39, 129.52, 127.93, 123.87, 122.58, 122.23, 45.89, 29.21, 25.73, 25.57. HR-MS (ESI, *m/z*); calcd. for C₁₆H₁₇N₃O₃+Na = 322.1162; obtained = 322.1184 [M+Na]⁺. *R_f* = 0.40 (dichloromethane).

6. Synthesis and characterization data for products (Scheme VII.15)

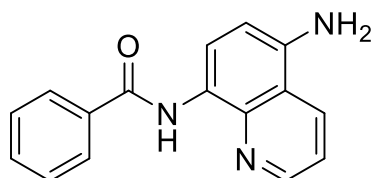
6.1 Gram-scale nitration of substrate **1**

A 100 mL round bottom flask was charged with of substrate **1** (1.89 g, 7.62 mmol), $\text{Co}(\text{NO}_3)_2 \cdot 6\text{H}_2\text{O}$ (443 mg, 20 mol%, 1.52 mmol), *tert*-butyl nitrite (4.10 mL, 90%, 4.0 equiv., 30.48 mmol) and 50 mL of acetic acid. The flask was sealed with a septum and the reaction stirred at room temperature for 18 hours. After this period the reaction mixture was diluted with ethyl acetate (200 mL) and extracted using brine (100 mL). The aqueous layer was then further extracted with ethyl acetate (2 x 100 mL), the organic layers combined, dried over magnesium sulfate and the solvent removed under reduced pressure. The Residue was suspended in 100 mL of boiling ethanol and the precipitate collected, dried under reduced pressure and recrystallized by slow diffusion of pentane into a chloroform solution of the collected precipitate (**1a** as a pale yellow solid; 1.35 g, 61%). The solvent from the ethanolic filtrate was removed under reduced pressure and the residue recrystallized in the same manner as product **1a** (**1b** as a white solid; 410 mg, 18%). See previous sections for characterization of these products.

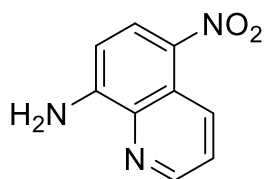
6.2 Upgrading of products **1a** and **1b**

The following describes the procedures for the synthesis of **1c**, **A**, **B** and **C**.

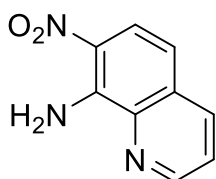
N-(5-aminoquinolin-8-yl)benzamide (**1c**)



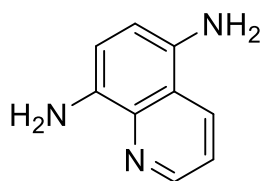
In a sealed round bottom flask product **1a** (300mg, 1.02 mmol) was dissolved in degassed ethyl acetate (10mL) and Pd/C (100 mg, 20 wt%) was added. The reaction was then placed under an atmosphere of hydrogen (1 atm, ballon) and stirred overnight. When the reaction was complete (TLC: dichloromethane, the reaction mixture was filtered through celite®, and the celite® was further washed with dichloromethane until the filtrate ran clear. The solvent from the combined organic filtrates was removed under reduced pressure and the resulting residue was purified by column chromatography using ethyl acetate:hexane (70:30) as eluent, resulting in a pale yellow solid (233 mg, 86%). ^1H NMR (D_6 -DMSO, 400 MHz, 298 K); δ = 10.30 (m, 1H), 8.89 (dd, 1H, $^3J_{\text{HH}} = 4.2$, $^4J_{\text{HH}} = 1.6$), 8.63 (dd, 1H, $^3J_{\text{HH}} = 8.5$, $^4J_{\text{HH}} = 1.6$), 8.43 (d, 1H, $^3J_{\text{HH}} = 8.3$), 8.03-7.98 (m, 2H), 7.66-7.56 (m, 3H), 7.53 (dd, 1H, $^3J_{\text{HH}} = 4.3$, $^3J_{\text{HH}} = 8.5$), 6.77 (d, 1H, $^3J_{\text{HH}} = 8.3$), 5.91 (br s, 2H). ^{13}C $\{^1\text{H}\}$ NMR (D_6 -DMSO, 100 MHz, 298 K); δ = 164.14, 149.30, 141.79, 140.02, 135.53, 132.37, 132.03, 129.35, 127.29, 123.86, 120.12, 120.06, 118.10, 107.37. HR-MS (ESI, m/z); calcd. for $\text{C}_{16}\text{H}_{13}\text{N}_3\text{O} + \text{Na}$ = 286.0956; obtained = 286.0952 $[\text{M} + \text{Na}]^+$. R_f = 0.78 (ethyl acetate:hexane; 70:30).

5-Nitroquinolin-8-amine (A)

Product **1a** (1.00 g, 3.41 mmol) was dissolved in ethanol (50 mL) in a 100 mL round-bottom flask. To the solution was added concentrated hydrochloric acid (11 mL). The resulting mixture was then refluxed at 100°C for 24 h. After this time the crude was concentrated under reduced pressure and cooled to 0°C, at which point 2M NaOH was added dropwise until the pH was alkaline. The solution was extracted with ethyl acetate (3 x 100 mL), dried over magnesium sulfate and the solvent removed under reduced pressure. The resulting residue was purified by column chromatography using dichloromethane as eluent, resulting in an orange solid (599 mg, 93%). ¹H NMR (D₆-DMSO, 400 MHz, 298 K); δ = 9.28 (dd, 1H, ³J_{HH} = 8.9 ⁴J_{HH} = 1.6), 8.84 (dd, 1H, ³J_{HH} = 4.1, ⁴J_{HH} = 1.6), 8.48 (d, 1H, ³J_{HH} = 9.1), 7.80 (dd, 1H, ³J_{HH} = 8.9, ³J_{HH} = 4.1), 7.78 (br s, 2H), 6.86 (d, 1H, ³J_{HH} = 9.1). ¹³C {¹H} NMR (D₆-DMSO, 100 MHz, 298 K); δ = 154.23, 148.06, 135.51, 132.81, 131.32, 130.11, 125.96, 123.96, 106.25. HR-MS (ESI, *m/z*); calcd. for C₉H₇N₃O₂+Na = 212.0430; obtained = 212.0429 [M+Na]⁺. *R_f* = 0.50 (dichloromethane). CAS: 42606-38-2. This compound is known and the data described is in agreement with the previous reports.^[13]

7-Nitroquinolin-8-amine (B)

Product **1b** (320 mg, 1.09 mmol) was dissolved in ethanol (25 mL) in a 50 mL round-bottom flask. To the solution was added concentrated hydrochloric acid (5 mL). The resulting mixture was then refluxed at 100°C for 24 h. After this time the crude was concentrated under reduced pressure and cooled to 0°C, at which point 2M NaOH was added dropwise until the pH was alkaline. The solution was extracted with ethyl acetate (3 x 50 mL), dried over magnesium sulfate and the solvent removed under reduced pressure. The resulting residue was purified by column chromatography using dichloromethane as eluent, resulting in an orange solid (163 mg, 84%). ¹H NMR (D₆-DMSO, 400 MHz, 298 K); δ = 8.90 (dd, 1H, ³J_{HH} = 4.3 ⁴J_{HH} = 1.7), 8.40 (br s, 2H), 8.33 (dd, 1H, ³J_{HH} = 8.2, ⁴J_{HH} = 1.7), 8.02 (d, 1H, ³J_{HH} = 9.5), 7.75 (dd, 1H, ³J_{HH} = 8.2, ³J_{HH} = 4.3), 7.07 (d, 1H, ³J_{HH} = 9.5). ¹³C {¹H} NMR (D₆-DMSO, 100 MHz, 298 K); δ = 149.21, 145.19, 139.44, 136.98, 131.47, 126.58, 125.96, 122.37, 113.98. HR-MS (ESI, *m/z*); calcd. for C₉H₇N₃O₂+Na = 212.0430; obtained = 212.0433 [M+Na]⁺. *R_f* = 0.68 (dichloromethane). CAS: 42606-37-1. This compound is known and the data described is in agreement with the previous reports.^[13]

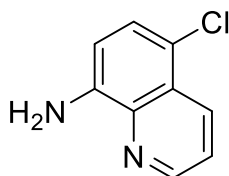
Quinoline-5,8-diamine (C)

In a sealed round bottom flask product A (500mg, 2.64 mmol) was dissolved in degassed ethyl acetate (15mL) and Pd/C (100 mg, 20 wt%) was added. The reaction was then placed under an atmosphere of hydrogen (1 atm, ballon) and stirred overnight. When the reaction was complete (TLC: dichloromethane, the reaction mixture was filtered through celite[®], and the celite[®] was further washed with ethyl acetate until the filtrate ran clear. The solvent was removed under reduced pressure and the resulting residue was purified by column chromatography using ethyl acetate as eluent, resulting in a brown solid (346 mg, 83%). ¹H NMR (D₆-DMSO, 400 MHz, 298 K); δ = 8.70 (dd, 1H, ³J_{HH} = 4.1, ⁴J_{HH} = 1.7), 8.40 (dd, 1H, ³J_{HH} = 8.5, ⁴J_{HH} = 1.7), 7.37 (dd, 1H, ³J_{HH} = 8.5, ³J_{HH} = 4.1), 6.74 (d, 1H, ³J_{HH} = 8.0), 6.62 (d, 1H, ³J_{HH} = 8.0), 5.02 (br s, 4H). ¹³C {¹H} NMR (D₆-DMSO, 100 MHz, 298 K); δ = 147.30, 138.66, 136.18, 134.79, 131.67, 119.54, 119.45, 111.29, 110.33. HR-MS (ESI, *m/z*); calcd. for C₉H₇N₃+H = 158.0713; obtained = 158.0726 [M+H]⁺. *R_f* = 0.40 (ethyl acetate). CAS: 162880-45-7. This compound has been reported previously.^[14]

7. Synthesis and characterization data for 5-substituted-8-aminoquinolines

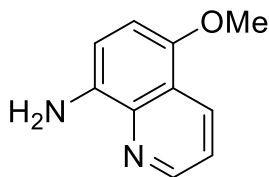
5-chloro and 5-methoxy-8-aminoquinoline were prepared according to the literature procedure.^[12] Substrates **1a** and **1c** were synthesized as products during this work and as such were prepared as described in Scheme 3 (main text).

5-Chloro-8-aminoquinoline



In a sealed round bottom flask 5-chloro-8-nitroquinoline (500mg, 2.40 mmol) was dissolved in degassed ethyl acetate (15mL) and Pd/C (100 mg, 20 wt%) was added. The reaction was then placed under an atmosphere of hydrogen (1 atm, balloon) and stirred overnight. When the reaction was complete (TLC: dichloromethane, the reaction mixture was filtered through celite®, and the celite® was further washed with ethyl acetate until the filtrate ran clear. The solvent was removed under reduced pressure and the resulting residue was purified by column chromatography using dichloromethane as eluent, resulting in a pale yellow solid (385 mg, 90%). ¹H NMR (CDCl₃, 400 MHz, 298 K); δ = 8.82 (dd, 1H, ³J_{HH} = 4.2, ⁴J_{HH} = 1.6), 8.50 (dd, 1H, ³J_{HH} = 8.5, ⁴J_{HH} = 1.6), 7.51 (dd, 1H, ³J_{HH} = 8.5, ³J_{HH} = 4.2), 7.41 (d, 1H, ³J_{HH} = 8.2), 6.86 (d, 1H, ³J_{HH} = 8.2), 5.04 (br s, 2H). ¹³C {¹H} NMR (CDCl₃, 100 MHz, 298 K); δ = 147.79, 143.31, 138.79, 132.91, 127.25, 126.55, 122.09, 118.07, 109.47. HR-MS (ESI, *m/z*); calcd. for C₉H₇N₂Cl+H = 179.0371; obtained = 179.0374 [M+H]⁺. *R_f* = 0.32 (dichloromethane). CAS: 5432-09-7. This compound is known and the data described is in agreement with the previous reports.^[15]

5-Methoxy-8-aminoquinoline

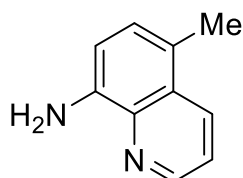


This compound was prepared from 5-methoxy-8-nitroquinoline (500 mg, 2.45 mmol) using the procedure described above for the preparation of 5-chloro-8-aminoquinoline and was purified by column chromatography using ethyl acetate:hexane (60:40) as eluent, resulting in a yellow solid (354 mg, 83%). ¹H NMR (CDCl₃, 400 MHz, 298 K); δ = 8.83 (dd, 1H, ³J_{HH} = 4.2, ⁴J_{HH} = 1.8), 8.53 (dd, 1H, ³J_{HH} = 8.5, ⁴J_{HH} = 1.8), 7.40 (dd, 1H, ³J_{HH} = 8.5, ³J_{HH} = 4.2), 6.89 (d, 1H, ³J_{HH} = 8.2), 6.75 (d, 1H, ³J_{HH} = 8.2), 4.65 (br s, 2H), 3.95 (s, 3H). ¹³C {¹H} NMR (CDCl₃, 100 MHz, 298 K); δ = 148.10, 147.06, 139.15, 137.39, 130.83, 121.16, 120.45, 109.70, 106.39, 55.94. HR-MS (ESI, *m/z*); calcd. for C₁₀H₁₀N₂O+H = 175.0866; obtained = 175.0872 [M+H]⁺. *R_f* = 0.54 (ethyl acetate:hexane; 60:40). CAS: 30465-68-0. This compound is known and the data described is in agreement with the previous reports.^[12]

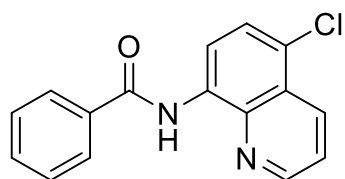
5-Methyl-8-aminoquinoline:

This compound was prepared by a Skraup reaction using 5-methyl-2-nitroaniline and subsequent reduction of the 5-methyl-8-nitroquinoline as described above for the synthesis of 5-chloro-8-aminoquinoline.

Synthesis of 5-methyl-8-nitroquinoline: Glycerol (5 mL, 68.6 mmol, 2.4 equiv.) was heated to 150 °C for 1 hour in a round-bottom flask and then cooled to 110 °C. 5-methyl-2-nitroaniline (5.0 g, 29 mmol) and NaI (87 mg, 0.6 mmol) were then added and the mixture was again heated to 150 °C with vigorous stirring. Thereafter, concentrated sulfuric acid (3.6 mL, 66.7 mmol, 2.3 equiv.) was added and the reaction was left for a further 45 minutes. The reaction was allowed to cool to room temperature, diluted with water (250 mL) and extracted with CH₂Cl₂ (3 x 100 mL). The combined organic layers were washed with brine, dried over magnesium sulfate and concentrated under reduced pressure. The crude was then purified by silica gel chromatography using dichloromethane (R_f = 0.29) as eluent. (3.11 g, 57%). ¹H NMR (CDCl₃, 400 MHz, 298 K); δ = 9.08 (dd, 1H, ³ J_{HH} = 4.2, ⁴ J_{HH} = 1.7), 8.42 (dd, 1H, ³ J_{HH} = 8.6, ⁴ J_{HH} = 1.7), 7.97 (d, 1H, ³ J_{HH} = 7.7), 7.59 (dd, 1H, ³ J_{HH} = 8.6, ³ J_{HH} = 4.2), 7.45 (dq, 1H, ³ J_{HH} = 7.7, ⁴ J_{HH} = 0.9), 2.77 (d, 1H, ⁴ J_{HH} = 0.9). ¹³C {¹H} NMR (CDCl₃, 100 MHz, 298 K); δ = 152.06, 140.29, 139.79, 132.73, 128.13, 125.52, 123.70, 122.33, 19.08. HR-MS (ESI, m/z); calcd. for C₁₀H₈N₂O₂+H = 189.0659; obtained = 189.0655 [M+H]⁺. R_f = 0.41 (dichloromethane). CAS: 65745-69-9. This product has been previously reported.^[16]



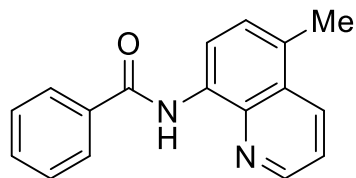
The final compound was prepared from 5-methyl-8-nitroquinoline (500 mg, 2.65 mmol) using the procedure described above for the preparation of 5-chloro-8-aminoquinoline and was purified by column chromatography using ethyl acetate:hexane (60:40) as eluent, resulting in a yellow solid (391 mg, 93%). ¹H NMR (CDCl₃, 400 MHz, 298 K); δ = 8.81 (dd, 1H, ³ J_{HH} = 4.2, ⁴ J_{HH} = 1.7), 8.25 (dd, 1H, ³ J_{HH} = 8.5, ⁴ J_{HH} = 1.7), 7.43 (dd, 1H, ³ J_{HH} = 8.5, ³ J_{HH} = 4.2), 7.18 (dq, 1H, ³ J_{HH} = 7.6, ⁴ J_{HH} = 0.9), 6.87 (d, 1H, ³ J_{HH} = 7.6), 2.58 (d, 1H, ⁴ J_{HH} = 0.9). ¹³C {¹H} NMR (CDCl₃, 100 MHz, 298 K); δ = 147.01, 142.26, 138.98, 132.62, 127.48, 122.36, 120.89, 109.84, 17.90. HR-MS (ESI, m/z); calcd. for C₁₀H₁₀N₂+H = 159.0917; obtained = 159.0931 [M+H]⁺. R_f = 69 (ethyl acetate:hexane; 60:40). CAS: 85656-64-0. This product has been previously reported.^[16]

N-(5-chloroquinolin-8-yl)benzamide (17)

This substrate was made according to the general procedure described above for the synthesis of substrate 1. 5-chloro-8-aminoquinoline (241 mg, 1.35 mmol) and benzoyl chloride (190 mg, 1.35 mmol) were used (320 mg, 84 % of a yellow solid). ¹H NMR (CDCl₃, 400 MHz, 298 K); δ = 10.67 (br s, 1H), 8.90-8.87 (m, 2H), 8.57 (dd, 1H, ³ J_{HH} = 6.9, ⁴ J_{HH} = 1.6), 8.11-8.06 (m, 2H), 7.67 (m,

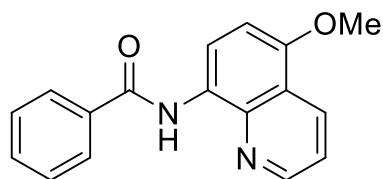
5H). ^{13}C $\{^1\text{H}\}$ NMR (CDCl_3 , 100 MHz, 298 K); δ = 165.36, 148.75, 139.26, 134.85, 133.84, 133.41, 132.01, 128.85, 127.28, 125.96, 124.47, 122.49, 116.44. HR-MS (ESI, m/z); calcd. for $\text{C}_{16}\text{H}_{11}\text{ClN}_2\text{O}+\text{Na}$ = 305.0452; obtained = 305.0450 $[\text{M}+\text{Na}]^+$. R_f = 0.66 (dichloromethane).

***N*-(5-methylquinolin-8-yl)benzamide (18)**



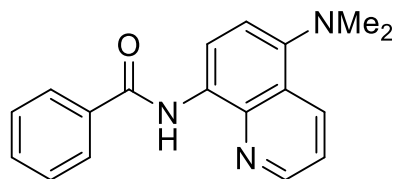
This substrate was made according to the general procedure described above for the synthesis of substrate **1**. 5-methyl-8-aminoquinoline (314 mg, 1.99 mmol) and benzoyl chloride (279 mg, 1.99 mmol) were used (403 mg, 77 % of an orange solid). ^1H NMR (CDCl_3 , 400 MHz, 298 K); δ = 10.75 (br s, 1H), 8.87 (dd, 1H, $^3J_{\text{HH}}$ = 4.2, $^4J_{\text{HH}}$ = 1.1), 8.84 (d, 1H, $^3J_{\text{HH}}$ = 7.8), 8.35 (dd, 1H, $^3J_{\text{HH}}$ = 8.5, $^4J_{\text{HH}}$ = 1.6), 8.14-8.07 (m, 2H), 7.63-7.56 (m, 3H), 7.55 (dd, 1H, $^3J_{\text{HH}}$ = 8.5, $^3J_{\text{HH}}$ = 4.2), 7.43 (dq, 1H, $^3J_{\text{HH}}$ = 8.7, $^4J_{\text{HH}}$ = 0.8), 2.67 (d, 1H, $^4J_{\text{HH}}$ = 0.8). ^{13}C $\{^1\text{H}\}$ NMR (CDCl_3 , 100 MHz, 298 K); δ = 165.33, 147.78, 139.07, 135.32, 133.02, 132.89, 131.73, 128.78, 128.45, 127.53, 127.31, 127.28, 121.25, 116.33, 18.23. HR-MS (ESI, m/z); calcd. for $\text{C}_{17}\text{H}_{14}\text{N}_2\text{O}+\text{Na}$ = 285.0998; obtained = 285.1006 $[\text{M}+\text{Na}]^+$. R_f = 48 (dichloromethane).

***N*-(5-methoxyquinolin-8-yl)benzamide (19)**



This substrate was made according to the general procedure described above for the synthesis of substrate **1**. 5-methoxy-8-aminoquinoline (500 mg, 2.87 mmol) and benzoyl chloride (403 mg, 2.87 mmol) were used (625 mg, 78 % of a yellow solid). ^1H NMR (CDCl_3 , 400 MHz, 298 K); δ = 10.51 (br s, 1H), 8.88 (d, 1H, $^3J_{\text{HH}}$ = 8.5), 8.86 (dd, 1H, $^3J_{\text{HH}}$ = 4.3, $^4J_{\text{HH}}$ = 1.7), 8.60 (dd, 1H, $^3J_{\text{HH}}$ = 8.4, $^4J_{\text{HH}}$ = 1.7), 8.13-8.07 (m, 2H), 7.62-7.52 (m, 3H), 7.47 (dd, 1H, $^3J_{\text{HH}}$ = 8.4, $^3J_{\text{HH}}$ = 4.3), 6.90 (d, 1H, $^3J_{\text{HH}}$ = 8.6), 4.02 (s, 3H). ^{13}C $\{^1\text{H}\}$ NMR (CDCl_3 , 100 MHz, 298 K); δ = 165.09, 150.45, 148.74, 139.48, 135.39, 131.61, 131.30, 128.76, 128.03, 127.28, 120.79, 120.53, 116.73, 104.39, 55.79. HR-MS (ESI, m/z); calcd. for $\text{C}_{17}\text{H}_{14}\text{N}_2\text{O}_2+\text{Na}$ = 301.0947; obtained = 301.0941 $[\text{M}+\text{Na}]^+$. R_f = 0.40 (dichloromethane). This compound is known and the data described is in agreement with the previous reports.^[17]

***N*-(5-(dimethylamino)quinolin-8-yl)benzamide (1d)**

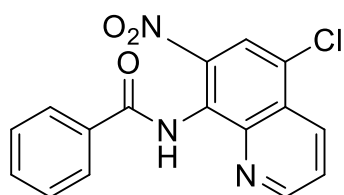


This substrate was prepared by N-methylation of compound **1c**, using a modified N-methylation procedure to that reported by Opatz and co-worker.^[2] To a solution of **1c** (275 mg, 1.04 mmol) in acetonitrile (5 mL), water (2 mL) and aqueous formaldehyde solution (0.8 mL, 37 %), was added sodium cyanoborohydride (190 mg, 3.0 mmol) at 0 °C in small portions. Finally, acetic acid (0.2 mL) was added dropwise and the mixture was

allowed to warm to room temperature and stirred overnight. Subsequently, saturated citric acid solution (10 mL) was added and the reaction stirred for a further 48 hours. After this period, the reaction mixture was adjusted to pH = 10 with sodium hydroxide solution and extracted with ethyl acetate (3 x 40 mL). The combined organic layers were further washed with brine (50 mL), dried over magnesium sulfate and the solvent removed under reduced pressure. The crude reaction product was purified by column chromatography, using dichloromethane as eluent to give analytically pure compound (212 mg, 70 % of a pale yellow solid). ^1H NMR (CDCl_3 , 400 MHz, 298 K); δ = 10.65 (br s, 1H), 8.86 (d, 1H, $^3J_{\text{HH}} = 8.4$), 8.86 (dd, 1H, $^3J_{\text{HH}} = 4.2$, $^4J_{\text{HH}} = 1.7$), 8.62 (dd, 1H, $^3J_{\text{HH}} = 8.5$, $^4J_{\text{HH}} = 1.7$), 8.12-8.08 (m, 2H), 7.62-7.54 (m, 3H), 7.50 (dd, 1H, $^3J_{\text{HH}} = 8.5$, $^3J_{\text{HH}} = 4.2$), 7.20 (d, 1H, $^3J_{\text{HH}} = 8.4$), 2.90 (s, 6H). ^{13}C $\{^1\text{H}\}$ NMR (CDCl_3 , 100 MHz, 298 K); δ = 165.20, 148.07, 145.81, 139.91, 135.40, 133.11, 131.65, 130.06, 128.76, 127.24, 123.82, 120.70, 116.67, 115.02, 45.43. HR-MS (ESI, m/z); calcd. for $\text{C}_{18}\text{H}_{17}\text{N}_3\text{O}+\text{H} = 292.144$; obtained = 292.1434 $[\text{M}+\text{H}]^+$. $R_f = 0.24$ (dichloromethane).

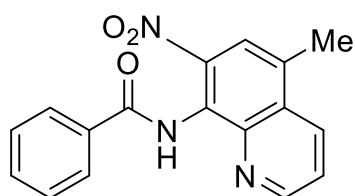
8. Synthesis and characterization data for products (Table VII.13)

N-(5-chloro-7-nitroquinolin-8-yl)benzamide (17b)



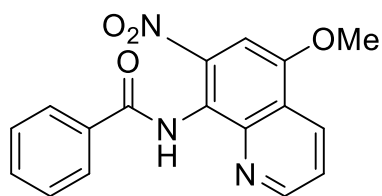
This compound was prepared by the general nitration protocol described above starting from substrate **17** (141mg, 0.5 mmol) to yield a white powder (155 mg, 95 %). ^1H NMR (CDCl_3 , 400 MHz, 298 K); δ = 10.37 (br s, 1H), 9.02 (dd, 1H, $^3J_{\text{HH}} = 4.2$, $^4J_{\text{HH}} = 1.6$), 8.66 (dd, 1H, $^3J_{\text{HH}} = 8.5$, $^4J_{\text{HH}} = 1.6$), 8.16 (s, 1H), 8.14-8.09 (m, 2H), 7.78 (dd, 1H, $^3J_{\text{HH}} = 8.5$, $^3J_{\text{HH}} = 4.2$), 7.68-7.62 (m, 1H), 7.61-7.54 (m, 2H). ^{13}C $\{^1\text{H}\}$ NMR (CDCl_3 , 100 MHz, 298 K); δ = 165.06, 150.79, 141.06, 133.74, 133.09, 132.92, 128.95, 128.03, 127.88, 127.67, 127.51, 126.28, 124.76, 122.03. HR-MS (ESI, m/z); calcd. for $\text{C}_{16}\text{H}_{10}\text{ClN}_3\text{O}_3 + \text{Na} = 350.0303$; obtained = 350.0298 $[\text{M} + \text{Na}]^+$. $R_f = 0.55$ (dichloromethane).

N-(5-methyl-7-nitroquinolin-8-yl)benzamide (18b)



This compound was prepared by the general nitration protocol described above starting from substrate **18** (131 mg, 0.5 mmol) to yield a white powder (130 mg, 85 %). ^1H NMR (CDCl_3 , 400 MHz, 298 K); δ = 10.37 (br s, 1H), 8.93 (dd, 1H, $^3J_{\text{HH}} = 4.2$, $^4J_{\text{HH}} = 1.6$), 8.37 (dd, 1H, $^3J_{\text{HH}} = 8.5$, $^4J_{\text{HH}} = 1.6$), 8.11-8.08 (m, 2H), 7.84 (d, 1H, $^4J_{\text{HH}} = 0.9$), 7.64 (dd, 1H, $^3J_{\text{HH}} = 8.5$, $^3J_{\text{HH}} = 4.2$), 7.64-7.54 (m, 1H), 7.56-7.52 (m, 2H), 2.70 (s, 3H). ^{13}C $\{^1\text{H}\}$ NMR (CDCl_3 , 100 MHz, 298 K); δ = 165.14, 149.87, 140.83, 140.20, 133.47, 133.22, 132.63, 130.67, 129.14, 128.87, 127.96, 126.26, 123.66, 121.76, 18.23. HR-MS (ESI, m/z); calcd. for $\text{C}_{17}\text{H}_{13}\text{N}_3\text{O}_3 + \text{Na} = 330.0849$; obtained = 330.0848 $[\text{M} + \text{Na}]^+$. $R_f = 0.39$ (dichloromethane).

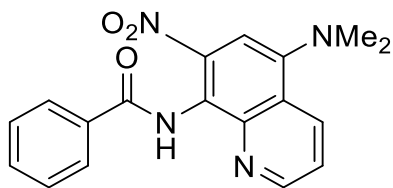
N-(5-methoxy-7-nitroquinolin-8-yl)benzamide (19b)



This compound was prepared by the general nitration protocol described above starting from substrate **19** (139 mg, 0.5 mmol) to yield a white powder (155 mg, 96 %). ^1H NMR (CDCl_3 , 400 MHz, 298 K); δ = 10.11 (br s, 1H), 8.97 (dd, 1H, $^3J_{\text{HH}} = 4.2$, $^4J_{\text{HH}} = 1.7$), 8.66 (dd, 1H, $^3J_{\text{HH}} = 8.5$, $^4J_{\text{HH}} = 1.7$), 8.14-8.09 (m, 2H), 7.66-7.59 (m, 2H), 7.59-7.54 (m, 2H), 7.38 (s, 1H), 4.10 (s, 3H). ^{13}C $\{^1\text{H}\}$ NMR (CDCl_3 , 100 MHz, 298 K); δ = 165.25, 151.38, 150.80, 141.42, 133.64, 132.49, 131.62, 128.83, 128.48, 127.91, 123.21, 122.73, 121.67, 99.94, 56.34. HRMS (ESI, m/z); calcd. for $\text{C}_{17}\text{H}_{13}\text{N}_3\text{O}_4 + \text{Na} = 346.0798$; obtained = 346.0803 $[\text{M} + \text{Na}]^+$. $R_f = 0.36$ (dichloromethane).

***N*-(5-(dimethylamino)-7-nitroquinolin-8-yl)benzamide (1db)**

This compound was prepared by the general nitration protocol described above starting



from substrate **1d** (146 mg, 0.5 mmol) to yield a white powder (135 mg, 80 %). $^1\text{H NMR}$ (CDCl_3 , 400 MHz, 298 K); δ = 10.65 (br s, 1H), 9.15 (s, 1H), 8.96 (dd, 1H, $^3J_{\text{HH}} = 4.2$, $^4J_{\text{HH}} = 1.7$), 8.73 (dd, 1H, $^3J_{\text{HH}} = 8.5$, $^4J_{\text{HH}} = 1.7$), 8.11-8.06 (m, 2H), 7.64-7.56 (m, 4H), 2.98 (s, 6H).

$^{13}\text{C} \{^1\text{H}\}$ NMR (CDCl_3 , 100 MHz, 298 K); δ = 165.27, 150.21, 143.59, 140.59, 138.25, 134.84, 134.54, 132.16, 131.56, 12.19, 127.29, 126.85, 122.51, 111.53, 43.36. HRMS (ESI, m/z); calcd. for $\text{C}_{18}\text{H}_{16}\text{N}_4\text{O}_3 + \text{Na} = 359.1115$; obtained = 359.1114 $[\text{M} + \text{Na}]^+$. $R_f = 0.52$ (dichloromethane).

9. X-ray crystallography data

Crystallographic data for compounds **11b** (CCDC-1438116), **13b** (CCDC-1438117) and **15a** (CCDC-1438118) can be obtained free of charge from the Cambridge Crystallographic Data Centre (CCDC) via www.ccdc.cam.ac.uk/data_request/cif. Furthermore, the corresponding CIF files have been included in the Supplementary Digital Material included in the attached CD.

9.1 X-Ray structure of 11b

Yellow crystals were grown by slow diffusion of pentane into a chloroform solution of the compound, and used for low temperature (100(2) K) X-ray structure determination. The measurement was carried out on a *BRUKER SMART APEX CCD* diffractometer using graphite-monochromated Mo $K\alpha$ radiation ($\lambda = 0.71073 \text{ \AA}$) from an x-Ray Tube. The measurements were made in the range 2.590 to 28.324° for θ . Full-sphere data collection was carried out with ω and ϕ scans. A total of 18366 reflections were collected of which 2946 [$R(\text{int}) = 0.0307$] were unique. Programs used: data collection, Smart^[18]; data reduction, Saint+^[19]; absorption correction, SADABS^[20]. Structure solution and refinement was done using SHELXTL^[21].

The structure was solved by direct methods and refined by full-matrix least-squares methods on F^2 . The non-hydrogen atoms were refined anisotropically. The H-atoms were placed in geometrically optimized positions and refined freely.

Table S34. Crystallographic data of **1aa**.

Chemical formula	$\text{C}_{14}\text{H}_9\text{N}_3\text{O}_4$
fw (g mol⁻¹)	283.24
T (K)	100(2)
Space group	Monoclinic, P 21/c
<i>a</i> (Å)	5.2240(4)
<i>b</i> (Å)	8.1944(6)
<i>c</i> (Å)	28.014(2)
α (deg.)	90
β (deg.)	92.3080(10)
γ (deg.)	90
<i>V</i> (Å³)	1198.22(15)
$\rho_{\text{calcd.}}$ (g cm⁻³)	1.570
λ (Å)	0.71073
R_1 [$I > 2\sigma(I)$]	0.0373
wR_2 [$I > 2\sigma(I)$]	0.0970

9.2 X-Ray structure of 13b

Colorless crystals were grown by slow diffusion of pentane into a chloroform solution of the compound, and used for low temperature (100(2) K) X-ray structure determination. The measurement was carried out on a *BRUKER SMART APEX CCD* diffractometer using graphite-monochromated Mo $K\alpha$ radiation ($\lambda = 0.71073 \text{ \AA}$) from an x-Ray Tube. The measurements were made in the range 2.544 to 28.348° for θ . Full-sphere data collection was carried out with ω and ϕ scans. A total of 8005 reflections were collected of which 2480 [$R(\text{int}) = 0.0174$] were unique. Programs used: data collection, Smart^[18]; data reduction, Saint+^[19]; absorption correction, SADABS^[20]. Structure solution and refinement was done using SHELXTL^[21].

The structure was solved by direct methods and refined by full-matrix least-squares methods on F^2 . The non-hydrogen atoms were refined anisotropically. The H-atoms were placed in geometrically optimized positions and refined freely.

Table S35. Crystallographic data of **1aa**.

Chemical formula	$\text{C}_{11}\text{H}_9\text{N}_3\text{O}_3$
fw (g mol⁻¹)	231.21
T (K)	100(2)
Space group	Monoclinic C c
<i>a</i> (Å)	10.0842(8)
<i>b</i> (Å)	16.0119(12)
<i>c</i> (Å)	7.0635(5)
α (deg.)	90
β (deg.)	116.3620(10)
γ (deg.)	90
<i>V</i> (Å³)	1021.92(13)
$\rho_{\text{calcd.}}$ (g cm⁻³)	1.503
λ (Å)	0.71073
R_1 [I > 2σ(I)]	0.0290
wR_2 [I > 2σ(I)]	0.0780

9.3 X-Ray structure of 15a

Colorless crystals were grown by slow diffusion of pentane into a chloroform solution of the compound, and used for low temperature (173(2) K) X-ray structure determination. The measurement was carried out on a *BRUKER SMART APEX CCD* diffractometer using graphite-monochromated Mo $K\alpha$ radiation ($\lambda = 0.71073 \text{ \AA}$) from an x-Ray Tube. The measurements were made in the range 2.235 to 28.392° for θ . Full-sphere data collection was carried out with ω and ϕ scans. A total of 10121 reflections were collected of which 3308 [R(int) = 0.0306] were unique. Programs used: data collection, Smart^[18]; data reduction, Saint+^[19]; absorption correction, SADABS^[20]. Structure solution and refinement was done using SHELXTL^[21].

The structure was solved by direct methods and refined by full-matrix least-squares methods on F^2 . The non-hydrogen atoms were refined anisotropically. The H-atoms were placed in geometrically optimized positions and forced to ride on the atom to which they are attached, other C-H hydrogens were refined freely.

Table S36. Crystallographic data of **1aa**.

Chemical formula	C ₁₄ H ₁₅ N ₃ O ₃
fw (g mol⁻¹)	273.29
T (K)	173(2)
Space group	Triclinic, P -1
a (Å)	8.466(10)
b (Å)	9.632(11)
c (Å)	9.683(11)
α (deg.)	85.531(19)
β (deg.)	67.313(17)
γ (deg.)	71.304(19)
V (Å³)	689.2(14)
$\rho_{\text{calcd.}}$ (g cm⁻³)	1.317
λ (Å)	0.71073
R₁ [I > 2sigma(I)]	0.0600
wR₂ [I > 2sigma(I)]	0.1645

10. Kinetic Isotope Effect (KIE) experiment

H-D exchange for the synthesis of the deuterated aminoquinoline (*selective 5,7-deuteration*) was performed using the methodology reported by Lautens and co-workers.^[22] This compound was then used for the synthesis of **D₂-1** as described above (Page S4). Figure S170 represents the ¹H NMR spectra obtained for **D₂-1** (96% deuterium incorporation).

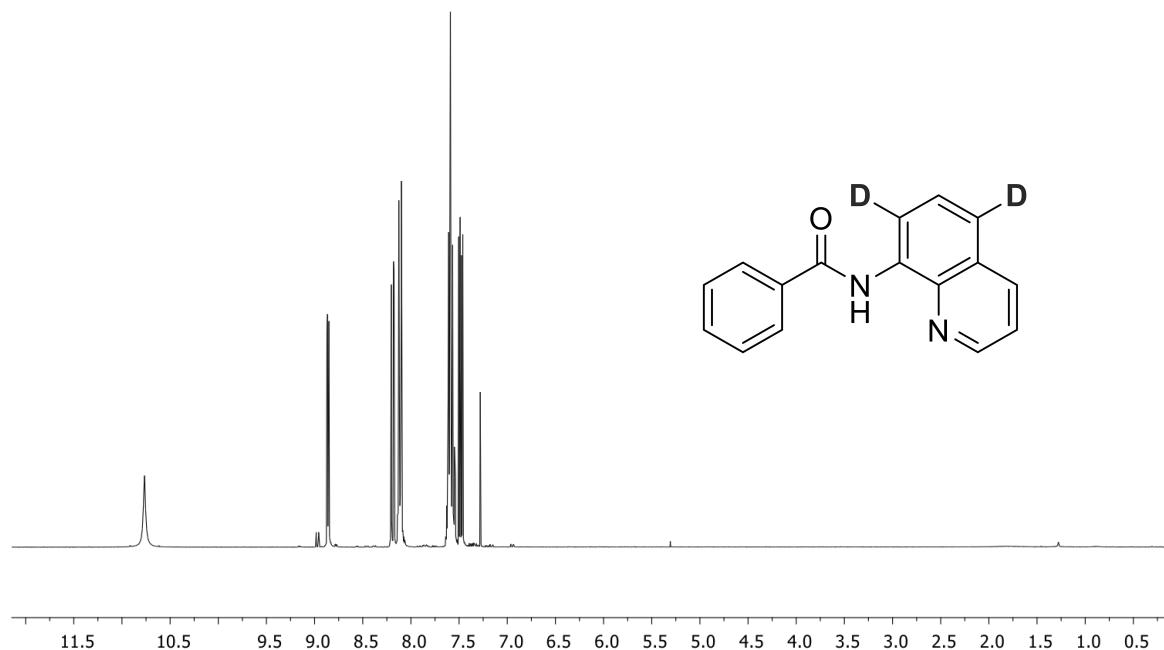


Figure S70. ¹H NMR of substrate **D₂-1** (CDCl₃, 298 K, 300 MHz).

A competitive reaction was carried out between substrates **1** and **D₂-1**, under the optimized reaction conditions, in order to obtain the k_H/k_D value. The ¹H NMR spectrum for this result is shown in Figure S71. The value of k_H/k_D was calculated to be 0.97 (using TMB as internal standard), which is consistent with the results obtained by Stahl and co-workers for the copper-catalyzed chlorination of the same substrate.^[23]

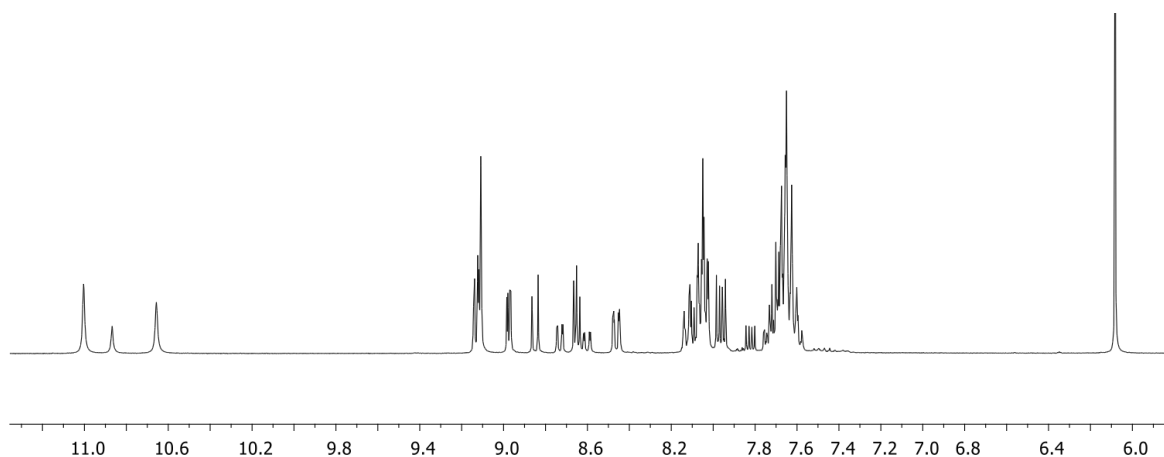


Figure S71. ¹H NMR spectrum used for the determination of the k_H/k_D value, using TMB as internal standard (CDCl₃, 298 K, 300 MHz).

11. References

- (1) Grigorjeva, L.; Daugulis, O. *Org. Lett.* **2014**, *16*, 4684.
- (2) N. Otto, N.; T. Opatz, T. *Beilstein J. Org. Chem.* **2012**, *8*, 1105.
- (3) Yapi, A.-D.; Desbois, N.; Chezal, J.-M.; Chavignon, O.; Teulade, J.-C.; Valentin, A.; Blache, Y. *Eur. J. Med. Chem.* **2010**, *45*, 2854.
- (4) Wang, J.; Yin, X.; Wu, J.; Wu, D.; Pan, Y. *Tetrahedron* **2013**, *69*, 10463.
- (5) Grigorjeva, L.; Daugulis, O. *Org. Lett.* **2015**, *17*, 1204.
- (6) Grigorjeva, L.; Daugulis, O. *Org. Lett.* **2014**, *16*, 4688.
- (7) Katayev, D.; Pfister, K. F.; Wendling, T.; Gooßen, L. *J. Chem. Eur. J.* **2014**, *20*, 9902.
- (8) Vangapandu, S.; Jain, M.; Jain, R.; Kaur, S.; Singh, P. P. *Bioorg. Med. Chem.* **2004**, *12*, 2501.
- (9) Xiong, H.-Y.; Besset, T.; Cahard, D.; Pannecoucke, X. *J. Org. Chem.* **2015**, *80*, 4204.
- (10) Zhang, J.; Chen, H.; Wang, B.; Liu, Z.; Zhang, Y. *Org. Lett.* **2015**, *17*, 2768.
- (11) Zhu, Q.; Ji, D.; Liang, T.; Wang, X.; Xu, Y. *Org. Lett.* **2015**, *17*, 3798.
- (12) He, G.; Zhang, S.-Y.; Nack, W. A.; Li, Q.; Chen, G. *Angew. Chem. Int. Ed.* **2013**, *52*, 11124.
- (13) Sosič, I.; Mirković, B.; Arenz, K.; Štefane, B.; Kos, J.; Gobec, S. *J. Med. Chem.* **2013**, *56*, 521.
- (14) Shimizu, T.; Watanabe, M. **1994**, EP614915A1.
- (15) Aihara, Y.; Tobisu, M.; Fukumoto, Y.; Chatani, N. *J. Am. Chem. Soc.* **2014**, *136*, 15509.
- (16) Ikeda, M.; Yamagishi, M.; Bayomi, S. M. M.; Miki, Y.; Sumida, Y.; Tamura, Y. *J. Chem. Soc., Perkin Trans. I: Org. Bio-Org. Chem.* **1983**, *2*, 349.
- (17) Allu, S.; Swamy, K. C. K. *J. Org. Chem.* **2014**, *79*, 3963.
- (18) Bruker Advanced X-ray Solutions. SMART: Version 5.631, **1997-2002**.
- (19) Bruker Advanced X-ray Solutions. SAINT +: Version 6.36A, **2001**.
- (20) Sheldrick, G. M. *Empirical Absorption Correction Program*, Universität Göttingen, **1996**, Bruker Advanced X-ray Solutions. SADABS Version 2.10, **2001**.
- (21) Sheldrick, G. M. *Program for Crystal Structure Refinement*, Universität Göttingen, **1997**, Bruker Advanced X-ray Solutions. SHELXTL Version 6.14, **2000-2003**. SHELXL-2013 (Sheldrick, **2013**).
- (22) Martins, A.; Lautens, M. *Org. Lett.* **2008**, *10*, 4351.
- (23) Seuss, A. M.; Ertem, M. Z.; Cramer, C. J.; Stahl, S. S. *J. Am. Chem. Soc.* **2013**, *135*, 9797.